Optimized Synthesis and Characteristics of Novel Thermoplastic Polymers for Solid Formulation

Inaugural Dissertation

for Attaining the Academic Degree of

„Doctor rerum naturalium“ (Dr. rer. nat.)

in Chemistry

Submitted in the Department 09

Chemistry, Pharmaceutical Science, Geography, and Geosciences

at the Johannes Gutenberg-University Mainz

Tristan Alexei Marquetant

born in Mannheim

Mainz, 2025

Dekan:

[redacted]

Erstgutachter:

[redacted]

Zweitgutachter:

[redacted]

Tag der mündlichen Prüfung:

20.02.2025

Eigenständigkeitserklärung

Hiermit erkläre ich, Tristan Alexei Marquetant, dass ich die vorliegende Arbeit mit dem Titel: **Optimized Synthesis and Characteristics of Novel Thermoplastic Polymers for Solid Formulation** selbstständig verfasst und keine anderen als die angegebenen Quellen und Hilfsmittel (dazu zählen auch KI-basierte Anwendungen und Werkzeuge) benutzt habe. Sämtliche wörtlichen und sinngemäßen Übernahmen und Zitate sind kenntlich gemacht und nachgewiesen (dies gilt auch für Texte, die durch generative KI, wie Chat GPT erzeugt wurden). Ich versichere, dass ich keine Hilfsmittel verwendet habe, deren Nutzung die Prüferin oder der Prüfer explizit ausgeschlossen hat. Folgende KI-Tools habe ich wie entsprechend beschrieben verwendet:

Tool	**Genutzt für…**	**Warum?**	**Wann?**
DeepL Translate	Übersetung von Begriffen von deutsch auf englisch und umgekehrt	Verständnis wissenschaftlicher Arbeiten und Hilfe bei Formulierung englischer Sätze	Über die gesamte Arbeit hinweg
DeepL Write	Neuformulierung meiner Textentwürfe	Bessere Lesbarkeit und Verständlichekeit	Über die gesamte Arbeit hinweg
ChatGPT	Neuformulierung meiner Textentwürfe	Bessere Lesbarkeit und Verständlichkeit	Über die gesamte Arbeit hinweg
MyGPT@Merck	Neuformulierung einer Textentwürfe	Bessere Lesbarkeit und Verständlichkeit	Über die gesamte Arbeit hinweg

Mit Abgabe der vorliegenden Leistung übernehme ich die Verantwortung für das eingereichte Gesamtprodukt. Ich verantworte damit auch jegliche KI-generierten Inhalte, die ichin meine Arbeit übernommen habe. Die Richtigkeit übernommener (KI-generierter) Aussagen und Inhalte habe ich nach bestem Wissen und Gewissen geprüft.

Mir ist bekannt, dass ein Verstoß gegen die genannten Punkte prüfungsrechtliche Konsequenzen hat und insbesondere dazu führen kann, dass die Promotionsleistung als mit „nicht bestanden“ bewertet wird. Die Einschreibung kann für bis zu zwei Jahre widerrufen werden, wenn Studierende zweimal oder häufiger bei Prüfungsleistungen täuschen (§69 Abs. 4 und 5 HoschSchG).

Vorwort

Diese Arbeit wurde unter der Betreuung von [redacted] im Zeitraum von Oktober 2020 bis Januar 2025 am Department Chemie der Johannes Gutenberg-Universität (JGU) Mainz in Kooperation mit der Merck Life Science KGaA in Darmstadt verfasst. Die Arbeit ist in Englisch verfasst. Der Hauptteil der Forschungsarbeit wurde in den Laboratorien der Merck Life Science KGaA durchgeführt. Wesentliche Teile der Arbeit wurden im Rahmen des „PolyPrint“ Verbundprojekts unter der Begleitmaßnahme „ProMatLeben-WIN“ des Bundesministeriums für Bildung und Forschung durchgeführt.

D77 – Dissertation Johannes Gutenberg-Universität Mainz

Abbreviations

Abbreviation	Meaning
T_{exp}	heating phase
ΔT_{prep}	initial cooling phase
^{13}C-NMR	carbon-13 nuclear magnetic resonance spectroscopy
^{1}H-NMR	H-1 nuclear magnetic resonance spectroscopy
Å	Ångström
acac	acetylacetonate
ACVA	4,4′-Azobis(4-cyanovaleric acid)
ADME	absorption, distribution, metabolism, and excretion
AmPEG	allyl poly(ethylene glycol) monomethyl ether
AP	amorphous polymer
API	active pharmaceutical ingredient
appl.	application
ARC	accelerating rate calorimeter
ASD	amorphous solid dispersion
ATRP	atom Transfer Radical Polymerization
AUC	area under curve
BCS	viopharmaceutics Classification System
BHT	dibutylhydroxytoluene
Caff	caffeine
CAP	cellulose acetate phthalate
CC	crystalline carrier
$c_{Caff,max}$	maximum concentration of caffeine
CDI	*N,N*′-Carbonyldiimidazol
$c_{KTZ,max}$	maximum concentration of ketoconazole
d	doublet
Đ	dispersity index
Da	Dalton
DCC	*N,N*′-Dicyclohexylcarbodiimide
DMA	dynamic mechanical analysis
DMAc	*N,N*-Dimethylacetamide
DMAP	4-(Dimethylamino)pyridine
DMF	*N,N*-Dimethylformamide
DMSO	dimethyl sulfoxide
DoE	design of experiments
DOSY NMR	diffusion ordered nuclear magnetic resonance spectroscopy
DSC	differential scanning calorimetry
e.g.	exempli gratia
EDC-HCl	1-Ethyl-3-(3-dimethylaminopropyl)carbodiimide
EMA	European Medicines Agency
eq.	equivalent
et al	et alii
Exp	experimental
Extr.	extrudable range
FaSSIF	Fasted State Simulated Intestinal Fluid
FDA	U.S. Food and Drug Administration
FDM	fused deposition modeling
Abbreviation	Meaning

FPT	freeze-pump-thaw
FRP	free radical polymerization
G'	storage modulus
G"	loss modulus
GC	gas chromatography
GPC	gel permeation chromatography
ɣ	angular frequency
hept	heptet
HMBC-NMR	heteronuclear multiple-bond correlation NMR spectroscopy
HME	hot melt extrusion
HPC	hydroxypropyl cellulose
HPLC	high pressure liquid chromatography
HPMC	hydroxypropyl methylcellulose
HPMCAS	hydroxypropyl methylcellulose acetate succinate
HQ	hydroquinone
HSQC-NMR	heteronuclear single quantum coherence NMR spectroscopy
Hygr.	hygroscopicity
I(X)	integral of X
Im	imidazol
Init.	initiator
iPrOH	*iso*-propanol
k_{xy}	reaction rate constant
KTZ	ketoconazol
M	molarity
m	multiplet
$M^{\#}$	monomer #
MALS	multi angle light scattering
MCC	microcrystalline cellulose
mDSC	modulated differential scanning calorimetry
MEHQ	4-methoxyphenol
misc	miscellaneous
Mod. Deg.	modification degree
M_p	maximum molecular weight
mPEG	poly(ethylene glycol) monomethyl ether
mPEG2 aa	2-[2-(2-Methoxyethoxy)ethoxy]acetic acid
mPEG550	mPEG with molecular weight of 550 g/mol
mPEGMA	poly(ethylene glycol) monomethyl ether methacrylate
MS	mass spectrometry
MTBE	methyl *tert*-butyl ether
M_w	mass average molar mass
MWCO	molecular weight cut off
n.a.	not available
n.d.	not determined
NaH	sodium hydride
NaOH	sodium hydroxide
NCE	new chemical entity
NMP	1-methylpyrrolidin-2-one
NMR	Nuclear Magnetic Resonance
OH-groups	hydroxyl groups
Abbreviation	Meaning
PAA	polyacrylic acid

PDI	poly dispersity index
PEG	polyethylene glycol
PEO	polyethylene oxide
PMMA	poly(methyl methacrylate)
ppm	parts per million
prec	precursor
PTFE	polytetrafluoroethylene
PVA	poly vinylalcohol
PVA-co-PVAc	poly(vinylacetate-co-vinylalcohol)
PVAc-co-PVP	poly(vinylacetate-co-vinylpyrrolidone)
PVAP	polyvinyl acetate phthalate
PVP	poly vinylpyrrolidone
PVP	poly vinylpyrrolidone
PVP-co-PVA	poly(vinylpyrrolidone-co-vinylalcohol)
q	quartet
quant.	quantitative
r_x	ratio of monomer x
RAFT	reversible addition−fragmentation chain-transfer
RDRP	controlled reversible-deactivation radical polymerization
RI	refractive index
rM-X	molar ratio of Monomer X
sap. Kollidon	saponified Kollidon VA64
SD	standard deviation
SD	standard deviation
SFP	surfactant polymer
SFP	surfactant
SNR	signal to noise ratio
Sol.	solubility
SP	swellable polymer
t	triplet
$T_{1000\ Pa\ s}$	temperature at melt viscosity of 1000 Pa s
$T_{10000\ Pa\ s}$	temperature at melt viscosity of 10000 Pa s
T_{deg}	degradation temperature
TFA	trifluoroacetic acid
T_g	glass transition temperature
TGA	thermogravimetric analysis
TGA-GC-MS	TGA coupled with GC and MS
TGA-IR	TGA coupled with infrared spectroscopy
theo	theoretical
Tm	melting temperature
TMS	tetramethylsilane
Tonset	onset temperature
Tproc	processing temperature
U(H)PLC	ultra high pressure liquid chromatography
USP	US Pharmacopeia
VAc	vinyl acetate
VAc	vinyl acetate
VBenz	vinyl benzoate
Abbreviation	Meaning
VCM	vacuum compression molding
VP	vinyl pyrrolidone

VP	vinyl pyrrolidone
w%	weight percent
WIP	water insoluble polymer
XRD	x-ray diffraction
δ	phase angle
ΔT	temperatuer difference
ηmelt	melt viscosity
λ	wavelength
ω	strain rate

Table of Contents

1 Zusammenfassung

Die vorliegende Arbeit widmet sich einer der wesentlichen Herausforderungen in der Formulierung fester Darreichungsformen: der schlechten Löslichkeit von neu entwickelten Wirkstoffen (APIs). Das Problem der geringen Löslichkeit ist insbesondere bei BCS-Klasse-II-Wirkstoffen entscheidend, da es die therapeutische Wirksamkeit von Medikamenten durch Begrenzung ihrer Bioverfügbarkeit direkt beeinträchtigt. Die Forschungsarbeit fokussiert sich gezielt auf die Forschung durch die Entwicklung und Nutzung speziell angepasster Polymere, insbesondere in Form von amorphen Feststoffdispersionen (ASDs), um die Löslichkeit der APIs zu verbessern.

Getrieben von der Notwendigkeit, sowohl die Löslichkeit von Wirkstoffen als auch die Herstellungsprozesse zu optimieren, ist das Hauptziel der Arbeit, thermoplastische Polymere zu entwickeln, die darauf abzielen, die Verarbeitbarkeit von Wirkstoffen in pharmazeutischen Extrusionsanwendungen zu verbessern und dessen Verarbeitungstemperaturen zu senken. Dies beinhaltet die Synthese modifizierter Polymere und eine eingehende Analyse der resultierenden Struktur-Eigenschafts-Beziehungen, die ihre Funktionalität bei der Verbesserung der Wirkstofflöslichkeit und Verarbeitbarkeit beeinflussen.

Der erste Teil der Studie legt den Grundstein, indem er sich auf die Synthese und die ausführliche Charakterisierung modifizierter Polymere konzentriert, insbesondere solcher, die von Polyvinylpyrrolidon-co-Vinylalkohol (PVP-co-PVA) abgeleitet sind. Dies wird durch rigorose Charakterisierungstechniken wie Kernspinresonanz (NMR) Spektroskopie, dynamische Differenz-Kalorimetrie (DSC), thermogravimetrische Analyse (TGA) und Schmelzrheologie sichergestellt, um die physikochemischen Eigenschaften der Polymere und ihre Wechselwirkungen mit Wirkstoffen qualitativ zu verstehen. Die Ergebnisse zeigen die erfolgreiche Synthese einer Reihe von neuartigen Polymeren mit unterschiedlichen Zusammensetzungen, die nicht nur eine verbesserte Löslichkeit eines Modellwirkstoffs zeigen, sondern auch geeignete mechanische und thermische Eigenschaften für Extrusionsprozesse aufweisen. Die Analyse dieser Struktur-Eigenschafts-Beziehungen zeigt, dass die Löslichkeitsverbesserungen durch die Variation der molekularen Architektur der Polymere direkt beeinflusst werden können, einschließlich der Monomertypen, die ihre Glasübergangstemperaturen, Viskosität und thermische Stabilität beeinflussen.

Der zweite Teil der Arbeit umfasst die Synthese von Polymeren durch freie radikalische Polymerisation, die eine gezielte Veränderung der molekularen Struktur ermöglicht und die Polymer-Eigenschaften signifikant beeinflusst. Die maßgeschneiderte Synthese dieser Polymere zielt darauf ab, Eigenschaften zu optimieren, die für Extrusionsprozesse entscheidend sind, wie Glasübergangstemperatur, thermische Stabilität und Schmelzviskosität. Eine skalierbare Synthese-Plattform wird entwickelt, die bis zu vier

Comonomere umfasst. Die Monomer-Auswahl enthält Vinylacetat, *N*-Vinylpyrrolidon, das hydrophile Poly(ethylenglycol)methacrylat und das hydrophobe, aromatische Vinylbenzoat, welche in unterschiedlichen Anteilen in die Polymere eingebaut werden. In einer explorativen statistischen Versuchsplanung (DoE) werden die spezifischen Einflüsse der verschiedenen Comonomere bewertet und eine vielversprechende Polymerzusammensetzung identifiziert. Kandidaten mit herausragender Löslichkeitsvermittlung wurden identifiziert, und die zuvor entwickelte Struktur-Eigenschafts-Beziehung wurde bestätigt.

Die Arbeit diskutiert eingehend das Potenzial dieser Polymere, die pharmazeutischen Extrusionstechniken bei niedrigeren Temperaturen voranzutreiben und betont ihre Fähigkeit, die Löslichkeit eines Modellwirkstoffs zu verbessern und damit potenziell die Bioverfügbarkeit von Medikamenten zu erhöhen. Die Interaktion zwischen den Polymeren und Wirkstoffen, beeinflusst durch die chemischen und physikalischen Eigenschaften der Polymere, wird kritisch erforscht, um zu verstehen, wie diese Interaktionen optimiert werden können, um den Wirkstofftransport zu verbessern.

Zusammenfassend zeigt die in dieser Studie durchgeführte Forschung die Entwicklung neuartiger pharmazeutischer Materialien, wobei insbesondere die Synthese von thermoplastischen Polymeren betont wird, die die doppelten Anforderungen an eine verbesserte Wirkstofflöslichkeit und eine effektive Extrusionsverarbeitung erfüllen. Die Ergebnisse tragen nicht nur zum akademischen Bereich der Polymerchemie und pharmazeutischen Wissenschaften bei, sondern haben auch praktische Auswirkungen und bieten erste Einblicke für die pharmazeutische Industrie, wie eine mögliche, maßgeschneiderte Lösung der Herausforderungen im Forschungsfeld schlecht wasserlöslicher Wirkstoffe aussehen könnte.

Ausblickend wird vorgeschlagen, weitere Forschungen zu anderen Monomer-Systemen durchzuführen, die die Polymer-Eigenschaften noch weiter verbessern könnten. Darüber hinaus kann der vorgeschlagene Syntheseprozess als Plattform dienen, um vielfältige Monomere zu integrieren, die die spezifischen Anforderungen erfüllen. Es wird auch empfohlen, Langzeitstabilitätsstudien und In-vivo-Tests durchzuführen, um die klinische Relevanz der entwickelten Polymere vollständig zu bestimmen.

2 Abstract

The present study presents a detailed exploration aimed at tackling one of the significant challenges in pharmaceutical sciences, namely the poor solubility of active pharmaceutical ingredients (APIs). The issue of poor solubility is pivotal in the case of BCS class II APIs as it directly impacts the therapeutic efficacy of drugs by limiting their bioavailability. The thesis methodically advances the research field by the utilization of tuned polymers, specifically in the form of amorphous solid dispersions (ASDs), to enhance API solubility.

The first part of this study lays the groundwork by focusing on the synthesis and detailed characterization of modified polymers, particularly those derived from polyvinylpyrrolidone-co-vinyl alcohol (PVP-co-PVA). The modification agents include functional groups such as substituted amines, aromatic moieties, polyethylene glycol groups, and alkyl chains. This is complemented by characterization techniques such as Nuclear Magnetic Resonance (NMR) spectroscopy, Differential Scanning Calorimetry (DSC), Thermogravimetric Analysis (TGA), and melt rheology to understand the polymers' physicochemical properties and their interactions with APIs. The findings reveal the successful synthesis of a series of novel polymers with varied compositions that not only demonstrate enhanced solubility with a model API but also exhibit suitable mechanical and thermal properties for extrusion processes. The analysis of these structure-property relationships shows that the solubility enhancements can be influenced by varying the polymers' molecular architecture, including monomer types and chain configurations that affect their glass transition temperatures, viscosity, and thermal stability.

The second part of the thesis includes the synthesis of polymers through free radical polymerization which allows for controlled variation of molecular structure thus affecting the polymer properties significantly. The tailored synthesis of these polymers aims to optimize properties crucial for extrusion processes such as glass transition temperature, thermal stability, and melt viscosity. A scalable synthesis is developed incorporating up to four comonomers. The comonomer selection consists of vinyl acetate, *N*-vinyl pyrrolidone, a hydrophilic polyethylene glycol methacrylate and a hydrophobic aromatic vinyl benzoate. Polymers are generated with varying ratios of these comonomers respectively. In an explorative design of experiments (DoE) approach, the specific influences of the different comonomers are evaluated and one high potential polymer composition is identified. Candidates with outstanding dissolution performance have been identified and the structure-property relationship previously developed was proven.

This thesis thoroughly discusses the potential of these polymers to advance pharmaceutical extrusion techniques at lower temperatures, emphasizing their capability to enhance the solubility of a model API and thereby potentially increase the bioavailability of drugs. The nuanced interaction between the

polymers and APIs, influenced by the polymers' chemical and physical properties, is critically explored to understand how these interactions can be optimized to enhance drug delivery systems.

Driven by the necessity to optimize both drug solubility and manufacturing processes, the thesis' primary objective is to engineer thermoplastic polymers tailored for decreasing the HME processing temperatures in the formulation of APIs. This involves the synthesis of modified polymers and an in-depth analysis of the structure-property relationships that influence their functionality in enhancing API solubility and processability.

In conclusion, the research encapsulated in this study demonstrates the development of novel pharmaceutical materials, particularly emphasizing the synthesis of thermoplastic polymers that meet the dual requirements of enhanced API solubility and effective extrusion processability. The findings not only contribute to the academic field of polymer chemistry and pharmaceutical sciences but also hold practical implications, offering first insights for a potential solution of challenges in the field of solid formulation of poorly water-soluble drugs.

Looking ahead, exploring other monomeric systems and their influence on the polymer/API interaction may enable the formulation of a given API to tailor the dissolution behavior and its manufacturing. Furthermore, the proposed synthesis process can serve as a platform to incorporate diverse monomers fulfilling the specific prerequisites posed by researchers. For the definition of those requirements, predictive, machine learning formulation tools may be employed to accelerate the discovery of the ideal structure, and the developed synthesis platform can then be used for the tailored synthesis thereof. It is also recommended to conduct long-term stability studies and in vivo trials to fully determine the clinical relevance of the developed polymers.

3 Introduction

3.1 Polymers in Solid Formulation

The endeavor to enhance the bioavailability of poorly water-soluble active pharmaceutical ingredients (APIs) is an ever-present challenge in the pharmaceutical industry. A significant number of pipeline drug candidates revealed by drug discovery programs, particularly those in the Biopharmaceutics Classification System Class II (BCS-II), exhibit poor water-solubility.[1] This severely hampers their respective bioavailability and thus their clinical efficacy.[2] Therefore, innovative solutions in drug formulation are vital. In this context, polymers offer a broad arsenal of means to tailor the delivery and the performance of these new drug products.

Since polymers were first mentioned by Staudinger[3], they evolved to have an extraordinary impact in a plethora of applications all over the world (Figure 1b). There is a steady influx of new use cases for this substance class and the production volume of polymers increased eightfold since 1976 to 400 million metric tons per year (Figure 1a). Today, Polymers are ubiquitous in everyday life, especially in packaging materials, clothing, or construction, and ever-present in various research fields, such as biodegradable polymers, smart and high-performance materials, or excipients in pharmaceutical formulation. This study deals with polymers in the field of pharmaceutical formulation, where polymers act as excipients in the formulation of active pharmaceutical ingredients.

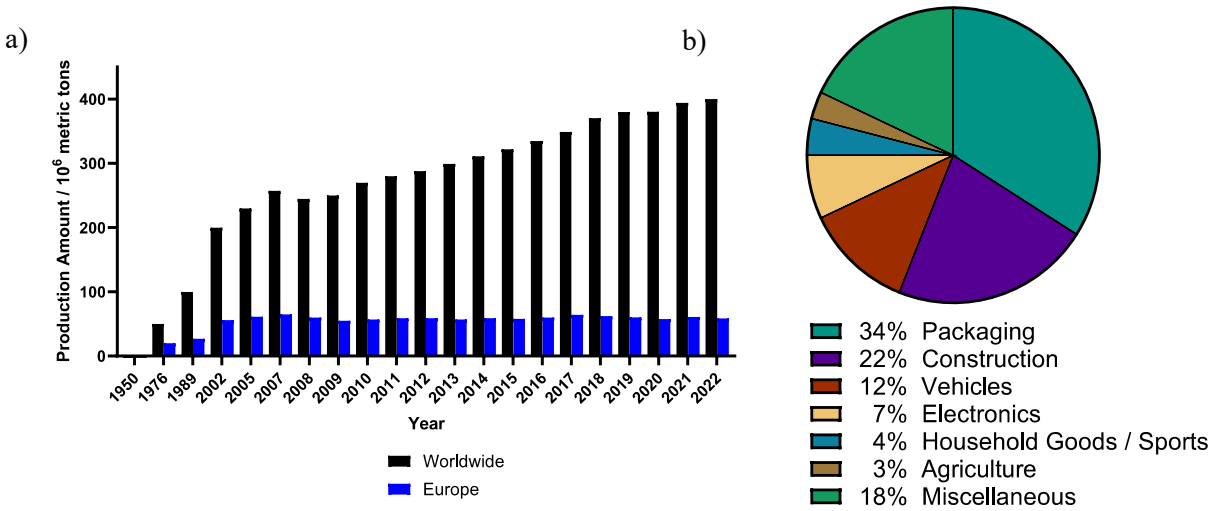

Figure 1: a) Worldwide production volume polymers in 2022[4]; b) Utilization of produced polymers in different working areas.

After their first utilization as film-formers for tablet coatings[5-7] in the late 1930s, polymers have revolutionized the field of drug delivery. Soon after, in the 1950s, polymers such as cellulose acetate phthalate were used for enteric coatings[8-10] and the first publications concerning poly vinylpyrrolidone

(PVP)[11, 12] emerged. The foundation was laid for polymers to become one of the most potent classes of compounds in solid formulation. Polymers offer a diverse set of functions in the development of pharmaceutical formulations including the enhancement of the efficacy, bioavailability, solubility, stability, and delivery of APIs. They take the role as excipients, which by definition are inactive substances and serve as the vehicle or medium for an API. Their applications are manifold, acting as binders, disintegrants, fillers and coating agents, where they contribute to ideal mechanical strength, the ideal release profile and bioavailability of drugs.[8-10, 13-35] Microcrystalline cellulose (MCC), first used in the 1960s, is a prominent entity used as a filler or binder with the ability to ensure structural integrity of a dosage form during ingestion and dissolution. Polymers like hydroxypropyl methylcellulose (HPMC) are widely used as matrices in controlled release formulations to modulate the release kinetics of an API resulting in reduced dosing frequencies and sustained therapeutic effect. These excipients offer structural flexibility as they may be functionalized leading to favorable properties regarding their properties such as their hydrophilicity.[5, 6, 8, 9, 23, 36-41]

After the first mentioning of polymers like PVP[11] or PVA in the 1950s, they later became pivotal in the creation of amorphous solid dispersions, where an API is molecularly dispersed in the polymer matrix.[29, 37, 42-51] Lactam based polymers such as Kollidon® VA64, Kollidon® PVP K30, or Soluplus® show amphiphilic properties due to the polyvinyl pyrrolidone moieties present in the two former polymers and polyvinyl lactam moieties present in the latter polymer.[52-55]

ASDs facilitate an increased drug dissolution, absorption, and stability of manufactured oral dosage forms enabling sophisticated and patient-centric therapeutic options. In the context of ASDs developed today, polymers are not merely inert carriers but exceptionally active, non-toxic participants in enhancing the clinical performance of APIs.[22] Through polymer-API interactions, they are capable and invaluable in keeping an API in a high-energy amorphous state, while preventing recrystallization and thus increasing the solubility manifold.[56] The increase in bioavailability through an increase of the solubility governs the rate and extent of which an API is absorbed by the body. There are several polymers commonly used in solid formulation (Table 1).[57]

Table 1 A selection of commonly used polymers in solid formulation.[34, 46, 58-61] Sol.: Solubility; Hygr: Hygroscopicity; Extr.: Extrudable Range

Family	Name	Polymer type	M_w / g mol^{-1}	Sol.	Hygr.	T_g / °C	T_{deg} / °C	Extr / °C
Polyvinyl-lactams	Kollidon®	12 PF	2000 to 3000	Water soluble	High	72	196	
	Kollidon®	17 PF	7000 to 11000			140	217	
	Kollidon®	25	28000 to 34000			153	166	
	Kollidon®	30	44000 to 54000			160	171	
	Kollidon®	90F	1000000 to 1500000			177	194	
	Kollidon®	VA64	45000 to 70000	Water soluble	High	105	270	162-186
	Soluplus®		90000 to 140000	Water soluble	High	72	278	148-185
Cellulosic polymers	HPMC	Pharmacoat	606 to 10000	Water soluble	high	139	244	
	Methocel	K100LV	25000			147, 168	259	
	Methocel	K100M	150000			96,173	259	
	HPC	Klucel LF	95000	Water soluble	High	0	170-200	
	HPMCAS	Shin-etsu AQOAT MF	18000	> pH 5	Low	122	204	
	HPMCP	HP-55	456000	> pH 5	Low	147	194	
	CAP		2534	> pH 6	Low	175	200	150-175
(Meth-) Acrylates	Eudragit®	E PO	47000	Gastric fluid > pH 5	Low	52	250	122-150
	Eudragit®	L100	125000	> pH 6	Low	195	176	
	Eudragit®	S100	125000	> pH 7	Low	173	173	
	Eudragit®	L100-55	320000	> pH 5.5	Low	111	176	190 - 210
Other polymers	PVAP		47000 to 60700	> pH 5	Low	42.5	150	
	PAA		1800 to 450000	Water soluble	Low	126	200	
	PEG/PEO		1000 to 7000000	Water soluble	Low	T_m 55-66	>200	
	Parteck®	MXP 4-88	32000	Water soluble	Mediu m	T_g 68, T_m 163	>230	162 - 186

3.2 Active Pharmaceutical Ingredients in Solid Formulation

APIs are the foundation of pharmacotherapy and embody the essential component for the therapeutic effect of a medication. The journey of a chemical component to become an API used in therapy is full of obstacles. While during early drug development the druglikeness of the chemical molecule itself may be estimated (e.g. Lipinski's rule of five[62]), in later stages, the absorption, distribution, metabolism and excretion (ADME) criteria become increasingly relevant. Along with the targeted pharmacological effect of a new chemical entity (NCE), a significant challenge is ensuring its high bioavailability (absorption). Drug candidates in the development pipeline are demonstrating severe solubility challenges, as around 75% are poorly water soluble.[1, 63] 60% to 70% of which can be assigned to BCS class II due to their high permeability but poor solubility in the target medium and their respective therapeutic active dose.[2, 64-66] Without changing the chemical structure of an API, it is critical to develop formulations using excipients resulting in high solubility, thereby increasing the bioavailability and therapeutic efficacy of a given API. There is no one-size fits all solution in terms of capable excipients, as the API chemistry space is vast[67] and the best solution strongly depends on the formulation type, performance and API characteristics. Solid formulations administered orally include tablets, capsules, and granules, which offer convenient means of drug delivery. A broad portfolio of excipients is used as benchmarks in formulation development to be able to develop the ideal formulation for a given API and manufacturing technique. The formulation of any API is a complex challenge, as the excipient needs to simultaneously provide sufficient stability and enhance the solubility of the API to reach the targeted therapeutic effect.

APIs are classified based on their solubility and permeability considering FDA approved guidelines.[68] The solubility of an API is characterized by the solubility of the highest single therapeutic dose in 250 mL or less aqueous media over a pH range of 1.2 to 6.8 at 37 °C. The lowest solubility obtained over the pH range is considered for the classification. Permeability of an API is preferentially tested in *in vivo* human pharmacokinetic studies, *e.g.*, absolute bioavailability or mass balance. It can also be assessed by validated and standardized *in vitro* methods or, e.g. calculated by *in silico* methods.[69] If a high absorption rate of the therapeutic dose is detected or calculated, the API is considered to have high permeability.

An overview of the evolution of this system and its first mentioning is given in by Shekhawat and Pokharka.[70] After the first mentioning of dissolution methods by Noyes-Whitneys[71] in 1897, the dissolution and permeability testing methods underwent several alterations and theoretical discussions[2] and before the BCS guidelines and standardized testing methods were introduced by the FDA in 2000.[72] Utilizing these guidelines, APIs can be classified in four groups (Figure 2).[72-75]

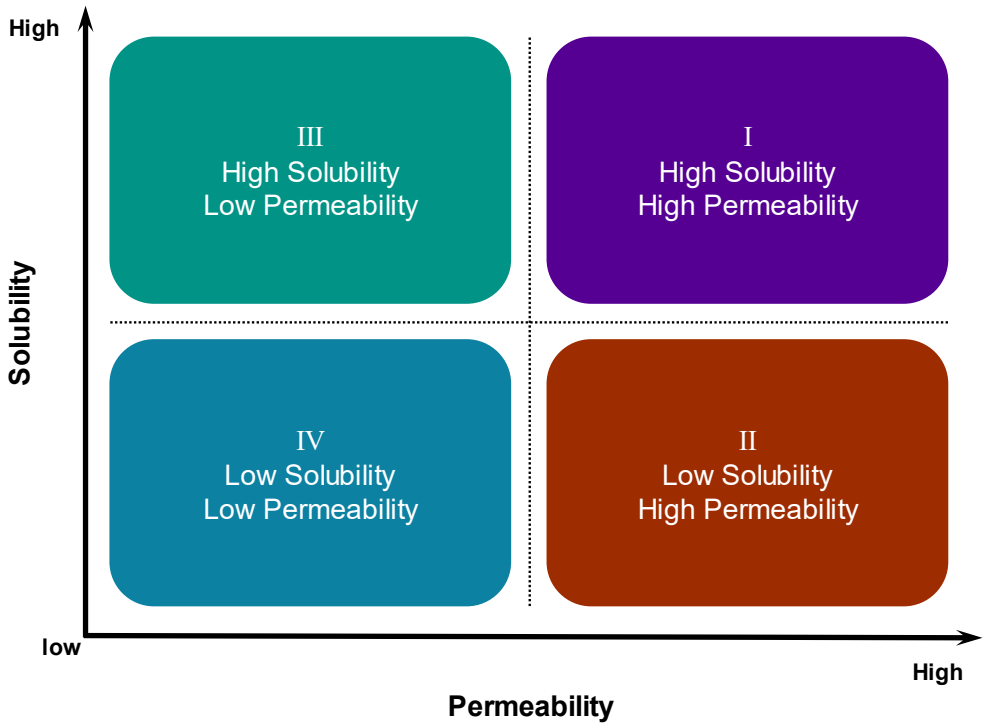

Figure 2: BCS classes and general properties of compounds belonging to the classes. [75]

BCS-I compounds show high solubility and high permeability, but only about 10% of drug substances in the pipeline show these properties. The fraction of drug substances in the pipeline can be assigned to the BCS-III, where permeability is low, but solubility is high. With 10% to 20%, BCS-IV is the second largest group of drug substances. These substances show low solubility and low permeability. Most drug substances in development belong to BCS-II, where solubility is low, but permeability high. 60% to 70% of current drug substances in the pipeline show these properties.[64, 74, 75] While the majority of drug substances in the pipeline belong to BCS-II, only around 30% of drugs on the market belong to this class (Figure 3).[63] This underlines the need for excipients in solid formulation to improve the bioavailability of drug substances in the pipeline. BCS-II drugs on the market include prominent examples like ibuprofen, which are sold in very high volumes annually (Table 2).

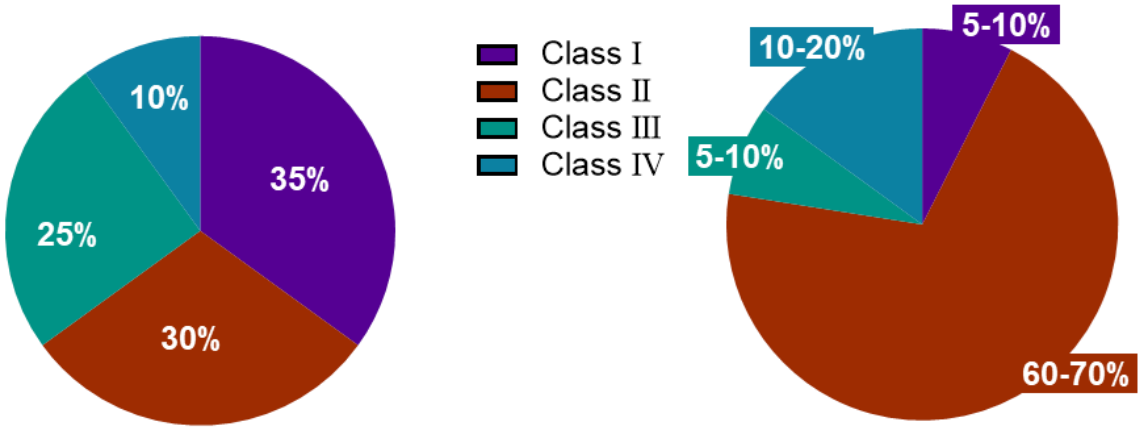

Figure 3: Distribution of BCS class categorization of drugs on market (left) and drug candidates in pipeline (right).

Table 2: A small collection of examples for each of the BCS classes I to IV.[73, 76, 77]

Class I	Class II	Class III	Class IV
Acetyl salicylic acid	Azithromycin	Amoxicillin	Chlorothiazide
Bisoprolol Fumarate	Carbamazepine	Atenolol	Ciprofloxacin
Caffeine	Carvedilol	Cetirizine	Ciprofoxacin
Codein	Danazole	Cimetidine	Folic Acid
Cyclophosphamide	Diclofenac	Dicloxacillin	Furosemide
Diazepam	Fluconazole	Enalapril	Hydrochlorothiazide
Levofloxacin	Ibuprofen	Famotidine	Mebendazole
Metronidazole	Ketoprofen	Pyrazinamide	Methotrexate
Primaquine Phosphate	Nifedipine	Ranitidine HCl	Ritonavir

The chemical structures of the compounds in BCS-II include various chemical motifs and a chemical space can be defined as demonstrated by Lipinski.[67] Overall, the compounds showing low solubility can be characterized as hydrophobic and include moieties like aromats, double bonds, ether groups, halogen substituents and/or long aliphatic chains. In drug development, various strategies can be employed to improve an APIs performance in terms of ADME including permeability and solubility, as was summarized in-depth by Di *et al.*[78] Typical strategies employed during early drug development for solubility enhancement include salt formation[79] and prodrug formation[80], whereas strategies for the increase of the permeability include, but are not limited to, the variation of substitution[81, 82], prodrug formation[80, 83, 84], the reduction of basicity[85] or an increase in lipophilicity.[86]

This thesis deals with the model compounds caffeine and ketoconazole (Table 3). Caffeine is a BCS-I compound with high solubility and high permeability. Ketoconazole is a BCS-II compound with high permeability but low solubility.[46, 87]

Table 3: Model compounds utilized in this thesis.

	Caffeine (Caff)	Ketoconazole (KTZ)
Structure	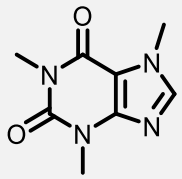	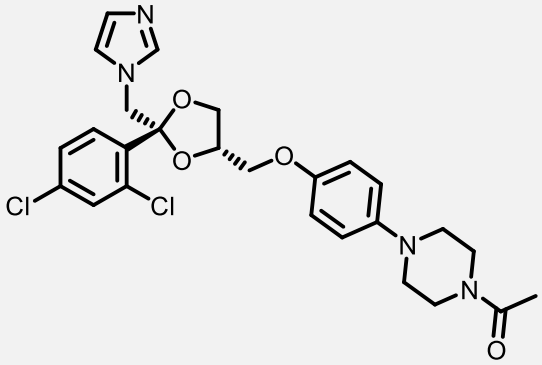
BCS Class	**I**	**II**
Solubility in Water	20 g L^{-1} (High)	0.005 g L^{-1} (Low)
Melting Point	235 to 237 °C	148 to 152 °C
T_g	n.a.	45 °C
T_{deg}	285 °C	345 °C
Permeability	High	High

3.3 Improving the solubility of an API

There are many techniques in solid formulation to improve the solubility of an API[42, 88] and extensive literature is available reviewing different approaches to tackle this challenge.[89] The most prominent ways are the reduction of the particle size, the incorporation into (amorphous) solid dispersions[87], the formation of an API salt[75, 79, 90], the inclusion in cyclodextrin complexes[91], the incorporation into co-crystals[75], the disruption of crystal formation[92] or lipid-based formulations.[77]

By reducing the particle size, thereby increasing the surface area the solvent can interact with, the dissolution rate can be enhanced. Techniques such as micronization and nanonization, are used for this

purpose. Incorporating an API in its amorphous form into a carrier matrix at the solid state can lead to higher solubilities. Amongst other things, the carrier matrix helps with maintaining a solubilized state, while it may also have a favorable influence on the processing parameters. In the amorphous state, the energy needed for breaking the crystal lattice during solubilization is not needed, so the solubility of the amorphous form is higher. When the API can be converted into a salt, the pH and thereby the solubility may change. When changing the pH at the site of dissolution, a higher rate can be achieved. When using cyclodextrins, inclusion complexes are generated, where the hydrophobic API is trapped inside the cavity of the cyclodextrin. The apparent solubility of the API incorporated in the complex increases due to the hydrophilic outer surface of the cyclodextrin. Another strategy is the co-crystallization utilizing a crystal co-former, where the API is held in crystal lattice by non-covalent interactions. These new solid forms are shown to have increased solubility and altered dissolution rates compared to the pure API.

This present study aims to improve an API's solubility by incorporation into an amorphous solid dispersion, where the amorphous API is dispersed in the amorphous carrier matrix. Matrix former used in this thesis are polymers which themselves are amorphous and soluble in water. The first solid dispersion was reported by Sekiguchi and Obi in 1961 increasing sulfathiazole solubility by forming an eutectic mixture of the API with an easily soluble carrier, urea.[93] Here, two phases of crystalline material are present. This was followed by the first amorphous solid dispersion using an amorphous carrier, poly vinylpyrrolidone, and a crystalline API in 1969.[94] These two cases were the basis for the first two classes of solid dispersions (Figure 4).[77] The third class consists of both amorphous polymer and API and includes a polymer with surfactant properties.[33, 95] In the fourth class a water insoluble or a swellable polymer is added to the mixture. Changing to an amorphous carrier matrix from a crystalline one, greatly increases the solubility and the dissolution rate of the API. Due to a phenomenon called "super saturation", delayed precipitation of the API is a common challenge in solid dispersions which leads to low stability. The API is solubilized first, and drug concentration is high, but due to super saturation of the solution, a metastable state, the API has the desire to revert to a more stable state leading to recrystallization. By addition of a surfactant polymer, this unwanted precipitation can be reduced, and the overall stability of the dispersion is increased. Adding a swellable or poorly water-soluble polymer to the formulation increases the control over the release kinetics and makes controlled release formulation possible while securing a high dissolution rate.

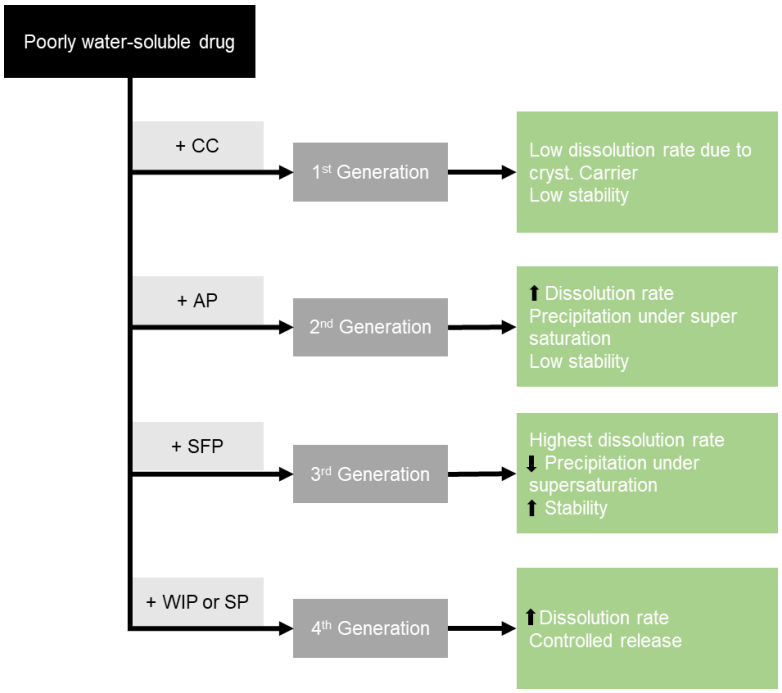

Figure 4: Composition and properties of four generations of solid dispersions. CC: crystalline carrier, AP: amorphous polymer, SFP: surfactant polymer, WIP: water insoluble polymer, SP: swellable polymer, SF: surfactant, (↑): increase, (↓): decrease. (adapted from *Vo et al.*)[33]

In general, the dissolution rates observed for the different generations of solid dispersions offer deep insight into their respective advantages (Figure 6).[96] By comparing the dissolution profile of a crystalline API and an amorphous API, it is evident, that by amorphization, the maximum drug concentration is increased greatly. The crystalline API dissolves steadily until the maximum solubility is reached and the concentration does not change afterwards. Considering the amorphous API, the maximum concentration is reached quickly, due to an increased apparent solubility of the amorphous API compared to the crystalline form leading to a super saturated solution. This effect is termed “spring effect”. The higher concentration rapidly decreases by re-crystallization of the amorphous form until the API concentration reaches that of the crystalline form.[97] Adding a matrix former, e.g. a polymer, can increase the maximum equilibrium concentration of the API in solution and additionally can act as a crystallization inhibitor. The result is a prolonged time at higher concentrations of API in solution. This effect is termed “parachute effect”. The ideal polymer in a formulation thereby increases the maximum concentration reached over time compared to the pure amorphous API and keeps this higher concentration for as long as possible. For the comparison of the different dissolution behaviors and performances, the area under the curve (*AUC*) as an indicator may be used. High *AUC* values indicate good solubility of the compound in the medium.

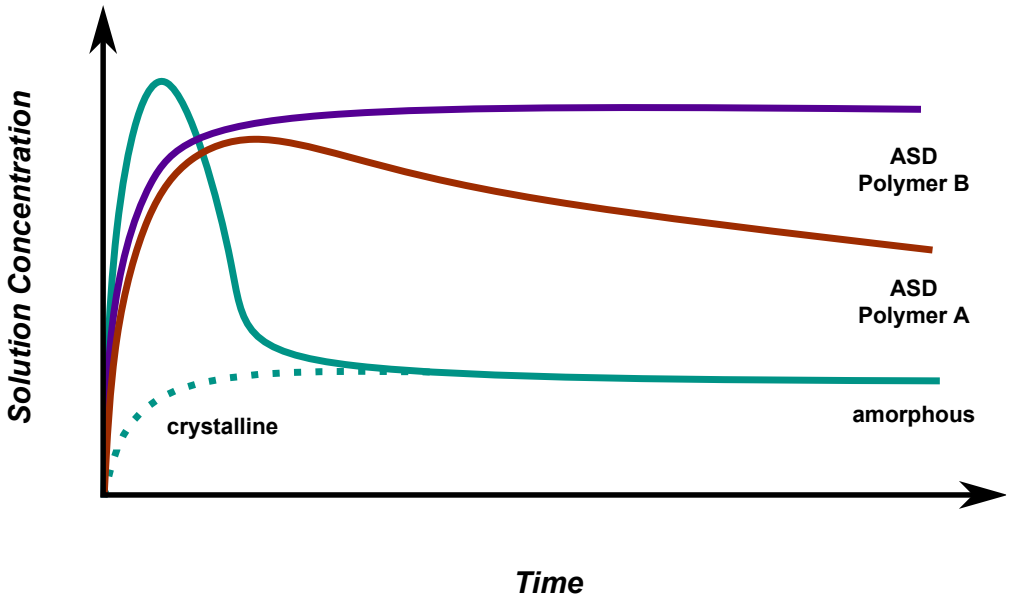

Figure 5: Schematic visualization of theoretical solution profiles of a crystalline API (green, dashed) and a pure amorphous API (green). Additional dissolution profiles of ASD's formulated with a polymer A (red) and polymer B (purple). The amorphous formulations have a "spring effect", and polymer A exerts a parachute effect while polymer B completely inhibits recrystallization and maintains the same degree of supersaturation. Adapted from *Shah et al.*[46]

The different generations of solid dispersions mentioned in literature are classified based on their respective composition (Figure 4).[96] A common concept is their general differences in dissolution behavior in conjunction with their composition as illustrated by Laitinen *et al.*[46] or Vo *et al.* [33] (Figure 6). In this concept, the drug release of a pure, crystalline API, has a linear curve progression. In the first generation of SDs, where e.g., a crystalline matrix former is added to the crystalline API, an increase in the dissolution rate especially in the early period of dissolution, can be observed. A maximum is reached followed by a decline but ultimately stays at high drug release values. Considering the second generation of SDs, where both API and matrix former are amorphous, the maximum is larger, and the initial dissolution rate is higher compared to first generation SDs. Also here, a decline in drug release follows leading to similarly high drug release values. The decline after the maximum indicates reprecipitation of the API, which is slightly reduced in second generation SDs compared to first generation APIs. Considering the third generation of SDs, the dissolution rate and maximum drug released is increased even further. The distinct difference compared to earlier generations is the low amount or non-existing recrystallization of API in these formulations. Finally, fourth generation SDs modulate the release kinetics to achieve controlled release with a linear increase in drug release. Formulating an API can increase a polymers solubility in a medium manifold. Compared to pure API, the slope is larger in these SDs. In the SDs of the first, second and third generation, the Spring-Parachute Effect[64] is pronounced in different strengths, but in each of those formulations, the favorable effect of super saturation can be

observed, as the amount of drug released can be modulated to result in amounts which are several times higher than the pure API.[77, 98]

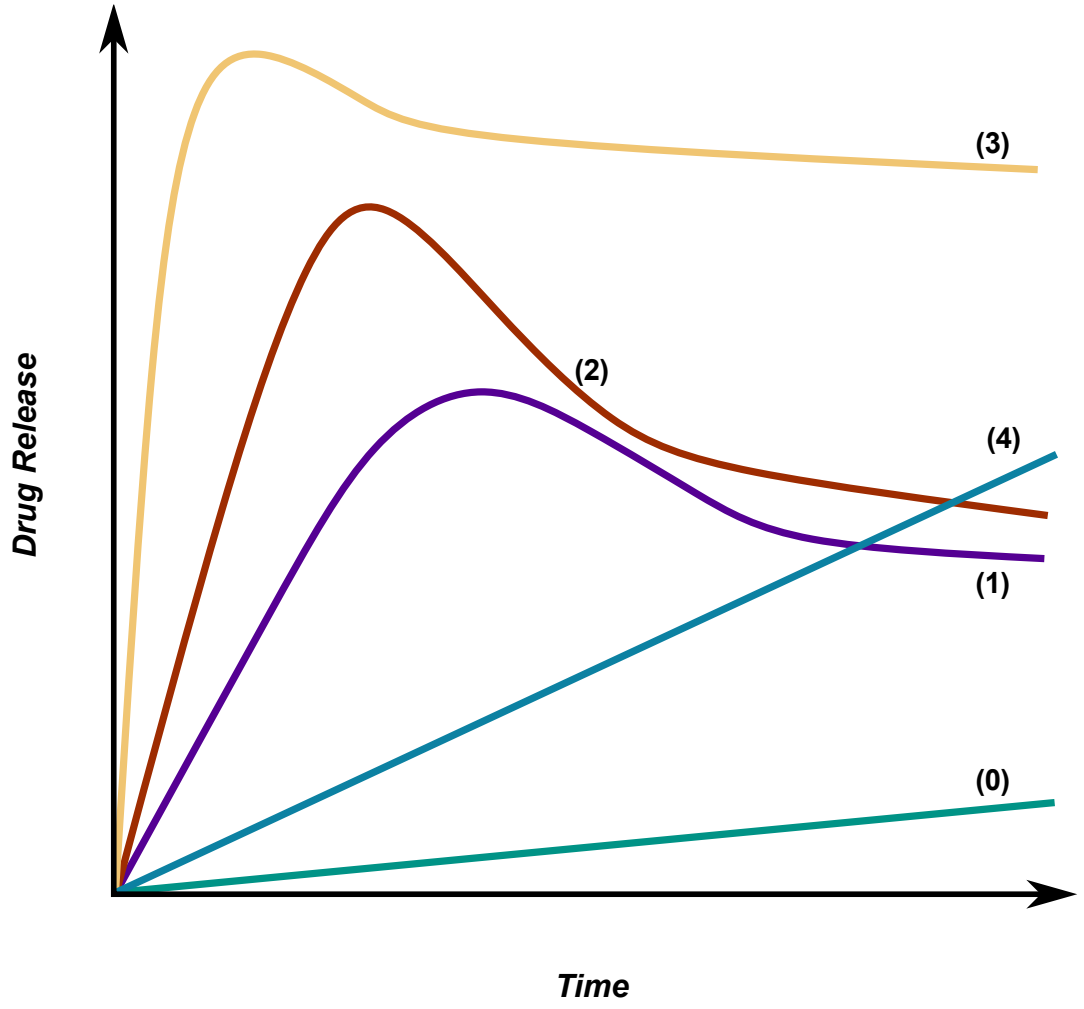

Figure 6: Adapted from *Vo et al.*[33] Schematic representation of dissolution profiles of different generations of solid dispersions in saturated conditions. (0) pure API; (1) 1st generation ASD with improved dissolution rate; (2) 2nd generation ASD with improved dissolution profiled and corresponding showing of „spring effect"; (3) 3rd generation ASD with improved dissolution capability mainly due to faster dissolution rate and lower rate of precipitation ("parachute effect") in supersaturated state; (4) 4th generation ASD with controlled, linear release.

The Spring Parachute Effect is an essential effect, which enables formulation scientist to develop drug products of poorly water soluble APIs.[89, 99] There is a plethora of ASDs commercially available today for a diverse group of drug substances as summarized by Baghel *et al.*[100]. Kollidon® VA64 is a prominent polymer in the field of ASDs (Table 4). Polymers and APIs mentioned above have been successfully incorporated into formulations and brought to market.[33, 34, 45, 48]

Table 4: Selection of marketed ASDs including matrix forming polymer Kollidon® VA64 and corresponding manufacturing technologies.[100]

Drug Substance	Preparation Method	Comments / Benefits
Ketoconazole	HME	Spring-Parachute effect carrier controlled, then burst release
Itraconazole	Electrospinning	Complete amorphization
Dipyridamole	Solvent evaporation	H-bonding with the drug
Ritonavir	HME	
Suvorexant	HME	
Sofosbuvir/Velpatasvir	Spray Drying	
Elbasvir/Grazoprevir	Spray Drying	

Amorphous solid dispersion are produced in various ways and can be divided in solvent based techniques and fusion techniques (Figure 7).[101] Next to the fusion based melt extrusion, the most commonly used solvent based manufacturing technique on large and intermediate scales is spray drying[102, 103]. Which of the processing techniques is used depends on various API characteristics e.g. solubility in organic solvents, thermal sensitivity, chemical structure, [100]

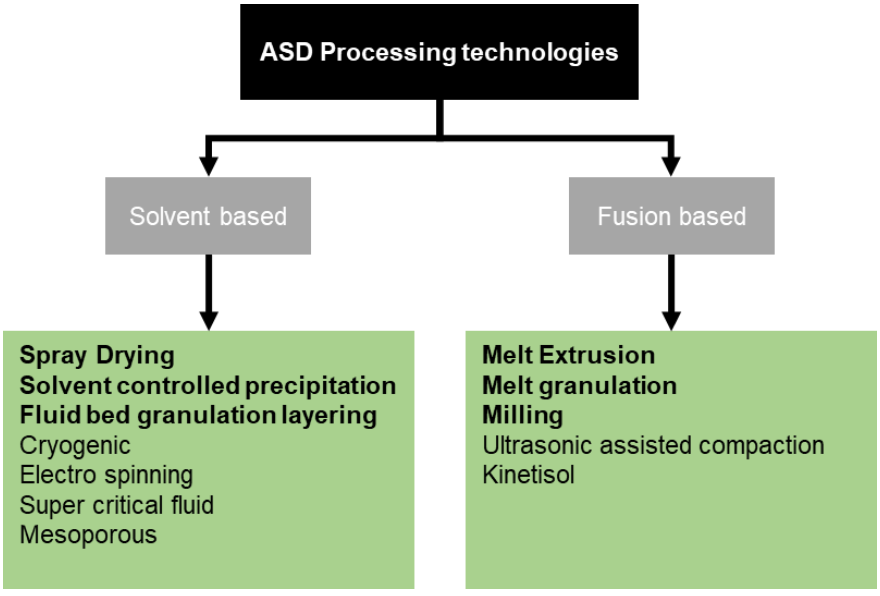

Figure 7: Commonly used processing technologies in the manufacturing of ASDs. Technologies denoted in bold are most commonly used (Adapted from *Shah et al.*).[46]

Solvent based methods involve the preparation of a solution of the API and the matrix former generating the ASD after the removal of the solvent. This enables mixing of the components on a molecular level increasing the solubility and stability of the product. The thermal stress imposed is low compared to

fusion methods, as the applied organic solvents typically have low boiling points. Due to this, thermally sensitive APIs can be manufactured without the risk of decomposition. Spray drying has emerged as a technology with high potential to be used on larger scales in the production ASDs.[102, 103] Here, a solution or suspension is converted into a dry powder in a single step providing control over process variables. These variables have a significant influence on the stability of a formulation[32] and also on powder properties including the size, density, shape, flow properties and crystallinity.[102, 104] The quick removal of solvent during the process leads to an entrapment of API molecules in the matrix former which has a favorable effect on crystallization prevention and can lead to an amorphous state of the API. Formation of crystalline forms, imperfect crystals, or metastable crystals is also possible.[104] Next to the manufacturing parameters, the chemical nature of the API has a significant influence on the morphologies formed, as outlined by Baird *et al.*[105] and Mahlin *et al.*[106] amongst others. In addition to the favorable effects on the formulation and its performance, spray drying offers low manufacturing costs, the opportunity be used in continuous manufacturing and offers an ease of scale-up.[32]

Fusion based methods for solubility enhancement exist since their first mentioning in 1961[93] and the modern equivalent technology is the hot melt extrusion (HME).[25] In pharmaceutical HME for the manufacturing of ASDs, a physical mixture of an API and the respective excipients is mixed extensively, molten and a filament is generated using an extruder (Figure 8). The physical mixture is transported via e.g., conveying, mixing, and kneading units through the barrel to the die and the filament is discharged onto a conveyor belt. The combination of these units is modified based on the specific needs of the manufacturing process and the materials used therein.[101] The extruder components are inert, both chemically and physically.

In addition to the thermal energy introduced into the system to melt the formulation, high shear stress is applied during conveying. Excipients and APIs used in an HME process must withstand the process without degradation to facilitate high performance of the formulation. In contrast to more traditional fusion methods, the melt can be directly formed into shapes like implants, pellets, or oral dosage forms.[101] Most commonly, the produced filaments are granulated and milled after extrusion before oral dosage forms are produced.

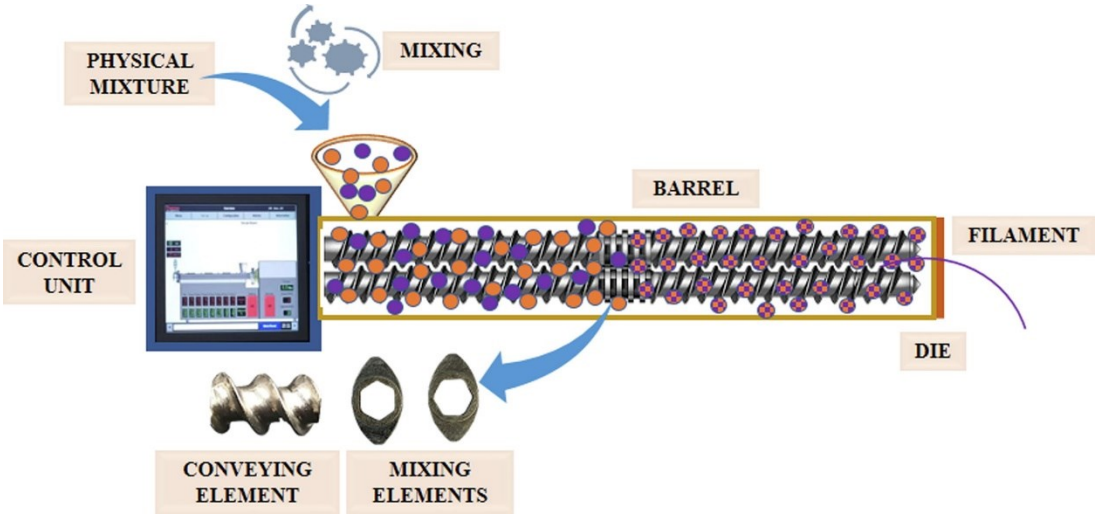

Figure 8: Schematic illustration of a co-rotating twin screw extruder. Taken with permission from *Bandari et al.*[107]

For an extrusion process to be successful it is of utmost importance, that the API is miscible in the polymer in the molten state. For a given API/polymer combination, solubility parameters which are either known in literature, determined by experiments, or modelled using computational methods can be used to predict the compatibility of a system. Compared to solvent based manufacturing techniques, hot melt extrusion uses no organic solvent, comparably fewer processing steps are needed (e.g. no drying or compression of ingredients) and due to high shear rates and temperatures, the components of the mixture are thoroughly mixed.[108] HME is exceptionally useful for the production of filaments, where the polymer is distributed in crystalline or amorphous form in the preferably amorphous polymer resulting in a (amorphous) solid dispersion or even molecularly dispersed in a solid solution.[109] Nowadays, continuous manufacturing is an upcoming trend in pharmaceutical manufacturing[110] and HME is used already as one element for e.g. tramadol hydrochloride controlled release tablets in a melt granulation[15], co-extrusion in an implant manufacturing process[111], or a continuous twin screw granulation[112].

One other usage of filaments produced by pharmaceutical extrusion consisting of an API and polymeric excipients is the 3d printing in a fused deposition modeling (FDM) process.[113] The generated filaments are optionally spun onto a spool and guided into the printing head of the printer via gear rolls. The printer head itself is heated, and the melted polymer is discharged via the nozzle onto a build platform in layers to form the desired printlet. Using a FDM process, printlets of varying size and consecutively varying doses can be manufactured enabling the batch printing of tailored dosage forms, which can be personalized based on the patient's constitution.

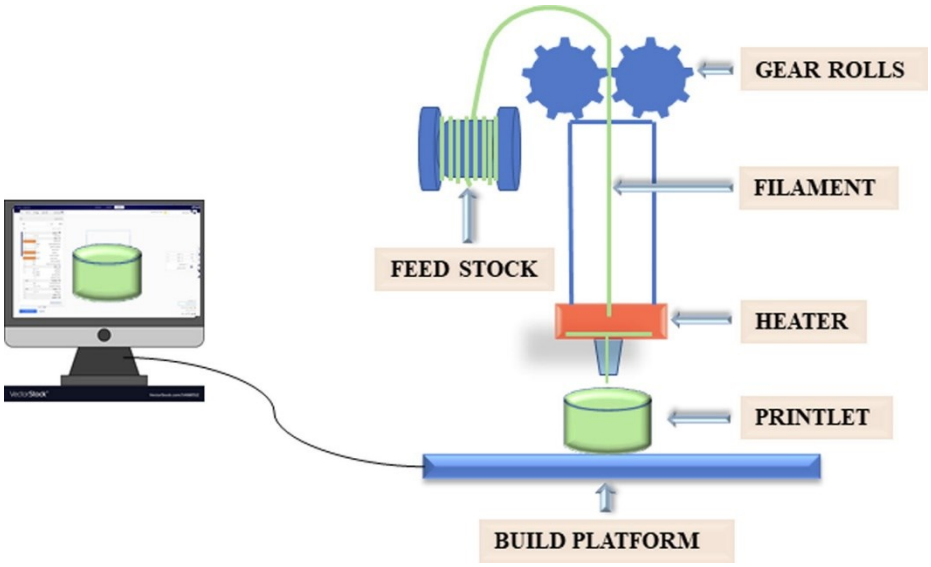

Figure 9: Schematic representation of a FFF 3d printer. Taken with permission from *Bandari et al.*[107]

Spray drying and hot melt extrusion are the most frequently utilized thermal processes in solid formulation. In these processes, thermal stability of the API is a crucial parameter. Mao *et al.* investigated 683 approved oral drug substances concerning their melting temperatures and 62% of investigated APIs showed a melting temperature over 150 °C (Figure 10).[114] Some APIs with high melting points are prone to degradation near this temperature. This illustrates a challenge in current research considering these high melting point APIs. By developing an appropriate formulation for high melting point APIs using e.g. polymers, it is possible to reduce the processing temperature below the API degradation temperatures.[115, 116] Formulations are typically processed above the processing temperature of the polymer. The processing temperature of a polymer is dependent on the manufacturing technique and usually above the respective glass transition temperature or melting temperature if melting point present. It is desired to process APIs at sufficiently low temperatures, to prevent any degradation. The manufacturing around these substance specific temperatures may induce degradation and this needs to be avoided.[115, 116] Finding the ideal excipient combination for the formulation of newly developed APIs is subject of extensive research.[117-119]

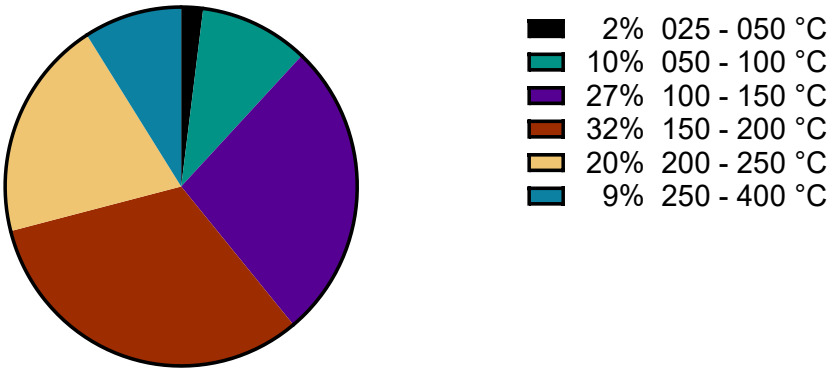

Figure 10: Melting point distribution of 683 approved oral drug substances. The highest number of drugs have a melting point in the range of 140 °C to 160 °C (14%).[114]

3.4 Polymer Properties relevant for the preparation of ASDs

Polymers used in solid formulation are of crucial importance to facilitate the drug delivery of poorly soluble drug substances. As outlined before, HME and FDM induce thermal and mechanical stress in both the excipient and the API. Therefore, one challenge is the processing of all components without degradation or alteration of the material.[59] In addition to the stability aspect of the polymer during manufacturing, a variety of other properties are important for the application in solid formulation (Figure 11).[57, 120] Polymer specific properties include thermo-physical and thermo-mechanical properties. A collection of polymer families and marketed products in the field of HME was published by Simoes *et al.*[118, 119] Bandari *et al.*[107] outlined additional necessary prerequisites of a formulation for the application in FDM. Finding the ideal polymer for a specific API in a formulation is a core activity in drug product development. The marketed and utilized polymers today are no one-size fits all solution and for each novel drug substance several polymers need testing.[121] For a novel polymer to be viable in HME, it has to possess distinct advantages compared to marketed products. Some of the challenges in formulation development may be solved by new structural motifs directly influencing the formulation's properties. One of the biggest challenges to solve is the poor water solubility of APIs in the pipeline.

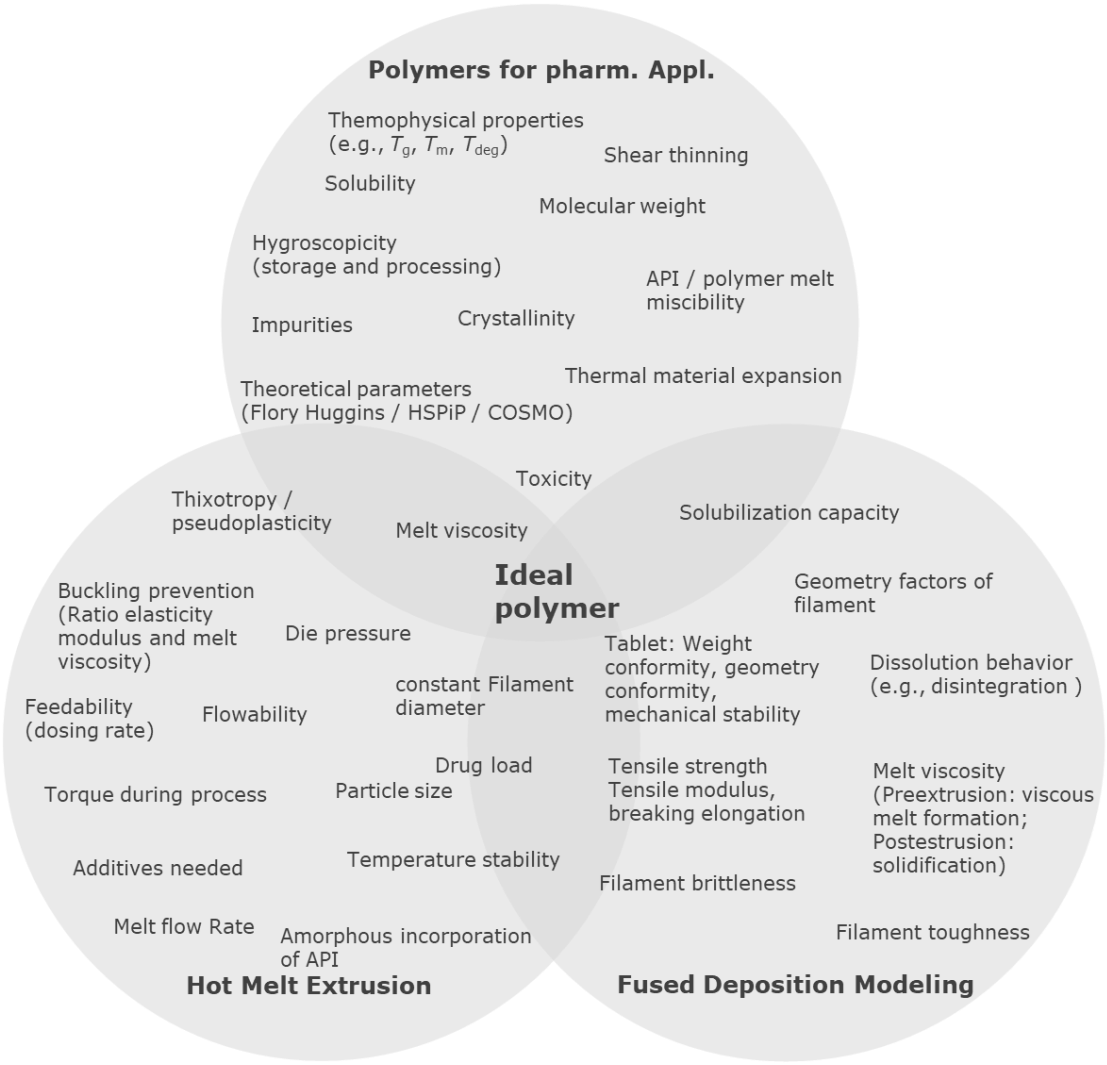

Figure 11: Selection of relevant polymer and formulation properties for the processing of a solid formulation by HME and FDM as outlined by Quodbach *et al.*[120]

As outlined by Quodbach *et al.*[120], there exists a variety of different properties the ideal polymer in solid formulation may fulfil. A selection of the mentioned properties will be thoroughly investigated in this thesis and the specific polymer properties are summarized in Table 5.

Table 5: Polymer parameters considered in this thesis and their impact on the formulation capability in ASDs.

Parameter	Abbr.	Method	Impact on formulation
Glass transition temperature	T_g	DSC	Lower Limit for processing
Melting temperature	T_m	DSC	If absent, amorphousness, otherwise lower Limit for processing
Degradation Temperature	T_{deg}	TGA	Upper limit for processing
Melt viscosity	η_{melt}	Melt rheology	
Storage modulus	G'	Melt rheology	
Loss modulus	G''	Melt rheology	
Temperature @1000 Pa s	$T_{1000\ Pa\ s}$	Melt rheology	Lower limit in extrusion
Temperature @10000 Pa s	$T_{10000\ Pa\ s}$	Melt rheology	Upper limit in extrusion
Phase angle	δ	Melt rheology	Measure for degradation behavior
Mean molecular weight distribution	M_w	GPC	
Maximum molecular weight	M_p	GPC	
Poly dispersity index	$Đ$	GPC	
Max. Caffeine Concentration	$c_{Caff,max}$	Caff. (BCS-I) Assay	Solubility of formulation and immediate release capabilities
Max. KTZ Concentration	$c_{KTZ,max}$	KTZ (BCS-II) Assay	Dissolution enhancement
Area Under Curve	AUC	KTZ (BCS-II) Assay	Dissolution Capability
Extrudability		Small-Scale Extrusion	Practical extrudability
Torque (Small Scale)		Small-Scale Extrusion	Practical extrudability
Extrudability		Intermediate Scale Extrusion	Practical extrudability

Some properties of the polymer itself and its chemical moieties present in it, have an influence on the performance during processing and application. In a formulation consisting of an amorphous polymer and crystalline API, the combination of glass transition temperature and degradation temperature of the polymer in conjunction with the degradation temperature of the API is a good estimate for the possible processing range of the formulation. Considering only the polymer, amorphousness is a major advantage as the polymer does not have crystalline character which usually serves as potential seed crystals for the recrystallization of the API. A polymer can only be processed if the temperature is either above the glass transition temperature, or, if present, above the melting temperature. Next to T_g and T_{deg}, the melt

viscosity is of integral importance. Kolter *et. al*[121] defined the extrudable range between 10000 Pa s and 1000 Pa s. Low melt viscosities lead to lower die pressures and lower torque during the extrusion, which in turn enables the combination with viscosity increasing APIs. Due to the lower torque and die pressure, the mechanical stress is reduced. In general, the stability profile of the polymer must fit the thermal properties of the API and the extrusion temperature ideally should be 30 °C below the degradation of the formulation components.[22, 25, 107, 119, 121] Typical extrusion temperatures are between 100 °C and 170 °C.[122] Agrawal *et al.* reported that a T_g at 50 °C above room temperature is favorable considering the storage stability of a formulation.[123] For common API/polymer combinations the T_g lies in the range between 50 °C and 180 °C.[121] A high solubility in water is favorable for the dissolution behavior of the formulation. Furthermore, solubility in organic solvents enables the processing and expands the usability across diverse fusion based and solvent based manufacturing techniques.[118] Most polymers used in the field have broad molecular weight distributions with a high dispersity index. This is due to the synthesis process utilized in their production. The Kollidon® family by BASF, and the poly vinyl alcohols (Merck, Kuraray)[124] are all synthesized on a large scale by radical polymerization. The Eudragit® family by Evonik (methacrylates), are either synthesized by radical polymerization or anionic polymerization. It seems, that a broad molecular weight distribution typically obtained by radical polymerization, may have a favorable influence in the formation of ASDs. The innate polymer properties mentioned may originate from the respective chemical motifs found in the marketed products. Next to these properties, processing parameters like screw design and speed, and especially the melt viscosity is of integral importance for pharmaceutical HME.[58, 59, 107, 121, 125-127] There is a plethora of different polymer properties which are integral to the successful development of a formulation and extensive research is being conducted for each new drug substance.

Widely used analysis techniques considering thermo-physical and mechanical properties include, but are not limited to, DSC, mDSC TGA, DMA, melt rheology and XRD. [49, 51, 128] DSC and mDSC measurements are conducted in closed crucibles. A sample is heated together with a reference in a controlled chamber with a specific heating rate. A comparative heat flow is detected which is dependent on the samples heat capacity and the heating rate at which the experiment is performed. When a glass transition temperature or a melting temperature is present, a spontaneous change in heat flow occurs due to the respective phase transition. A sample is heated twice during one measurement. The first heating cycle is used to remove any thermal history the sample inherits and ensures comparability between different polymer samples. The glass transition temperature constitutes the range in temperature where the glass transition occurs. It is a property of the amorphous region of a polymer. This transition is the reversal (and gradual) change of a material's state. At colder temperatures the polymer behaves like a glass while at rising temperatures, higher than the T_g range, it is in a viscous or rubbery state. In the

glassy state, the polymer is hard and brittle due to lack of mobility. In the rubbery or viscous state, mobility increases, and the material becomes soft and flexible. In a semi-crystalline polymer, like PVA-co-PVAc (Parteck® MXP), a melting point is present. The melting point is a property of the crystalline region of a polymer and is greater than the glass transition temperature. Above the melting point, the polymer chains move more freely, and the polymer softens eventually turning into a liquid. The temperatures of the described phase transitions are generally used as an estimate for the lower temperature limit in a potential extrusion. Furthermore, the T_g is a first indicator concerning the storage stability of the polymer, as generally, a T_g at least 50 °C above storage temperature is favored to ensure lasting stability.

In TGA, a sample is heated in a controlled chamber, while a balance registers any mass loss during the experiment. The degradation of a sample is generally accompanied by a mass loss during the measurement. Multiple "steps" in the mass curve indicate that more than one degradation process is involved. This is exceptionally clear when the first derivative is taken into account, as local minima and maxima can then be observed. Copolymers such as PVA-co-PVAc or PVAc-co-PVP have acetate moieties bound via an ester in their backbones. With the help of hyphenated measurement techniques such as TGA-GC-MS or TGA-IR, the resulting degradation products can be identified. In a multistep degradation process, these esters are cleaved by elimination forming double bonds and/or carbonyl groups in the backbone.[129] This can be applied to other copolymers carrying ester bound side chains such as methacrylates.[130]. It is of utmost importance for the integrity of the formulation and thus its safety, that no degradation takes place during the manufacturing. Therefore, the onset of degradation is the thermal event to estimate the upper limit of a potential extrusion.

In addition to the characterization *via* DSC and TGA, melt rheology plays a crucial role in the characterization of novel polymers in the field. [58, 60, 61] Especially temperature sweep measurements can be used to predict the polymers manufacturing window in extrusion. As outlined by *Kolter*,[121] a melt viscosity between 10000 Pa s and 1000 Pa s is ideal for extrusion. A broad window at comparably lower temperatures (Table 1) is favored for the careful processing of thermolabile APIs. During the measurement on a plate rheometer, the temperature of the polymer sample is increased in a controlled manner (temperature sweep) while oscillation frequency and amplitude are constant. The relative values of the storage modulus (*G'*) compared to the loss modulus (*G''*) characterize the viscoelastic behavior of the polymer. For amorphous polymers, *G''* is relatively higher than *G'* in a specific temperature range between two crossover points. For (semi-)crystalline polymers, *G'* is higher than *G''* in a temperature range where crystalline phases are present. The phase angle increases over the course of the measurement until a maximum is reached. The phase angle decreases again suggesting the beginning of degradation. The temperature difference between T(10000 Pa s) and T(1000 Pa s) is defined as the extrudable range ΔT and the specific temperatures indicate the lower and upper limit of extrudability as

an estimate for intermediate extrusion.

In GPC measurements, the molecular weight distribution of a sample is determined. A combination of columns of differenz pore sizes are used to separate species of varying molecular weight. The interaction of the lower molecular weight species with the columns is stronger, leading to higher retention times. Due to the interaction with the columns, the different species are separated. Utilizing a refractive index (RI) detector, a calibration against polymer standards of similar nature is necessary. When using a MALS (multi-angle light scattering) detector, an absolute determination of the molecular weight distribution is possible. For polymers, a distribution is obtained, and the distribution's dispersity index (PDI, *Đ*) strongly depends on the nature of the polymerization. It is a measure for the heterogeneity of the sample and calculated by the division of the weight average molecular weight M_w and the number average molecular weight M_n obtained during GPC measurements. For free radical polymerization a high *Đ* (≥ 1.5), therefore a broad distribution is usually obtained, whereas for controlled polymerizations a low *Đ* (~ 1.0) is possible. Most of the polymers utilized in the manufacturing of ASDs have high *Đ* and broad molecular weight distributions (Table 1). This may indicate, that a broad PDI is favorable compared to lower PDIs for the polymers used in the manufacturing *via* HME. Furthermore, a favorable effect on the dissolution capabilities of these polymers may be exerted by the small molecular weight fractions.

The abovementioned properties mainly influence the manufacturing of said formulations. The maximum concentration in both the caffeine assay and the KTZ assay which was developed by Auch *et al.*,[131]can be viewed as an indicator on how the formulation will perform in later in-vivo assays. The USP dissolution assay is used to examine the polymer specific dissolution capabilities in terms of its release kinetics and its overall capability to enhance the solubility of a poorly soluble API. The small-scale formulation and amorphization of the API in the polymer matrix is a good simulation of the entity used in later in-vitro and in-vivo assays. By changing the chemical structure of the polymer, a direct influence in these assays is plausible.

3.5 Synthesis and utilization of PVP-co-PVAc in solid formulation

One of the most prominent examples of polymers utilized in pharmaceutical solid formulation is Kollidon® VA64 (**PVAc-co-PVP**), which is a copolymer consisting of vinyl pyrrolidone (**VP**) and vinyl acetate (**VAc**) monomers. Kollidon® VA64 exhibits remarkable properties, which make it a potent matrix former, when used in conjunction with poorly soluble APIs in the field of pharmaceutical extrusion. To date, it is used in a wide range of different formulations and drug products as summarized

extensively by Saha *et al.*[97] and Zhang *et al.*[34] amongst other publications[55, 132]. As outlined in the latter publication, Kollidon® VA64 is the excipient used in 37% of investigated drug products (Figure 12).

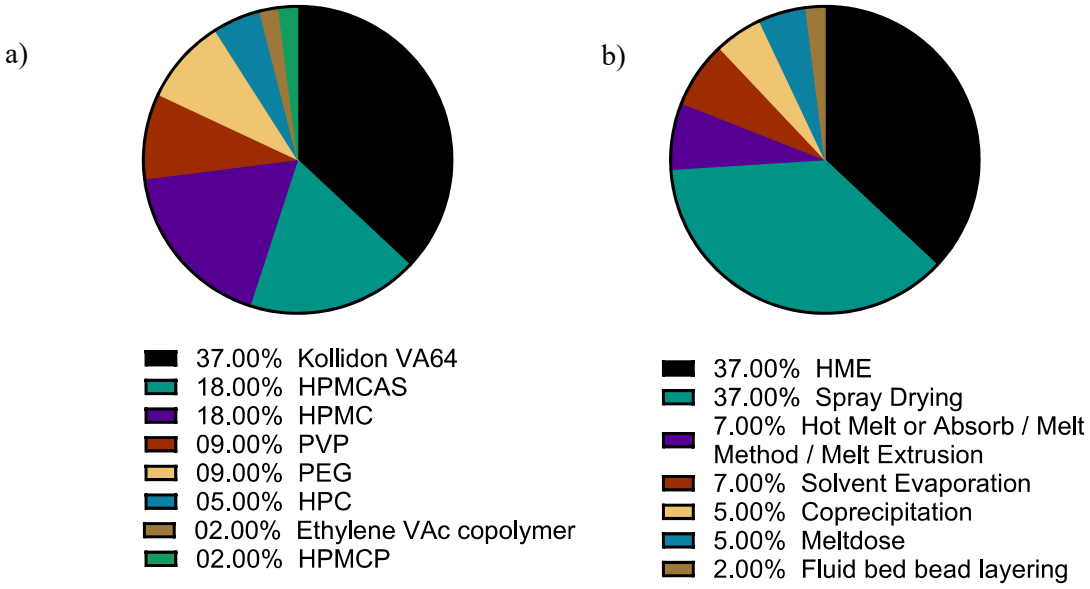

Figure 12: Analysis of FDA-approved drug products showing the distribution of (A) polymers (B) manufacturing processes, employed by pharmaceutical industries.[97]

As early as 1996, Kollidon® VA64 was used in the EMA approved formulation of film coated tablets in a HME process containing Ritonavir by AbbVie Germany GmbH Co. KG.[133] The USP entry[134] and the technical information sheet[54, 134] offer insight into supplementary properties and the distinct characterization of the material as well as some applications.[87] Bühler[52, 135] summarizes the synthesis, properties, and applications of the different BASF products containing *N*-Vinyl-2-pyrrolidon. A selection of relevant properties for this study considering Kollidon® VA64 (Figure 12-PVAc) is summarized in the table below.

Table 6: Selection of relevant properties of PVP-co-PVAc (Kollidon® VA64) for this study.[34]

Parameter	Method	Value	Lit.
Molecular weight (M_w)	Light Scattering	45000 to 70000 g mol^{-1}	34, 136
Molecular weight (M_w)	GPC	15000 to 20000 g mol^{-1}	13
Hygroscopicity	Dynamic Vapor Sorption	High	137
Glass transition temperature (T_g)	DSC	105 °C	138
Degradation temperature (T_{deg})	TGA	270 °C	137
Extrudable range (ΔT)	Melt Rheology	155-200 °C	52, 121

3.5.1 Radical polymerization of copolymers

Copolymers are synthesis products incorporating at least two covalently bound monomers obtaining a macromolecular chain or network and are generated by copolymerization. They are of great importance for the manufacturing of tailored products with distinct properties due to the chemical versatility of available monomers and possible chemical motifs. The simplicity at which comonomers can be combined in a single product, results in a broad spectrum of possible product types, compositions, and applications. Introducing even small amounts of comonomer can drastically change the product's properties. These properties include, but are not limited to thermal properties, mechanical properties, its solubility, or its solvent resistance. By utilizing building blocks carrying functional groups, post-polymerization modification can be enabled. This is facilitated by e.g., the incorporation of alcohol, acid or amine groups into the backbone which can be modified by targeted chemical reactions.

In general, copolymers can be divided in five groups. Alternating, statistical or gradient polymers are mainly obtained by the simultaneous polymerization of two monomers. These polymer architectures are typically obtained by free radical polymerization. Block copolymers consist of at least two domains which consist of solely one monomer. They are usually obtained by living polymerization with high control over the progress of the reaction and the monomer incorporation. Graft copolymers are defined by a backbone where several pendant groups are attached at various positions. For each of the architectures, various concepts can be followed, and various polymerization techniques[139, 140] (anionic-, free radical-, ATRP[140], RAFT, and cationic polymerization) can be utilized.

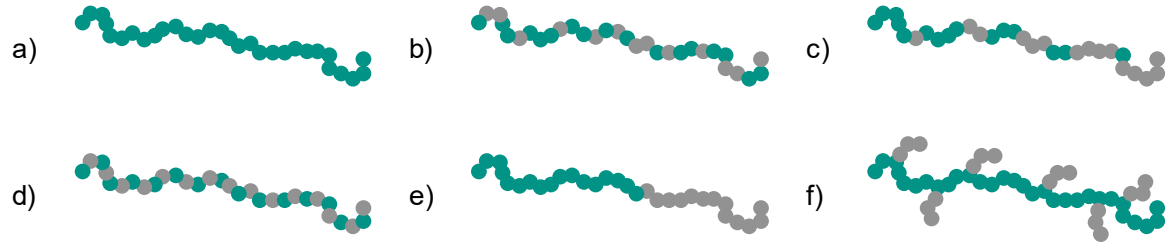

Figure 13: Schematic illustration of the five main types of copolymers. a) Homopolymer; b) statistical copolymer; c) gradient copolymer; d) alternating copolymer; e) block copolymer f) one possible graft copolymer (grafting from[140]). Grey: M^1; Blue: M^2. Adapted from Koltzenburg, Maskos, Nuyken *et al.*[139]

In radical polymerization of at least two monomers, the reactivity of each monomer and the reaction conditions have a direct influence on the resulting copolymer architecture (statistical, gradient, block or alternating). In general, apart from few exceptions, the monomer composition at the beginning of a polymerization is not equivalent to the monomer composition found in the copolymer product. This is mainly due to the uncontrolled nature of the growth reactions occurring in radical polymerization. Increasing the number of monomers present in the reaction results in a higher number of possible reaction pathways and thereby more complex microstructures (Scheme 1). The explanation of the separate reaction steps is very well known in literature[139] and only propagation steps will be explained in the following paragraph. The case explained assumes equimolar starting concentration and four monomers present in the reaction.

After the decomposition of the initiator and the formation of the radical initiating species, a reaction with each kind of the present monomers M^1 to M^4 is possible. This reaction leads to a reactive chain end with a terminal radical M^1, M^2, M^3 or M^4 which itself may also react with each of the present monomers. The terminal monomers react according to their specific reactivity ratios in the system with each other. This may lead to a favored reaction of the terminal M^1 radical with additional free M^1 monomer or any other favored reaction. The same is true for each other combination of radical chain ends and present monomers. For each combination, a rate constant k_{xy} (x: $M^{\#}$ at reactive chain end; y: $M^{\#}$ free monomer) can be formulated. The monomers are incorporated into the polymer backbone in accordance with their reactivity ratios. Monomers with higher reactivity are incorporated faster, than those with low reactivity.

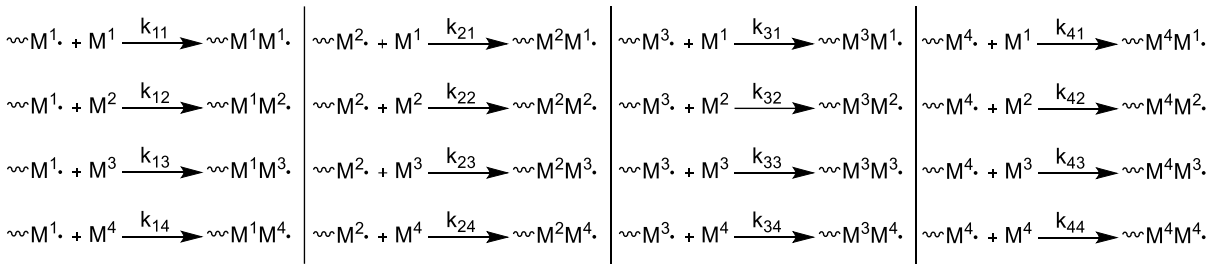

Scheme 1: Possible propagation pathways in radical polymerizations with 4 monomers M^1 to M^4.

The following paragraph is limited to two monomers due to the vastly increasing complexity with each additional monomer. Only the concept will be explained. Next to the specific reactivity ratios of the monomers at equivalent concentrations, the concentration of the monomers at each time point is directly influencing the course of the reaction. The highly reactive monomer is predominantly incorporated into the chain while its concentration gradually decreases. With decreasing concentration of the reactive monomer, the less reactive monomer is incorporated with higher probability. This behavior can be described with the following equation valid for systems with two monomers M^1 and M^2:

$$\frac{d[M^1]}{d[M^2]} = \frac{[M^1]k_{11}[P - M^1\,\bullet] + k_{21}[P - M^2\,\bullet]}{[M^2]k_{22}[P - M^2\,\bullet] + k_{12}[P - M^1\,\bullet]} \tag{1}$$

For each time point during the reaction the rate at which a monomer is incorporated into the polymer (k_{xy}) can be determined. By introducing the copolymerization parameters r_1 and r_2 with the assumption of equilibrium radical concentration, this equation can be simplified. The copolymerization parameters are equal to the ratio of the propagation rates considering the reaction with the same kind of monomer and the propagation rate considering cross reaction. These parameters characterize the behavior of a terminal radical to react with the same kind of monomer leading to the relative reactivity between the two monomers in question. After simplification, the general Mayo-Lewis-Equation for a system consisting of two monomers is obtained:

$$\frac{d[M^1]}{d[M^2]} = \frac{[M^1](r_1[M^1] + [M^2])}{[M^2](r_2[M^2] + [M^1])} \qquad r_1 = \frac{k_{11}}{k_{12}} \qquad r_2 = \frac{k_{22}}{k_{21}} \tag{2}$$

This equation is only viable, as long as the terminal active chain end is considered without the inclusion of potential influences of other previously reacted monomers on the same chain. It delivers a good approximation for the polymer constitution at conversions lower that 5%, but if the copolymerization parameters are unknown for a system, it can give a first estimation of the monomer distribution in the final copolymer. When considering more than two monomers, more reaction pathways are possible and the equation becomes drastically more complex resulting in additional reaction rate constants and copolymerization parameters.[141-144] By determining each respective copolymerization parameter of a monomer system, the resulting microstructure may be estimated and tailored microstructures in a polymer system can be obtained.

This is especially true if controlled radical polymerization techniques such as RAFT, ATRP or NMP are conducted. These controlled polymerizations offer precise control over the initiation, propagation and termination processes occurring during the generation of the copolymer. A uniform chain growth can be secured which ultimately leads to narrow molecular weight distributions and a low dispersity index. High control over the respective reaction pathways is obtained by the addition of carefully chosen additives to the reaction mixture which depend on the polymerization technique chosen. These inimers and transmers serve several purposes in a controlled radical polymerization including the ability to control the targeted molecular weight or the dispersity index of a synthesized polymer. Free radical polymerization functions without one of these additives and the associated precise reaction conditions, but one loses the ability to carefully control the polymer structure and dispersity of the molecular weight distribution. Free radical polymerization is a robust technique with a high tolerance of impurities and monomers without the addition of specialized catalysts. Kollidon® VA64 is synthesized by free radical polymerization[124], a facile way to receive a copolymer with sufficient control over the resulting polymer microstructure.

In chain growth polymerizations, e.g. free radical polymerizations, high molecular weight polymers are obtained at low conversions (Figure 14). In the early stages of polymerization, directly after initiation, the concentration of radicals is high, leading to the fast growth of the polymer chains. Propagation reactions occur (Scheme 1) leading to high molecular weight polymer chains. Due to termination reactions such as disproportion or recombination, the molecular weight no longer rises. The uncontrolled nature of the reaction without control over termination reactions leads to broad molecular weight distributions. In contrast, the molecular weight in a controlled radical polymerization (or controlled reversible-deactivation radical polymerization, RDRP) steadily rises in a linear progression during the reaction process. High molecular weight polymers are obtained towards the end of the reaction time. In summary, free radical polymerization is a robust polymerization process withstanding a variety of impurities and can be conducted in a cost-effective way on a technical scale. The uncontrolled nature of this polymerization technique leads to broad molecular weight distributions which influence the chemical and mechanical properties of the product. The controlled radical polymerization enables the synthesis of narrow distributed (block-) copolymers with high control over the chain architecture. Specially designed additives are needed for these kinds of polymerizations leading to higher costs at a technical scale. Furthermore, RDRP is less robust regarding impurities. RDRP is exceptionally well suited for specialty polymers where highest control over the polymer architecture plays an important role for the desired application.

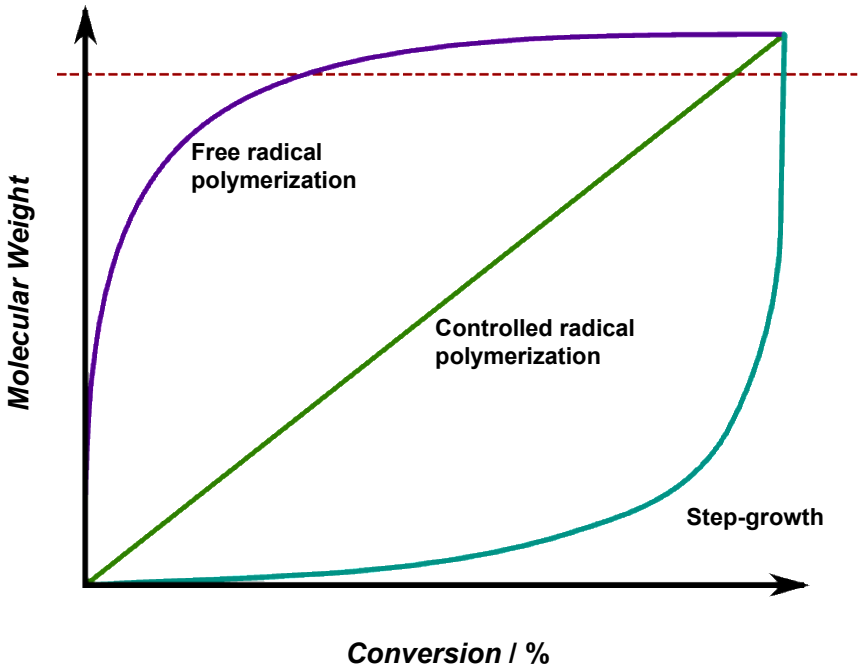

Figure 14: Illustration of molecular weight over conversion or time for different polymerization mechanisms. Above the red dotted line, high molecular weight polymers are obtained.

Free radical polymerization was chosen as the polymerization technique for the research conducted in this thesis for several reasons:

- Commercially available products are synthesized via free radical polymerization.
- Broad molecular weight distribution may have favorable influence on performance.
- Compatibility with a wide range of monomers.
- Robust polymerization regarding impurities and conditions.
- Next to initiator, unreacted monomer and solvent, no other residuals
- Scalable up to several tons of product.
- No specialized equipment needed.
- No specialized additive needed.
- Cost-effective synthesis on larger scales.

3.6 Postpolymerization modification: *N,N′*-Carbonyldiimidazol

N,N′-Carbonyldiimidazol (CDI) is a very well-known reagent in peptide chemistry for the formation of amide bonds between carboxylic acids and amino functions and was reported by Staab[145] in the 1950s. In the past, CDI served as a reagent to enable bioconjugation linking polymers to biomolecules such as proteins to facilitate their application in drug delivery and diagnostics. Furthermore, it has been used in polymer synthesis for the post polymerization modification of suitable functional groups resulting in new functionalities in sidechains or the crosslinking within polymer matrices. Wittmar[146] was able to functionalize poly (vinyl alcohol) (PVA) utilizing a variety of amines using NMP as the solvent.

CDI serves as a substitution to phosgene in organic chemistry and its reactivity is comparable to acyl halides. The high reactivity of the compound can be explained by the high degree of electrophilicity of the imidazole ring. Due to the electron-withdrawing influence of the carbonyl group adjacent to the imidazole ring, the positive charge on the ring carbon atoms is enhanced and thus CDI is susceptible to nucleophilic attack.

Multiple functional groups readily react with CDI to form activated intermediates (Scheme 2). The most prominent substance classes which are used in combination with CDI are carboxylic acids, amines and alcohols. Activated intermediates for follow-up reactions are obtained in a nucleophilic substitution mechanism. Amines and alcohols react with CDI releasing one equivalent imidazole. Carboxylic acids react with CDI releasing one equivalent imidazole and one equivalent carbon dioxide, which also promotes the reaction.

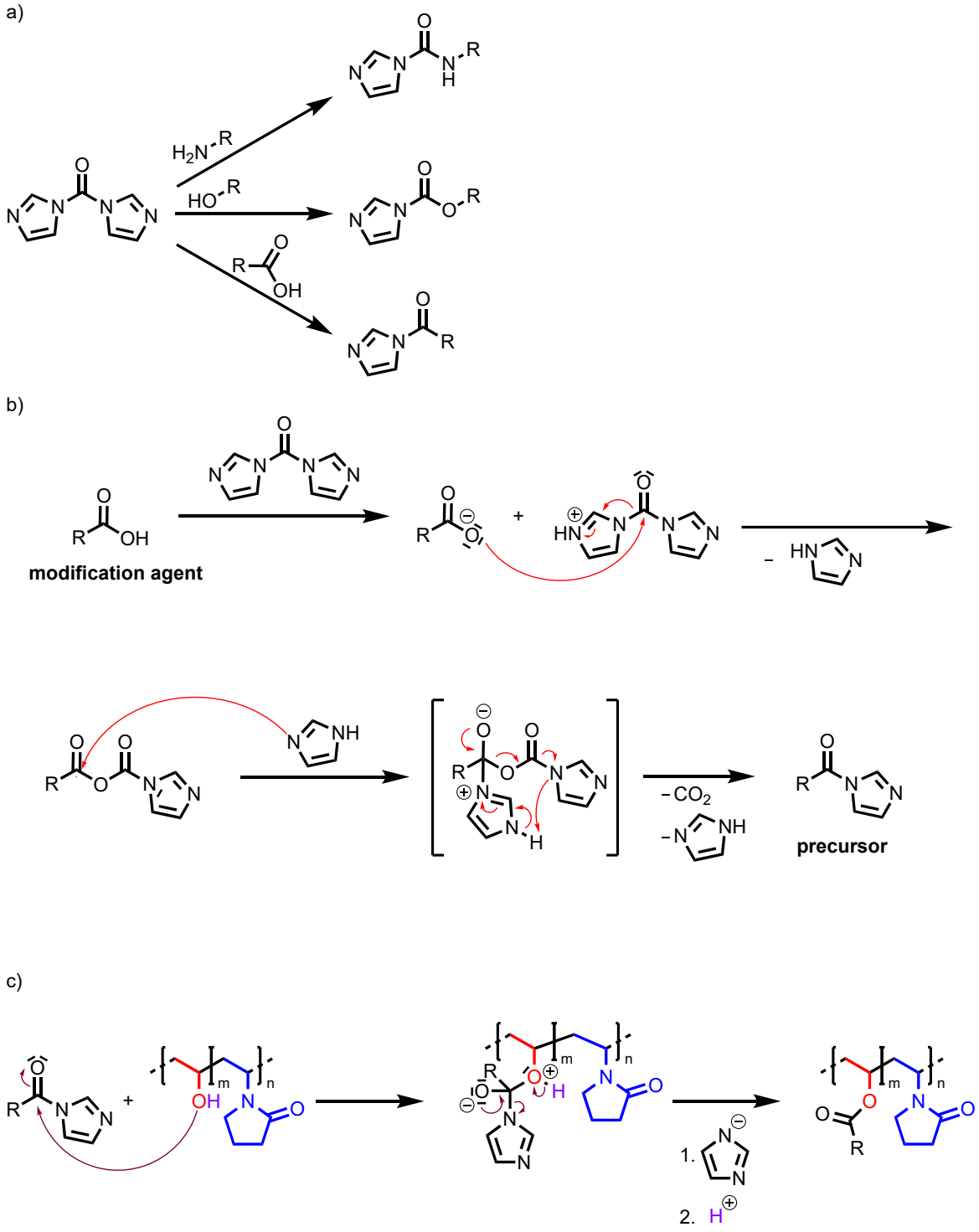

Scheme 2: a) General reaction for the synthesis of activated intermediates of carboxylic acids (activated amide), amines (activated urea), and alcohols (activated carbamate) using CDI; b) A possible reaction mechanism was proposed by Staab[145] and includes the formation of a mixed anhydride of the modification agent and CDI by nucleophilic attack by the deprotonated (by CDI) carboxylic acid. After the abstraction of one eq. imidazole, the imidazole nitrogen interacts *via* an intermolecular nucleophilic attack with the modification agent carbonyl carbon. Elimination of carbon dioxide yields the precursor. c) Final polymer modification of hydroxyl carrying PVA-co-PVP. After the nucleophilic attack of the hydroxyl moiety onto the carbonyl group in the precursor, a tetrahedral intermediate is formed. An imidazole-anion is lost followed by rapid loss of a proton yielding an ester and an equivalent of imidazole.

CDI is a versatile reagent used in several different synthesis strategies including esterification, amide bond formation, and urethane formation. The facile activation of otherwise less reactive species offers a variety of pathways in the modification of alcohol groups in polymer sidechains as present in PVA-co-PVAc or PVA-co-PVP.[146-148] CDI chemistry is utilized to modify polymers, introducing specific functional groups that may enhance the polymer's interaction with the API. The modified polymers can significantly impact the solubility, stability, and bioavailability of the drug when used in a formulation.

There are other postpolymerization modification methods imaginable for the modification of PVA-co-PVP. Considering the modification targeting the hydroxyl moiety, other techniques are imaginable. The esterification is also possible in a Steglich-type esterification utilizing EDC-HCl (1-Ethyl-3-(3-dimethylaminopropyl)carbodiimide) or DCC (*N*,*N*'-Dicyclohexylcarbodiimide) and DMAP (4-(Dimethylamino)pyridine). Due to the acute toxicity of DMAP, this kind of reaction type is unfavored, as DMAP needs to be removed completely before using the synthesis product in the pharmacological context.

Another type of reaction is the Williamson ether synthesis utilizing a strong base such as NaH (sodium hydride) in conjunction with halogenated modification agents. Halogenated modification agents are readily available on a commercial scale. Alcohol cannot be used as a solvent in this reaction and due to limited solubility of PVAc-co-PVP this reaction would need to be conducted using DMF, DMAc or DMSO. In a recent study by Yang *et al.*[149], the explosion hazard considering the use of NaH with DMF or DMSO was investigated again. Even at lower temperatures between 56 and 200 °C, a substantial safety hazard was observed and during experiments using the DMSO/NaH mixture, the utilized accelerating rate calorimeter (ARC) cell ruptured. Due to this, this reaction type is not suited for the synthesis on larger scales.

A different approach would be the radical grafting from polymerization targeting the methyne carbon on the PVA-co-PVAc backbone. In different studies by Markley[150], Wheeler *et al.*[151], and Liu *et al.* [152], a PVA derivative was functionalized by free radical polymerization. In recent studies conducted at Merck Life Science KGaA, this reaction type was deemed as not feasible due to difficulties in the formation of product. Other modification strategies such as copper catalyzed azide-alkyne click chemistry are not compatible due to missing functional groups and the introduction of metal centers which need thorough removal in the pharmaceutical context. In summary, there are many different approaches to modify a PVA derivative. From these approaches, the modification via CDI chemistry is the most favorable due to the diverse pool of modification agents, non-toxic residuals, and its ability to be performed on larger scales. One drawback is the synthesis in the solvent DMF, but purification by dialysis may bring the residuals level below the maximum amount as denoted in the ICH-Q3C guidelines.[153]

4 Aim of Work

Enhancing the bioavailability of poorly water-soluble APIs is one of the major challenges in solid formulation. 70% to 90% of drug substances in the research pipeline are poorly water soluble. 60% to 70% of new drug substances (NCEs) can be assigned to the BCS class II showing high bioavailability but low solubility. This results in limited pharmaceutical efficacy and in a need for the development of solubility enhancing excipients.[64, 74, 75] The main function of these biocompatible and non-toxic excipients, most commonly polymers, is the increase of the API solubility to reach therapeutically effective doses and to ensure the capability to manufacture oral dosage forms on an industrial scale. The polymers in use serve as a mediator between the hydrophobic, poorly soluble API and the aqueous physiological environment. The commercially available polymer landscape includes synthetic and cellulose based polymers carrying a diverse spectrum of chemical moieties (Table 1). Many of which are well-known in the field and currently used in marketed drug products. In this context, polymers offer a versatile platform for the development of advanced drug delivery systems.

At this point in time, finding the best polymer for the formulation of a NCE is a time and financially intensive endeavor. Especially, as there is no one size fits all solution in terms of excipients. A prediction of a polymer's performance in a formulation thereby reducing the number of required experiments is one subject matter in current research. By utilizing small scale screening tools, a polymer in conjunction with a model API can be assessed, but a comprehensive structure-property relationship to chemical structures included in the polymers is not yet available. This thesis aims to move a step closer to being able to predict the performance of an API by considering the innate chemical moieties.

One other pressing challenge is the low solubility of most NCEs in development. Low solubility limits the pharmaceutical efficacy and the bioavailability. In addition to that, the processability of the formulation via HME can present a significant challenge. NCEs of low melting (Figure 10) point are prone to degradation during thermal and mechanical stress. Especially the processing of APIs in the temperature range between 90 °C and 150 °C is of great interest, as a multitude of APIs have melting points above 150°C[114], which results in high processing temperatures and thereby poses a risk for the integrity of the API during processing and formulation.

One aspect this thesis is dealing with, is the post-polymerization modification of a copolymer consisting of vinyl pyrrolidone and vinyl alcohol for the solubility enhancement of a poorly soluble model API (Section 4). Ultimately the aim is to develop a comprehensive understanding of how modifications of the base polymer PVA-co-PVP influence the polymer properties. Furthermore, how these properties influence its interaction with the API to improve the solubility of the poorly water-soluble model compound. This thesis pursues the development of a qualitative structure-property relationship by systematic modification of the base polymer to assess the specific influences of chemical structures

introduced into the copolymer-backbone. The copolymers Parteck® MXP (PVA-co-PVAc), consisting of vinyl alcohol and vinyl acetate monomers and Kollidon® VA64 (PVAc-co-PVP), a polyvinyl pyrrolidone and polyvinyl acetate copolymer, are well-known excipients in the field of solid formulation. In light of the elaborate research conducted in the past concerning PVAc-co-PVP and PVA-co-PVAc and its extensive utilization in solid formulation, this thesis seeks to address the modification of a related vinyl alcohol derivative to further tailor the properties of the polymer. By aqueous saponification, the vinyl acetate moieties in PVAc-co-PVP may be removed to obtain the vinyl alcohol derivative (PVA-co-PVP). The systematic investigation will explore how various chemical structure elements affect its physicochemical properties, its processing conditions, and the resultant dissolution capabilities. By utilizing different chemical entities such as hydrophobic (*e.g.*: cinnamate or palmitate) or mPEG (with increasing mPEG chain length) substituted carboxylic acids and amines, the development of a structure-property relationship is investigated. To evaluate the qualitative influence of each of these groups onto the polymer properties is the main subject matter of the first chapter. The polymer modifications carrying diverse types of chemical motifs in various modification degrees will be extensively characterized in terms of their physico-chemical properties using techniques such as DSC, TGA and melt rheology. The investigation of the resulting properties, namely the glass transition temperature and the degradation temperature, intends to predict the polymer's properties during melt rheological measurements and consecutively during small-scale and intermediate scale extrusion. The target range in terms of glass transition temperature is between 80 and 90 °C, while thermal stability should be given above 200 °C. Combined with a melt viscosity between 1000 Pa s and 10 000 Pa s in this temperature range leads to a broad window in which the polymer can be processed via HME. With solubility capabilities in processability at low temperatures enabling the manufacturing of thermally labile APIs. Ultimately, a high dissolution capability for a poorly soluble API ketoconazole (KTZ) with low manufacturing temperatures are desired. Furthermore, the process is transferred to pilot scale to enable the synthesis of sufficient amounts of material for an intermediate scale extrusion. This includes development of a scalable process for the saponification and modification.

Another aspect of this thesis is the synthesis of innovative thermoplastic polymers specifically designed for the manufacturing at lower temperatures and the solubility enhancement of poorly water-soluble APIs. To address these challenges, this thesis focuses on the development of novel polymer carriers, which have the ability to maintain the API in its amorphous state. This ideally leads to enhanced dissolution properties of the API and reduces the processing temperatures to circumvent the thermal instability of the same. This aspect of this thesis addresses several key objectives. The first objective is the development of a bottom-up synthesis platform for the targeted generation of multifunctional copolymers by free radical polymerization. The synthesis process developed must be scalable and capable of being executed resulting in up to one metric ton of product. The second essential objective

in this section of the thesis is the refinement of the qualitative structure-property relationship. By means of an explorative design of experiments (DoE) approach, the distinct influence of the monomers in the generated copolymers is characterized. On the journey to a polymer with optimized properties for manufacturing and dissolution enhancement, DoE serves as a tool enable the deliberate synthesis of polymer entities with favorable properties in terms of dissolution enhancement and manufacturability. The synthesized polymers are composed of up to four comonomers carrying functional groups which exert a favorable influence on the API solubility and processing temperature. As a proof of concept, two monomers, namely vinyl acetate and *N*-vinyl-2-pyrrolidone, were utilized. Transitioning from two to four comonomers leads to additional degrees of freedom to adjust the resulting performance in terms of HME manufacturing and super saturation. To address the desired glass transition temperature between 80 and 90 °C, a mPEG derivative (allyl mPEG or mPEG methacrylate) is incorporated. Vinyl benzoate is utilized as a fourth monomer to facilitate high solubility properties with regards to the API KTZ. The development of a robust free radical polymerization process enables the facile introduction of multiple different monomers into the copolymer in a single reaction step. Lastly, the research aims to develop a synthesis process which can be scaled up to the ton scale, as these polymers serve as excipients for the processing by hot melt extrusion which itself is a widespread and scalable manufacturing technique of solid dosage forms.

Ultimately, this thesis will provide an essential understanding of the role of chemical motifs in polymeric materials in the manufacturing of the same by HME and in enhancing the solubility of poorly water-soluble APIs. It aims to build a connection between a chemical structure present in an excipient and the resulting properties in manufacturing and application. The knowledge gained in this thesis may lead to the development of new drug delivery systems for novel poorly soluble NCEs in today's pipeline.

5 Structure-property relationship in modified PVP-co-PVA

5.1 Introduction

Understanding how a chemical moiety in a polymer impacts its performance in pharmaceutical applications including extrusion and solubility enhancement of a model API, is essential for the formulation of new poorly water-soluble APIs. One aim of this thesis is to establish a connection between the polymer structure and the resulting properties of chemical motifs present for their processing in pharmaceutical extrusion and subsequent solubilization of a model API.

The polymer entities were synthesized in a post polymerization reaction starting from a base polymer carrying a vinyl alcohol moiety in its backbone (PVA-co-PVP). The vinyl alcohol derivative was obtained by saponification of PVAc-co-PVP (Kollidon® VA64). PVAc-co-PVP itself is widely used and tested in the solid formulation of poorly soluble APIs.[18, 21, 87, 109, 123, 154-158] It is successfully employed in formulations in conjunction with chemically diverse API's.[53, 87, 97 34] An advantage in using this excipient is its amphiphilicity making it soluble in various organic solvents, e.g. 2-propanol, butanol, chloroform and more hydrophilic solvents like water. This facilitates trouble-free processing and handling of the material. Amorphousness of both polymer and API in a formulation has advantages with respect to bioavailability and processability. PVAc-co-PVP is an amorphous polymer, leading to the absence of seed crystals for premature recrystallization of the API. Also, amorphousness with a T_g around 103 °C means, that no melting point is present and the processing temperatures were found to be 160 °C to 180 °C by Kolter *et al.* [121] and Bühler[135].

The hydroxyl moieties in the polymer backbone, which are generated by saponification, are ideal for a targeted post-polymerization modification. Considering the polymers marketed today, various comonomers are present in the respective chemical structures. A post-polymerization modification of a PVA-co-PVP polymer enables the introduction of functional groups by reaction on this specific site. The reaction center offers great flexibility in terms of reactants as carboxylic acids, amines or alcohols are well-known substance classes and a plethora of variations known and may be used as modification agents. The pool of commercially available modification agents is vast and functional groups such as amines, alcohols, carboxylic acids, alkyl chains, aromats or mPEG moieties are imaginable. By introducing these groups, the polymer properties might be influenced favorably for the manufacturing of physical mixtures of polymers and APIs via HME. In this thesis, a variation of multiple groups are introduced into the backbone including hydrophilic mPEG derivatives, polar amines, hydrophobic aromatic groups or alkyl groups and miscellaneous CH-acidic modification agents like ketones or esters. Multiple binding sites exist on the PVA-co-PVP backbone, thereby enabling the partial functionalization of the hydroxyl moieties. As a result, each modification can be probed based on its specific influence of

the modification agent onto the properties of the resulting polymer in proportion to the number of present moieties. The generated polymers include structures which are present in marketed products in the research field like vinyl pyrrolidone in Kollidon® VA64 or PVP K30, vinyl alcohol as in Parteck® MXP or Kollicoat® IR and PEG structures as in Soluplus® or Kollicoat® IR. As a majority of NCE are poorly water soluble, hydrophobic moieties may have the potential to form favorable interactions with the API and increase their solubility.

The polymers were assessed based on key properties for the targeted manufacturing technique via HME. These properties include the processing temperature, thereby the degradation behavior as well as the glass transition temperature and the melt rheological behavior. From the generated polymer library, a selection was processed in small-scale extrusion and subsequently the synthesis was scaled to 200 g product following an extrudability test via an intermediate-scale extrusion. Additionally, polymer-API interactions play a crucial role in the solubilization of a given API. These interactions were characterized by a dissolution assay using ketoconazole as model API. The release kinetics were tested utilizing a readily soluble API, caffeine.

5.2 Results and Discussion

The processing temperature of polymer matrices in the field of amorphous solid dispersions is of great importance to improve the processability of physical mixtures loaded with thermally labile APIs. In addition to this, the solubilizing effect of the polymer with regards to the API in aqueous media is of key interest for the effectiveness in the application in solid dispersions. In this study, a PVA-co-PVP derivative was used as the base co-polymer, as obtained from the saponification of PVAc-co-PVP, and by its modification via CDI-chemistry, its properties were influenced (Figure 15). A multitude of different modifications were synthesized and evaluated to establish a structure-property relationship of chemical motifs onto the performance in solubility enhancement. An understanding of the specific groups influencing the solubility enhancement and processability was generated. The targeted processing techniques of these novel polymers include FDM 3d printing and extrusion.

Polymer entities were synthesized in three steps from a commercially available Polyvinyl acetate-co-poly(*N*-vinyl-2-pyrrolidone) (PVP-co-PVAc) starting material. The starting material bearing acetate moieties was saponified leading to the base polymer polyvinyl alcohol-co-poly(*N*-vinyl-2-pyrrolidone) (PVP-co-PVA) (Scheme 3a). Hydroxyl moieties present in the base polymer were then partially modified via CDI-chemistry (Scheme 3b and c) utilizing esters or amines carrying various functional groups. The result of this modification is a terpolymer with a functional comonomer. The modification agents for the OH-moieties in PVP-co-PVA can be categorized in groups according to their chemical nature: mPEG-acids, hydrophobic acids, alkyl amines and miscellaneous.

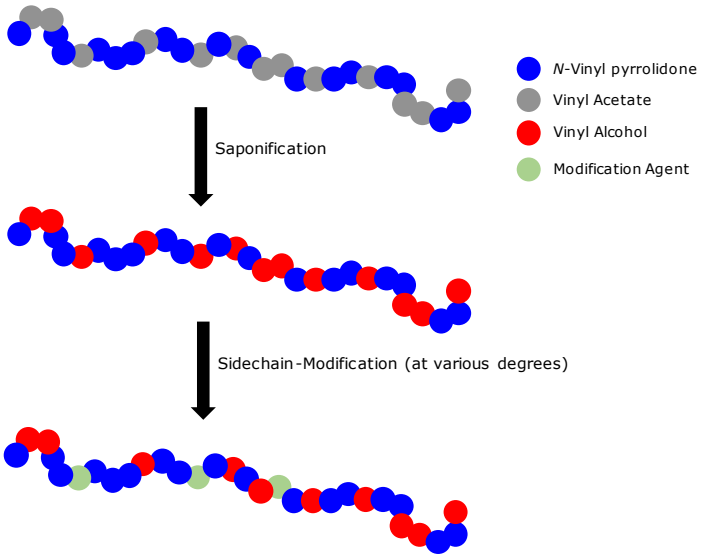

Figure 15: Schematic illustration of the synthesis procedure starting from a PVAc-co-PVP copolymer, which after saponification to obtain PVA-co-PVP, is modified in various degrees and different monomers.

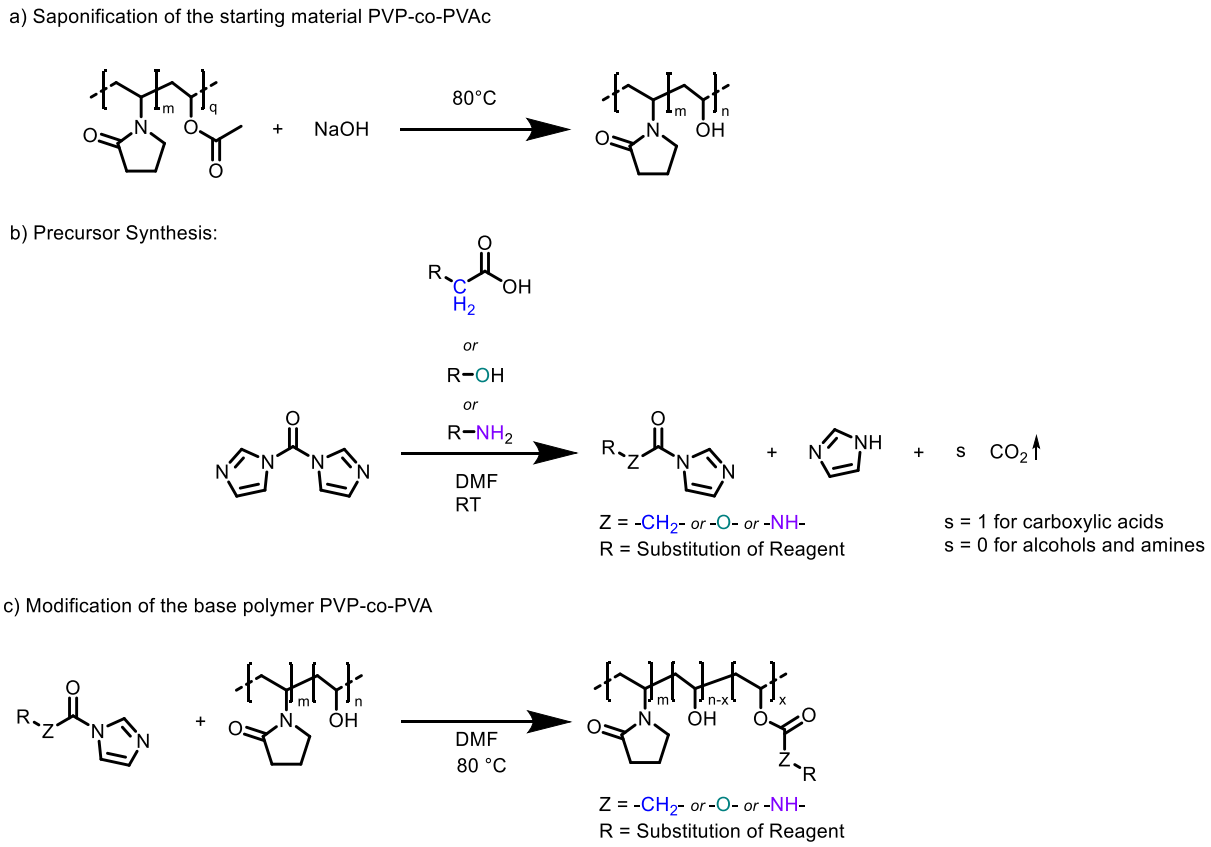

Scheme 3: Schematic overview of modification process

As outlined in the introduction of this chapter, one of the key properties for novel polymers in the field of extrusion is their processability. Each polymer was evaluated regarding its glass transition temperature T_g and degradation temperature T_{deg} with the aim to reach low processing temperatures for a later extrusion. If a polymer fulfilled the requirements, a small-scale extrusion was conducted to further evaluate its performance for the anticipated manufacturing technology. The polymer entities were assessed and candidates with the highest potential were identified, directly leading to a chemical structure motif influencing the processability.

By comparing the terpolymers with the starting material and base polymer as benchmarks, the advantages of these modifications are outlined. The starting material and base polymer were analyzed extensively facilitating a direct comparison with obtained modifications. The starting material, the resulting polymers for each group, and the analysis of these polymers will be discussed in the following subchapters. Synthesized polymers were analyzed regarding their spectroscopic properties, their physico-chemical properties, and their molecular weight distribution. Analysis techniques utilized include nuclear magnetic resonance spectroscopy (NMR), differential scanning calorimetry (DSC), thermogravimetric analysis (TGA), gel permeation chromatography (GPC), Melt rheology and dissolution behavior. The exact ranges for each of these properties were defined (Table 7) and the

polymers were each assessed concerning these features. Synthesis protocols can be found in Section 8. To investigate their applicability in intermediate scale extrusion, the synthesized polymers were milled and extruded on a small scale if the requirements were met. Furthermore, the polymers fulfilling the targets were synthesized on a larger scale (200 g), followed by intermediate-scale extrusion.

Table 7: Target criteria and acceptable ranges for the assessment of a polymer entity. The factors concerning NMR, DSC, TGA are strongly discriminating. Factors for the dissolution properties are targeted and need to be investigated.

Method	Target criteria	Target reached	Acceptable
NMR	Successful reaction	Yes	
DSC	$T_g \geq 80 – 90$ °C	80 – 90 °C	± 25 °C
DSC	No T_m Amorphousness	No T_m	
Extrusion (Mini Extruder)	Transparent filaments	Yes, low torque	Yes, increased torque
Melt viscosity	η_{melt} = 1000 – 10000 Pa s @ 0.1 rad s^{-1}	1000 – 10000 Pa s	
TGA	$T_{deg} \geq 200$ °C	≥ 200 °C	190 °C – 200 °C
Dissolution	80% release ≤ 30 min	≤ 30 min	≥ 30 min, ≤ 60 min
Process window	40 – 50 °C difference T_{deg} and $\eta_{melt,\ 10000\ Pa\ s}$	40 – 50 °C	30 – 40 °C
ASD Screening KTZ	Supersaturation potential	Yes	Yes

5.2.1 Selection process for pharmaceutical extrusion

A polymer's ability to be processed at low temperatures (90 °C to 150 °C) and their capability to improve the solubility of a poorly water-soluble API in acidic aqueous solution is of key interest for the application in solid formulation of oral dosage forms. The polymers synthesized in this study were assessed based on their thermophysical properties, their thermomechanical properties, and their solubilizing properties (Figure 16). Candidates with high potential were extruded on a small scale on a 3 mm twin-screw extruder (*Three-Tec Mini-Extruder*, 3 mm). If a polymer entity met most of the prerequisites posed in the introduction of this chapter, a larger batch (100 g to 200 g) was synthesized to enable the testing of its performance on an intermediate scale extruder (*Pharma 11*, Thermo Fisher, 11 mm). 50 to 60 g material is needed to test one setting in terms of temperature and screw speed on the 11 mm extruder. This experiment merely proofs the extrudability of a material based on one set of settings during the extrusion. For an optimization of the extrusion process, much larger quantities (1000 g to 1500 g) of material are needed. The effort of scaling a synthesis process starting from 5 g of material to ten-, twenty- or a hundredfold the amount of material is an exceptionally complex, time-consuming, and laborious endeavor. Therefore, a deep understanding of the polymers thermal behavior is mandatory to estimate an appropriate range for a successful extrudability test. Next to the processability, solubilizing properties of a polymer in relation to a poorly water-soluble model API is a key factor. A polymer candidate with high potential has the ability to increase a model API's solubility

in aqueous acidic environment to increase its solubility to therapeutically effective values and thus increase the API's bioavailability. Only if most of these prerequisites are met and a preliminary extrudability on the intermediate scale extruder is given, an upscaling of the batch process to 1000 g is reasonable.

The polymers synthesized during this study are first assessed in terms of their properties on a small scale. DSC measurements and TGA measurements were used to develop an understanding of the available temperature range between degradation and fusibility, which in turn is used for further analysis. Consecutive melt rheological measurements and small-scall extrusion were used to narrow down the estimated temperature range in which the extrudability test is most probable to succeed. In addition to these tests concerning the processability of a polymer, the solubilizing properties are investigated utilizing a dissolution assay developed by cooperation partners at Merck Life Science KGaA. Model compounds used are the BCS-I compound caffeine for the evaluation of the performance for immediate release, and ketoconazole to assess the dissolution enhancement of a poorly water soluble BCS-II compound.

As part of this project, cooperation partners executed parts of the experiments and analysis procedures. The extrusion experiments on an intermediate scale and rheological measurements were conducted by Alessandro-Giuseppe Elia (*Merck Life Science KGaA*), Nadine Gottschalk (*Merck Life Science KGaA*) and Florian Hess (*Merck Life Science KGaA*). Dissolution Experiments and related vacuum compression molding preparations (VCM, *MeltPrep*) were conducted by Nabil Lamrabet (*Merck Life Science KGaA*). Oliver Stranowsky (*Merck Electronics KGaA*) conducted the reactions on larger scales (> 100 g) and the consecutive dialysis.

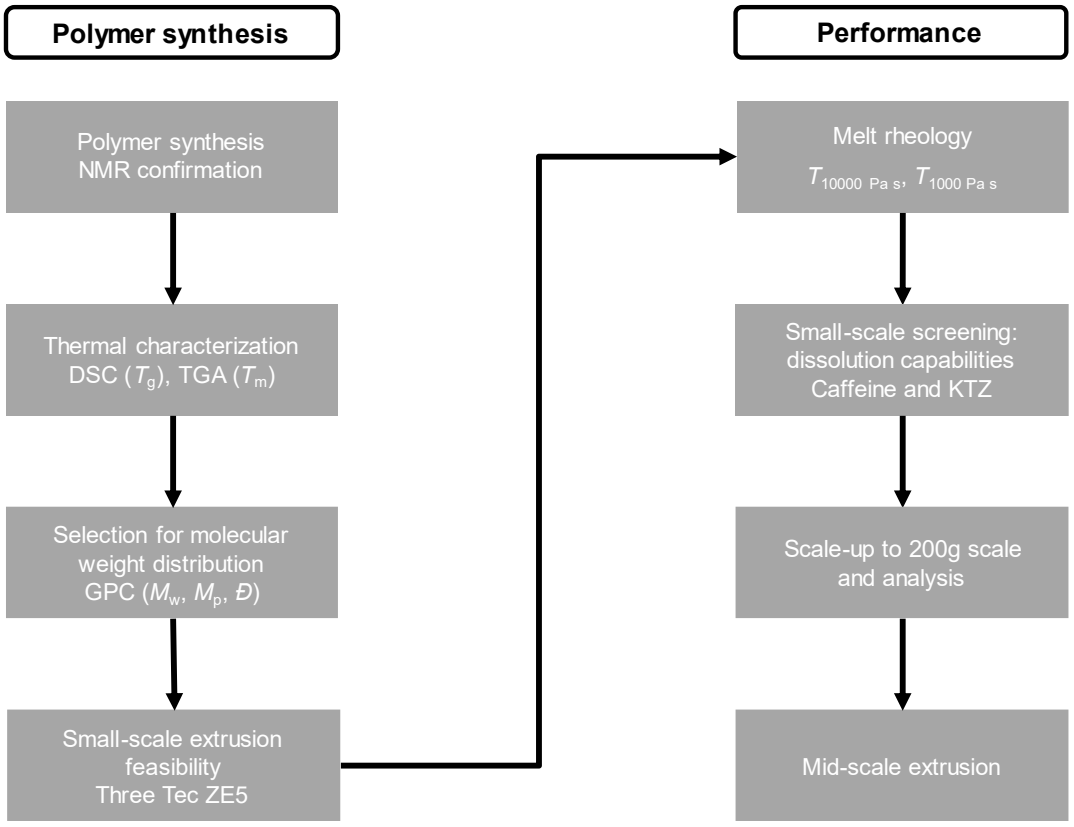

Figure 16: Illustration of the polymer assessment. If polymer properties are far from the defined specifications, the consecutive activities will not be conducted.

5.2.2 Analysis of the starting material PVP-co-PVAc

Commercially available PVP-co-PVAc (Kollidon® VA64, BASF SE) served as the starting material and was analyzed in detail to facilitate direct comparison with terpolymers synthesized and thus display the influence of the introduced comonomer on the polymer's properties. PVP-co-PVAc was saponified to form the base polymer, which in turn was utilized for the modification. PVP-co-PVAc is marketed as a copolymer with a distribution of 60% VP and 40% VAc. To confirm this, quantitative ^{1}H-NMR and quantitative ^{13}C-NMR was used. The signal of residual water (corresponding to HDO-d_1) in DMSO-d_6 in ^{1}H-NMR spectroscopy shows resonance around 3.3 ppm and shifts depending on water content (Appendix, Figure 1).[63] The PVP-signal b^3 overlaps strongly with water, so trifluoroacetic acid (TFA) was used as an additive in the ^{1}H-, HSQC- and HMBC-NMR analysis if not otherwise stated. The ^{1}H-NMR utilizing TFA suggests a VAc/VP distribution of 57% VP and 43% VAc (Figure 17, signals b^3 and b^4, c^3), whereas the acetate methyl singlet (c^3) overlaps strongly with the pyrrolidone methylene multiplet (b^4). Therefore, additional quantitative ^{13}C-measurements were conducted (Figure 18). In the ^{13}C-NMR spectrum, the two carbonyl-carbons in VAc (C^4) and VP (B^6) were used for the evaluation. These two signals do not overlap with any other signals and the visually estimated signal to noise ratio

is large (SNR > 10), therefore an evaluation with these singlets is appropriate. A distribution of 55% VP and 45% of VAc comonomers is obtained (Figure 18) and consecutive calculations are based on this distribution. In this work, three different batches of PVP-co-PVAc were used for synthesis (Table 9). The respective ^{13}C-NMR-spectra show similar distributions for VP and VAc and these batches were treated as the same material for batch calculation purposes (Appendix, Figure 2, Appendix, Figure 3, Appendix, Figure 4).

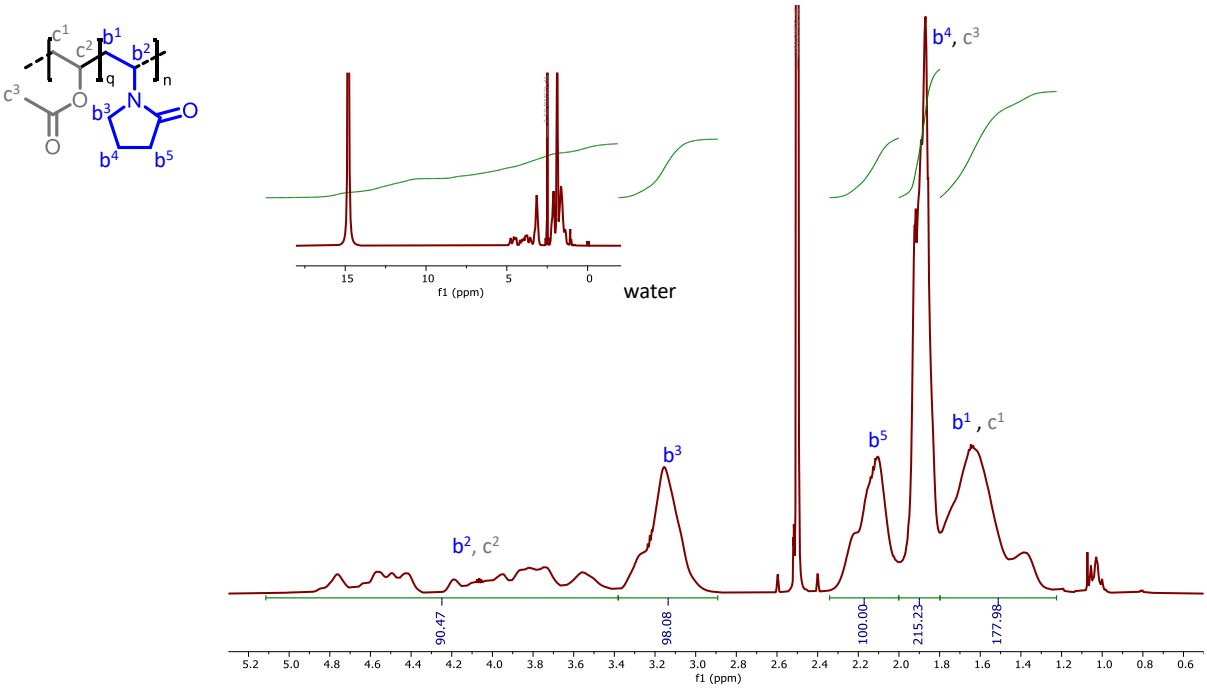

Figure 17: Quantitative ^{1}H-NMR spectrum of commercially acquired, pure PVP-co-PVAc (Kollidon® VA64) with the addition of TFA to force a shift of proton signal corresponding to residual water. Normalized to methylene moiety b^5. Calculation based on VAc methyl moiety c^3 and VP methylene moiety b^5.

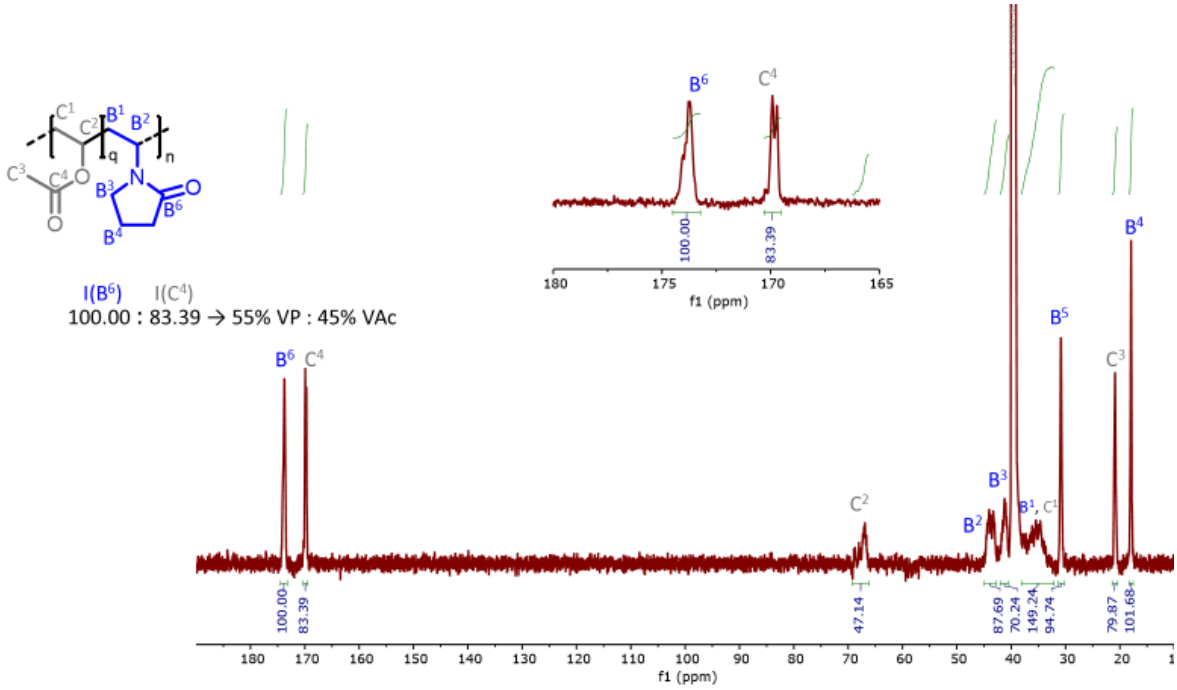

Figure 18: Quantitative ^{13}C-NMR spectrum of PVP-co-PVAc (Kollidon® VA64) at a concentration of 200 mg mL^{-1}. 512 scans with addition of Cr(acac)$_3$ as relaxation agent to reduce T_2 relaxation and increase resolution at a relaxation delay of 15 s. Calculations based on carbonyl groups in VP (B^6) and VAc (C^4).

To further confirm the specifications given by the supplier and to define a starting point for comparison for later polymers, PVP-co-PVAc was analyzed concerning its molecular weight distribution by GPC using RI detection with PMMA calibration standards and MALS detection. In later experiments, monomodal distributions and a shift of M_w to higher molecular weights in comparison to the starting material is a sign for successful reaction. There were different batches used in this thesis, which were analyzed separately. The batches showed very similar molecular weight distributions (Appendix, Figure 5) and properties. All elugrams show a monomodal distribution without additional peaks in the low molecular weight region. The molecular weight of the batches is close to $M_w = 32000$ g mol^{-1} with a dispersity index $Đ = 3.9$ (Figure 19c). Additional measurements were conducted utilizing MALS detection leading to a molecular mass of $M_w = 36000$ g mol^{-1} and a dispersity index of $Đ = 2.5$ (Figure 19c). Batch calculation for consecutive saponification (Chapter 5.2.3) were conducted based on this molecular weight ($M_{w,MALS}$), indifferent of which batch was used for the synthesis.

The thermal behavior was characterized by DSC, TGA and melt rheology. The excipient PVP-co-PVAc is prevalent in the field of solid formulation.[52, 97, 132, 137] A first indicator for a polymer's processing range is its thermophysical behavior in DSC and TGA measurements. Utilizing DSC, the glass transition and melting temperature can be determined. The glass transition temperature or, if present, the melting temperature gives an estimate on where the lower limit of a polymer processing window is located. PVP-co-PVAc shows no melting range, indicating amorphousness of the polymer in the measured

temperature range between 0 °C and 250 °C. The glass transition temperature of PVP-co-PVAc is at 106 °C (Figure 19a). This suggests that the polymer is suitable for extrusion of thermolabile API's. The absence of a melting point is a significant advantage over other polymers bearing a melting point, as the amorphous state is intrinsic for these polymers and does not need to be induced by HME.

The upper limit of a samples processing range is its degradation temperature (T_{deg}). This temperature is determined by TGA. To ensure thermal stability during the targeted extrusion temperatures in the process, a T_{deg} over 200 °C is advantageous. PVP-co-PVAc shows an onset of degradation at T_{deg} = 236 °C (Figure 19b). Considering the temperature range between T_g and T_{deg}, a first notion of the polymer's processing range is obtained. At first glance, the temperature difference of 130 °C suggests a broad applicability.

In addition to the thermophysical characterization via DSC and TGA, temperature sweep melt rheology measurements were used to predict the polymers performance in extrusion. The extrudable range is defined as the temperature range where the melt has a viscosity between 10000 Pa s and 1000 Pa s.[121] During the measurements on a plate rheometer, the temperature of the polymer sample is increased in a controlled manner while oscillation frequency and amplitude are constant. The extrudable range obtained from melt rheology is between the upper limit of extrudability at T(10000 Pa s) = 161 °C and the lower limit at T(1000 Pa s) = 186 °C, resulting in a processing range in extrusion of ΔT = 24 °C (Figure 19d). The relative values of the storage modulus (G') compared to the loss modulus (G'') characterize the viscoelastic behavior of the polymer. For PVAc-co-PVP, G'' is higher than G' in the temperature range from 130 °C to 232 °C, where the two curves intersect. This indicates that the polymer is amorphous and has no melting point. The phase angle increases over the course of the measurement until a maximum is reached at 201 °C. The phase angle decreases again suggesting the beginning of degradation.

For more information about the analysis techniques and methods, the reader is referred to section 8.1.2. A summary of the analytical data is given in Table 9.

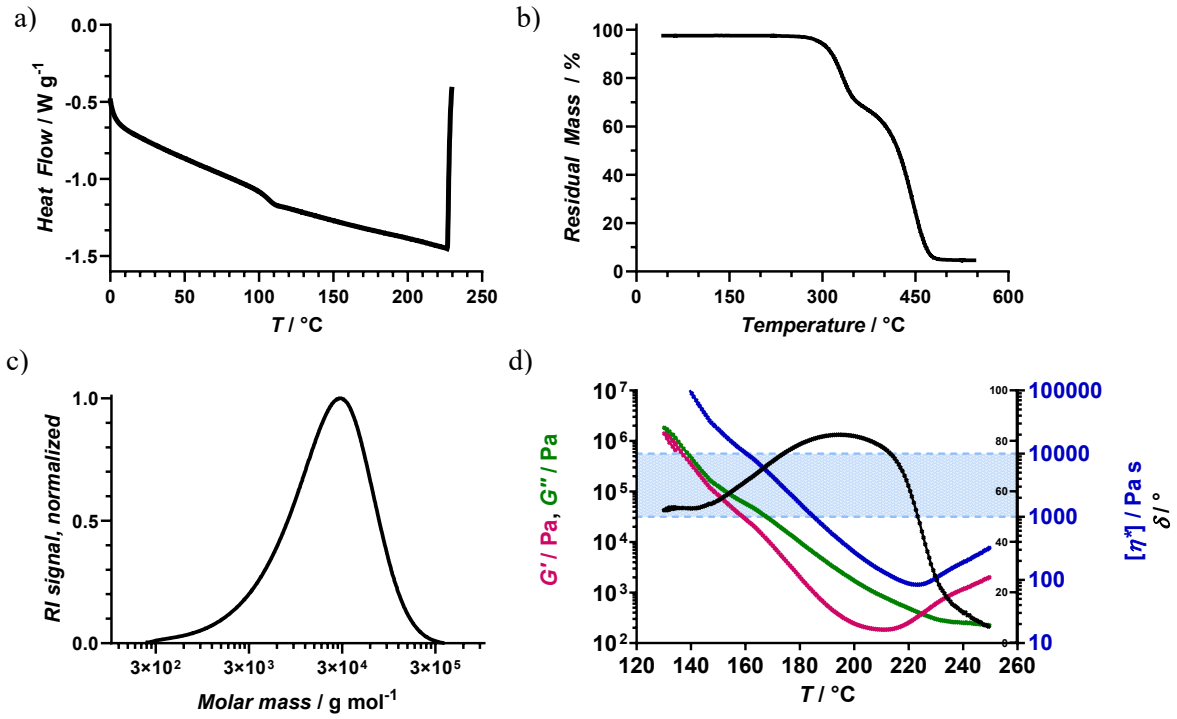

Figure 19: a) DSC thermogram of the second heating cycle for PVAc-co-PVP with a heating rate of 10 K min^{-1}. Glass transition temperature of this sample is 106 °C and no melting temperature is visible. B) TGA thermogram of PVAc-co-PVP. The degradation temperature is 236 °C. c) RI detection; DMAc/0.6 g L^{-1} LiBr, PMMA Standards, M_w = 32000 g mol^{-1}, Đ = 3.9. d) Plots of melt viscosity, phase angle, G' and G'' of PVP-co-PVAc. T(1000 Pa s) = 186 °C; T(10000 Pa s) = 161 °C. Dashed lines indicate the range between 1000 and 10000 Pa s

The extrusion of PVAc-co-PVP leads to yellow filaments that are very brittle. Lab-scale mini extrusion was possible above 130 °C with moderate average torque values of 1.5 N m. The intermediate-scale extrusion can be conducted at a temperature of 190 °C with low die pressures and moderate torque.

Table 8: Analytical summary of PVAc-co-PVP batches used in this thesis.

Name	NMR Ratio VP/VAc	GPC MALS M_w / g mol $^{-1}$	GPC MALS Đ	GPC RI M_w / g mol $^{-1}$	GPC RI Đ	GPC RI M_w / g mol $^{-1}$	DSC T_g / °C
Batch 1	55%/45%	36000	2.5	33000	3.8	27000	107
Batch 2	55%/45%			31000	3.7	22000	106
Batch 3	56%/44%			33000	3.6	28000	110

5.2.3 Obtaining the base Polymer PVA-co-PVP: Saponification of the starting material PVAc-co-PVP

In this thesis, polymers were synthesized in a three-step reaction starting from PVP-co-PVAc. The first step includes a saponification reaction of the acetate functions on the backbone of the polymer (Scheme 4). Consecutively, modifications were synthesized utilizing a PVP-co-PVA copolymer and a variety of carboxylic acids or amines. PVP-co-PVAc was saponified overnight using a basic 1 M sodium hydroxide solution at 80 °C. After precipitation from acetone and dialysis against water, lyophilization led to the product as a pale-yellow solid. Multiple batches were synthesized over the course of this thesis and were used interchangeably, as complete saponification was successful in all cases.

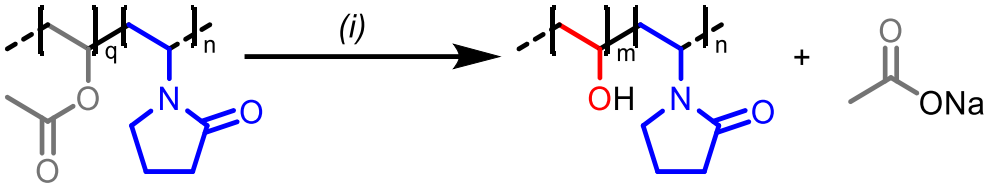

Scheme 4: Saponification reaction of PVAc-co-PVP; (i) PVAc-co-PVP (1 eq based on moles acetate in reactant, see Section 8.2.1.2), 1 M NaOH (1.75 eq), water, 80 °C, 24 h.

The methyl group of acetate (c^3) in the starting material shows resonance between 1.81 and 2.01 ppm as a singlet in the ^{1}H-NMR spectrum, whereas the signal of the methylene proton b^4 of VP overlaps strongly (Figure 17). To confirm the success of the reaction, HSQC-NMR spectroscopy was conducted and the absence of the acetate resonance signals around 1.81/17.57 ppm (Figure 21) in the product spectrum (Figure 22) serves as sufficient confirmation, that full saponification took place. This yields a product whose resonance signals for b^5 and b^4 have a very similar integral (Figure 20) which further confirms successful reaction. This product serves as the base for every modification reaction described in this chapter. Additional saponification-reaction batches were synthesized in the same way. PVA-co-PVP served as the base polymer for all modification reactions discussed in this chapter. A summary of the analytical data is given in Table 9.

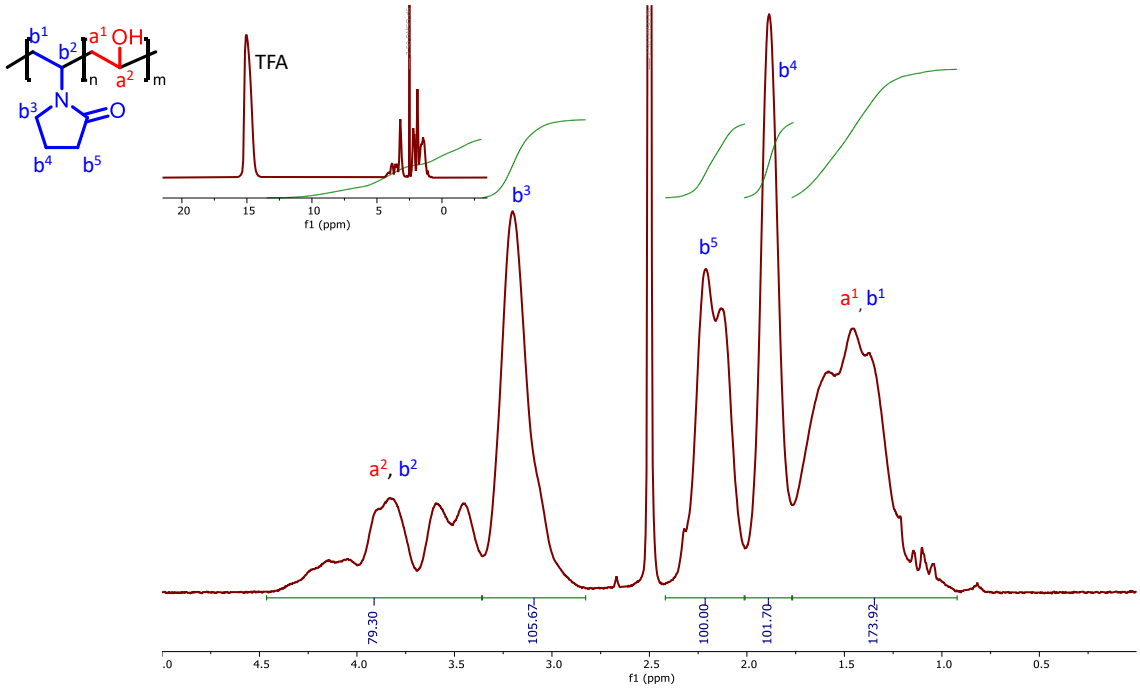

Figure 20: Quantitative ^{1}H-NMR spectrum of PVA-co-PVP normalized to methylene moiety b^5. Considering the signal for the b^4 methylene protons, the absence of an underlying signal between 2.0 ppm and 1.75 ppm suggests complete saponification. Addition of TFA to shift the signal corresponding to exchangeable hydroxyl protons to higher chemical shifts (signal around 15 ppm).

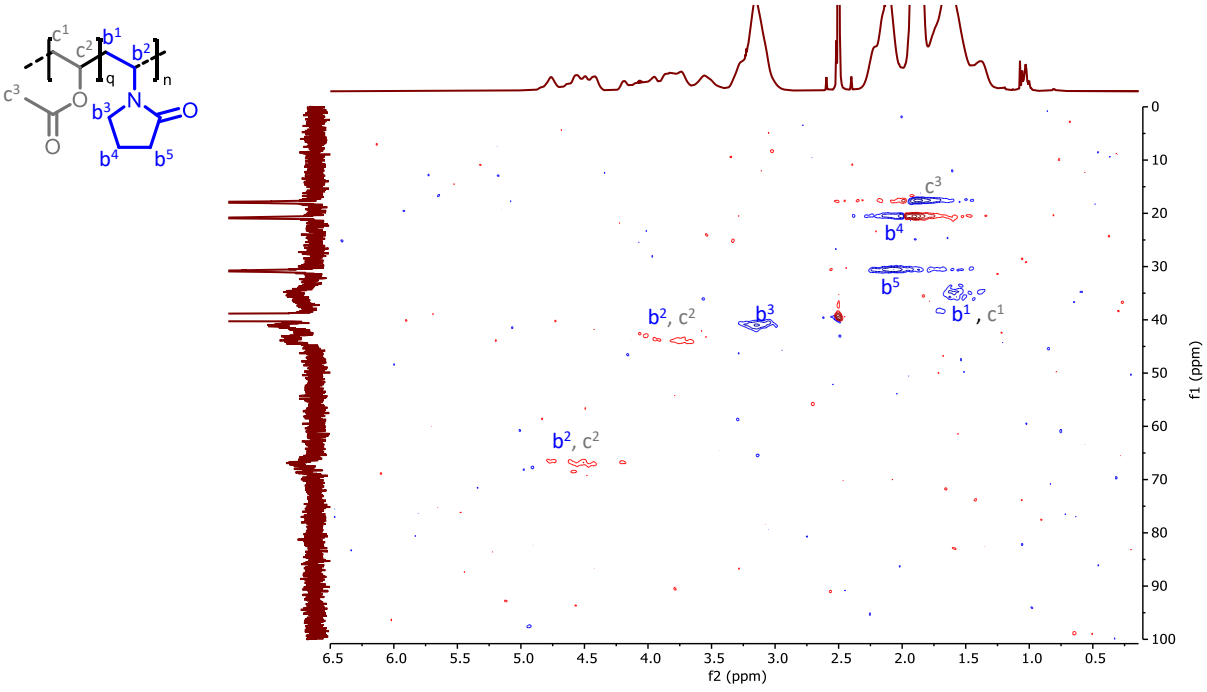

Figure 21: HSQC-NMR spectrum of PVAc-co-PVP (Kollidon® VA64). VAc acetate proton signal c^3 clearly visible underlying the VP methylene proton signal b^4.

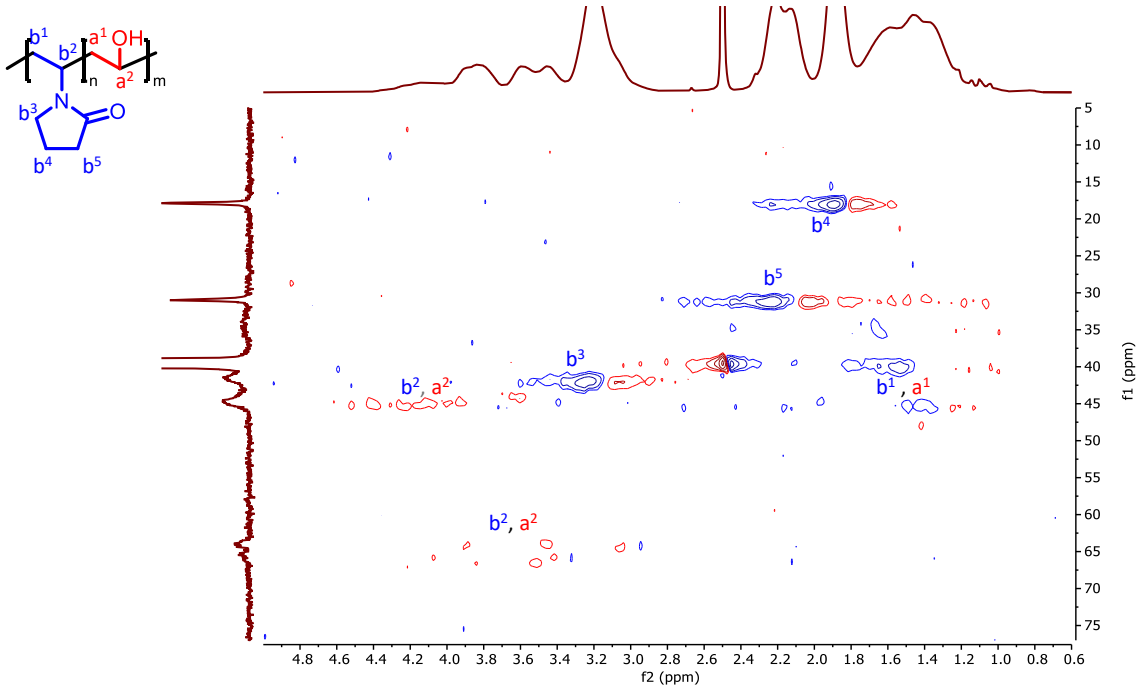

Figure 22: HSQC-NMR spectrum of PVA-co-PVP. No VAc acetate proton signal c^3 visible underlying the VP methylene proton signal b^4 indicating complete saponification.

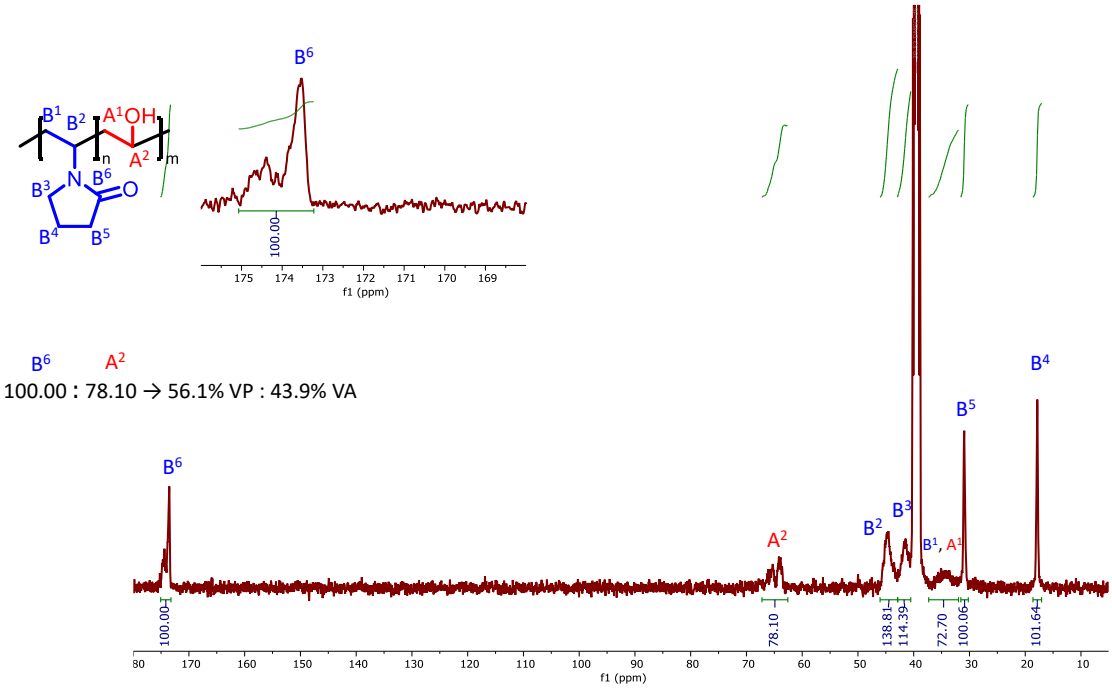

Figure 23: Quantitative ^{13}C-NMR spectrum of PVA-co-PVP at a concentration of 200 mg mL^{-1}. 512 scans with addition of $Cr(acac)_3$ as relaxation agent to reduce T_2 relaxation and increase resolution at a relaxation delay of 15 s. Calculations based on carbonyl groups in VP (B^6) and methyne groups VAc (A^2). Absence of VAc carbonyl group around 170 ppm indicates complete saponification.

DSC analysis of PVA-co-PVP showed a T_g at 139 °C and amorphousness as no melting temperature range can be observed (Figure 24a). The saponification of PVAc-co-PVP to obtain the PVA derivative

leads to an increase of the T_g from 106 °C to 139 °C. This is likely due to the intramolecular hydrogen bonding of the hydroxyl moieties in the PVA product. One objective of the modifications was to decrease this T_g again to facilitate processing in lower temperature ranges.

The thermal stability of the polymer did not change significantly after the saponification. A degradation temperature T_{deg} = 228 °C is obtained in thermogravimetric analysis in a three-step degradation (Figure 24b). This leads to a broad temperature difference between the glass transition and degradation temperatures of ΔT = 92 °C.

PVA-co-PVP was analyzed regarding its molecular mass distribution using RI detection and PMMA standards. The elugram shows a monomodal distribution without additional peaks in the low molecular weight region. The molecular weight of the exemplary batch is M_w = 29000 g mol^{-1} with a dispersity index of $Đ$ = 3.5 (Figure 24c). In addition to RI detection, MALS detection was utilized to determine the molecular weight of PVA-co-PVP. A molecular mass of M_w = 30000 g mol^{-1} and a dispersity index of $Đ$ = 1.9 was obtained (Appendix, Figure 6). Batch calculation for modifications (Section 8.2.1.4) was conducted based on this molecular weight, indifferent of which saponification batch was used for the process.

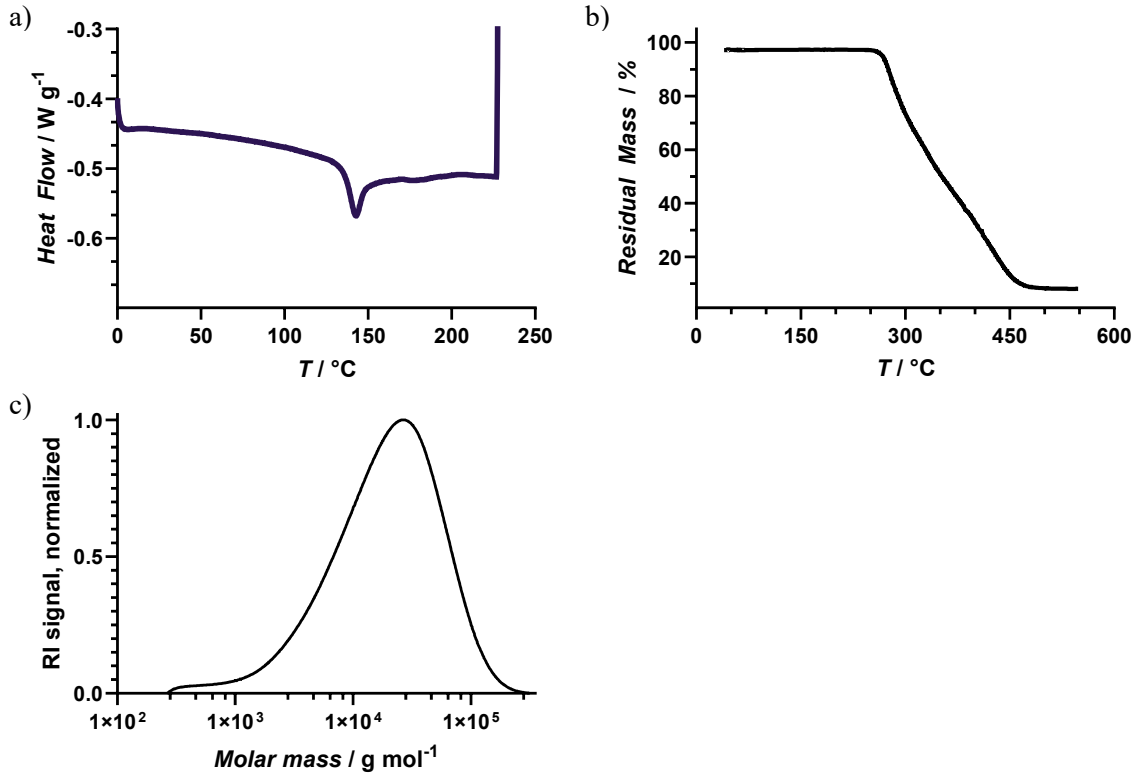

Figure 24: Characterization of PVA-co-PVP: a) Exemplary DSC thermogram of PVP-co-PVA. Glass transition temperature at T_g = 139 °C; b) TGA thermogram of PVP-co-PVA. Degradation temperature at T_{deg} = 228 °C; c) GPC-Elugram of PVP-co-PVA with normalized RI signal. Measurement calibrated against PMMA standards in DMAc with 0.6 g L^{-1} LiBr; M_w = 29000 g mol^{-1} and dispersity index $Đ$ = 3.5.

Table 9: Summary table for starting material and base polymers used for the synthesis of modified PVA derivatives.

	Batch	M-I	M-II	DSC		TGA	GPC	
				T_g / °C	T_m / °C	T_{deg} / °C	M_w / g mol^{-1}	$Đ$
PVAc-co-PVP	1	VP	VAc	106	n.d.	236	33000	3.8
PVAc-co-PVP	2	VP	VAc	110	n.d.	236	33000	3.9
PVAc-co-PVP	3	VP	VAc	106	n.d.	236	33000	3.6
PVA-co-PVP	1	VP	VA	136	n.d.	228	29000	3.5
PVA-co-PVP	2	VP	VA	137	n.d.	221	29000	3.5

5.2.4 Benchmarks

The comparison of novel synthesized polymers with marketed products in the research field as benchmarks is of great importance. In a given API system, the various polymers offer diverse advantages in terms of processability and dissolution capabilities. The aspect of dissolution is strongly dependent on the chemical nature of the polymer and the API used. The polymers predominantly used in solid formulation are polyvinyl lactams, polyvinyl alcohols, poly methacrylates and cellulose based polymers. The base polymer consists of vinyl pyrrolidone and vinyl alcohol moieties, chemical structures present in prominent excipients in the field. Candidates of each group of excipients and especially the marketed products Parteck® MXP (PVA-co-PVAc) and Kollidon VA64 (PVAc-co-PVP), which carry the chemical moieties of the base polymer, were tested in conjunction with the model API KTZ. Each polymer utilized has its own benefit with regards to processability and dissolution capabilities. In formulation development of a new chemical entity, many different polymer systems, and combinations of the same are tested to discover the composition with the highest overall performance. One tool to predict the dissolution performance of a polymer was developed by *Auch et al.*[131], a melt-based screening assay. In this assay, the API and the polymer are mixed and melted into discs, simulating their manufacturing by HME, and preferably leading to an amorphous state of both the API and the polymer. The dissolution capabilities of these specimen are then tested in a medium simulating the physiological environment of interest.

Utilizing VCM, a disc consisting of polymer and API at a drug load of 40% is prepared and tested in fasted state simulated intestinal fluid (FaSSIF) in a time frame of 120 minutes. Samples are taken at various timepoints, and the API concentration is analyzed by HPLC. The selection of tested polymers provide insight into the research space created by the variety of chemical structures and properties. Broadly, the polymers can be classified according to their chemical structures as described in the introduction of this thesis (Table 1). Along with the different monomers present in the polymers, the products also show varying properties such as their molecular weight, solubility, which are relevant for their dissolution behavior. The thermophysical properties are most important for the processing by e.g. spray drying or HME. Kollidon® VA64 (PVAc-co-PVP), PVP K30 (PVP) and Soluplus® (vinyl acetate-co-vinyl caprolactam-graft-poly ethylene glycol) are polymers including vinyl lactams as monomers. The products Eudragit® E PO (Butyl methacrylate-co-dimethylaminoethyl methacrylate-co-methyl methacrylate) and Eudragit® L-100-55 (methacrylic acid-co-ethyl acrylate) can be attributed to the (meth-) acrylates. HPMC-AS HF (hydroxypropyl methylcellulose substituted with 12 % Acetyl, 7 % Succinoyl, dissolving at pH ≥ 6.5), HPMC HP 50 (hydroxypropyl methylcellulose substituted with 6-10 % hydroxy propoxy, 20-24 % methoxy, 21-27% phthalyl, dissolving at pH ≥ 5.0) and CAP (Cellulose acetate phthalate, 22-26% acetyl, 30-36% phthalyl) are cellulosic excipients. Parteck® MXP

(PVA-co-PVAc) as well as Kollicoat® IR (PVA-graft-PEG) include vinyl alcohol as one of their comonomers. In testing this diverse group of polymers, the behavior of the API can be probed.

Pure KTZ is virtually insoluble in the FaSSIF medium, and the polymers CAP and HPMC HP-50 did not improve the solubility (Figure 25). The polymers Eudragit® E PO, Soluplus®, Eudragit® L 100-55 and HPMC-AS HF only slightly increase the solubility of KTZ with a highest *AUC* of 4400 observed for Soluplus®. A slightly higher increase in solubility is achieved by formulating KTZ with Parteck® MXP and the base polymer PVP-co-PVAc with *AUC* around 6600 to 8300. A further increase is observed when PVP K30 or Kollicoat® IR is used with *AUC* values around 17000 to 17600. The highest solubility enhancement in this system has been observed when Kollidon® VA64 is used with an *AUC* of 40000. In the tested system, Kollidon® VA64 has outstanding super saturation capabilities compared to other benchmarks tested. This shows that the tested polymers of varying structure, molecular weight and solubility behave very differently when combined with KTZ. There may be several reasons for the high solubility enhancement of Kollidon® VA64 including its molecular weight distribution, its good solubility in the testing medium or favorable polymer API interactions.

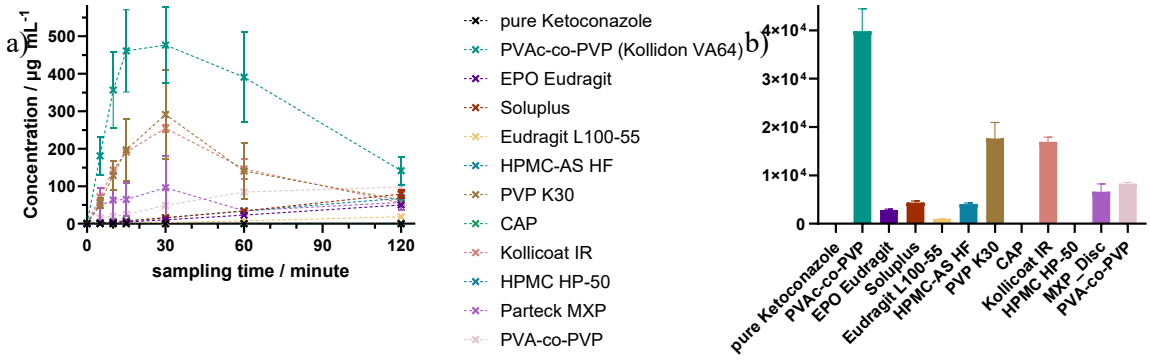

Figure 25: Dissolution capabilities of selected benchmarks in comparison to pure, crystalline API. Amorphous sample discs were prepared by VCM. Non-sink dissolution of amorphized samples through melt-quenching in FaSSIF at pH 6.5 at 37 °C. Concentration of 0.75 mg drug per mL medium, +/- SD (n = 3), drug: Ketoconazole at 40% drug load; HPLC analysis at λ = 225 mm. Discs were prepared by MeltPrep method and used as is. Dashed lines incorporated to guide the reader's eye; b) Corresponding *AUC* of the dissolution measurements for comparison of dissolution capability.

To further investigate the performance of Kollidon® VA64 (PVAc-co-PVP), the molecular weight distribution of the polymer was considered. As mentioned in earlier chapters (Figure 19), the polymer shows a dispersity index of $Đ = 3.7$, which indicates a broad distribution, but is to be expected for a product synthesized by free radical polymerization. The mean molecular weight observed is $M_w = 31000$ g mol^{-1} with a maximum at $M_p = 21000$ g mol^{-1}. The broad distribution also includes a significant number of small oligomers which may have a favorable influence on the dissolution capabilities. In general, polymer chains of the same polymer species with lower molecular weight are dissolved quicker than larger species.

In order to further understand the specific dissolution properties of different molecular weight fractions, commercially available PVAc-co-PVP was subject to a multistep dialysis utilizing dialysis tubes of different pore sizes. Utilizing three tubes, with pore sizes of 12 kDa to14 kDa, 25 kDa and 50 kDa respectively, three fractions were isolated during the dialysis against water. The fractions were analyzed independently in terms of their molecular weight, dissolution performance and melt rheological properties. The dialysis process was tested first on a small scale with 10 g material and then transferred to a cooperating laboratory. 300 g material were dialyzed by Oliver Stranowsky (*Merck Electronics KGaA*), as larger amounts of material were needed and asked for by another cooperating laboratory at *Merck Life Science KGaA* where extrusion experiments on an intermediate scale are planned.
Starting with the molecular weight distribution of the commercial product, the first step of the dialysis using the 12 kDa to 14 kDa tubes removes the weight fraction of very low molecular weight. This is followed by the dialysis of the retentate using the 25 kDa tubes. The resulting permeate (**F1**) is lyophilized and the retentate is further dialyzed against 14 kDa tubes to receive the permeate fractions **F2-1** and **F2-2** and the retentate fraction **F3**. The aqueous fractions were lyophilized and analyzed.

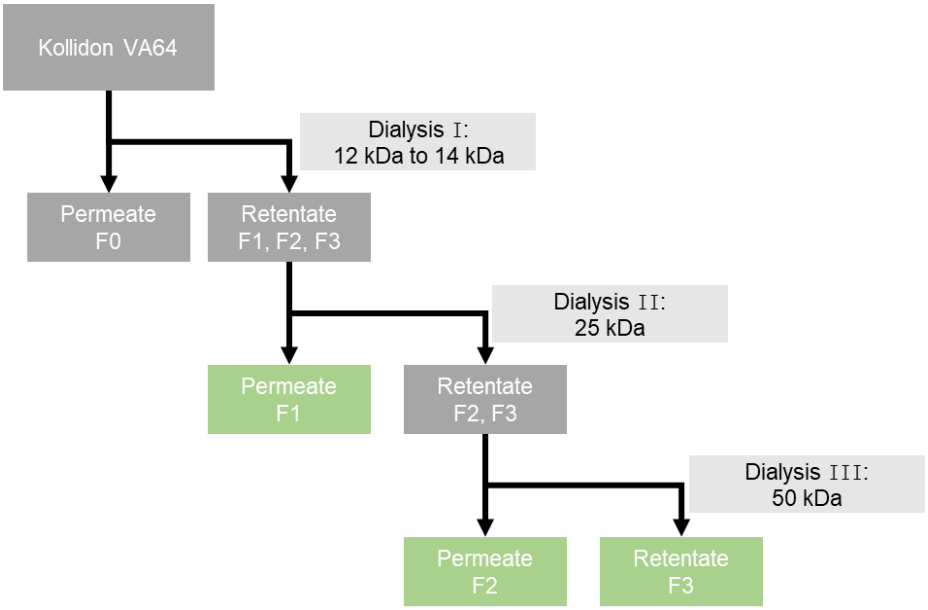

Figure 26: Schematic overview of sequential dialysis conducted utilizing commercially obtained Kollidon® VA64 (PVAc-co-PVP). The solvent used for each of the three dialysis steps is water. Dialysis fluid was exchanged at least thrice collecting the generated permeate. The fraction F1, F2 and F3 (green boxes) were isolated by lyophilization of the aqueous solutions. The fractions were analyzed by GPC, melt rheology and used in a dissolution assay.

The molecular weight distributions differ significantly from crude PVAc-co-PVP and are more narrow compared to crude PVAc-co-PVP as confirmed by GPC (Figure 27). The fraction **F1** is mainly comprised of low molecular weight species with a maximum at $M_p = 4000$ g mol^{-1} (Table 10). The fractions **F2-1** and **F2-2** with their maximum at 20000 g mol^{-1} and 7000 g mol^{-1} respectively include large amounts of intermediate size species and species of high molecular weight. These high molecular

weight species are mainly found in **F3**, where low molecular weight fractions were removed by dialysis and mainly high molecular weight fractions were observed. The bimodal curve progression for the fractions **F2-1** and **F2-2** may result from minor spillages of retentate during the dialysis processes. In addition to this, dialysis is no quantitative separation technique like for example preparative GPC and large molecules can still penetrate the dialysis membranes even though the molecular weight cutoff of the tubes should prevent this. In summary, the differences in the molecular weight distributions of the four fractions is significant and the fractions were each subject to rheological measurements.

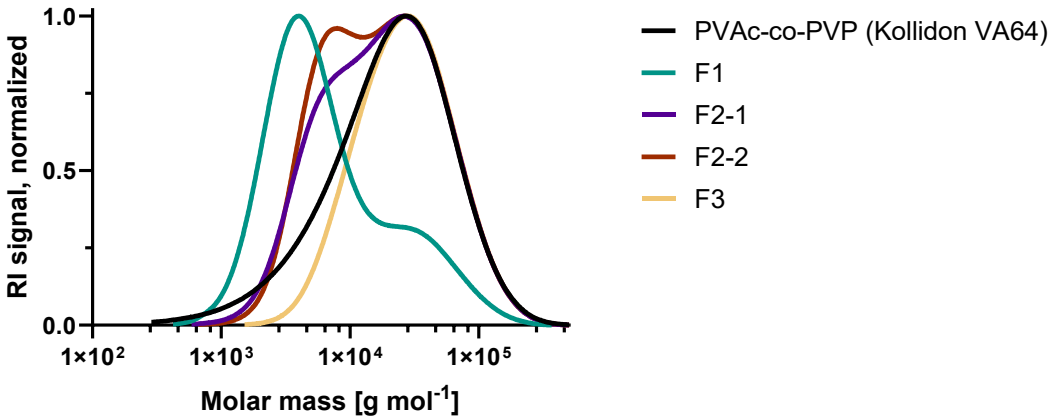

Figure 27: Fractionation of PVP-co-PVAc after sequential dialysis.

The melt rheological measurements were conducted by Alessandro-Giuseppe Elia (*Merck Life Science KGaA*). The temperature at which the polymer melt reaches a melt viscosity of η = 1000 Pa s and the temperature at which η = 10000 Pa s is reached are of great importance for the processability. The isolated fractions may be extruded separately, as their melt viscosity reaches the extrudable range (Figure 28). In addition to that, *G''* is higher than *G'* in the measured temperature range indicating amorphousness of the samples. This is to be expected, as the same is true for PVAc-co-PVP. The measured phase angle and its progression is also similar for the fraction when compared to PVAc-co-PVP.

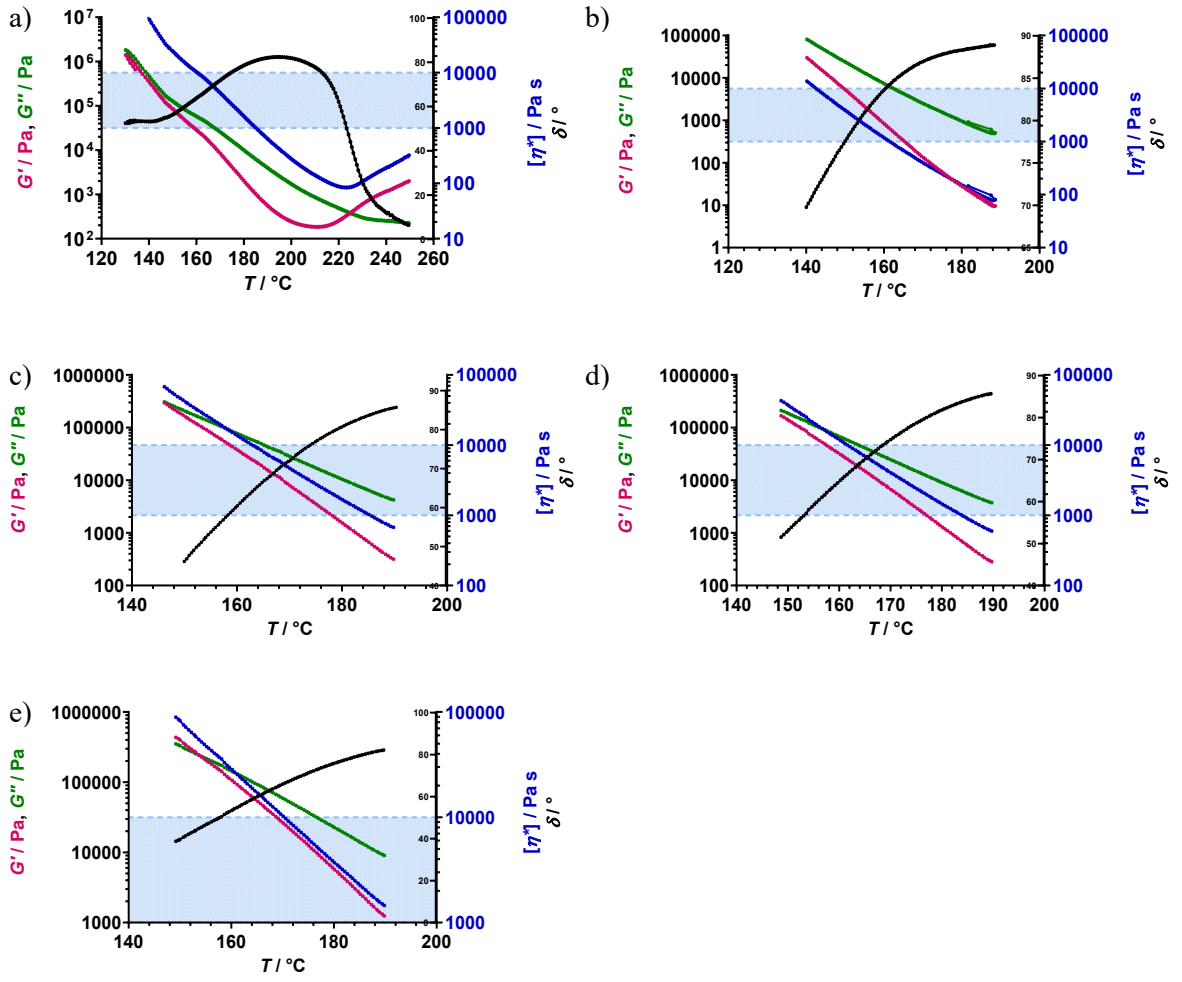

Figure 28: Melt rheology measurements for the separate fractions of PVP-co-PVAc. a) PVP-co-PVAc b) **F1**; c) **F2-1**; d) **F2-2**; e) **F3**. Data obtained from analysis can be found in Table 10.

The extrudable range of PVAc-co-PVP is between $T_{10000\ Pa\ s}$ = 161 °C and $T_{10000\ Pa\ s}$ = 186 °C (Table 10) In comparison to crude PVAc-co-PVP, **F1** reaches a melt viscosity of η = 10000 Pa s at lower temperatures of $T_{10000\ Pa\ s}$ = 142 °C and η = 1000 Pa s is reached at $T_{1000\ Pa\ s}$ = 161 °C. Considering the fraction **F2-1** and **F2-2**, the extrudable range is similar to that of PVAc-co-PVP. And the higher molecular weight fraction **F3** is extrudable at higher temperature of 170 °C to 189 °C. These results indicate that lower molecular weight fractions are extrudable at lower temperatures when compared to the same polymer with higher molecular weight. Additionally, it can be argued, that the inclusion of lower molecular weight fractions leads to favorable properties concerning the melt rheological properties of the final product and low molecular weight molecules in a polymer distribution act as an internal plasticizer, enabling processing at lower temperatures.

Table 10: Summary of fractions obtained by sequential dialysis of PVP-co-PVAc.

Sample	M_w / g mol^{-1}	M_p / g mol^{-1}	$Đ$	$T_{\eta = 1000\ Pa\ s}$ / °C	$T_{\eta = 10000\ Pa\ s}$ / °C
PVP-co-PVAc	33000	26000	3.9	186	161
F1	15000	4000	3.5	161	142
F2-1	30000	23000	2.7	185	162
F2-2	29000	7000	2.8	184	162
F3	38000	26000	2.0	>189	170

Each fraction was tested in the KTZ assay to investigate their super saturation potential. The assay was executed by Nabil Lamrabet (*Merck Life Science KGaA*). The curve progression of the respective fraction differs from that of PVAc-co-PVP. The fractions **F1**, **F2-1** and **F2-2** have a slower onset while the onset of **F3** is faster when compared to PVAc-co-PVP. In the case of PVAc-co-PVP and **F2-1**, the maximum concentration is reached after 30 min, compared to a concentration maximum after 60 min for the samples **F2-2** and **F1**. Considering **F3**, the peak concentration is reached after 10 min. These results indicate, that in the tested system, the different molecular weight fractions can modulate the release API release kinetics. The maximum concentration of 200 µg mL^{-1}was observed for **F3** compared to 164 µg mL^{-1} for PVAc-co-PVP. The maximum concentration for the other fractions **F1**, **F2-1**, and **F2-2** are lower with 90 µg mL^{-1}, 90 µg mL^{-1} and 120 µg mL^{-1} respectively. Apart from **F3**, the maximum concentrations reached are significantly lower than for PVAc-co-PVP. The high molecular weight fraction, the retentate after the sequential dialysis, shows the quickest onset and highest API concentration and thus the largest spring effect. Also, the retentate has the quickest decline in API concentration after reaching the maximum, indicating a poor parachute effect to keep the API in solution. In contrast, the original PVP-co-PVAc fraction shows a API-concentration maximum which is nearly as high as in the retentate fraction, but shows a slower decline in API concentration, thereby possessing a pronounced parachute effect. These results indicate that high molecular weight fractions are favorable for high maximum concentrations of API and low molecular weight fractions are necessary to keep the API in solution or otherwise premature precipitation occurs. The combination of large molecular weight species, increasing the spring effect and lower molecular weight fractions prolonging the solvation of the API (parachute effect) seems to have favorable effects on the overall performance.

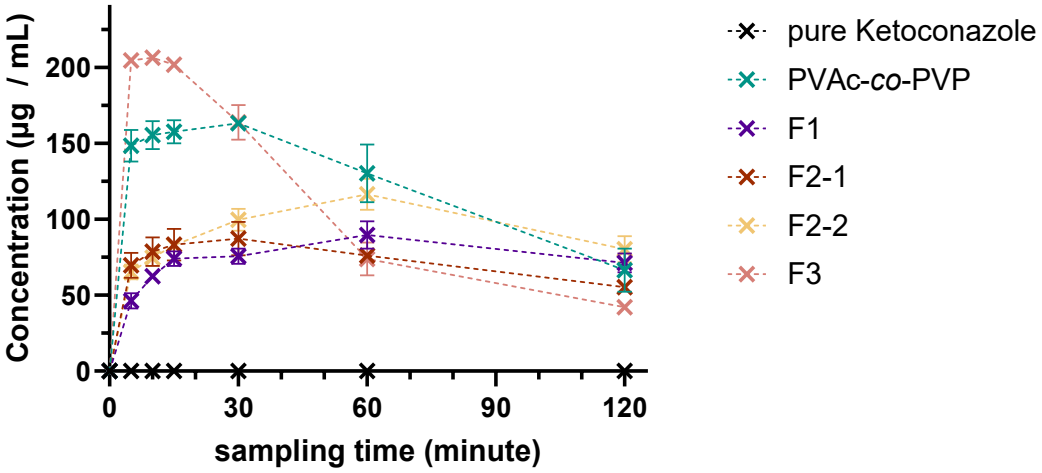

Figure 29: Dissolution capabilities of PVAc-co-PVP in comparison with fractions obtained from sequential dialysis and pure, crystalline API. Non-sink dissolution of amorphized samples through melt-quenching in FaSSIF at pH 6.5 at 37 °C, 6 mg of drug in 8 mL medium, +/- SD (n = 3), drug: Ketoconazole at 40% drug load; HPLC analysis at λ = 225 mm. Discs were milled before assay. Dashed lines incorporated to guide the reader's eye.

In summary, low molecular weight fractions have a favorable effect on the processing temperatures as indicated by the melt rheology measurements. Higher molecular weight fractions need higher temperatures to be extruded. These fractions (**F3**) in PVP-co-PVAc occur be responsible for the quick onset and thus the prominent spring effect in PVP-co-PVAc. The lower molecular weight fractions **F1** **F2-**1 and **F2-2** seem to be responsible for the control over the following decline in API concentration after reaching a maximum concentration and thereby have a favorable influence on the parachute effect, prolonging the solvation of the API.

5.2.5 Modification of PVP-co-PVA: Introducing chemical motifs and their influence on the polymer properties

By modification of the base polymer PVP-co-PVA its properties in terms of processability can be influenced. Additionally, polymer API interaction may be influenced favorably by monomers present in the polymer. One objective was to reduce the glass transition temperature, and therefore the processing temperature in thermal processes like HME. Different groups of modification agents were employed and evaluated based on their influence on the thermophysical parameters. Another objective of this study was the influence of polar and hydrophobic comonomers on the interaction with a model API in a dissolution assay.

The second step of the two-step modification process is an esterification using activated intermediates like amides, carbamates, and ureas. These intermediates were synthesized right before the addition to the saponified polymer (Scheme 5). The respective carboxylic acid, alcohol or amine was added in

portions to a suspension of *N,N'*-carbonyl diimidazole in anhydrous DMF. The activated intermediate was formed nearly quantitatively in 1 h at room temperature. DMF was removed under vacuo from the crude solution containing the imidazole activated intermediate and analyzed by ^{1}H-NMR and HSQC-NMR spectroscopy. High conversion was achieved in this case (91%, Figure 30) and the product solution was therefore used in all modification reactions without further purification. After the reaction, the imidazole proton signals show a small increase in their chemical shift and can be compared to the product signals as assigned in the spectrum.

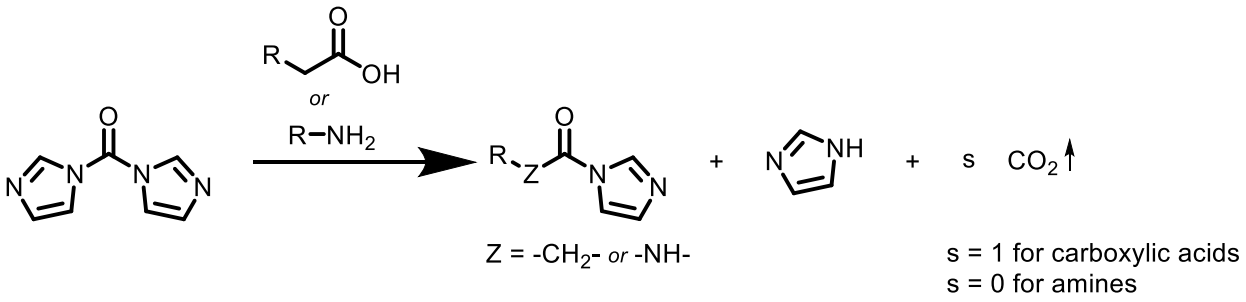

Scheme 5: General reaction scheme for the synthesis of the activated intermediate. The reaction product can be classified as an amide when using carboxylic acids, carbamate when using alcohols and urea when using amines. R corresponds to the respective agent used.

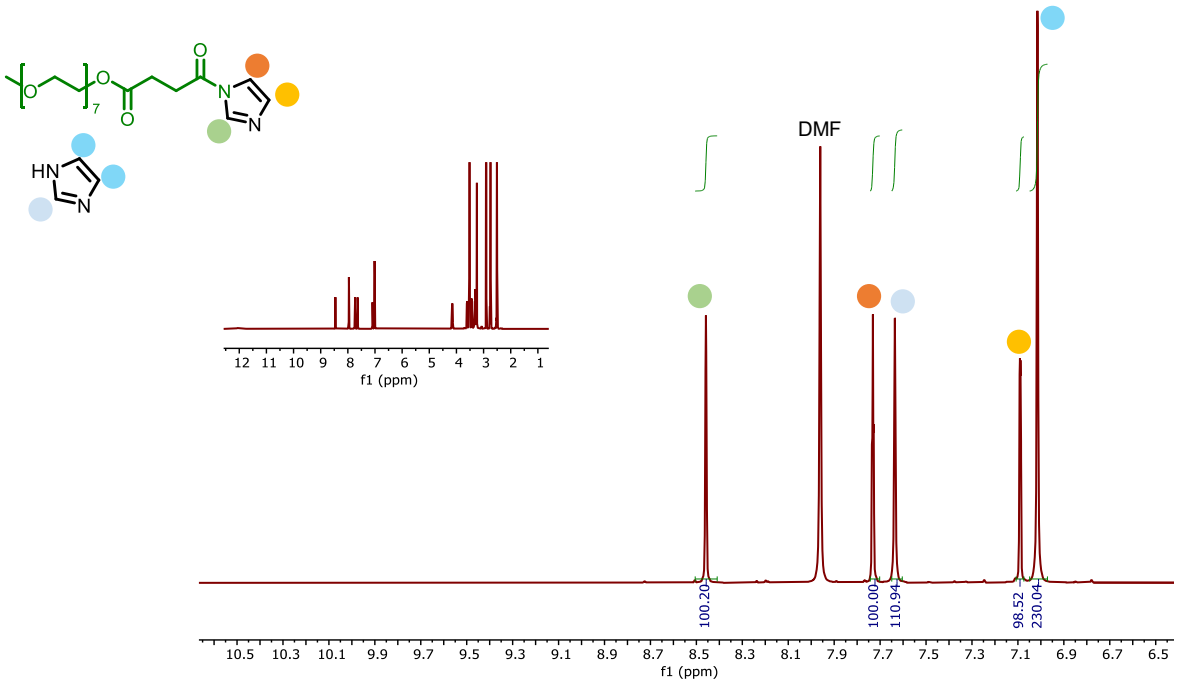

Figure 30: Exemplary ^{1}H-NMR evaluation of the crude solution containing precursor compound corresponding to mPEG-III. 91% Conversion.

The modification reaction itself was conducted utilizing a *Radley's Tornado Overhead Stirring System* reaction station, where six batches can be prepared simultaneously. The objective was to synthesize modified PVA derivatives where a fraction of the vinyl alcohol (VA) moieties present in the polymer are reacted to form a terpolymer (Scheme 6). Multiple polymers were synthesized simultaneously with increasing VA modification degree. The reaction was conducted in DMF at 80 °C and the previously synthesized precursor was added in the respective quantity to achieve the desired modification degree of VA. The emerging comonomer (ester, carbamate, or carbonate) in these modified polymers bears chemically different end-groups and influences the polymer's thermophysical and mechanical properties. The polymer was isolated after removing the solvent DMF, followed by a dialysis against water and the final removal of water by lyophilization. A variety of modification agents were utilized, and four groups can be derived: mPEG derivatives, alkyl amines, hydrophobic acids, miscellaneous acids (Table 11).

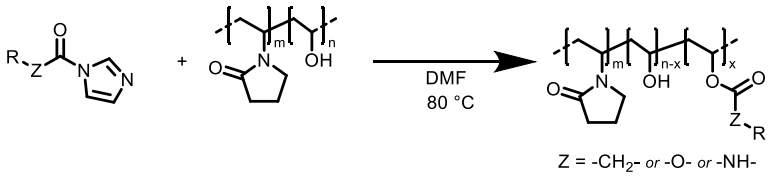

Scheme 6: General reaction scheme for the synthesis of PVA derivatives using CDI-activated intermediates. Reaction conditions and synthesis protocol adapted from literature.[145, 146, 159]

Table 11: Overview of modification agents used for PVA-co-PVP post polymerization modification.

mPEG derivatives Glass transition and processing temperature	**Substituted amines** Polar interaction with model API	**Hydrophobic acids** Hydrophobic polymer API interaction	**Miscellaneous acids**
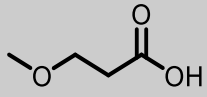 3-methoxypropanoic acid **mPEG-I**	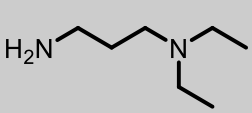 N^1,N^1-diethylpropane-1,3-diamine **amine-I**	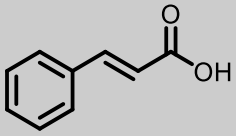 cinnamic acid **apolar-I**	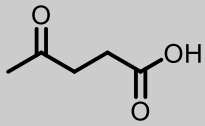 4-oxopentanoic acid **misc-I**
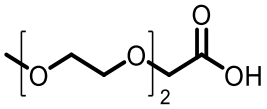 2-(2-(2-methoxyethoxy)ethoxy)acetic acid **mPEG-II**	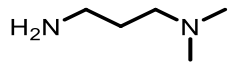 N^1,N^1-dimethylpropane-1,3-diamine **amine-II**	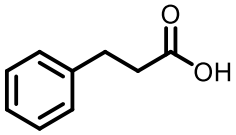 3-phenylpropanoic acid **apolar-II**	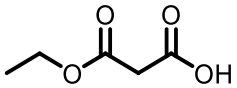 3-ethoxy-3-oxopropanoic acid **misc-II**
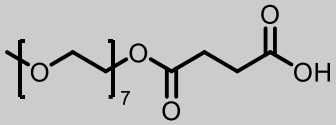 mPEG350 succinate **mPEG-III**	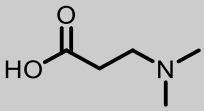 3-(dimethylamino)propanoic acid **amine-III**	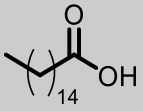 palmitic acid **apolar-III**	
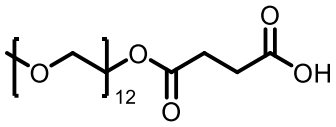 mPEG550 succinate **mPEG-IV**		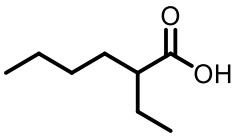 ethyl hexanoic acid **apolar-IV**	

A glass transition temperature between 80 °C and 90 °C is favorable for the processing of thermally labile APIs. The melt viscosity needs to be in an acceptable range at lower temperatures between 120 °C and 180 °C. Furthermore, thermal stability during processing is necessary. Another challenge in formulation development is the solubility enhancement of poorly soluble APIs. One approach is to stabilize the metastable amorphous form of the API thereby increasing the solubility of the API drastically. Using a polymer which is amorphous itself has the advantage, that in a best case, no seed crystals are present at any stage during the formulation. APIs in development include a variety of chemical moieties in their structure, such as polar and hydrophobic groups. A polymer interacting with

the API may result in the stabilization of the amorphous state and subsequently increase the solubility of the API. These interactions are based on the functional groups present in an API. The majority of APIs in development are considered to be part of BCS class II or IV and are practically insoluble in water. By incorporating these APIs in amorphous polymer matrices, it is possible to achieve concentrations in the range of pharmaceutical efficacy. The polymer API interactions relevant for this thesis are polar interactions and hydrophobic interactions. In terms of polar interactions, specifically the hydrogen bonding or polar interactions between amine functions and the API. In the case of KTZ (Table 3), hydrogen bonds may be formed by the imidazole function and the amide group. Other polar groups in the molecular structure include the ether bonds and the substituted aromatic rings. KTZ is a poorly water-soluble API indicating high hydrophobicity. Therefore, hydrophobic interactions of the polymer with chemical motifs such as the aromatic groups may have a favorable influence on the API solubility.

The modification agents utilized in this thesis can be categorized based on functional groups and thus, their interaction with the API. The first group are the mPEG derivatives 3-methoxypropanoic acid (MeO propanoic acid, **mPEG-I**), 2-(2-(2-methoxyethoxy)ethoxy)acetic acid (mPEG2 aa, **mPEG-II**), mPEG350 succinate (mPEG7 succinate, **mPEG-III**), and mPEG550 succinate (mPEG12 succinate, **mPEG-IV**), carrying an increasing length of the PEG chain. mPEG additives are generally used for their plasticizing effect during manufacturing, so this modification is introduced to have a reducing effect concerning T_g and therefore the reduction in processing temperature in the extrusion. The mPEG moiety also might have a favorable influence on the API solubility due to its polarity. Alkyl amines are polar species, and therefore may have a favorable polar interaction with the polar structures in the model API. The modification agents include amines and a carboxylic acid which are compatible with the modification strategy via CDI. In N^1,N^1-diethylpropane-1,3-diamine (**amine-I**) and N^1,N^1-dimethylpropane-1,3-diamine (**amine-II**) different alkyl substitutions at the tertiary amine are tested, whereas with 3-(dimethylamino)propanoic acid (**amine-III**), a carboxylic acid is used. The hydrophobic acids utilized in this thesis range from aromatic to alkyl apolar carboxylic acids. 3-phenylpropanoic acid (**apolar-II**) and cinnamic acid (**apolar-I**) may interact with the aromatic groups present in KTZ resulting in favorable properties regarding the solubility. The alkyl substituted carboxylic acids palmitic acid (**apolar-III**) and ethyl hexanoic acid (**apolar-IV**) are used for a potential interaction with the apolar API. The miscellaneous acids 4-oxopentanoic acid (**misc-I**) and 3-ethoxy-3-oxopropanoic acid (**misc-II**) carry multiple functional groups and their influence was investigated separately. The specific influence was investigated by synthesis of various polymers with different modification degrees and chemical nature of the modification agent. A structure-property relationship was established to facilitate the optimization and tailoring of the polymer properties for the application in processing via extrusion and solubility enhancement.

5.2.5.1 mPEG derivatives

5.2.5.1.1 Synthesis

Modifications of PVP-co-PVA were synthesized with acids bearing different PEG chain lengths (Scheme 7). **mPEG-I** and **mPEG-II** are commercially available and were used as received. **mPEG-III** and **mPEG-IV** were synthesized beforehand. The detailed synthesis protocol can be found in Section 8.2. A total of 16 polymers were synthesized for this group, ranging in modification degree from 5 to 13% of available OH-groups. The analytical characterization will be given in the following section.

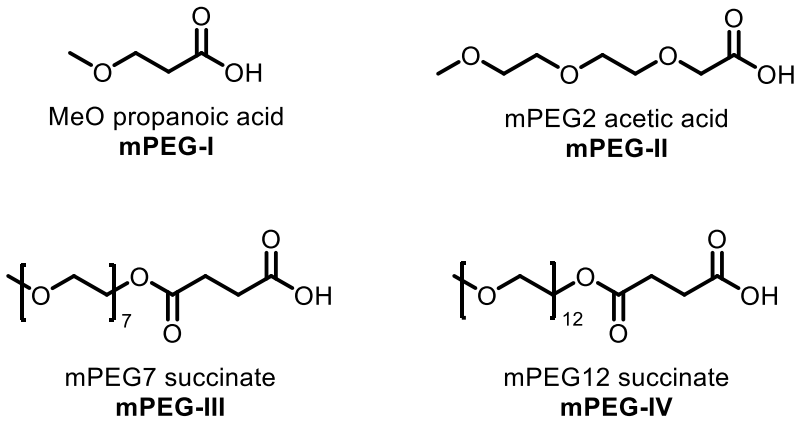

Scheme 7: mPEG derivatives used in this work for the modification of PVP-co-PVA via esterification.

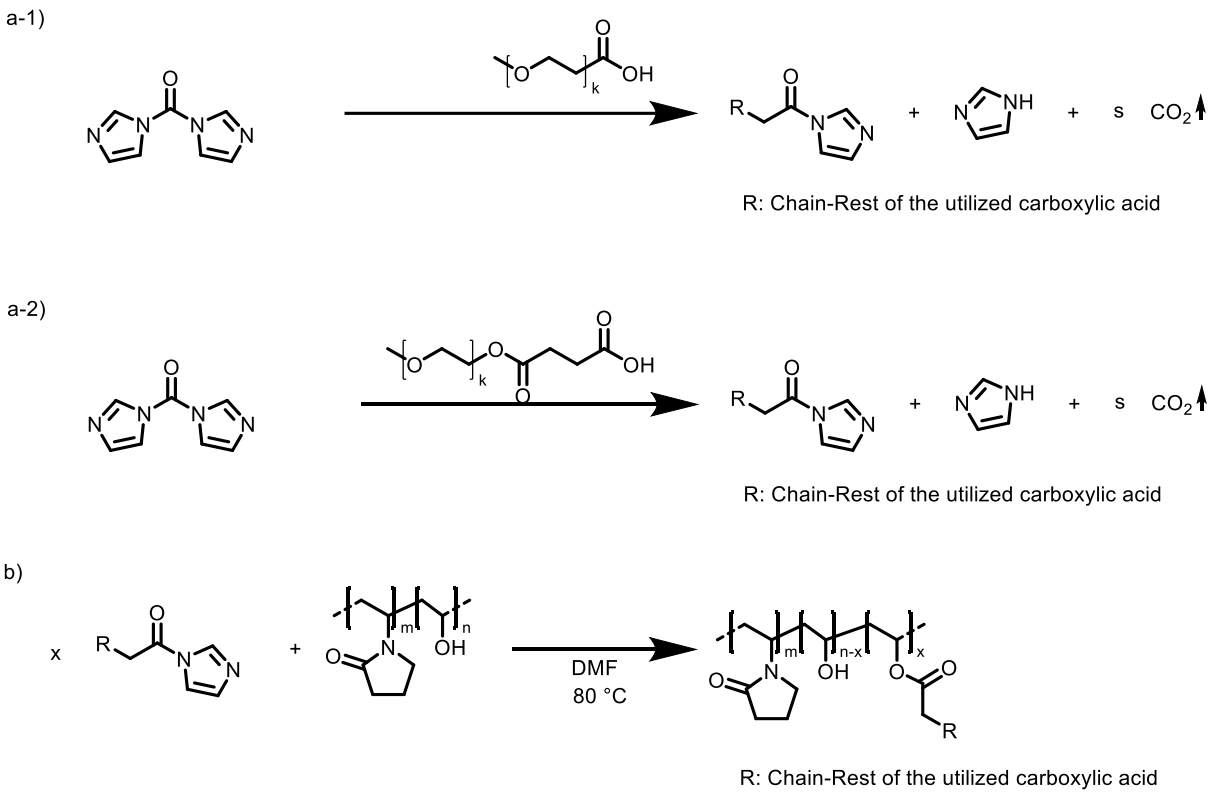

Scheme 8: General reaction scheme for the modification of PVP-co-PVA using carboxylic acids. The rest R differs according to the acid utilized in the reaction; a-1) shows the synthesis of the precursor utilizing substituted carboxylic acids to form a *N*-acyl imidazole, where carbon dioxide evolution can be noticed; a-2) shows the synthesis of the precursor utilizing mPEG substituted succinates forming a *N*-acyl imidazole, where carbon dioxide evolution can be noticed b) shows the final modification reaction leading to the modified copolymer. Multiple polymers were synthesized with varying moles of the activated intermediate to give polymers with varying x-monomer amount in the polymer dependent on the amount a of intermediate employed during the reaction.

The modification product was analyzed via quantitative ^{1}H-, ^{13}C-, HSQC, and HMBC NMR spectroscopy. The signals of the mPEG-moiety strongly overlap with other signals in ^{1}H-NMR. By comparison of the multiplet for the methylene protons b^{5} in VP and the subtraction thereof from the signal around the methylene protons b^{3}, the integral fraction belonging to the methyl protons c^{8} can be obtained and thereby the amount of modified OH-groups can be calculated (Figure 31). Signals corresponding to residual imidazole at 9.09 ppm and 7.67 ppm as well as residual DMF around 2.88 ppm are visible, but do not influence the evaluation. Comparing the results obtained by quantitative ^{1}H-NMR for each other mPEG derivative (**mPEG-I**, **-III** and **-IV**) the same calculation method can be utilized and similar spectroscopic methods were used (see Appendix, Figure 7, Appendix, Figure 9). A library of all obtained analytical results for the modified polymers is given in Table 12.

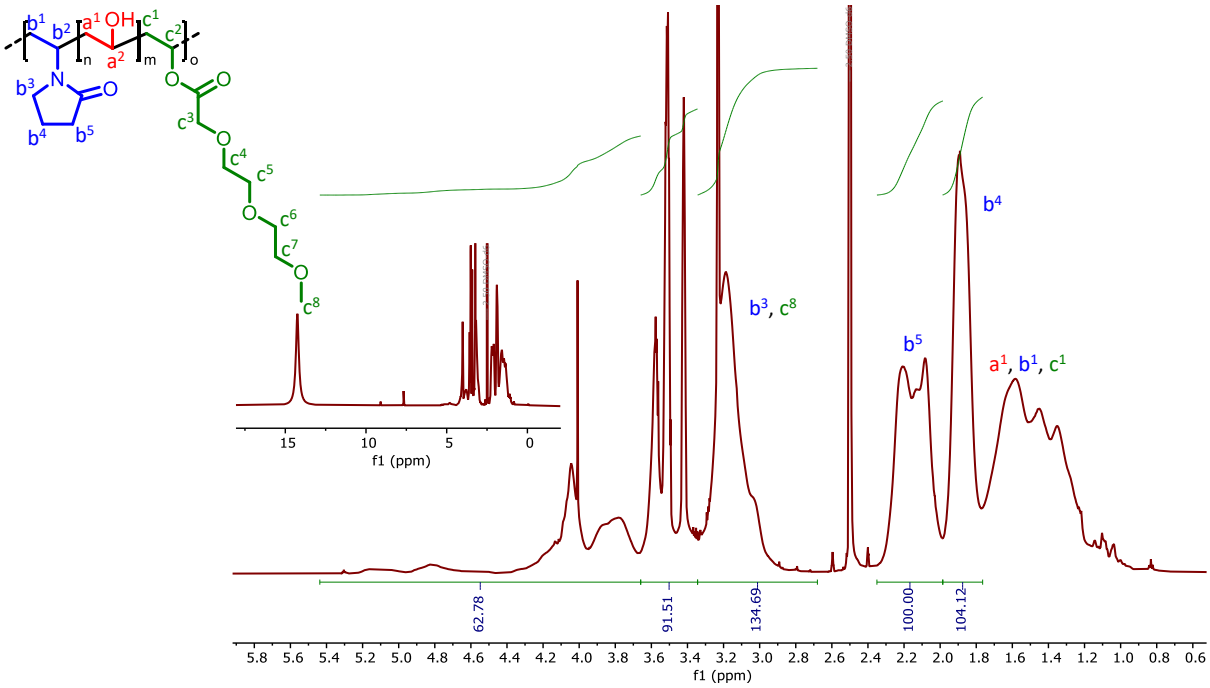

Figure 31: Exemplary quantitative ^{1}H-NMR spectrum of **mPEG-II** modified PVP-co-PVA. Modification degree 13.1%.

5.2.5.1.2 Characterization

All modifications obtained were characterized regarding their thermophysical behavior utilizing DSC. A collection of all thermograms obtained for modifications using mPEG derivatives can be found in the appendix (Appendix, Figure 11) and a summary of analytical data is given at the end of this chapter (Table 12). A melting point is absent in all DSC thermograms indicating amorphousness of the polymers. The modification using mPEG derivatives greatly reduced the glass transition temperature and the lowest T_g achieved was 54 °C (**mPEG-IIId**). These findings support the previously described proposition, that this kind of modification can be used to achieve a reduction of the processing temperatures.

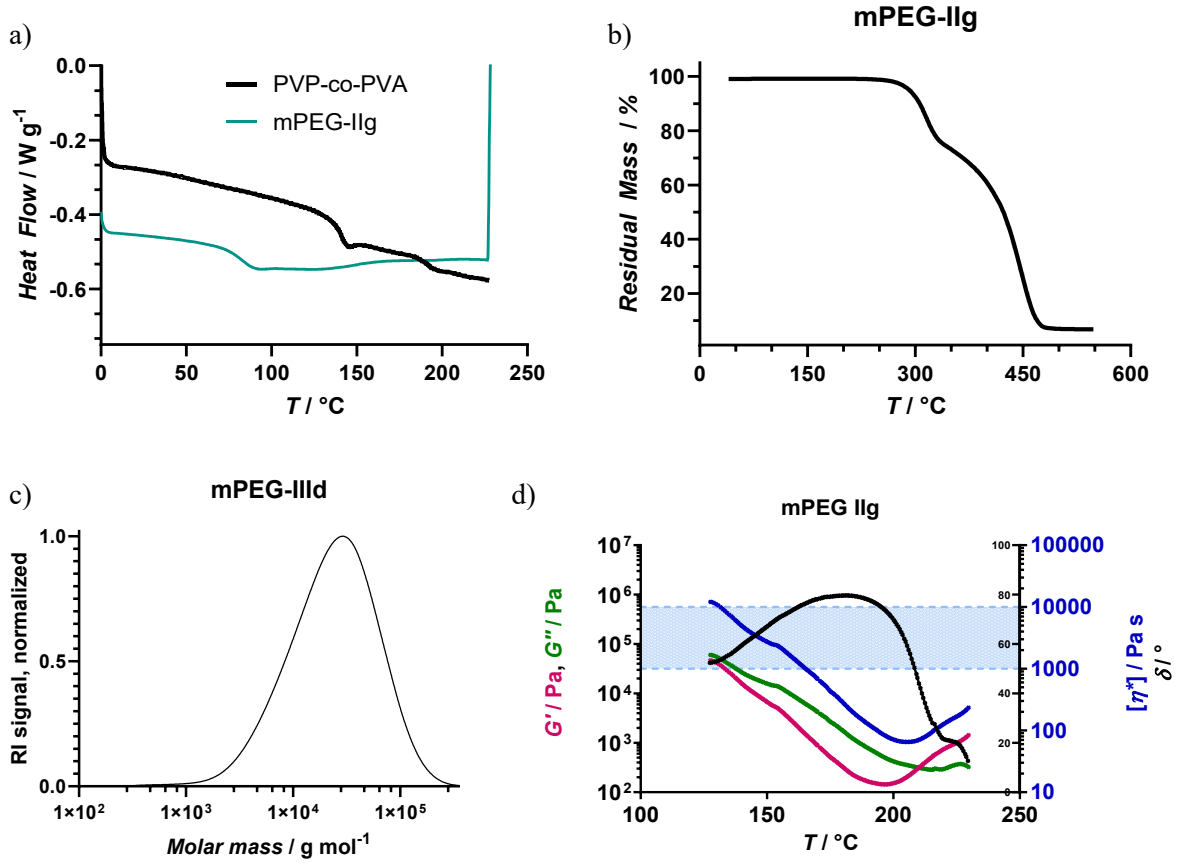

Figure 32: a) DSC of **mPEG-IIg**, T_g = 83 °C; b) TGA thermogram of **mPEG-IIg**. Degradation starts at 220 °C; c) GPC elugram for **mPEG-IId**. Mw = 35000 g mol^{-1}, $Đ$ = 2.6; d) Rheogram of **mPEG-IIg**, T(10000 Pa s) = 129 °C, T(1000 Pa s) = 160 °C.

The samples were analyzed utilizing thermogravimetric analysis. The modified polymers analyzed degrade in a two-step degradation process, whereas PVP-co-PVA degrades in a single-step degradation (Figure 19). This second degradation step may result from the degradation of the newly formed side chain, an ester bond, after the modification. It is evident, that the modification does not significantly decrease the thermal stability of the polymer. The lowest temperature obtained was T_{deg} = 189 °C (**mPEG-IIIe**). This means, that a modification of the base polymer with a mPEG derivative leads to a slight reduction of the degradation temperature. In most cases, the degradation temperature stays above 200 °C and these polymers fit the chosen specifications (Table 12).

Table 12: Compilation of thermo-physical data observed for polymers carrying mPEG moieties.

	Yield / %	Mod. Deg. / % of -OH	T_g (DSC) / °C	T_{deg} (TGA) / °C	M_w (GPC) / g mol^{-1}	M_p (GPC) / g mol^{-1}	$Đ$ (GPC)
mPEG-Ia	85	5.0	130	233	42000	30000	2.8
mPEG-Ib	80	6.0	129	236	44000	30000	2.8
mPEG-IIa	92	6,9	120	233			
mPEG-IIb	87	8,9	112	227			
mPEG-IIc	81	9,0	107	220			
mPEG-IId	75	10,8	111	210	35000	27000	2.6
mPEG-IIe	72	11,6	97	205			
mPEG-IIf	65	13,1	90	192	38000	28000	2.6
mPEG-IIg	91	13,3	83	208	38000	29000	2.5
mPEG-IIIa	62	7.7	79	208			
mPEG-IIIb	72	9.8	67	218			
mPEG-IIIc	80	9.5	74	207			
mPEG-IIId	69	10.0	54	191	40000	31000	3.1
mPEG-IIIe	54	10.6	58	189			
mPEG-IVa	62	6.3	70	209			
mPEG-IVb	68	9.6	64	196			
mPEG-IVc	79	8.9	60	190	34000	27000	5.8

For each different modification agent, at least one sample was analyzed by GPC. Due to the nature of the reaction, namely a modification of its free hydroxyl moieties, monomodal distributions are expected. Also, an increase in molecular mass (M_w) is to be expected, as the molecular mass of the monomer bearing the mPEG derivative increases. Indeed, for all measured samples the molecular masses increases and a monomodal distribution is obtained. Together with the spectroscopic results it can be concluded that the modification reaction was successful.

For one polymer, namely **mPEG-IIg**, the melt viscosity is in the optimal range for extrusion in the temperature range between $T_{10000\ Pa\ s}$ = 129 °C and $T_{1000\ Pa\ s}$ = 160 °C with a resulting processing range of ΔT = 31 °C. *G'* values are lower than the *G''* values up to 210 °C suggesting amorphousness in the temperature range usable for extrusion. The phase angle reaches its maximum at $\delta(80°)$ = 181 °C indicating degradation at temperatures above that. The maximum is reached below the degradation temperature obtained from TGA, which indicates, that mechanical stress induces degradation.

By modification of the hydroxyl moieties in PVA-co-PVP, the glass transition temperature is significantly lowered with increasing PEG chain length and increasing modification degree (Figure 33). Consequently, the glass transition temperature can be controlled while the degradation temperature

remains nearly unchanged. mPEG modification of PVP-co-PVA is of great importance for the optimization of the processing temperatures for thermal processes like HME. Due to the decrease in glass transition temperature, the processing temperature is also reduced, which enables the processing of thermally labile APIs.

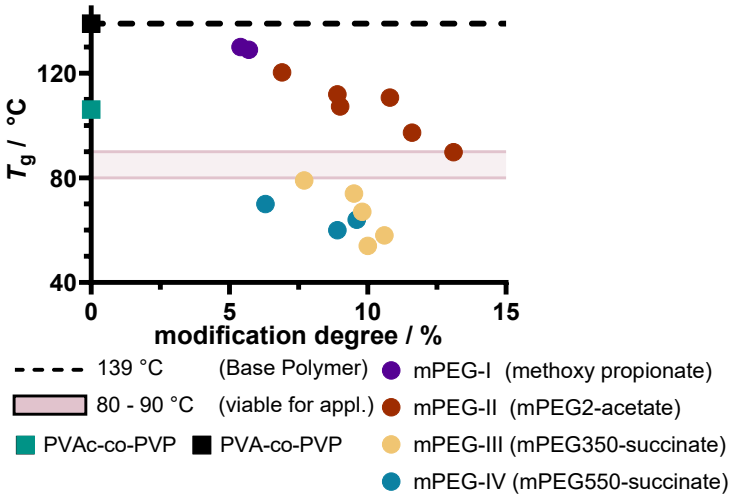

Figure 33: Glass transition temperatures against modification degree for each synthesized polymer with amine comonomers. Dashed black line is shown to guide the reader's eye and black square indicates the respective glass transition temperature of PVP-co-PVA before modification. The glass transition temperature of PVAc-co-PVP is indicated in green. The red box marks the targeted temperature range.

The modification utilizing mPEG derivatives leads to a decrease in T_{deg}. The base polymer shows a degradation above 221 °C and a prerequisite for a broad manufacturing temperature range is a T_{deg} above 200 °C. Especially the mPEG-III and mPEG-IV modified polymers at higher modification degrees show degradation temperatures below 200 °C. These polymers are not optimal for a manufacturing by HME. The polymers modified with **mPEG-II** in conjunction with the greatly reduced T_g makes them the ideal entities for tests by HME.

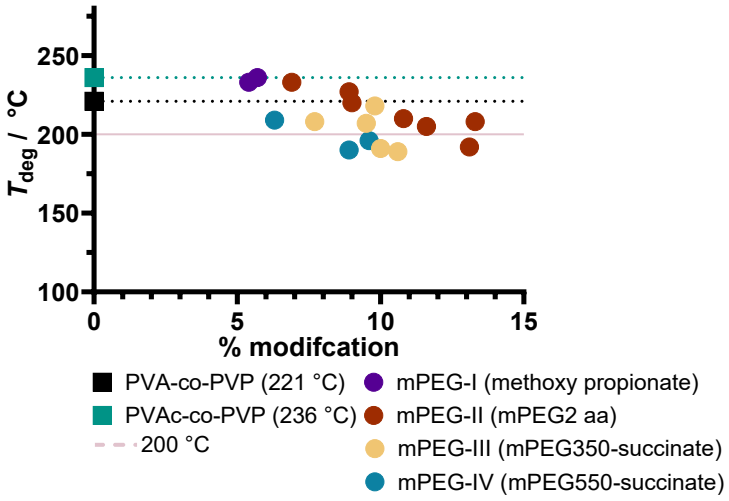

Figure 34: Degradation temperatures against modification degree for each synthesized polymer with mPEG comonomers. Pointed lines (black and green) are shown to guide the eye indicating the degradation temperatures of the starting material PVAc-co-PVP and of the base polymer PVA-co-PVP. The pink line at 200 °C is the temperature above which the polymer should be stable for enabling a broad manufacturing range.

5.2.5.1.3 Extrusion

Four entities were subject to small scale extrusion experiments to prove their viability in later intermediate scale extrusion. In a twin-screw extruder with three heating zones, the temperature was set close to the T_g obtained by DSC. The material was milled utilizing a cryo-mill and introduced into the extruder at 200 revolutions per min (RPM). The material was discharged onto a conveyor belt via a 1.5 mm nozzle. The filaments were characterized visually concerning their color and translucence. As the charging of the material into the extruder barrel is performed manually, the thickness of the extrudate needs to be controlled by adjustment of the conveyor belt speed. The flowability of the different polymer melts vary greatly, so irregular filaments are obtained. Their brittleness is tested manually directly after the cooling phase.

The polymers **mPEG-IIe** and **mPEG-IIf** both were extrudable in the temperature range tested (Table 13 and Table 14). The lower starting point in temperature was chosen close to the respective T_g and increased in increments of at least 10 °C. Both polymers showed extrudability at temperatures close to T_g with low average torque (1.4 N m and 1.3 N m). Opaque, yellow filaments were obtained indicating incomplete melting. Increasing the temperature led to slightly decreased average torque in both cases, while the filaments were transparent from the second temperature setting onward. The filaments were less brittle compared to pure PVP-co-PVAc, but were unable to be bent before breaking. Further analysis of their brittleness was not conducted. In summary, both specimens were extrudable on a small-scale twin-screw extruder in the temperature range above the respective T_g.

Table 13: Summary of Extrusion experiment for mPEG modified polymer mPEG-IIe (T_g = 97 °C, T_{deg} = 205 °C).

Polymer	**mPEG-IIe**	**mPEG-IIe**	**mPEG-IIe**
Temperature / °C	100/100/100	80/110/110	90/120/120
RPM / min^{-1}	200	200	200
average torque / Nm	1.4	1.3	1.15
nozzle / mm	1.5	1.5	1.5
Appearance	yellow	yellow	yellow
Translucence	opaque	transparent	transparent
Flexibility	brittle	brittle	brittle
Filament			
Extrusion possible	**Yes**	**Yes**	**Yes**

Table 14: Summary of Extrusion experiment for mPEG modified polymer mPEG-IIf. (T_g = 90 °C, T_{deg} = 192 °C).

Polymer	**mPEG-IIf**	**mPEG-IIf**	**mPEG-IIf**
Temperature / °C	90/100/100	90/110/110	90/120/120
RPM / min^{-1}	200	200	200
average torque / Nm	1.3	1.15	1.2
nozzle / mm	1.5	1.5	1.5
Appearance	yellow	yellow	yellow
Translucence	opaque	transparent	transparent
Flexibility	brittle	brittle	brittle
Filament			
Extrusion possible	**Yes**	**Yes**	**Yes**

The polymers **mPEG-IIIc** and **mPEG-IVb** were extruded in similar fashion as other mPEG modified polymers. Starting at a temperature close to the T_g, it was possible to obtain transparent yellow filaments

at 120 °C. **mPEG-IIIc** was extrudable forming transparent filaments with little die swelling and low torque of 0.8 N m. Also, the filaments were more flexible than PVP-co-PVA (Table 15). **mPEG-IVb** was also extrudable forming transparent filaments at 120 °C with little die swelling. The filaments, which were more flexible than **mPEG-IIIc** filaments, were sticky to touch, indication hygroscopicity and water solubility of the polymer. The average torque was low at 0.8 N m, comparable to the extrusion parameters when extruding **mPEG-IIIc**.

Table 15: Summary of Extrusion experiment for mPEG modified polymer mPEG-IIIc (T_g = 74 °C, T_{deg} = 207 °C).

Polymer	**mPEG-IIIc**	**mPEG-IIIc**	**mPEG-IIIc**
Temperature / °C	60/90/90	60/110/110	75/120/120
RPM / min^{-1}	200	200	200
average torque / Nm	1.0	0.8	0.8
nozzle / mm	1.5	1.5	1.5
Appearance	yellow	yellow	yellow
Translucence	opaque	Semi-transparent	transparent
Flexibility	brittle	flexible	flexible
Filament			
Extrusion possible	**Yes**	**Yes**	**Yes**

Table 16: Summary of Extrusion experiment for mPEG modified polymer mPEG-IVb (T_g = 64 °C, T_{deg} = 196 °C).

Polymer	**mPEG-IVb**	**mPEG-IVb**	**mPEG-IVb**
Temperature / °C	60/100/100	65/110/110	70/120/120
RPM / min^{-1}	200	200	200

average torque / Nm	0,8	0,8	0,8
nozzle / mm	1.5	1.5	1.5
Appearance	yellow	yellow	yellow
Translucence	opaque	Semi-transparent	transparent
Flexibility	flexible	flexible	flexible
Filament	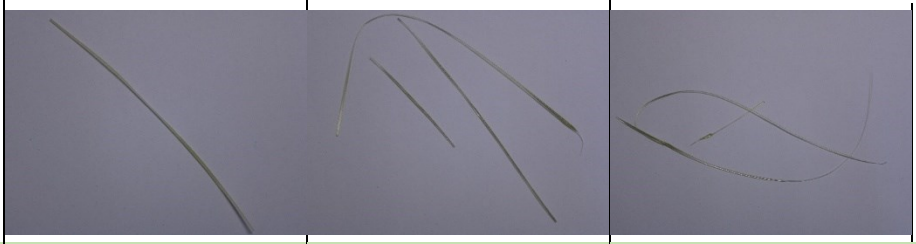		
Extrusion possible	**Yes**	**Yes**	**Yes**

5.2.5.1.4 Scale-Up

A polymer with high potential demonstrated by its properties in terms of T_g, T_{deg}, its amorphousness, its melt rheological behavior and performance during the lab-scale extrusion is **mPEG-IIf** (Table 17). The synthesis procedure was transferred to a cooperation partner and the synthesis and dialysis was performed by Oliver Stranowsky (*Merck Electronics KGaA*). The precursor synthesis was conducted in a 1 L round-bottom flask, while the modification reaction was executed using a 10 L double jacketed apparatus. The dialysis was conducted in two 60 L PE barrels. Consecutive lyophilization yielded 182 g (60%) of **mPEG-IIg**. The synthesis of **mPEG-IIg** showed good reproducibility compared to **mPEG-IIf** as the polymer properties in terms of modification degree, T_g, and T_{deg} are similar for both polymer specimen. GPC measurements showed similar distributions and mean molecular weight. The melt rheological characterization (Figure 32d) yielded a processing window of $\Delta T = 31$ °C between 129 °C and 160 °C, which is in good agreement to the posed prerequisites in Section 5.1. The extrusion on intermediate scale of **mPEG-IIg**, conducted by Alessandro-Guiseppe Elia (*Merck Life Science KGaA*), on the Pharma 11 extruder was possible with low torque and low die pressure at low temperatures of 135 °C.

Table 17: Analytical data of lab-scale batch mPEG-IIf in comparison to upscaled 200 g batch mPEG-IIg.

		mPEG-IIf 5 g	**mPEG-IIg 200 g**
NMR	Modification degree	11%	10%
GPC	M_w	38000 g mol^{-1}	38000 g mol^{-1}

DSC	$T_g \geq$ 80-90 °C	90 °C	83 °C
DSC	No T_m, amorphous	no T_m	no T_m
Mini Extruder	Transparent filaments	low torque	
TGA	$T_{deg} \geq$ 200 °C	192 °C	208 °C
Melt viscosity	η_{melt} =1000 – 10000 Pa s @ 0.1 rad s^{-1}	n.d.	129-160°C
Process window	η_{melt} < 10 000 Pa s; below T_{deg} > 40-50°C	n.d.	Δ = 31 °C
Intermediate-scale Extrusion		n.d.	Low torque low die pressure

5.2.5.1.5 Dissolution experiments

A polymer utilized in the field of solid formulation of oral dosage forms needs to fulfill various roles, including the control of the release kinetics of a pharmaceutical ingredient and the enhancement of poor solubility in a given physiological medium. Next to the influence of a polymer in the interplay with an API, the polymer itself possesses solubility characteristics which lead to various release kinetics and polymer/API interactions may lead to a favorable influence on the APIs dissolution profile. In this study, two aspects of the polymer solubility characteristics are investigated. The polymer-based release kinetics and its influence on the solubility of a poorly soluble API. The testing assays were developed in a cooperating department (*Merck Life Science KGaA*) adapted from literature[131, 160] and the experiments were conducted by Nabil Lamrabet (*Merck Life Science KGaA*).

The release kinetics of a polymer to be utilized in an immediate release formulation can be probed conducting dissolution experiments with an analyte with high solubility. Caffeine is suitable as analyte with a high solubility of 20 g L^{-1}.[161] A sample specimen is created consisting of the polymer and a known amount of analyte where the amount of dissolved caffeine over time is determined via externally calibrated UV-VIS spectroscopy. The BCS-I compound caffeine is readily soluble in the testing medium HCl. In this testing assay, 10w% drug load was used with a sample polymer. The physical mixture was amorphized by heating above a polymer specific temperature via a vacuum compression molding method (VCM, *MeltPrep*). The polymer/API melt is pressed to a disc using a piston in the apparatus. The melted disc resembles the high density in a filament or 3d printed tablet and is used as is for the assay. In a dissolution apparatus (USP paddle method), the test specimen is submerged in HCl, and the absorbance of caffeine at specific timepoints in measured. Utilizing this assay, the polymer-based release kinetics can be assessed. A detailed description of the procedure is given in Section 8.

Modified polymers are compared to the base and marketed polymer to assess their overall dissolution kinetic and to unravel potential changes in solubility due to the introduction of a modification in their side chain (Figure 35). The sample PVAc-co-PVP shows a quick onset in caffeine absorbance reaching 99% ± 6% release after 15 minutes with a maximum of 104% during the measurement time. This indicates its good capability in an immediate release formulation. In the same manner, PVA-co-PVP also shows a quick onset to 83% ± 11% release after 15 minutes approaching 90% until the end of the measurement time., so the saponification of acetate groups in the side chain do not significantly change the release kinetics. **mPEG-IIg** reached 94% ± 10% release after 10 minutes with a maximum of 114% at 360 minutes. Values slightly above 100% may be the result of unwanted absorption of the modification agent at 272 nm, which is the wavelength used for detection of the caffeine carbonyl transition bands.[162, 163] n-π* and/or π-π* transitions as can be found in carbonyl groups or aromatic systems usually show an absorption band around these wave lengths and the modification agent **mPEG-II** possesses an ester bond.[164] After saponification, PVP-co-PVA has less carbonyl groups than PVP-co-PVAc, which may be the reason for a lower maximum absorbance during the testing. The progression of the curves do not differ significantly, suggesting, that **mPEG-IIg** has the same release kinetics as the starting material PVP-co-PVAc.

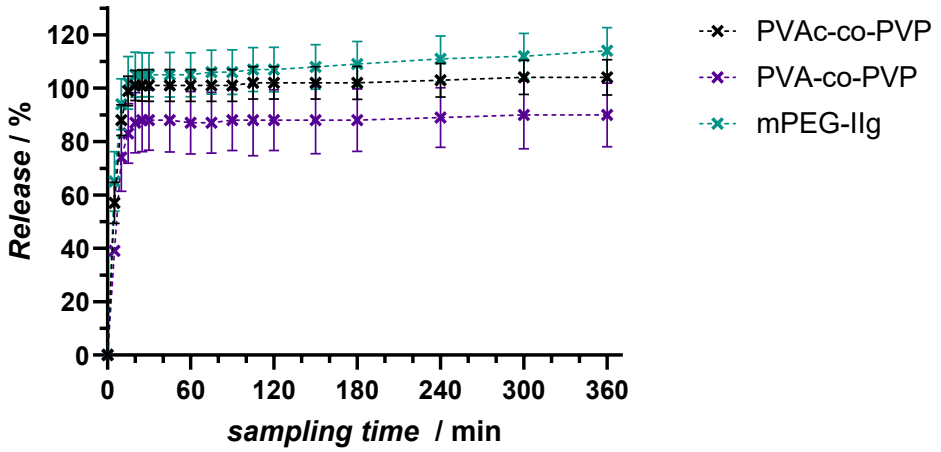

Figure 35 Release kinetics of selected polymers in comparison with benchmark PVAc-co-PVP (Kollidon® VA64) in caffeine assay. Amorphous sample discs were prepared by VCM. Non-sink dissolution of amorphized samples through melt quenching in 0.1 M HCl at 37 °C, 75 rpm and 900 mL medium. Drug: Caffeine at 10% drug load in 300 mg specimen, arithmetic means ± SD (n = 3). UV-VIS Analysis at λ = 227 mm. Discs were prepared by MeltPrep method and used as is. Dashed lines incorporated to guide the reader's eye.

Next to the dissolution kinetics, a polymer's capability in terms of the dissolution enhancement regarding a model API is of great interest. Poorly water-soluble APIs typically include hydrophobic moieties in their chemical structure. Furthermore, the thermodynamic stable phase is the arrangement in crystal lattices, which in turn leads to a significantly lower solubility in aqueous media. Incorporating these APIs in polymer matrices, which exhibit the ability of preventing crystal formation, increases their aqueous solubility. In doing so, BCS-II compounds become biologically available and can have their therapeutic effect. By this, the influence of the polymer/API interaction on the supersaturation behavior is tested. The ability to increase the solubility of an API over the course of a given time frame is known as solubility enhancement. The difference in performance of a polymer in dissolution testing is dependent on the API system it is used in. *Auch et al.*[131] developed a melt-based screening assay for the prediction of polymer performance in a model API system.

The API is incorporated into the polymer matrix by vacuum compression molding (VCM, *MeltPrep*). Ketoconazole (KTZ, Table 3), a small molecule API with multiple hydrophobic moieties including halogenated aromatic rings and aromatic ether groups, is used as the model API. The physical mixture with 40w% drug load is amorphized via VCM, which mimics the density of extruded filaments or a 3d printed tablet. This assay helps to understand the dissolution enhancement capabilities of a polymer on a screening approach utilizing small amounts of sample. A detailed description of the procedure is given in Section 8. The concentration of KTZ released from the polymer matrix in the dissolution medium is analyzed by HPLC and measured at six time points over the course of 120 minutes. Pure KTZ is practically insoluble in water (17 µg/ml)[165], so the incorporation into a polymer matrix is used to assess the solubility enhancement properties of a sample polymer. An area under the curve (*AUC*) is calculated by integrating the curves of each polymer. The results obtained by this assay are specific for the model API system in use. Changing the model API and present interaction sites may lead to a change in polymer/API interaction and thus lead to differences in the performance of each polymer.

The polymers tested in this section have a favorable influence on the API dissolution (Figure 36). PVAc-co-PVP and **mPEG-IIg** show a quick onset of the API concentration with a maximum after 30 minutes and a concentration of 480 ± 100 µg mL^{-1} and 240 ± 20 µL mL^{-1} respectively. PVA-co-PVP does not show a maximum in the measurement time and reaches a concentration of 100 ± 10 µL mL^{-1} after 120 minutes. For the polymers PVAc-co-PVP and **mPEG-IIg** a spring-parachute effect can be noticed, as the maximum is reached quickly followed by a prolonged decrease of the API concentration in solution. The slope after the minimum in the case of PVAc-co-PVP is larger negative than for **mPEG-IIg** indicating a prolonged spring effect for the modified polymer. The area under the curve (*AUC*) is a good indicator on the dissolution capabilities of a polymer in this system. The *AUC* of PVAc-co-PVP is 40000 ± 5000 whereas the *AUC* for **mPEG-IIg** is 22000 ± 3000 further underlining the increased

a) b)

performance of PVAc-co-PVP. The overall performance of PVAc-co-PVP is better than **mPEG-IIg** as the maximum concentration and therefore bioavailability is higher. All tested polymers have the ability of super saturation of the testing solution considering the model API KTZ, but PVAc-co-PVP demonstrated the best capabilities in terms of solubility enhancement.

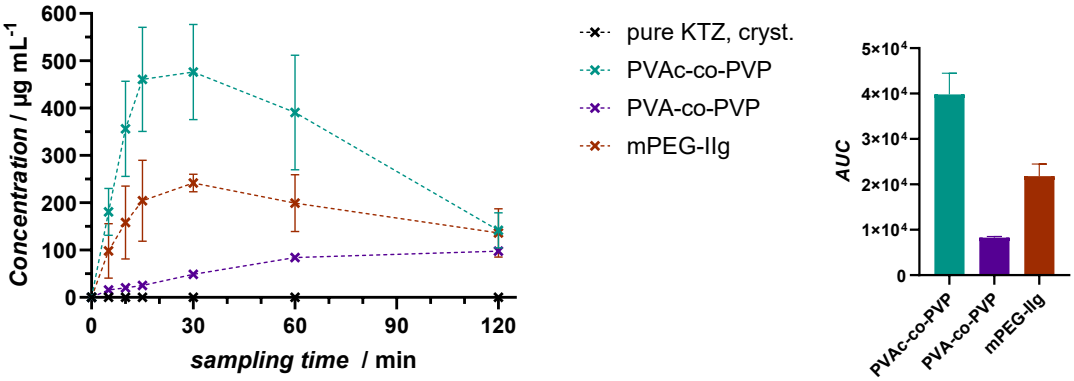

Figure 36: a) Dissolution capabilities of selected polymers and benchmark PVAc-co-PVP (Kollidon® VA64) in comparison to pure, crystalline API. Amorphous sample discs were prepared by VCM. Non-sink dissolution of amorphized samples through melt-quenching in FaSSIF at pH 6.5 at 37 °C. Concentration of 0.75 mg drug per mL medium, arithmetic means ± SD (n = 3), drug: Ketoconazole at 40% drug load; HPLC analysis at λ = 225 mm. Discs were prepared by MeltPrep method and used as is. Dashed lines incorporated to guide the reader's eye; b) Corresponding *AUC* of the dissolution measurements for comparison of dissolution capability.

When compared to other benchmark polymers (See Section 5.2.4, page 57) it is evident, that the modified polymer has indeed a solubility enhancing effect on the model API, as can be observed in terms of the respective *AUC* (Figure 37). The *AUC* resulting from solubility experiments is a good indicator on the performance of a given polymer and is strongly dependent on the polymer/API interactions and consecutively on the API used during the experiments. In the tested system utilizing KTZ, the modified polymer shows increased super saturation capabilities compared to other marketed products such as vinyl pyrrolidone based PVP K30, the vinyl alcohol derivatives Parteck® MXP, Kollicoat® IR and the methacrylate based products Eudragit® E PO and Eudragit® L100-55. Considering the starting material PVAc-co-PVP (Kollidon® VA64), the mPEG modification has a lower effect in terms of solubility enhancement. This indicates that the various combinations of chemical moieties present in Parteck® MXP, Kollicoat® IR, Eudragit® E PO and Eudragit® L100-50 have a less favorable effect on the solubility of KTZ when compared to Kollidon® VA64. As outlined in a previous chapter, the marketed products not only differ in their chemical composition in terms of monomers, but also in their solubility, molecular weight, functional groups, and polarity. This further suggests that not only the chemical structure of the comonomers substantially influences the performance in an API system but also other factors are essential for a solubility enhancing effect. In subsequent dissolution studies only PVAc-co-PVP and PVA-co-PVP will be compared to the synthesized polymers as the

chemical structures of these benchmarks are the most similar and PVAc-co-PVP is the best performing excipient in the selection tested.

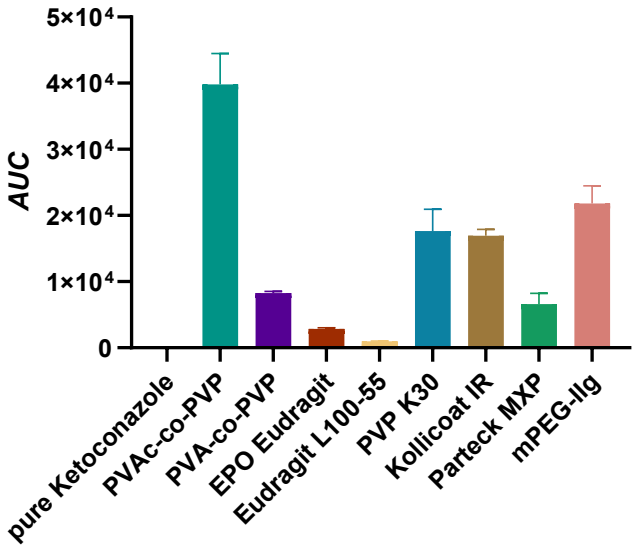

Figure 37: *AUC* of a selection of benchmark products resulting from dissolution experiments with KTZ (n=3) including error bars of the separate measurements. Structural information concerning the benchmarks can be found in the introduction and Section 5.2.4.

5.2.5.1.6 Conclusion

In conclusion, mPEG modifications of PVP-co-PVA show remarkable improvements for the processing of the polymers as confirmed by small scale extrusion and melt rheology measurements. The synthesis via CDI-chemistry was successful, while the glass transition temperature could be decreased to close to 60 °C compared to 139 °C as observed in the marketed polymer PVP-co-PVAc. The scale-up to amounts of 200 g was successful as confirmed various analysis techniques. PVAc-co-PVP has a higher dissolution performance compared **mPEG-IIg**, so mPEG modification may be used for the reduction in processing temperature to reach the targeted range between 80 °C and 90 °C. The modification improves the solubility of KTZ compared to the starting material, when used as a polymer matrix in combination with KTZ. It has higher solubility capabilities compared to most benchmarks tested (Figure 37), but not Kollidon® VA64.

5.2.5.2 Substituted Amines

5.2.5.2.1 Synthesis

The second group of modification agents which was investigated were substituted amines. The substituted alkyl amines were used because the introduction of a polar amine function in the sidechain of the resulting polymer may have a favorable influence on the polymer-API interaction. Additionally, amines are compatible with the CDI-modification reaction and can be used according to the synthesis procedure outlined before. One alkyl substituted amino acid, 3-(dimethylamino)propanoic acid (**amine-III**), and two alkylamines, namely N^1,N^1-diethylpropane-*1,3*-diamine (**amine-I**) and N^1,N^1-dimethylpropane-1,3-diamine (**amine-II**) were used for the modification. In total, 14 polymers were synthesized with a modification degree of 1% to 13%. The analytical characterization will be given in the following section.

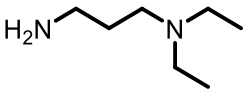

N^1,N^1-diethylpropane-1,3-diamine
amine-I

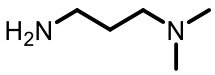

N^1,N^1-dimethylpropane-1,3-diamine
amine-II

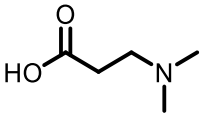

3-(dimethylamino)propanoic acid
amine-III

Scheme 9: Alkyl amino functionalized modification agents used in this thesis.

The synthesis of these modifications closely follows the procedure using carboxylic acid, but no carbon dioxide is generated during the synthesis of the precursor with amines (Scheme 10). The resulting product, an activated urea derivative reacts in the same way with the hydroxyl moieties in PVP-co-PVA, generating a carbamate comonomer. **amine-III**, reacts the same way as the previously mentioned mPEG acids to form ester comonomers (Scheme 8).

a)

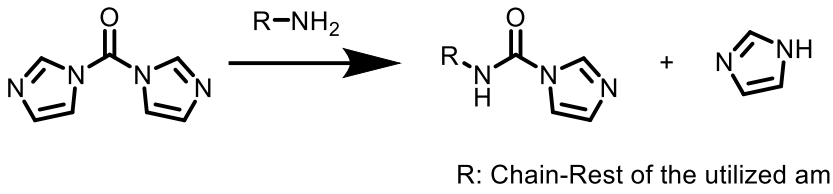

b)

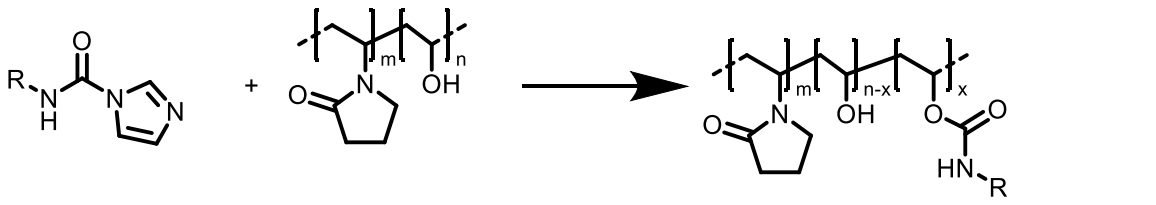

Scheme 10: General reaction scheme for the modification of PVP-co-PVA using amines. The rest R differs according to the amine utilized in the reaction; a) shows the synthesis of the precursor utilizing substituted amines with the formation of an urea; b) shows the final modification reaction leading to the modified copolymer. Multiple polymers were synthesized with varying moles of the activated intermediate to give polymers with varying x-monomer amount in the polymer dependent on the amount a of intermediate employed during the reaction..

The modification product was analyzed via quantitative ^{1}H-, ^{13}C-, HSQC, HMBC and DOSY NMR spectroscopy. The quantitative ^{1}H-NMR of **amine-IIe** shows the typical PVP-co-PVA signals as described in Section 5.2.3 and additionally a broad signal between 2.73 *ppm* and 2.93 *ppm* where the protons c^{3}, c^{5} and c^{6} show resonance (Figure 38). Comparing the results obtained by quantitative ^{1}H-NMR For each other amine derivative (**amine-I**, **amine-II** and **amine-III**) the same calculation method can be utilized and similar spectroscopic methods were used (see Appendix, Figure 24). A summary of all analytical results for the modified polymers is given in Table 18.

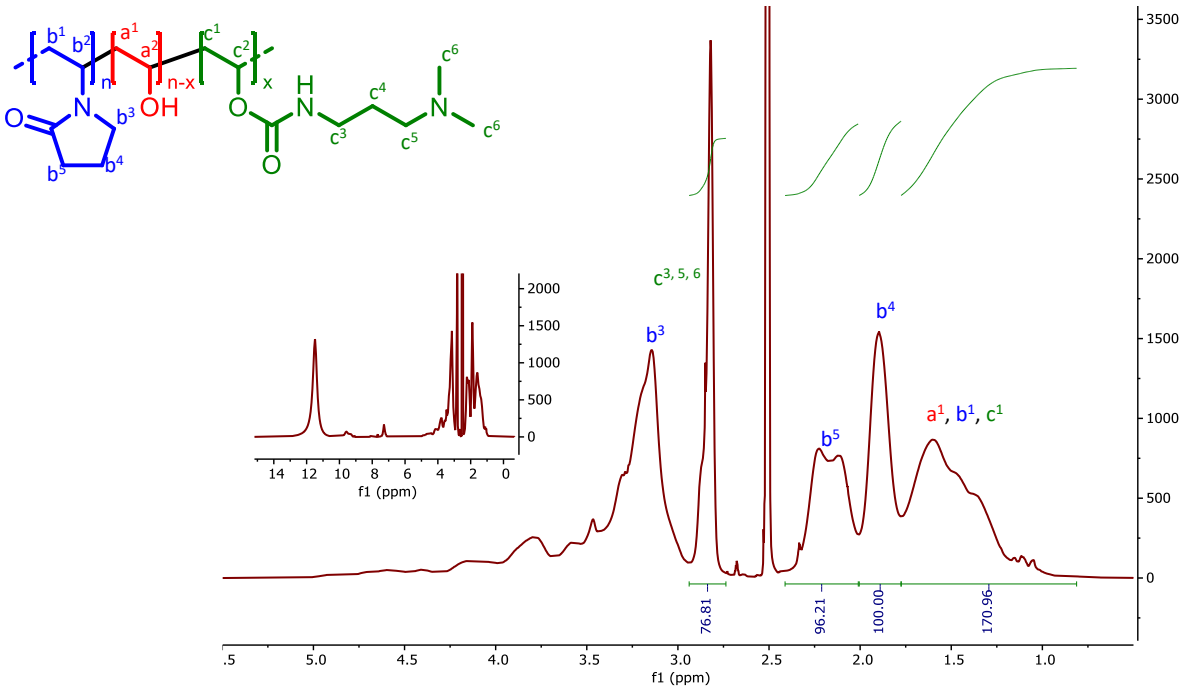

Figure 38: Quantitative ^{1}H-NMR spectrum of amine-IIf. Modification degree is 7.4%.

5.2.5.2.2 Characterization

Amine modified polymers obtained were characterized regarding their thermophysical behavior utilizing DSC. A collection of all thermograms obtained for modifications using amine derivatives can be found in the appendix (Appendix, Figure 25, Appendix, Figure 26 and Appendix, Figure 27) and a summary of analytical data is given at the end of this chapter (Table 18). No melting point is visible in the DSC thermograms indicating amorphousness in all cases. The modification using amine has a lower reducing effect on the glass transition temperature in comparison to mPEG derivatives. Though, with increased amine content in the polymer, a reduction of the glass transition temperature is observed. The lowest glass transition measured was for **amine-IIf** with a T_g = 108 °C compared to the glass transition temperature of the starting material PVP-co-PVA T_g = 139 °C (Figure 39a).

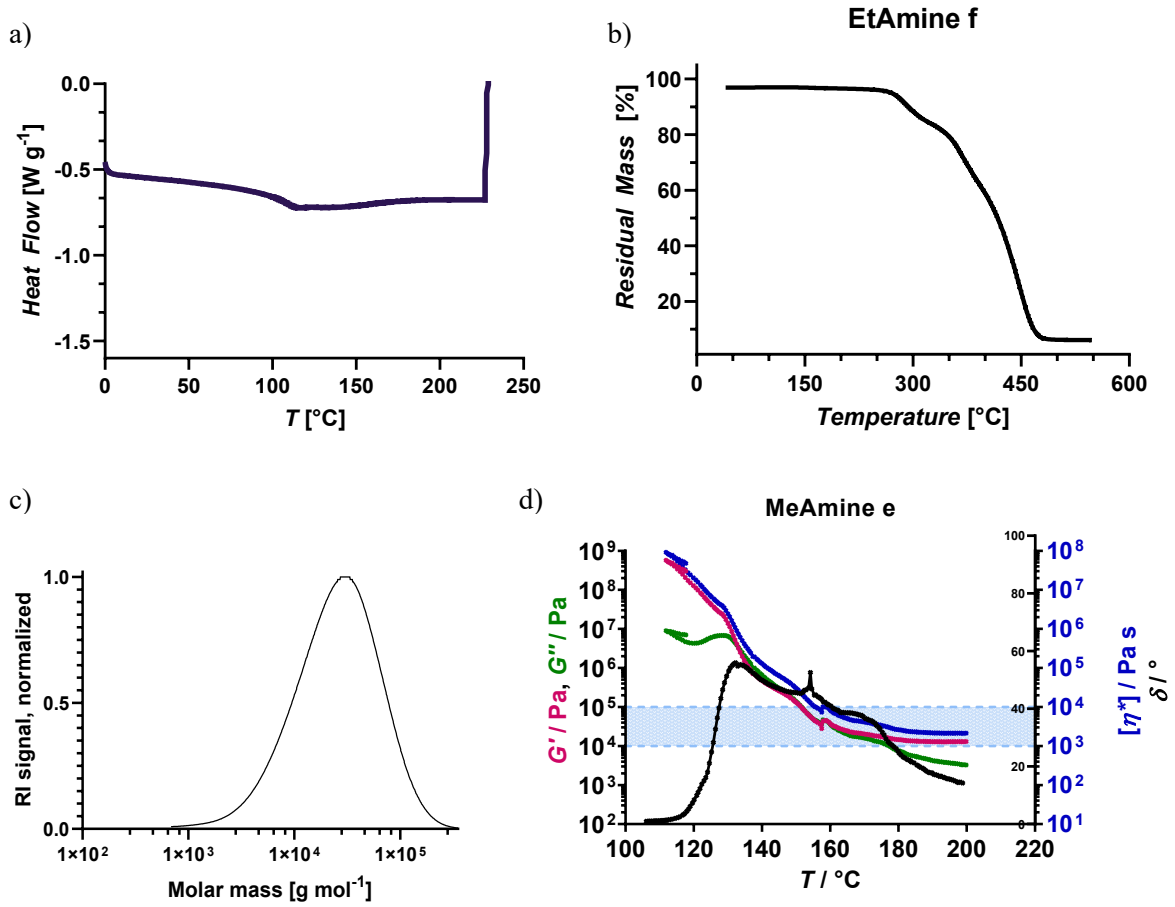

Figure 39: a) DSC thermogram of **amine-II f**, T_g = 108 °C; b) TGA thermogram of **amine-If**. Degradation starts at 199 °C; c) **amine-IIf**, Mw = 36000 g mol^{-1}, D = 2.5; d) Rheogram of **amine-IIe**, measurement inconclusive due to strong bubble formation.

All polymers were analyzed utilizing thermogravimetric analysis (Figure 39b). The analyzed polymers degrade in a two-step degradation process, whereas PVP-co-PVA degrades in a single-step degradation (Figure 19). This second degradation step may result from the degradation of the newly formed side chain after the modification. Amine modification reduced the thermal stability of the polymer from 226 °C to as low as 186 °C. Apart from the polymers **amine-IId**, **amine-IIe** and **amine-IIf**, with 9%, 9% and 12% modification degree respectively, the onset of degradation is above 200 °C, which is in line with previously defined specifications.

Table 18: Compilation of analytical data obtaines for amine derivative modified copolymers.

	Yield / %	Mod. Deg. / % of -OH	T_g / °C	T_{deg} / °C	M_w / g mol^{-1}	M_p / g mol^{-1}	$Đ$
amine-Ia	83	1.4	137	220			
amine-Ib	70	4.2	133	208			
amine-Ic	52	6.4	130	202			
amine-Id	63	8.7	125	195			
amine-Ie	42	9.4	123	186	37000	29000	2.9
amine-If	49	11.6	124	199			
amine-IIa	81	2.0	129	225			
amine-IIb	66	4.0	128	214			
amine-IIc	43	4.6	118	207			
amine-IId	53	5.9	124	216			
amine-IIe	44	6.0	122	215	35000	27000	2.5
amine-IIf	40	7.4	108	208	36000	28000	2.5
amine-IIIa	82	13.0	134	225			
amine-IIIb	61	13.0	136	231	38000	29000	2.6

At least one polymer of each modification type was analyzed by GPC (Figure 39c). As hydroxyl moieties in the base polymer are modified to form a new comomer, monomodal distributions with an increase in molecular mass were obtained (M_w). Compared to the base polymer an increase of up to 8000 g mol^{-1} can be observed (**amine-IIIb**)

Together with the spectroscopic data obtained, it can be concluded, that all modification reactions were successful.

Melt rheology measurements were conducted for the polymer **amine-IIe** and **amine-Ie**, but in both cases bubble formation occurred during the measurement and thereby no reliable conclusion about the processing range can be made (Figure 39d). The curves have abrupt leaps in their progression, which could be due to an incomplete filling of the slit during the melting period, bubble formation or a reaction under thermal stress of the polymer.

By hydroxyl modification in PVA-co-PVP, it was possible to reduce the glass transition temperature (Figure 40), which was more pronounced with higher modification degrees, while the polymers mostly remained thermally stable and degradation was observed above 200 °C (Figure 41). Especially the amine-II modified polymers at higher modification degrees show degradation temperatures below 200 °C. Despite their thermal stability, the glass transition temperature does not reach the targeted temperature range. Therefore, amine modification may not be ideal for a significant reduction in processing temperatures but may have an influence on the polymers API interaction, as will be discussed in a later chapter.

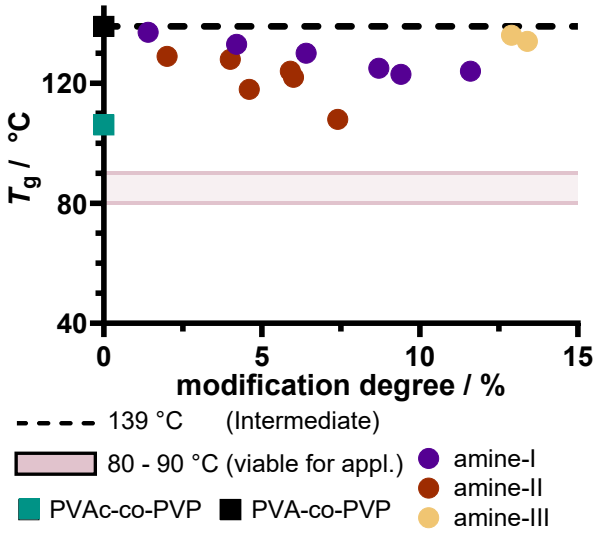

Figure 40: Glass transition temperatures against modification degree for each synthesized polymer with amine comonomers. Dashed black line is shown to guide the reader's eye and symbol indicates the glass transition temperature of PVP-co-PVA before modification. The glass transition temperature of PVAc-co-PVP is indicated in green. The red box marks the targeted temperature range.

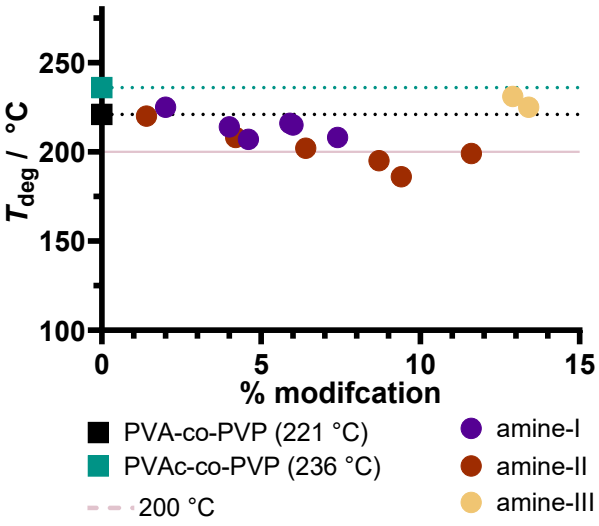

Figure 41: Degradation temperatures against modification degree for each synthesized polymer with amine comonomers. Pointed lines (black and green) are shown to guide the eye indicating the degradation temperatures of the starting material PVAc-co-PVP and of the base polymer PVA-co-PVP. The pink line at 200 °C is the temperature above which the polymer should be stable for enabling a broad manufacturing range.

5.2.5.2.3 Extrusion

Two entities of amine modified polymers were subject to small scale extrusion experiments using a twin-screw extruder. The extrusion temperature was set close to, but above the T_g of the respective polymer. A 1.5 mm nozzle was used, and the filaments were characterized visually. The extrusion of **amine-Ie** and **amine-IIf** led to brownish-yellow filaments with strong die swelling. The filaments were

brittle and the average torque values were increased ranging from 1.5 N m to 1.7 N m with high torque spikes during the extrusion of **amine-IIf**. A strong amine swell was noticed during the extrusion indicating premature degradation even below the T_{deg}. This is very unfavorable, as premature degradation and or chemical reaction during the extrusion may change the polymer properties substantially. In addition, the filaments were brittle, similar to PVP-co-PVA, which is also disadvantageous for the processing of the polymer. These results and the bubble formation during the melt rheology measurements both suggest that these polymers do not fit the specifications for the anticipated manufacturing *via* extrusion and were therefore not further investigated.

Table 19: Summary of Extrusion experiment for amine modified polymer **amine-Ie** (T_g = 123 °C, T_{deg} = 186 °C).

Polymer	**amine-Ie**	**amine-Ie**	**amine-Ie**
Temperature / °C	90/140/140	90/145/145	95/155/155
RPM / min^{-1}	200	200	200
average torque / Nm	1.7	1.6	1.5
nozzle / mm	1.5	1.5	1.5
Appearance	Brownish-yellow	yellow	yellow
Translucence	opaque	transparent	transparent
Flexibility	brittle	brittle	brittle
Filament	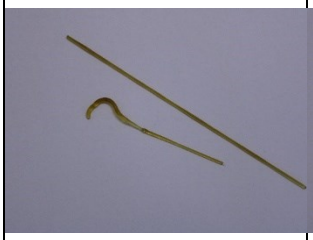	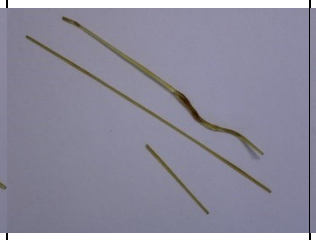	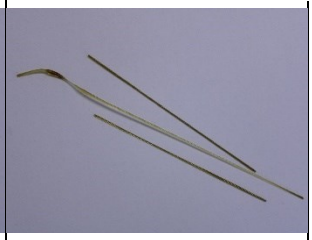
Extrusion possible	**Yes**	**Yes**	**Yes**

Table 20: Summary of Extrusion experiment for amine modified polymer **amine-IIf** (T_g = 108 °C, T_{deg} = 208 °C).

Polymer	**amine-IIf**	**amine-IIf**	**amine-IIf**
Temperature / °C	70/100/100	70/110/110	70/120/120
RPM / min^{-1}	200	200	200
average torque / Nm	1.4	1.5	1.7
nozzle / mm	1.5	1.5	1.5

Appearance	Brownish green	Brownish green	Brownish green
Translucence	opaque	transparent	transparent
Flexibility	brittle	brittle	brittle
Filament			
Extrusion possible	**No**	**No**	**no**

5.2.5.2.4 Conclusion

Due to the amine smell observed during the extrusion, the brittleness of the produced filaments and the bubble formation during melt rheology measurements, the group of polymers bearing amines in their sidechain was not investigated further. Premature thermal degradation or chemical degradation during processing cannot be tolerated for a potential application.

5.2.5.3 Hydrophobic acids

5.2.5.3.1 Synthesis

The ability to increase a poorly soluble API's solubility in solution is another key property of a matrix polymer for the pharmaceutical application of excipients in solid formulation. Most API's bear hydrophobic moieties and the aim of the modification using hydrophobic acids is to increase the hydrophobic interaction of the model API with the polymer and increase its solubility. As shown before, mPEG derivatives and, to an extent, substituted amines have a favorable influence on the polymers processability. The group of hydrophobic acids was chosen because of their potential to have favorable interactions with the API and to increase its solubility. The aromatic compounds cinnamic acid (**apolar-I**) and hydro cinnamic acid (**apolar-II**) were used for their aromatic moiety, palmitic acid (**apolar-III**), ethyl hexanoic acid (**apolar-IV**) and stearic acid (**apolar-V**) for their long hydrophobic alkyl chain, which may also decrease the processing temperatures. In total, 14 polymers were synthesized with a modification degree of 2% to 28%. The analytical characterization will be given in the following section. A summary of all analytical results for the modified polymers is given in Table 21.

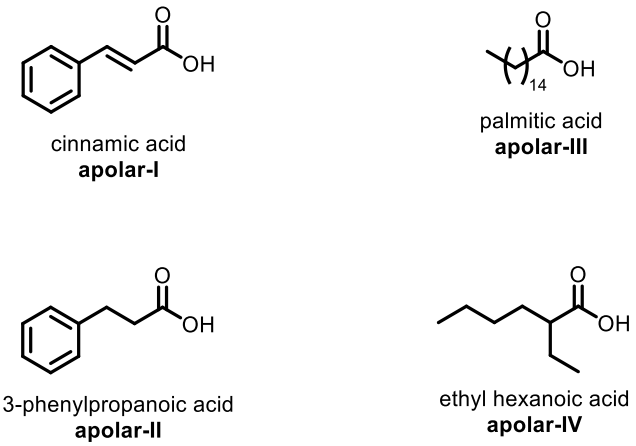

Scheme 11: Hydrophobic acid derivatives used in this work for the modification of PVP-co-PVA via esterification.

Modification of hydroxyl groups using hydrophobic acids was obtained in the same way as described in section 5.2.5.1 by utilizing the generated carbamate intermediates in the modification reaction with PVP-co-PVA (Scheme 8). Due to low solubility in the reaction medium in the case of calcium(II) di(stearate), no polymers were obtained. ^{1}H-, ^{13}C-, HSQC, HMBC NMR spectroscopy was used for the identification of the products. The quantitative ^{1}H-NMR of **apolar-Id** shows the typical resonance signals of PVP-co-PVA and additionally, the aromatic and double bond protons show resonance in the range of 8.06 ppm to 7.12 ppm (c^{3-7}) resulting in a modification degree of 6%. The remaining signals can be assigned to residual DMF and imidazole impurities (Figure 42). Polymers with a modification degree between 3%

and 11% were obtained. Modifications bearing the hydro cinnamic acid (**apolar-II**) function show similar resonance for the aromatic protons (Appendix, Figure 38) leading to modification degrees between 8% and 11% (Appendix, Figure 38 and Appendix, Figure 39).

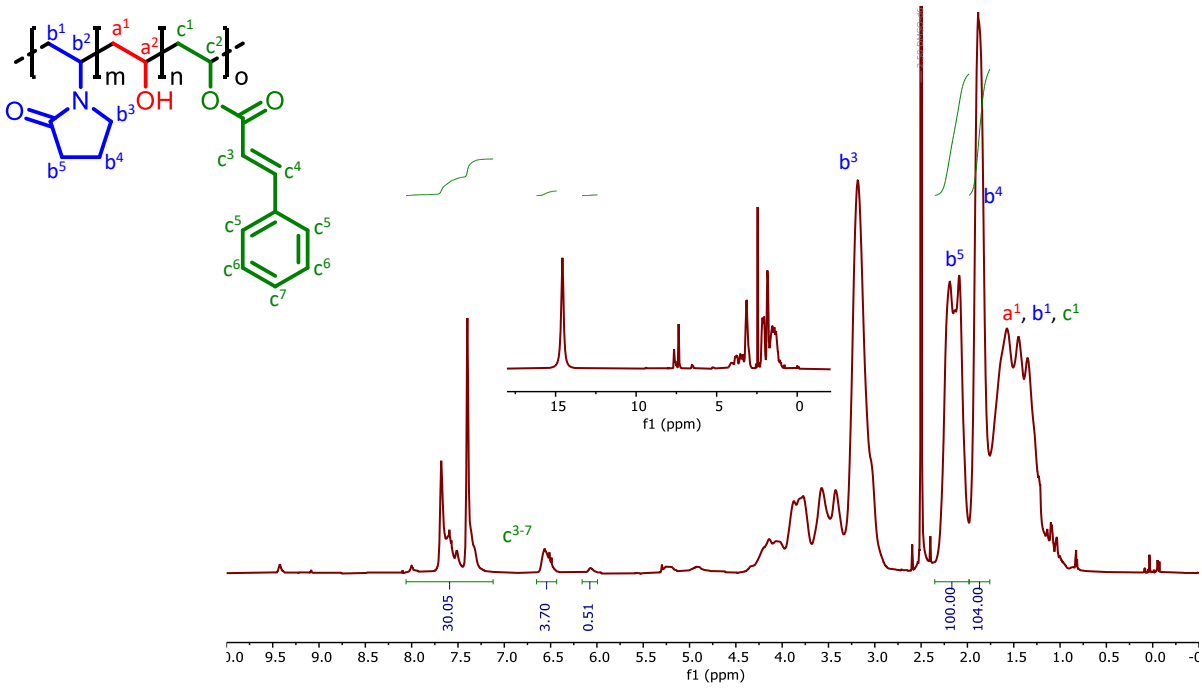

Figure 42: Exemplary quantitative ^{1}H-NMR spectrum of **apolar-I** modified PVP-co-PVA. Modification degree 6.0%.

The ^{1}H-NMR of polymers modified with palmitic acid (**apolar-III)** were analyzed by ^{1}H-NMR spectroscopy. In the spectrum showing the usual PVA-co-PVP signals, the singlet between 0.93 ppm and 0.79 ppm can be attributed to the methyl group of the alkyl chain and was used for the quantification (c^{15}, Figure 43). Modification degrees in the ranges of 4% to 28% of residual hydroxyl moieties were obtained (Appendix, Figure 34, Appendix, Figure 35). In the case of the ethyl hexanoic acid modification (**apolar-IV**), a modification degree of 2% was obtained by evaluating the methylene c^{7} protons between 0.92 ppm and 0.68 ppm (Appendix, Figure 36, Appendix, Figure 37).

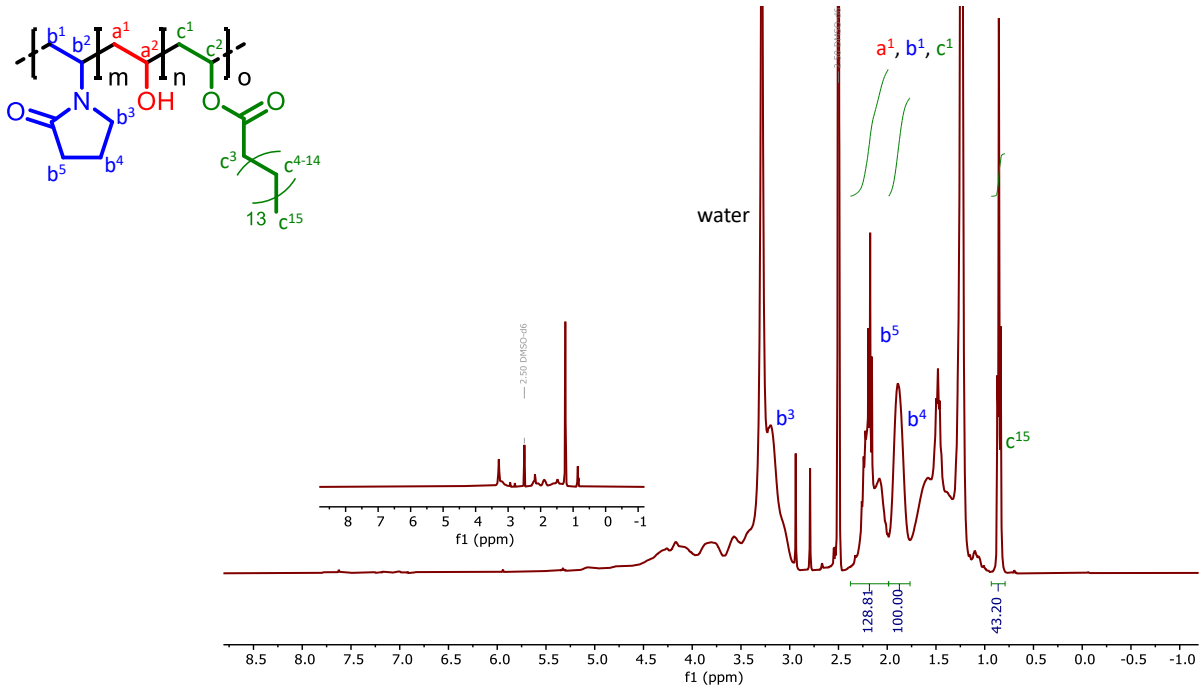

Figure 43: Exemplary quantitative ^{1}H-NMR spectrum of **apolar-III** modified PVP-co-PVA. Modification degree 28.3%.

5.2.5.3.2 Characterization

Modified polymers utilizing hydrophobic acid derivatives were characterized regarding their thermophysical behavior using DSC. A summary of analytical data is given at the end of this chapter (Table 21).

A melting point is visible in the DSC thermograms of the **apolar-III** group indicating semi-crystallinity (Appendix, Figure 42). All other polymers, namely the groups **apolar-I**, **apolar-II**, and **apolar-IV** do not show a melting range in DSC measurement, thus indicating amorphousness of the polymers (Figure 44a, Appendix, Figure 40, Appendix, Figure 41 and Appendix, Figure 43). The terpolymers bearing a hydrophobic comonomer show a reduction in their glass transition temperature with increasing modification degree. Especially palmitic acid has a large reducing effect on the polymers' glass transition temperature. The polymer **apolar-IIIc** with a glass transition temperature of 75 °C showed the lowest T_g of all polymers discussed in this section, but this group of polymers showed melting points in the range between 141 °C and 175 °C (Appendix, Figure 42).

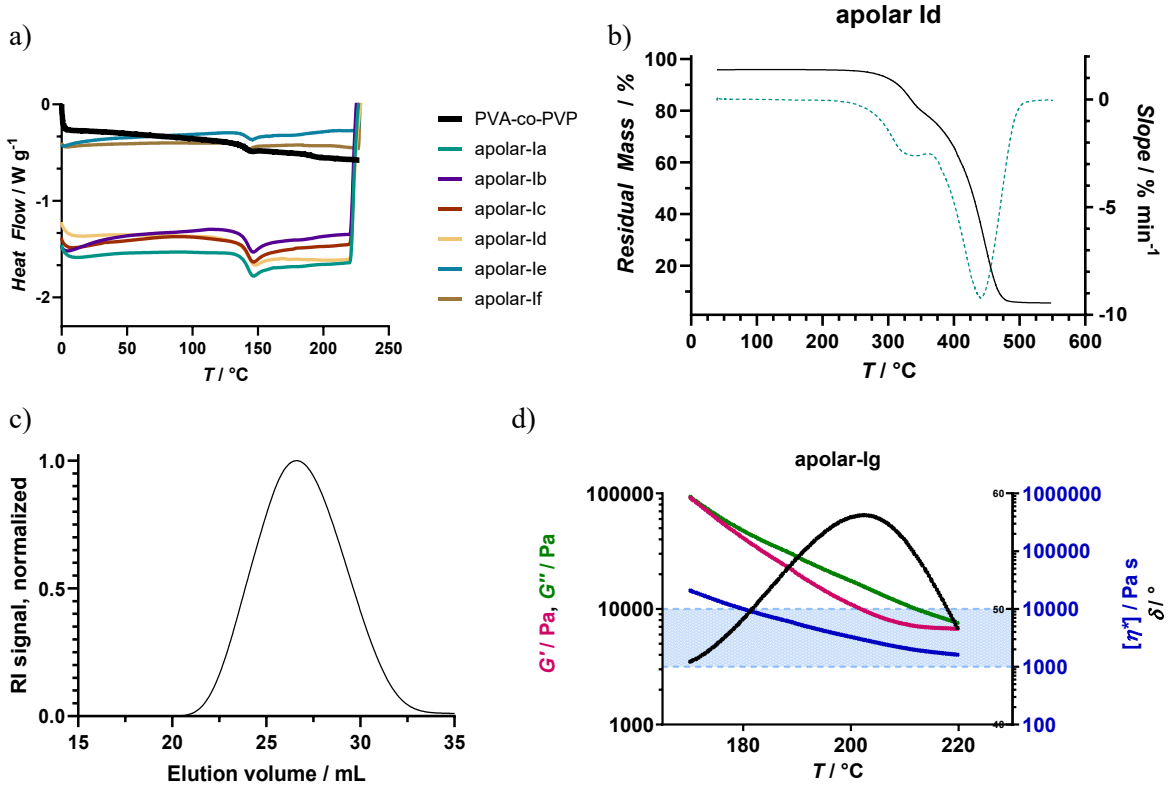

Figure 44: a) DSC of **apolar-I** modified polymers **a** to **f**, $T_{g,a}$ = 142 °C, $T_{g,b}$ = 141 °C, $T_{g,c}$ = 142 °C $T_{g,d}$ = 142 °C, $T_{g,e}$ = 140 °C, $T_{g,f}$ = 137 °C; b) TGA thermogram of **apolar-Id**. Degradation starts at 213 °C; c) GPC elugram for **apolar-Id**. Mw = 37000 g mol^{-1}, Đ = 2.4; d) Rheogram of **apolar-Ig**, T(10000 Pa s) = 180 °C, T(1000 Pa s) not reached during measurement.

The polymers were analyzed concerning their thermal stability. The polymers analyzed degrade in a two-step degradation process, whereas PVP-co-PVA degrades in a single-step degradation (Figure 19). This second degradation step may result from the degradation of the newly formed side chain after the modification. **apolar-Ie**, **apolar-If** and **apolar-IIIc** show a reduced T_{deg} of 175 °C, 178 °C and 141 °C respectively. The other polymers in this group show a T_{deg} near 230 °C and at least above 200 °C indicting sufficient thermal stability as defined by the targeted specifications.

The polymer **apolar-Id** was analyzed by GPC to investigate the success of the modifications. A polymer with a mean molecular mass of M_w = 37000 g mol^{-1} and a dispersity index $Đ$ = 2.4 was formed during the reaction. The polymers **apolar-IIa**, **apolar-IIb**, **apolar-IIIc**, **apolar-IVa** and **apolar-IVb** also show an increase in molecular weight after the modification to up to 37000 g mol^{-1}. The increase in molecular weight in comparison to the base polymer PVP-co-PVA indicates successful modification. In correspondence with the NMR spectroscopic data for each modification agent, it can be concluded, that the modification reactions of the base polymer PVP-co-PVA were successful.

Table 21: Compilation of analytical data gathered for apolar modified copolymers.

	Yield / %	Mod. Deg. / % of -OH	T_g (DSC) / °C	T_m (TGA) / °C	T_{deg} (TGA) / °C	M_w (GPC) / g mol^{-1}	M_p (GPC) / g mol^{-1}	Đ (GPC)
apolar-Ia	89	2.8	142	-	243			
apolar-Ib	88	5.0	141	-	245			
apolar-Ic	84	5.8	142	-	228			
apolar-Id	73	6.0	142	-	213	37000	29000	2.4
apolar-Ie	64	6.6	140	-	175			
apolar-If	49	10.9	137	168	178			
apolar-IIa	62	1.0	115		210	28000	21000	3.2
apolar-IIb	56	2.0	106		211	33000	28000	3.3
apolar-IIIa	68	4.2	121	179	238			
apolar-IIIb	67	18.0	123	163	238			
apolar-IIIc	85	28.3	75	141	141	37300	29400	2.4
apolar-IVa	42	2.0	136		210	30440	25240	3.1
apolar-IVb	40	2.2	134		220	30630	25200	3.1

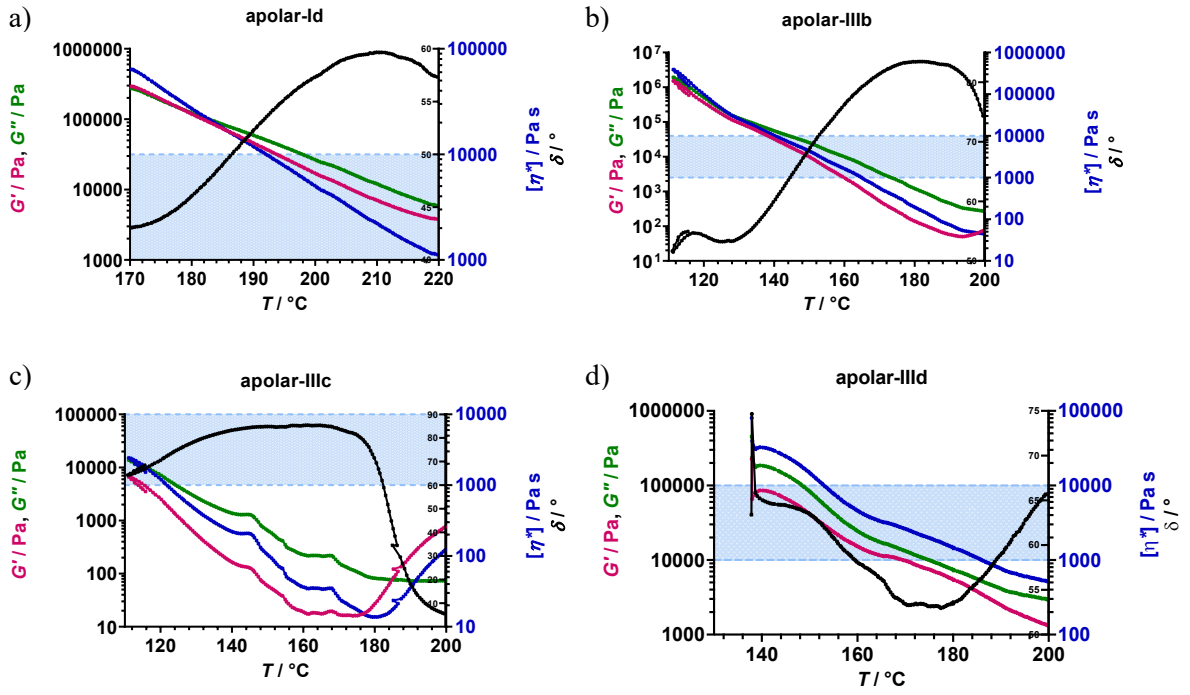

Figure 45: a) Rheogram of **apolar-Id**, T(10000 Pa s) = 192 °C, T(1000 Pa s) = 220 °C; b) Rheogram of **apolar-IIIb**, T(10000 Pa s) = 141 °C, T(1000 Pa s) = 165 °C; c) Rheogram of **apolar-IIIc**, T(10000 Pa s) > 116 °C, T(1000 Pa s) = 122 °C; d) Rheogram of **apolar-III d**, T(10000 Pa s) = 153 °C, T(1000 Pa s) = 186 °C.

Melt rheology measurements were conducted for selected polymer entities (Figure 45a). **apolar-Id** shows a discrete declining progression of both ***G'*** and ***G''***, with ***G''*** being higher than ***G'*** above 178 °C

indicating amorphousness at temperatures above this threshold. 10000 Pa s in melt viscosity is reached at $T_{\eta=10000\ Pa\ s}$ = 192 °C and 10000 Pa s is reached at 220 °C, which is a substantial increase in processing temperature for this polymer modification compared to the base polymer PVP-co-PVAc. A maximum in phase angle is visible around 210 °C indicating degradation, as was confirmed by TGA, where a T_{deg} = 213 °C was obtained. This temperature is lower than the degradation temperature of PVP-co-PVA (T_{deg} = 221 °C), indicating a decreasing influence on the T_{deg} by the modification using **apolar-I**, cinnamic acid.

The polymers **apolar-IIIb**, **apolar-IIIc**, **apolar-IIId** were measured regarding their rheological behavior. **apolar-IIIc** had low viscosities (> 1000 Pa s above 120 °C) during the whole temperature range in the measurement and was running from the shearing gap in the instrument. Therefore, a measurement of the processing range was not possible. The polymer **apolar-IIIc** may be extruded at even lower temperatures than 120 °C, which was lower than the targeted range of the defined specifications. The polymer **apolar-IIIb** showed a processing range of 141 °C to 165 °C during melt rheology measurements. *G'* is smaller than *G''* in the temperature range measured indicating amorphousness. **apolar-IIId** showed a processing range between 153 °C and 186 °C and also *G'* is smaller than *G''* in the measurement window, which indicates amorphousness.
The modification using hydrophobic acid derivatives has a decreasing effect on the glass transition temperature compared to the starting material (Figure 46). The modification using cinnamic acid slightly decreases the glass transition temperature with increasing modification degree. At 11% modification with cinnamic acid resulted in a small decrease of only 2°C from 139 °C to 137 °C compared to the starting material. In the case of hydro cinnamic acid a strong decreasing influence on the glass transition temperature was observed. At 11% modification a decrease of 33 °C to a T_g = 106 °C was observed. Modifications utilizing ethyl hexanoic acid as modification showed low modification degrees of 1% to 2% and thus a low difference in T_g by 5 °C. Palmitic acid modification had the largest effect in the reduction of the glass transition temperature, where a 28% modification decreased the glass transition temperature to 75 °C. It can be concluded that for the modification using hydro cinnamic acid and palmitic acid a strong reducing effect on the glass transition effect was observed, whereas the modifications with cinnamic acid only had a slight reducing effect. No effect can be ascribed to ethyl hexanoic acid, as no polymer could be synthesized bearing more than 2% modified hydroxyl functions and therefore no significant change was observed.

The modification introducing apolar moieties has a slight reducing effect on the glass transition temperature (Figure 46). Especially for **apolar-III** modified polymers a pronounced effect was observed. Utilizing **apolar-I**, only a minor decreasing effect was observed. The influence in T_g was also observed during melt rheology experiments, where **apolar-III** showed reduced processing temperatures

and **apolar-I** showed little effect compared to the benchmark polymer PVAc-co-PVP. **apolar-III** polymers showed a melting range in DSC measurements, which may lead to challenges in their extrudability, as usually an extrusion is only feasible above the melting range. In terms of their degradation temperature (Figure 47), it is evident, that at higher modification degrees, the thermal stability is below the targeted 200 °C for the modification with apolar-I and apolar-III. Apart from these entities, the polymers are stable above 200 °C. In conclusion, apolar modification with **apolar-I** cannot be used for the reduction in processing temperatures as only slight reduction in glass transition temperature is visible. In conjunction with the degradation behavior, only a narrow range for processing can be utilized. Despite this, the aromatic moiety may have a favorable influence on the dissolution performance. This will be described in a later chapter.

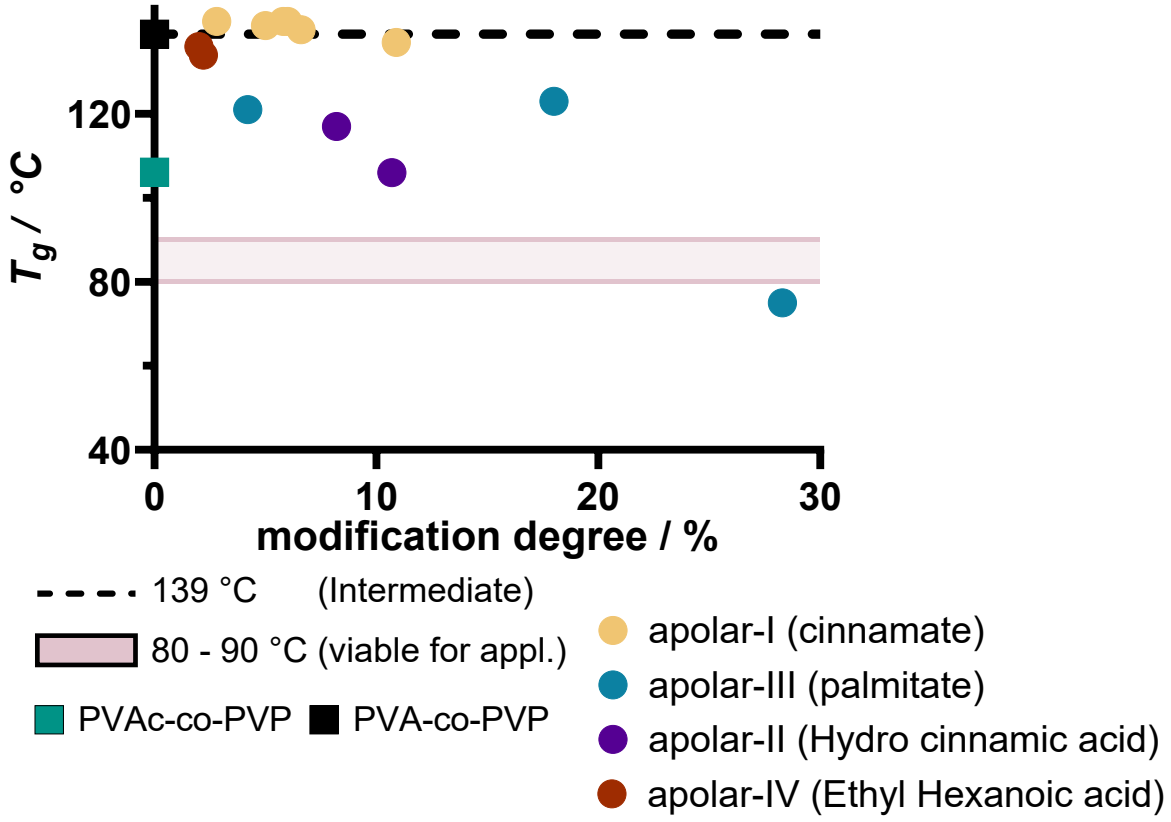

Figure 46: Glass transition temperatures against modification degree for each synthesized polymer with apolar comonomers. Dashed black line is shown to guide the reader's eye and symbol indicates the glass transition temperature of PVP-co-PVA before modification. The glass transition temperature of PVAc-co-PVP is indicated in green. The red box marks the targeted temperature range.

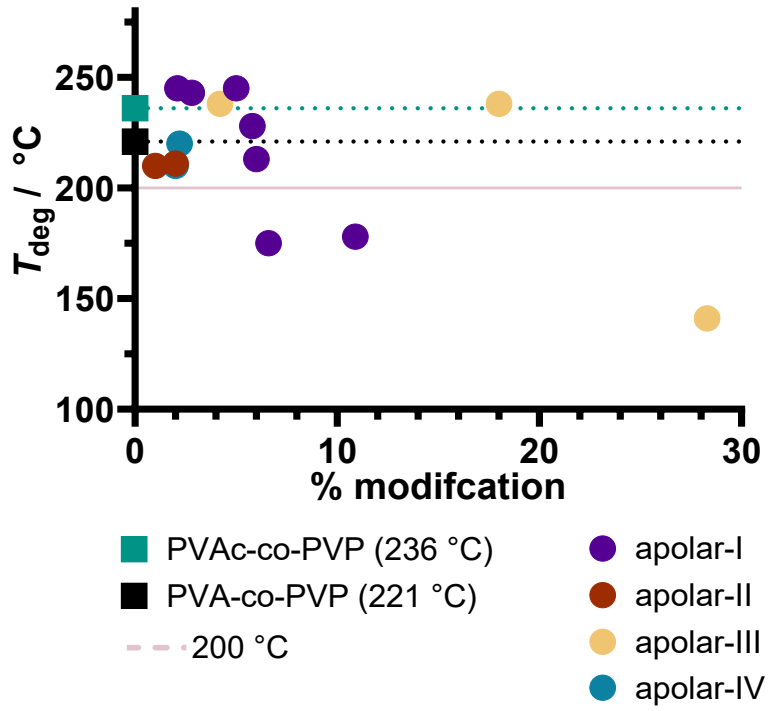

Figure 47: Degradation temperatures against modification degree for each synthesized polymer with hydrophobic acid comonomers. Pointed lines (black and green) are shown to guide the eye indicating the degradation temperatures of the starting material PVAc-co-PVP and of the base polymer PVA-co-PVP. The pink line at 200 °C is the temperature above which the polymer should be stable for enabling a broad manufacturing range.

5.2.5.3.3 Extrusion

The polymers **apolar-Id** and **apolar-IIIb** were extruded using a small-scale twin-screw extruder at 300 revolutions per minute. Extrusion of cinnamic acid modified **apolar-Id** resulted in brown, moderately transparent filaments at higher temperatures of 165 °C. The filaments were brittle and die swelling occurred during the extrusion. At lower temperatures no extrusion was possible due to high average torque values near 1.85 N m and formation of opaque extrudates. The average torque decreased by increasing the temperature and the filament were transparent at higher temperatures. The residence time of the polymer was long compared to mPEG modified entities indicating lower flowability of the polymer melt. During the extrusion of palmitic acid functionalized **apolar-IIIb** between 130 °C and 140 °C, transparent filaments were obtained with little die swelling and low average torque values between 1.0 N m and 0.8 N m. The yellow filaments were less brittle than PVP-co-PVA.

Table 22: Summary of Extrusion experiment for amine modified polymer **apolar-Id** (T_g = 142 °C, T_{deg} = 213 °C).

Polymer	**apolar-Id**	**apolar-Id**	**apolar-Id**
Temperature / °C	100/145/145	100/155/155	100/165/165
RPM / min^{-1}	300	300	300
average torque / Nm	1.85	1.35	1.1
nozzle / mm	1.5	1.5	1.5
Appearance	brown	brown	brown
Translucence	opaque	transparent	transparent
Flexibility	brittle	brittle	brittle
Filament			
Extrusion possible	**No**	**Yes**	**Yes**

Table 23: Summary of Extrusion experiment for amine modified polymer **apolar-IIIb** (T_g = 123 °C, T_{deg} = 238 °C).

Polymer	**apolar-IIIb**	**apolar-IIIb**
Temperature / °C	120/130/130	115/140/140
RPM / min^{-1}	300	300
average torque / Nm	1.0	0.8
nozzle / mm	1.5	1.5
Appearance	Greenish yellow	brown
Translucence	Transparent	transparent
Flexibility	Flexible	flexible
Filament		
Extrusion possible	**Yes**	**Yes**

5.2.5.3.4 Scale-Up

Polymers with high potential in this group are **apolar-I** modified and **apolar-III** modified polymers (Table 24). Polymers carrying **apolar-I** and **apolar-III** in their side chain showed lower water solubility

in dissolution tests and during synthesis. This led to a threefold increased use of water during dialysis of the crude reaction product. This can be attributed to the hydrophobic nature of both moieties introduced into the side chain. Due to the increased amount of water required to dissolve the functionalized polymer, a direct transfer of the synthesis procedure was not possible. The dialysis of three times the amount of aqueous solution was not feasible in the setting of the cooperating process development laboratory. Therefore, polymers with lower modification degrees were synthesized and dialyzed by Oliver Stranowsky (*Merck Electronics KGaA*) with the aforementioned procedure without any other alterations. The polymers **apolar-Ig** and **apolar-IIIc** were obtained in moderate yields of 80% (189 g) and 72% (160 g) respectively. The synthesis showed good reproducibility considering the targeted modification degree and the thermal properties of the polymers were as expected. The mean molecular weight is in the expected range. Small-scale Extrusion of **apolar-Ib** lead to increased torque values and melt rheological measurements indicated possible extrusion at higher temperature above 180 °C. Even though high temperatures are needed for the extrusion, the cinnamic acid modification may be interesting for their potential in solubility enhancement. The extrusion, conducted by Alessandro-Giuseppe Elia (*Merck Life Science KGaA*) utilizing **apolar-Ig** was not possible as the maximum torque threshold of the *Pharma 11* extruder was exceeded. The intermediate-scale extrusion of **apolar-IIIc** was possible with high torque and low die pressure at high temperatures of 190 °C. Both polymers may be interesting for their performance in solubility enhancement, but the modification does not reduce the processing temperatures and thus, to not fit the prerequisites for a candidate with high potential (Section 5.1).

Table 24: Analytical data of lab-scale apolar modified polymers in comparison to the respective upscaled 200 g batches.

		apolar-Ib	apolar-Ig	apolar-IIIb	apolar-IIId
NMR	Modification degree	5.0%	2.1%	18.0%	4.2%
GPC	M_w				
DSC	$T_g \geq$ 80-90 °C	141 °C	135 °C	123 °C	125 °C
DSC	No T_m, amorphous	no T_m	no T_m	163 °C	no T_m
Mini Extruder	Transparent filaments	increased torque	n.d.	low torque	n.d
TGA	$T_{deg} \geq$ 200 °C	245 °C	n.d	238 °C	n.d
Melt viscosity	η_{melt} =1000 – 10000 Pa·s @ 0.1 rad s^{-1}	192- >220°C	180-220°C	141-165°C	153-186°C
Process window	η_{melt} < 10 000 Pa s; below T_{deg} > 40-50°C	Δ = 28 °C	Δ =35 °C	Δ = 24.5 °C	Δ =33 °C
intermediate-Scale Extrusion		n.d.	Torque limit exceeded	n.d.	High torque low die pressure

5.2.5.3.5 Dissolution experiments

The polymers **apolar-Id**, **apolar-Ig**, **apolar-IIIc**, and **apolar-IIId** were tested in the aforementioned assays (5.2.5.1.5, p79) conducted by Nabil Lamrabet (*Merck Life Science KGaA*). Polymers **apolar-Id** and **apolar-Ig** show values over 100% realease (Figure 48). This is not possible, as no more than 100% of caffeine used in the formulation of the test specimen can be released during the assay. The wavelength utilized for the detection of the UV-active transitions present in caffeine is 272 nm. The modifications include the introduction of another π-electron system, the conjugated aromat *trans*-cinnamic acid, which also has UV-active bands at this wavelength and interferes with the measurement method. Therefore, the results obtained for these polymers are not indicative of the real release kinetics of the polymer samples.

The palmitic acid modified polymers **apolar-IIId** and **apolar-IIIc** were analyzed concerning their release kinetics (Figure 49). **Apolar-IIIc** shows a slower onset of release approaching the maximum after 150 min and 116 ± 16%. **Apolar-IIId** shows a faster onset of release approaching the maximum after 90 minutes and 193 ± 9%. Both polymers show values over 100%, which may be attributed to absorption of the modification agent palmitic acid in the tested wavelength. Therefore, the results are not indicative of the real release kinetics of the polymer samples.

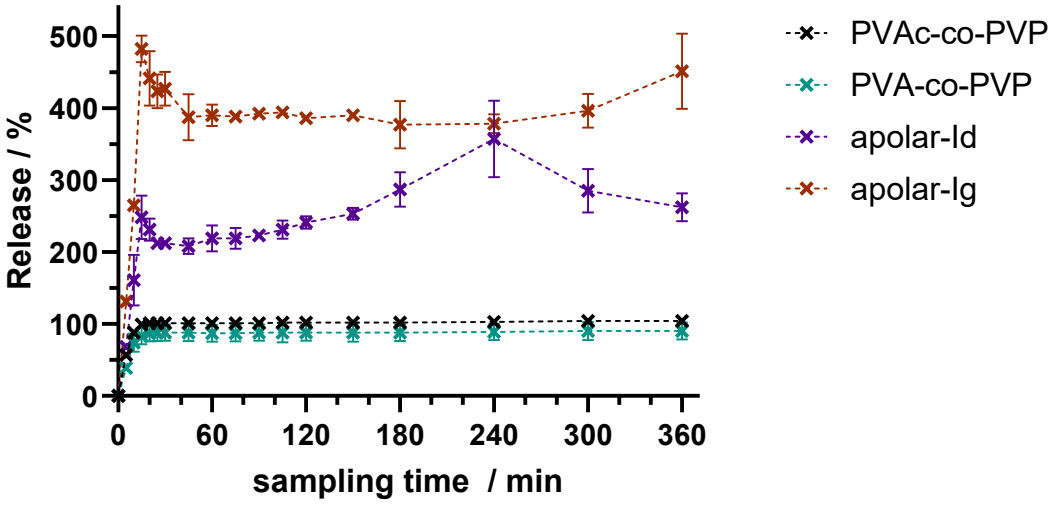

Figure 48: Release kinetics of selected polymers in comparison with benchmark PVAc-co-PVP (Kollidon® VA64) in caffeine assay. Amorphous sample discs were prepared by VCM. Non-sink dissolution of amorphized samples through melt quenching in 0.1 M HCl at 37 °C, 75 rpm and 900 mL medium. Drug: Caffeine at 10% drug load in 300 mg specimen, arithmetic means ± SD (n = 3). UV-VIS Analysis at λ = 227 mm. Discs were prepared by MeltPrep method and used as is. Dashed lines incorporated to guide the reader's eye.

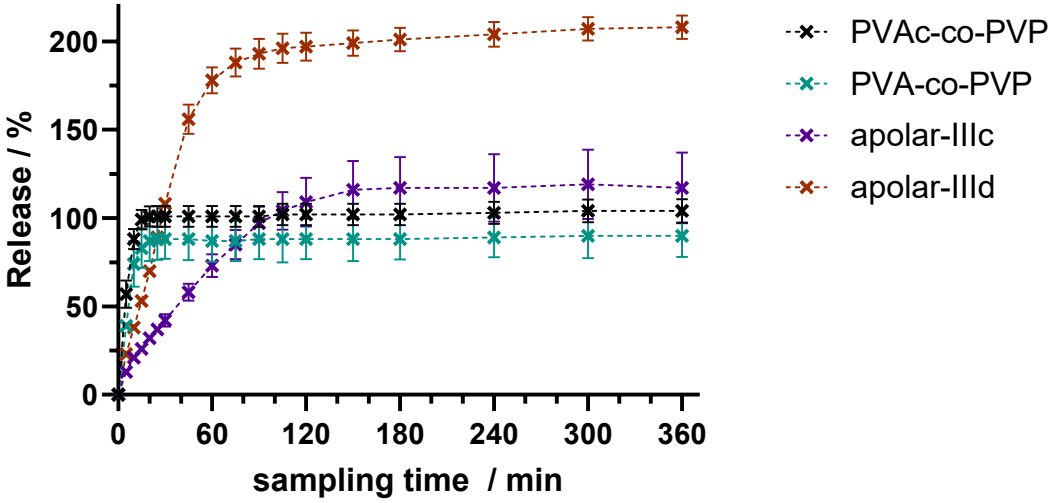

Figure 49: Release kinetics of selected polymers in comparison with benchmark PVAc-co-PVP (Kollidon® VA64) in caffeine assay. Amorphous sample discs were prepared by VCM. Non-sink dissolution of amorphized samples through melt quenching in 0.1 M HCl at 37 °C, 75 rpm and 900 mL medium. Drug: Caffeine at 10% drug load in 300 mg specimen, arithmetic means ± SD (n = 3). UV-VIS Analysis at λ = 227 mm. Discs were prepared by MeltPrep method and used as is. Dashed lines incorporated to guide the reader's eye.

Utilizing the previously mentioned assay to test the performance of the polymer matrix in terms of solubility enhancement, **apolar-IIIc** and **apolar-IIId** were tested incorporating KTZ as API. The assays were conducted by Nabil Lamrabet (*Merck Life Science KGaA*).

Comparing apolar modified polymers with the starting material PVAc-co-PVP, a longer onset time can be observed. This may result from slower solubility in the testing medium and therefore slower release, which was also observed for **apolar-III** modified polymers during the caffeine assay. The maximum in concentration is reached after 60 minutes considering the polymers **apolar-Id**, **apolar-Ig** and **apolar-IIId**. During the measurement time, no maximum was observed for **apolar-IIIc**, which may be reached on a later time point. No statement can be made about the behavior after 120 minutes. The maximum concentration reached while testing modified polymers is lower than for the starting material PVAc-co-PVP. The AUC is similar for **apolar-I** modified polymers in the range of 22000 to 25000 for **apolar-Ig** and **apolar-Id** respectively, while the **apolar-III** modified polymers reach an AUC of 14000 in both cases. Comparing the modified polymers with PVAc-co-PVP, possessing an AUC of 40000 ± 5000, suggests, that the modified polymers have a lower capability in terms of supersaturation, but still lead to a strong improvement compared to crystalline KTZ. All polymers show an improvement compared to crystalline KTZ, but **apolar-I** modified polymers demonstrate a higher capability than **apolar-III** modifications. In comparison to **mPEG-IIg**, **apolar-Id** has an increased performance considering the *AUC* resulting in an increase of 22000 ± 3000 to 25000 ± 3000 and also the maximum concentration is increased from 241 ± 19 µg mL^{-1} to 285 ± 56 µg mL^{-1}. These results indicate that **apolar-I** (cinnamic acid) modifications have a stronger polymer/API interaction than **mPEG-II** modifications, even with a lower modification degree (compare 6% for **apolar-Id** and 9**%** for **mPEG-IIg**).

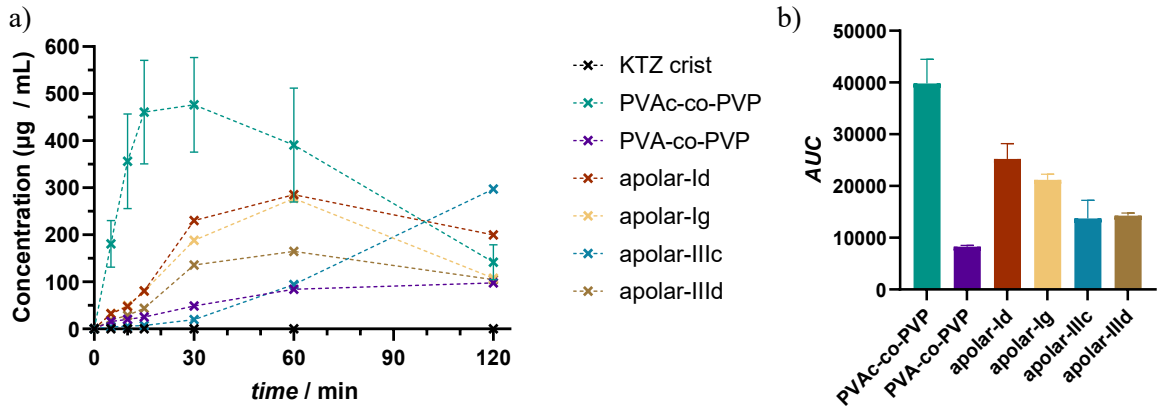

Figure 50: a) Dissolution capabilities of selected polymers and benchmark PVAc-co-PVP (Kollidon® VA64) in comparison to pure, crystalline API. Amorphous sample discs were prepared by VCM. Non-sink dissolution of amorphized samples through melt-quenching in FaSSIF at pH 6.5 at 37 °C. Concentration of 0.75 mg drug per mL medium, arithmetic means ± SD (n = 3), drug: Ketoconazole at 40% drug load; HPLC analysis at λ = 225 mm. Discs were prepared by MeltPrep method and used as is. Dashed lines incorporated to guide the reader's eye; b) Corresponding *AUC* of the dissolution measurements for comparison of dissolution capability.

5.2.5.3.6 Conclusion

In conclusion, polymers modified with cinnamic acid and palmitic acid were extrudable in the temperature range tested. The glass transition temperature of the PVP-co-PVA base polymer is not

significantly changed by modification with cinnamic acid, but greatly reduced by modification with palmitic acid. Cinnamic acid can not be used for the reduction of the processing temperature, while palmitic acid may be utilized for the reduction of the processing temperature. High modification degrees of palmitic acid lead to the formation of a melting point as observed in DSC measurements, which may be due to interactions between the palmitic acid groups in a singular polymer chain or between different polymer chains. Due to this reason, only low amounts of palmitic acid should be introduced into the side chain to retain amorphousness after the modification. Extrusion experiments in small-scale as well as larger scale led to high torque for both **apolar-I** and **apolar-III** modification, rendering these polymers unfit for pharmaceutical extrusion. High temperatures were needed for the processing of the polymers, which also make them unfit for the objective of process temperature reduction. The apolar modifications induce increased polymer/API interactions as confirmed by dissolution experiments with KTZ when comparing with the base polymer PVA-co-PVP. Furthermore, even at lower modification degrees (6% in **apolar-Id**), the polymers in this group show increased performance compared to mPEG modifications at higher modification degrees (9**%** for **mPEG-IIg**) in both *AUC* and maximum API-concentration. Even though, extrusion was not possible at intermediate scale due to high torque, **apolar** modifications have a favorable influence on the dissolution capabilities compared to all other modified polymers. Especially **apolar-I** modified polymers enhance the solubility of KTZ compared to tested benchmarks.

5.2.5.4 Miscellaneous acids

5.2.5.4.1 Synthesis

Next to the previously discussed modification agents, other functional groups and chemical motifs were tested concerning their influence on the properties of PVA-co-PVP. These modification agents bear additional carbonyl groups, namely a keto-, or an ester group. The modification agents used were 4-oxopentanoic acid (**misc-I**) and 3-ethoxy-3-oxopropanoic acid (**misc-II**) (Scheme 12). These modification agents were used in an analogous manner as other carboxylic acids utilized in this study (Scheme 8). Polymers with a modification degree of 1% (**misc-Ia)** and 2% (**misc-Ib**) were obtained using **misc-I**. By using **misc-II**, two polymers were obtained with a modfication degree of 4% (**misc-IIa**) and 7% (**misc-IIb**). These findings were confirmed by ^{1}H-NMR spectroscopy. The analytical characterization will be given in the following section. A summary of all analytical results for the modified polymers is given in Table 25.

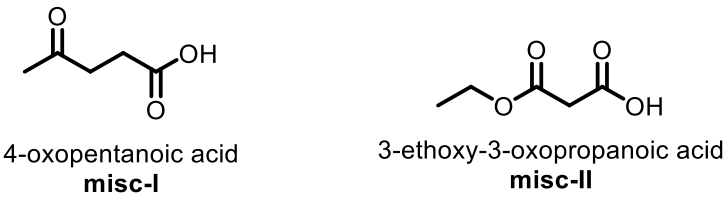

Scheme 12: Miscellaneous acid derivatives used in this work for the modification of PVP-co-PVA via esterification.

For the analysis of the modification degree in **misc-Ia** and **misc-Ib**, the methylene c^{3} proton signal between 2.66 ppm and 2.56 ppm was utilized (Figure 51). The proton signal c^{5} between 1.22 ppm and 1.15 ppm was utilized for the analysis of **misc-IIa** and **misc-IIb** (Figure 52).

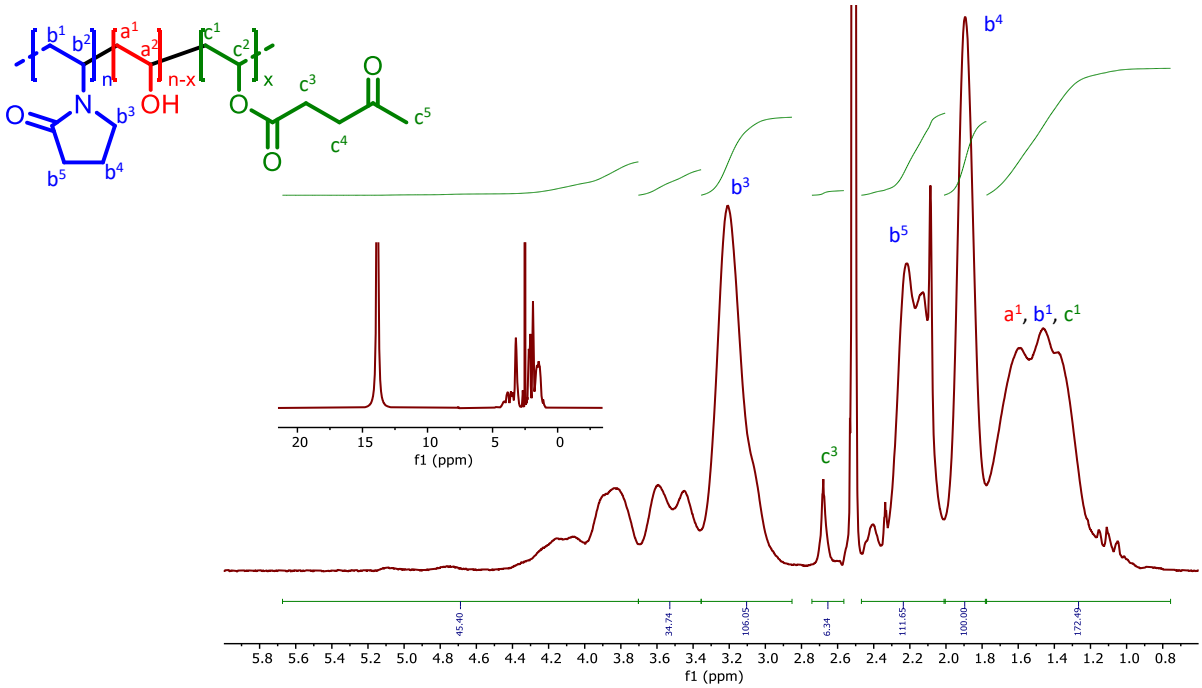

Figure 51: Exemplary quantitative ^{1}H-NMR spectrum of **misc-Ia** modified PVP-co-PVA. Modification degree 1.0%.

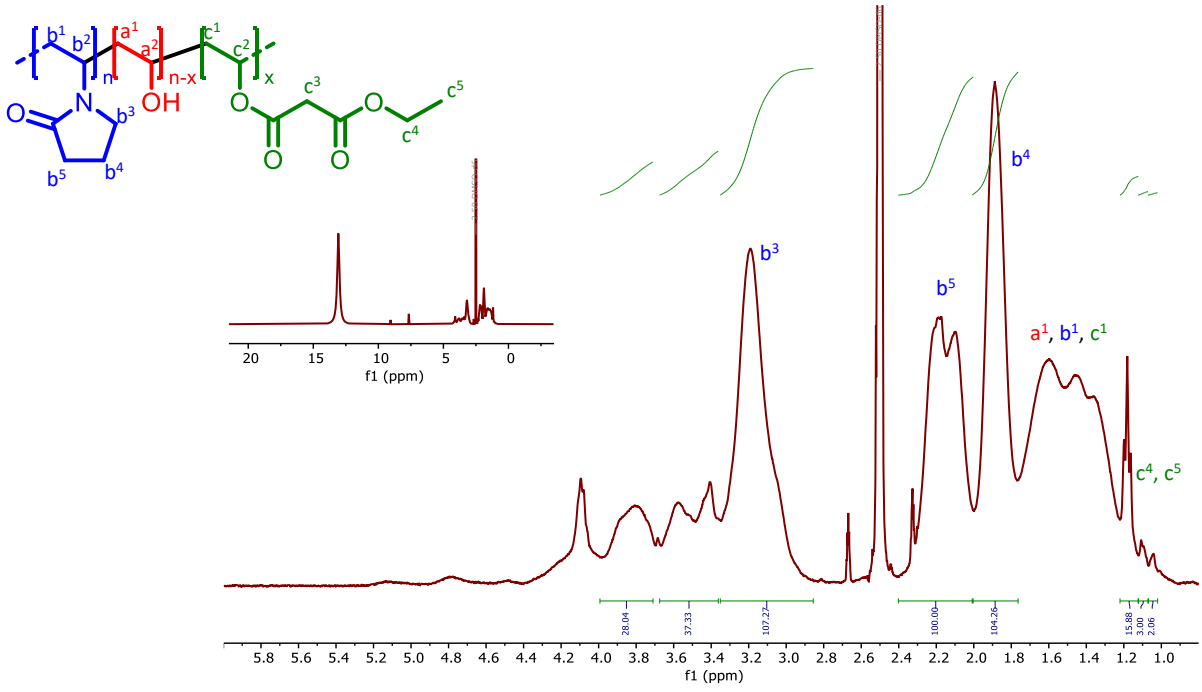

Figure 52: Exemplary quantitative ^{1}H-NMR spectrum of **misc-IIa** modified PVP-co-PVA. Modification degree 4.0%.

5.2.5.4.2 Characterization

The polymer modifications were analyzed by DSC, TGA, and GPC. Modification degrees for **misc-I** modified polymers were very low, and DSC analysis showed little reduction of the glass transition temperature from 139 °C to 133 °C (Figure 53a). Thermal stability remained high at around 229 °C as

confirmed by TGA measurements (Figure 53b). The average molecular weight increased slightly to M_w = 31000 g mol^{-1} (Figure 53c). Due to the low changes in the polymer properties, no further analysis was conducted.

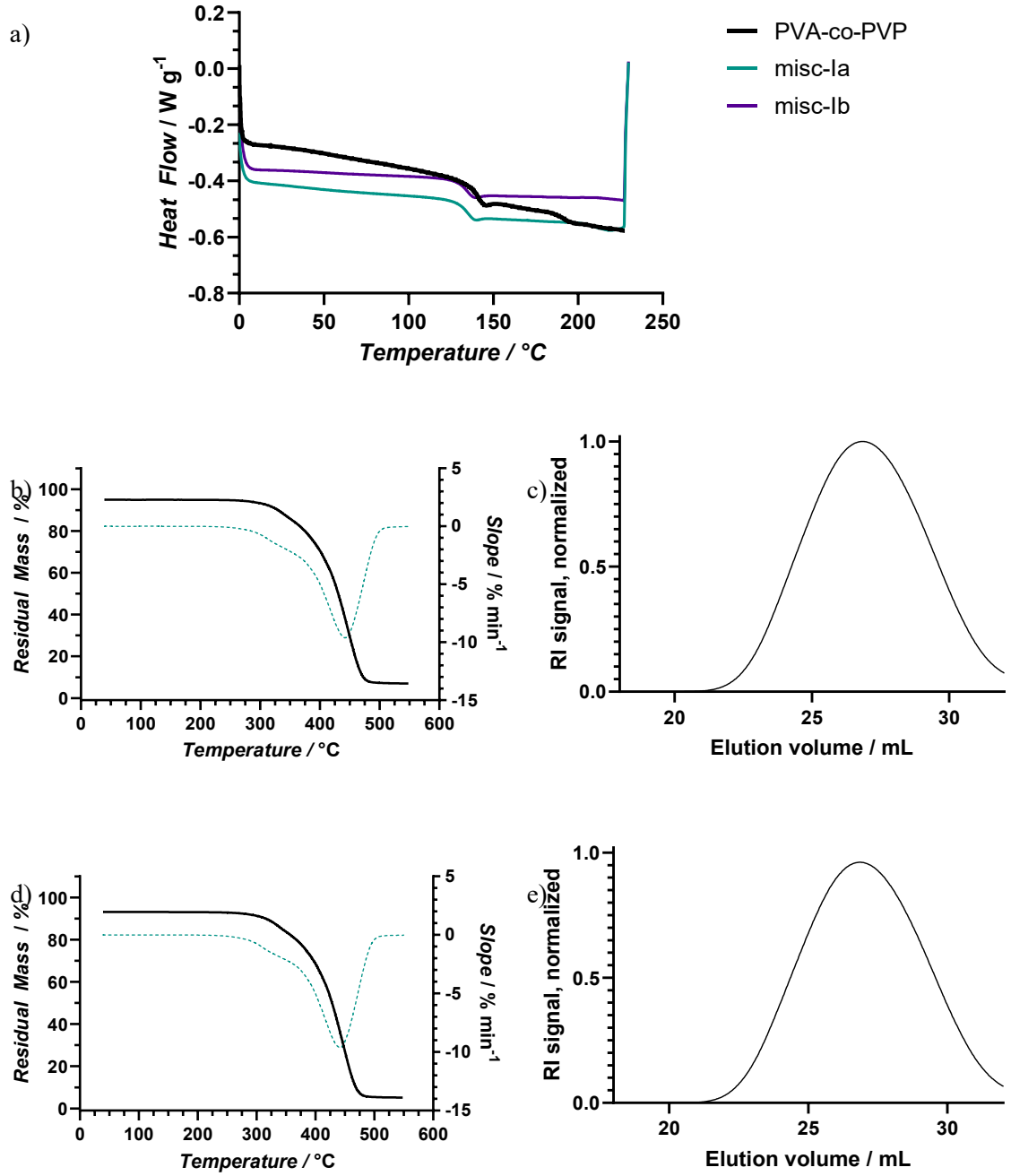

Figure 53 a) DSC of **misc-I** modified polymers, $T_{g,a}$ = 133 °C, $T_{g,a}$ = 133 °C; b) TGA thermogram of **misc-Ia**. Degradation starts at $T_{deg,a}$ = 229 °C; c) GPC elugram for **misc-I**. $M_{w,a}$ = 31000 g mol^{-1}, $Đ_a$ = 3.1; d) TGA thermogram of **misc-Ib**. Degradation starts at $T_{deg,b}$ = 232 °C; e) GPC elugram for **misc-Ib**. $M_{w,b}$ = 31000 g mol^{-1}, $Đ_a$ = 2.6.

Misc-IIa and **Misc-IIb** showed slightly increase glass transition temperatures compared to the base polymer PVP-co-PVA at T_g = 143 °C and T_g = 147 °C respectively. The analyzed polymers analyzed degrade in a two-step degradation process, whereas PVP-co-PVA degrades in a single-step degradation (Figure 19). This second degradation step may result from the degradation of the newly formed side chain after the modification. The thermal stability decreased substantially, as degradation was visible via TGA at T_{deg} = 124 °C and T_{deg} = 126 °C. Furthermore, the average molecular weight sharply increased to M_w = 60000 g mol^{-1} and 138000 g mol^{-1}. In addition to high molecular weight, the dispersity index increased significantly to $Đ$ = 4.9 and $Đ$ = 9.4. The surprisingly high increase in average molecular weight to more than double, while observing a relatively low modification degree of 4% and 7% indicate crosslinking. This could have happened via the α-acidic proton present in the maleic acid derivative **misc-II**, as imidazole forms during the precursor synthesis and the modification reaction and generates a basic environment in the non-aqueous solvent DMF. Due to this, and the relatively low thermal stability, **misc-IIa** and **misc-IIb** were not analyzed further, as the specifications are not met.

Table 25: Compilation of analytical data obtained for miscellaneous modified polymers.

	Yield / %	Mod. Deg. / % of -OH	T_g (DSC) / °C	T_{deg} (TGA) / °C	M_w (GPC) / g mol^{-1}
misc-Ia	66	1.0	133	229	30750
misc-Ib	76	2.0	133	232	30600
misc-IIa	88	4.0	143	124	
misc-IIb	83	7.0	147	126	

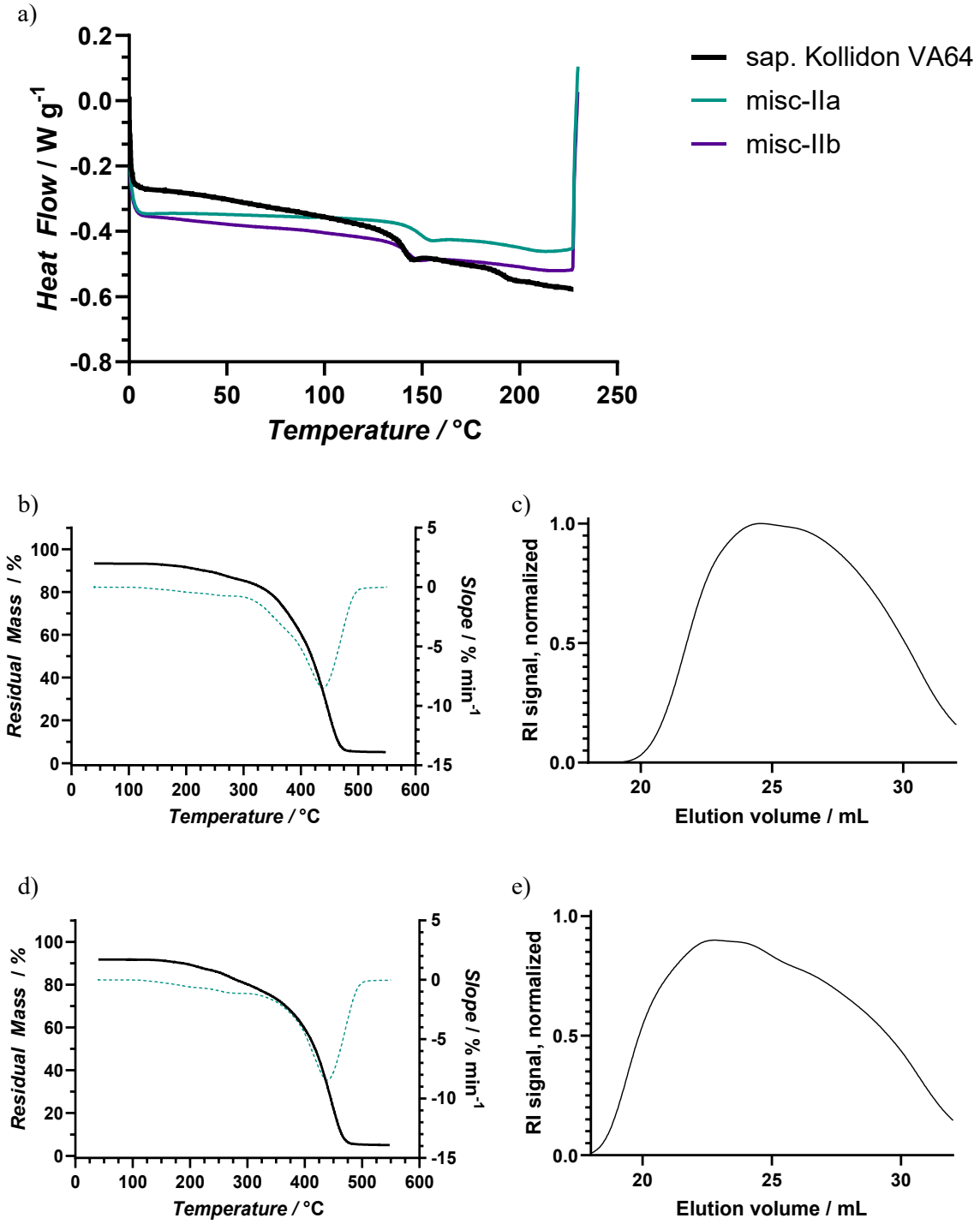

Figure 54: a) DSC of **misc-II** modified polymers, $T_{g,a}$ = 143 °C, $T_{g,a}$ = 147 °C; b) TGA thermogram of **misc-IIa**. Degradation starts at $T_{deg,a}$ = 124 °C; c) GPC elugram for **misc-IIa**. M_w = 59800 g mol^{-1}, M_p = 59000 g mol^{-1}, $Đ$ = 4.9; d) TGA thermogram of **misc-IIb**. Degradation starts at $T_{deg,b}$ = 126 °C; e) GPC elugram for **misc-IIb** , M_w = 138000 g mol, M_p = 126000 g mol^{-1}, $Đ_a$ = 9.4.

5.2.5.5 Qualitative Trends and Structure Property Relationships

The different groups of modification agents each showed an impact on the resulting polymers properties such as the processing temperatures in form of altered T_g, T_{deg}, $T_{1000\ Pa\ s}$, $T_{10000\ Pa\ s}$ and their dissolution properties such as the dissolution kinetics in the caffeine tests or the respective AUC in combination with the model API KTZ. Qualitative trends can be observed and can be summarized (Table 26). The miscellaneous modifications were omitted due to the strong increase in their molecular weight during the modification reaction using **misc-II** and the low modification degrees obtained with **misc-I**.

Assessing the overall performance of the modification using mPEG derivatives, it can be concluded, that introducing these moieties into the polymer backbone strongly decreases the processing temperature range accompanied with a decrease in glass transition and only a slight decrease in terms of thermal stability. The incorporation of these chemical entities into the backbone has a favorable effect on the overall manufacturability, even at low modification degrees. mPEG modification does not change the dissolution kinetics in caffeine tests significantly but increases the maximum concentration of KTZ as observed by an increase of AUC in KTZ dissolution testing and when compared to the base polymer PVA-co-PVP. PVAc-co-PVP outperforms all mPEG modified polymers in KTZ dissolution tests.

Modification with substituted amines leads to a slight decrease in T_g and T_{deg} and melt rheology measurements indicate no significant change in their processing range. No significant improvement was observed when PVA-co-PVP was modified with these entities, therefore the dissolution properties were not tested.

The hydrophobic (apolar) modification by aromatic and alkyl substituted carboxylic acid was assessed separately. The introduction of aromatic groups into the backbone of PVA-co-PVP leads to a slight decrease in thermal stability, while the T_g mostly remained unchanged. Despite these properties, melt rheology measurements showed an increase in the required temperature to achieve melt viscosities, where an extrusion is possible. **apolar-I** modification caused higher solubility of KTZ in dissolution tests, with increased KTZ concentration and AUC compared to PVA-co-PVP.

Apolar alkyl modification of PVA-co-PVA led to a strong decrease in T_g with increasing modification degree. A slight decrease in T_{deg} at low modification degrees and a very strong decrease at higher modification degrees (**apolar-IIIc**). The modification led to a delayed release of caffeine which can be attributed to lower solubility and an increase in KTZ maximum concentration as well as AUC. Despite the improvements observed for apolar modifications compared to PVA-co-PVP, PVAc-co-PVP outperforms all apolar modified polymers in KTZ dissolution tests.

Table 26: Qualitative trends observed after the modification of PVA-co-PVP with a multitude of different agents. Upwards arrows indicate an increase, downwards arrows indicate a decrease in the specific property. Arrows pointing to the right indicate no significant change in the property. The impact on a property is judged based on the properties of the base polymer with the aim to influence the target property to fulfil the proposed ideal properties defined in Section 5.2. Green arrows indicate a strong influence, yellow arrows a weak influence on the property.

Group	**Impact on polymer property considering target property (arrow indicates direction)**				
	Glass transition T_g	Thermal stability T_{deg}	Processing Temperature $T_{1000\ Pa\ s}$ and $T_{10000\ Pa\ s}$	Dissolution kinetics Time until 90% release of caffeine	*AUC* KTZ dissolution compared to PVA-co-PVP
mPEG derivatives	Strong decrease	Slight decrease	Strong decrease	equally as fast	increase in performance
Substituted Amines	Slight decrease	Slight decrease	No significant change	not analyzed	not analyzed
apolar acids aromats	No significant change	Slight decrease	Increased processing Temp.	inconclusive due to measurement method	Strong increase in performance
apolar acids alkyl	strong decrease	Slight decrease	Strong decrease	delayed release	increase in performance

In summary, no single modification resulted in the ideal polymer for the solubility enhancement of KTZ and the reduction of the processing temperatures. In terms of processing temperatures, mPEG modifications led to polymers with the highest potential. More precisely, **mPEG-II** (mPEG2 aa) modification led to a moderate decrease in degradation temperature and a strong decrease in glass transition temperature with increasing modification degree leading to processing temperatures during extrusion which fit the proposed target properties. Qualitatively, **mPEG-II** modification had no negative effect on the solubility in organic solvents of the resulting polymer. The modification using **apolar-I**

(cinnamic acid) had the most significant impact on the dissolution performance rendering this kind of modification to have the most potential for further development. In an attempt to combine the favorable influences of more than one modification agent, **mPEG-II** and **apolar-I** may be used simultaneously to achieve a decrease in processing temperature and a significant increase in dissolution performance.

5.2.5.6 Combined mPEG and hydrophobic modification

5.2.5.6.1 Synthesis

By modification with mPEG derivatives the processing temperatures can be influenced significantly as highlighted in Section 5.2.5.1. Furthermore, hydrophobic moieties in a polymer have a favorable influence on the performance in dissolution enhancement as discussed in section 5.2.5.6. **mPEG-II** and **apolar-I** were utilized in the same reaction mixture for the modification of PVP-co-PVA (Scheme 13). Both modification agents were used simultaneously to improve the processing temperatures on the one hand, and on the other hand induce favorable polymer/API interactions for the solubility enhancement.In Section 5.2.5.1, a modification degree of 13% of **mPEG-II** was found to decrease the glass transition temperature of the resulting polymer to 90 °C, which is in line with the targeted specifications. Therefore, it was aimed to reach this modification degree for **mPEG-II** while varying the modification degree of **apolar-I** to determine its influence on the processing temperatures. Precursors were synthesized separately and used as discussed in previous section in the modification reactions. In total, 10 polymers were synthesized with a modification degree of 6% to 13% **mPEG-II** and 0.5% to 5% **apolar-I**. The analytical characterization will be given in the following section. A summary of all analytical results for the modified polymers is given in Table 27.

2-(2-(2-methoxyethoxy)ethoxy)acetic acid
mPEG2 acetic acid
mPEG II

cinnamic acid
apolar-I

Scheme 13: Hydrophobic acid derivative and mPEG derivative used in this work for the modification of PVP-co-PVA in combined modification strategy.

As described in previous chapters, the modification degree of **mPEG-II** was determined by the proton signal for the methoxy group (d^8) in the ^1H spectrum 2.84 and 3.34 ppm and the degree of modification of **apolar-I** by the signals for the aromatic protons between 7.19 and 8.19 ppm (Figure 55). Spectra of remaining polymers can be found in the Appendix.

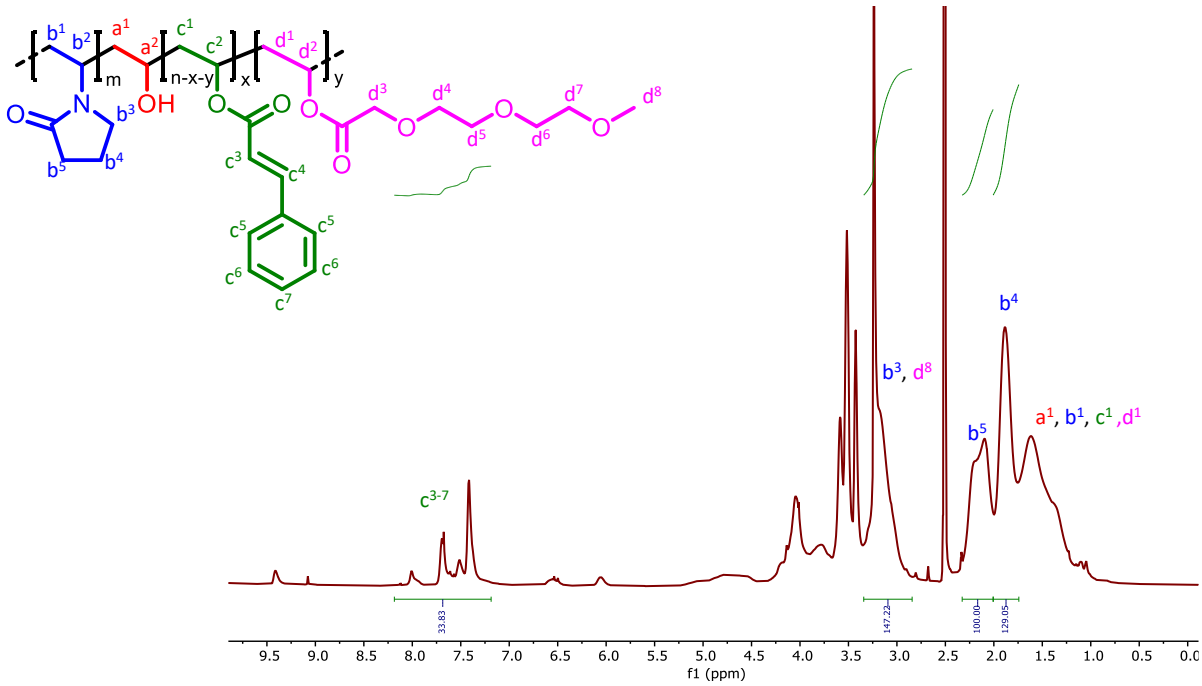

Figure 55: NMR Combined Modification

5.2.5.6.2 Characterization

DSC analysis showed the expected reduction in glass transition temperature with increasing modification degree of **mPEG-II**, as observed in previous modifications using **mPEG-II** (Table 12). The influence on the T_g by the separate modification agents cannot be characterized independently, but it can be argued, that the reducing influence on the T_g by **mPEG-II** is larger than **apolar-I** has on the T_g. The modification with **mPEG-II** was utilized to reduce the processing temperatures to fit the specifications. The lowest T_g observed was 59 °C for **mPEG-II/apolar-Ii** with a modification degree of 10% **mPEG-II**, while the highest was 190 °C for **mPEG-II/apolar-Ia** with a modification degree of 6% **mPEG-II**. These results are in line with the results obtained for **mPEG-II** modifications. A melting range was observed for **mPEG-II/apolar-If** around 187 °C.

The polymers analyzed degrade in a two-step degradation process, whereas PVP-co-PVA degrades in a single-step degradation (Figure 19). This second degradation step may result from the degradation of the newly formed side chains after the modification as was also observed while using one of the modification agents. The degradation temperatures of obtained for the polymer entities are reduced compared to PVA-co-PVP, but very close to 200 °C in all cases. This aspect is tolerable for the manufacturing *via* extrusion.

GPC analysis of **mPEG-II/apolar-Id** showed an increase of the mean molecular weight compared to PVP-co-PVA (29000 g mol^{-1}) to M_w = 57000 g mol^{-1}. The decrease in glass transition temperature and the increase in mean molecular weight while the degradation temperature remains above 200 °C in most

cases, indicate a successful modification of the base polymer to form polymers fitting the specifications. The polymer **mPEG-II/apolar-Id** appears to be the polymer entity with the highest potential for later application in pharmaceutical extrusion and was reproduced 4 times to obtain a larger amount of material. The polymers **mPEG-II/apolar-Ig** to, **mPEG-II/apolar-Ij** were synthesized in an identical way to **mPEG-II/apolar-If** and good reproducibility was observed after analysis via NMR, DSC and TGA.

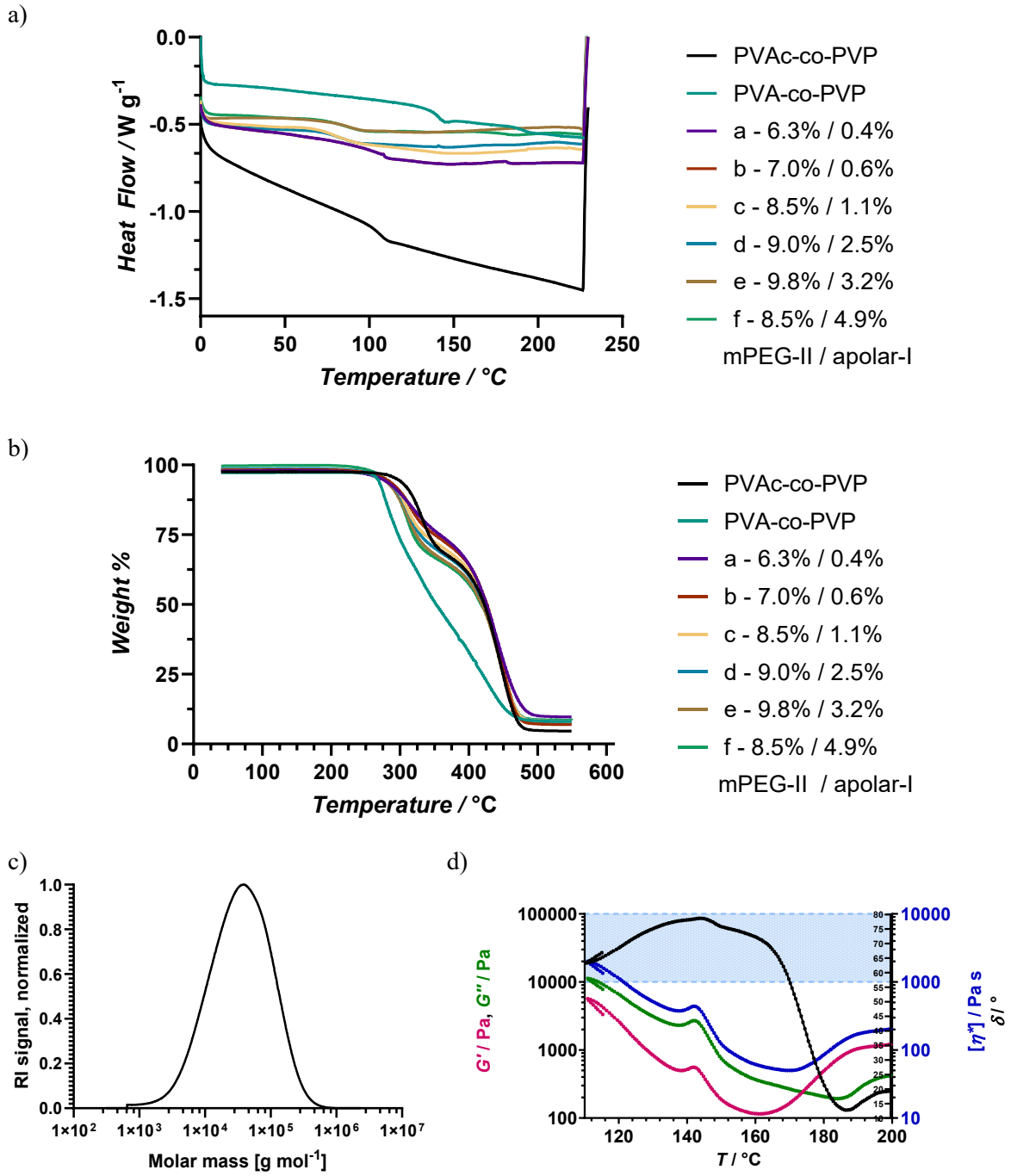

Figure 56: a) DSC of **mPEG-II/apolar-I** modified polymers; b) TGA thermograms of **mPEG-II/apolar-I** modified polymers; c) GPC elugram of **mPEG-II/apolar-Id**. M_w = 56000 g mol^{-1}, M_p = 36000 g mol^{-1}, $Đ$ = 3.2; Additional analytical data such as glass transition temperatures and degradation temperatures can be found in Table 27.

By modification of the hydroxyl moieties in PVA-co-PVP with mPEG-II, the glass transition temperature is significantly lowered with increasing PEG modification degree (Figure 57). Consequently, the glass transition temperature can be controlled while the degradation temperature remains nearly unchanged and above 200 °C for most of the polymers (Figure 58). The simultaneous

modification with apolar-I does not have a strong decreasing effect on the thermal stability as was observed in the modification with apolar-I only. The combined modification with mPEG-II and apolar-I leads to polymers with favorable glass transition temperatures in the range viable for extrusion and additionally their degradation temperature remains above 200 °C. These circumstances make them viable for further testing in melt rheology.

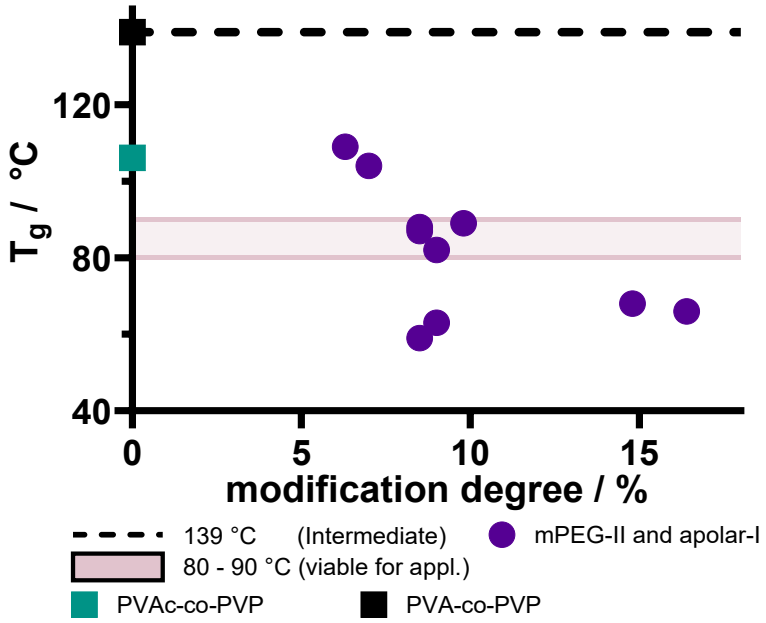

Figure 57: Glass transition temperatures against modification degree for each synthesized polymer with a combined mPEG-II and apolar-I modification. Dashed black line is shown to guide the reader's eye and symbol indicates the glass transition temperature of PVP-co-PVA before modification. The glass transition temperature of PVAc-co-PVP is indicated in green. The red box marks the targeted temperature range.

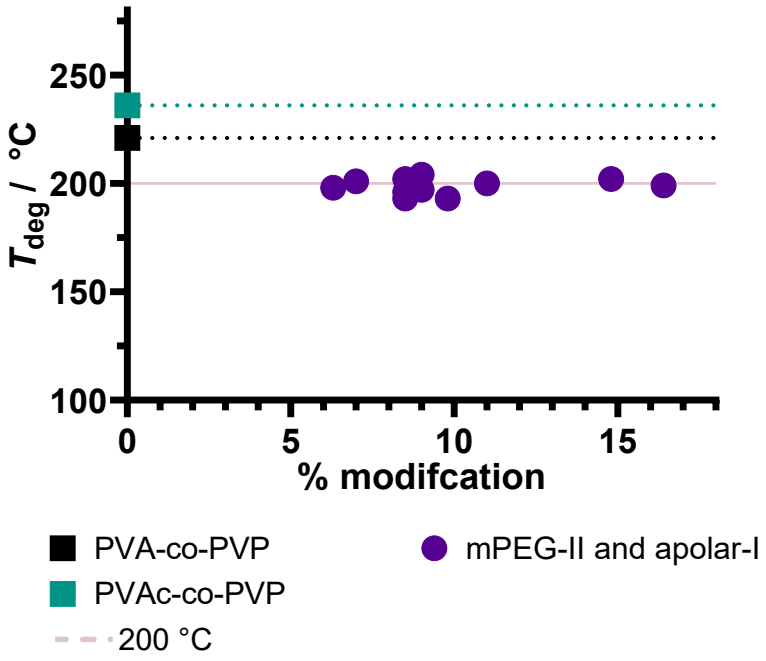

Figure 58: Degradation temperatures against modification degree for each synthesized polymer with a combined mPEG-II and apolar-I modification. Pointed lines (black and green) are shown to guide the eye indicating the degradation temperatures of the starting material PVAc-co-PVP and of the base polymer PVA-co-PVP. The pink line at 200 °C is the temperature above which the polymer should be stable for enabling a broad manufacturing range.

Table 27: Summary of analytical data obtained for polymers with mPEG and apolar modification.

Polymer	Yield (%)	Mod. Deg.	Mod. Deg.	T_g	T_m	T_{onset}	M_w	M_p	$Đ$
mPEG-II/apolar-Ia	57	6.3	0.4	109	-	198			
mPEG-II/apolar-Ib	60	7.0	0.6	104	-	201			
mPEG-II/apolar-Ic	56	8.5	1.1	87	-	193			
mPEG-II/apolar-Id	52	9.0	2.5	82	-	197	57000	37000	3.1
mPEG-II/apolar-Ie	52	9.8	3.2	89	-	193			
mPEG-II/apolar-If	53	8.5	4.9	88	187	196			
mPEG-II/apolar-Ig	63	14.8	3.1	68		202			
mPEG-II/apolar-Ih	55	16.4	2.0	66		199			
mPEG-II/apolar-Ii	41	8.5	2.8	59		202			
mPEG-II/apolar-Ij	59	9.0	2.0	63		204			

The polymers **mPEG-II/apolar-Id** and **mPEG-II/apolar-Ii** were subject to melt rheological characterization (Figure 59). *G'* is below *G''* in both cases until an intersection is observed at high temperatures (192 °C Figure 59a; 174 °C Figure 59b) indicating amorphousness of the polymers in the temperature range below. The processing temperature of **mPEG-II/apolar-Id** is between T(10000 Pa s) = 129 °C and T(1000 Pa s) = 168 °C with a maximum phase angle of δ(61°) = 168 °C

and a resulting range of $\Delta T = 39$ °C. The lower temperature threshold for extrusion of **mPEG-II/apolar-Ii** T(1000 Pa s) = 121 °C while the upper limit was not reached in the measured temperature range. The maximum phase angle was observed at δ(79°) = 144 °C. This can be explained by a larger modification degree of **mPEG-II** in **mPEG-II/apolar-Ii**. The polymer **mPEG-II/apolar-Ii** was flowing out of the measurement slit in the temperature range measured, which also indicates very low melt viscosity. The phase angles indicate slight degradation at these lower temperatures even though the degradation temperatures observed were higher and near 200 °C.

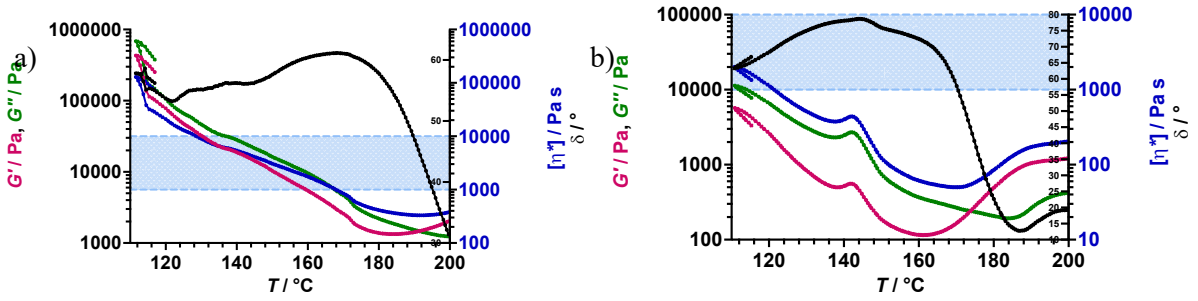

Figure 59: a) Rheogram of **mPEGII/apolar-Id**, T(10000 Pa s) = 129 °C, T(1000 Pa s) = 168 °C; b) Rheogram of **mPEGII/apolar-Ii**, T(10000 Pa s) ≤ 115 °C, T(1000 Pa s) = 121 °C.

The modification of PVP-co-PVA using **mPEG-II** and **apolar-I** lead to polymers with low processing temperature and moderately high thermal stability. These polymer entities were further tested in dissolution experiments, as the specifications were met.

5.2.5.6.3 Extrusion

Polymers showing **mPEG-II** and **apolar-I** after modification of PVP-co-PVA (**mPEG-II/apolar-Ie**) was extruded using a twin-screw labscale extruder. A low T_g enabled an extrusion as low as 120 °C at moderately high average torque values of 1.6 N m obtaining transparent brown filaments. Die swelling occurs during the extrusion and brittle filaments were obtained. The average torque values decrease while increasing the temperature during the extrusion at 300 rpm. Cinnamic acid in the polymer sidechain caused the brown discoloration as can be observed for extrudates formed by the extrusion of **apolar-Id**. The low extrusion temperatures can be attributed to mPEG-II present in the polymer as can be observed when extruding other mPEG modified polymers (**mPEG-IIe**, **mPEG-IIf**, **mPEG-IIIc** and **mPEG-IVb**). Though **mPEG** modified polymers are more flexible than PVP-co-PVAc after extrusion, the presence of **apolar-I** makes the filaments much more brittle.

Table 28: Extrusion mPEG-II/apolar-Ie

Polymer	**mPEG-II/apolar-Ie**	**mPEG-II/apolar-Ie**	**mPEG-II/apolar-Ie**
Temperature / °C	80/110/110	75/120/120	80/150/150
RPM / min^{-1}	300	300	300
average torque / Nm	1.75	1.6	1.5
nozzle / mm	1.5	1.5	1.5
Appearance	brown	brown	brown
Translucence	Opaque	Transparent	transparent
Flexibility	brittle	brittle	brittle
Filament	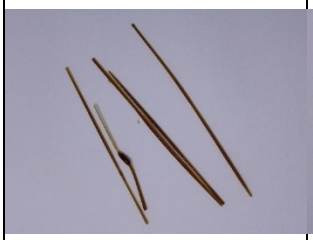		
Extrusion possible	**no**	**Yes**	**Yes**

5.2.5.6.4 Scale-Up

A polymer in this group was synthesized on a larger scale (Table 29). Polymers with **mPEG-II** in their sidechain showed low processing temperatures during small- and intermediate-scale extrusion. **Apolar-I** modified polymers showed an increased capability for solubility enhancement. Therefore, these modification techniques were combined. Firstly, the polymer **mPEG-II/apolar-Ig** was resynthesized in a multi-batch procedure pooling 4 batches of nearly 15 g material in moderate overall yield (55%, **mPEG-II/apolar-I-Pool**). The synthesis showed good reproducibility as shown by NMR, DSC and TGA (see Table 27 for complete analytical data, **mPEG-II/apolar-Ig, -h, -i, -j**). The pooled batch showed a T_g = 61 °C and a processing range between 115 °C and 200 °C, which can be attributed to the increased modification degree of **mPEG-II**. The T_g value is lower that the prerequisites targeted. The pooled product was subject to a limited intermediate-scale extrusion experiment due to the low amount of material at one extruder setting conducted by Alessandro-Giuseppe Elia (*Merck Life Science KGaA*) at 150 °C. Herein, low torque and low die pressure was observed. The filaments showed strong brown discoloration, which was expected, as the same was observed during the extrusion of **apolar-I** modified polymers. Another large scale batch was synthesized by Oliver Stranoswky (*Merck Electronics KGaA*) in moderate yields of 51% (**mPEG-II/apolar-Ik**). Analysis showed good reproducibility compared to other batches aiming at the same polymer product (Table 29).

Table 29: Analytical data of lab-scale mPEG/apolar modified polymers in comparison to the respective upscaled 200 g batches.

		mPEG-II/apolar-Id **10 g**	**mPEG-II/apolar-I-Pool** **55 g**	**mPEG-II/apolar-Ik** **200 g**
NMR	**Modification degree**	9.0%/2.5%	15.9%/1.3%	11%/1.0%
GPC	M_w	56000	58000	43000
DSC	T_g **≥ 80 – 90 °C**	82 °C	61 °C	73 °C
DSC	**No** T_m**, amorphous**	no T_m	no T_m	no T_m
Mini Extruder	**Transparent filaments**	low torque	n.d.	n.d.
TGA	T_{deg} **≥ 200 °C**	197 °C	200 °C	227 °C
Melt viscosity	η_{melt} **= 1000 – 10000 Pa s @ 0.1 rad** s^{-1}	129 – 168 °C	115 - > 200 °C	n.d.
Process window	η_{melt} **< 10000 Pa s; below** T_{deg} **> 40 – 50 °C**	ΔT = 39 °C	ΔT = 85 °C	n.d.
Intermediate-scale Extrusion		n.d.	Low torque low die pressure	n.d.

5.2.5.6.5 Dissolution experiments

One polymer of this group was tested in dissolution assays (**mPEG-II/apolar-I-Pool**) by Nabil Lamrabet (*Merck Life Science KGaA*). After a quick onset, 350±16% release was reached after 25 minutes (Figure 60). This is not possible and results from the unwanted detection of transitions derived from the modification agents cinnamic acid (**apolar-I**). Therefore, the results obtained are not indicative of the real release kinetics of the polymer sample.

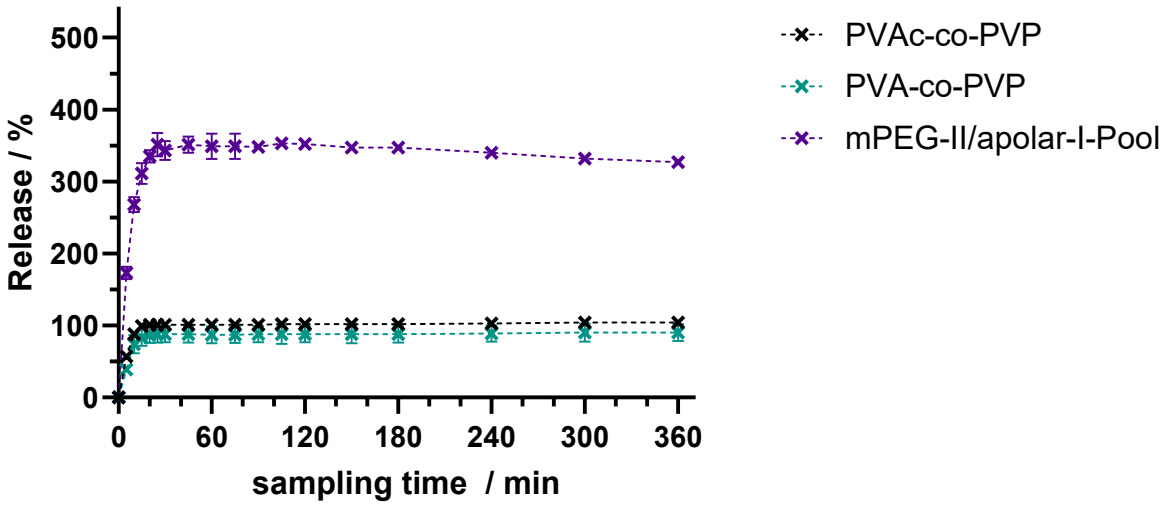

Figure 60: Release kinetics of selected polymers in comparison with benchmark PVAc-co-PVP (Kollidon® VA64) in caffeine assay. Amorphous sample discs were prepared by VCM. Non-sink dissolution of amorphized samples through melt quenching in 0.1 M HCl at 37 °C, 75 rpm and 900 mL medium. Drug: Caffeine at 10% drug load in 300 mg specimen, arithmetic means ± SD (n = 3). UV-VIS Analysis at λ = 227 mm. Discs were prepared by MeltPrep method and used as is. Dashed lines incorporated to guide the reader's eye.

The same polymer was analyzed regarding its solubility enhancement capabilities. **mPEG-II/apolar-I-Pool** showed a slower onset than PVAc-co-PVP with a low maximum concentration of 110±20µg mL^{-1} after 60 minutes (Figure 61). The *AUC* for **mPEG-II/apolar-I-Pool** is also very low with 9600 compared to 40000 obtained for PVAc-co-PVP. Comparing these results with previously obtained for the other modifications, the course of the curve is as expected, showing a maximum with a slower onset, probably resulting from cinnamate modification. These results show, that the anticipated increase of solubility enhancement by combining the two modification agents was not possible in this case.

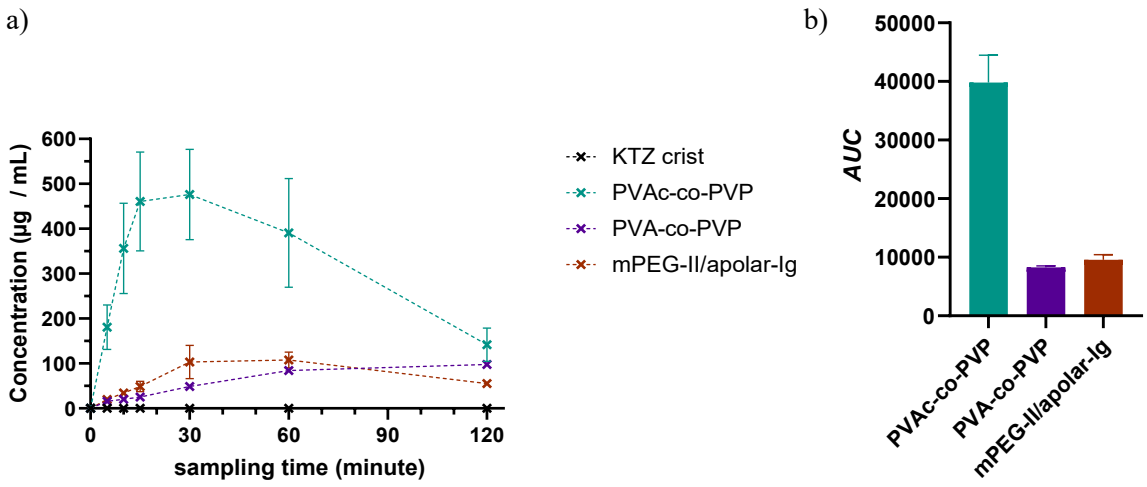

Figure 61: a) Dissolution capabilities of selected polymers and benchmark PVAc-co-PVP (Kollidon® VA64) in comparison to pure, crystalline API. Amorphous sample discs were prepared by VCM. Non-sink dissolution of amorphized samples through melt-quenching in FaSSIF at pH 6.5 at 37 °C. Concentration of 0.75 mg drug per mL medium, arithmetic means ± SD (n = 3), drug: Ketoconazole at 40% drug load; HPLC analysis at λ = 225 mm. Discs were prepared by MeltPrep method and used as is. Dashed lines incorporated to guide the reader's eye; b) Corresponding *AUC* of the dissolution measurements for comparison of dissolution capability. Arithmetic means ± SD (n = 3).

5.2.5.6.6 Conclusion

In conclusion, polymers with combined modifications of **mPEG** and **apolar** show improved processing temperatures due to the incorporation of **mPEG-I**. The glass transition temperature is greatly reduced while degradation temperatures stay close to 200 °C. Melt rheological measurements also indicated reduced processing temperatures compared to the marketed polymer PVP-co-PVAc. The reproducibility was given in upscaled reactions. The dissolution experiments indicate, that the modification degree of **apolar-I** is too low with 1% to observe a meaningful improvement in solubilization. Considering higher modification degrees as was shown in Section 5.2.5.3, a more pronounced effect was visible. By incorporating higher modification with **apolar-I** the synergy of the reducing effect of **mPEG-I** can be used in additional studies. High modification degrees of **mPEG-I** led to processing ranges as low as 115 °C and a broad window of 85 °C before degradation occurs. These polymers are fitting for the manufacturing of thermolabile APIs.

5.2.6 Synthesis of 3 kg product on pilot Scale

Large amounts of material is needed for the optimization of an extrusion process using the polymer alone and in combination with an API. As indicated before (Section 5.2.1), the scale-up of a synthesis process is very time consuming, laborious and expensive. Therefore, the ideal polymer needed to be chosen for the synthesis on a 3 kg scale. Considering all synthesized polymers and their individual properties in terms of their feasibility for solubility enhancement and simultaneously their processability, the polymer with the most potential is **mPEG-IIg**. It showed one of the most favorable property combinations, as its processing temperature is sufficiently low, while its dissolution capabilities are increased significantly, when compared to the base polymer PVA-co-PVP. Also, its reproducibility was given in repeated experiments making the success of an upscaled process more likely. The synthesis procedure was upscaled to amounts of 1 kg of base polymer and conducted in four batches in the cooperating laboratory by Oliver Stranowsky (*Merck Electronics KGaA)*. After confirming reproducibility of the synthesis process by analysis via NMR, DSC, TGA and GPC (Table 30), the batches were unified. The individual batches were analyzed by GPC leading to molecular weights of 63000 g mol^{-1} to 104000 g mol^{-1}, which is higher than anticipated considering the synthesis protocol of **mPEG-IIh** was utilized and scaled to 1 kg of base polymer. Other properties like the glass transition temperature are near the target range around T_g = 96 °C. Processing temperatures as obtained by melt rheology measurements are between 142 and 171 °C with a temperature difference of 29 °C fulfilling the requirements posed. The corresponding data can be found in the appendix. The pooled product was further analyzed utilizing the dissolution assays. In the caffeine assay, mPEG-II-Pool shows a similar course of the curve as **mPEG-IIg** indicating similar dissolution behavior (Figure 62). Furthermore, in the KTZ assay, it showed a slower onset compared to **mPEG-IIg** but otherwise similar behavior (Figure 63). The pooled product was subject to intermediate-scale extrusion experiments by Alessandro-Guiseppe Elia (*Merck Life Science KGaA*). Due to the increased molecular weight, high torque values were obtained and the extrusion was only possible near the upper limit of torque. By adding 20% plasticizer (PEG2000) an extrusion at low torque was facilitated.

Table 30: Analytical data obtained for upscaled synthesis batches.

Target criteria	mPEG-IIf Lab	mPEG-IIh 200g	mPEG-IIj	mPEG-IIk	mPEG-III	mPEG-IIm	mPEG-II Pool
Modification degree	10%	11%	10.3%	9.2%	10%	10%	
Yield reaction	5 g (65%)	182 g (86%)	948 g (83%)	909 g (80%)	895 g (79%)	925 g (81%)	3651g (80%)
T_g ≥ 80-90 °C	90 °C	87°C	91	99	95	96	96
No T_m, amorphous	no T_m	no T_m	no T_m	no T_m	no T_m	no T_m	no T_m
T_{deg} ≥ 200 °C	192 °C	208 °C	209	207	202	210	204
M_w / g mol^{-1}	38000	38000	104000	63000	70000	80000	79000
M_P / g mol^{-1}	28000	28000	83000	38000	42000	69000	45000
$Đ$	2.5	2.6	7.6	5.0	6.0	5.6	5.9
$T_{10kPas, 1kPas}$ @ 0.1 rad s^{-1}	n.d.	129 - 160°C	130-160 °C	139-169°C	142-171°C	126-157°C	142-171
Yield after milling	n.d.	166 g (83%)	871 g (92%)	857 g (95%)	846 g (96%)	820 g (89%)	3259 (89%)
$\Delta T = \eta_{10k\ Pa\ s} - \eta_{1k\ Pa\ s}$	n.d.	Δ= 31 °C	Δ = 30 °C	Δ = 30 °C	Δ = 30 °C	Δ = 31 °C	Δ = 29 °C

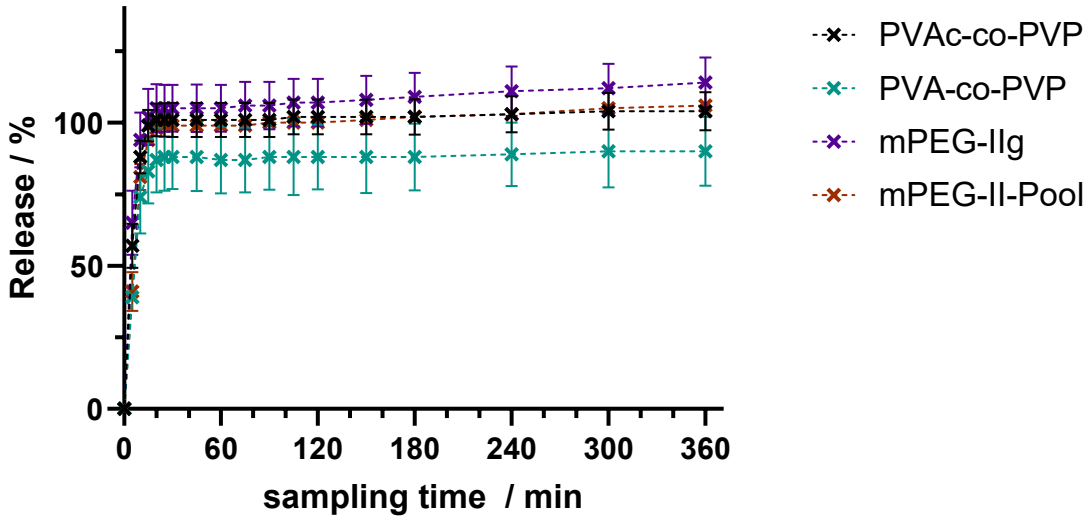

Figure 62: Release kinetics of selected polymers in comparison with benchmark PVAc-co-PVP (Kollidon® VA64) and the lab-scale batch in caffeine assay. Amorphous sample discs were prepared by VCM. Non-sink dissolution of amorphized samples through melt quenching in 0.1 M HCl at 37 °C, 75 rpm and 900 mL medium. Drug: Caffeine at 10% drug load in 300 mg specimen, arithmetic means ± SD (n = 3). UV-VIS Analysis at λ = 227 mm. Discs were prepared by MeltPrep method and used as is. Dashed lines incorporated to guide the reader's eye.

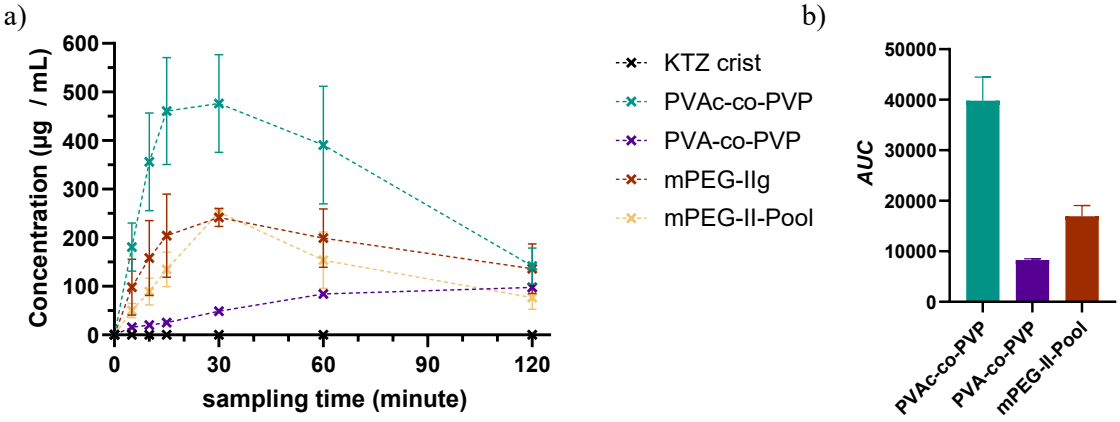

Figure 63: a) Dissolution capabilities of selected polymers and benchmark PVAc-co-PVP (Kollidon® VA64) in comparison to pure, crystalline API. Amorphous sample discs were prepared by VCM. Non-sink dissolution of amorphized samples through melt-quenching in FaSSIF at pH 6.5 at 37 °C. Concentration of 0.75 mg drug per mL medium, arithmetic means ± SD (n = 3), drug: Ketoconazole at 40% drug load; HPLC analysis at λ = 225 mm. Discs were prepared by MeltPrep method and used as is. Dashed lines incorporated to guide the reader's eye; b) Corresponding *AUC* of the dissolution measurements for comparison of dissolution capability.

5.3 Conclusion

The base polymer PVA-co-PVP was modified with a variety of modification agents, being able to establish a qualitative structure-property relationship. The specific influences are summarized in Table 31. The results obtained showed clearly, that mPEG modification at higher modification degrees around 10% led to an extraordinary improvement in terms of the processability of the resulting polymer *via* extrusion. By using apolar agents, namely *trans*-cinnamic acid, the dissolution performance in terms of solubility enhancement of KTZ in the testing assay could be improved, even at lower modification degrees around 6%. It may be possible to further improve the dissolution performance by increasing the ratio of present apolar moieties in the polymer. During the synthesis of all modifications, a low modification efficiency was observed, as high excess of modification agent needed to be used to reach high modification degrees. The highest combined modification degree of hydroxyl functions obtained was 18% in the polymer **mPEG-II/apolar-Ih** (mPEG aa/cinnamic acid modification), even though the batch was calculated to result in 100% modified OH-groups. Also, the highest modification degree obtained by modification with apolar agents was 18% in the polymer **mPEG-IIIc** (mPEG350 succinate modification), which resulted in significantly reduced water solubility. It was not possible to reach higher modification degrees by increasing the amount of modification agent utilized during the synthesis. Solubilizing effects of the polymers improved when higher amounts of **apolar-I** (cinnamic modification) were present in the polymer. Higher modification degrees than 6% may lead to better performance in the dissolution assay using KTZ. Furthermore, the saponification of acetate groups in the starting material led to significant decrease in solubility performance as can be observed by the performance of PVA-co-PVP in the dissolution assays. This means, that the acetate groups also play a crucial role in the solubilization of the poorly soluble KTZ. A polymer bearing pyrrolidone, acetate, mPEG and an aromatic/hydrophobic moiety could be ideal to combine the favorable influences on the processability of the polymer and additionally increase the solubilizing effect on an API. The modification with mPEG derivatives were capable of reaching the targeted glass temperature range between 80 and 90 °C while also being extrudable. Utilizing cinnamic acid increased the dissolution capabilities but hindering extrusion. The combined modification thereby enabled low temperatures during processing via HME showing extrudability while reaching the targeted range in terms of glass transition temperature between 80 °C and 90 °C in the case of **mPEG** modified entities. Especially the **apolar-I** modified polymers facilitated increased solubilization of KTZ during the assay when compared to all benchmarks with the exception of Kollidon® VA64. This study outlines the importance of various moieties to be present in a polymer structure. Lowering the processing temperature and reaching the targeted temperature window was facilitated by **mPEG** (mPEG2 aa) modifications. The polymer's ability to solubilize a poorly soluble model API increasing its water solubility was greatly improved by

apolar-I (cinnamate) and **apolar-III** (palmitate) modification. In summary, a tailored polymer can be synthesized utilizing a combination of multiple functionalities of hydrophilic and hydrophobic sidechains to obtain an entity which can be manufactured at low temperatures while also enhancing the water solubility of a poorly soluble API.

Table 31: Summary of the qualitative influence of each modification agent onto the thermophysical properties compared to the base polymer PVA-co-PVP. The respective influence on the dissolution performance and the melt rheological properties for each modification agent are compared to PVAc-co-PVP.

Structure Modification Agent	**Modification name**	**Influence on polymer thermophysical properties (Compared to PVA-co-PVP)**	**Influence on dissolution performance and HME (Compared to PVAc-co-PVP)**
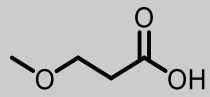	mPEG-I	Slight T_g reduction Slight T_{deg} reduction Increase in M_w and M_p	Not tested
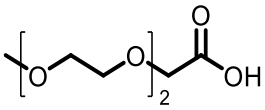	mPEG-II	Strong T_g reduction Slight T_{deg} reduction Increase in M_w and M_p	Strong reduction in $T_{10000\ Pa\ s}$ and $T_{1000\ Pa\ s}$ Improved dissolution
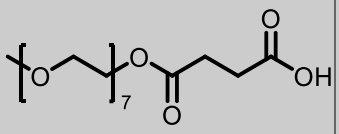	mPEG-III	Strong T_g reduction Slight T_{deg} reduction Increase in M_w and M_p	Strong reduction in $T_{10000\ Pa\ s}$ and $T_{1000\ Pa\ s}$ Dissolution not tested
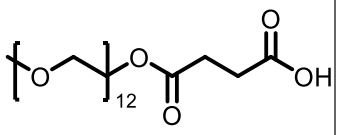	mPEG-IV	Strong T_g reduction Slight T_{deg} reduction Increase in M_w and M_p	Strong reduction in $T_{10000\ Pa\ s}$ and $T_{1000\ Pa\ s}$ Dissolution not tested
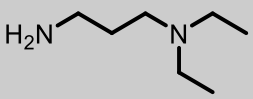	amine-I	No T_g reduction Slight T_{deg} reduction Increase in M_w and M_p	Not tested
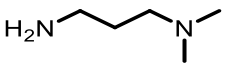	amine-II	No T_g reduction Slight T_{deg} reduction Increase in M_w and M_p	Not tested
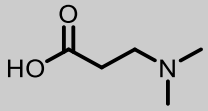	amine-III	No T_g reduction Slight T_{deg} reduction Increase in M_w and M_p	Not tested
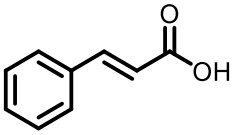	apolar-I	Slight T_g increase Slight T_{deg} increase Increase in M_w and M_p	Increase in $T_{10000\ Pa\ s}$ and $T_{1000\ Pa\ s}$ Improved dissolution

Structure Modification Agent	**Modification name**	**Influence on polymer thermophysical properties** (Compared to PVA-co-PVP)	**Influence on dissolution performance and HME** (Compared to PVA-co-PVP)
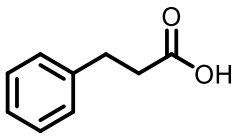	apolar-II	No T_g reduction Slight T_{deg} reduction Increase in M_w and M_p	Not tested
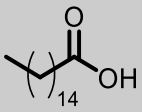	apolar-III	Strong T_g reduction Slight T_{deg} reduction Increase in M_w and M_p	Decrease in $T_{10000\ Pa\ s}$ and $T_{1000\ Pa\ s}$ Improved dissolution
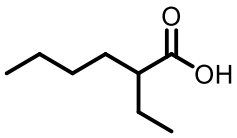	apolar-IV	No T_g reduction Slight T_{deg} reduction Increase in M_w and M_p	Not tested
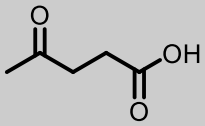	misc-I	No T_g reduction Slight T_{deg} reduction Increase in M_w and M_p	Not tested
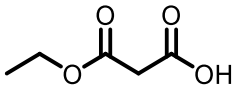	misc-II	Slight T_g increase Strong T_{deg} reduction Strong Increase in M_w and M_p, crosslinking	Not tested
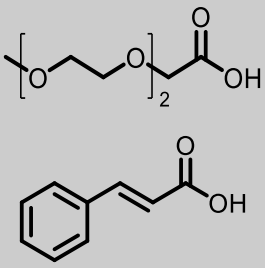	mPEG-II/apolar-I	Strong T_g reduction Strong T_{deg} reduction Increase in M_w and M_p	Decrease in $T_{10000\ Pa\ s}$ and $T_{1000\ Pa\ s}$ Improved dissolution

6 The Journey to an Optimized Polymer for Dissolution Enhancement of a model API

6.1 Introduction

The synthesis of a polymer with tailored material properties poses a great opportunity to facilitate the solubility enhancement of a poorly water-soluble API. By tailoring the advantageous properties of the polymer to optimize its processability and subsequently its influence on the solubility of a model API, it can be formulated and administered via an oral dosage form. Utilizing the previously established structure property relationship (Section 5) and keeping the respective limitations posed in mind, a synthesis process of polymers with specially tailored properties for the pharmaceutical extrusion and consequently the solubility enhancement of a poorly soluble model API was developed.

The entities were synthesized in a free radical polymerization process and consisted of up to four monomers with the aim of controlling their processability and their performance in a dissolution assay. An understanding of the influences of monomers present in the polymer was generated by an explorative design of experiments approach leading to an ideal monomer distribution in the polymer for the processing technique extrusion. Targeted key properties include the processing temperature, consequently the degradation behavior as well as the glass transition temperature and the melt rheological behavior. Furthermore, the polymer-API interactions play a crucial role as these interactions enhance the API's solubility in the tested medium. The processing technique investigated is the pharmaceutical extrusion, so thermal and especially mechanical stability is of great interest. The extruded materials were subsequently subject to dissolution experiments investigating their influence on a model API's solubility.

6.2 Results and discussion

The established structure-property relationship (Section 0) was utilized in order to synthesize novel polymers with optimized processability and dissolution behavior. Based on the findings outlined in chapter 5, a bottom-up synthesis strategy of a polymer system was established. Utilizing the trends discovered during the development of these structure-property relationships, a polymer family derived from PVAc-co-PVP was investigated. By incorporating the chemical motifs identified as favorable, namely mPEG and aromatic moieties in the side chain, a polymer was designed to meet the prerequisites posed for the manufacturing in pharmaceutical extrusion and the intended dissolution enhancement of a poorly soluble API.

Free radical polymerization of more than one monomer strongly depends on the reactivity of the present species with each other and themselves. Where applicable, known copolymerization parameters were

utilized to assess the individual behavior in copolymerization. As a proof of concept, VP and VAc were polymerized following a slightly adapted synthesis procedure from literature.[166, 167] Furthermore, the incorporation of one additional hydrophobic/aromatic or hydrophilic (mPEG) was tested. Finally, an explorative design of experiments approach was followed in order to identify the ideal ratios to obtain a polymer composition which fulfills the ideal properties defined in the following section 6.1. A selection of polymers was subject to dissolution experiments characterizing their influence on the solubility of a poorly soluble API.

6.2.1 Definition of optimized properties

By analyzing several benchmark polymers currently used in solid dosage forms, a set of crucial properties were devised. These properties include thermophysical and physicochemical properties (Table 32).[120] Analysis methods utilized for the characterization consist of NMR, DSC, TGA, melt rheology measurements and a dissolution assay. As outlined in the introduction, a vast majority of APIs currently in development are poorly water soluble and thermolabile, which results in a need for excipients which can be processed at lower temperatures and increase the aqueous solubility of a specific API. The processing range of a polymer via extrusion is defined by its melt viscosity and only in the range between η_{melt} = 1000 Pa s and η_{melt} = 10000 Pa s an extrusion is feasible.[121] For a first impression of the polymers processability, the glass transition temperature T_g as well as the degradation temperature T_{deg} are of great importance. For processing at low temperatures, the optimal glass transition temperature lies between 80 °C and 90 °C, and at least 50 °C above room temperature, to improve storage stability and mitigate moisture absorption from the environment. A thermal stability up to 200 °C is necessary as extrusion is a mechanically and thermally demanding processing technique and degradation during processing is unwanted. To characterize the polymer's performance in the dissolution in combination with the API, an assay was developed with 40% drug load.

Table 32: Target criteria for polymers synthesized via free radcial polymerization for pharmaceutical extrusion.

Target	Method
Successful reaction	NMR
T_g ≥ 80-90 °C	Thermal analysis (DSC)
No T_m Amorphousness	Thermal analysis (DSC)
T_{deg} ≥ 200 °C	Thermal analysis (TGA)
Transparent extrudate	Extrusion (Mini Extruder)
Amorphous drug loading ≥ 40%	ASD Screening
Supersaturation potential (Yes / No)	Non-sink dissolution
η_{melt} = 1000 – 10000 Pa s at < 160 °C	Melt rheology

6.2.2 Synthesis strategy: free radical polymerization

To develop a polymer meeting the prerequisites for dissolution enhancement, a synthetic route was pursued that involved the free radical polymerization of up to four distinct monomers. Due to upper limitations in the modification degree, which were achievable during the post-polymerization reaction described in Section 0, free radical polymerization starting from carefully chosen monomers, was employed. This synthesis route allowed the facile adjustment of the polymer compositions and enabled the synthesis of a broad range of tailored polymers. Free radical polymerization (FRP) is a well-established synthesis technique, and an abundance of knowledge is available for most commercially available comonomers. Radical copolymerization can be conducted in various ways as outlined in the introductory chapter. The system researched in this study was limited to free radical polymerization, due to its robustness concerning the monomer choice and impurity profile of utilized chemicals. Considering the benchmark polymer PVAc-co-PVP, which is itself synthesized *via* free radical polymerization on a large scale, the specifications posed in terms of control over the polymer structure and dispersity are rather broad. In addition to that, no specific and/or demanding conditions are needed for the synthesis procedure which enables the transfer to larger scales without the need for specialized equipment. The development of a process enabling the cost-effective production of large quantities of product is one crucial factor in the development of novel polymers in the present research field. For these reasons and the advantage to tailor the polymer backbone based on high potency monomers, free radical polymerization serves as an ideal platform for the research endeavor.

PVP-co-PVAc was used as a benchmark in dissolution performance and the modification reactions were

based on a close derivative of PVP-co-PVAc. Therefore, polymers synthesized in this section show close resemblances to PVP-co-PVAc with the addition of favorable comonomers with hydrophilic moieties to improve the processability and aromatic moieties to improve the dissolution performance.

PVP-co-PVAc is a well-established and widely used excipient in solid formulation. It consists of the building blocks **M-I** (*N*-vinyl-2-pyrrolidone) and **M-II** (vinyl acetate), which were used in this study as a starting point for the development of novel polymers. As described in Section 0, modifications of a PVP-co-PVA derivative with hydrophilic and aromatic moieties improved the polymer's performance in the desired processing technology. The monomers **M-III** (poly (ethylene glycol) methyl ether methacrylate, M_n = 300 g mol^{-1}) and **M-V** (allyl (poly (ethylene glycol) methyl ether)), M_n = 300 g mol^{-1}) bear a poly(ethylene glycol) group, aiming to decrease the glass transition temperature and thus the processing temperature, when incorporated in a polymer or when added as a plasticizer. Furthermore, the degradation temperatures obtained were not significantly changed when used in post-polymerization modification reactions (Section 5.2.5.1), which further emphasizes their usefulness. The monomer **M-IV** (vinyl benzoate) bears a hydrophobic, aromatic moiety, which has a favorable influence on the dissolution performance (Section 5.2.5.3). The combination of these hydrophilic and hydrophobic comonomers in the interplay with the comonomers **M-I** and **M-II** was utilized to synthesize polymers with optimized properties for extrusion and dissolution enhancement.

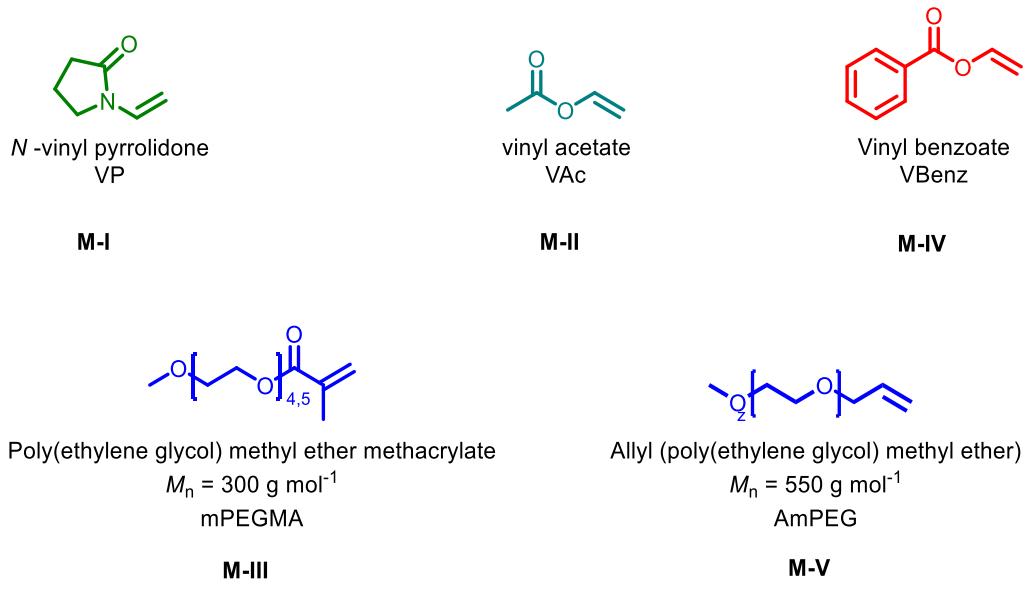

Figure 64: Vinyl and acrylate monomers used in this work for the radical polymerization.

6.2.2.1 Development of the synthesis process

The reaction pathway and thus the monomer distribution in a polymer prepared by the copolymerization of more than one comonomer is strongly dependent on the respective reactivity parameter in a given

system.[166, 168-172] A great difference in reactivity parameter can lead to blocky copolymers, where one monomer is incorporated at a much higher probability than the other. For many copolymer systems utilizing two monomers, these parameters are known in literature.[166, 173-175] For novel polymers these are unknown and need to be determined experimentally or the parameters need to be calculated[170-172, 176] Various methods can be employed, e.g. the (*extended*) *Kelen Tüdös*[177, 178] method, the *Mayo-Lewis* method[179], the *Q-e Scheme*[180], the *Fineman-Ross* method[181] or a method established by *Mao*[182]. For the monomers used in this present study, reactivities in different systems are known in literature and the real reactivity could be roughly estimated.[166, 171-173, 176] M-I and M-II are very well-known comonomers and M-III is a methacrylate with much higher reactivity, so utilizing the literature values were used to roughly approximate their reactivity in the comonomer system.

The polymers in this section were prepared using an adapted synthesis protocol found in the literature.[166, 167] As monomers with significantly different reactivities were used in this study, the addition of the respective comonomers into the reaction vessel was controlled throughout the synthesis process corresponding to the respective reactivity of the monomer. A detailed description of each synthesis process is given in Section 8.2 and a compilation of the analytical data for all polymers in this section is given in Table 43. The polymers synthesized in this section were analyzed using ^{1}H-NMR, ^{13}C-NMR spectroscopy, and GPC to confirm the success of the reaction. Subsequent thermophysical characterization was performed by DSC, TGA, and melt rheology measurements for a selection of copolymers. Multiple reaction conditions were tested to develop a synthesis process enabling the facile synthesis of a polymer with four monomers with the ability to be scale to larger amounts of product.

In a first attempt, synthesizing a PVAc-co-PVP derivative, the monomers **M-I** and **M-II** were polymerized in 1,4-dioxane at 70 °C using 4,4-Azobis(4-cyanovaleric acid) (ACVA) as the initiator (Scheme 14). A polymer consisting of 74 mol% **M-I** and 26 mol% **M-II** was targeted after the precipitation from ice-cold CPME. During the reaction, liquid droplets were visible around the condenser indicating evaporation of the reactant **M-II**. ^{1}H-NMR spectroscopy confirmed this observation as a monomer distribution of 93 mol% to 7 mol% (**M-1**/**M-II**) was obtained (Figure 65) with a yield of 60%. For the evaluation of the distribution, the integrals of the b^{3} methyl protons of **M-II** and the a^{4} methylene protons of **M-1** were compared.

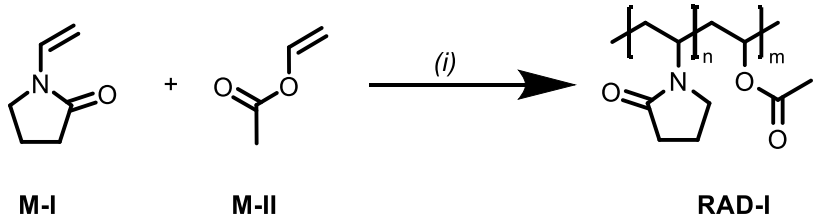

M-I **M-II** **RAD-I**

Scheme 14: Copolymerization of the monomers M-I and M-II; (i) M-I (255 eq.), M-II (78 eq.), ACVA (1 eq.), 1,4-Dioxane, 75 °C, 6 h. Solutions degassed by three freeze-pump-thaw cycles.

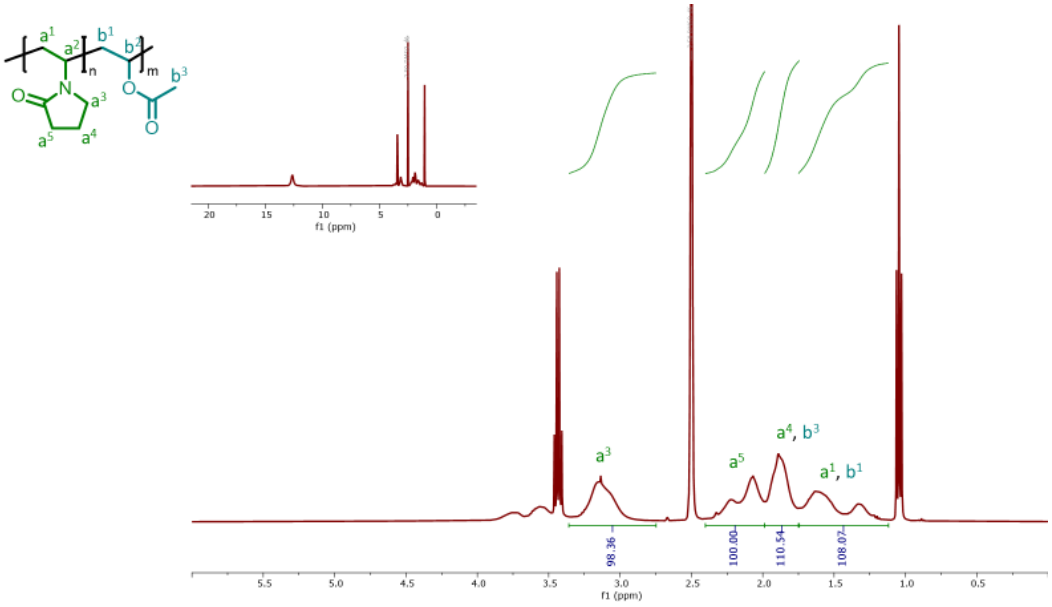

Figure 65: ^{1}H-NMR spectrum of RAD-I normalized to M-I methylene moiety a^5 with addition of TFA. Calculation based on M-I methylene group a^5 and M-II methyl group b^3.

The mean molecular weight of **RAD-I** was determined by GPC calibrated against PMMA standards. Its mean molecular weight is $M_w = 70000$ g mol^{-1} with a dispersity index of $Đ = 3.5$ in a monomodal distribution. As outlined in the introductory chapter, this broad distribution is to be expected in free radical polymerization reactions and was not further optimized.[183] The temperature for the first degradation step obtained via TGA measurements is $T_{deg,1} = 124$ °C, and the second $T_{deg,2} = 267$ °C. Although the monomer ratio in **RAD-I** is significantly skewed to **M-I** and too little **M-II** was incorporated, the fundamentals of the synthesis process were used in subsequent experiments.

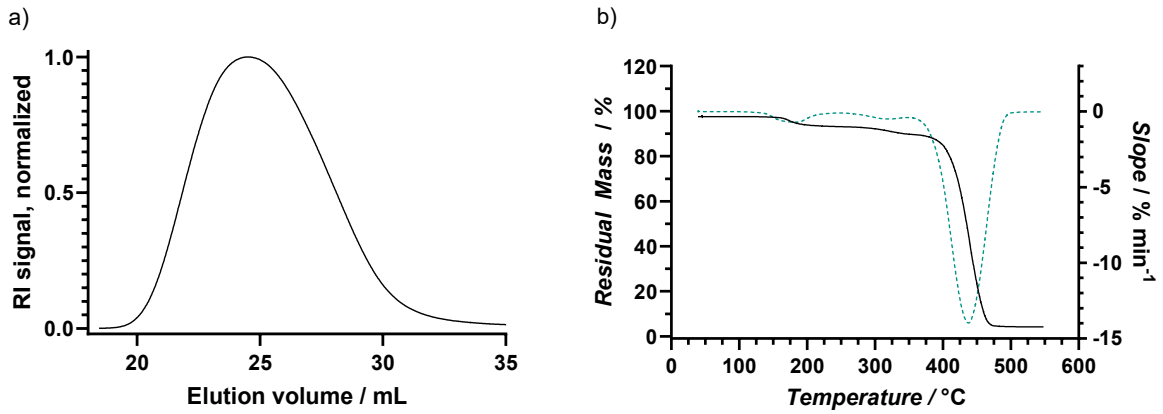

Figure 66: Characterization of RAD-I: a) GPC-Elugram of RAD-I with normalized RI signal. Measurement calibrated against PMMA standards in DMAc with 0.6 g L^{-1}LiBr. $M_w = 71000$ g mol^{-1} b) TGA thermogram of RAD-I (black) and the respective 1st derivative (blue) with a $T_{deg} = 124$ °C and 267 °C (right)

The polymer **RAD-II** was synthesized utilizing the comonomers **M-I**, **M-II** and **M-V** with ACVA as the initiator system in 2-propanol targeting a polymer distribution of 55%/35%/10% (**M-I**/**M-II**/**M-V**) (Scheme 15). After precipitation from MTBE the polymer was obtained in low yields of %. NMR analysis of the previously mentioned protons for **M-I** and **M-II** as well as the methoxy protons of **M-V** lead to a comonomer distribution of 70%/12%/18% (**M-I**/**M-II**/**M-V**). Low ratio of **M-II** once again indicating the loss of the comonomer during the reaction (Figure 67).

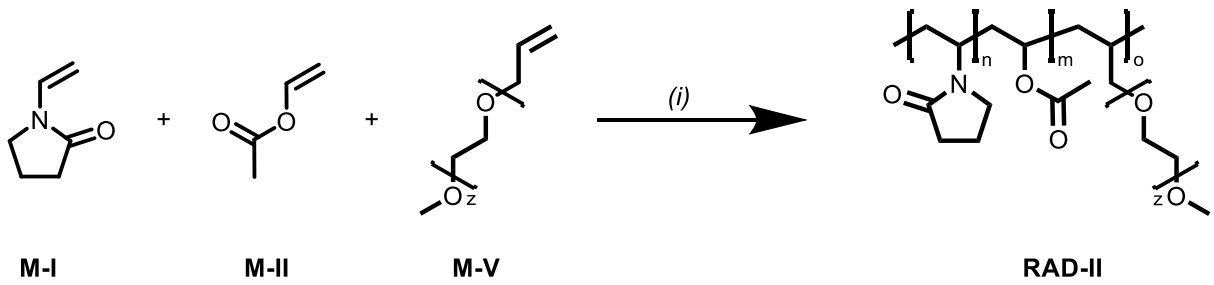

Scheme 15: Copolymerization of the monomers M-I, M-II, and M-V; (i) M-I (183 eq.), M-II (117 eq.), M-V (33 eq), ACVA (1 eq.), 1,4-Dioxane, 75 °C, 6 h. Solutions degassed by three freeze-pump-thaw cycles.

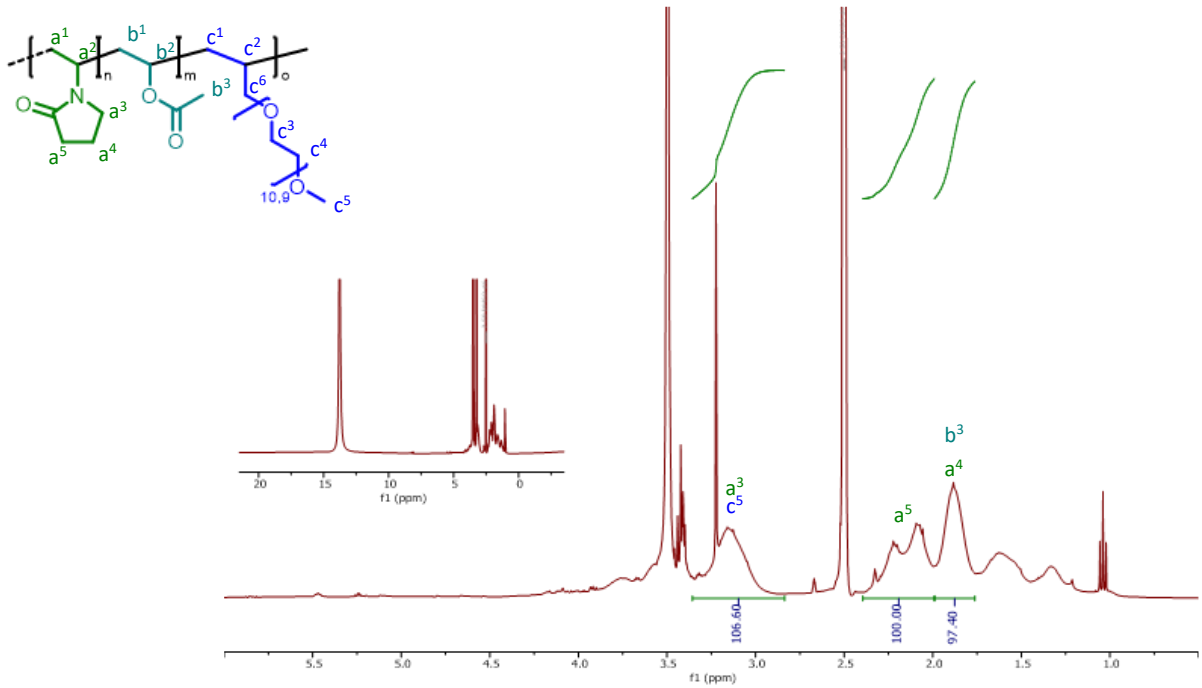

Figure 67: ^{1}H-NMR spectrum of RAD-II normalized to methoxy moiety present in mPEG comonomer M-V with addition of TFA. Calculation based on integrated signals corresponding to methyl group b^3 in VAc M-II and methylene group a^5 of VP M-I.

GPC measurements resulted in a low mean molecular weight of the product at M_w = 6100 g mol^{-1} with shouldering to lower molecular weight indicating low conversion. A low degradation temperature was observed at T_{deg} = 127 °C (Figure 68) with a multi-step degradation pattern.

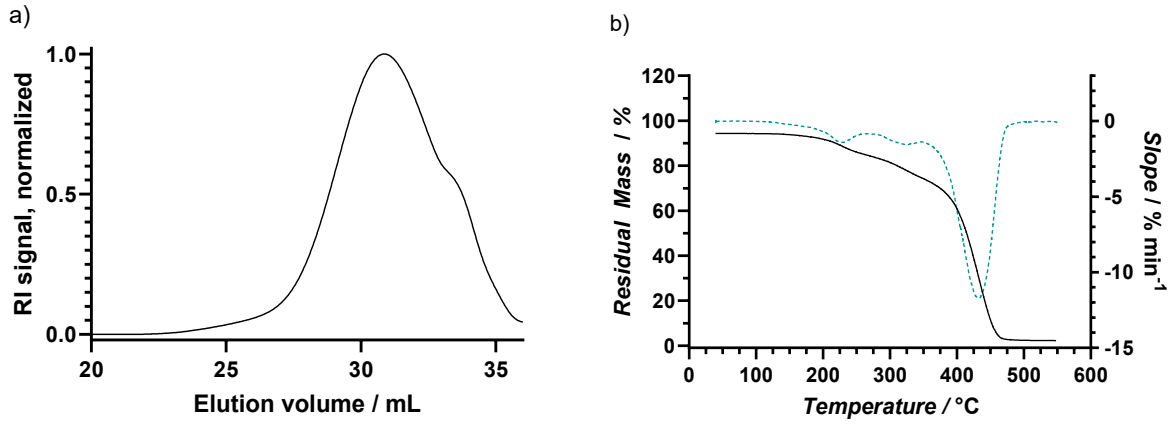

Figure 68 Characterization of RAD-II: a) GPC-Elugram of RAD-I with normalized RI signal. Measurement calibrated against PMMA standards in DMAc with 0.6 g L^{-1}LiBr; M_w = 6100 g mol^{-1} b) TGA thermogram of RAD-I (black) and the respective 1st derivative (blue) with a T_{deg} = 127 °C.

Due to the formation of a low molecular weight polymer, the mPEG monomer was changed to a mPEG ester of methacrylic acid, which has a much higher reactivity than the allyl monomer. Due to the significant difference in reactivity of vinyl monomers and (meth-)acrylates, a syringe pump was used for the introduction of the more reactive methacrylate monomer to control the incorporation of mPEG functions into the polymer.[173] For the terpolymer **RAD-III**, a monomer distribution of 55%/35%/10% (**M-I**, **M-II**, **M-III**) was targeted (Scheme 16). The reaction in iPrOH with ACVA as the initiator lead to a polymer with a monomer distribution of 60%/30%/10% after precipitation from MTBE in 78% yield (Figure 69). The NMR spectrum was evaluated as previously discussed for **RAD-II.** The monomer distribution closely resembles the anticipated and the incorporation of **M-III** could be influenced by the addition via syringe pump. As the reactivity of a methacrylate is higher than of a vinyl monomer, the monomers introduced into the reaction mixture are consumed first. Additionally, **M-II** was incorporated in sufficient manner, which was facilitated by an increase in N_2 pressure in the apparatus during the reaction in comparison to the synthesis of **RAD-I** and **RAD-II** and no excessive liquid droplets on the condenser were observed.

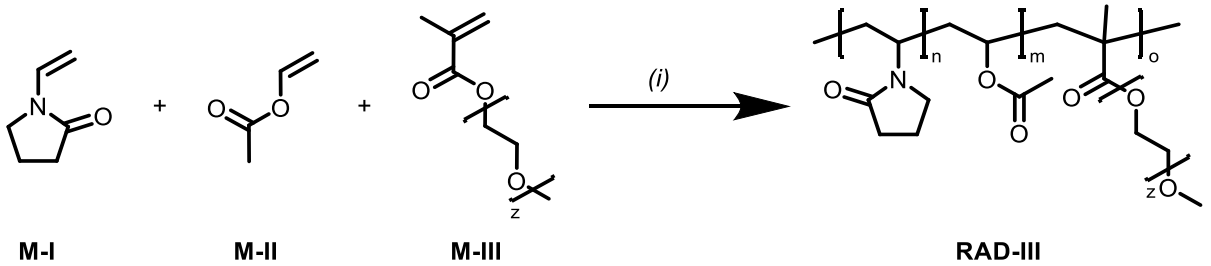

Scheme 16: Copolymerization of the monomers M-I, M-II, and M-III; (i) M-I (183 eq.), M-II (117 eq.), M-III (33 eq), ACVA (1 eq.), iPrOH, 75 °C, 6 h. Solutions degassed by three freeze-pump-thaw cycles.

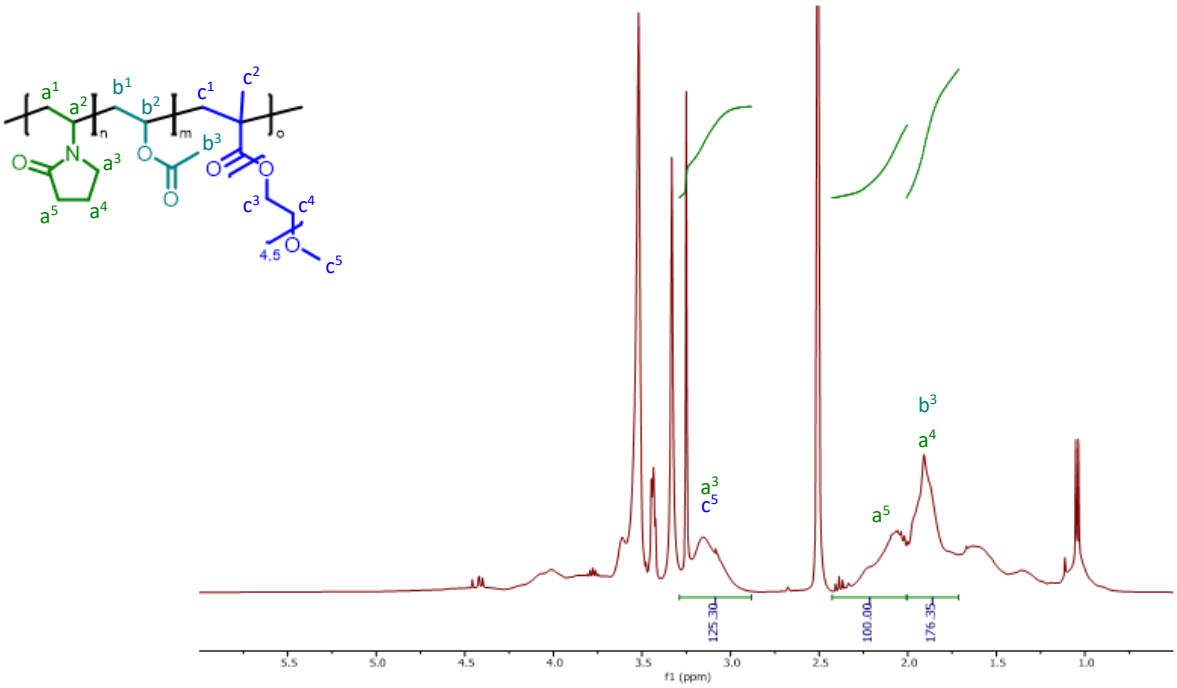

Figure 69: ^{1}H-NMR spectrum of RAD-III normalized to M-I methylene moiety a^5. Monomer distribution in copolymer calculated based on integrated signals corresponding to methyl group b^3 and methoxy group c^5.

A polymer with a mean molecular weight of M_w = 29000 g mol^{-1} with a dispersity index $Đ$ = 3.6 was obtained as confirmed by GPC. This is in good agreement with the anticipated polymer properties (Figure 70). A glass transition temperature of T_g = 43°C was obtained by DSC and a degradation temperature of T_{deg} = 269 °C was obtained by TGA. This further demonstrates the T_g reducing effect of mPEG moieties, when present in the polymer. Also, no significant influence on the degradation temperature can be observed, which shows the suitability of this monomer for the synthesis of thermally stable polymers for extrusion. A glass transition temperature of T_g = 43 °C is too low for the extrusion, which further demonstrates, that already with a 10 mol% ratio of mPEG in the polymer transition temperature can be shifted to very low temperatures. As shown, aromatic moieties tend to increase the glass transition temperature of the final polymer. Therefore, these two influences need to be balanced when combined in order to obtain an optimal polymer.

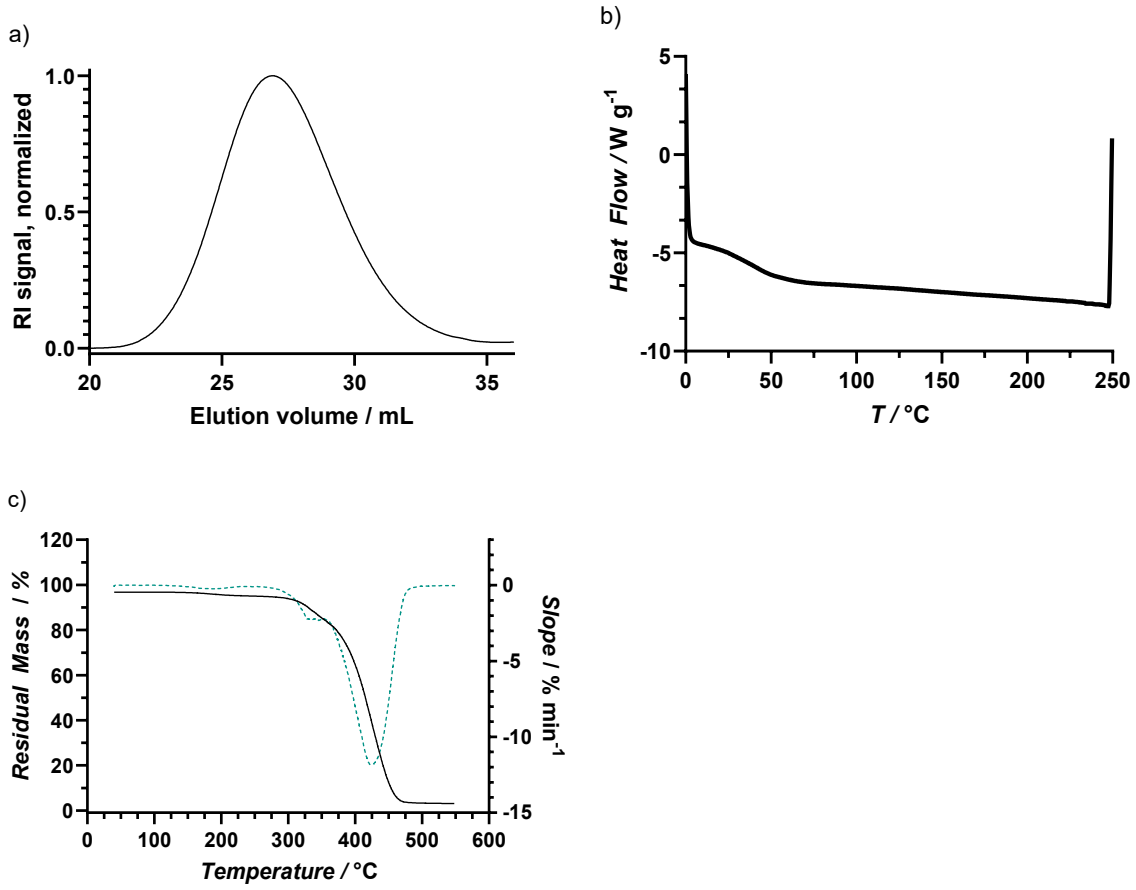

Figure 70: Characterization of RAD-III: a) GPC-Elugram of RAD-III with normalized RI signal. Measurement calibrated against PMMA standards in DMAc with 0.6 g L^{-1}LiBr; M_w = 30000 g mol^{-1} b) DSC thermogram of RAD-III with a T_g = 43 °C c) TGA thermogram of RAD-III (black) and the respective 1st derivative (blue) with a T_{deg} = 269 °C.

The quaterpolymer **RAD-IV** was synthesized incorporating **M-I**, **M-II**, **M-III**, and **M-IV** as comonomers into one polymer targeting a distribution of 60% 20% 10% 10%. A polymer with monomer ratios of 60%/21%/11%/8% (**M-I**/**M-II**/**M-III**/**M-IV**) was obtained as confirmed by ^{1}H-NMR spectroscopy (Figure 71). In addition to the signals observed for **M-I**, **M-II**, and **M-III** as elaborated for the polymers **RAD-II** and **RAD-III**, the proton signals between 7.3 ppm and 8.0 ppm corresponding to the aromatic protons of **M-IV** were used for the evaluation.

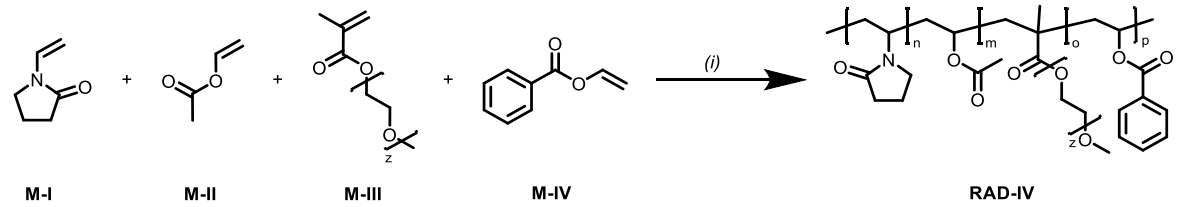

Scheme 17: Copolymerization of the monomers M-I, M-II, M-III, and M-IV; (i) M-I (200 eq.), M-II (67 eq.), M-III (33 eq), M-IV (33 eq), ACVA (1 eq.), iPrOH, 75 °C, 6 h. Solutions degassed by three freeze-pump-thaw cycles.

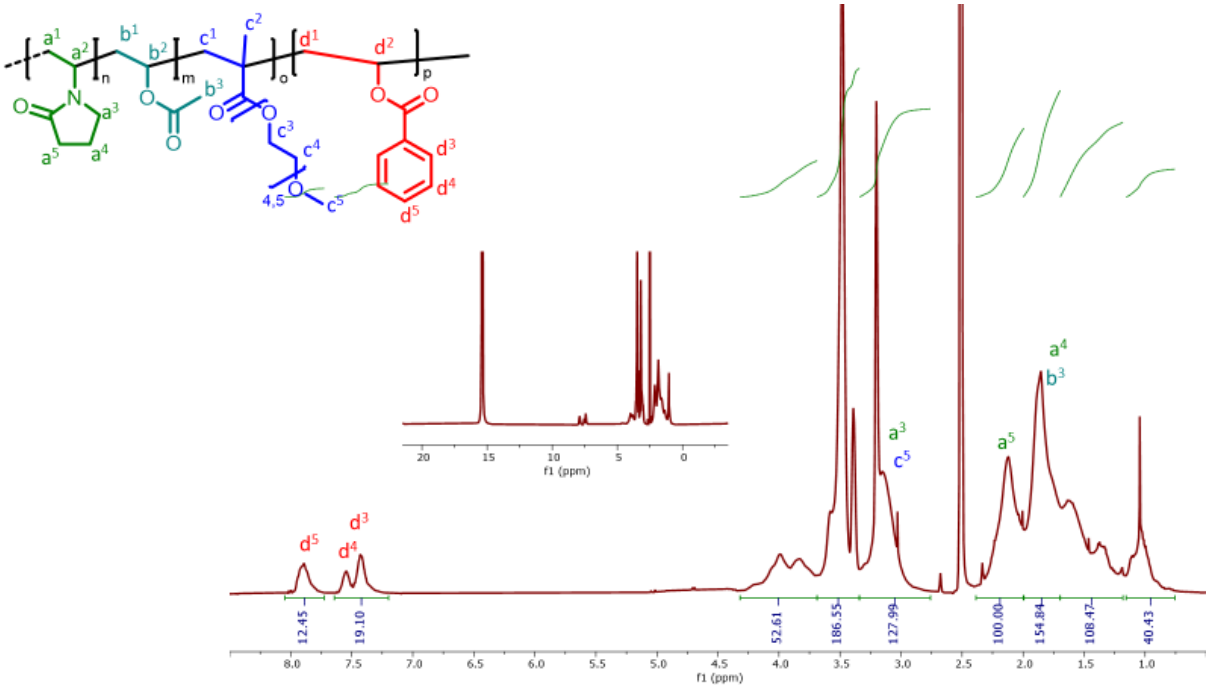

Figure 71: ^{1}H-NMR spectrum of RAD-IV normalized to M-I methylene moiety a^5. Monomer distribution in copolymer calculated based on integrated signals corresponding to methyl group b^3 of M-II, methoxy group c^5 of M-III and the aromatic protons d^3 to d^5 of M-IV.

The polymer has a mean molecular weight of $M_w = 38000$ g mol^{-1} and a dispersity index of $Đ = 3.3$. DSC measurements showed a glass transition temperature of 82 °C and TGA measurements showed a $T_{deg} = 194$ °C. Utilizing this monomer system, it was possible to synthesize a quaterpolymer which meets the anticipated comonomer distribution with high molecular weights a glass transition temperature in the expected range while having sufficient thermal stability. For degassing before the initiation of the polymerization during preparation was done by three cycles of freeze pump thaw.

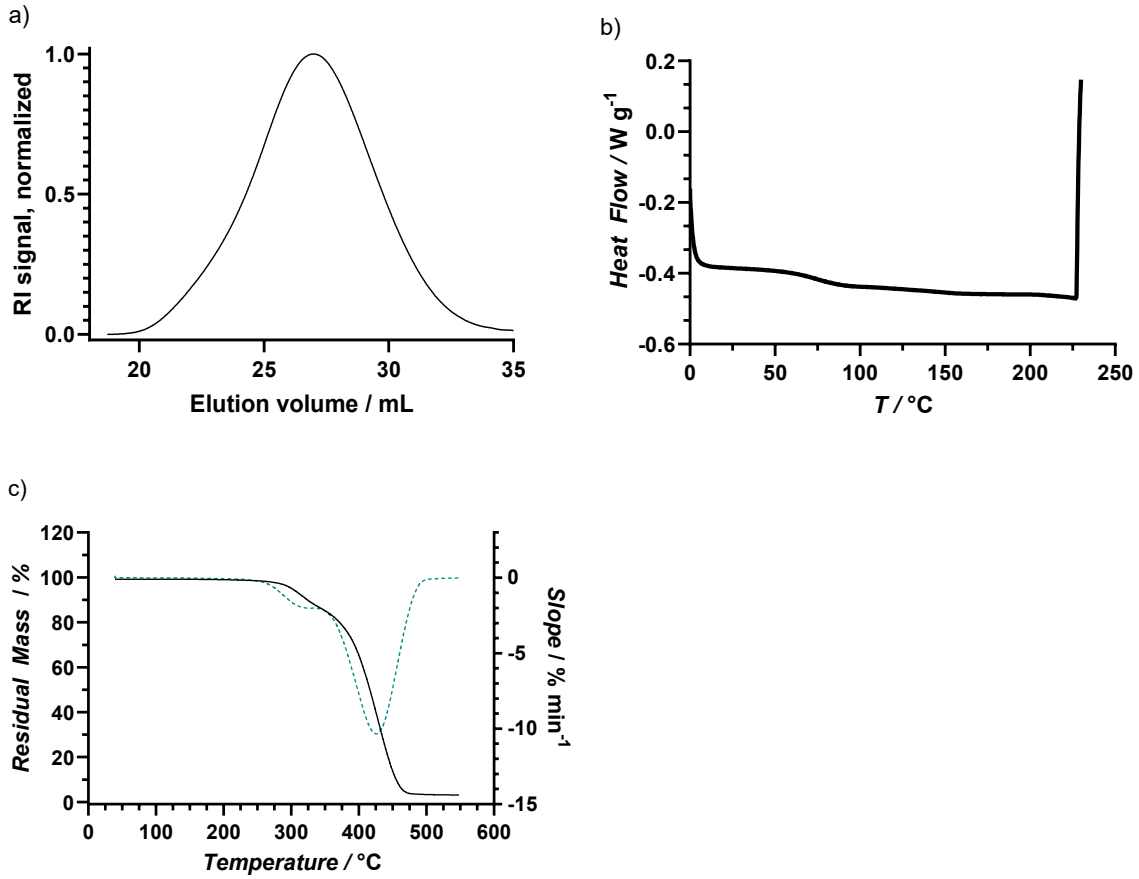

Figure 72: Characterization of RAD-IV: a) GPC-Elugram of RAD-IV with normalized RI signal. Measurement calibrated against PMMA standards in DMAc with 0.6 g L^{-1}LiBr; M_w = 38000 g mol^{-1} b) DSC thermogram of RAD-IV with a T_g = 82 °C c) TGA thermogram of RAD-IV (black) and the respective 1st derivative (blue) with a T_{deg} = 194 °C.

During the preparation of quaterpolymer **RAD-V** the solutions were degassed using nitrogen in contrast to the preparation of **RAD-IV**, where three cycles of freeze-pump-thaw was conducted. The same comonomer distribution (60/20/10/10, M-I/M-II/M-III/M-IV) was targeted. As confirmed by NMR spectroscopy, a polymer with the distribution 61%/22%/11%/6% was obtained. The monomer distributions show no significant differences (Figure 73).

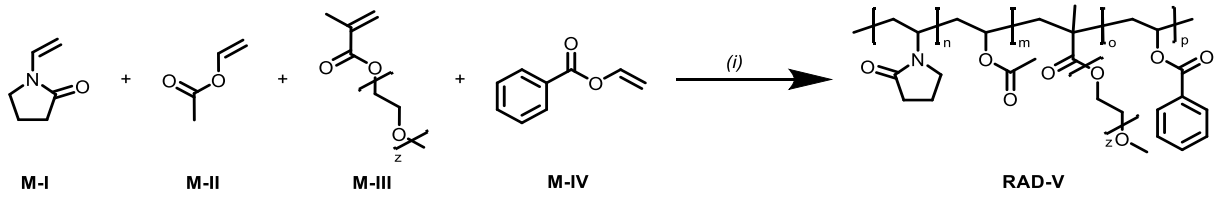

Scheme 18: Copolymerization of the monomers M-I, M-II, M-III, and M-IV; (i) M-I (200 eq.), M-II (67 eq.), M-III (33 eq), M-IV (33 eq), ACVA (1 eq.), iPrOH, 75 °C, 6 h. Solutions degassed by nitrogen bubbling.

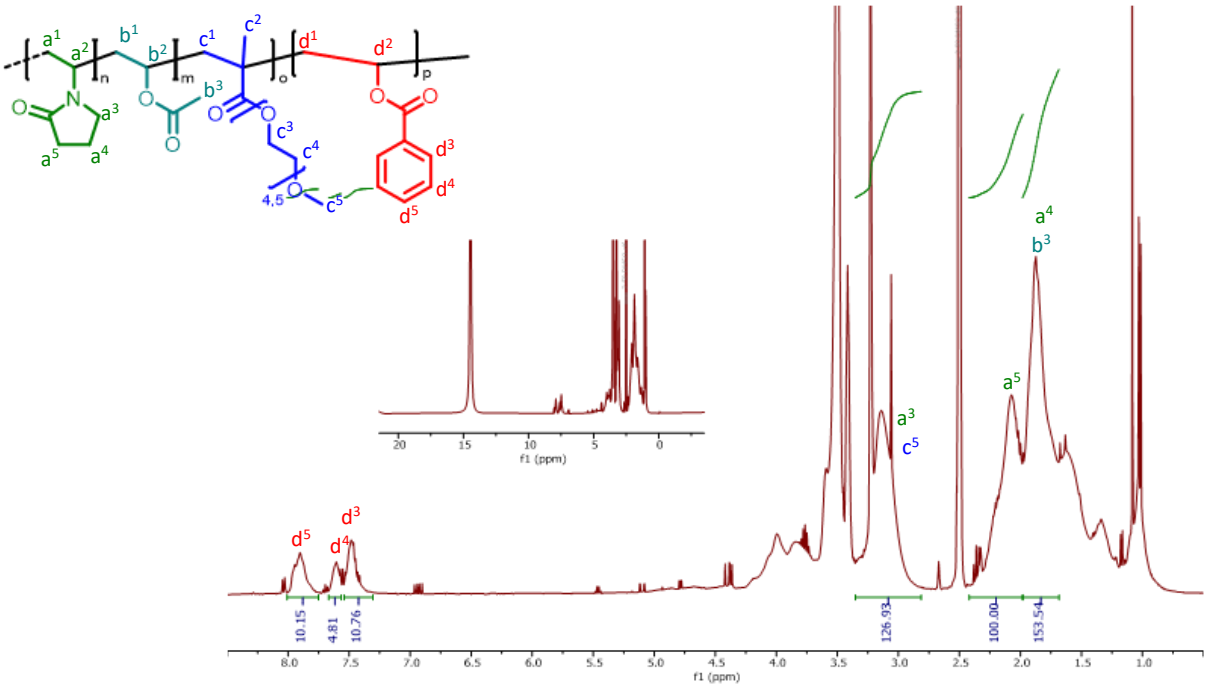

Figure 73: ^{1}H-NMR spectrum of RAD-V normalized to M-I methylene moiety a^5. Monomer distribution in copolymer calculated based on integrated signals corresponding to methyl group b^3 of M-II, methoxy group c^5 of M-III and the aromatic protons d^3 to d^5 of M-IV. Impurities correspond to residual MTBE.

The molecular weight of **RAD-V** is 42000 g mol^{-1} with a dispersity of 3.6 and the glass transition temperature was observed to be 85 °C (Figure 74). Also, these results show no significant difference compared to the preparation using freeze pump thaw for degassing. The polymers described in the following sections were prepared degassing the solutions with nitrogen.

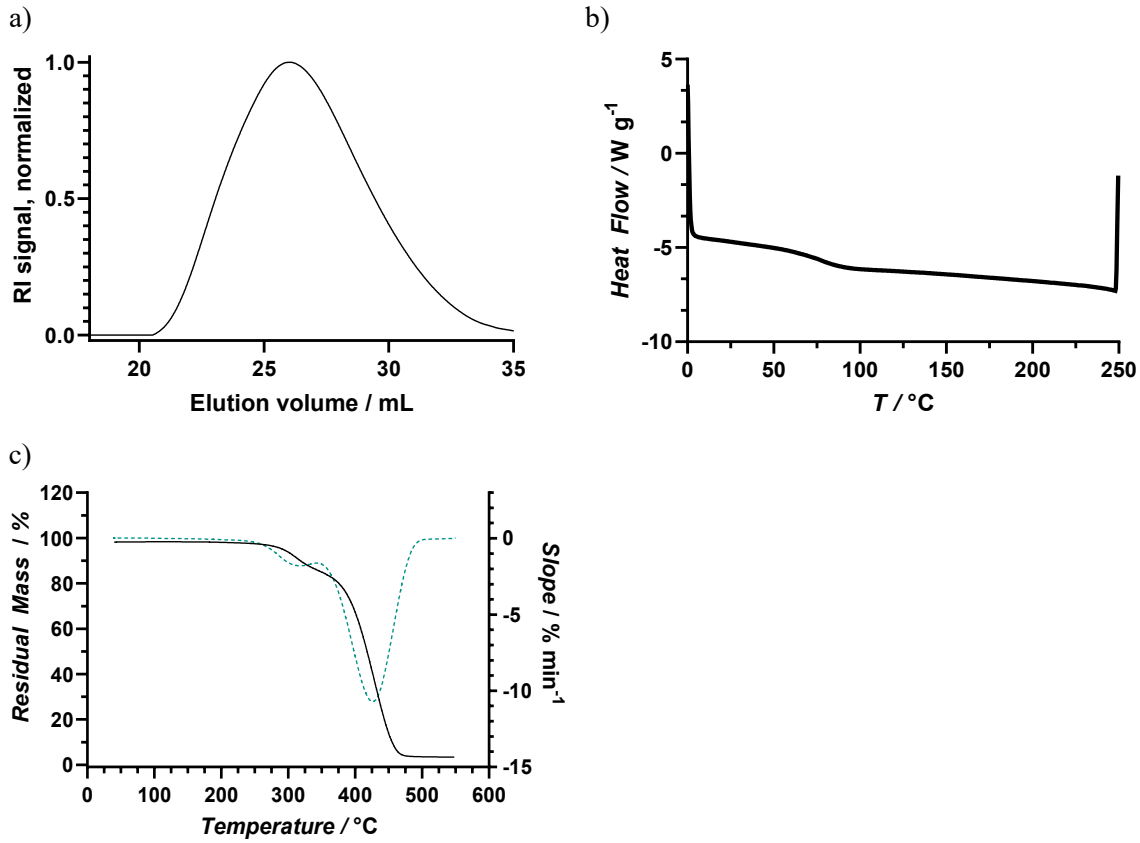

Figure 74: Characterization of RAD-V: a) GPC-Elugram of RAD-V with normalized RI signal. Measurement calibrated against PMMA standards in DMAc with 0.6 g L^{-1}LiBr; M_w = 42000 g mol^{-1} b) DSC thermogram of RAD-IV with a T_g = 85 °C c) TGA thermogram of RAD-V (black) and the respective 1st derivative (blue) with a T_{deg} = 195 °C.

As elaborated in the previous section, a synthesis process was developed for the synthesis of quaterpolymers with the monomer **M-I**, **M-II**, **M-III**, and **M-IV** without the removal of the inhibitor (Figure 75). The final synthesis protocol includes the preparation of multiple feeds which each are degassed using a nitrogen stream through the solutions. In order to reduce the probability of the formation of monomer blocks in the polymer, the different monomers are charged into the reaction vessel according to their respective reactivity via a dropping funnel or a syringe pump. During the reaction, five feeds are added to the reaction mixture to influence the comonomer concentration throughout the reaction time of 6 h. At a given timepoint during the reaction additional initiator is introduced. After the reaction, the polymer was isolated via precipitation from cold MTBE to obtain the polymer in high yields. A more detailed description of the synthesis process can be found in Section 8.

Theoretical safety considerations were performed to estimate if a safe execution of the polymerization is possible on a lab-scale and on a kilogram scale. Process parameters like the dosing times, the reaction times and reaction temperature as well as substance specific parameters like the individual substance amounts and boiling points were considered. The amount introduced via syringe pump was partitioned based on the addition time of Feed 2. Heat capacities were estimated based on values of similar chemical

structures. The calculation resulted in adiabatic temperature increases 19 K after the introduction of Feeds 1 and 2 and 5 K after the introduction of Feeds 3 and 4 respectively. The temperature increases in conjunction with the solvent iPrOH at the reaction temperature are suitable for the upscaling of a lab-scale process to kilogram scale. The calculation of the maximum heat flow resulted in values of 6.5 W kg^{-1} after Feed 1 and 2 and 1 W kg^{-1} after Feed 3 and 4 which is also suitable for the upscaling of the reaction.

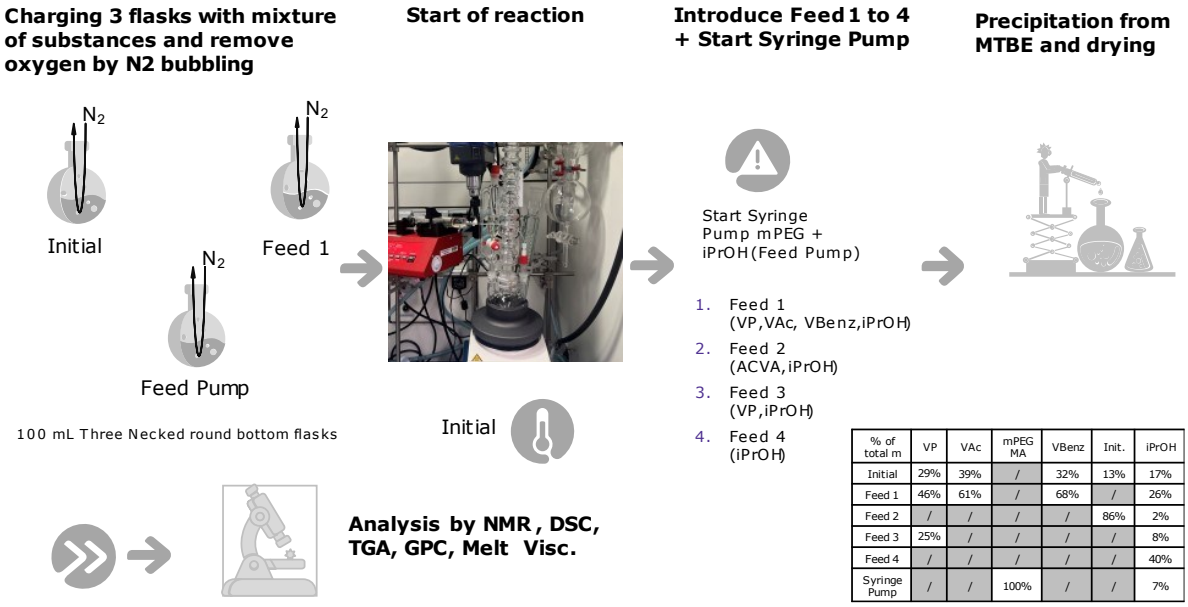

% of total m	VP	VAc	mPEGMA	VBenz	Init.	iPrOH
Initial	29%	39%	/	32%	13%	17%
Feed 1	46%	61%	/	68%	/	26%
Feed 2	/	/	/	/	86%	2%
Feed 3	25%	/	/	/	/	8%
Feed 4	/	/	/	/	/	40%
Syringe Pump	/	/	100%	/	/	7%

Figure 75: Schematic overview of the final process utilized for the synthesis of quaterpolymers reducing the probability of the formation of blocky sections due to reactivity differences of the respective monomers.

In summary polymers consisting of two to four monomers were successfully synthesized while optimizing the synthesis process (Table 33). By controlling the time of introduction of the degassed monomer solution during the process and the amount of introduced, the monomer ratios in the resulting polymer can be influenced. On the basis of the structure-property relationship resulting from previous studies, the successfully developed process as a result from the synthesis of the polymers **RAD-I** to **RAD-V**, is used to vary the monomer ratios in to optimize the properties of the resulting polymers.

Table 33: Summary of analytical data obtained for polymers synthesized by free radical polymerization as a proof of concept for the development of the synthesis process and the polymerization using up to four monomers. Synthesis protocols can be found in Section 8.2; n.d. means not detected.

	RAD-I	**RAD-II**	**RAD-III**	**RAD-IV**	**RAD-V**
Monomer 1	VP	VP	VP	VP	VP
Monomer 2	VAc	VAc	VAc	VAc	VAc
Monomer 3	-	AmPEG	mPEGMA	mPEGMA	mPEGMA
Monomer 4	-	-	-	VBenz	VBenz
rVP Exp	93	70	60	60	61
rVAc Exp	7	11	30	22	22
rPEG Exp	-	18	10	11	11
rAr Exp	-	-	-	8	6
rVP theo	76	55	55	60	60
rVAc theo	24	35	35	20	20
rPEG theo	-	10	10	10	10
rAr theo	-	-	-	10	10
Yield / %	60	8	78	49	52
Mass / g	3.02	0.2	9.8	6.01	6.71
T_g / °C	130	n.d.	43	82	85
T_{deg} / °C	124/ 267	141/261	270	194	195
$M_{w,theo}$ / g mol^{-1} †	35000	48000	40000	43000	43000
$M_{w,exp}$ / g mol^{-1}	71000	6000	30000	38000	42000
$Đ$	3.5	3.6	3.2	3.3	3.6
$M_{p,exp}$ / g mol^{-1}	60000	4000	27000	23000	32000

† Note, that the theoretical molecular weight is estimated and based on 100% conversion and is only viable if one initiator molecule starts exactly one polymer chain without taking into account side reactions, which lead to premature termination of the growing chain.

6.2.3 Quaternary Polymer Systems: Design of experiments

6.2.3.1 Setup of the Design and Synthesis

Aromatic moieties and hydrophilic moieties have a distinct influence onto the resulting polymer properties. In the last chapters this influence could be observed e.g. when using mPEG derivatives as comonomers, the processing temperature was greatly reduced. In Section 5, aromatic modifications led to a slight increase in glass transition temperatures. To further investigate and characterize this influence on the processing temperatures, an explorative design of experiments (DoE) was set up.

Table 34: Illustration of parameters varied in the DoE and their estimated influence on the properties of the resulting polymer.

Monomer	**Vinyl pyrrolidone** **M-I**	**Vinyl acetate** **M-II**	**mPEG methacrylate (hydrophilic)** **M-III**	**Vinyl benzoate (hydrophobic)** **M-IV**
Variation	None, constant at 60%	40% to 20%	0% to 10%	0% to 10%
Objective for Variation		Dependent on M-III and M-IV ratio Increased hydrophobicity	Increased hydrophilicity Reduction of processing temperature Decrease of T_g Decrease of processing temperature Decrease of $T_{1,10000\ Pa\ s}$	Increased hydrophobicity Increased hydrophobic interactions with API Increased Dissolution Performance
Other assumed effects		No significant influence on degradation Reduced solubility	Increased solubility No significant influence on degradation	Reduced solubility slight increase in T_g No significant influence on degradation

In addition to the thermophysical properties, the melt rheology is of great importance for the manufacturing in pharmaceutical extrusion. The thermophysical properties T_g and T_{deg} only give a crude impression of the performance in extrusion. The polymers **RAD-VII** to **RAD-XVII** were prepared in a similar manner as **RAD-V** (Scheme 18). A summary of the analytical data obtained is given in Table 43 and the corresponding evaluations and graphs not shown in this section can be found in the Appendix (Section 12.2.1). One exemplary set of data corresponding to the data gathered for each polymer is given below. The polymer **RAD-XV** was synthesized utilizing the same synthesis process compared to **RAD-VI**. A comonomer distribution of 60%/25%/5%/10%, **M-I**/**M-II**/**M-III**/**M-IV** was targeted and after the precipitation from MTBE the resulting polymer was analyzed. NMR analysis yielded a polymer with the comonomer distribution 60%/25%/7%/8%/ **M-I**/**M-II**/**M-III**/**M-IV** with a yield of 70%.

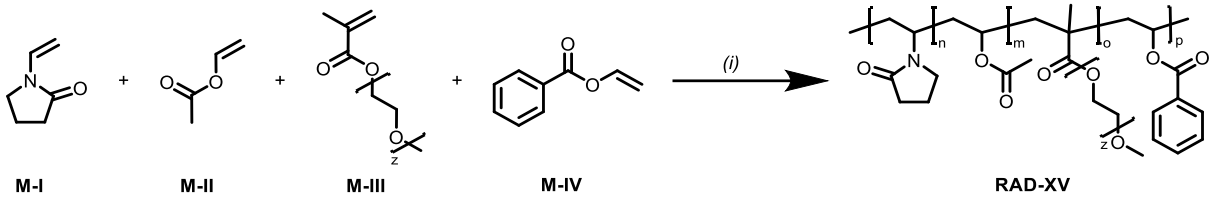

Scheme 19: Copolymerization of the monomers M-I, M-II, M-III, and M-IV for the formation of RAD-XV; (i) M-I (200 eq.), M-II (83 eq.), M-III (17 eq), M-IV (33 eq), ACVA (1 eq.), iPrOH, 75 °C, 6 h. Solutions degassed by nitrogen bubbling.

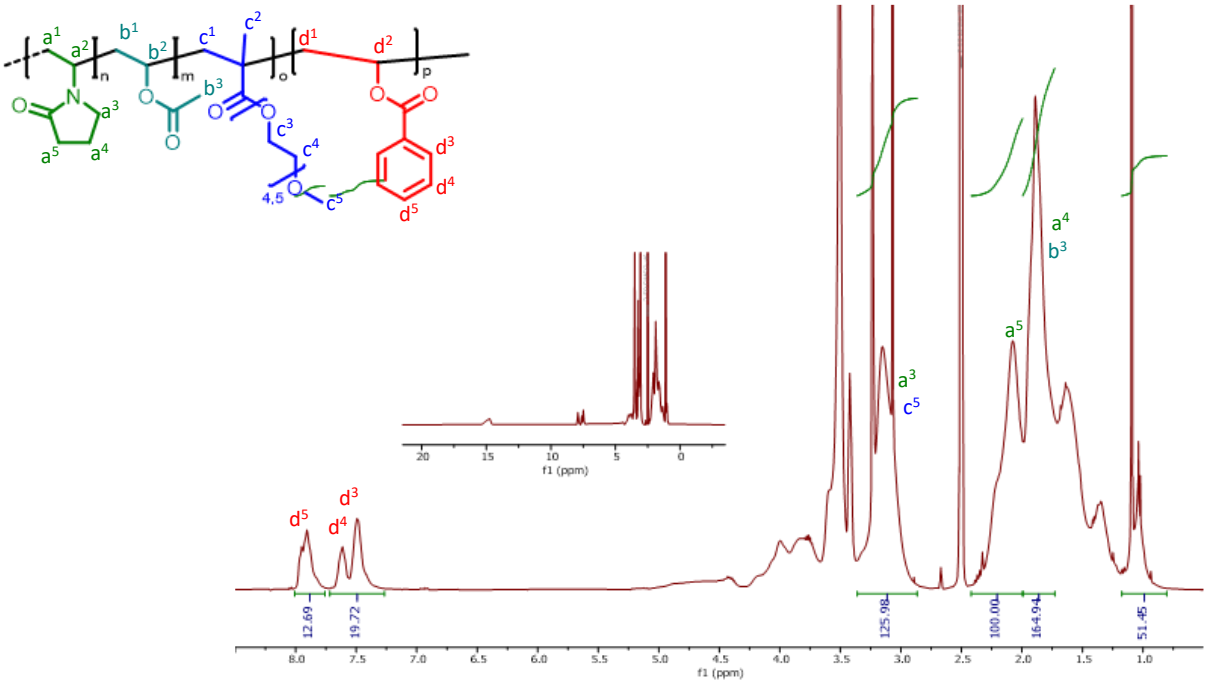

Figure 76: ^{1}H-NMR spectrum of RAD-XV normalized to M-I methylene moiety a^5 with the addition of TFA. Monomer distribution in copolymer calculated based on integrated signals corresponding to methyl group b^3 of M-II, methoxy group c^5 of M-III and the aromatic protons d^3 to d^5 of M-IV.

The polymer showed a mean molecular weight of M_w = 25000 g mol^{-1} with a dispersity index $Đ$ = 2.9 and thus matching the anticipated polymer properties (Figure 77). **RAD-XV** possesses a glass transition temperature of T_g = 97 °C without a melting point and a degradation temperature of T_{deg} = 221 °C. Melt rheology measurements confirmed the amorphousness of the polymer (G" above G') and the polymer reached at $T_{1,10000\ Pa\ s}$ = 132 °C and should be extrudable until $T_{2,1000\ Pa\ s}$ = 157 °C, leading to a processing temperature range of $T_{process}$ = 25 °C.

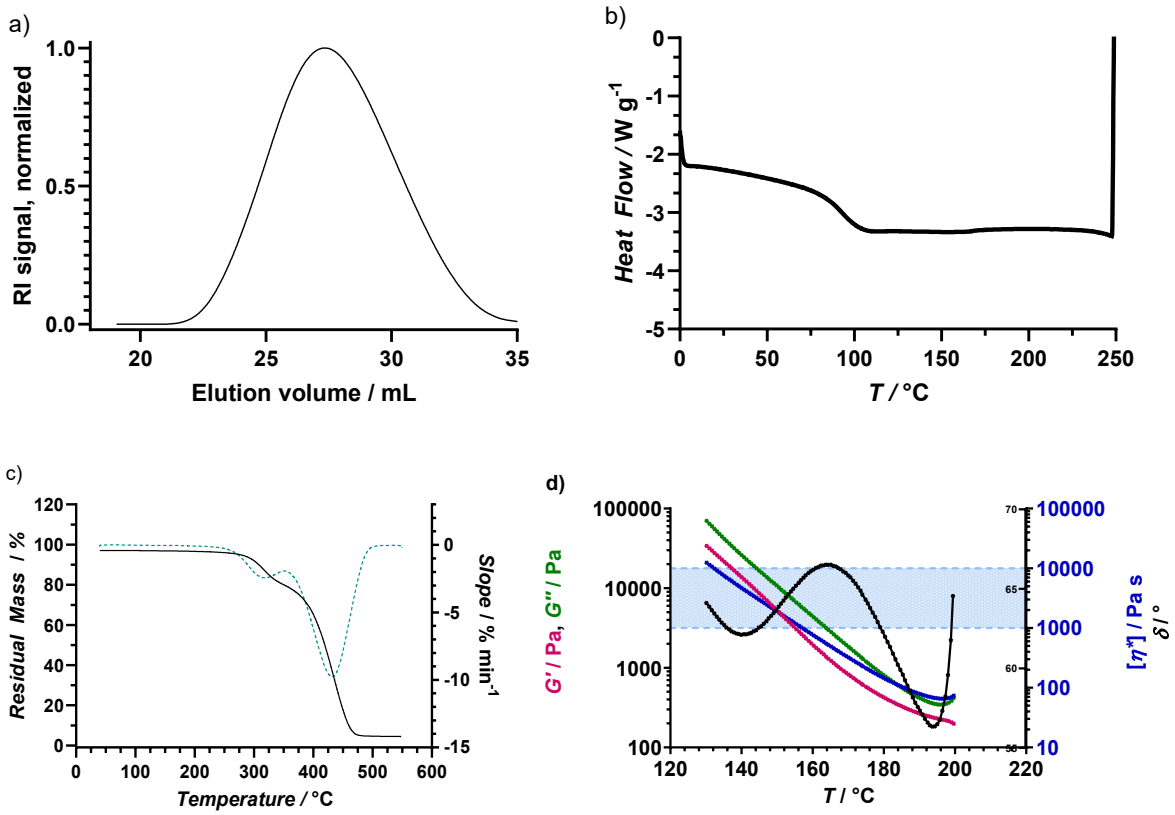

Figure 77: Characterization of RAD-XV: a) GPC-Elugram of RAD-XV with normalized RI signal. Measurement calibrated against PMMA standards in DMAc with 0.6 g L^{-1}LiBr; M_w = 25000 g mol^{-1} b) DSC thermogram of RAD-XV with a T_g = 97 °C c) TGA thermogram of RAD-XV (black) and the respective 1st derivative (blue) with a T_{deg} = 221 °C. d) Melt rheogram of RAD-XV, $T_{1,10000\ Pa\ s}$ = 157 °C $T_{2,1000\ Pa\ s}$ = 132 °C blue area confined by dashed lines indicates melt viscosity between η_{melt} = 1000 Pa s and η_{melt} = 10000 Pa s, blue: melt viscosity η_{melt}, red: G', blue: G'', black: phase angle.

The program MODDE was used for the setup of the DoE and the corresponding statistical evaluation. A quadratic D-optimal model with a statistic G-efficiency of 60.488 was chosen for the elucidation of the influences the hydrophilic and hydrophobic comonomer has on the resulting polymer properties. The D-optimal model with interaction was chosen to also analyze the interaction parameters between the separate factors (Table 35). In the design, the molar ratios of the comonomer **M-I**, **M-II**, **M-III**, and **M-IV** in the batch of a polymer preparation were varied. **M-III** and **M-IV** were varied from 0.00 to 0.10 each. In dependance to that, **M-I** was varied from 0.20 to 0.40. The **M-I** fraction was kept at 0.60 for all polymers. e.g., if the **M-III** and **M-IV** fraction was each 0.10, the **M-II** fraction results to 0.20, while the **M-I** fraction remains at 0.60. The number of repeating units were kept constant at 333 and the molar amounts of each monomer present in the respective polymer were calculated according to their ratios. With 11 experiments in the DoE including 3 center points an experiment list is produced, where each line represents a polymer which was prepared according to the randomized running order generated by the program (Table 36). This explorative DoE approach was limited to 4 responses, while one of them remained constant throughout the preparation of the experiments. The free radical polymerization of

multiple monomers has a plethora of degrees of freedom, as many different factors play a crucial role in the execution of chemical reactions. This DoE approach was utilized to get a first idea of the system only, because the addition of one or more factors would lead to a great increase in experiments which need to be executed. In previous studies, a qualitative structure-property relationship was developed which in turn was tested here in a statistical manner with a real-world problem. The statistical area was limited to three factors to enable the generation of a compact DoE system, whose execution was feasible in a reasonable time frame including all analytics and the statistical evaluation.

Table 35: Factors defined for the DoE.

Name	Abbreviation	Units	Type	Use	Variation Settings
Ratio M-I	rVP	Fraction	Formulation	Constant	0.6
Ratio M-II	rVAc	Fraction	Formulation	Controlled	0.2 to 0.4
Ratio M-III	rPEG	Fraction	Formulation	Controlled	0 to 0.1
Ratio M-IV	rAr	Fraction	Formulation	Controlled	0 to 0.1

Table 36: Worksheet as generated by MODDE for the execution of the DoE.

Sample No	Run Order	Ratio VP rM-I	Ratio VAc rM-II	Ratio mPEGMA rM-III	Ratio VAr rM-IV			
RAD-VII	10	0.60	0.40	0.00	0.00	1	0	0
RAD-VIII	1	0.60	0.35	0.00	0.05	¾	0	½
RAD-IX	4	0.60	0.35	0.05	0.00	¾	½	0
RAD-X	2	0.60	0.30	0.00	0.10	½	0	1
RAD-XI	9	0.60	0.30	0.05	0.05	½	½	½
RAD-XII	6	0.60	0.30	0.05	0.05	½	½	½
RAD-XIII	5	0.60	0.30	0.05	0.05	½	½	½
RAD-XIV	8	0.60	0.30	0.10	0.00	½	1	0
RAD-XV	11	0.60	0.25	0.05	0.10	¼	½	1
RAD-XVI	3	0.60	0.25	0.10	0.05	¼	1	½
RAD-XVII	7	0.60	0.20	0.10	0.10	0	1	1

The responses considered for the optimization are measured by DSC (T_g), TGA (T_{deg}), melt rheology measurements and mean molecular weight M_w. The melt rheology measurement provides information about the temperature at which the polymer melt reaches a melt viscosity of $\eta_{melt,T1}$ = 10000 Pa s and $\eta_{melt,T2}$ = 1000 Pa s, whose difference leads to the polymer's processing temperature in extrusion (Table 37).

Table 37: Responses as defined for the evaluation of the data generated by the DoE data.

Name	Abbreviation	Units	Condition	Objective	Min	Target	Max
T_g	T_g	°C	Required	Target	65	70	80
T_{deg}	T_{deg}	°C	Observed	Predicted	190		
$T_{1, (10000\ Pa\ s)}$	T_1	°C	Required	Target	120	130	140
$T_{2, (1000\ Pa\ s)}$	T_2	°C	Observed	Predicted	120		220
M_w	Mw	g/mol	Observed	Predicted			
Process Window	Tproc	°C	Observed	Predicted	10		

6.2.3.2 Analytical summary

After the preparation and the characterization of all polymers (Table 38 and Table 39), the influences of each factor (Table 35) on the responses (Table 37) were evaluated. The preparation was successful for each experiment number after a preparation in iPrOH with ACVA as the initiator and a precipitation step for purification. The feed contents were adapted to the presence of the monomers. **M-III** was always introduced via syringe pump and **M-IV** was introduced in the same manner as **M-II** and **M-I**, due to the reactivities being similar in vinyl monomers. The individual ratios for the monomers were obtained by NMR spectroscopy (Table 38). Comparing these with the targeted monomer distribution as defined during the DoE setup (Table 36), the obtained monomer ratios in the polymer are each close to target. r**M-I** is slightly higher than expected and r**M-II** is slightly lower than expected for most of the polymers, which was observed during the development of the synthesis process. The ratios for r**M-III** and r**M-IV** are close to target. Due to the uncontrolled nature of the free polymerization reaction, this is an expected result. As the observed ratios are close to the targeted ratios in each case and the individual difference of the obtained ratios compared to their targeted is low (Figure 78), these polymers are suitable for further analysis and were considered for the DoE evaluation.

Table 38: Results Table DoE. rM-I = VP; M-II = VAc; M-III = mPEGMA; M-IV = VBenzoate; *n*, *m*, *o*, *p* corresponds to the number of the respective monomers present in the polymer structure.

	rM-I exp	rM-I theo	rM-II exp	rM-II theo	rM-III exp	rM-III theo	rM-IV exp	rM-IV theo
RAD-VII	77%	60%	23%	40%	0%	0%	0%	0%
RAD-VIII	69%	60%	27%	35%	0%	0%	4%	5%
RAD-IX	70%	60%	22%	35%	8%	5%	0%	0%
RAD-X	66%	60%	26%	30%	0%	0%	8%	10%
RAD-XI	66%	60%	25%	30%	5%	5%	4%	5%
RAD-XII	65%	60%	24%	30%	7%	5%	4%	5%
RAD-XIII	70%	60%	21%	30%	5%	5%	4%	5%
RAD-XIV	64%	60%	23%	30%	13%	10%	0%	0%
RAD-XV	60%	60%	25%	25%	7%	5%	8%	10%
RAD-XVI	60%	60%	23%	25%	14%	10%	3%	5%
RAD-XVI	60%	60%	20%	20%	14%	10%	6%	10%

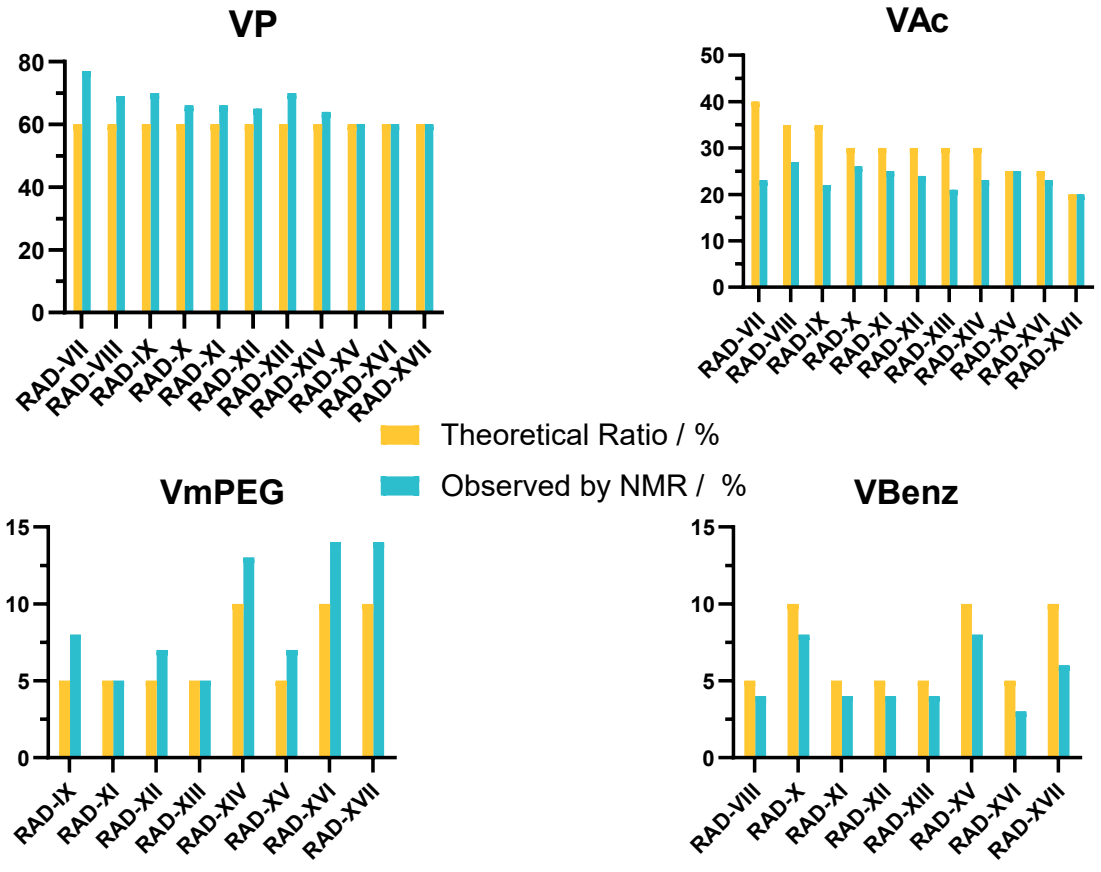

Figure 78: Comparison of targeted monomer ratio with observed monomer ratio for the monomers M-1, M-II, M-III and M-IV considering the polymers RAD-VII to RAD-XVII.

The thermophysical properties resulted in e.g., glass transition temperatures T_g which were in the expected range from low 38 °C at high ratios of **M-III** in the polymer to high 131 °C without **M-III** and

M-IV in the polymer (Table 39, Line 11 and 1). The influence of **M-III** in the reduction of the T_g is clearly visible, as higher ratios of the mPEG monomer in the polymer lead to substantial decreases in glass transition temperature (Figure 79a). The transition temperatures for polymers with the same amount of **M-III** are not identical which indicates that an additional influence on the T_g by one of the other monomers is present. When comparing T_{deg} of the polymer **RAD-VII** which includes only **M-I** and **M-II** as building blocks, the introduction of other monomers, **M-III** and **M-IV** respectively, did not have a significant influence on their degradation. The T_{deg} of each polymer is in the range of 192 °C to 226 °C, indicating sufficient thermal stability as a basis for a broad processing window (Figure 79b). The molecular weight of the polymers was small in some cases and lower than the estimated (Figure 79c). The estimation of the average molecular weight is based on a free radical polymerization, where one initiator molecule starts a singular chain, and where 100% conversion is reached. In addition to that, side reactions, or premature terminations were not accounted for in the estimation. In reality, free radical polymerizations seldom have 100% conversion, and a significant number of initiated chains do not polymerize without side reactions. This also leads to broad molecular weight distributions compared to controlled polymerization, which the high dispersity indices $Đ$ for the polymers demonstrate. In a best-case scenario, polymers of the same molecular weight are compared to each other, as then, the difference in molecular weight of the polymers does not have an influence on the dissolution performance. Also, the number of repeating units would be in a similar order leading to a similar amount of hydrophilic or hydrophobic moieties in the side chain of the polymer. Even though polymers were obtained with a $M_{w,exp}$ in the range of 11000 g mol^{-1} to 32000 g mol^{-1}, all polymers were used in the evaluation of the DoE.

Table 39: Compilation of analytical data obtained for polymers synthesized in the scope of the DoE and were used for the evaluation.

#	rM-I/rM-II/ rM-III/rM-IV	T_g / °C	T_{deg} / °C	$M_{w,\ theo.}$† / g mol^{-1}	$M_{w,\ exp.}$ / g mol^{-1}	Đ	$M_{p,\ exp.}$ / g mol^{-1}	T_1 / °C	T_2 / °C	T_{proc} / °C
RAD-VII	77/23/ 0/0	131	226	34000	12000	2.5	11000	160	183	23
RAD-VIII	69/27/ 0/4	121	212	35000	11000	2.5	10000	152	176	24
RAD-IX	70/22/ 8/0	87	223	37000	21000	2.9	16000	136	157	21
RAD-X	66/26/ 0/8	126	226	36000	12000	2.3	10000	152	177	25
RAD-XI	66/25/ 5/4	94	192	38000	14000	2.9	22000	126	146	20
RAD-XII	65/24/ 7/4	97	200	38000	16000	2.3	14000	125	148	23
RAD-XIII	70/21/ 5/4	103	225	38000	26000	2.1	12000	136	161	25
RAD-XIV	64/23/13/0	66	214	41000	31000	2.9	26000	119	143	24
RAD-XV	60/25/ 7/8	97	221	39000	25000	2.9	20000	132	157	25
RAD-XVI	60/23/14/3	68	224	42000	32000	3.0	25000	109	133	24
RAD-XVII	60/20/14/6	38	220	43000	19000	2.4	15300	73	89	17

† Note, that the theoretical molecular weight is estimated and based on 100% conversion and is only viable if one initiator molecule starts exactly one polymer chain without taking into account side reactions, which lead to premature termination of the growing chain.

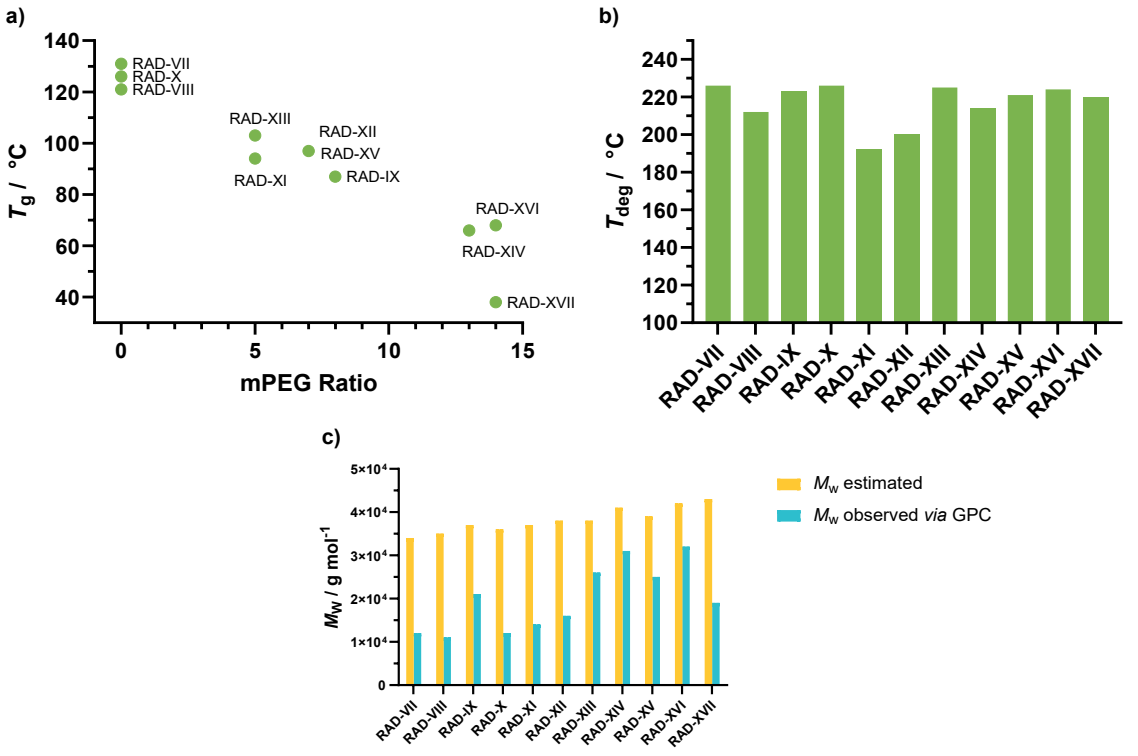

Figure 79: Glass transition temperature against the mPEG ratio. A clear decreasing influence at rising mPEG ratios can be observed.

The melt rheological Considering the analytical data obtained from melt rheology measurements, sufficiently broad ranges where extrusion is feasible were observed (Figure 80). Melt rheology

measurements were conducted by Alessandro-Giuseppe Elia (*Merck Life Science KGaA*). The lower limit of extrusion ($T_{1,1000\ Pa\ s}$) is roughly 30 °C higher than the observed T_g, which makes the T_g a good tool for a first estimate, but rheology measurements are a crucial tool to judge a polymer's extrudability. All polymers reach $T_{2,10000\ Pa\ s}$ before they start to degrade.

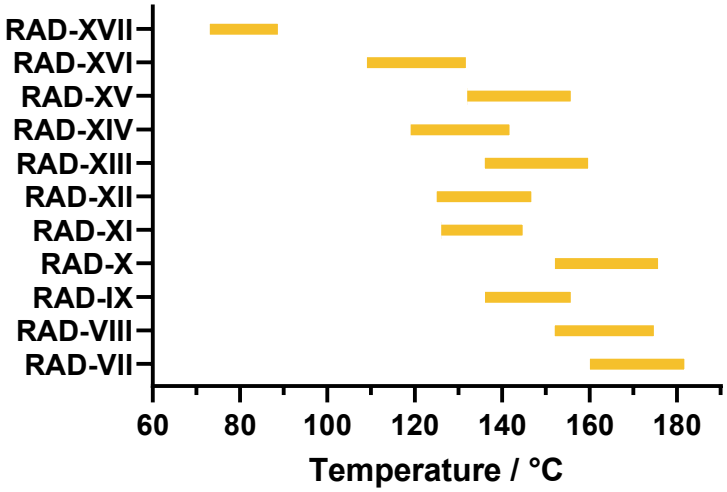

Figure 80: Melt rheological determination of the processing temperature of the polymers used in the DoE. The bar indicates the temperature range where the melt viscosity is between 1000 Pa s and 10000 Pa s.

In summary, the developed process for the targeted synthesis of polymers with distinct ratios of up to four monomer was successful for the eleven polymers needed in the DoE approach. The targeted monomer ratios could be observed in the synthesized polymers as confirmed by NMR and the thermal behavior resembles those known from previous experiments. Considering the previously established structure-property relationship, the trends elaborated were also visible in these polymers.

6.2.3.3 Program assisted evaluation of experimental results

During the analysis of a design of experiments dataset, multiple factors play a key role in the assessment of how good the statistical fit for each response is. A summary of fit plot gives a first impression on the validity of the model, which is high, if the bar for each response is at least above 0.5 (Figure 81). The summary of fit is a result of the analysis of each response on the basis of their residuals, their coefficients and their reproducibility. In each step of the evaluation, definite outliers are removed from the statistical model to increase the model's grade. In the following section, the summary of fit will be discussed. The detailed illustration of each response is given in Section 12.2.2 in the appendix.

The R^2-value (green bar) is a measure for the "Goodness-of-the-fit", assessing how close the actual data is to the regression line of the model. For T_g, T_{deg}, T_1, T_2 and M_w, R^2 is high meaning that the model can explain the variability around the mean in a good manner. For the processing temperature range

$T_{proc} = (T_1\text{-}T_2)$, the R^2 value is low, meaning that the model does not fit the data well. As T_{proc} is derived from T_1 and T_2 whose R^2 value is high, one can assume that the model is valid also for T_{proc}. One reason for low R^2 might be the differences between the center-points (Table 38, experiment 5-7).

The Q^2 (dark blue bar) is a measure for the "Goodness-of-prediction" showing how well the model predicts new data and assesses the variation of the response predicted by the model. Q^2 is around 0.8 for T_g and T_{deg}, indicating good prediction power of the model for these responses. It is around 0.6 to 0.5 for T_1 and T_2 indicating moderate predicting ability and captures a substantial portion of the variation of these responses. Q^2 in the case of M_w is 0.35 which indicates that the model has some, yet lower predictive power that for the other responses. For the processing temperature, the Q^2-value is negative, meaning that the present model has no predictive power. As the processing temperature is a derived response from T_1 and T_2, this is not surprising as even for those two source responses only moderate predictive power is obtained. The overall predictive power of the model is moderate to high and is sufficiently great for the real-world system of free radical polymerization when taking into account the low number of factors employed in the model.

The yellow bar in the histogram corresponds to the "Model Validity" and is an indicator for how valid the model is and if there is a "Lack-of-Fit" present. A perfect fit would result in a value of 1 and a substantial lack of fit would lead to a value below 0.25. As can be seen in the summary of fit (Figure 81, yellow bar), the model validity is above 0.55 in all cases and at its maximum for T_{deg} at 0.9. This shows, that the pure error is in the same range as the model error in all cases and the statistical model can be described as valid. To increase the model validity, more experiments would need to be conducted and/or more factors need to be considered in setting up the model. Taking a glance at the residuals (Figure 84), which directly influence the model validity, shows that most of the results considered are inside the 4 Standard Deviation (4 SD) range. The separate points in the respective figures are close to 0, show no clustering and show no systematic pattern. This also indicates, that the model validity is high for each response.

The last set of bars in the histogram (light blue) corresponds to the reproducibility. The reproducibility is defined as the variation of the response under the same condition, meaning the variation in the center-points of the model. Excluding the process temperature response, all other values for the reproducibility are above 0.9 and thus, reproducibility is given. As the process temperature is a derived response, and its Q^2 value is very low, its reproducibility can be neglected without questioning the high grade of the model.

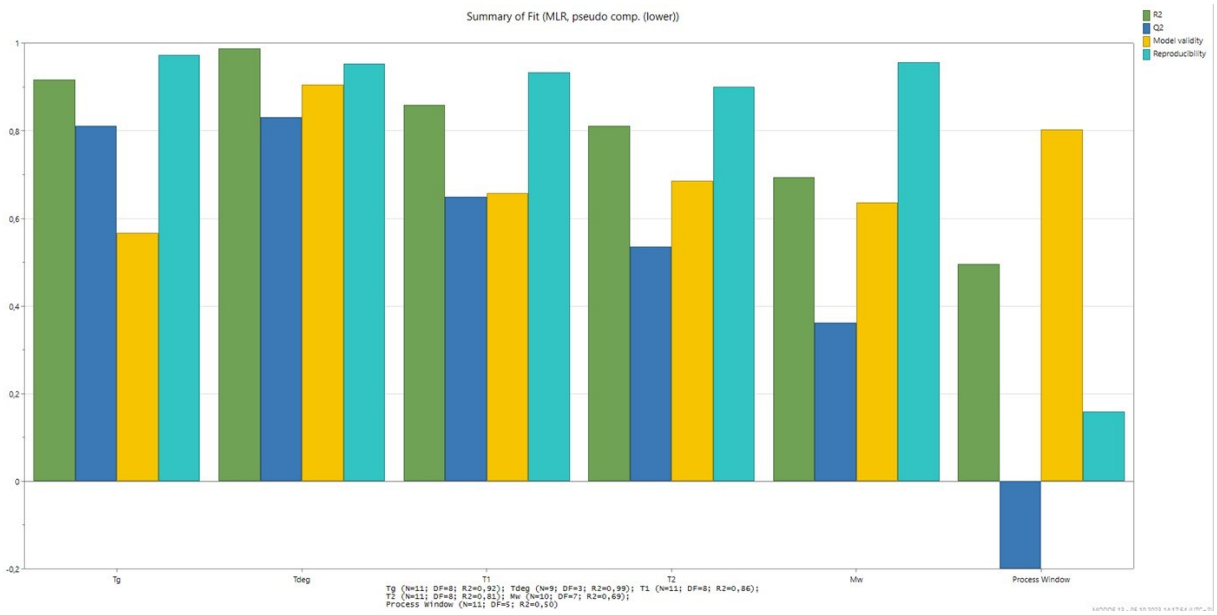

Figure 81: Summary of fit DoE

Each response is analyzed regarding their coefficients separately. If the error bar is significantly larger than the bar corresponding to the interaction (e.g. rVAc*rVAc, see T_{deg}, Figure 82), the interaction is not considered in the evaluation of the model. The coefficient values corresponding to the factors cannot be excluded. This way, the coefficients are cleaned from the interaction parameters where the error bar is significantly higher than the actual coefficient. This yields a more accurate model, and its predictability is increased.

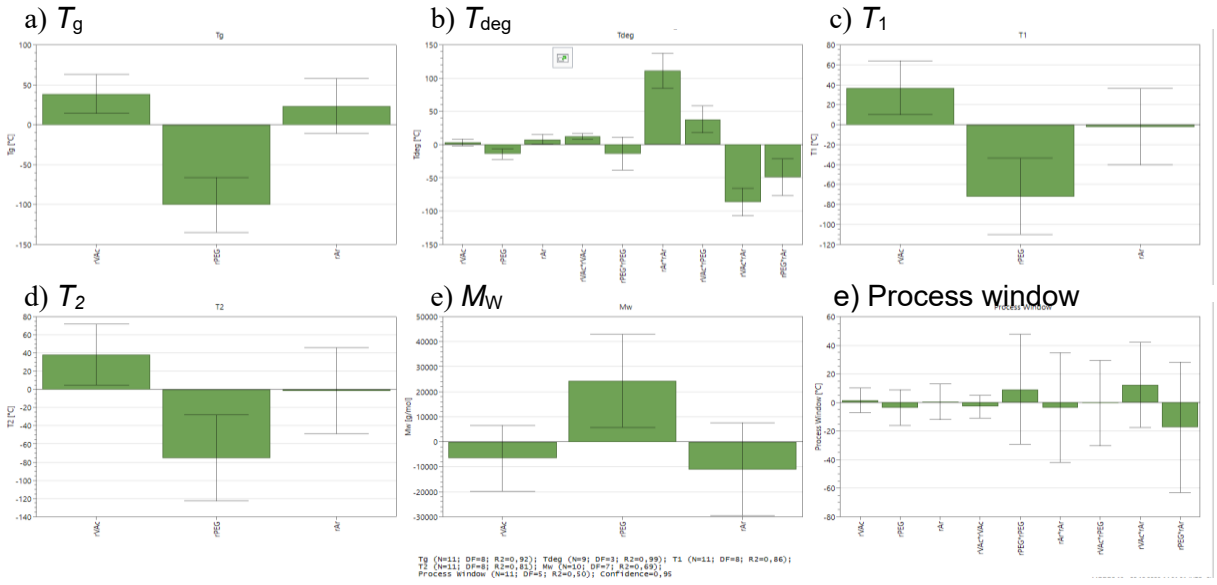

Figure 82: Coefficients Plots

In the overview plot (Figure 83) a summary is given corresponding to the response T_g. The red dotted lines in section a) are the boundaries set for the minimum, maximum and target value for a given response. The values are nicely spread, and it can be seen clearly, that there is an optimal polymer configuration possible to achieve the target criteria. On the right end side of the graph (Figure 83a, 9-11), the replicates can be seen, which have quite similar T_g values and show good reproducibility. The residual normal probability (Figure 83d) shows, that nearly each measurement lies inside the boundaries and close to an ideal straight line.

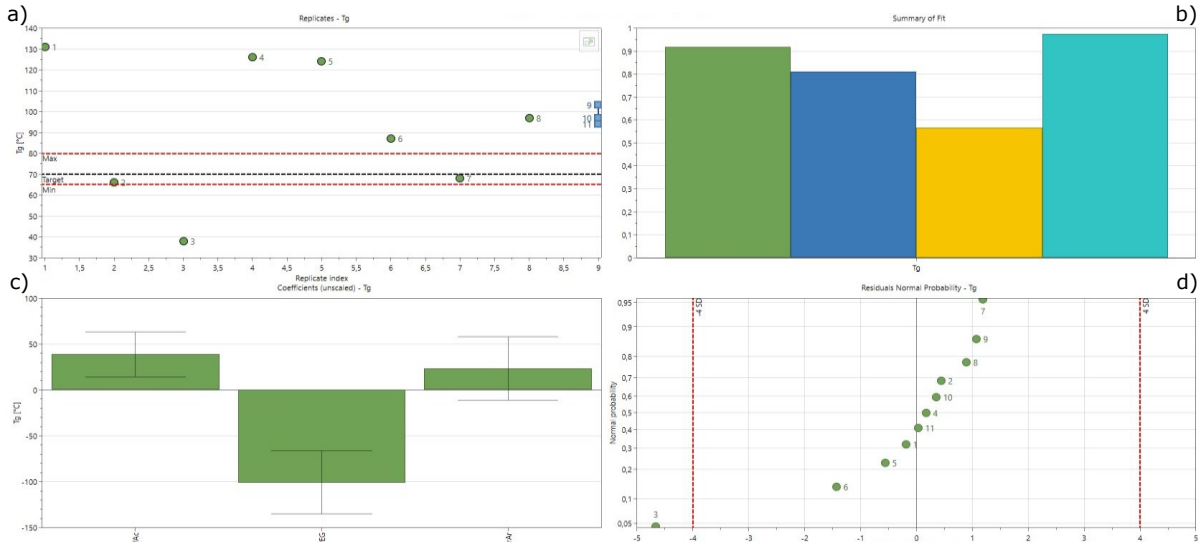

Figure 83: MODDE evaluation for factor T_g. a) Replicates, red dashed lines indicate the maximum and minimum set for the factor, the black dashed line indicates the target value, blue squares represent the center points and indicate reproducibility; b) Summary of fit, R^2 (dark green), Q^2 (dark blue), Model validity (yellow), Reproducibility (turquoise); c) Coefficients obtained for the specific experiments and used for the evaluation, error bars result from the MODDE evaluation; d) Residuals Normal Probability, dashed red lines indicate 4 standard deviations.

A good indicator for the validity of the model in question are the residuals for each response (Figure 84). The residuals in all cases are scattered around 0 and only a small number of outliers were identified, which were subsequently omitted in the evaluation (Number of removed outliers: T_{deg}: 2; M_w: 1). The position of the residuals mimics straight lines, which indicate a good model and good fit. In addition to mimicking a straight line the coordinates of the residuals themselves are spread across the whole coordinate space indicating a fitting depiction of the gathered data and a positive influence on the validity of the model.

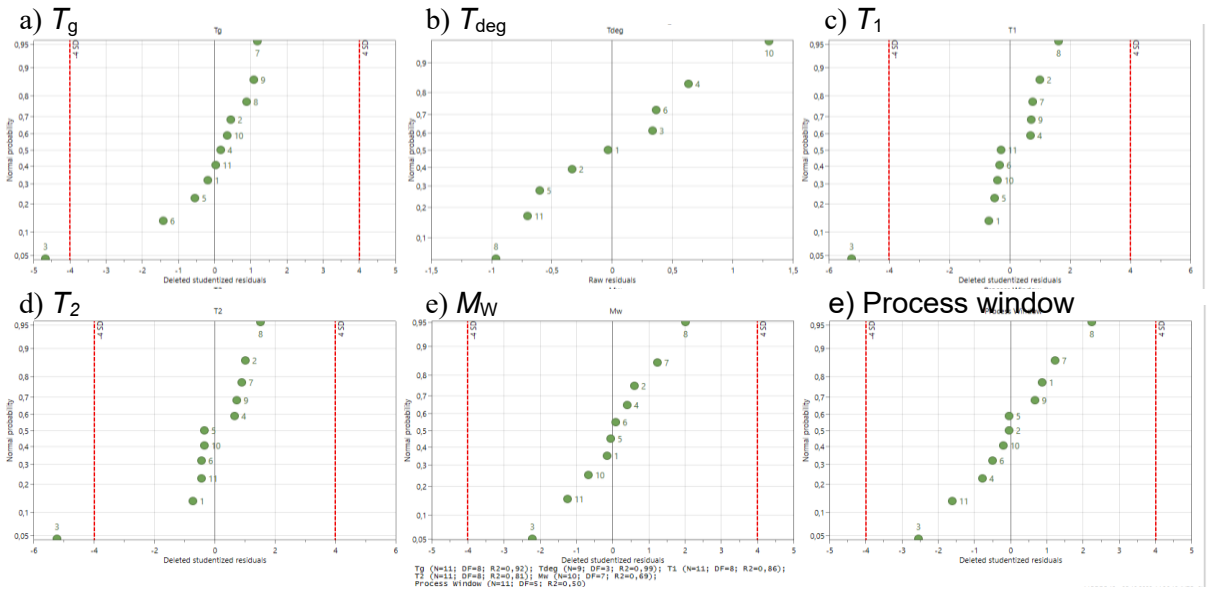

Figure 84: Residuals Normal Probability, dashed red lines indicate 4 standard deviations. One plot for each factor utilized in the model.

6.2.3.4 *Finding the optimized polymer: Sweet Spot Synthesis*

On the journey to find a more optimized polymer, the sweet spot analysis of a given system using DoE, is a well-known tool to enable the facile analysis of the design space. One other use case of the sweet spot analysis is to confirm the presumed high validity and high predictive power of the model (Figure 85). This is confirmed by synthesizing a polymer of the proposed constitution, followed by analysis and subsequent evaluation of its performance.

The most important responses were chosen from the model and an upper and lower boundary was set for the analysis (Figure 86). The factors T_g and T_1 are the most important properties to facilitate low processing temperatures of the polymer. Therefore, these were chosen to find the optimal monomer distribution for the optimization of the processing temperatures (Figure 86). An optimization with a target glass transition temperature of 70 °C and a target temperature of 130 °C at 10000 Pa s in melt viscosity was conducted resulting in a sweet spot area (Figure 85, bright green).

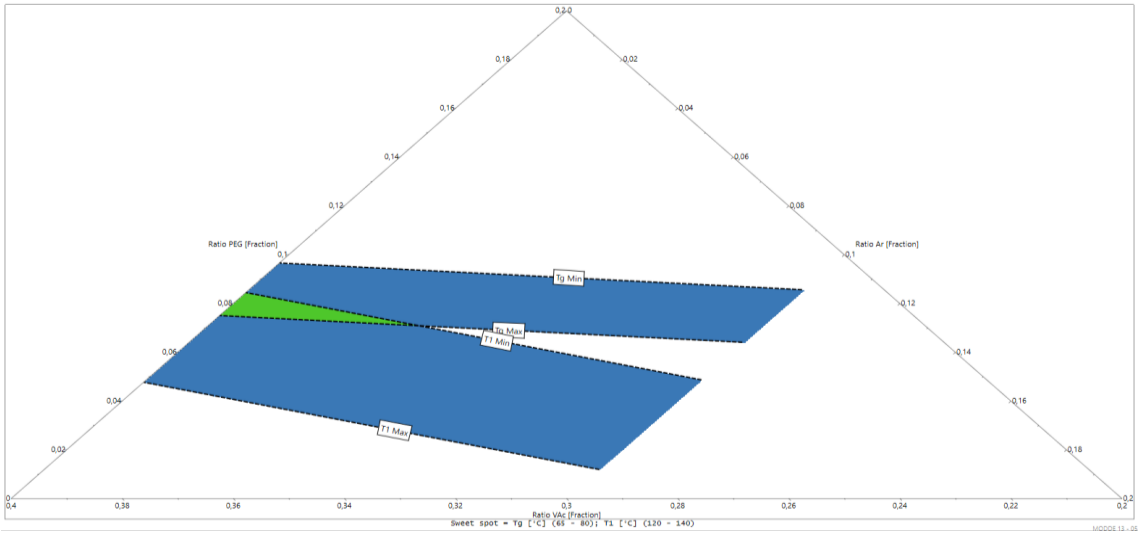

Figure 85: Sweet Spot Plot. Bright green area indicates design space where both criteria and set prerequisites corresponding to T_g and T_1 are met. The blue area indicates the design space where one criterion is met. Upper and lower limits set were: T_g = 65 °C to 80 °C with a target at 70 °C; T_1 = 120 °C to 140 °C with a target at 130 °C.

	Name	Abbreviation	Units	Condition	Objective	Min	Target	Max	Predicted min	Predicted max	Response range
1	**Tg**	Tg	°C	Required	Target	65	70	80	55,0606	132,393	
2	**Tdeg**	Tdeg	°C	Observed	Predicted	190			203,764	226,033	
3	**T1**	T1	°C	Required	Target	120	130	140	92,1515	166,085	
4	**T2**	T2	°C	Observed	Predicted	120		220	113,451	190,385	
5	**Mw**	Mw	g/mol	Observed	Predicted				10411,7	28088,3	
6	**Process Window**	Tproc	°C	Observed	Predicted	10			18,7579	25,6923	

Figure 86: Responses chosen (T_g and T_1) for the sweet spot analysis with upper and lower boundaries. White underlayed cells in column Min, Target and Max indicate the chosen responsed for the sweet spot analysis.

A polymer composition with a high ratio of **M-IV** (aromatic moiety, vinyl benzoate) inside the boundaries of the sweet spot area was chosen for the confirmation of the DoE model. In an identical synthesis process, the polymer was prepared on three different time points. The resulting polymers **RAD-XVIII**, **RAD-XIX**, and **RAD-XX** were analyzed regarding the relevant polymer properties for verification of the prediction and additionally, the confirmation of the model (Table 40). More detailed results can be found in the Appendix Section 12.2.2.2.

Table 40: Summary of analytical data for the sweet spot synthesis including deviations of the three experiments. See Appendix, Figure 94 for corresponding analytical data.

Parameter	Target	Achieved	
Ratio M-I	60 %	62%	± 2%
Ratio M-II	30%	24%	± 2%
Ratio M-III	5%	9%	± 1%
Ratio M-IV	5%	4%	± 0%
M_W / g mol^{-1}		28000	± 4000
$Đ$		3.0	± 0.3
T_g / °C	80-90	88	± 2
T_{deg} / °C	>200	225	± 5

The results obtained for the polymers synthesized as the sweet spot match the properties predicted by the Design of Experiments model. The model was able to predict the ratios for a polymer with optimized properties. Also, the reproducibility was given for these three polymers. This further underlines the robustness and predictive power of the model.

6.2.3.5 Confirming the polymer properties: Extrusion

Each polymer synthesized during the design of experiments approach was extruded on a small-scale twin screw extruder (Section 12.2.3). In general, the extrusion was set up to start at the lower extrudable temperature $T_{1,10000\ Pa\ s}$. The polymer was fed into the extruder until around 10 cm of filament was produced. After the successful production of a filament strand, the temperature was increased in steps of 10 °C. Another 10 cm of filament was produced. This was proceeded until at least the higher temperature of extrudability $T_{2,1000\ Pa\ s}$ was reached. In some cases, the temperature was increased further above this temperature. For each temperature point, filament was collected and judged based on the appearance, the opacity, and flexibility in a qualitative way.

As can be observed from the various photographs and descriptions in the respective table (Table 72), one can say that the extrusion temperature directly links to the temperatures predicted by melt rheology measurements. Not only is this analysis technique a good way to predict the extrudability, it also is sufficiently precise to predict the lower temperature of extrudability on a laboratory scale mini twin screw extruder.

6.2.3.6 DoE as a tool to find an optimized polymer

In conclusion, with the utilization of the model, a polymer with optimized properties was predicted and successfully synthesized. The polymer showed properties as were predicted by the model. One can argue, that a good model for the design space was generated with high validity and high predictive power. The model has the ability to correctly predict a polymers property in terms of the glass transition temperature and lower boundary of processability via extrusion. The deliberate preparation of the sweet spot polymer in the design space was successful and the targeted properties were achieved. Chemical reactions have many more degrees of freedom than the ones used in the set-up of the design space and can only be portrayed in a majorly simplified way. As can be seen from the summary of fit (Figure 81), even with this simplification, the present design of experiments leads to a statistical fit, which is able to correctly evaluate a monomer's influence on the processing temperatures. The mPEG methacrylate monomer **M-III** has a strong decreasing effect on the processing temperature. The monomers **M-I** and **M-II** have an increasing effect on the processing temperature, whereas the increase of **M-II** is a more powerful effect. This is also true for the factors T_1 and T_2.

6.2.4 Dissolution enhancement of poorly water-soluble API's

In solid formulation, next to the optimization of a polymer's processability, its capability in terms of the dissolution enhancement regarding a model API is of great interest. New active pharmaceutical ingredients are typically poorly water soluble and consist of a multitude of hydrophobic moieties in their chemical structure. These structures and their tendency to form insoluble crystal systems lead to a need in polymers exhibiting capabilities for preventing this crystallization and increasing this low solubility. Only when solubilized, BCS-II compounds are biologically available, and have an effect as a pharmaceutical agent.

A testing assay was developed adapted from literature[131, 160] utilizing simulated gastric fluid as medium, where a polymer entity is combined with an API, to monitor its dissolution behavior. The model compound chosen for these tests is ketoconazole (Table 3), a small molecule API bearing multiple hydrophobic moieties including halogenated aromatic rings and aromatic ether groups. In this testing assay, the API is mixed with a sample polymer in a physical mixture with 40w% drug load. This mixture is then amorphized utilizing a vacuum compression molding method (VCM, *Meltprep*), where the mixture is heated to a polymer specific temperature above the glass transition temperature and with the help of vacuum and a piston, a thin disc is created. This disc mimics a small piece of filament usually produced during an extrusion. In contrast to the dissolution assay described in Section 0, the discs generated by VCM are milled and tested in the assay, so the results obtained in this chapter can not be compared to the results obtained in Section 0. This assay enables the investigation of dissolution capabilities in small scales and imitates the large-scale production of filaments via extrusion in solid formulation and their consecutive milling before manufacturing the actual tablets. A detailed description of the procedure is given in Section 8.

From the polymers prepared during the design of experiment, three polymers were chosen and compared to a benchmark. As two of the monomers utilized in the quaterpolymers are also used in the marketed product Kollidon® VA64 (PVP-co-PVAc), it seems natural to compare the novel polymers with this polymer entity. The polymers **RAD-IX**, **RAD-XI**, and **RAD-XV** were chosen due to the increasing ratio of the aromatic moiety **M-IV** and otherwise similar ratio of the other comonomer **M-I**, and **M-III** (Table 41). Furthermore, their average molecular weight is in the same range and therefore the fraction of low molecular weight species in the monomodal distribution is of similar size. This enables comparability, as the influence of small molecular weight fractions onto the dissolution performance is minimized. The dissolution experiments and the evaluations were conducted by Nabil Lamrabet (*Merck Life Science KGaA*).

Table 41: Polymers utilized in dissolution assay.

#	**rM-I** VP exp	**rM-II** VAc exp	**rM-III** mPEG exp	**rM-IV** VBenz exp	DSC T_g / °C	TGA T_{deg} / °C	GPC $M_{w,\ theo.}$ / g mol^{-1}	$M_{w,\ exp.}$ / g mol^{-1}	Melt Viscosity T_1 / °C	T_2 / °C	T_{proc} / °C
Kollidon® VA64	0.55	0.45			135	226		31000			
RAD-IX	0.70	0.22	0.08	0.00	87	223	37000	21000	136	157	21
RAD-XI	0.66	0.25	0.05	0.04	94	192	37000	26000	126	146	20
RAD-XV	0.60	0.25	0.07	0.08	97	221	39000	25000	132	157	25

All polymers have favorable influences on the dissolution behavior of the model API. All polymers show a spring-parachute effect, were the API-concentration in the solution quickly increases and reaches a maximum before the concentration declines. The polymers differ in their onset time until the maximum concentration of API is reached. PVP-co-PVAc has a quick onset reaching high concentrations after 10 minutes with a maximum after 30 minutes. The polymer **RAD-IX** has a slower onset in the first 30 minutes with a maximum after 60 minutes. The polymer **RAD-XI** shows a similar behavior to **RAD-IX** but reaches the maximum concentration at the 30 minute sample point. **RAD-XV** also reaches the maximum concentration after 60 minutes with a similar course of the curve compared to the other tested polymers. Comparing the three polymers generated during the DoE investigation, one can clearly observe a trend at which the maximum concentration in solution increases with the aromatic comonomer content. The quaterpolymers take longer than PVP-co-PVAc to reach the maximum API-concentration. The negative slope during the decline in API concentration is lower for **RAD-XV**, which indicates a longer parachute phase and higher API concentration for a longer period in time. The initial increase in API concentration (*spring effect*) of the novel polymers is spread across a longer time frame. The longer onset time of the novel polymers could correlate with a decreased water solubility of the final test specimen because of the introduced hydrophobic moiety, although the exact solubility was not tested. In comparison to the pure API, which has a very low solubility in the dissolution medium, all tested polymers have strong abilities in terms of super saturation of the testing solution.

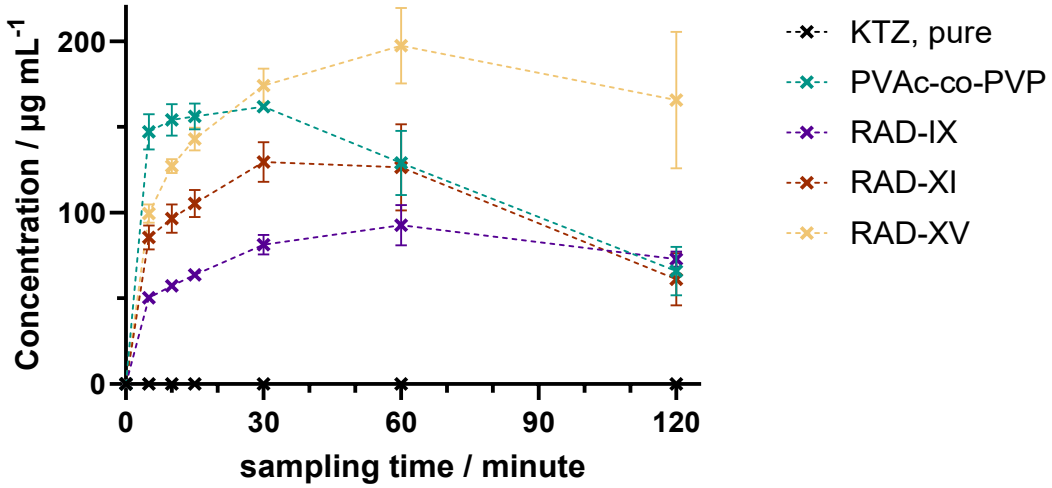

Figure 87: Dissolution capabilities of selected polymers and benchmark PVAc-co-PVP (Kollidon® VA64) in comparison to pure, crystalline API. Non-sink dissolution of amorphized samples through melt-quenching in FaSSIF at pH 6.5 at 37 °C, 6 mg of drug in 8 mL medium, arithmetic means ± SD (n = 3), drug: Ketoconazole at 40% drug load; HPLC analysis at λ = 225 mm. Discs were milled before assay. Dashed lines incorporated to guide the reader's eye.

By calculating the *AUC* for the polymers used for dissolution experiments (Figure 88, and Table 42), it is evident that dissolution capability is improved with increasing **M-IV** content. The polymer **RAD-XV** with 8% aromatic **M-IV** content performs better than the benchmark PVAc-co-PVP with an *AUC* of 20300 ± 1400 and 14500 ± 800 respectively. These results suggest, that in the chosen polymer/API system using KTZ as the API, the novel polymer has increased dissolution capabilities and can be processed at lower temperatures compared to PVAc-co-PVP.

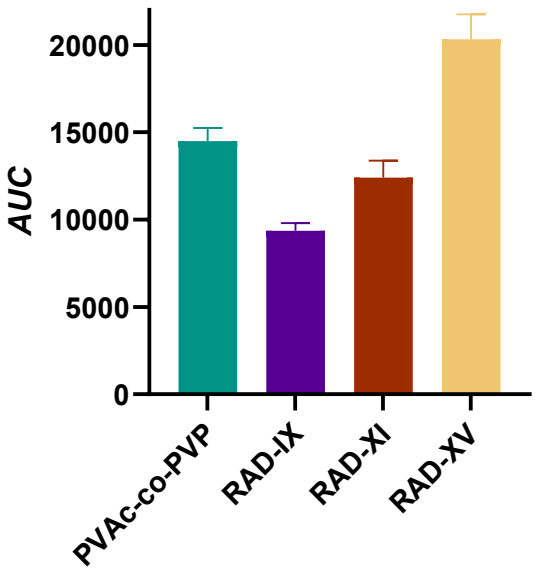

Figure 88: *AUC* of Benchmark PVAc-co-PVP and polymers synthesized in DoE. *AUC* was calculated utilizing the "area under curve" functionality in the program GraphPad Prism. Arithmetic means ± SD (n = 3)

Table 42: *AUC* of DoE polymers in comparison to PVAc-co-PVP as benchmark

Polymer	AUC
PVAc-co-PVP	14500 ± 800
RAD-IX	9400 ± 400
RAD-XI	12400 ± 1000
RAD-XV	20300 ± 1400

6.2.5 Proof-of-concept: Synthesis at Pilot-Scale

As elaborated in Section 6.2.4, a higher amount of aromatic moiety in the polymer leads to an increased maximum API-concentration in the tested medium. Although the onset time until the maximum concentration is reached seems to be longer the more aromatic comonomer is present, this may be tuned by the molecular weight distribution as elaborated in Section 5.2.4. To further investigate the ideal polymer for the processing via extrusion and subsequently the dissolution enhancement of a poorly soluble API, a polymer with high aromatic content was synthesized. The synthesis process was thereby transferred to a process development laboratory, upscaling the quantity synthesized in one batch. This also served as a proof-of-concept, if the synthesis process can be transferred to larger reactors using the current procedure (Scheme 20).

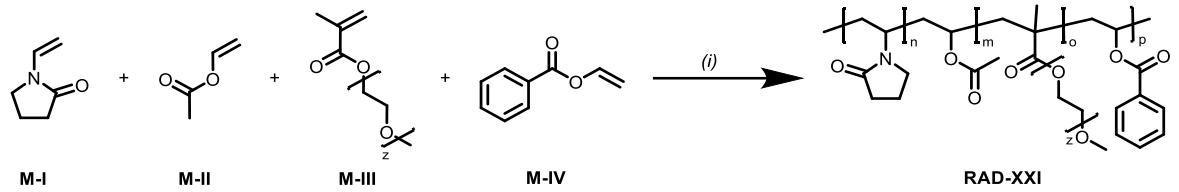

Scheme 20: Copolymerization of the monomers M-I, M-II, M-III, and M-IV; (i) M-I (167 eq.), M-II (83 eq.), M-III (17 eq), M-IV (67 eq), ACVA (1 eq.), iPrOH, 75 °C, 6 h.

The targeted polymer **RAD-XXI** has the comonomer distribution of 50%/25%/5%/20% (**M-I**/**M-II**/**M-III**/**M-IV**). As confirmed by ^{1}H-NMR the copolymerization in a 150 g scale with the identical process as described in Section 6.2.2.1 was successful resulting in a copolymer with the comonomer distribution of 49%/30%/5%/16% (**M-I**/**M-II**/**M-III**/**M-IV**). After precipitation from MTBE the polymer could be isolated in 78% yield. GPC analysis showed a polymer with a mean molecular weight of M_w = 26000 g mol^{-1} and a dispersity index of $Đ$ = 2.8, which is in good agreement with the anticipated molecular weight. The polymer shows a T_g = 96 °C while the thermal stability is high with a T_{deg} = 211 °C (Figure 89).

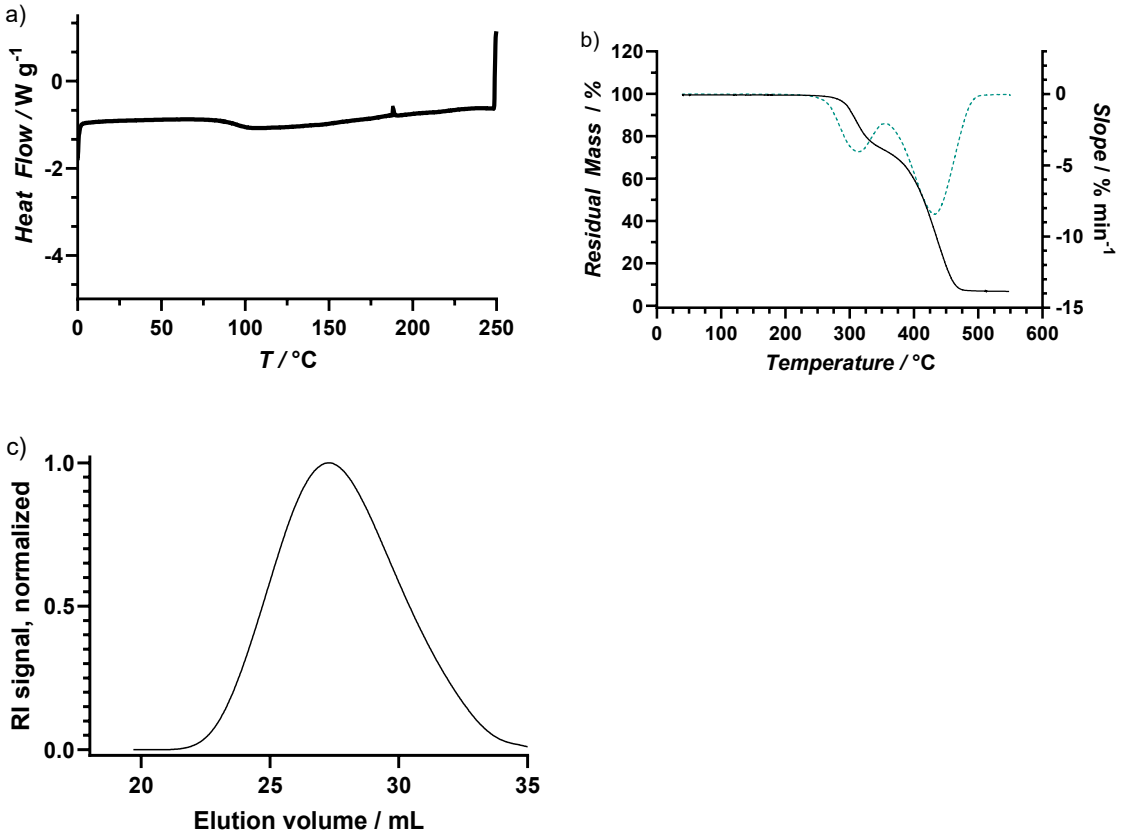

Figure 89: Characterization of RAD-XXI: a) DSC thermogram of RAD- XXI with a T_g = 96 °C; b) TGA thermogram of RAD-XXI (black) and the respective 1st derivative (blue) with a T_{deg} = 211 °C; c) GPC-Elugram of RAD- XXI with normalized RI signal. Measurement calibrated against PMMA standards in DMAc with 0.6 g L^{-1}LiBr; M_w = 26000 g mol^{-1}.

Polymer **RAD-XXI** was analyzed concerning its super saturation potential utilizing the assay elaborated in Section 6.2.4 (Figure 90). In comparison to polymers with less aromatic ratios in the backbone, the onset of the concentration increase is longer. In the measured timeframe of 120 minutes, **RAD-XXI** does not show a maximum, whereas the polymers **RAD-IX**, **RAD-XI**, **RAD-XV**, and PVP-co-PVAc all show a maximum API concentration in this time frame. One reason for this may be a lower solubility in the testing medium due to the increased presence of hydrophobic moieties in the backbone. The curve progression of **RAD-XXI** allows the assumption, that a maximum in API concentration will be reached at a later stage, after the 120 minute mark. As no maximum can be observed in the time frame of the assay, no statement can be made about the overall performance of the polymer **RAD-XXI**. The lesser performance of **RAD-XXI** is also visible in the $AUC = 12600 \pm 700$ (Figure 91), where the value is below that of **RAD-XV**, even though the **M-IV** ratio is higher. One would expect the polymer-API interaction to be greater than in the other cases with a lower number of aromatic moieties in the backbone, whereas higher numbers of aromatic moieties supposedly lead to a higher concentration of API and thus a higher dissolution enhancement in this polymer/API system.

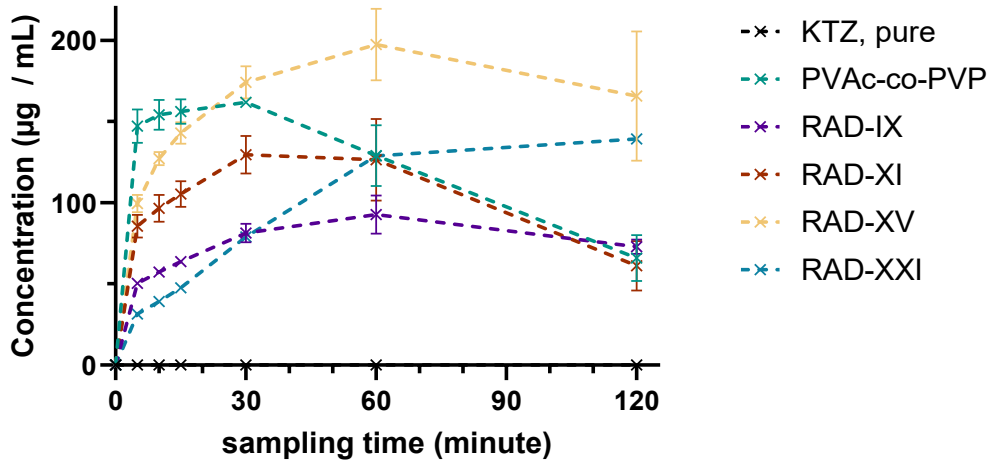

Figure 90: Super Saturation potential of polymers prepared by radical polymerization in comparison to PVP-co-PVAc and pure KTZ. Non-sink dissolution of amorphized samples through melt-quenching in FaSSIF at pH 6.5 at 37 °C, 6 mg of drug in 8 mL medium, arithmetic means ± SD (n = 3), drug: Ketoconazole at 40% drug load; HPLC analysis at λ = 225 mm. Discs were milled before assay. Dashed lines incorporated to guide the reader's eye.

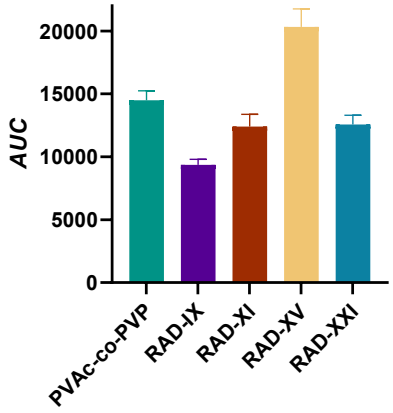

Figure 91 *AUC* of Benchmark PVAc-co-PVP, the polymers synthesized during the DoE, and the polymer synthesized on larger scale. M-IV ratio increases from left to right. *AUC* was calculated utilizing the "area under curve" functionality in the program GraphPad Prism. Arithmetic means ± SD (n = 3)

The transfer of the synthesis process from lab-scale with preparations of 10 g product to the pilot-scale laboratory with a preparation of 100 g product was effortless. It was possible to transfer the procedure directly to a double jacketed reaction vessel preparing ten times as much product as on laboratory scale. Also the purification method, a precipitation step from cold MTBE could be transferred and the resulting yield was comparable to the yield obtained on a small scale. The calculation considering safety aspects of the upscaling using a double jacketed reaction vessel resulted in suitable adiabatic temperature increases and maximum heat flows.

6.3 Conclusion

A free radical polymerization process with the aim to synthesize a polymer consisting of up to four different monomers resulting in optimized properties for pharmaceutical extrusion and dissolution enhancement of a poorly soluble API was developed. The development of the synthesis protocol was successful, as a process was found which enables the facile synthesis of a polymer, where the individual monomer distribution in the polymer fits the targeted. The synthesis protocol is robust, as no inhibitor needs to be removed and the solutions only need degassing by nitrogen flow, without the need of the freeze-pump thaw technique. By utilizing this synthesis protocol, it was possible to set up an explorative design of experiments (DoE) with the aim of finding a polymer with optimized properties for pharmaceutical extrusion. Consequently, a polymer synthesis platform was developed directed at the synthesis of tailored polymers for usage in the statistical analysis of the separate influences of the included monomers. The DoE was used as a tool to characterize the specific influence of the incorporated monomers on thermophysical and thermomechanical properties of the polymers. During the DoE, the ratios of the four utilized monomers in the polymer composition were varied. The monomer ratios in the final polymer in terms of **M-I** (*N*-vinyl-2-pyrrolidone, VP) was kept constant at 60%; **M-III** (poly (ethylene glycol) methyl ether methacrylate, M_n = 300 g mol, mPEGMA) and **M-IV** (vinyl benzoate, VBenz) were varied from 0% to 10% and thus, **M-II** (vinyl acetate, VAc) was varied from 40% to 20%. By statistical analysis, the distinct influences on the thermomechanical and thermophysical properties were devised.

As the ratio of VP (**M-I**) was kept stable at 60 mol%, no distinct influence can be attributed. VAc (**M-II**) has a substantial reducing effect on the T_g in the considered range. An increase in mPEGMA (**M-III**) in the polymer lead to a strong decrease in the transition temperature. In absence of mPEGMA (**M-III**) and VBenz (**M-IV**), a polymer (**RAD-VII**, 77% VP/23% VAc/0% mPEGMA/0% VBenz) with a T_g of 131 °C was obtained whereas the lowest observed T_g was 38 °C in polymer **RAD-XVII** (60% VP/20% VAc/14% mPEGMA/6% VBenz) with 14% mPEGMA (**M-III**). This reduction in T_g directly influences the processing temperature during extrusion as extrusion temperatures of as low as 60 °C were achievable in **RAD-XVII** (60% VP/20% VAc/14% mPEGMA/6% VBenz). The DoE evaluation showed that the incorporation of the monomers VAc (**M-II**) and VBenz (**M-IV**) increased the T_g of the resulting polymer, in direct contrast to the reducing effect of mPEGMA (**M-III**). These tendencies are also true for the properties $T_{1,10000\ Pa\ s}$ and $T_{2,1000\ Pa\ s}$. The influence of the monomers concerning M_w of the polymer cannot be reliably characterized, as more information of the system is needed. It can be argued that monomer VAc (**M-II**), with its comparably higher molecular weight than the other monomers, has the strongest impact on the final molecular weight per incorporated monomer.

Overall, the DoE showed high validity and strong predictive power as demonstrated by the correct

prediction of the polymer properties fulfilling the prerequisites of the sweet-spot area. It was possible to use the design to predict a polymer composition leading to a polymer with optimized properties for pharmaceutical extrusion. Furthermore, the reproducibility was shown by repeating the synthesis of the optimized polymer three times resulting in low deviations in the respective properties of the polymer. During development of the synthesis method, it was evaluated, if each step was feasible on a larger scale. In cooperation with partners at *Merck Electronics KGaA*, a transfer of the synthesis protocol was possible and could be conducted in a double jacketed apparatus. Increasing the batch size tenfold and synthesizing a polymer with a monomer distribution of 49% VP, 30% VAc, 5% mPEG and 16% VBenz (**M-I**/**M-II**/**M-III**/**M-IV**) was successful.

In terms of dissolution performance, a clear trend was visible in that increasing the ratio of VBenz (**M-IV**) in a polymer directly leads to an increase in the *AUC* and the maximum KTZ concentration. The *area under curve* (*AUC*) can be obtained by integrating the area under the dissolution curve in a given time frame. Due to different possible curvatures of the API concentration over time in the process of the dissolution testing (see different classes of ASDs and curve progressions in Figure 5 and Figure 6), the area is a indicator for the overall dissolved amount of API during the assay. High *AUC* values thereby indicate strong dissolution enhancing behavior and are desired of a polymer. Additionally, a high maximum concentration (maximum of the curve) is desired. The KTZ content in solution is analyzed by UPLC with UV detection ($n = 3$). In polymers of similar average molecular weight, the *AUC* observed increased from 9400 ± 400 for **RAD-IX** (70% VP/22% VAc/8% mPEGMA/0% VBenz) in the absence of **M-IV** to 20300 ± 1400 for **RAD-XV** (60% VP/25% VAc/7% mPEGMA/8% VBenz) consisting of 8% **M-IV**. **RAD-XV** performed better than the benchmark PVAc-co-PVP in this assay and polymer/API system. When the **M-IV** ratio was increased to 16% in **RAD-XXI** (49% VP/30% VAc/5% mPEGMA/16% VBenz), no maximum, and a slow initial increase in KTZ concentration could be observed during the measurement time. The observed *AUC* at 12600 ± 700 was lower than for **RAD-XV** with a lower ratio of **M-IV**. The curve progression indicates slow solubilization of the polymer in the medium, which may be due to high apolar monomer content in the polymer.

All in all, it was possible to use the structure-property relationship established in preceding investigations (Section 5) to apply the devised trends to synthesize a polymer with tailored abilities for pharmaceutical extrusion. Furthermore, by drawing from the insights gained, a polymer with exceptional dissolution performance in the given system was obtained exceeding benchmark performances. This study outlines the capabilities of an explorative design of experiments approach as a tool to generate knowledge about a complex copolymer system, which facilitates the deliberate synthesis of a polymer with optimized properties.

Table 43: Summary table for copolymers obtained via free radical polymerization using the monomers M-I, M-II, M-III and M-IV.

	rM-I VP	**rM-II VAc**	**rM-III PEG**	**rM-IV Ar**	**DSC**	**TGA**	**GPC**		**Melt Viscosity**		
#	exp	exp	exp	exp	T_g / °C	T_{deg} / °C	$M_{w,\,exp.}$ / g mol^{-1}	$Đ$	T_1 / 10k Pa s	T_2 / 1k Pa s	$T_{process}$ / °C
RAD-I	93%	7%	-	-	130	124/ 267	71000	3.5	n.a.	n.a.	n.a.
RAD-III	60%	30%	10%	-	43	137 / 269	30000	3.2	n.a.	n.a.	n.a.
RAD-IV	60%	22%	11%	8%	85	202	38000	3.3	n.a.	n.a.	n.a.
RAD-V	61%	22%	11%	6%	44	194	42000	3.6	n.a.	n.a.	n.a.
RAD-VII	77%	23%	-	-	131	226	12000	2.5	160	183	23
RAD-VIII	69%	27%	-	4%	121	212	11280	2.5	152	176	24
RAD-IX	70%	22%	8%	-	87	223	20670	2.9	136	157	21
RAD-X	66%	26%	-	8%	126	226	11950	2.3	152	177	25
RAD-XI	66%	25%	5%	4%	94	225	26450	2.9	126	146	20
RAD-XII	65%	24%	7%	4%	97	200	16010	2.3	125	148	23
RAD-XIII	70%	21%	5%	4%	103	192	13740	2.1	136	161	25
RAD-XIV	64%	23%	13%	-	66	214	30370	2.9	119	143	24
RAD-XV	60%	25%	7%	8%	97	221	25100	2.9	132	157	25
RAD-XVI	60%	23%	14%	3%	68	224	31900	3.0	109	133	24
RAD-XVII	60%	20%	14%	6%	38	220	19480	2.4	73	89	17

7 Conclusion & Outlook

The development of novel thermoplastic polymers specifically designed to reduce the manufacturing temperature, the solubility and ultimately the bioavailability of poorly water-soluble APIs was investigated. These polymers, tailored in their molecular structure, have proven to be effective in the manufacturing of formulations at lower processing temperatures compared to some commercially available products and to be effective in enhancing the solubility of KTZ, a BCS-II compound. Analytical techniques such as NMR, DSC, TGA, GPC and melt rheology played a pivotal role in characterizing these polymers, allowing for a detailed understanding of their physico-chemical properties. The caffeine and KTZ dissolution studies further enabled the investigation of their effectiveness in solubility enhancement.

One element focused on the elucidation of the structure-property relationship of post polymerization modifications of PVA-co-PVP, highlighting how specific chemical motifs in a polymer structure influence the processability of a polymer. In addition to that, the influence of these specific modifications was investigated with respect to their influence in the solubility enhancement of KTZ. By modification with chemically diverse modification agents, a qualitative structure-property relationship was established enabling the targeted synthesis of a polymer with favorable physico-chemical properties for the manufacturing of solid formulations via HME.

PVA-co-PVP, which served as the base polymer for post-polymerization modifications, was synthesized from PVAc-co-PVP. The reproducibility of the saponification reaction was shown by analysis of five separate batches. PVAc-co-PVP was successfully saponified to form the base polymer PVA-co-PVP on an intermediate scale of up to 1 kg. The synthesis protocol and purification process by dialysis and lyophilization was transferred to partnering pilot laboratories and optimized for larger scale production. In addition to that, the technology transfer facilitated the synthesis of sufficient polymer quantities of selected modified entities for an intermediate extrusion on an 11 mm twin screw extruder.

Modifications utilizing thirteen different modification agents at varying modification degrees, which are categorized in four distinct groups, namely mPEG acids, apolar acids, amine functionalized carboxylic acids and miscellaneous acids (keto and ester carrying acids), were synthesized and characterized.

The following key points concerning the structure-property relationship were identified considering the modification of the base polymer PVA-co-PVP with carboxylic acid derivatives with increasing modification degrees:

- Modification with **mPEG** derivatives leads to reduced glass transition temperatures in the targeted range between 80 °C and 90 °C
- Melt rheological measurements predicted HME processability (η_{melt} between 1000 °Pa s and 10000 Pa s) as low as 130 °C for **mPEG-III** modification
- Longer "PEG" chain lengths lead to more pronounced reduction in T_g and lower processing temperatures
- mPEG modification increases the dissolution capabilities compared to base polymer. Higher solubilization was observed compared to all Benchmarks except from Kollidon® VA64
- Hydrophobic **apolar** modification, especially **apolar-II**, hindered processability by HME showing increased torque.
- **apolar-II** modification greatly improved solubilization of KTZ with respect to the base polymer
- **apolar-III** modification led to semi-crystalline entities rendering the polymers not viable for the application in HME
- Substituted amines, ketones and esters did not show sufficient benefits to be further considered

Considering the library of synthesized polymers, a selection of four candidates with increased potential in HME were identified and synthesized on a scale of 200 g. These polymers were investigated considering their behavior in an extrusion at intermediate scale (Pharma 11) and in assays utilizing the model API's caffeine and KTZ ketoconazole. The devised structure property relationship is true for the model system using KTZ. In systems utilizing other APIs with a different set of chemical moieties, the devised effects may change and need to be evaluated separately.

Another aspect built upon the previous findings by exploring the synthesis and characterization of novel thermoplastic polymers designed and optimized specifically for improved processability and enhanced dissolution capabilities. It was possible to synthesize these polymers with control over their composition in a free radical polymerization process. Polymers consisting of up to four monomers of differing nature were synthesized and the process was transferred and executed once at scales of 100 g in a pilot laboratory. An explorative DoE approach was successfully employed as a tool to quantify the specific influence of each of the four monomers onto the polymer properties. The synthesis process employed in the DoE was developed with scalability in mind and with respect to its compatibility to monomers of vastly different reactivities. These monomers were selected based on the structure-property relationship established in the earlier chapter. The limitations in modification degree occurring in previous studies

were overcome by direct inclusion of the specific monomers into the backbone of the polymer. Due to the outstanding performance of PVAc-PVP, a derivative thereof was synthesized with the inclusion of a mPEG and an aromatic comonomer in addition to VP (**M-I**) and VAc (**M-II**). The mPEG comonomer (**M-III**) was utilized for an optimized and lower processing temperature, whereas the aromatic moiety (**M-IV**) was incorporated to induce favorable polymer-API interactions. The explorative DoE approach supported the previous findings in that mPEG monomers are integral for the reduction in processing temperature. The mPEG induced reduction in T_g outweighs any increasing effect by VAc or the aromatic comonomer and reduces the overall processing temperature as confirmed by melt rheology measurements significantly. This means, that with increasing mPEG ratio in the polymer, the T_g and thus, the processing temperature can be controlled. Another trend visible during analysis is the increase in super saturation potential with increasing benzoate content as confirmed during the testing assay with KTZ. **RAD-XV** outperformed the commercially available benchmark PVAc-co-PVP in the tested model system considering dissolution capabilities and the processing range between 132 °C and 157 °C can be labeled as low. Overall, the tailored synthesis of optimized polymers for the targeted application was successful and major insights into the polymer-API system have been gained. The technology transfer from lab-scale to pilot-scale was possible with ease and the synthesis on a larger scale of 100 g was successful with possibilities of further scaling the synthesis process.

In summary, the results obtained in this thesis deepened the understanding concerning the specific influence of a chemical moiety onto the polymer's performance in HME and dissolution. A broad polymer library was generated outlining the effects of a modification qualitatively. Utilizing the conclusion drawn, a DoE system was set up to advance the insight leading to a polymer structure bearing a benzoate, a mPEG, acetate and pyrrolidone group. The scalable production process can be used as a synthesis platform to facilitate the synthesis of a wide array of different polymer compositions with optimized properties.

Looking forward, this thesis opens several pathways for further investigation and development. One area is continuing the optimization of polymer properties by exploring additional monomer combinations. The monomers utilized in the present study include VAc and VP, which are also utilized in prominent products in the field and their behavior in the body is known and studied extensively. They are used in several different products, not only in the field of solid formulation and their health risk is minimal. A derivative of mPEGMA, grafted mPEG is utilized in, e.g. Kollicoat® IR. Its physiological behavior is therefore known. In recent times, more and more studies have suggested, that humans may suffer adverse effects of PEG or even form anti-PEG antibodies.[184-193] If substitution becomes obligatory in the future, this poses a significant challenge for the pharmaceutical industry.

A monomer not currently utilized in any product in the field is VBenz leading to the question on how it

behaves in physiological environment. Therefore, it is of utmost importance to investigate the pharmacological effect of the generated polymer and its degradation products forming during metabolization. If the ester bond is cleaved, benzoate may be formed, which is known to be harmful. Therefore, substitution of VBenz could be explored. A chemically similar compound is styrene, which itself is used in pharmacology in the form of nano particles or microspheres. It constitutes a pharmacologically known monomer, and its influence on the resulting polymer properties should be similar to that of VBenz. These considerations lead to a need to explore other comonomers to refine the polymer properties, but also regulatory considerations play a significant role in the future development of novel polymeric excipients. Next to the plethora of conditions to be fulfilled before a new excipient is admitted to the regional pharmacopoeias, ICH guidelines play a significant role in pharmaceutical development.[153] One aspect are impurities, side-products or residual solvents, each with their allowed upper limit. This may lead to increased research effort in order to remove any harmful residual from the otherwise well performing excipient. Continued collaboration and complying with regulatory bodies is essential as new polymer systems are introduced into the market. Biocompatibility tests are of utmost importance for any new excipient.

Another pathway is to deepen the understanding regarding the polymer-API interactions. So far, limited experimental data with two model APIs was generated. To further the understanding on how and at which site the polymers interact with an API, a library of APIs could be tested to extend the amount of information. With the help of molecular dynamics simulations, a deeper insight into the specific interactions in the model system consisting of API and polymer could be visualized and predicted. As polymers are large molecules, exact calculation of these interactions is currently not possible due to the sheer number of degrees of freedom, but theoretical calculations are conducted and can be experimentally verified.[87, 139, 194] Employing multiple APIs in experiments with the same polymer may lead to a more robust structure-property relationship as the performance of a polymer in conjunction with a different API than KTZ may differ greatly. In terms of theoretical considerations, generative AI is a hot topic in current research and development. With the help of generative AI, preclinical testing in terms of toxicity prediction and ADME prediction for pharmacokinetics could be undertaken by a future AI model.[195]

An anchor point is the outstanding performance of PVAc-co-PVP. The onset-time in dissolution studies is very quick, as observed in this thesis. This fact may indicate, that species of lesser molecular weight have indeed a great impact onto the dissolution performance. The onset-time of Kollidon®VA64 is shorter, than that obtained for novel polymers investigated in this study. So the spiking of these novel polymers with small molecular weight species could have a favorable influence on the release kinetics. Researchers may obtain the ability to precisely tune the release kinetics of a novel polymer to control the API release affording highest pharmacological efficiency.

3d printing is an upcoming technology in the field of solid formulation. Once a deep understanding of the polymer-API interaction is generated and the platform approach for the design of novel polymers is investigated further, it is imaginable to tailor the properties of the polymer-API combination in such a way, that the targeted manufacturing of oral dosage forms may open the way for personalized medicine and possibly the pediatric field.

In conclusion, this thesis has established a structure-property relationship which can be exploited to further the field of novel polymers in the formulation of poorly water-soluble APIs. The facile and scalable synthesis process incorporating up to four comonomers can be applied to a variety of different chemical structures and may be used as a synthesis platform with vast possibilities for the tailored synthesis of polymers for NCEs. The study performed constitutes only one steppingstone on a long way for the completion of a structure-property relationship considering an arbitrary API and a polymer. The insights generated may help future researchers to construct a synthesis platform with the ability to generate polymers with tailored properties for any given API.

8 Experimental part

8.1 Materials and methods

8.1.1 Materials

Table 44: Commercially acquired PVAc-co-PVP batches utilized for the synthesis of modified polymers in this thesis.

Substance Name	Abbreviation	Company	Name	Batch no.
Kollidon® VA64	PVP-co-PVAc	BASF	Batch 1	54167356PO_01
Kollidon® VA64	PVP-co-PVAc	BASF	Batch 2	00183656PO_G3
Kollidon® VA64 fine	PVP-co-PVAc	BASF	Batch 3	38908697V0

All solvents and chemicals were obtained from commercial sources and used as received unless otherwise stated. The list of suppliers includes *Sigma-Aldrich* (Sigma-Aldrich Chemie GmbH, Taufkirchen), *VWR* (VWR International GmbH, Darmstadt) *Creative PEGWorks* (Creative PEGWorks Durham, North Carolina, USA). Chemicals used were purchased in highest purities if not otherwise stated. Anhydrous dimethyl formamide was used for the modifications with ureas and carbamates. CDI was stored under inert gas. Vinyl acetate (3 – 20 ppm HQ as inhibitor, Sigma Aldrich) was either passed through basic aluminum oxide prior to use to remove inhibitor or used as received. Vinyl pyrrolidone (100 ppm NaOH as inhibitor, Sigma Aldrich) was either passed through acidic aluminum oxide prior to use to remove inhibitor or used as received. Vinyl benzoate (≤ 20 ppm HQ, ≤ 50 ppm MEHQ as inhibitor, Sigma Aldrich) was either passed through basic aluminum oxide prior to use to remove inhibitor or used as received. mPEGMA (M_n = 300 g mol^{-1}, 300 ppm BHT, 100 ppm MEHQ, Sigma Aldrich) and allylmPEG (Allyl (poly(ethylene glycol) methyl ether), (M_n = 550 g mol^{-1}, CreativePEGWorks) was either passed through basic aluminum oxide prior to use to remove inhibitor or used as received. Deuterated solvents were purchased from *Sigma Aldrich* with or with-out TMS-standard and used as received. Water was demineralized utilizing a Milli-Q® IQ 7000 (ZIQ7000T0) demineralizer. Dialysis tubes were purchased from *Carl Roth* (Carl Roth GmbH, Karlsruhe).

8.1.2 Methods

8.1.2.1 NMR

NMR experiments were performed on *BRUKER Avance III 400*, *BRUKER Avance II HD 300* and *BRUKER Avance III 700* (Bruker Corporation, Billerica, Massachusetts), at the Central analytics department at Merck Life Science KGaA Darmstadt using DMSO-*d6* ($\delta_{DMSO\text{-}d6}$ = 2.500 ppm), $CDCl_3$ (δ_{CDCl3} = 7.260 ppm) or D_2O (δ_{D2O} = 4.800 ppm) as solvents. The chemical shifts (δ) are reported in parts per million (ppm) relative to the residual solvent protons (^{1}H NMR) or the deuterium coupled ^{13}C solvent signal ($^{13}C^1$H NMR). Following abbreviations were used for the declaration of the spin multiplicities: s (singlet), d (doublet), t (triplet), q (quartet), hept (heptet), m (multiplet) and the appropriate combinations of these. Polymer signals are generally very broad and no discrete spin multiplicities may be assigned. This will be indicated by assigning broad to the respective signal. Coupling constants (J) are stated in Hertz (Hz). NMR experiments were analysed using *MESTRENOVA v.14.3.1*. Each spectrum was referenced to the solvent signal. A phase correction was applied and the baseline was corrected using the Splines method.

The measurements were conducted in cooperation with the central analytics department and with the support of the colleagues Dr. Andreas Marx, Harald-Arthur Rosignol, Markus Knoth, Julia Kraus, Kevin Jährling, Petra Kroy, and Colin Neumeuer.

8.1.2.2 GPC

GPC measurements were conducted on an Agilent 1100 system equipped with a G1310A Pump, a G1313A and a Agilent 1260 G7162A RI detector (Agilent Technologies Deutschland GmbH, Waldbronn). The column were temperature controlled by an Extrema TCC6500 column oven. Additionally, a Biotech 2-Ch Degasi was used. Three GRAM columns (100 Å, 1000 Å, 1000 Å) and a GRAM precolumn were used for separation. Solvent for elution was DMAc with 0.6 g L^{-1} LiBr at 70 °C oven temperature. Calibration was done by utilizing 3 vials from the PSS PMMA ReadyCal-Kits low (yellow vial, 46800 kDa, 8350 kDa, and 2380 kDa) and high (green vial, 2200000 kDa, 340000 kDa, and 41400 kDa; white vial, 608000 kDa, 88500 kDa, 9680 kDa) before each sequence. 100 µL of sample was injected into the instrument at a flow rate of 1 ml min^{-1} and a runtime of 45 minutes. Each sample was dissolved in the eluent at a concentration of 5 mg mL^{-1} (e.g. 20 mg in 4 mL). If dissolution was incomplete overnight, the sample was heated to 50 °C. Each polymer was measured once. Data was recorded and evaluated using WinGPC UniChrom Version 8.30. For MALS detection, a WYATT Technology Europe GmbH DAWN 8 detector was used. Method development was conducted at the

Central Analytics department at Merck KGaA by Erik Althapp and Melanie Dietz testing various sets of columns and additives.

8.1.2.3 TGA

TGA was measured by the on a Netzsch TG 209 F1 Libra in a nitrogen atmosphere using Proteus Analysis Software Version 8.0.1 software. Measurement was conducted in open 85 µL Al crucibles. The heating rate was 10 °C/min in a range of temperature between 30 and 550 °C. Before each measurement the sample was heated up to 110 °C for 5 minutes and to 125 °C for 2 minutes. After cooling down to 40 °C and holding for 15 minutes the actual measurement was conducted while heating to 550 °C. The preheating step to 110 °C was included for the removal of residual water before the measurement and the heating step to 125 °C to remove other residual solvents.

Table 45 Temperature program for TGA measurements in this thesis. Step #7 was utilized for the evaluation of T_{deg}.

Step #	Action (@10 K min^{-1})
1	Dynamic increase to 110 °C
2	Isothermal @110 °C; 5 min
3	Dynamic increase to 125 °C
4	Isothermal @125 °C; 2 min
5	Dynamic decrease to 40 °C
6	Isothermal @40 °C; 15 min
7	Dynamic increase to 550 °C

The measurements were conducted thrice, and the mean value of each significant temperature was taken. The degradation can be observed in section 7 of the utilized method. To obtain the degradation temperature, the slope of the thermogram's first derivative was evaluated. Once the slope showed a significant change (~0.5 K/min), this temperature was defined as T_{deg} and it was assumed, that degradation began.

8.1.2.4 DSC

DSC measurements were performed on a *Mettler Toledo DSC 3* calorimeter, in a closed aluminum crucible, under nitrogen atmosphere. The calibration was carried out with high purity Indium. The

glass transition temperature was determined by the inflection point of the heating curve defined by tangents at the second heating curve of the following temperature program (measurement section 9). Heating rate was 10 K min^{-1} if not otherwise stated. The measurements were conducted thrice, and the mean value of each significant temperature was taken. Each dataset was analyzed with the STAR-E software.

Step #	Action (@10 K min^{-1})
1.	Dynamic increase to 110 °C
2.	Isothermal @110 °C; 5 min
3.	Dynamic increase to 125 °C
4.	Isothermal @125 °C; 1 min
5.	Dynamic decrease to 0 °C
6.	Isothermal @0 °C; 4 min
7.	Dynamic increase to 200 °C
8.	Dynamic decrease to 0 °C
9.	Dynamic increase to 230 °C

8.1.2.5 Lyophilization

The aqueous solutions were lyophilized using a *Christ Epsilon 2-12D* instrument utilizing up to 10 L aqueous solution in rectangular metal dishes. A schematic representation of the process is given below. Initial freezing occurs at -40 °C, without vacuum. The temperature is set to -20 °C and -20 °C is reached after 6 h of freezing. From there, main drying begins at 0.37 mbar pressure and every 5 to 10 h the temperature is increased stepwise by 5 °C until +5 °C is reached. The temperature is then increased stepwise by 5 °C every 2 h until +30 °C is reached. Secondary drying is conducted at a pressure of 0.0010 mbar and +30 °C for at least 12 h for a total drying time of 90 to 140 h depending on the loading of the instrument.

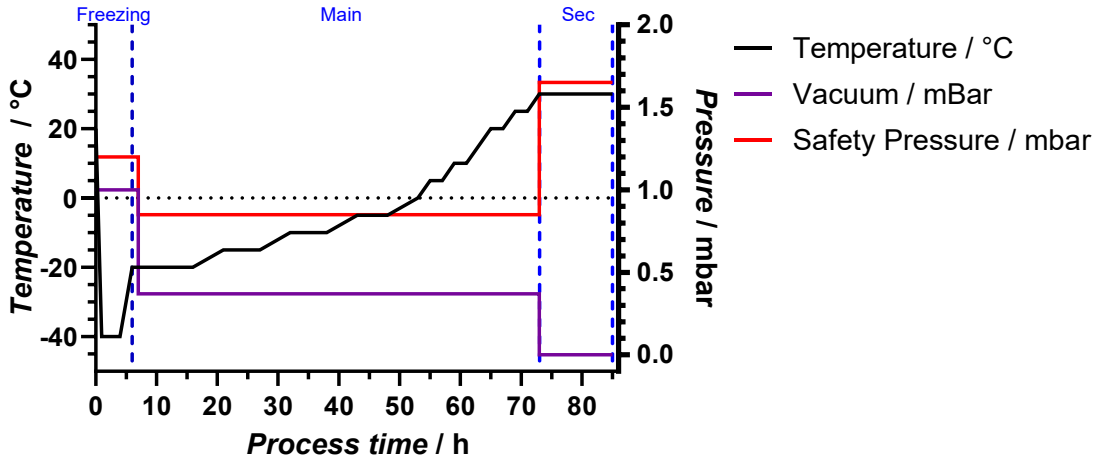

Figure 92: Lyophilization process utilized for the drying of synthesized polymers. Process can be divided into freezing, main drying, and secondary drying (Sec).

8.1.2.6 Cryo Mill

Polymers for extrusion were milled using a *Retsch* Cryo Mill operating under liquid nitrogen cooling. This greatly increases the polymers brittleness and facilitates easier milling. Milling temperature was reached by precooling for 6 minutes at a frequency of 5 s^{-1}. Five milling cycles of 2 minutes with a frequency of 30 s^{-1} and intermediate cooling of 1 minute at 5 s^{-1} were conducted. Each polymer was milled in the same way.

8.1.2.7 Extrusion

The polymer powders were extruded using a twin screw ThreeTec Extruder ZE5 HMI. Before each extrusion, the polymer was milled and dried in a vacuum drying oven at 50 °C. It was attempted, that the powder was continuously fed into the twin-screw extruder, so that the material is conveyed evenly through the 2 mm nozzle. The Three-Tec Cooling Conveyer Belt was adjusted in velocity to achieve filaments of uniform thickness. Temperature and rpm (revolutions per minute) were varied during the course of the extrusion with reference to DSC and TGA results to investigate the polymers thermo-mechanical behavior. A conveyer belt was utilized for the extrudate to be conveyed after it was pressed through the nozzle.

Intermediate extrusions conducted by Alessandro-Giuseppe Elia were conducted on a 11 mm twin screw extruder (Pharma 11, Thermo Fisher Scientific, Waltham, MA, USA) equipped with a gravimetric feeder (Congrav OP1-S, Brabender GmbH & Co. KG, Duisburg, Germany), an automatic conveyor belt (Brabender GmbH & Co. KG, Duisburg, Germany), and an industry standard screw design for mixing,

kneading and melting was utilized.[196] The polymer powders were dried before the extrusion using a vacuum drying oven at 50 °C.

8.1.2.8 Melt Rheology

Rheological studies were performed on an Thermo Fisher Scientific (USA) Haake™ Mars™ Rheo 60 rheometer. Data was processed using the software *HAAKE RheoWin 4.87.0006.* The measurements were conducted by Alessandro-Giuseppe Elia (*Merck Life Science KGaA*) and Florian Hess (*Merck Life Science KGaA*). It was equipped with aluminum single use plates with a diameter of 25 mm. Each measured sample was milled using an IKA Tube mill 100 (IKA-Werke GmbH & Co. KG, Staufen, Germany) or a cryo mill (Section 8.1.2.6) prior to use and dried for at least 24 h in a vacuum drying oven at 50 °C. Approximately 550 mg of sample was placed on the lower plate and heated to the starting temperature as defined by the methods below. A sample mass of ≈550 mg was utilized. Temperature sweep measurements were conducted. After loading, the top plate was lowered to a gap height of 1 mm. Excess material was trimmed. The starting temperature was maintained for 5 min. Viscosity (η_{melt}), phase angle delta (δ), the storage modulus (*G'*), and the loss modulus (*G''*) were determined during each measurement. For each sample, the temperature range was defined in relation to the sample's thermal properties as T_g as obtained by DSC. The following methods were used for the samples with a heating rate of 5 °C min^{-1} for the initial cooling phase (ΔT_{prep}) and 2 °C min^{-1} for the heating phase (T_{exp}) where data is obtained. To reduce the duration of thermal stress during cooling phase, a higher heating rate was used. The upper plate oscillation was set to a constant strain rate of ω = 0.1% and an angular frequency of ɣ = 0.1 rad s^{-1}.

Table 46: Measurement parameters for temperature sweep of polymers analyzed in this thesis.

Polymer	ΔTprep / °C	Duration / min	ΔTexp / °X	Duration / min
PVAc-co-PVP	190		190.00 - 140.00	25
PVA-co-PVP	160.00 - 110.00	10	110.00 - 200.00	45
amine-Ie				
amine-IIe				
apolar-IIIb				
mPEG-IIg				
mPEG-IIId				
mPEG-II-POOL				
mPEG-II-upscale				
mPEG-II-upscale				

Polymer	ΔTprep / °C	Duration / min	ΔTexp / °X	Duration / min
mPEG-Ic				
apolar-Id	150.00 - 110.00	8	110.00 - 200.00	45
apolar-IIIc				
mPEG-II/apolar-Id				
mPEG-II/apolar-Ii				
mPEG-IIg	150.00 - 130.00	4	130.00 - 230.00	50
apolar-IIId	160.00 - 140.00	4	140.00 - 200.00	30
apolar-Id	190.00 - 170.00	4	170.00 - 220.00	25
apolar-Ig				
F1	180		190.00 - 140.00	25
F2-1	190		190.00 - 140.00	25
F2-2	190		190.00 - 140.00	25
F3	190		190.00 - 140.00	25
RAD-VIII	180		180.00 - 60.00	60
RAD-X				
RAD-XI				
RAD-XII				
RAD-XIII				
RAD-IX	200		200.00 - 130.00	35
RAD-VI				
RAD-VIII				
RAD-XIV				
RAD-XV	145		145.00 - 100.00	22.5
RAD-XVI	110		110.00 - 60.00	25

8.1.2.9 Vacuum Compression Molding (VCM, MeltPrep)

Vacuum compression molding (VCM) experiments were conducted by Nabil Lamrabet (*Merck Life Science KGaA*). A MeltPrep system (MeltPrep GmbH, Graz, Austria) including heating plate, vacuum pump, disc insert and cooling apparatus was utilized for the preparation of cylindrical samples of thermoplastic polymers from powders or granules. The polymers were milled using the aforementioned cryo mill protocol or an IKA Tube mill 100 (IKA-Werke GmbH & Co. KG, Staufen, Germany) before

the VCM preparations. The melting vessel was coated using PTFE films. To facilitate thorough homogenization, a Tubula Mixer T2C (Willi A. Bachofen, Muttenz, Switzerland), or a Speed Mixer DAC 150SP (Hauschild, Hamm, Germany) was charged with the sample mixture. The 25 mm insert was used and all inner surfaces are covered in PTFE films and approximately 1000 mg of sample mixture. The piston is inserted, and the vessel is evacuated to remove any air bubbles present. The sample is heated in accordance with the specific thermal properties above the T_g for an appropriate period of time to facilitate complete melting. After cooling, the sample is extracted. The sample specimen are then either milled in the case of the polymers synthesized by free radical polymerization or used without milling in the case of polymer modifications. Milled samples simulate the pharmaceutical production of tablets by pressing, whereas without milling, a filament slice can be simulated. The following times were used for the measurements of benchmark polymers and adapted slightly based on the T_g for the sample preparation including synthesized polymers.

Table 47: Melting time and temperature for benchmark polymers during VCM preparations. T_g and T_m values based on experimental data and literature [46, 58-61, 121]

	T_g / °C	Melting time / min	VCM Temperature / °C
Eudragit EPO	52	7	200
Kollidon VA64	105	7	190
Kollicoat IR	45, T_m = 208 °C	7	200
PVP K30	160	7	215
Parteck MXP	68, T_m = 155 - 193	8	200
Soluplus	72	7	200
Eudragit L100-55	111	7	200

8.1.2.10 Caffeine Dissolution Assay

The assay and the measurements were conducted by Nabil Lamrabet (*Merck Life Science KGaA*). The assay is conducted using discs consisting of caffeine and the polymer sample at 10% drug load with a total sample weight of 300 mg. Utilizing a Sotax AT7 Smart Semi-Automated dissolution tester (Sotax, Aesch, Switzerland) in conjunction with a Agilent 8453 Photometer (Agilent Technologies Deutschland GmbH, Waldbronn) and a Hellma flow cell (5 mm light path, type 170.700-QS, Hellma GmbH & Co. KG, Müllheim) the caffeine dissolution was tested. The paddle method (USP) was used. The discs were tested against 900 mL of 0.1 M HCl dissolution volume at a stirring speed of 75 revolutions per minute over the course of 6 h at 37 °C. Online UV-VIS detection was utilized to determine the concentration of released caffeine and the absorbance is measured at a wavelength of λ = 272 nm. By internal calibration

utilizing standard solutions of caffeine, the performance of a polymer in terms of caffeine release can be characterized.

8.1.2.11 KTZ Dissolution Assay and HPLC Analytics

The assay and the measurements were conducted by Nabil Lamrabet (*Merck Life Science KGaA*). The assay is conducted using discs prepared by VCM consisting of KTZ and the polymer sample at 40% drug load. For the measurements concerning modified polymers, small discs were prepared. For measurements of polymers produced by free radical polymerization, the discs were milled beforehand. FaSSIF medium is prepared according to the instructions by Biorelveant. FaSSiF, sample vials and shaker are tempered to 37 °C. 15 mg of sample is introduced into the sample vials (corresponds to 40% drug load at an API content of 6 mg). 8 mL FaSSiF is added and the TH15 shaker (Bühler) is set to 37 °C. At time points of 5, 10, 15, 30, 60 and 120 min 1 mL is taken by syringe a filtered through a 0.45 µm PTFE filter. 1 mL into charged into a HPLC vial and 250 µL into a second which is diluted with 250 µL ethanol.

Analytical reversed phase high performance liquid chromatography was performed on an Agilent 1260 Infinity II system. A Waters xBridge C8 3.5 µm column is used. The instrument consisted of an in-line degasser, a binary pump system, and a UV/VIS-detector. Detection was conducted at $\lambda = 225$ nm. As solvents water/formic acid (999:1 v/v) and acetonitrile/formic acid (999:1 v/v) are utilized. Gradient conditions were 90% aqueous to 90% organics and back to 90% aqueous. The separations were performed at 37 °C. Solvents used were in HPLC quality and ultrapure water was generated by a Milli-Q device. The API concentration based on an internal calibration with standard solutions, where the area is directly related to the resulting concentration. The analyses showed linearity in the range tested with a $R^2 \geq 0.9990$. Each polymer entity was measured three times.

8.2 Synthesis

8.2.1 Modification of PVA-co-PVP

8.2.1.1 General batch calculation

The batch calculation for each modification of PVA-co-PVP and the saponification of PVAc-co-PVP is based on the GPC and NMR analysis results obtained for PVAc-co-PVP. The distribution obtained by NMR (Section 5.2.1), namely 55% VP and 45% VAc directly relates to the distribution of VP/VA in the saponified product, as complete saponification was achieved. The molecular mass distribution of the saponification product PVP-co-PVAc with its mean molecular weight at M_w = 36000 g / mol^{-1}(Section 5.2.1) was utilized to calculate the number of VA moieties and therefore the available OH groups for modification. Based on the molecular weight of the saponified product PVP-co-PVA of M_w = 30000 g mol^{-1} and the number of available OH-groups, the molar amount of utilized modification agent can be calculated (Table 48). The modification degree is given with regards to the targeted number of modified OH-groups. The calculations are based on the molecular weight distribution as obtained from GPC and the integral ratios as obtained from quantitative ^{13}C-NMR and ^{1}H-NMR.

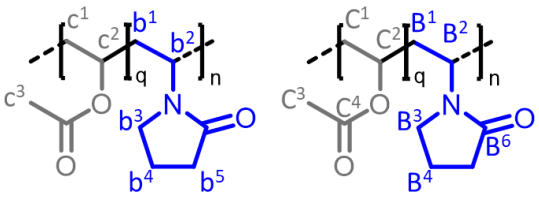

Scheme 21: Chemical structure of starting material PVAc-co-PVP

^{1}H NMR (700 MHz, DMSO) δ [ppm]=5.12–3.39 (m, 2H, b^{2}, c^{2}), 3.22 (d, *J* = 93.1 Hz, 2H, b^{3}), 2.34–2.00 (m, 2H, b^{5}), 2.00–1.81 (m, 5H, b^{4}, c^{3}), 1.81–1.24 (m, 4H, b^{1}, c^{1}).

^{13}C NMR (101 MHz, DMSO) δ [ppm]=173.69 (s, 1C, B^{6}), 169.76 (d, *J* = 20.9 Hz, 1C, C^{4}), 69.24-65.90(m, 1C, C^{2}), 45.12-42.30 (m, 1C, B^{2}), 42.03-40.56 (m, 1C, B^{3}), 38.23-32.65 (m, 1C, B^{1}, C^{1}), 30.82 (s, 1C, B^{5}), 20.86 (s, 1C, C^{3}), 17.91 (s, 1C, B^{4}).

Table 48: Calculation amount of OH groups.

Calculation of the number of repeating units (GPC and NMR)		
	M / g/mol	**Comment/assumptions**
Vinylpyrrolidone (VP)	111.14	55% contained in PVP-co-PVAc
Vinylacetate (VAc)	86.09	45% contained in PVP-co-PVAc
Hybrid repeating unit	99.87	0.45 x M(vinyl acetate) + 0.55 x M(vinyl pyrrolidone)
Kollidon® VA64 (GPC) / g mol^{-1}	36000	Taken from GPC MALS Measurements
before acetate cleavage		
Number of repeating units	360	
Number of VP repeating units	198	NMR Evaluation: 55% VP
Number of VAc repeating units	162	NMR Evaluation: 45% VAc
after acetate cleavage		
Vinylalcohol (VA)	44.05	
PVP-co-PVA (GPC) / g mol^{-1}	29000	all acetate gropus are cleaved; estimate by calculation

8.2.1.2 SOP Saponification of PVAc-co-PVP

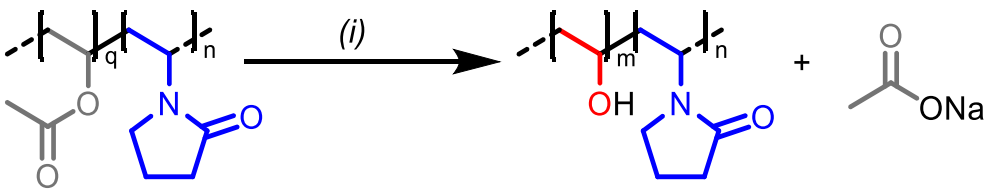

Scheme 22: : Chemical structure of reactant PVAc-co-PVP with annotated protons (top left) and carbons (top right); Saponification reaction of PVAc-co-PVP; (i) PVAc-co-PVP (1 eq based on moles of acetate moiety in reactant, see Section 8.2.1.2), 1 M NaOH (1.75 eq), water, 80 °C, 24 h (bottom)

The calculation of molar amounts is based on the NMR/GPC evaluation of the starting material PVAc-co-PVP as elaborated in the previous section (Table 48). 180 g PVAc-co-PVP (6 mmol, 0.006 eq; 0.924 mol and 1 eq based on amount of calculated acetate moieties present in the polymer) were charged into a three-necked round bottom flask equipped with a stirring bar and a reflux condenser. 1 L of 1 M NaOH solution (total 1.617 mol, was added, and the mixture was stirred at room temperature until the polymer was dissolved. Another 400 mL of 1 M NaOH were added under stirring. Reaction mixture was heated at 80 °C for 24 hours. Reaction was terminated by removing the heating plate. The polymer was partially precipitated by adding 250 mL of the reaction mixture dropwise into 2 L of acetone over a period of 10 minutes. Subsequently the dispersion was stirred until an orange rubbery precipitate was formed. The clear supernatant was decanted, and the precipitate was dried under ambient conditions. This was repeated until all the product was precipitated. The precipitated polymer was dissolved in water and dialyzed against water using tubes with pore sizes of 12 kDa to 14 kDa. The dialysis water was

removed thrice over a period of three days and lyophilization yielded the pure product. Yield: 138 g (95%)

Table 49: Saponification batch description

Batch-no.	Amount (PVAc-co-PVP) / g (mmol)	Yield / g (%)
SAP-I	180 (5 mmol)	138 (95%)
SAP-II	1400 (39 mmol)	947 (82%)
SAP-III	1400 (39 mmol)	940 (81%)
SAP-IV	1400 (39 mmol)	1157 (99%)

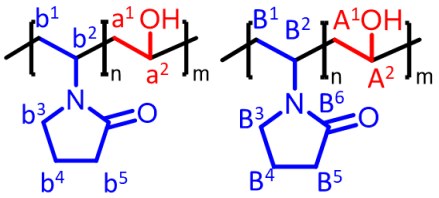

Scheme 23:Chemical structure of PVA-co-PVP with annotated protons.

^{1}H NMR (400 MHz, DMSO) δ [ppm]=4.46-3.36 (m, 2H, b^2, a^2), 3.36-2.83 (m, 2H, b^3), 2.42-2.01 (m, 2H, b^5), 2.01-1.77 (m, 2H, b^4) 1.77-0.92 (m, 4H, b^1, a^1).

^{13}C NMR (101 MHz, DMSO) δ [ppm]= 175.23-173.28 (m, 1C, B^6), 67.24-63.40(m, 1C, A^2), 46.24-43.00(s, 1C, B^2), 43.00-40.64 (s, 1C, B^3), 38.51-31.59 (m, 1C, A^1, B^1), 31.60-30.14(s, 1C, B^5), 18.76-17.09 (s, 1C, B^4).

8.2.1.3 SOP Synthesis of activated intermediates

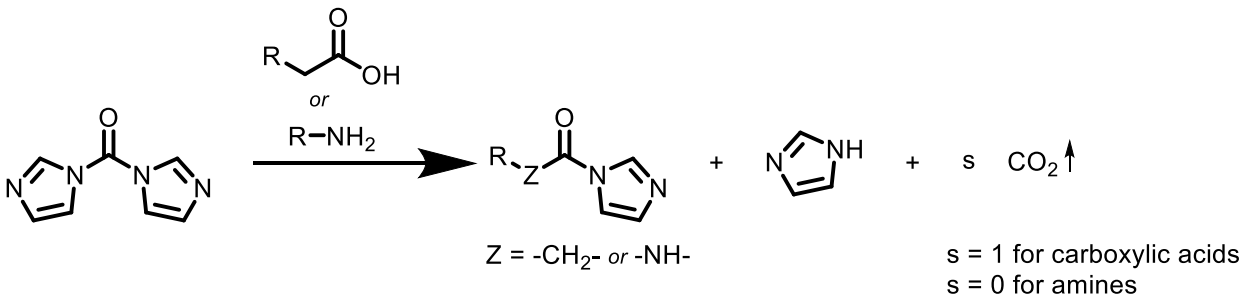

Scheme 24: General reaction scheme for the synthesis of the activated intermediate. The reaction product can be classified as an amide when using carboxylic acids, and urea when using amines. R corresponds to the respective agent used.

The following reaction description was utilized for the synthesis of activated intermediates. The molar amount of chemicals used is calculated based on the consecutive modification of PVA-co-PVP in two to six separate batches executed at the same time using *Radley's Tornado Reaction Station*. In the following subchapters the respective molar amounts for the modifications are noted. The synthesis was adapted according to literature.[146] Briefly, an oven-dried three-necked round bottom flask, equipped with a gas inlet and magnetic stirrer was charged with dry DMF under a nitrogen atmosphere. Then, carbonyl diimidazole (CDI) was introduced into the solvent forming a suspension. The modification agent (carboxylic acid or amine) was introduced at room temperature in portions. The reaction mixture was stirred for 1 hour at room temperature. Utilizing carboxylic acids, carbon dioxide evolution was observed. This is not the case, when using amines. A clear, colored solution was obtained. It was used without further purification after quantification via ^{1}H-NMR. The solution was kept under nitrogen until used in the modification reaction.

mPEG-I precursor

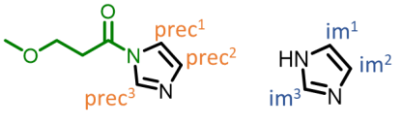

Scheme 25: Structure of activated amide corresponding to mPEG-I.

^{1}H NMR (700 MHz, DMSO) δ [ppm] = 8.45 (s, 1H, prec^{3}), 7.95 (DMF), 7.72 (d, *J* = 1.5 Hz, 1H, prec^{1}), 7.69 (s, 1H, im^{3}), 7.07 (d, *J* = 1.7 Hz, 1H, prec^{2}), 7.04 (dd, *J* = 1.1 Hz, 2H, im^{1}, im^{2}).

mPEG-II precursor

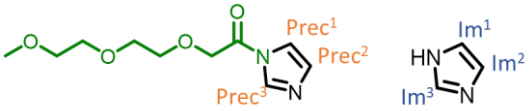

Scheme 26: Structure of activated amide corresponding to mPEG-II.

^{1}H NMR (700 MHz, DMSO) δ [ppm] = 8.37 (s, 1H, prec^{3}), 7.95 (DMF), 7.69 (d, *J* = 1.5 Hz, 1H, prec^{1}), 7.64 (s, 1H, im^{3}), 7.08 (d, *J* = 1.6 Hz, 1H, prec^{2}), 7.01 (d, *J* = 1.1 Hz, 3H, im^{1}, im^{2}).

mPEG-III precursor

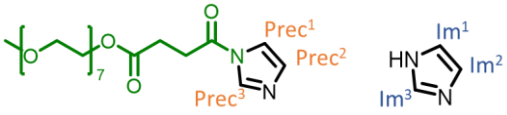

Scheme 27: Structure of activated amide corresponding to mPEG-III.

^{1}H NMR (700 MHz, DMSO) δ [ppm] = 8.45 (s, 1H, prec^{3}), 7.95 (DMF), 7.72 (d, *J* = 1.5 Hz, 1H, prec^{1}), 7.63 (s, 1H, im^{3}), 7.08 (d, *J* = 1.7, 0.8 Hz, 1H, prec^{2}), 7.01 (dd, *J* = 1.1 Hz, 2H, im^{1}, im^{2}).

mPEG-IV precursor

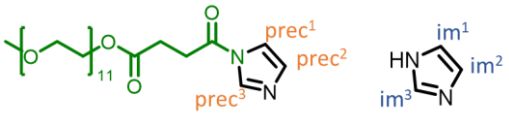

Scheme 28: Structure of activated amide corresponding to mPEG-IV.

^{1}H NMR (400 MHz, DMSO) δ [ppm] = 8.45 (s, 1H, prec^{3}), 7.95 (DMF), 7.72 (d, *J* = 1.5 Hz, 1H, prec^{1}), 7.64 (s, 1H, im^{3}), 7.08 (d, *J* = 1.7, 0.8 Hz, 1H, prec^{2}), 7.01 (dd, *J* = 1.1 Hz, 2H, im^{1}, im^{2}).

apolar-I precursor

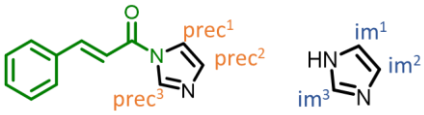

Scheme 29: Structure of activated amide corresponding to apolar-I.

^{1}H NMR (400 MHz, DMSO) δ [ppm] = 8.75 (s, 1H, prec^{3}), 7.94 (DMF), 7.68 (d, *J* = 1.5 Hz, 1H, prec^{1}), 7.64 (s, 1H, im^{3}), 7.15 (d, *J* = 1.7, 0.8 Hz, 1H, prec^{2}), 7.01 (dd, *J* = 1.1 Hz, 2H, im^{1}, im^{2}).

amine-I precursor

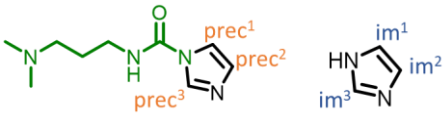

Scheme 30: Structure of activated amide corresponding to amine-I.

^{1}H NMR (400 MHz, DMSO) δ [ppm] = 8.23 (s, 1H, prec^{3})), 7.95 (DMF), 7.66 (d, *J* = 1.5 Hz, 1H, prec^{1}), 7.64 (s, 1H, im^{3}), 7.12f (d, *J* = 1.7, 0.8 Hz, 1H, prec^{2}), 7.09-7.01 (m, 3H, prec^{2}, im^{1}, im^{2}).

amine-I precursor

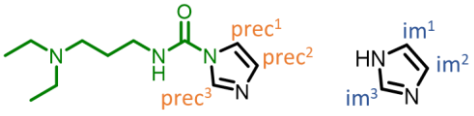

Scheme 31: Structure of activated amide corresponding to amine-II.

^{1}H NMR (400 MHz, DMSO) δ [ppm] = 8.21 (s, 1H, prec^{3}), 7.95 (DMF), 7.64 (d, *J* = 1.5 Hz, 1H, prec^{1}), 7.64 (s, 1H, im^{3}), 7.12–6.95 (m, 3H, prec^{2}, im^{1}, im^{2}).

8.2.1.4 SOP Modification Reactions of PVP-co-PVA

8.2.1.4.1 Modification of PVA-co-PVP with activated intermediates

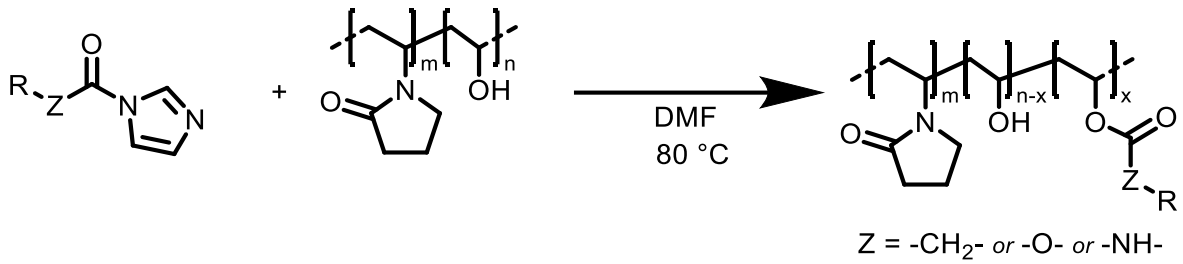

Scheme 32: Schematic synthesis scheme for the modification of PVA-co-PVP with the corresponding activated intermediates investigated in this work.

The molar amount of modification agent is based on the targeted modification degree of present OH moieties in the base polymer PVA-co-PVP. The number of OH-functions is itself based on the NMR/GPC evaluation of PVAc-co-PVP (Table 48). The modification was adapted and executed according to literature.[146] Depending on the number of simultaneous reactions, oven-dried two-necked round bottom flasks, equipped with a magnetic stirrer, were charged with 60 mL DMF and PVAc-co-PVP. The reaction mixture was heated to 80 °C and the appropriate amount of precursor/DMF solution was introduced utilizing volumetric pipettes. Precursor was added corresponding to the targeted modification degree. The targeted modification degree corresponds to the equivalents of activated intermediate used compared to the hydroxyl functions in the saponified PVAc-co-PVP (Table 50). A variable amount of DMF was added to each reaction vessel so the total reaction volume resulted in 100 mL. The reaction was stirred at 80 °C for three days. DMF was removed under reduced pressure and the crude polymer mixture was dissolved in Milli-Q water. Dialysis of the polymer was conducted over the course of three days exchanging the water thrice. After the dialysis, the product was isolated by lyophilization. Batch calculations can be found in Table 50.

8.2.1.4.2 Batch calculations

Table 50: Batch calculations for the synthesis of modified PVA's

Batch no.	PVA-co-PVP			-OH			Precursor 1				Precursor 2				
	M / g mol^{-1}	*m* / g	*n* / µmol	#VA	n / **m**mol	eq.	*M* / g mol^{-1}	*m* / g	*n* / µmol	eq.	*M* / g mol^{-1}	*m* / g	*n* / µmol	eq.	**Yield / g (%)**
amine-Ia	29000	5	172	162	27.9	1.0	196.25	0.93	4.74	0.10					9.1(83)
amine-Ib	29000	5	172	162	27.9	1.0	196.25	2.79	14.21	0.30					7.7(70)
amine-Ic	29000	5	172	162	27.9	1.0	196.25	4.64	23.68	0.50					5.7(52)
amine-Id	29000	5	172	162	27.9	1.0	196.25	6.50	33.15	0.70					6.9(63)
amine-Ie	29000	5	172	162	27.9	1.0	196.25	7.43	37.88	0.80					4.6(42)
amine-If	29000	5	172	162	27.9	1.0	196.25	9.29	47.35	1.00					5.4(49)
amine-IIa	29000	5	172	162	27.9	1.0	224.31	1.06	4.74	0.10					8.9(81)
amine-IIb	29000	5	172	162	27.9	1.0	224.31	3.19	14.21	0.30					8.7(66)
amine-IIc	29000	5	172	162	27.9	1.0	224.31	5.31	23.68	0.50					6.6(43)
amine-IId	29000	5	172	162	27.9	1.0	224.31	7.44	33.15	0.70					9.2(53)
amine-IIe	29000	5	172	162	27.9	1.0	224.31	8.50	37.88	0.80					8.1(44)
amine-IIf	29000	5	172	162	27.9	1.0	224.31	10.62	47.35	1.00					8.2(40)
amine-IIIa	29000	10	345	162	55.9	1.0	196.25	0.93	4.74	0.10					11.3(82)
amine-IIIb	29000	10	345	162	55.9	1.0	196.25	2.79	14.21	0.30					10.6(61)
apolar-Ia	29000	5	172	162	27.9	1.0	198.23	0.47	2.37	0.10					4.7(89)
apolar-Ib	29000	5	172	162	27.9	1.0	198.23	0.94	4.74	0.20					4.9(88)
apolar-Ic	29000	5	172	162	27.9	1.0	198.23	1.41	7.10	0.30					5(84)
apolar-Id	29000	5	172	162	27.9	1.0	198.23	2.35	11.84	0.50					4.8(73)
apolar-Ie	29000	5	172	162	27.9	1.0	198.23	3.75	18.94	0.80					4.8(64)
apolar-If	29000	5	172	162	27.9	1.0	198.23	4.69	23.68	1.00					3.9(49)
apolar-Ig	29000	200	6897	162	1117.2	1.0	198.23	56.90	287.05	0.30					186(69)
apolar-IIa	29000	10	345	162	55.9	1.0	200.24	6.68	33.35	0.60					10.3(62)
apolar-IIb	29000	10	345	162	55.9	1.0	200.24	8.90	44.47	0.80					10.7(56)
apolar-IIc	29000	10	345	162	55.9	1.0	200.24	11.13	55.59	1.00					#WERT!
apolar-IIIa	29000	5	172	162	27.9	1.0	306.49	0.73	2.37	0.10					3.9(68)
apolar-IIIb	29000	5	172	162	27.9	1.0	306.49	1.45	4.73	0.20					4.3(67)
apolar-IIIc	29000	5	172	162	27.9	1.0	306.49	2.18	7.11	0.30					6.1(85)

Batch no.	PVA-co-PVP			*-OH*			Precursor 1				Precursor 2				
	M / g mol^{-1}	*m* / g	*n* / µmol	#VA	n / **m**mol	eq.	*M* / g mol^{-1}	*m* / g	*n* / µmol	eq.	*M* / g mol^{-1}	*m* / g	*n* / µmol	eq.	**Yield / g (%)**
apolar-IIId	29000	200	6897	162	1117.2	1.0	306.49	34.24	111.72	0.10					160(49)
apolar-IVa	29000	10	345	162	55.9	1.0	194.28	8.64	44.47	0.80					10.8(42)
apolar-IVb	29000	10	345	162	55.9	1.0	194.28	10.80	55.59	1.00					10.6(39)
misc-Ia	29000	10	345	162	55.9	1.0	166.18	4.62	27.79	0.50					8.4(66)
misc-Ib	29000	10	345	162	55.9	1.0	166.18	7.39	44.47	0.80					10.9(76)
misc-IIa	29000	10	345	162	55.9	1.0	182.18	2.53	13.90	0.50					5.8(88)
misc-IIb	29000	10	345	162	55.9	1.0	182.18	4.05	22.24	0.80					6.2(83)
mPEG-Ia	29000	5	172	162	27.9	1.0	154.17	0.73	4.74	0.20					4.9(86)
mPEG-Ib	29000	5	172	162	27.9	1.0	154.17	1.10	7.13	0.30					4.9(80)
mPEG-IIa	29000	5	172	162	27.9	1.0	228.25	0.42	1.84	0.08					4.9(92)
mPEG-IIb	29000	5	172	162	27.9	1.0	228.25	1.27	5.56	0.23					5.1(87)
mPEG-IIc	29000	5	172	162	27.9	1.0	228.25	2.11	9.24	0.39					5.2(81)
mPEG-IId	29000	5	172	162	27.9	1.0	228.25	2.95	12.92	0.54					5.3(75)
mPEG-IIe	29000	5	172	162	27.9	1.0	228.25	3.37	14.76	0.62					5.3(72)
mPEG-IIf	29000	5	172	162	27.9	1.0	228.25	4.22	18.49	0.78					5.2(65)
mPEG-IIg	29000	187	6448	162	1044.6	1.0	228.25	190.75	835.70	0.80					182(91)
mPEG-IIh	29000	10	345	162	55.9	1.0	228.25	6.98	30.57	0.55					12.1(49)
mPEG-IIIa	29000	5	172	162	27.9	1.0	501.56	1.19	2.37	0.10					5.5(91)
mPEG-IIIb	29000	5	172	162	27.9	1.0	501.56	1.78	3.55	0.15					5.6(85)
mPEG-IIIc	29000	5	172	162	27.9	1.0	501.56	2.97	5.92	0.25					6(79)
mPEG-IIId	29000	5	172	162	27.9	1.0	501.56	4.16	8.29	0.35					6.4(74)
mPEG-IIIe	29000	5	172	162	27.9	1.0	501.56	5.94	11.84	0.50					6.4(63)
mPEG-II-upscale	29000	800	27586	162	4469.0	1.0	228.25	561.02	2457.93	0.55					947.9(83)
mPEG-II-upscale	29000	800	27586	162	4469.0	1.0	228.25	561.02	2457.93	0.55					909.1(80)
mPEG-II-upscale	29000	800	27586	162	4469.0	1.0	228.25	561.02	2457.93	0.55					895(79)
mPEG-II-upscale	29000	800	27586	162	4469.0	1.0	228.25	561.02	2457.93	0.55					925(81)
mPEG-IVa	29000	5	172	162	27.9	1.0	699.80	1.66	2.37	0.10					5.8(87)
mPEG-IVb	29000	5	172	162	27.9	1.0	699.80	3.31	4.74	0.20					6.2(74)
mPEG-IVc	29000	5	172	162	27.9	1.0	699.80	4.97	7.10	0.30					6.5(66)
mPEG-II/apolar-Ia	29000	5	172	162	27.9	1.0	228.25	4.32	18.94	0.80	198.23	0.47	2.37	0.10	5.4(57)

Batch no.	PVA-co-PVP			*-OH*			Precursor 1				Precursor 2				
	M / g mol^{-1}	*m* / g	*n* / µmol	#VA	n / **m**mol	eq.	*M* / g mol^{-1}	*m* / g	*n* / µmol	eq.	*M* / g mol^{-1}	*m* / g	*n* / µmol	eq.	**Yield / g (%)**
mPEG-II/apolar-Ib	29000	5	172	162	27.9	1.0	228.25	4.32	18.94	0.80	198.23	0.94	4.74	0.20	5.9(60)
mPEG-II/apolar-Ic	29000	5	172	162	27.9	1.0	228.25	4.32	18.94	0.80	198.23	2.35	11.84	0.50	6.2(56)
mPEG-II/apolar-Id	29000	5	172	162	27.9	1.0	228.25	4.32	18.94	0.80	198.23	3.75	18.94	0.80	6.5(52)
mPEG-II/apolar-Ie	29000	5	172	162	27.9	1.0	228.25	4.32	18.94	0.80	198.23	4.69	23.68	1.00	6.9(52)
mPEG-II/apolar-If	29000	5	172	162	27.9	1.0	228.25	4.32	18.94	0.80	198.23	5.63	28.41	1.20	7.5(53)
mPEG-II/apolar-Ig	29000	10	345	162	55.9	1.0	228.25	4.32	18.94	0.80	198.23	5.63	28.41	0.60	15.3(63)
mPEG-II/apolar-Ih	29000	10	345	162	55.9	1.0	228.25	4.32	18.94	0.80	198.23	5.63	28.41	0.60	13.5(55)
mPEG-II/apolar-Ii	29000	10	345	162	55.9	1.0	228.25	4.32	18.94	0.80	198.23	5.63	28.41	0.60	10(41)
mPEG-II/apolar-Ij	29000	10	345	162	55.9	1.0	228.25	4.32	18.94	0.80	198.23	5.63	28.41	0.60	14.4(59)
mPEG-II/apolar-Ik	29000	200	6897	162	1117.2	1.0	228.25	178.51	782.07	0.70	198.23	66.44	335.17	0.30	201(51)

8.2.1.4.3 NMR evaluation PVA-co-PVP modifications

In the following section the NMR signals for each polymer modification are given. During the reaction, the targeted modification degree was varied leading to the same overall signals in ^{1}H-NMR spectroscopy. The signals for each of the modification agents is given for one exemplary polymer, as only the relative integral corresponding to the modified side chain changes when the modification degree increases. The signals are each annotated to the protons present in the structure.

mPEG modifications

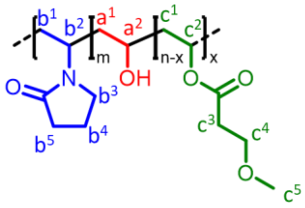

Scheme 33: Chemical structure of PVA-co-PVP modified with **mPEG-I**.

mPEG-I: ^{1}H NMR (700 MHz, DMSO) δ [ppm] = 5.21-3.35 (broad m, 3H, a^2, b^2, c^2), 3.55-3.47 (s, 2H, c^4), 3.35-2.83 (broad m, 2H, b^3, c^5), 2.48-2.33 (s, 2H, c^3), 2.33-2.01 (broad m, 2H, b^5), 2.01-1.76 (broad m, 2H, b^4), 1.77-0.70 (broad m, 6H, a^1, b^1, c^1).

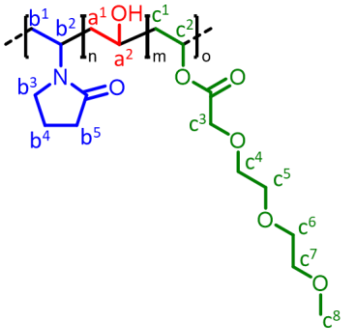

Scheme 34: Chemical structure of PVA-co-PVP modified with **mPEG-II**.

mPEG-II: 1H NMR (700 MHz, DMSO) δ [ppm] = 5.44-3.66 (broad m, 5H, a^2, b^2, c^2, c^3), 3.66-3.34 (broad m, 8H, c^{4-7}), 3.34-2.68 (broad m, 5H, b^3, c^8), 2.35-1.98 (broad m, 2H, b^5), 1.99-1.76 (broad m, 2H, b^4), 1.76-0.89 (broad m, 6H, a^1, b^1, c^1).

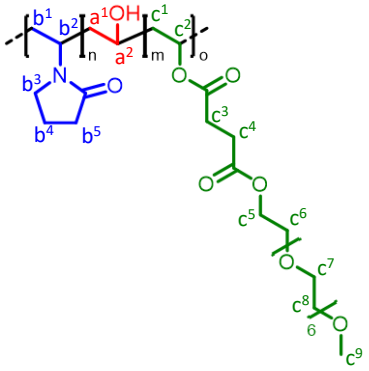

Scheme 35: Chemical structure of PVA-co-PVP modified with **mPEG-III**.

mPEG-III: 1H NMR (400 MHz, DMSO) δ [ppm] = 5.44-3.69 (broad m, 5H, a^2, b^2, c^2, b^5), 3.69-3.35 (broad m, 26H, c^{6-8}), 3.36-2.90 (broad m, 5H, b^3, c^9), 2.62-2.52 (broad m, DMSO, 4H, c^3, c^4), 2.35-2.01 (broad m, 2H, b^5), 2.00-1.75 (broad m, 2H, b^4), 1.75-0.92 (broad m, 3H, a^1, b^1, c^1).

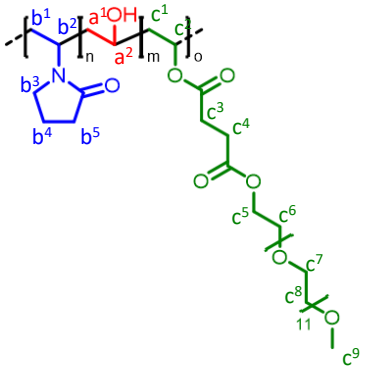

Scheme 36: Chemical structure of PVA-co-PVP modified with **mPEG-IV**.

mPEG-IV: 1H NMR (400 MHz, DMSO) δ [ppm] = 5.19-3.65 (broad m, 5H, a^2, b^2, c^2, b^5), 3.65-3.36 (broad m, 46H, c^{6-8}), 3.36-2.85(broad m, 5H, b^3, c^9), 2.70-2.39 (broad m, DMSO, 4H, c^3, c^4), 2.39-1.99 (broad m, 2H, b^5), 1.99-1.77, (broad m, 2H, b^4), 1.77-0.67 (broad m, 3H, a^1, b^1, c^1).

apolar modifications

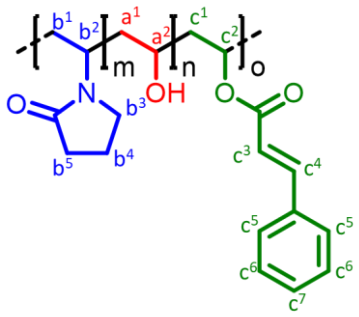

Scheme 37: Chemical structure of PVA-co-PVP modified with **apolar-I**.

apolar-I: ^{1}H NMR (700 MHz, DMSO) δ [ppm] = 8.06-7.12 (broad m, 5H, c^{4-6}), 6.65-6.43 (broad m, 1H, c^{7}), 6.16-5.99 (broad m, 5H, c^{3}), 5.37-3.33(broad m, 3H, a^{2}, b^{2}, c^{2}), 3.34-2.66 (broad m, 2H, b^{3}), 2.35-1.98 (broad m, 2H, b^{5}), 1.98-1.76 (broad m, 2H, b^{4}), 1.75-0.87 (broad m, 3H, a^{1}, b^{1}, c^{1}).

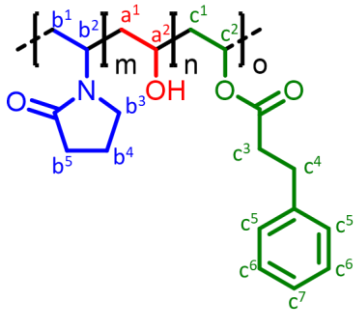

Scheme 38: Chemical structure of PVA-co-PVP modified with **apolar-II**.

apolar-II: 1H NMR (400 MHz, DMSO) δ [ppm] = 7.68-7.61 (broad m, 5H, c^{5-7}), 7.31-7.10 (broad m, 5H, c^{5-7}), 5.22-3.35 (broad m, 3H, a^{2}, b^{2}, c^{2}), 3.36-2.92 (broad m, 2H, b^{3}), 2.93-2.72 (broad s, 2H, c^{4}), 2.5 (DMSO, broad s, 1H, c^{3}), 2.36-1.99 (broad m, 2H, b^{5}), 1.99-1.75 (broad m, 2H, b^{4}), 1.75-0.89 (broad m, 3H, a^{1}, b^{1}, c^{1}).

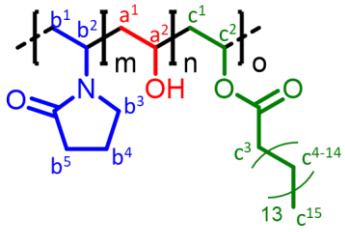

Scheme 39: Chemical structure of PVA-co-PVP modified with **apolar-III**.

apolar-III: 1H NMR (400 MHz, DMSO) δ [ppm] = 4.81-3.37 (broad m, 3H, a^2, b^2, c^2), 3.37-2.89 (water, broad m, 2H, b^3), 2.42-2.00 (broad m, 2H, b^5), 1.99-1.76 (broad m, 2H, b^4), 1.76-0.94 (broad m, 30H, a^1, b^1, c^1, $c^{3\text{-}14}$), 0.91-0.79 (broad m, 3H, c^{15}).

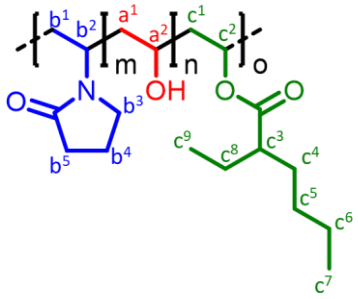

Scheme 40: Chemical structure of PVA-co-PVP modified with **apolar-IV**.

apolar-IV: 1H NMR (400 MHz, DMSO) δ [ppm] = 5.08-3.36 (broad m, 3H, a^2, b^2, c^2), 3.35-2.86 (broad m, 2H, b^3), 2.39-2.00 (broad m, 2H, b^5), 2.00-1.77 (broad m, 2H, b^4), 1.77-0.98 (broad m, 6H, a^1, b^1, c^1, c^4, c^5 c^6, c^8), 1.17-1.13 (broad t, 3H, c^9) , 1.13-1.07 (broad t, 3H, c^9), 1.07-1.02 (broad t, 3H, c^9), 0.92-0.75 (broad m, 3H, c^7).

amine modifications

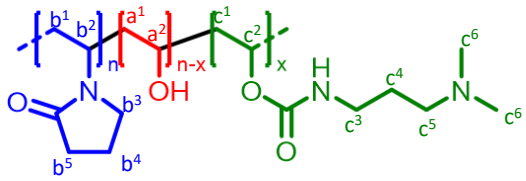

Scheme 41: Chemical structure of PVA-co-PVP modified with **amine-I**.

amine-II: 1H NMR (700 MHz, DMSO) δ [ppm] = 5.28-3.44 (broad m, 3H, a^2, b^2, c^2), 3.44-2.96 (broad m, 2H, b^3), 2.94-2.74 (broad m, 10H, c^3, c^5, c^6), 2.41-2.01 (broad m, 2H, b^5), 2.00-1.78(broad m, 2H, b^4), 1.78-0.81 (broad m, 5H, a^1, b^1, c^1, c^4).

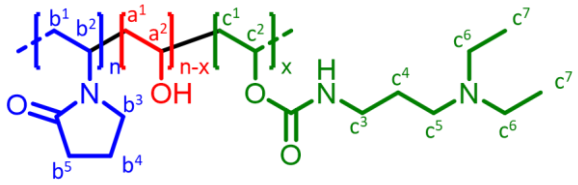

Scheme 42: Chemical structure of PVA-co-PVP modified with **amine-II**.

amine-II: 1H NMR (400 MHz, DMSO) δ [ppm] = 5.10-3.36 (broad m, 3H, a^2, b^2, c^2), 3.36-2.81 (broad m, 2H, b^3), 2.43-2.02 (broad m, 2H, b^5), 2.03-1.78 (broad m, 2H, b^4), 1.78-1.23 (broad m, 5H, a^1, b^1, c^1, c^4)., 1.22-1.11 (broad m, 6H, c^7).

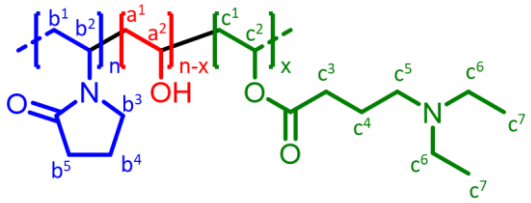

Scheme 43: Chemical structure of PVA-co-PVP modified with **amine-III**.

amine-III: 1H NMR (700 MHz, DMSO) δ [ppm] = 4.53-3.35 (broad m, 3H, a^2, b^2, c^2), 3.36-2.85 (broad m, 12H, b^3, c^3, c^5, c^6), 2.38-2.01 (broad m, 2H, b^5), 2.01-1.78 (broad m, 2H, b^4), 1.76-0.93 (broad m, 5H, a^1, b^1, c^1, c^4), 1.19-0.98 (broad m, 3H, c^7).

miscellaneous modifications

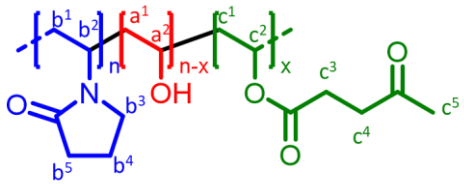

Scheme 44: Chemical structure of PVA-co-PVP modified with **misc-I**.

misc-I: 1H NMR (400 MHz, DMSO) δ [ppm] = 5.67-3.36 (broad m, 3H, a^2, b^2, c^2), 3.36-2.85 (broad m, 2H, b^3), 2.74-2.57 (broad d, 2H, c^3), 2.47-2.00 (broad m, 7H, b^5, c^4, c^5), 2.01-0.76 (broad m, 6H, a^1, b^1, c^1).

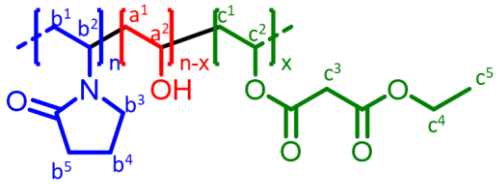

Scheme 45: Chemical structure of PVA-co-PVP modified with **misc-II**.

misc-II: 1H NMR (400 MHz, DMSO) δ [ppm] = 5.34-3.71 (broad m, 5H, a^2, b^2, c^2, c^4), 3.67-3.36 (broad m, 2H, b^3), 3.35-2.86 (broad m, 2H, c^3), 2.40-2.00 (broad m, 2H, b^5), 2.01-1.76 (broad m, 2H, b^4), 1.76-1.22 (broad m, 6H, a^1, b^1, c^1), 1.22-1.12 (broad m, 3H, c^5).

combined modifications mPEG-II and apolar-II

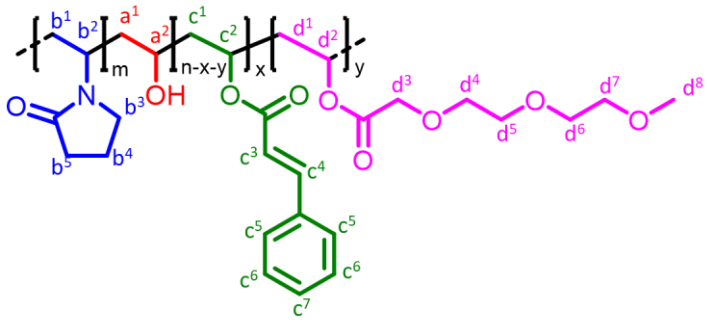

Scheme 46: Chemical structure of PVA-co-PVP modified with **mPEG-II/apolar-I**.

mPEG-II/apolar-I: 1H NMR (400 MHz, DMSO) δ [ppm] = 8.19-7.19 (broad m, 5H, c^{4-6}), 6.71-6.39 (broad m, 1H, c^7), 6.14-5.92 (broad m, 1H, c^3), 5.33-3.66 (broad m, 6H, a^2, b^2, c^2, d^2, d^3), 3.66-3.35 (broad m, 8H, d^{4-7}), 3.34-2.84 (broad m, 5H, b^3, d^8), 2.33-2.01 (broad m, 2H, b^5), 2.01-1.74 (broad m, 2H, b^4), 1.74-0.85 (broad m, 6H, a^1, b^1, c^1, d^1).

8.2.1.5 Synthesis of mPEG7 succinate and mPEG12 succinate

The modification agents mPEG7 succinate and mPEG12 succinate were synthesized starting from commercially available mPEG350 (M_w = 350 g mol^{-1}), mPEG550 (M_w 550 g mol^{-1}) and succinic anhydride. Pyridine was added to a solution of succinic anhydride in DCM at 0 °C. To this solution the respective mPEG was added and after stirring over 2 days, the product was isolated by extraction with DCM.

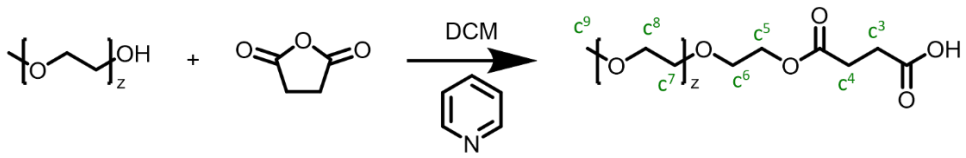

Scheme 47: Synthesis of mPEG7 succinate and mPEG12 succinate.

mPEG550-succinate: ^{1}H NMR (700 MHz, DMSO) δ [ppm] = 8.97-8.94 (pyridine), 8.67-8.62 (pyridine), 8.13-8.09 (pyridine), 4.13–4.09 (m, 1H, c^{5}), 3.61–3.56 (m, 1H, c^{6}), 3.53-3.47 (m, 44H, c^{7}, c^{8}), 3.23-3.21 (s, 3H, c^{9}), 2.48-2.43 (m, 4H, c^{3}, c^{4}).

8.2.2 General procedure for free radical polymerization experiments

The polymerization was conducted according to an adapted literature procedure.[166] Oven-dried glassware was utilized for all free radical polymerization reactions. The feed mixtures were prepared independently and in separate oven-dried flasks. The total molar ratios of utilized substances are summarized in Table 51. For each monomer combination the distribution of each reagent in the respective feed is given in Tables in the following subchapters. The following paragraph describes a typical reaction procedure. For Feed 2, the corresponding solvent was dried over 3 Å mol sieves. For the reactions leading to **RAD-I** and **RAD-II**, 1,4-Dioxane was used as solvent at a temperature of 70 °C. The remaining polymers were synthesized using 2-propanol (iPrOH) at 75 °C. After testing multiple solvents for the precipitation, MTBE was found to be ideal and used for the purification of each polymer discussed. The polymerizations were conducted at a mass concentration of c_w = 0.2 g mL^{-1} (*m*/*v*).

A three-necked round bottom flask was charged with the initial mixture consisting of a defined mole fraction of the monomers VP (**M-I**), VAc (**M-II**), where applicable VBenz (**M-IV**), a fraction of the initiator and a fraction of the solvent. A second three-necked round bottom flask was charged with Feed 1 consisting of VP, VAc, where applicable VBenz, and solvent. Feed 3, consisting of VP and solvent, was charged into a third round-bottom flask. The initiator was dispersed in the appropriate amount of solvent and kept under a nitrogen atmosphere. In polymerizations where mPEGMA (**M-III**) was used as a monomer, mPEGMA was dissolved in the appropriate amount of solvent in a fourth round-bottom flask. All round bottom flasks were degassed thrice using the freeze-pump-thaw (FPT) technique using a dry-ice acetone bath (**RAD-I**, **-II**, **-III**, and **RAD-IV**) or by nitrogen bubbling (**RAD-V** to **RAD-XXII**) and kept under nitrogen. The reagents were degassed via nitrogen bubbling if not otherwise stated in the respective subchapter.

The synthesis is conducted in the 100 mL three-necked round bottom flask containing the Initial Feed equipped with an air cooler, dropping funnel and a septum. In reactions where a syringe pump is utilized, the septum is exchanged for the connection with the syringe pump. The reaction is carried out in an inert atmosphere with slight nitrogen overpressure to prevent premature termination of the reaction. The reaction is started by heating the reaction vessel to the annotated temperature above the decomposition temperature of ACVA (Table 51). Feed 1 is transferred into the dropping funnel and the stopcock is opened after 0.75 hours of reaction time, introducing the monomer mixture on a time scale of 120 minutes. If a mPEGMA is used during the reaction, the syringe pump is started after 90 minutes with the appropriate flow rate to facilitate introduction of the monomer in 240 minutes. After the reaction proceeded for 2 hours, Feed 3 is charged into the same dropping funnel and opened so the mixture is introduced during a period of 120 minutes. Feed 2 is introduced via a nitrogen flushed syringe into the reaction mixture over the course of 30 minutes. After the reaction proceeded for 5 hours, the

dropping funnel is charged with Feed 4 and is introduced into the reaction mixture during a time period of 40 minutes. The reaction is terminated after 6 hours by opening the reaction vessel to the atmosphere while stirring to enable atmospheric oxygen to terminate the polymerization.

The solvent utilized for the purification is noted in Table 51 for each synthesized polymer. The polymer is isolated by precipitation from cold MTBE. Briefly, the solvent is removed under reduced pressure and four times the mass of utilized total monomer mass is added to the oily residue. The polymer is then added dropwise into 30 times the amount of previously added solvent volume of MTBE at -40 °C. A dry-ice isopropanol mixture is utilized for cooling. The polymer precipitates as a colorless solid and was separated from the liquid via vacuum filtration. Residual solvent is removed in a vacuum drying oven at 50 °C.

8.2.2.1 Batch calculations free radical polymerization

Table 51: Molar amounts utilized in free radical polymerization of up to four monomers.

Batch no.			M1			M2			M3			M4			Initiator								
	Solvent	$m(M)_{tot}$ / g	*m* / g	*n* / mol	*eq*	*m* / g	*n* / mol	*eq*	*m* / g	*n* / mol	*eq*	*m* / g	*n* / mol	*eq*	*m* / g	*n* / µmol	eq	V_{Solv} / mL	r(M1)	r(M2)	r(M2)	r(M2)	Yield / % (g)
RAD-I	1,4-Dioxane	5.0	4.03	36.23	253	0.97	11.44	80	0.00	0.00	0	0.00	0.00	0	0.04	143	1	25	76	24	0	0	3(60)
RAD-II	2-Propanol	2.5	1.04	9.40	183	0.52	5.98	117	0.94	1.71	33	0.00	0.00	0	0.01	51	1	13	55	35	10	0	0.2(8)
RAD-III	2-Propanol	12.5	6.30	56.70	183	3.11	36.08	117	3.09	10.31	33	0.00	0.00	0	0.09	310	1	63	55	35	10	0	9.8(78)
RAD-IV	2-Propanol	12.5	6.48	58.27	200	1.67	19.42	67	2.91	9.71	33	1.44	9.71	33	0.08	292	1	63	60	20	10	10	6.5(52)
RAD-V	2-Propanol	12.5	6.48	58.27	200	1.67	19.42	67	2.91	9.71	33	1.44	9.71	33	0.08	292	1	63	60	20	10	10	6.7(54)
RAD-VI	2-Propanol	15.0	9.89	89.00	200	5.11	59.34	133	0.00	0.00	0	0.00	0.00	0	0.13	445	1	75	60	40	0	0	9.2(61)
RAD-VII	2-Propanol	15.0	9.60	86.35	200	4.34	50.37	117	0.00	0.00	0	1.07	7.20	17	0.12	432	1	75	60	35	0	5	11.2(75)
RAD-VIII	2-Propanol	15.0	8.95	80.49	200	4.04	46.95	117	2.01	6.71	17	0.00	0.00	0	0.11	403	1	75	60	35	5	0	10.3(69)
RAD-IX	2-Propanol	15.0	9.60	86.35	200	4.34	50.37	117	0.00	0.00	0	1.07	7.20	17	0.12	432	1	75	60	35	0	10	9.7(64)
RAD-X	2-Propanol	15.0	8.70	78.32	200	3.37	39.16	100	1.96	6.53	17	0.97	6.53	17	0.11	392	1	75	60	30	5	5	10.5(70)
RAD-XI	2-Propanol	15.0	8.70	78.32	200	3.37	39.16	100	1.96	6.53	17	0.97	6.53	17	0.11	392	1	75	60	30	5	5	9.8(65)
RAD-XII	2-Propanol	15.0	8.70	78.32	200	3.37	39.16	100	1.96	6.53	17	0.97	6.53	17	0.11	392	1	75	60	30	5	5	8.8(58)
RAD-XIII	2-Propanol	15.0	8.16	78.32	200	3.16	36.73	100	3.67	12.24	33	0.00	0.00	0	0.11	392	1	75	60	30	10	0	6.7(45)
RAD-XIV	2-Propanol	15.0	8.48	78.32	200	2.74	31.77	83	1.91	6.35	17	1.88	12.71	33	0.11	382	1	75	60	25	5	10	10.5(70)
RAD-XV	2-Propanol	15.0	7.96	69.92	200	2.57	23.31	83	3.58	11.65	33	0.88	11.65	16	0.10	350	1	75	60	20	10	5	10.5(70)
RAD-XVI	2-Propanol	15.0	7.77	69.92	200	2.01	23.31	67	3.50	11.65	33	1.73	11.65	33	0.10	350	1	75	60	20	10	10	6.7(45)
RAD-XVII	2-Propanol	20.0	11.61	104.42	200	4.49	52.21	100	2.61	8.70	17	1.29	8.70	17	0.15	523	1	100	60	30	5	5	15(75)
RAD-XVIII	2-Propanol	20.0	11.61	104.42	200	4.49	52.21	100	2.61	8.70	17	1.29	8.70	17	0.15	523	1	100	60	30	5	5	13(65)
RAD-XIX	2-Propanol	20.0	11.61	104.42	200	4.49	52.21	100	2.61	8.70	17	1.29	8.70	17	0.15	523	1	100	60	30	5	5	17(85)
RAD-XX	2-Propanol	150.0	68.48	616.15	167	26.52	308.07	83	18.48	61.61	17	36.52	246.46	67	1.04	3701	1	750	50	25	5	20	118(91)

Tot: Total sum of monomer masses
MX: Monomer present in the synthesis
m(X): Mass
M monomer
I initiator ACVA

V_{solv}: Volume of solvent in reaction
n(X): molar amount of X
eq(X): equivalents of X
m(X): mass of X

8.2.2.2 RAD-I (M-I, M-II with FPT)

Table 52: Chemical substances used during the reaction and the distribution of amounts in the respective feeds. Initial denotes the mixture prepared in the beginning of the reaction.

% of total moles	VP	VAc	ACVA	Dioxane
Initial	29%	39%	14%	17%
Feed 1	46%	61%	/	26%
Feed 2	/	/	86%	2%
Feed 3	25%	/	/	8%
Feed 4	/	/	/	40%

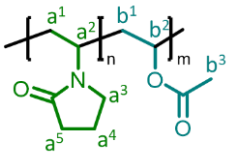

Scheme 48: Chemical structure of RAD-I.

RAD-I: ^{1}H NMR (400 MHz, DMSO) δ [ppm] = 3.95-3.35 (broad m, 2H, a^2, b^2), 3.36-2.75 (broad s, 2H, a^3), 2.40-1.99 (broad m, 2H, a^5), 1.99-1.74 (broad m, 5H, a^4, b^3), 1.75-1.12 (broad m, 4H, a^1, b^1).

8.2.2.3 RAD-II (M-I, M-II, M-V with FPT)

Table 53 Chemical substances used during the reaction and the distribution of amounts in the respective feeds. Initial denotes the mixture prepared in the beginning of the reaction.

% of total moles	VP	VAc	allylPEG	Init.	Dioxane
Initial	29%	39%	39	14%	17%
Feed 1	46%	61%	61	/	26%
Feed 2	/	/	/	86%	2%
Feed 3	25%	/	/	/	8%
Feed 4	/	/	/	/	40%

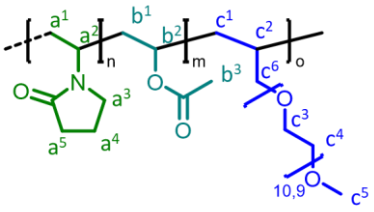

Scheme 49: Chemical structure of RAD-II

RAD-II: ^{1}H NMR (400 MHz, DMSO) δ [ppm] = 4.57-3.36 (broad m, 47H, a^2, b^2, c^3, c^4,), 3.36-2.84 (broad m, 5H, a^3, c^5), 2.39-1.99 (broad m, 4H, a^5, c^5), 1.99-1.76 (broad m, 5H, a^4, b^3), 1.75-1.12 (broad m, 8H, a^1, b^1, c^1, c^6).

8.2.2.4 RAD-III (M-I, M-II, M-III, with FPT)

Table 54: Chemical substances used during the reaction and the distribution of amounts in the respective feeds. Initial denotes the mixture prepared in the beginning of the reaction.

% of total m	VP	VAc	mPEGMA	Init.	iPrOH
Initial	29%	39%	/	14%	17%
Feed 1	46%	61%	/	/	26%
Feed 2	/	/	/	86%	2%
Feed 3	25%	/	/	/	8%
Feed 4	/	/	/	/	40%
Syringe Pump	/	/	100%	/	

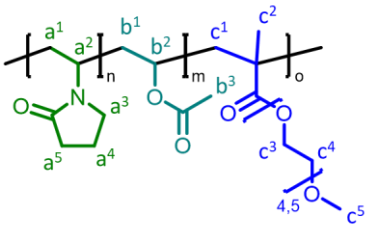

Scheme 50: Chemical structure of RAD-III.

RAD-III: ^{1}H NMR (400 MHz, DMSO) δ [ppm] = 4.95-3.29 (broad m, 22H, a^2, b^2, c^3, c^4), 3.29-2.88 (broad m, 5H, a^3, c^5), 2.43-2.00 (broad m, 4H, a^5, c^5), 2.01-1.71 (broad m, 5H, a^4, b^3), 1.71-1.15 (broad m, 6H, a^1, b^1, c^1, c^2).

8.2.2.5 RAD-IV (M-I, M-II, M-III, M-IV with FPT)

Table 55: Chemical substances used during the reaction and the distribution of amounts in the respective feeds. Initial denotes the mixture prepared in the beginning of the reaction.

% of total m	VP	VAc	mPEGMA	VBenz	Init.	iPrOH
Initial	29%	39%	/	32%	14%	17%
Feed 1	46%	61%	/	68%	/	26%
Feed 2	/	/	/	/	86%	2%
Feed 3	25%	/	/	/	/	8%
Feed 4	/	/	/	/	/	40%
Syringe Pump	/	/	100%	/	/	

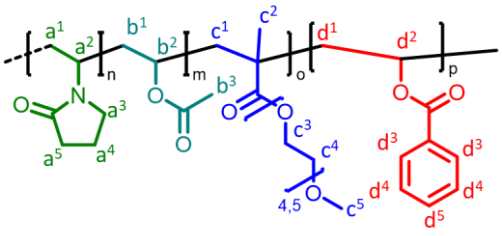

Scheme 51: Chemical structure of RAD-IV.

RAD-IV: ^{1}H NMR (400 MHz, DMSO) δ [ppm] = 8.05-7.73 (broad m, 2H, d^3), 7.64-7.20 (broad m, 3H, d^4, d^5), 4.32-3.34 (broad m, 23H, a^2, b^2, c^3, c^4,d^2), 3.34-2.76 (broad m, 5H, a^3, c^5), 2.39-1.99 (broad m,

4H, a^5, c^5), 2.00-1.70 (broad m, 5H, a^4, b^3), 1.70-1.18 (broad m,8H, a^1, b^1, c^1, d^1), 1.16-0.76 (Isopropanol, broad m, 3H, c^2).

8.2.2.6 RAD-V (M-I, M-II, M-III, M-IV)

Table 56: Chemical substances used during the reaction and the distribution of amounts in the respective feeds. Initial denotes the mixture prepared in the beginning of the reaction.

% of total m	VP	VAc	mPEGMA	VBenz	Init.	iPrOH
Initial	29%	39%	/	32%	14%	17%
Feed 1	46%	61%	/	68%	/	26%
Feed 2	/	/	/	/	86%	2%
Feed 3	25%	/	/	/	/	8%
Feed 4	/	/	/	/	/	40%
Syringe Pump	/	/	100%	/	/	

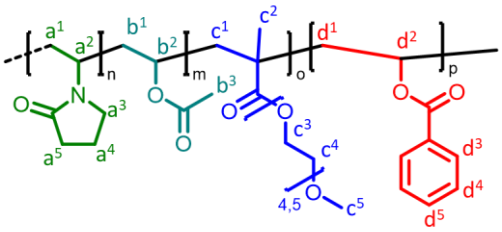

Scheme 52: Chemical structure of RAD-V.

RAD-V: ^{1}H NMR (400 MHz, DMSO) δ [ppm] = 8.01-7.75 (broad m, 2H, d^3), 7.67-7.31 (broad m, 3H, d^4, d^5), 5.16-3.35 (broad m, 23H, a^2, b^2, c^3, c^4,d^2), 3.35-2.81 (broad m, 5H, a^3, c^5), 2.42-1.98 (broad m, 4H, a^5, c^5), 1.98-1.68 (broad m, 5H, a^4, b^3), 1.69-0.76 (broad m,11H, a^1, b^1, c^1, d^1, c^2).

8.2.2.7 RAD-VI (M-I, M-II)

Table 57: Chemical substances used during the reaction and the distribution of amounts in the respective feeds. Initial denotes the mixture prepared in the beginning of the reaction.

% of total m	VP	VAc	Init.	iPrOH
Initial	29%	39%	14%	17%
Feed 1	46%	61%	/	26%
Feed 2	/	/	86%	2%
Feed 3	25%	/	/	8%
Feed 4	/	/	/	40%
Syringe Pump	/	/	/	

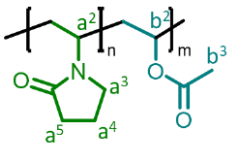

Scheme 53: Chemical structure of RAD-VI.

RAD-VI: ^{1}H NMR (400 MHz, DMSO) δ [ppm] = 9.59-9.43, 5.31-3.36, 3.36-2.83, 2.43-2.00, 2.00-1.78, 1.78-1.14, 1.14-0.94.

RAD-I: ^{1}H NMR (400 MHz, DMSO) δ [ppm] = 3.95-3.35 (broad m, 2H, a^2, b^2), 3.36-2.75 (broad s, 2H, a^3), 2.40-1.99 (broad m, 2H, a^5), 1.99-1.74 (broad m, 5H, a^4, b^3), 1.75-1.12 (broad m, 4H, a^1, b^1).

8.2.2.8 RAD-VII (M-I, M-II, M-IV)

Table 58: Chemical substances used during the reaction and the distribution of amounts in the respective feeds. Initial denotes the mixture prepared in the beginning of the reaction.

% of total m	VP	VAc	VBenz	Init.	iPrOH
Initial	29%	39%	32%	14%	17%
Feed 1	46%	61%	68%	/	26%
Feed 2	/	/	/	86%	2%
Feed 3	25%	/	/	/	8%
Feed 4	/	/	/	/	40%
Syringe Pump	/	/	/	/	

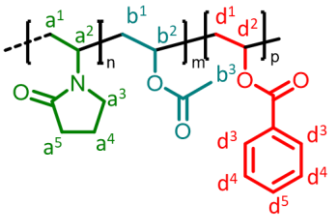

Scheme 54: Chemical structure of RAD-VII.

RAD-VII: ^{1}H NMR (400 MHz, DMSO) δ [ppm] = 8.01-7.78 (broad m, 2H, d^3), 7.68-7.36 (broad m, 3H, d^4, d^5), 5.21-3.38 (broad m, 3H, a^2, b^2, d^2), 3.38-2.79 (broad m, 2H, a^3), 2.41-1.99 (broad m, 2H, a^5), 1.99-1.76 (broad m, 5H, a^4, b^3), 1.75-0.96 (Isopropanol, broad m, 6H, a^1, b^1, d^1).

8.2.2.9 RAD-VIII (M-I, M-II, M-III)

Table 59: Chemical substances used during the reaction and the distribution of amounts in the respective feeds. Initial denotes the mixture prepared in the beginning of the reaction.

% of total m	VP	VAc	mPEGMA	Init.	iPrOH
Initial	29%	39%	/	14%	17%
Feed 1	46%	61%	/	/	26%
Feed 2	/	/	/	86%	2%
Feed 3	25%	/	/	/	8%
Feed 4	/	/	/	/	40%
Syringe Pump	/	/	100%	/	

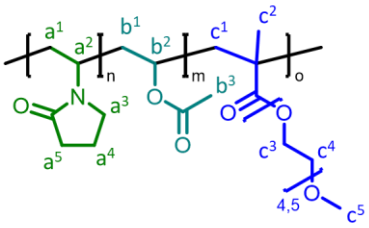

Scheme 55: Chemical structure of RAD-VIII.

RAD-VIII: ^{1}H NMR (400 MHz, DMSO) δ [ppm] = 4.99-3.38 (broad m, 22H, a^2, b^2, c^3, c^4), 3.37-2.83 (broad m, 5H, a^3, c^5), 2.39-1.99 (broad m, 4H, a^5, c^5), 2.00-1.77 (broad m, 5H, a^4, b^3), 1.77-0.93 (broad m, 9H, a^1, b^1, c^1, c^2).

8.2.2.10 RAD-IX (M-I, M-II, M-IV)

Table 60: Chemical substances used during the reaction and the distribution of amounts in the respective feeds. Initial denotes the mixture prepared in the beginning of the reaction.

% of total m	VP	VAc	VBenz	Init.	iPrOH
Initial	29%	39%	32%	14%	17%
Feed 1	46%	61%	68%	/	26%
Feed 2	/	/	/	86%	2%
Feed 3	25%	/	/	/	8%
Feed 4	/	/	/	/	40%
Syringe Pump	/	/	/	/	

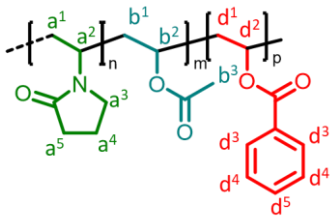

Scheme 56: Chemical structure of RAD-IX.

RAD-IX: ^{1}H NMR (400 MHz, DMSO) δ [ppm] = 8.03-7.77 (broad m, 2H, d^3), 7.69-7.30 (broad m, 3H, d^4, d^5), 5.03-3.38 (broad m, 3H, a^2, b^2, d^2), 3.38-2.74 (broad m, 2H, a^3), 2.41-1.99 (broad m, 2H, a^5), 1.99-1.73 (broad m, 5H, a^4, b^3), 1.73-0.96 (Isopropanol, broad m, 8H, a^1, b^1, d^1).

8.2.2.11 RAD-X (M-I, M-II, M-III, M-IV)

Table 61: Chemical substances used during the reaction and the distribution of amounts in the respective feeds. Initial denotes the mixture prepared in the beginning of the reaction.

% of total m	VP	VAc	mPEGMA	VBenz	Init.	iPrOH
Initial	29%	39%	/	32%	14%	17%
Feed 1	46%	61%	/	68%	/	26%
Feed 2	/	/	/	/	86%	2%
Feed 3	25%	/	/	/	/	8%
Feed 4	/	/	/	/	/	40%
Syringe Pump	/	/	100%	/	/	

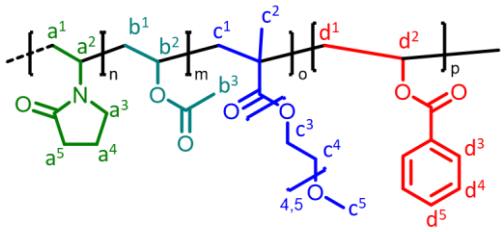

Scheme 57: Chemical structure of RAD-X.

RAD-X: ^{1}H NMR (400 MHz, DMSO) δ [ppm] = 8.01-7.77 (broad m, 2H, d^3), 7.69-7.32 (broad m, 3H, d^4, d^5), 5.21-3.37 (broad m, 23H, a^2, b^2, c^3, c^4,d^2), 3.36-2.88 (broad m, 5H, a^3, c^5), 2.40-1.99 (broad m, 4H, a^5, c^5), 2.00-1.74 (broad m, 5H, a^4, b^3), 1.74-0.88 (broad m,11H, a^1, b^1, c^1, d^1, c^2).

8.2.2.12 RAD-XI (M-I, M-II, M-III, M-IV)

Table 62 Content of solutions for free radical polymerization with 4 comonomers.

% of total m	VP	VAc	mPEGMA	VBenz	Init.	iPrOH
Initial	29%	39%	/	32%	14%	17%
Feed 1	46%	61%	/	68%	/	26%
Feed 2	/	/	/	/	86%	2%
Feed 3	25%	/	/	/	/	8%
Feed 4	/	/	/	/	/	40%
Syringe Pump	/	/	100%	/	/	

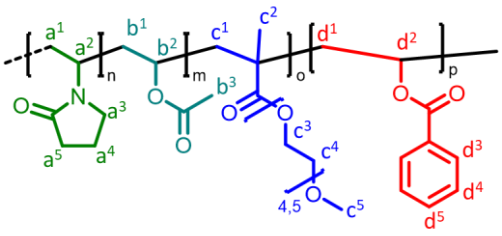

Scheme 58: Chemical substances used during the reaction and the distribution of amounts in the respective feeds. Initial denotes the mixture prepared in the beginning of the reaction.

RAD-XI: ^{1}H NMR (400 MHz, DMSO) δ [ppm] = 8.03-7.79 (broad m, 2H, d^3), 7.72-7.36 (broad m, 3H, d^4, d^5), 5.13-3.38 (broad m, 23H, a^2, b^2, c^3, c^4, d^2), 3.38-2.83 (broad m, 5H, a^3, c^5), 2.44-1.99 (broad m, 4H, a^5, c^5), 1.99-1.72 (broad m, 5H, a^4, b^3), 1.74-1.15(broad m,11H, a^1, b^1, c^1, d^1, c^2).

8.2.2.13 RAD-XII (M-I, M-II, M-III, M-IV)

Table 63: Chemical substances used during the reaction and the distribution of amounts in the respective feeds. Initial denotes the mixture prepared in the beginning of the reaction.

% of total m	VP	VAc	mPEGMA	VBenz	Init.	iPrOH
Initial	29%	39%	/	32%	14%	17%
Feed 1	46%	61%	/	68%	/	26%
Feed 2	/	/	/	/	86%	2%
Feed 3	25%	/	/	/	/	8%
Feed 4	/	/	/	/	/	40%
Syringe Pump	/	/	100%	/	/	

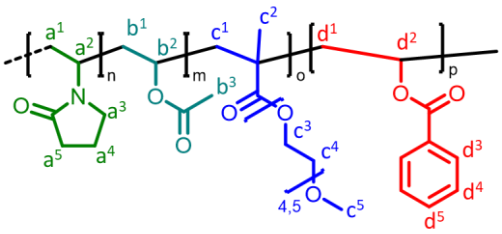

Scheme 59: Chemical structure of RAD-XII.

RAD-I: ^{1}H NMR (400 MHz, DMSO) δ [ppm] = 8.02-7.78 (broad m, 2H, d^3), 7.73-7.38 (broad m, 3H, d^4, d^5), 5.21-3.39 (broad m, 23H, a^2, b^2, c^3, c^4, d^2), 3.39-2.87 (broad m, 5H, a^3, c^5), 2.41-1.99 (broad m, 4H, a^5, c^5), 1.99-1.72 (broad m, 5H, a^4, b^3), 1.72-0.94 (broad m,11H, a^1, b^1, c^1, d^1, c^2).

8.2.2.14 RAD-XIII (M-I, M-II, M-III, M-IV)

Table 64: Chemical substances used during the reaction and the distribution of amounts in the respective feeds. Initial denotes the mixture prepared in the beginning of the reaction.

% of total m	VP	VAc	mPEGMA	Init.	iPrOH
Initial	29%	39%	/	14%	17%
Feed 1	46%	61%	/	/	26%
Feed 2	/	/	/	86%	2%
Feed 3	25%	/	/	/	8%
Feed 4	/	/	/	/	40%
Syringe Pump	/	/	100%	/	

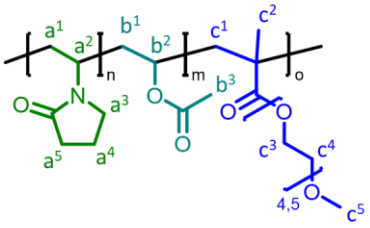

Scheme 60: Chemical structure of RAD-XIII.

RAD-XIII: ^{1}H NMR (400 MHz, DMSO) δ [ppm] = 5.16-3.37 (broad m, 22H, a^2, b^2, c^3, c^4), 3.36-2.89 (broad m, 5H, a^3, c^5), 2.39-1.99 (broad m, 4H, a^5, c^5), 1.99-0.77 (broad m, 6H, a^1, b^1, c^1, c^2).

8.2.2.15 RAD-XIV (M-I, M-II, M-III, M-IV)

Table 65: Chemical substances used during the reaction and the distribution of amounts in the respective feeds. Initial denotes the mixture prepared in the beginning of the reaction.

% of total m	VP	VAc	mPEGMA	VBenz	Init.	iPrOH
Initial	29%	39%	/	32%	14%	17%
Feed 1	46%	61%	/	68%	/	26%
Feed 2	/	/	/	/	86%	2%
Feed 3	25%	/	/	/	/	8%
Feed 4	/	/	/	/	/	40%
Syringe Pump	/	/	100%	/	/	

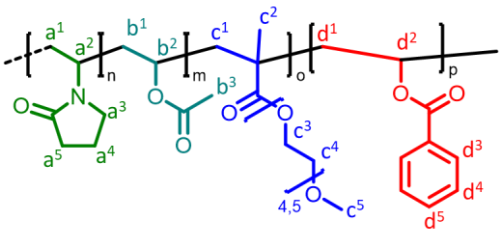

Scheme 61: Chemical structure of RAD-XIV.

RAD-XIV: ^{1}H NMR (400 MHz, DMSO) δ [ppm] = 8.01-7.76 (broad m, 2H, d^3), 7.72-7.27 (broad m, 3H, d^4, d^5), 5.19-3.38 (broad m, 23H, a^2, b^2, c^3, c^4,d^2), 3.36-2.87 (broad m, 5H, a^3, c^5), 2.42-1.99 (broad m, 4H, a^5, c^5), 1.99-1.73 (broad m, 5H, a^4, b^3), 1.73-1.17 (broad m, 8H, a^1, b^1, c^1, d^1, c^2), 1.17-0.80 (Isopropanol, broad m, 3H, c^2).

8.2.2.16 RAD-XV (M-I, M-II, M-III, M-IV)

Table 66: Chemical substances used during the reaction and the distribution of amounts in the respective feeds. Initial denotes the mixture prepared in the beginning of the reaction.

% of total m	VP	VAc	mPEGMA	VBenz	Init.	iPrOH
Initial	29%	39%	/	32%	14%	17%
Feed 1	46%	61%	/	68%	/	26%
Feed 2	/	/	/	/	86%	2%
Feed 3	25%	/	/	/	/	8%
Feed 4	/	/	/	/	/	40%
Syringe Pump	/	/	100%	/	/	

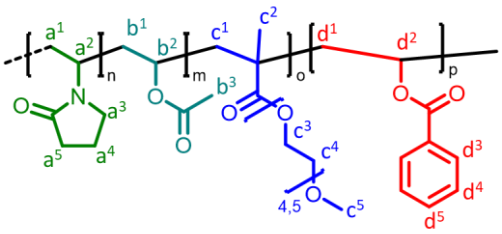

Scheme 62: Chemical structure of RAD-XV.

RAD-XV: ^{1}H NMR (400 MHz, DMSO) δ [ppm] = 8.04-7.75 (broad m, 2H, d^3), 7.75-7.31 (broad m, 3H, d^4, d^5), 5.30-3.36 (broad m, 23H, a^2, b^2, c^3, c^4, d^2), 3.36-2.82 (broad m, 5H, a^3, c^5), 2.41-1.99 (broad m, 4H, a^5, c^5), 1.99-1.69 (broad m, 5H, a^4, b^3), 1.69-0.86 (broad m,11H, a^1, b^1, c^1, d^1, c^2).

8.2.2.17 RAD-XVI (M-I, M-II, M-III, M-IV)

Table 67: Chemical substances used during the reaction and the distribution of amounts in the respective feeds. Initial denotes the mixture prepared in the beginning of the reaction.

% of total m	VP	VAc	mPEGMA	VBenz	Init.	iPrOH
Initial	29%	39%	/	32%	14%	17%
Feed 1	46%	61%	/	68%	/	26%
Feed 2	/	/	/	/	86%	2%
Feed 3	25%	/	/	/	/	8%
Feed 4	/	/	/	/	/	40%
Syringe Pump	/	/	100%	/	/	

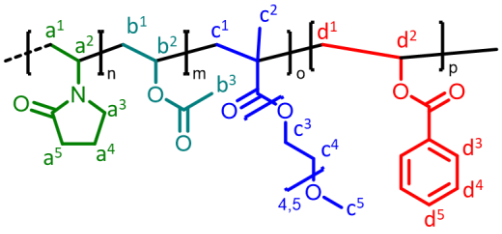

Scheme 63: Chemical structure of RAD-XVI.

RAD-XVI: ^{1}H NMR (400 MHz, DMSO) δ [ppm] = 8.07-7.74 (broad m, 2H, d^3), 7.69-7.34 (broad m, 3H, d^4, d^5), 5.33-3.37 (broad m, 23H, a^2, b^2, c^3, c^4, d^2), 3.27-2.91 (broad m, 5H, a^3, c^5), 2.43-2.00 (broad m, 4H, a^5, c^5), 2.00-1.70 (broad m, 5H, a^4, b^3), 1.70-0.68 (broad m,11H , a^1, b^1, c^1, d^1, c^2).

8.2.2.18 RAD-XVII (M-I, M-II, M-III, M-IV)

Table 68: Chemical substances used during the reaction and the distribution of amounts in the respective feeds. Initial denotes the mixture prepared in the beginning of the reaction.

% of total m	VP	VAc	mPEGMA	VBenz	Init.	iPrOH
Initial	29%	39%	/	32%	14%	17%
Feed 1	46%	61%	/	68%	/	26%
Feed 2	/	/	/	/	86%	2%
Feed 3	25%	/	/	/	/	8%
Feed 4	/	/	/	/	/	40%
Syringe Pump	/	/	100%	/	/	

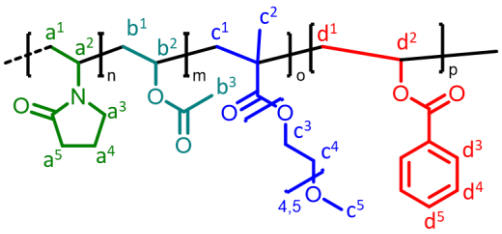

Scheme 64: Chemical structure of RAD-XVII.

RAD-XVII: ^{1}H NMR (400 MHz, DMSO) δ [ppm] = 8.05-7.81 (broad m, 2H, d^3), 7.65-7.33 (broad m, 3H, d^4, d^5), 5.63-3.34 (broad m, 23H, a^2, b^2, c^3, c^4, d^2), 3.35-2.82 (broad m, 5H, a^3, c^5), 2.43-2.00 (broad m, 4H, a^5, c^5), 2.00-1.70 (broad m, 5H, a^4, b^3), 1.71-0.76 (broad m,11H , a^1, b^1, c^1, d^1, c^2).

8.2.2.19 RAD-XVIII (M-I, M-II, M-III, M-IV)

Table 69: Chemical substances used during the reaction and the distribution of amounts in the respective feeds. Initial denotes the mixture prepared in the beginning of the reaction.

% of total m	VP	VAc	mPEGMA	VBenz	Init.	iPrOH
Initial	29%	39%	/	32%	14%	17%
Feed 1	46%	61%	/	68%	/	26%
Feed 2	/	/	/	/	86%	2%
Feed 3	25%	/	/	/	/	8%
Feed 4	/	/	/	/	/	40%
Syringe Pump	/	/	100%	/	/	

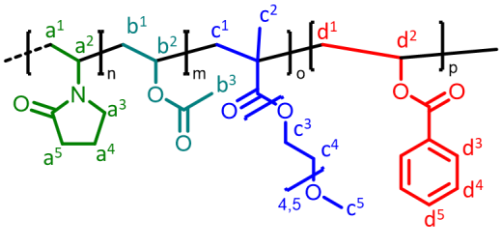

Scheme 65: Chemical structure of RAD-XVIII.

RAD-XVIII: ^{1}H NMR (400 MHz, DMSO) δ [ppm] = 8.03-7.79 (broad m, 2H, d^3), 7.70-7.40 (broad m, 3H, d^4, d^5), 5.58-3.36 (broad m, 23H, a^2, b^2, c^3, c^4, d^2), 3.37-2.83 (broad m, 5H, a^3, c^5), 2.42-1.99 (broad m, 4H, a^5, c^5), 1.99-1.73 (broad m, 5H, a^4, b^3), 1.72-0.85 (broad m,11H , a^1, b^1, c^1, d^1, c^2).

8.2.2.20 RAD-XIX (M-I, M-II, M-III, M-IV)

Table 70: Chemical substances used during the reaction and the distribution of amounts in the respective feeds. Initial denotes the mixture prepared in the beginning of the reaction.

% of total m	VP	VAc	mPEGMA	VBenz	Init.	iPrOH
Initial	29%	39%	/	32%	14%	17%
Feed 1	46%	61%	/	68%	/	26%
Feed 2	/	/	/	/	86%	2%
Feed 3	25%	/	/	/	/	8%
Feed 4	/	/	/	/	/	40%
Syringe Pump	/	/	100%	/	/	

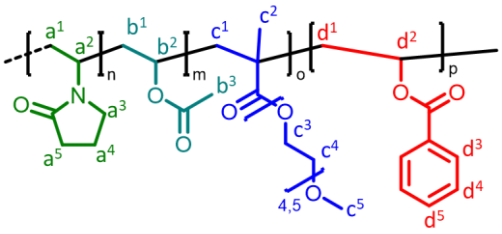

Scheme 66: Chemical structure of RAD-XIX.

RAD-XIX: ^{1}H NMR (400 MHz, DMSO) δ [ppm] = 8.00-7.79 (broad m, 2H, d^3), 7.71-7.41 (broad m, 3H, d^4, d^5), 5.26-3.37 (broad m, 23H, a^2, b^2, c^3, c^4, d^2), 3.37-2.79 (broad m, 5H, a^3, c^5), 2.42-2.00 (broad m, 4H, a^5, c^5), 2.00-1.72 (broad m, 5H, a^4, b^3), 1.72-0.84 (broad m,11H , a^1, b^1, c^1, d^1, c^2).

8.2.2.21 RAD-XX (M-I, M-II, M-III, M-IV)

Table 71: Chemical substances used during the reaction and the distribution of amounts in the respective feeds. Initial denotes the mixture prepared in the beginning of the reaction.

% of total m	VP	VAc	mPEGMA	VBenz	Init.	iPrOH
Initial	29%	39%	/	32%	14%	17%
Feed 1	46%	61%	/	68%	/	26%
Feed 2	/	/	/	/	86%	2%
Feed 3	25%	/	/	/	/	8%
Feed 4	/	/	/	/	/	40%
Syringe Pump	/	/	100%	/	/	

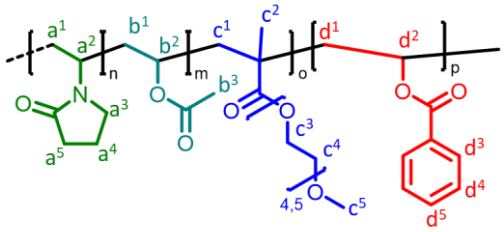

Scheme 67: Chemical structure of RAD-XX.

RAD-XX: ^{1}H NMR (400 MHz, DMSO) δ [ppm] = 8.00-7.79 (broad m, 2H, d^3), 7.71-7.41 (broad m, 3H, d^4, d^5), 5.26-3.37 (broad m, 23H, a^2, b^2, c^3, c^4, d^2), 3.37-2.79 (broad m, 5H, a^3, c^5), 2.42-2.00 (broad m, 4H, a^5, c^5), 2.00-1.72 (broad m, 5H, a^4, b^3), 1.72-0.84 (broad m,11H , a^1, b^1, c^1, d^1, c^2).

9 Figures

10 Tables

11 References

(1) Ting, J. M.; Porter, W. W., 3rd; Mecca, J. M.; Bates, F. S.; Reineke, T. M. Advances in Polymer Design for Enhancing Oral Drug Solubility and Delivery. *Bioconjug Chem* **2018**, *29* (4), 939-952.

(2) Amidon, G. L.; Lennernäs, H.; Shah, V. P.; Crison, J. R. A Theoretical Basis for a Biopharmaceutic Drug Classification: The Correlation of in Vitro Drug Product Dissolution and in Vivo Bioavailability. *Pharmaceutical Research* **1995**, *12* (3), 8.

(3) Staudinger, H. Über Polymerisation. *Berichte der deutschen chemischen Gesellschaft (A and B Series)* **1920**, *53* (6), 1073-1085.

(4) PlasticsEurope. *Weltweite und europäische Kunststoffproduktion in den Jahren von 1950 bis 2022 (in Millionen Tonnen)*. 2023. https://de.statista.com/statistik/daten/studie/167099/umfrage/weltproduktion-von-kunststoff-seit-1950/ (accessed 26.03.2024).

(5) Bass, S. L.; Goggin, W. C. Ethyl Cellulose Films and Plastics. *Transactions of The Electrochemical Society* **1938**, *74* (47).

(6) Koch, W. Properties and Uses of Ethylcellulose. *Industrial & Engineering Chemistry Research* **1937**, *29* (6).

(7) Reinhart, F. W.; Kline, G. M. Film-Forming Plastics. *Industrial and Engineering Chemistry* **1939**, *31* (12), 8.

(8) Doerr, D. W.; Serles, E. R.; Deardorff, D. L. Tablet coatings: cellulosic high polymers. *J Am Pharm Assoc Am Pharm Assoc* **1954**, *43* (7), 433-436.

(9) Malm, C. J.; Emerson, J.; Hiatt, G. D. Cellulose acetate phthalate as an enteric coating material. *J Am Pharm Assoc Am Pharm Assoc* **1951**, *40* (10), 520-525.

(10) Wagner, J. G.; Brignall, T. W.; Long, S. Enteric Coatings II. *Journal of the American Pharmaceutical Association (Scientific ed.)* **1959**, *48* (4), 244-249.

(11) Higuchi, T.; Kuramoto, R. Study of possible complex formation between macromolecules and certain pharmaceuticals. II. Polyvinylpyrrolidone with p-aminobenzoic acid, aminopyrine, benzoic acid, salicylic acid, p-hydroxybenzoic acid, m-hydroxybenzoic acid, citric acid, and phenobarbital. *Journal of the American Pharmaceutical Association (Scientific ed.)* **1954**, *43* (7), 398-401.

(12) Higuchi, T.; Kuramoto, R. Study of Possible Complex Formation between Macromolecules and Certain Pharmaceuticals*. *Journal of the American Pharmaceutical Association (Scientific ed.)* **1954**, *43* (7), 398-401.

(13) Arndt, O.; Kleinebudde, P. Influence of binder properties on dry granules and tablets. *Powder Technology* **2018**, *337*, 68-77.

(14) Browne, E.; Worku, Z. A.; Healy, A. M. Physicochemical Properties of Poly-Vinyl Polymers and Their Influence on Ketoprofen Amorphous Solid Dispersion Performance: A Polymer Selection Case Study. *Pharmaceutics* **2020**, *12* (5).

(15) Keen, J. M.; Foley, C. J.; Hughey, J. R.; Bennett, R. C.; Jannin, V.; Rosiaux, Y.; Marchaud, D.; McGinity, J. W. Continuous twin screw melt granulation of glyceryl behenate:

Development of controlled release tramadol hydrochloride tablets for improved safety. *Int J Pharm* **2015**, *487* (1-2), 72-80.

(16) Serrano, D. R.; Kara, A.; Yuste, I.; Luciano, F. C.; Ongoren, B.; Anaya, B. J.; Molina, G.; Diez, L.; Ramirez, B. I.; Ramirez, I. O.; et al. 3D Printing Technologies in Personalized Medicine, Nanomedicines, and Biopharmaceuticals. *Pharmaceutics* **2023**, *15* (2).

(17) Vithani, K.; Goyanes, A.; Jannin, V.; Basit, A. W.; Gaisford, S.; Boyd, B. J. An Overview of 3D Printing Technologies for Soft Materials and Potential Opportunities for Lipid-based Drug Delivery Systems. *Pharm Res* **2018**, *36* (1), 4.

(18) Debotton, N.; Dahan, A. Applications of Polymers as Pharmaceutical Excipients in Solid Oral Dosage Forms. *Med Res Rev* **2017**, *37* (1), 52-97.

(19) Melocchi, A.; Parietti, F.; Maroni, A.; Foppoli, A.; Gazzaniga, A.; Zema, L. Hot-melt extruded filaments based on pharmaceutical grade polymers for 3D printing by fused deposition modeling. *Int J Pharm* **2016**, *509* (1-2), 255-263.

(20) Nikolakakis, I.; Partheniadis, I. Self-Emulsifying Granules and Pellets: Composition and Formation Mechanisms for Instant or Controlled Release. *Pharmaceutics* **2017**, *9* (4).

(21) Al-Japairai, K.; Hamed Almurisi, S.; Mahmood, S.; Madheswaran, T.; Chatterjee, B.; Sri, P.; Azra Binti Ahmad Mazlan, N.; Al Hagbani, T.; Alheibshy, F. Strategies to improve the stability of amorphous solid dispersions in view of the hot melt extrusion (HME) method. *Int J Pharm* **2023**, *647*, 123536.

(22) Alshehri, S.; Imam, S. S.; Hussain, A.; Altamimi, M. A.; Alruwaili, N. K.; Alotaibi, F.; Alanazi, A.; Shakeel, F. Potential of solid dispersions to enhance solubility, bioavailability, and therapeutic efficacy of poorly water-soluble drugs: newer formulation techniques, current marketed scenario and patents. *Drug Deliv* **2020**, *27* (1), 1625-1643.

(23) Babu, N. R.; Nagpal, D.; Ankola, D.; Awasthi, R. Evolution of Solid Dispersion Technology: Solubility Enhancement Using Hydroxypropyl Methylcellulose Acetate Succinate: Myth or Reality? *Assay Drug Dev Technol* **2022**, *20* (4), 149-163.

(24) Bhalani, D. V.; Nutan, B.; Kumar, A.; Singh Chandel, A. K. Bioavailability Enhancement Techniques for Poorly Aqueous Soluble Drugs and Therapeutics. *Biomedicines* **2022**, *10* (9).

(25) Breitenbach, J. Melt extrusion: from process to drug delivery technology. *Eur J Pharm Biopharm* **2002**, *54* (2), 107-117. From NLM.

(26) Guzman, H. R.; Tawa, M.; Zhang, Z.; Ratanabanangkoon, P.; Shaw, P.; Gardner, C. R.; Chen, H.; Moreau, J. P.; Almarsson, O.; Remenar, J. F. Combined use of crystalline salt forms and precipitation inhibitors to improve oral absorption of celecoxib from solid oral formulations. *J Pharm Sci* **2007**, *96* (10), 2686-2702.

(27) He, Y.; Ho, C. Amorphous Solid Dispersions: Utilization and Challenges in Drug Discovery and Development. *J Pharm Sci* **2015**, *104* (10), 3237-3258.

(28) Luebbert, C.; Huxoll, F.; Sadowski, G. Amorphous-Amorphous Phase Separation in API/Polymer Formulations. *Molecules* **2017**, *22* (2).

(29) Newman, A.; Knipp, G.; Zografi, G. Assessing the performance of amorphous solid dispersions. *J Pharm Sci* **2012**, *101* (4), 1355-1377.

(30) Sareen, S.; Mathew, G.; Joseph, L. Improvement in solubility of poor water-soluble drugs by solid dispersion. *Int J Pharm Investig* **2012**, *2* (1), 12-17.

(31) Sinha, S.; Baboota, S.; Ali, M.; Kumar, A.; Ali, J. Solid Dispersion: An Alternative Technique for Bioavailability Enhancement of Poorly Soluble Drugs. *Journal of Dispersion Science and Technology* **2009**, *30* (10), 1458-1473.

(32) Sollohub, K.; Cal, K. Spray drying technique: II. Current applications in pharmaceutical technology. *J Pharm Sci* **2010**, *99* (2), 587-597.

(33) Vo, C. L.; Park, C.; Lee, B. J. Current trends and future perspectives of solid dispersions containing poorly water-soluble drugs. *Eur J Pharm Biopharm* **2013**, *85* (3 Pt B), 799-813.

(34) Zhang, J.; Guo, M.; Luo, M.; Cai, T. Advances in the development of amorphous solid dispersions: The role of polymeric carriers. *Asian J Pharm Sci* **2023**, *18* (4), 100834.

(35) Zhang, Y.; Luo, R.; Chen, Y.; Ke, X.; Hu, D.; Han, M. Application of carrier and plasticizer to improve the dissolution and bioavailability of poorly water-soluble baicalein by hot melt extrusion. *AAPS PharmSciTech* **2014**, *15* (3), 560-568.

(36) Bhardwaj, S. P.; Arora, K. K.; Kwong, E.; Templeton, A.; Clas, S. D.; Suryanarayanan, R. Mechanism of amorphous itraconazole stabilization in polymer solid dispersions: role of molecular mobility. *Mol Pharm* **2014**, *11* (11), 4228-4237.

(37) Bhujbal, S. V.; Mitra, B.; Jain, U.; Gong, Y.; Agrawal, A.; Karki, S.; Taylor, L. S.; Kumar, S.; Tony Zhou, Q. Pharmaceutical amorphous solid dispersion: A review of manufacturing strategies. *Acta Pharm Sin B* **2021**, *11* (8), 2505-2536.

(38) De Brabander, C.; Van Den Mooter, G.; Vervaet, C.; Remon, J. P. Characterization of ibuprofen as a nontraditional plasticizer of ethyl cellulose. *J Pharm Sci* **2002**, *91* (7), 1678-1685.

(39) Hughey, J. R.; Keen, J. M.; Miller, D. A.; Brough, C.; McGinity, J. W. Preparation and characterization of fusion processed solid dispersions containing a viscous thermally labile polymeric carrier. *Int J Pharm* **2012**, *438* (1-2), 11-19.

(40) Nayak, P.; Rajagopal, K.; Chang, D. Hydroxypropyl methyl cellulose derivatives stabilize fragment antibody against aggregation in spray dried formulations at elevated temperature and resist pH changes. *Eur J Pharm Biopharm* **2022**, *178*, 105-116.

(41) Zhang, J.; Xu, P.; Vo, A. Q.; Bandari, S.; Yang, F.; Durig, T.; Repka, M. A. Development and evaluation of pharmaceutical 3D printability for hot melt extruded cellulose-based filaments. *J Drug Deliv Sci Technol* **2019**, *52*, 292-302.

(42) Vasconcelos, T.; Sarmento, B.; Costa, P. Solid dispersions as strategy to improve oral bioavailability of poor water soluble drugs. *Drug Discov Today* **2007**, *12* (23-24), 1068-1075.

(43) Weuts, I.; Van Dycke, F.; Voorspoels, J.; De Cort, S.; Stokbroekx, S.; Leemans, R.; Brewster, M. E.; Xu, D.; Segmuller, B.; Turner, Y. T.; et al. Physicochemical properties of the amorphous drug, cast films, and spray dried powders to predict formulation probability of success for solid dispersions: etravirine. *J Pharm Sci* **2011**, *100* (1), 260-274.

(44) Miller, J. M.; Beig, A.; Carr, R. A.; Spence, J. K.; Dahan, A. A win-win solution in oral delivery of lipophilic drugs: supersaturation via amorphous solid dispersions increases apparent solubility without sacrifice of intestinal membrane permeability. *Mol Pharm* **2012**, *9* (7), 2009-2016.

(45) Van Den Mooter, G. The use of amorphous solid dispersions: A formulation strategy to overcome poor solubility and dissolution rate. *Drug Discov Today Technol* **2012**, *9* (2), e71-e174.

(46) Shah, N. S., H.; Choi, D. S.; Chokshi, H., Malick, A.W. *Amorphous Solid Dispersions*; Springer, 2014.

(47) Mendes, C.; Andrzejewski, R. G.; Pinto, J. M. O.; de Novais, L. M. R.; Barison, A.; Silva, M. A. S.; Parize, A. L. Impact of Drug-Polymer Interaction in Amorphous Solid Dispersion Aiming for the Supersaturation of Poorly Soluble Drug in Biorelevant Medium. *AAPS PharmSciTech* **2020**, *21* (5), 189.

(48) Pandi, P.; Bulusu, R.; Kommineni, N.; Khan, W.; Singh, M. Amorphous solid dispersions: An update for preparation, characterization, mechanism on bioavailability, stability, regulatory considerations and marketed products. *Int J Pharm* **2020**, *586*, 119560.

(49) Iyer, R.; Petrovska Jovanovska, V.; Berginc, K.; Jaklic, M.; Fabiani, F.; Harlacher, C.; Huzjak, T.; Sanchez-Felix, M. V. Amorphous Solid Dispersions (ASDs): The Influence of Material Properties, Manufacturing Processes and Analytical Technologies in Drug Product Development. *Pharmaceutics* **2021**, *13* (10).

(50) Alzahrani, A.; Nyavanandi, D.; Mandati, P.; Youssef, A. A. A.; Narala, S.; Bandari, S.; Repka, M. A systematic and robust assessment of hot-melt extrusion-based amorphous solid dispersions: Theoretical prediction to practical implementation. *Int J Pharm* **2022**, *624*, 121951.

(51) Tambe, S.; Jain, D.; Meruva, S. K.; Rongala, G.; Juluri, A.; Nihalani, G.; Mamidi, H. K.; Nukala, P. K.; Bolla, P. K. Recent Advances in Amorphous Solid Dispersions: Preformulation, Formulation Strategies, Technological Advancements and Characterization. *Pharmaceutics* **2022**, *14* (10).

(52) Bühler, V. *Kollidon*; BASF SE, 2008.

(53) Shendge, R. S.; Tagad, R. R.; Jagtap, P. S. A brief review on Kollidon. *Journal of Drug Delivery and Therapeutics* **2019**, *9* (2), 493-500.

(54) *Kollidon VA64/Kollidon VA64 Fine*; BASF SE - Technical Information, 2022.

(55) Strojewski, D.; Krupa, A. Kollidon(R) VA 64 and Soluplus(R) as modern polymeric carriers for amorphous solid dispersions. *Polim Med* **2022**, *52* (1), 19-29.

(56) Yang, F.; Su, Y.; Small, J.; Huang, C.; Martin, G. E.; Farrington, A. M.; DiNunzio, J.; Brown, C. D. Probing the Molecular-Level Interactions in an Active Pharmaceutical Ingredient (API) - Polymer Dispersion and the Resulting Impact on Drug Product Formulation. *Pharm Res* **2020**, *37* (6), 94.

(57) Thakkar, R.; Thakkar, R.; Pillai, A.; Ashour, E. A.; Repka, M. A. Systematic screening of pharmaceutical polymers for hot melt extrusion processing: a comprehensive review. *Int J Pharm* **2020**, *576*, 118989.

(58) Gupta, S. S.; Meena, A.; Parikh, T.; Serajuddin, A. T. M. Investigation of thermal and viscoelastic properties of polymers relevant to hot melt extrusion - I: Polyvinylpyrrolidone and related polymers. *J. Excipients and Food Chem.* **2014**, *6* (1), 32-45.

(59) Gupta, S. S.; Solanki, N.; Serajuddin, A. T. Investigation of Thermal and Viscoelastic Properties of Polymers Relevant to Hot Melt Extrusion, IV: Affinisol HPMC HME Polymers. *AAPS PharmSciTech* **2016**, *17* (1), 148-157.

(60) Meena, A.; Parikh, T.; Gupta, S. S.; Serajuddin, A. T. M. Investigation of thermal and viscoelastic properties of polymers relevant to hot melt extrusion - II: Cellulosic polymers. *Journal of Excipients and Food Chemistry* **2014**, *5* (1), 10.

(61) Parikh, T.; Gupta, S. S.; Meena, A.; Serajuddin, A. T. M. Investigation of thermal and viscoelastic properties of polymers relevant to hot melt extrusion - III: Polymethacrylates and polymethacrylic acid based polymers. *Journal of Excipients and Food Chemistry* **2014**, *5* (1), 9.

(62) Lipinski, C. A.; Lombardo, F.; Dominy, B. W.; Feeney, P. J. Experimental and computational approaches to estimate solubility and permeability in drug discovery and development settings. *Advanced Drug Delivery Reviews* **1996**, *23* (25).

(63) Thayer, A. M. Finding Solutions. *Chemical & Engineering News Archive* **2010**, *88* (22), 13-18.

(64) Babu, N. J.; Nangia, A. Solubility Advantage of Amorphous Drugs and Pharmaceutical Cocrystals. *Crystal Growth & Design* **2011**, *11* (7), 2662-2679.

(65) Martinez, M. N.; Amidon, G. L. A mechanistic approach to understanding the factors affecting drug absorption: a review of fundamentals. *J Clin Pharmacol* **2002**, *42* (6), 620-643.

(66) Ku, M. S. Use of the Biopharmaceutical Classification System in Early Drug Development. *American Association of Pharmaceutical Scientists* **2008**, *10* (1), 5.

(67) Lipinski, C. A. Drug-like properties and the causes of poor solubility and poor permeability. *Journal of Pharmacological and Toxicological Methods* **2000**, *44*, 15.

(68) U.S. Department of Health and Human Services Food and Drug Administration; Center for Drug Evaluation and Research (CDER); Center for Biologics Evaluation and Research (CBER). *M9 Biopharmaceutics Classification System Based Biowaivers*. U.S. Department of Health and Human Services Food and Drug Administration, 2021. https://www.fda.gov/regulatory-information/search-fda-guidance-documents/m9-biopharmaceutics-classification-system-based-biowaivers (accessed 2024 03.04.).

(69) Dokoumetzidis, A.; Valsami, G.; Macheras, P. Modelling and simulation in drug absorption processes. *Xenobiotica* **2007**, *37* (10-11), 1052-1065.

(70) Shekhawat, B. P.; Pokharkar, V. B. Understanding peroral absorption: regulatory aspects and contemporary approaches to tackling solubility and permeability hurdles. *Acta Pharm Sin B* **2017**, *7* (3), 260-280.

(71) Noyes, A. A.; Whitney, W. R. The rate of Solution of Solid Substances in their own Solutions. **1897**, 5.

(72) Dahan, A.; Miller, J. M.; Amidon, G. L. Prediction of solubility and permeability class membership: provisional BCS classification of the world's top oral drugs. *AAPS J* **2009**, *11* (4), 740-746.

(73) Samineni, R.; Chimakurthy, J.; Konidala, S. Emerging Role of Biopharmaceutical Classification and Biopharmaceutical Drug Disposition System in Dosage form Development: A Systematic Review. *Turk J Pharm Sci* **2022**, *19* (6), 706-713.

(74) Takagi, T.; Ramachandran, C.; Bermejo, M.; Yamashita, S.; Yu, L. X.; Amidon, G. L. A Provisional Biopharmaceutical Classification of the Top 200 Oral Drug Products in the United States, Great Britain, Spain, and Japan. *Molecular pharmaceutics* **2006**, *3* (6), 631-643.

(75) Lüdecker, D.; Briel, T. Improving API Solubility by Salt and Cocrystal Formation. **2023**, (MK_WP12169EN).

(76) Barends, D. M.; Shah, V. P.; Dressman, J.; Potthast, H.; Zheng, N.; Lionberger, R. A.; Mehta, M. U.; Yu, L. X.; Abrahamsson, B.; Welink, J.; et al. *Biowaiver Monographs 2004-2012*; International Pharmaceutical Federation, 2012.

(77) Saal, C.; Nair, A. *Solubility in Pharmaceutical Chemistry*; Walter de Gruyter GmbH, 2020.

(78) Di, L.; Kerns, E. H.; Carter, G. T. Drug-Like Property Concepts in Pharmaceutical Design. *Current Pharmaceutical Design* **2009**, *15* (19), 11.

(79) Hall, A.; Billinton, A.; Bristow, A. K.; Brown, S. H.; Chowdhury, A.; Cutler, L.; Giblin, G. M.; Goldsmith, P.; Hayhow, T. G.; Kilford, I. R.; et al. Discovery of brain penetrant, soluble, pyrazole amide EP1 receptor antagonists. *Bioorg Med Chem Lett* **2008**, *18* (14), 4027-4032.

(80) Stella, V. J.; Borchardt, R. T.; Hageman, M. J.; Oliyai, R.; Maag, H.; Tilley, J. W. *Prodrugs: Challenges and Rewards Part 2*; Springer, 2007.

(81) Qiao, J. X.; King, S. R.; He, K.; Wong, P. C.; Rendina, A. R.; Luettgen, J. M.; Xin, B.; Knabb, R. M.; Wexler, R. R.; Lam, P. Y. Highly efficacious factor Xa inhibitors containing alpha-substituted phenylcycloalkyl P4 moieties. *Bioorg Med Chem Lett* **2009**, *19* (2), 462-468.

(82) Carrico, D.; Ohkanda, J.; Kendrick, H.; Yokoyama, K.; Blaskovich, M. A.; Bucher, C. J.; Buckner, F. S.; Van Voorhis, W. C.; Chakrabarti, D.; Croft, S. L.; et al. In vitro and in vivo antimalarial activity of peptidomimetic protein farnesyltransferase inhibitors with improved membrane permeability. *Bioorg Med Chem* **2004**, *12* (24), 6517-6526.

(83) Hussain, M. A.; Aungst, B. J.; Shefter, E. Prodrugs for Improved Oral beta-Estradiol Bioavailability. *Pharmaceutical Research* **1988**, *5* (1), 4.

(84) Cundy, K. C.; Sastry, S.; Luo, W.; Zou, J.; Moors, T. L.; Canafax, D. M. Clinical pharmacokinetics of XP13512, a novel transported prodrug of gabapentin. *J Clin Pharmacol* **2008**, *48* (12), 1378-1388.

(85) Cox, C. D.; Breslin, M. J.; Whitman, D. B.; Coleman, P. J.; Garbaccio, R. M.; Fraley, M. E.; Zrada, M. M.; Buser, C. A.; Walsh, E. S.; Hamilton, K.; et al. Kinesin spindle protein (KSP) inhibitors. Part V: discovery of 2-propylamino-2,4-diaryl-2,5-dihydropyrroles as potent, water-soluble KSP inhibitors, and modulation of their basicity by beta-fluorination to overcome cellular efflux by P-glycoprotein. *Bioorg Med Chem Lett* **2007**, *17* (10), 2697-2702.

(86) Zhang, S.; Yang, X.; Coburn, R. A.; Morris, M. E. Structure activity relationships and quantitative structure activity relationships for the flavonoid-mediated inhibition of breast cancer resistance protein. *Biochem Pharmacol* **2005**, *70* (4), 627-639.

(87) Flugel, K.; Schmidt, K.; Mareczek, L.; Gabe, M.; Hennig, R.; Thommes, M. Impact of incorporated drugs on material properties of amorphous solid dispersions. *Eur J Pharm Biopharm* **2021**, *159*, 88-98.

(88) Rodriguez-Aller, M.; Guillarme, D.; Veuthey, J.-L.; Gurny, R. Strategies for formulating and delivering poorly water-soluble drugs. *Journal of Drug Delivery Science and Technology* **2015**, *30*, 342-351.

(89) Huang, Y.; Dai, W. G. Fundamental aspects of solid dispersion technology for poorly soluble drugs. *Acta Pharm Sin B* **2014**, *4* (1), 18-25.

(90) Di, L.; Fish, P. V.; Mano, T. Bridging solubility between drug discovery and development. *Drug Discov Today* **2012**, *17* (9-10), 486-495.

(91) Loftsson, T.; Brewster, M. E. Pharmaceutical applications of cyclodextrins: effects on drug permeation through biological membranes. *J Pharm Pharmacol* **2011**, *63* (9), 1119-1135.

(92) Finlay, M. R.; Acton, D. G.; Andrews, D. M.; Barker, A. J.; Dennis, M.; Fisher, E.; Graham, M. A.; Green, C. P.; Heaton, D. W.; Karoutchi, G.; et al. Imidazole piperazines: SAR and development of a potent class of cyclin-dependent kinase inhibitors with a novel binding mode. *Bioorg Med Chem Lett* **2008**, *18* (15), 4442-4446.

(93) Sekiguchi, K.; Obi, N. Studies on Absorption of Eutectic Mixture, I. A Comparison of the Behavior of Eutectic Mixture of Sulfathiazole and that of Ordinary Sulfathiazol in Man. **1967**, *9*.

(94) Simonelli, A. P.; Mehta, S. C.; Higuchi, W. I. Dissolution rates of high energy polyvinylpyrrolidone (PVP)-sulfathiazole coprecipitates. *J Pharm Sci* **1969**, *58* (5), 538-549.

(95) Malkawi, R.; Malkawi, W. I.; Al-Mahmoud, Y.; Tawalbeh, J. Current Trends on Solid Dispersions: Past, Present, and Future. *Adv Pharmacol Pharm Sci* **2022**, *2022*, 5916013.

(96) Williams, H. D.; Trevaskis, N. L.; Charman, S. A.; Shanker, R. M.; Charman, W. N.; Pouton, C. W.; Porter, C. J. Strategies to address low drug solubility in discovery and development. *Pharmacol Rev* **2013**, *65* (1), 315-499.

(97) Saha, S. K.; Joshi, A.; Singh, R.; Dubey, K. Review of industrially recognized polymers and manufacturing processes for amorphous solid dispersion based formulations. *Pharm Dev Technol* **2023**, *28* (7), 678-696.

(98) Alonzo, D. E.; Zhang, G. G.; Zhou, D.; Gao, Y.; Taylor, L. S. Understanding the behavior of amorphous pharmaceutical systems during dissolution. *Pharm Res* **2010**, *27* (4), 608-618.

(99) Boersen, N. n.; Lee, T.; Hui, H. Development of Preclinical Formulations for Toxicology Studies. In *A Comprehensive Guide to Toxicology in Preclinical Drug Development*, 2013; pp 69-86.

(100) Baghel, S.; Cathcart, H.; O'Reilly, N. J. Polymeric Amorphous Solid Dispersions: A Review of Amorphization, Crystallization, Stabilization, Solid-State Characterization, and Aqueous Solubilization of Biopharmaceutical Classification System Class II Drugs. *J Pharm Sci* **2016**, *105* (9), 2527-2544.

(101) Patil, H.; Tiwari, R. V.; Repka, M. A. Hot-Melt Extrusion: from Theory to Application in Pharmaceutical Formulation. *AAPS PharmSciTech* **2016**, *17* (1), 20-42.

(102) Araújo, R. R.; Teixeira, C. C. C.; Freitas, L. A. P. The Preparation of Ternary Solid Dispersions of an Herbal Drug via Spray Drying of Liquid Feed. *Drying Technology* **2010**, *28* (3), 412-421.

(103) Giovagnoli, S.; Palazzo, F.; Di Michele, A.; Schoubben, A.; Blasi, P.; Ricci, M. The influence of feedstock and process variables on the encapsulation of drug suspensions by spray-drying in fast drying regime: the case of novel antitubercular drug-palladium complex containing polymeric microparticles. *J Pharm Sci* **2014**, *103* (4), 1255-1268.

(104) Corrigan, O. I. Thermal analysis of spray dried products. *Thermochimica Acta* **1995**, *248*, 14.

(105) Baird, J. A.; Santiago-Quinonez, D.; Rinaldi, C.; Taylor, L. S. Role of viscosity in influencing the glass-forming ability of organic molecules from the undercooled melt state. *Pharm Res* **2012**, *29* (1), 271-284.

(106) Mahlin, D.; Ponnambalam, S.; Hockerfelt, M. H.; Bergstrom, C. A. Toward in silico prediction of glass-forming ability from molecular structure alone: a screening tool in early drug development. *Mol Pharm* **2011**, *8* (2), 498-506.

(107) Bandari, S.; Nyavanandi, D.; Dumpa, N.; Repka, M. A. Coupling hot melt extrusion and fused deposition modeling: Critical properties for successful performance. *Adv Drug Deliv Rev* **2021**, *172*, 52-63.

(108) Repka, M. A.; Battu, S. K.; Upadhye, S. B.; Thumma, S.; Crowley, M. M.; Zhang, F.; Martin, C.; McGinity, J. W. Pharmaceutical applications of hot-melt extrusion: Part II. *Drug Dev Ind Pharm* **2007**, *33* (10), 1043-1057.

(109) Crommelin, D. J. A. *Formulating Poorly Water Soluble Drugs*; Springer, 2012.

(110) Maniruzzaman, M.; Nokhodchi, A. Continuous manufacturing via hot-melt extrusion and scale up: regulatory matters. *Drug Discov Today* **2017**, *22* (2), 340-351.

(111) Krier, F.; Mantanus, J.; Sacre, P. Y.; Chavez, P. F.; Thiry, J.; Pestieau, A.; Rozet, E.; Ziemons, E.; Hubert, P.; Evrard, B. PAT tools for the control of co-extrusion implants manufacturing process. *Int J Pharm* **2013**, *458* (1), 15-24.

(112) Vercruysse, J.; Peeters, E.; Fonteyne, M.; Cappuyns, P.; Delaet, U.; Van Assche, I.; De Beer, T.; Remon, J. P.; Vervaet, C. Use of a continuous twin screw granulation and drying system during formulation development and process optimization. *Eur J Pharm Biopharm* **2015**, *89*, 239-247.

(113) Muehlenfeld, C.; Duffy, P.; Yang, F.; Zermeño Pérez, D.; El-Saleh, F.; Durig, T. Excipients in Pharmaceutical Additive Manufacturing: A Comprehensive Exploration of Polymeric Material Selection for Enhanced 3D Printing. *Pharmaceutics* **2024**, *16* (3).

(114) Mao, F.; Kong, Q.; Ni, W.; Xu, X.; Ling, D.; Lu, Z.; Li, J. Melting Point Distribution Analysis of Globally Approved and Discontinued Drugs: A Research for Improving the Chance of Success of Drug Design and Discovery. *ChemistryOpen* **2016**, *5* (4), 357-368.

(115) Huang, S.; O'Donnell, K. P.; Delpon de Vaux, S. M.; O'Brien, J.; Stutzman, J.; Williams, R. O., 3rd. Processing thermally labile drugs by hot-melt extrusion: The lesson with gliclazide. *Eur J Pharm Biopharm* **2017**, *119*, 56-67.

(116) Kyerematen, S. O.; Voges, K.; Dohrn, S.; Sobich, E.; Lander, U.; Weber, S.; Gessner, D.; Evans, R. C.; Degenhardt, M. A Hot-Melt Extrusion Risk Assessment Classification System for Amorphous Solid Dispersion Formulation Development. *Pharmaceutics* **2022**, *14* (5).

(117) Butreddy, A.; Bandari, S.; Repka, M. A. Quality-by-design in hot melt extrusion based amorphous solid dispersions: An industrial perspective on product development. *Eur J Pharm Sci* **2021**, *158*, 105655.

(118) Simoes, M. F.; Pinto, R. M. A.; Simoes, S. Hot-melt extrusion in the pharmaceutical industry: toward filing a new drug application. *Drug Discov Today* **2019**, *24* (9), 1749-1768.

(119) Simoes, M. F.; Pinto, R. M. A.; Simoes, S. Hot-Melt Extrusion: a Roadmap for Product Development. *AAPS PharmSciTech* **2021**, *22* (5), 184.

(120) Quodbach, J.; Bogdahn, M.; Breitkreutz, J.; Chamberlain, R.; Eggenreich, K.; Elia, A. G.; Gottschalk, N.; Gunkel-Grabole, G.; Hoffmann, L.; Kapote, D.; et al. Quality of FDM 3D Printed Medicines for Pediatrics: Considerations for Formulation Development, Filament Extrusion, Printing Process and Printer Design. *Ther Innov Regul Sci* **2022**, *56* (6), 910-928.

(121) Kolter, K.; Karl, M.; Grycke, A. *Hot-Melt Extrusion with BASF Pharma Polymers - Extrusion Compendium*; BASF SE, 2012.

(122) Cailleaux, S.; Sanchez-Ballester, N. M.; Gueche, Y. A.; Bataille, B.; Soulairol, I. Fused Deposition Modeling (FDM), the new asset for the production of tailored medicines. *J Control Release* **2021**, *330*, 821-841.

(123) Agrawal, A. M.; Dudhedia, M. S.; Zimny, E. Hot Melt Extrusion: Development of an Amorphous Solid Dispersion for an Insoluble Drug from Mini-scale to Clinical Scale. *AAPS PharmSciTech* **2016**, *17* (1), 133-147.

(124) Hallensleben, M. L.; Fuss, R.; Mummy, F. Polyvinyl Compounds, Others.

(125) Repka, M. A.; Bandari, S.; Kallakunta, V. R.; Vo, A. Q.; McFall, H.; Pimparade, M. B.; Bhagurkar, A. M. Melt extrusion with poorly soluble drugs - An integrated review. *Int J Pharm* **2018**, *535* (1-2), 68-85.

(126) Censi, R.; Gigliobianco, M. R.; Casadidio, C.; Di Martino, P. Hot Melt Extrusion: Highlighting Physicochemical Factors to Be Investigated While Designing and Optimizing a Hot Melt Extrusion Process. *Pharmaceutics* **2018**, *10* (3).

(127) LaFountaine, J. S.; McGinity, J. W.; Williams, R. O., 3rd. Challenges and Strategies in Thermal Processing of Amorphous Solid Dispersions: A Review. *AAPS PharmSciTech* **2016**, *17* (1), 43-55.

(128) Bharti, K.; Dubey, G.; Kumar, M.; Jha, A.; Manjit; Upadhyay, M.; Mali, P. S.; Kumar, A.; Bharatam, P. V.; Mishra, B. A multifaceted approach for grading of polymers for the development of stable amorphous solid dispersion of Riluzole. *Journal of Drug Delivery Science and Technology* **2023**, *90*.

(129) Holland, B. J.; Hay, J. N. The thermal degradation of poly(vinyl acetate) measured by thermal analysis-Fourier transform infrared spectroscopy. *Polymer* **2002**, *43*, 5.

(130) Czech, Z.; Agnieszka, K.; Ragańska, P.; Antosik, A. Thermal stability and degradation of selected poly(alkyl methacrylates) used in the polymer industry. *Journal of Thermal Analysis and Calorimetry* **2014**, *119* (2), 1157-1161.

(131) Auch, C.; Harms, M.; Mader, K. Melt-based screening method with improved predictability regarding polymer selection for amorphous solid dispersions. *Eur J Pharm Sci* **2018**, *124*, 339-348.

(132) Maddineni, S.; Battu, S. K.; Morott, J.; Majumdar, S.; Murthy, S. N.; Repka, M. A. Influence of process and formulation parameters on dissolution and stability characteristics of Kollidon(R) VA 64 hot-melt extrudates. *AAPS PharmSciTech* **2015**, *16* (2), 444-454.

(133) Communities, E. Summary of Community decisions on marketing authorizations in respect of medicinal products from 15 August 1996 to 15 September 1996. Official Journal of the European Communities: 1996; Vol. 39.

(134) United States Pharmacopeia, N. M. USP-NF Copovidone. 2022; p 7.

(135) Bühler, V. *Polyvinylpyrrolidone Excipients for Pharmaceuticals*; Springer, 2005.

(136) Parikh, T.; Gupta, S. S.; Meena, A. K.; Vitez, I.; Mahajan, N.; Serajuddin, A. T. Application of film-casting technique to investigate drug-polymer miscibility in solid dispersion and hot-melt extrudate. *J Pharm Sci* **2015**, *104* (7), 2142-2152.

(137) Nair, A. R.; Lakshman, Y. D.; Anand, V. S. K.; Sree, K. S. N.; Bhat, K.; Dengale, S. J. Overview of Extensively Employed Polymeric Carriers in Solid Dispersion Technology. *AAPS PharmSciTech* **2020**, *21* (8), 309.

(138) Piccinni, P.; Tian, Y.; McNaughton, A.; Fraser, J.; Brown, S.; Jones, D. S.; Li, S.; Andrews, G. P. Solubility parameter-based screening methods for early-stage formulation development of itraconazole amorphous solid dispersions. *J Pharm Pharmacol* **2016**, *68* (5), 705-720.

(139) Koltzenburg, S.; Maskos, M.; Nuyken, O. *Polymere: Synthese, Eigenschaften und Anwendungen*; Springer Spektrum Berlin, Heidelberg, 2024.

(140) Matyjaszewski, K.; Tsarevsky, N. V. Nanostructured functional materials prepared by atom transfer radical polymerization. *Nat Chem* **2009**, *1* (4), 276-288.

(141) Pujari, N. S.; Wang, M.; Gonsalves, K. E. Co and terpolymer reactivity ratios of chemically amplified resists. *Polymer* **2017**, *118*, 201-214.

(142) Braun, D.; Hu, F. Free radical quaterpolymerization of acceptor- and donor-monomers. *Polymer Bulletin* **2003**, (49), 8.

(143) Braun, D.; Hu, F. Polymers from non-homopolymerizable monomers by free radical processes. *Progress in Polymer Science* **2006**, *31* (3), 239-276.

(144) Hadjichristidis, N.; Hirao, A. *Anionic Polymerization - Principles, Practice, Strength, Consequences and Applications*; Springer, 2015.

(145) Staab, H. A. New Methods of Preparative Organic Chmistry IV. Syntheses Using Heterocyclic Amides (Azolides). *Angew. Chem. internat. Edit.* **1962**, *1* (7), 17.

(146) Wittmar, M. Charge modified, comb-like graft-polyesters for drug delivery and DNA vaccination: Synthesis and Characterization of Poly(vinyl dialkylaminoalkylcarbamate-co-vinyl acetate-co-vinyl alcohol)-graft-poly(D,L-lactide-co-glycolide)s. Ph.D. Thesis, Philipps-Universität Marburg, 2004.

(147) Alves, M. H.; Young, C. J.; Bozzetto, K.; Poole-Warren, L. A.; Martens, P. J. Degradable, click poly(vinyl alcohol) hydrogels: characterization of degradation and cellular compatibility. *Biomedical materials (Bristol, England)* **2012**, *7* (2), 024106. From NLM.

(148) Ossipov, D. A.; Hilborn, J. Versatile Funtionalization of Poly(vinyl alcohol) for Grafting of Biofuntional Building Blocks. *Polym. Prepr. (Am. Chem. Soc., Div. Polym. Chem.)* **2007**, *48* (2), 182-183.

(149) Yang, Q.; Sheng, M.; Henkelis, J. J.; Tu, S.; Wiensch, E.; Zhang, H.; Zhang, Y.; Tucker, C.; Ejeh, D. E. Explosion Hazards of Sodium Hydride in Dimethyl Sulfoxide, N,N-

Dimethylformamide, and N,N-Dimethylacetamide. *Organic Process Research & Development* **2019**, *23* (10), 2210-2217.

(150) Markley, T. J. Grafting reactions of vinyl acetate onto poly[(vinyl alcohol)-co- (vinyl acetate)]. Master Thesis. Lehigh University, 1994.

(151) Wheeler, O. L.; Lavin, E.; Crozier, R. N. Branching mechanisms in the polymerization of vinyl acetate. *J. Polym. Sci.* **1952**, *9* (2), 12.

(152) Liu, Y.; Liu, X.; Liu, Y.; Zhang, J.; Deng, K.; Liu, Z. Graft copolymerization of methyl acrylate onto poly(vinyl alcohol) initiated by potassium diperiodatoargentate(III). *Polym. Int.* **2004**, *53* (11), 1611-1616.

(153) Committee for Medicinal Products for Human Use. *ICH Q3C (R9) Residual solvents - Scientific guideline*. International Council for Harmonisation of Technical Requirements for Registration of Pharmaceuticals for Human Use, 2024. https://www.ema.europa.eu/en/ich-q3c-r9-residual-solvents-scientific-guideline (accessed 2024 15.07.).

(154) Nikghalb, L. A.; Singh, G.; Singh, G.; Kahkeshan, K. F. Solid Dispersion: Methods and Polymers to increase the solubility of poorly soluble drugs. *Journal of Applied Pharmaceutical Science* **2012**, *2* (10), 6.

(155) Chen, Y.; Liu, C.; Chen, Z.; Su, C.; Hageman, M.; Hussain, M.; Haskell, R.; Stefanski, K.; Qian, F. Drug-polymer-water interaction and its implication for the dissolution performance of amorphous solid dispersions. *Mol Pharm* **2015**, *12* (2), 576-589.

(156) Fu, Q.; Fang, M.; Hou, Y.; Yang, W.; Shao, J.; Guo, M.; Li, M.; Li, J.; Wang, Y.; He, Z.; et al. A physically stabilized amorphous solid dispersion of nisoldipine obtained by hot melt extrusion. *Powder Technology* **2016**, *301*, 342-348.

(157) Knopp, M. M.; Nguyen, J. H.; Mu, H.; Langguth, P.; Rades, T.; Holm, R. Influence of Copolymer Composition on In Vitro and In Vivo Performance of Celecoxib-PVP/VA Amorphous Solid Dispersions. *AAPS J* **2016**, *18* (2), 416-423.

(158) Lehmkemper, K.; Kyerematen, S. O.; Heinzerling, O.; Degenhardt, M.; Sadowski, G. Impact of Polymer Type and Relative Humidity on the Long-Term Physical Stability of Amorphous Solid Dispersions. *Mol Pharm* **2017**, *14* (12), 4374-4386.

(159) Hussain, M. A.; Liebert, T.; Heinze, T. Acylation of Cellulose with N,N′-Carbonyldiimidazole-Activated Acids in the Novel Solvent Dimethyl Sulfoxide/Tetrabutylammonium Fluoride. *Macromolecular Rapid Communications* **2004**, *25* (9), 916-920.

(160) Kipping, T.; Di Gallo, N.; Elia, A. G.; Knuettel, A.; Bauer, F. Novel Screening Tools for Hot Melt Extrusion – Early Prediction of Formulation Performance. *Merck KGaA, Germany* **2019**.

(161) Nonappa; Kolehmainen, E. Caffeine as a Gelator. *Gels* **2016**, *2* (1).

(162) Dobrinas, S.; Soceanu, A.; Popescu, V.; Stanciu, G.; Smalberger, S. Optimization of a UV-VIS spectrometric Method for Caffeine Analysis in Tea, Coffee and other Beverages. *Scientific Study & Research, Chemistry & Chemical Engineering, Biotechnology, Food Industry* **2013**, *14*.

(163) Ahmad Bhawani, S.; Fong, S. S.; Mohamad Ibrahim, M. N. Spectrophotometric Analysis of Caffeine. *Int J Anal Chem* **2015**, *2015*, 170239.

(164) Hesse, M.; Meier, H.; Zeeh, B. *Spektroskopische Methoden in der organischen chemie*; Georg Thieme Verlag, 2012.

(165) Sodeifian, G.; Sajadian, S. A.; Razmimanesh, F.; Hazaveie, S. M. Solubility of Ketoconazole (antifungal drug) in SC-CO(2) for binary and ternary systems: measurements and empirical correlations. *Sci Rep* **2021**, *11* (1), 7546.

(166) Taghizadeh, M. T.; Foroutan, M. Water-soluble Copolymers of N-vinylpyrrolidone and Vinyl Acetate: Synthesis, Characterization, and Monomer Reactivity at High Conversions. *Journal of Polymer Research* **2004**, *11*, 203–209.

(167) Zhong, Y.; Parikh, H.; Smith, T. E. Process for Providing Homogenenous Copolymers of Vinylpyrrolidone and Vinyl Acetate which Form Clear Aqueous Solutions Having a High Cloud Point. USA US5395904, 1995.

(168) Scott, A.; Penlidis, A. Computational Package for Copolymerization Reactivity Ratio Estimation: Improved Access to the Error-in-Variables-Model. *Processes* **2018**, *6* (1).

(169) Young, L. J. Copolymerization parameters. *Journal of Polymer Science* **2003**, *54* (160), 411-455.

(170) Yu, X.; Wang, X.; Chen, J. Support Vector Machine Regression for Reactivity Parameters of Vinyl Monomers. *J. Chil. Chem. Soc.* **2011**, *56* (3).

(171) Dube, M.; Sanayei, R. A.; Penlidis, A.; O'Driscoll, K. F.; Reilly, P. M. A microcomputer program for estimation of copolymerization reactivity ratios. *Journal of Polymer Science Part A: Polymer Chemistry* **2003**, *29* (5), 703-708.

(172) Ham, G. E. Calculation of copolymerization reactivity parameters from product probabilities. *Journal of Polymer Science Part A: General Papers* **2003**, *2* (9), 4181-4189.

(173) Garrett, T. A.; Park, G. S. Reactivity ratios for the copolymerization of vinyl acetate with methyl acrylate. *Journal of Polymer Science Part A-1: Polymer Chemistry* **2003**, *4* (10), 2714-2717.

(174) Haaf, F.; Sanner, A.; Straub, F. Polymers of N-Vinylpyrrolidone: Synthesis, Characterization and Uses. *Polymr Journal* **1985**, *17* (1), 10.

(175) Kokkorogianni, O.; Kontoes-Georgoudakis, P.; Athanasopoulou, M.; Polizos, N.; Pitsikalis, M. Statistical Copolymers of N-Vinylpyrrolidone and Isobornyl Methacrylate via Free Radical and RAFT Polymerization: Monomer Reactivity Ratios, Thermal Properties, and Kinetics of Thermal Decomposition. *Polymers (Basel)* **2021**, *13* (5).

(176) Kawauchi, S.; Akatsuka, A.; Hayashi, Y.; Furuya, H.; Takata, T. Determining the Q-e values of polymer radicals and monomers separately through the derivation of an intrinsic Q-e scheme for radical copolymerization. *Polymer Chemistry* **2022**, *13* (8), 16.

(177) Kelen, T.; Tüdos, F. Analysis of the Linear Methods for Determining Copolymerization Reactivity Ratios. I. A New Improved Linear Graphic Method. *Journal of Macromolecular Science: Part A - Chemistry* **1975**, *9* (1), 1-27.

(178) Tüdös, F.; Kelen, T.; Földes-Berezhnykh, T.; Turcsányi, B. Evaluation of High Conversion Copolymerization Data by a linear Graphical Method. *Reaction Kinetics and Catalysis Letters* **1975**, *2* (4), 9.

(179) Mayo, F. R.; Lewis, F. M. Copolymerization. I. A Basis for Comparing the Behavior of Monomers in Copolymerization; The Copolymerization of Styrene and Methyl Methacrylate. **1944**, *66*.

(180) Alfrey Jr., T.; Price, C. C. Relative reactivities in vinyl copolymerization. **1947**, *2* (1), 101-106.

(181) Fineman, M.; Ross, S. D. Linear method for determining monomer reactivity ratios in copolymerization. **1950**, *5* (2), 259-262.

(182) Mao, R.; Huglin, M. B. A new linear method to calculate monomer reactivity ratios by using high conversion copolymerization data: terminal model. *Polymer* **1993**, *34* (8), 1709-1715.

(183) Colombani, D. Chain-Growth Control in Free Radical Polymerization. *Prog. Polym. Sci.,* **1997**, *22*, 72.

(184) Zhang, P.; Sun, F.; Liu, S.; Jiang, S. Anti-PEG antibodies in the clinic: Current issues and beyond PEGylation. *J Control Release* **2016**, *244* (Pt B), 184-193.

(185) Kozma, G. T.; Shimizu, T.; Ishida, T.; Szebeni, J. Anti-PEG antibodies: Properties, formation, testing and role in adverse immune reactions to PEGylated nano-biopharmaceuticals. *Adv Drug Deliv Rev* **2020**, *154-155*, 163-175.

(186) Knop, K.; Hoogenboom, R.; Fischer, D.; Schubert, U. S. Poly(ethylene glycol) in drug delivery: pros and cons as well as potential alternatives. *Angew Chem Int Ed Engl* **2010**, *49* (36), 6288-6308.

(187) Kozma, G. T.; Meszaros, T.; Vashegyi, I.; Fulop, T.; Orfi, E.; Dezsi, L.; Rosivall, L.; Bavli, Y.; Urbanics, R.; Mollnes, T. E.; et al. Pseudo-anaphylaxis to Polyethylene Glycol (PEG)-Coated Liposomes: Roles of Anti-PEG IgM and Complement Activation in a Porcine Model of Human Infusion Reactions. *ACS Nano* **2019**, *13* (8), 9315-9324.

(188) Mohamed, M.; Abu Lila, A. S.; Shimizu, T.; Alaaeldin, E.; Hussein, A.; Sarhan, H. A.; Szebeni, J.; Ishida, T. PEGylated liposomes: immunological responses. *Sci Technol Adv Mater* **2019**, *20* (1), 710-724.

(189) Castells, M. C.; Phillips, E. J. Maintaining Safety with SARS-CoV-2 Vaccines. *N Engl J Med* **2021**, *384* (7), 643-649.

(190) Randriantsilefisoa, R.; Cuellar-Camacho, J. L.; Chowdhury, M. S.; Dey, P.; Schedler, U.; Haag, R. Highly sensitive detection of antibodies in a soft bioactive three-dimensional bioorthogonal hydrogel. *Journal of Materials Chemistry B* **2019**, *7* (20), 3220-3231.

(191) Yang, Q.; Jacobs, T. M.; McCallen, J. D.; Moore, D. T.; Huckaby, J. T.; Edelstein, J. N.; Lai, S. K. Analysis of Pre-existing IgG and IgM Antibodies against Polyethylene Glycol (PEG) in the General Population. *Anal Chem* **2016**, *88* (23), 11804-11812.

(192) Elsadek, N. E.; Abu Lila, A. S.; Ishida, T. Immunological responses to PEGylated proteins. In *Polymer-Protein Conjugates*, 2020; pp 103-123.

(193) Verhoef, J. J.; Carpenter, J. F.; Anchordoquy, T. J.; Schellekens, H. Potential induction of anti-PEG antibodies and complement activation toward PEGylated therapeutics. *Drug Discov Today* **2014**, *19* (12), 1945-1952.

(194) Fedors, R. F. A method for estimating both the solubility parameters and molar volumes of liquids. *Polymer Engineering & Science* **2004**, *14* (2), 147-154.

(195) Carroll, R.; Jaiswal, S.; Berman, A.; Spencer, J.; Anderson, K.; Moroney, J.; Behbahani, A.; White, J.; Beisenbayev, D. *How pharma can benefit from using GenAI in drug discovery*. 2024. https://www.ey.com/en_us/insights/life-sciences/how-pharma-can-benefit-from-using-genai-in-drug-discovery (accessed 03.07.2024).

(196) Hess, F.; Kipping, T.; Weitschies, W.; Krause, J. Understanding the Interaction of Thermal, Rheological, and Mechanical Parameters Critical for the Processability of Polyvinyl Alcohol-Based Systems during Hot Melt Extrusion. *Pharmaceutics* **2024**, *16* (4).

12 Appendix

12.1 Section 5: Structure-property relationship in modified PVA-co-PVP's

12.1.1 Additional analytical data base polymer

12.1.1.1 NMR

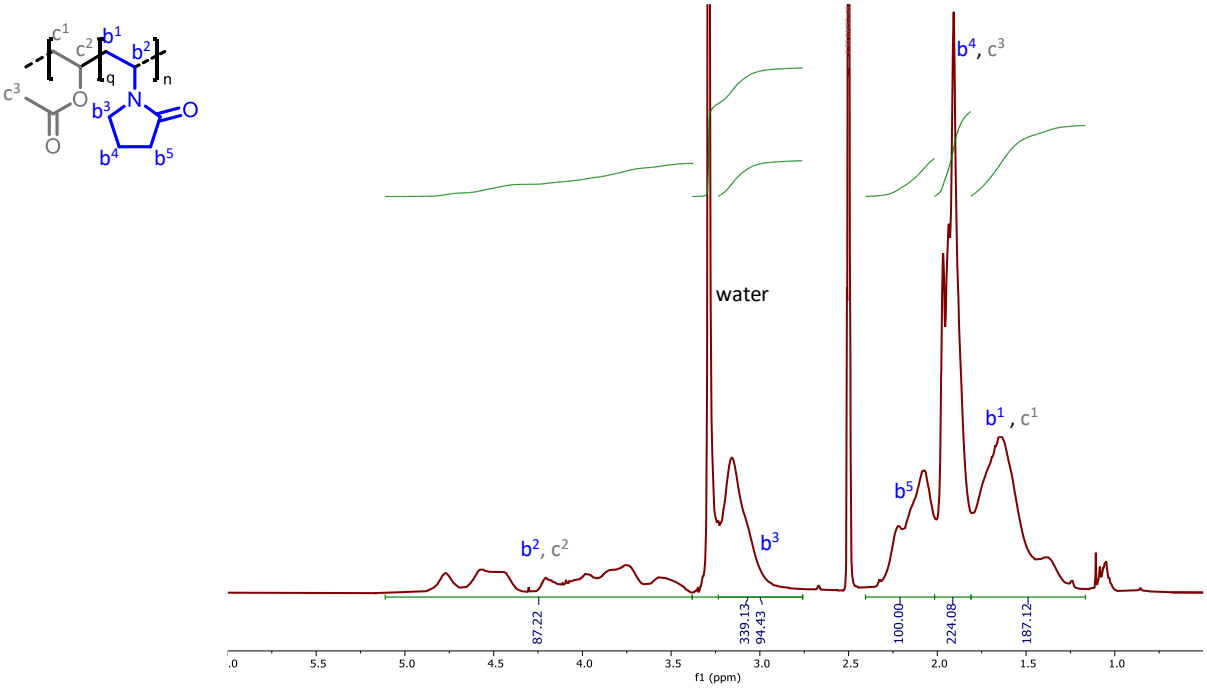

Appendix, Figure 1: Quantitative ^{1}H-NMR spectrum of commercially acquired, pure PVP-co-PVAc (Kollidon® VA64) normalized to methylene moiety b^5. Calculation based on VAc methyl moiety c^3 and VP methylene moiety b^5.

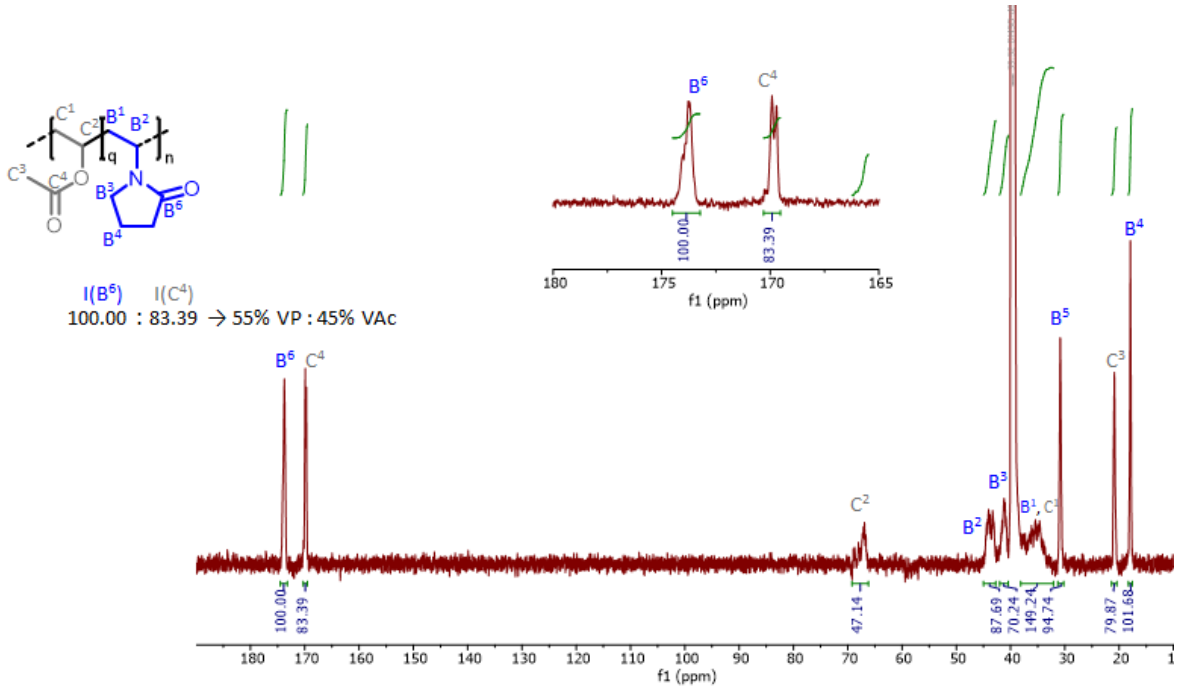

Appendix, Figure 2: Quantitative ^{13}C-NMR spectrum of commercially obtained batch of PVP-co-PVAc (Kollidon® VA64, Batch 1) at a concentration of 200 mg mL^{-1}. 512 scans with addition of Cr(acac)$_3$ as relaxation agent to reduce T_2 relaxation and increase resolution at a relaxation delay of 15 s. Calculations based on carbonyl groups in VP (B^6) and VAc (C^4).

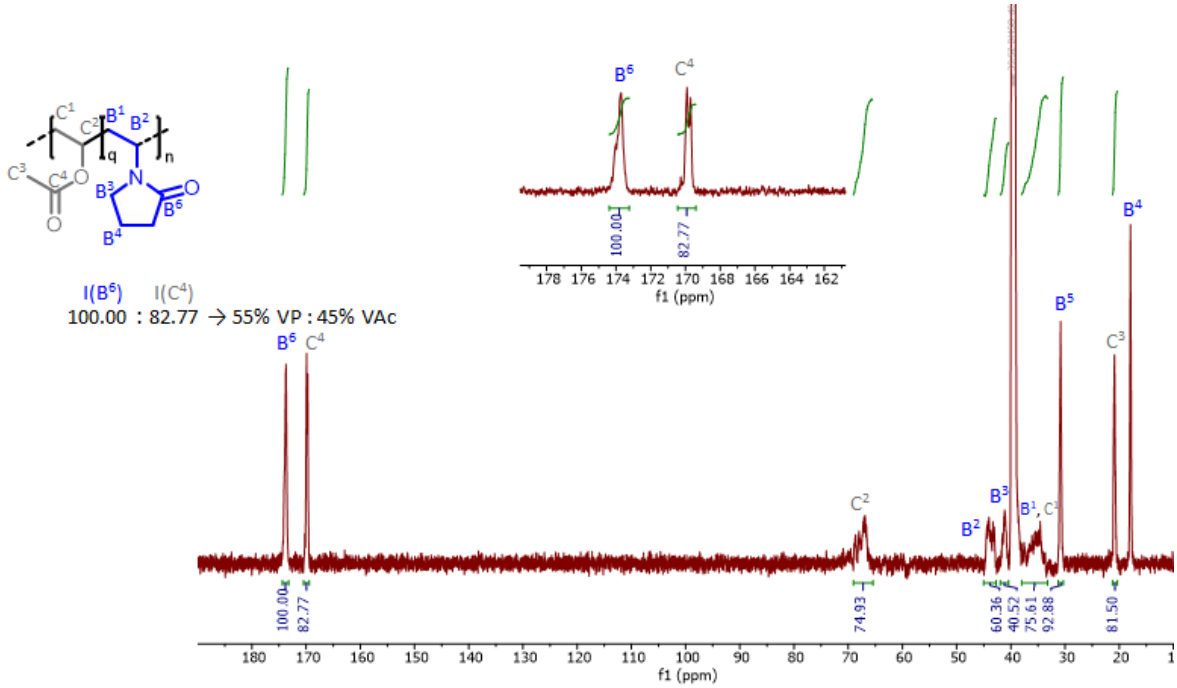

Appendix, Figure 3: Quantitative ^{13}C-NMR spectrum of commercially obtained batch of PVP-co-PVAc (Kollidon® VA64, Batch 2) at a concentration of 200 mg mL^{-1}. 512 scans with addition of Cr(acac)$_3$ as relaxation agent to reduce T_2 relaxation and increase resolution at a relaxation delay of 15 s. Calculations based on carbonyl groups in VP (B^6) and VAc (C^4).

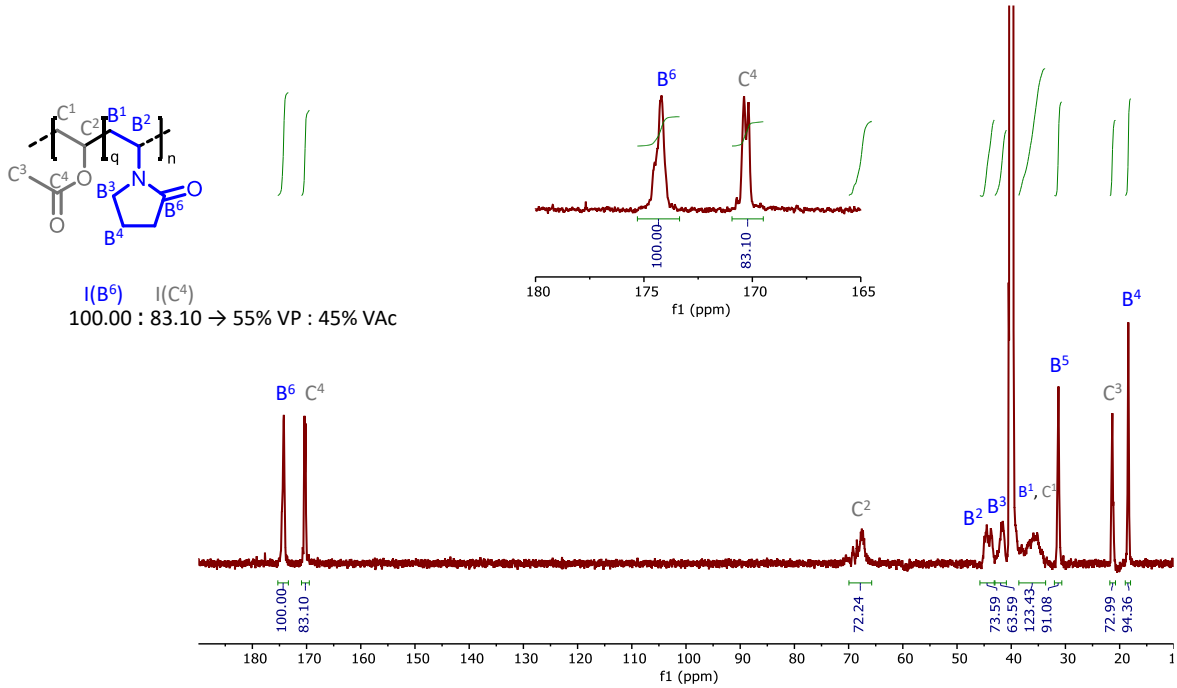

Appendix, Figure 4: Quantitative ^{13}C-NMR spectrum of commercially obtained batch of PVP-co-PVAc (Kollidon® VA64, Batch 3) at a concentration of 200 mg mL^{-1}. 512 scans with addition of Cr(acac)$_3$ as relaxation agent to reduce T_2 relaxation and increase resolution at a relaxation delay of 15 s. Calculations based on carbonyl groups in VP (B^6) and VAc (C^4).

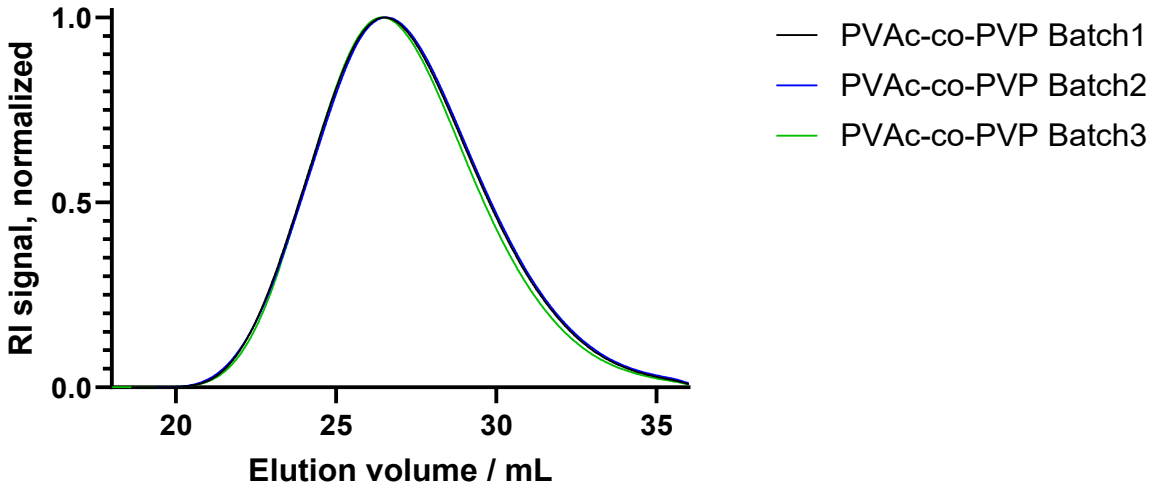

Appendix, Figure 5: Comparison of GPC elugrams of all batches of PVP-co-PVAc used in this thesis. $M_{w,Batch1}$ = 33000 g mol^{-1}, $M_{p,Batch1}$ = 27000 g mol^{-1}, $Đ_{Batch1}$ = 3.8 ; $M_{w,Batch2}$ = 33000 g mol^{-1}, $M_{p,Batch2}$ = 26000 g mol^{-1}, $Đ_{Batch2}$ = 3.9 ; $M_{w,Batch3}$ = 33000 g mol^{-1}, $M_{p,Batch3}$ = 26000 g mol^{-1}, $Đ_{Batch3}$ = 3.6.

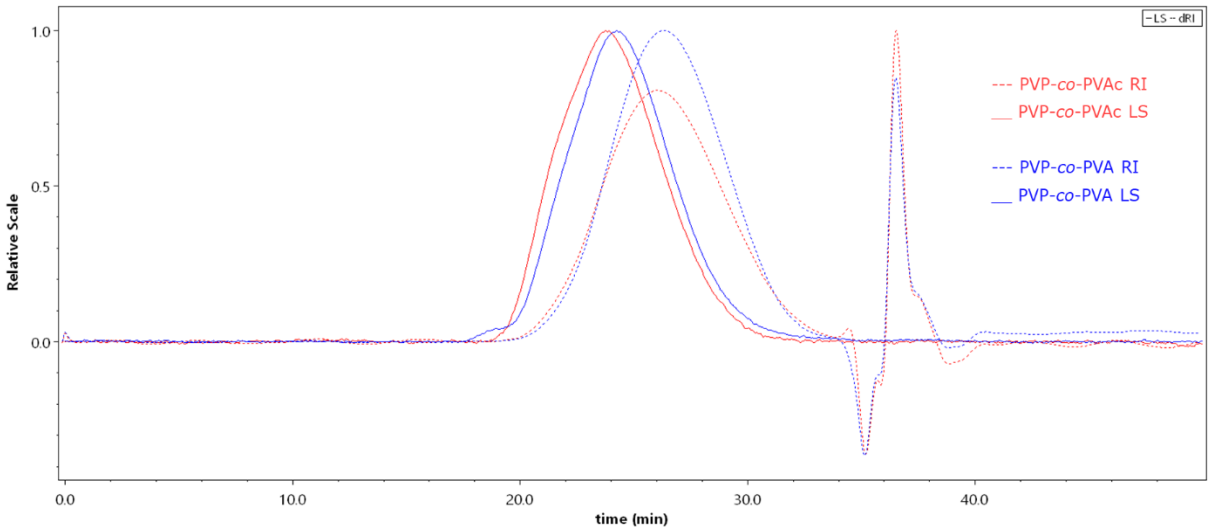

Appendix, Figure 6: MALS Chromatogram of PVP-co-PVAc (red) and PVP-co-PVA (blue). M_w (PVP-co-PVAc) = 36000 g mol^{-1}, Đ = 2.5; M_w (PVP-co-PVA) = 30000 g mol^{-1}, Đ = 1.9.

12.1.2 Additional analytical data mPEG modifications

12.1.2.1 NMR

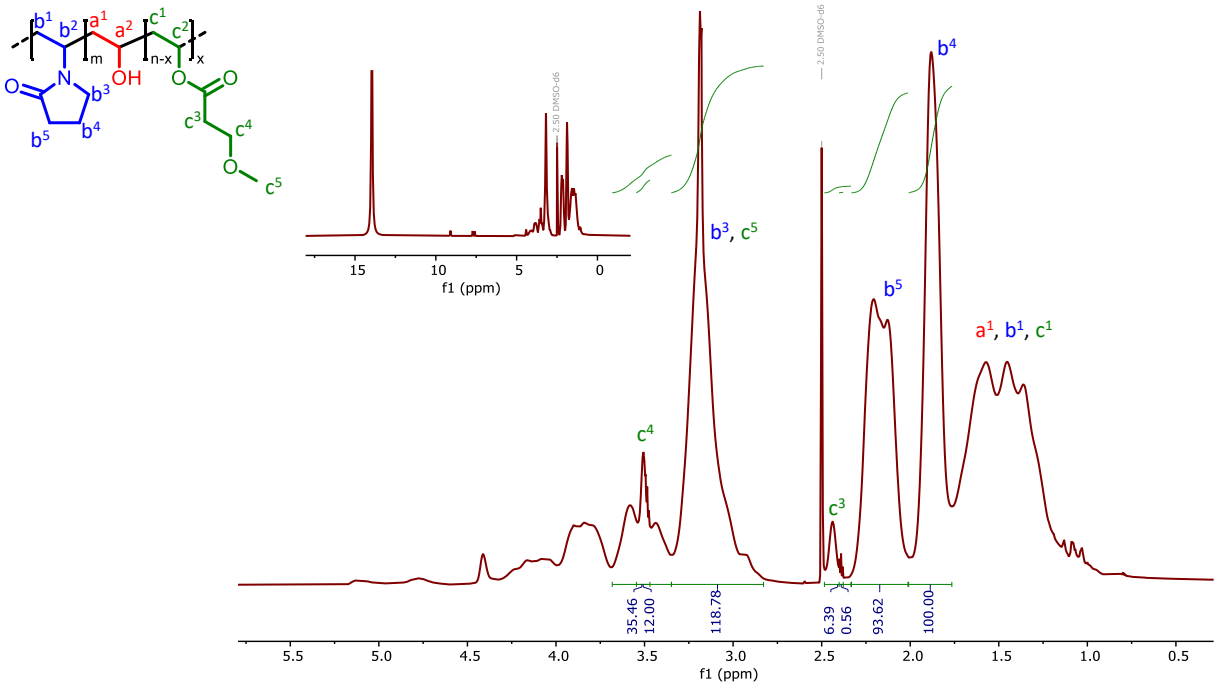

Appendix, Figure 7: Quantitative ^{1}H-NMR spectrum of mPEG-I modified PVP-co-PVA. Modification degree 5.4%.

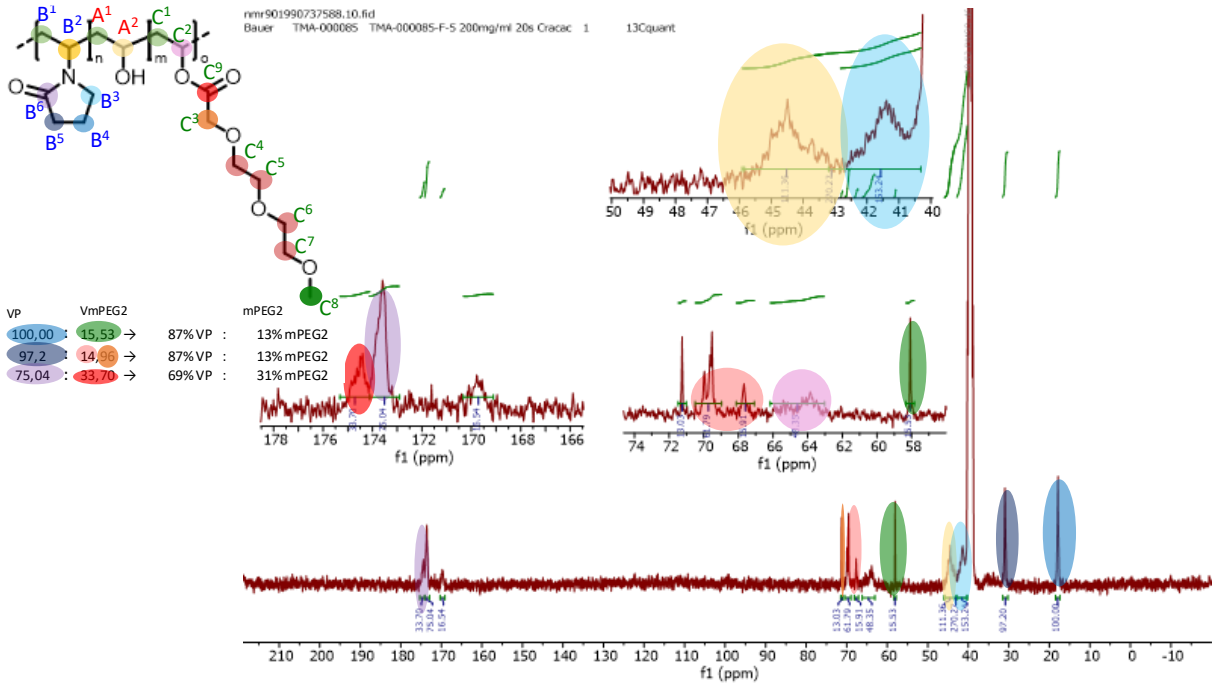

Figure 93: Quantitative ^{13}C NMR of mPEG II modified PVP-co-PVA. Modification degree 13%.

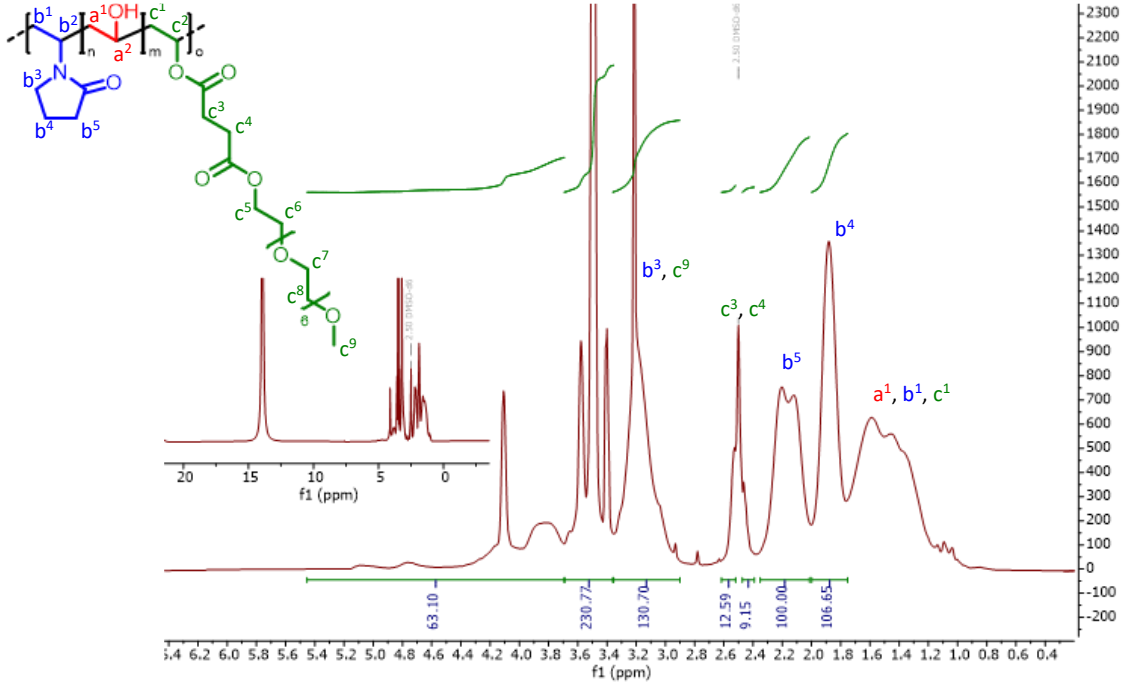

Appendix, Figure 8: Quantitative ^{1}H-NMR spectrum of mPEG-III modified PVP-co-PVA. Modification degree 10.6%.

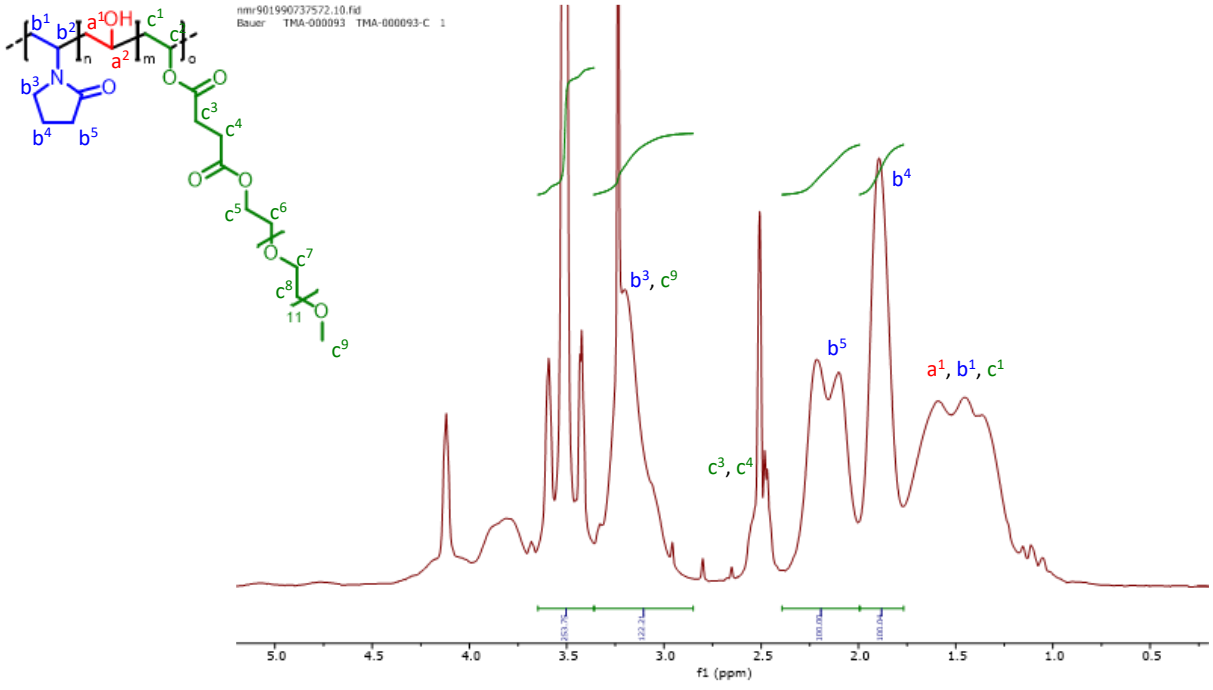

Appendix, Figure 9: Quantitative ^{1}H-NMR spectrum of mPEG-IV modified PVP-co-PVA. Modification degree 8.9%.

12.1.2.2 DSC

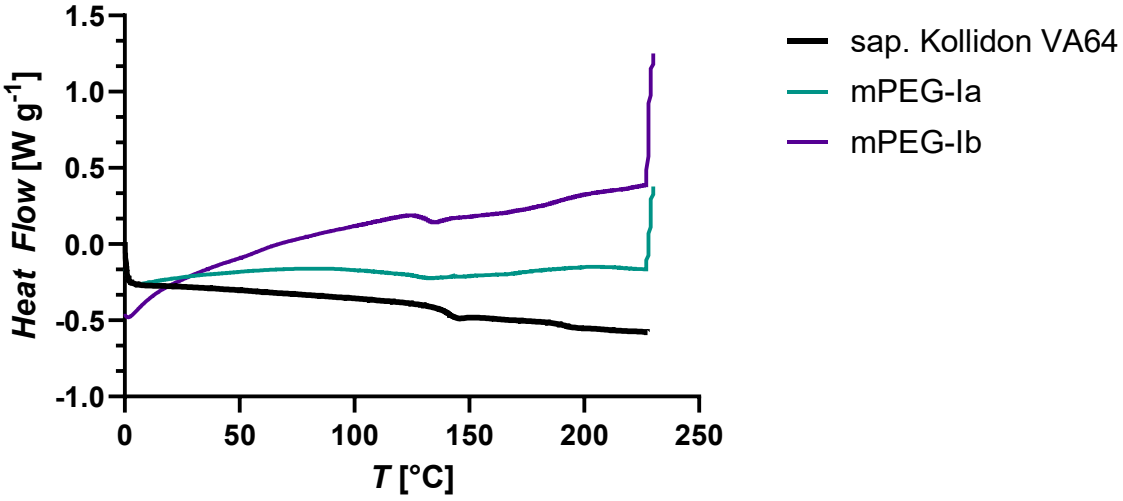

Appendix, Figure 10: DSC thermograms of all modifications using **mPEG I**; T_g (a) = 130 °C; T_g (b) = 129 °C.

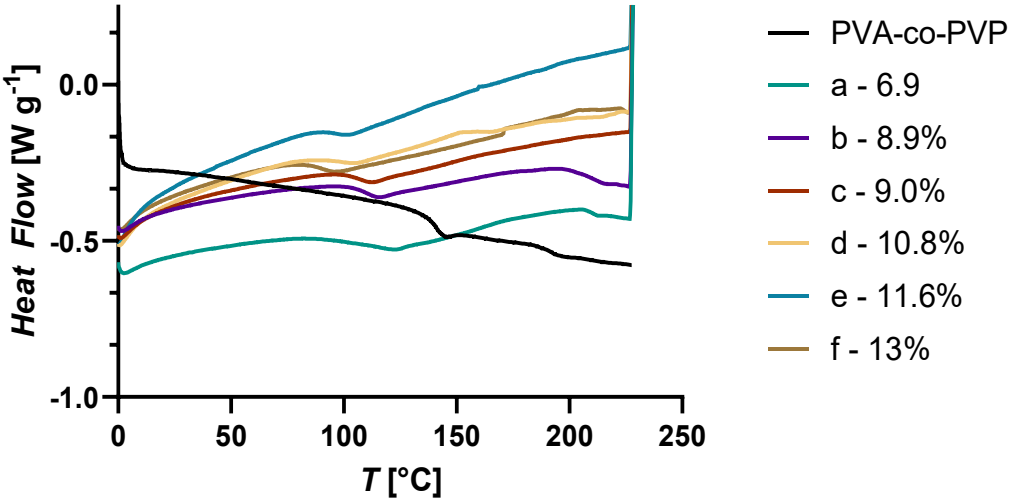

Appendix, Figure 11: DSC thermograms of all modifications using **mPEG-IIa** to **-f**; T_g(a) = 120 °C ; T_g(b) = 112 °C ; T_g(c) = 107 °C ; T_g(d) = 111 °C ; T_g(e) = 97 °C ; T_g(f)= 90 °C.

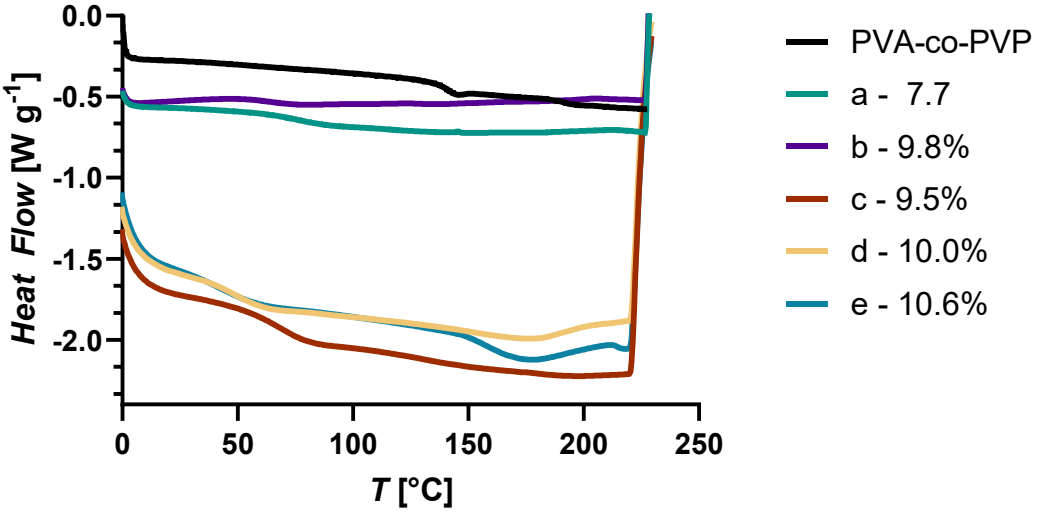

Appendix, Figure 12:DSC thermograms of all modifications using **mPEG-IIIa** to **-e** T_g(a) = 79 °C ; T_g(b) = 67 °C ; T_g(c) = 74 °C ; T_g(d) = 54 °C ; T_g(e) = 58 °C.

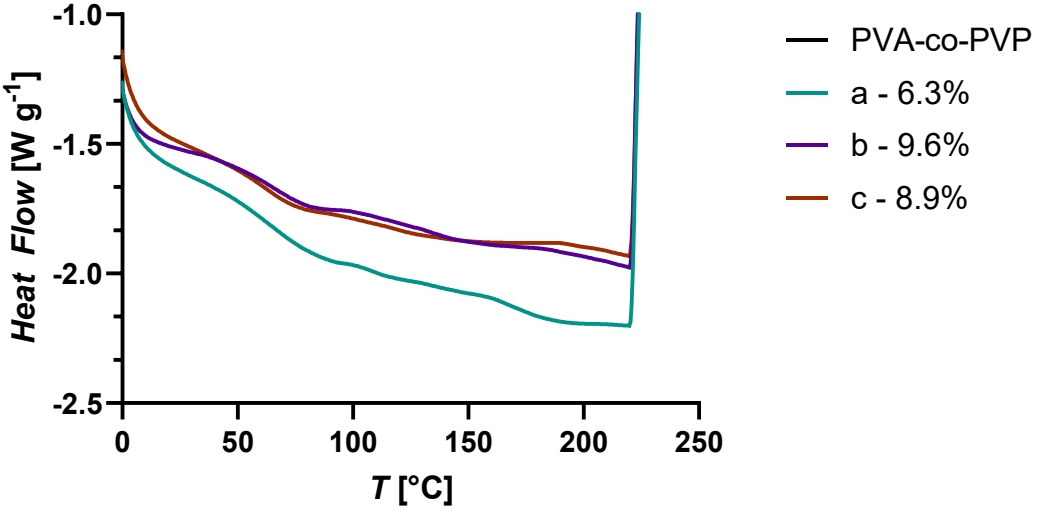

Appendix, Figure 13 DSC thermograms of all modifications using **mPEG-Ia** to –**c**; T_g(a) = 70 °C ; T_g(b) = 64 °C ; T_g(c) = 60 °C.

12.1.2.3 TGA

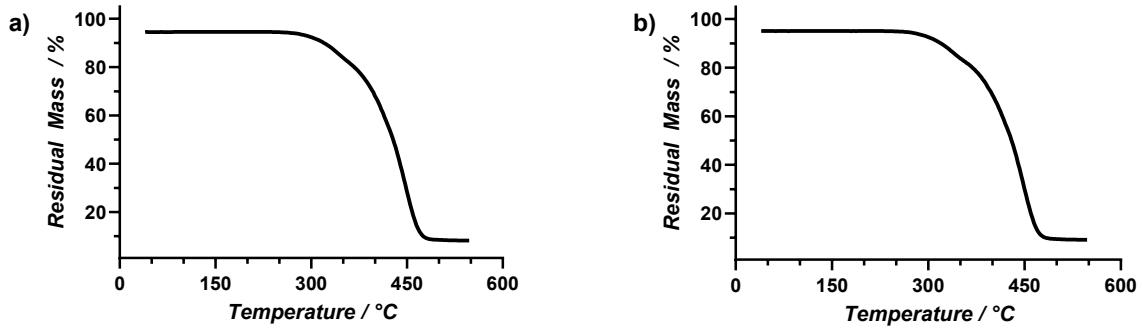

Appendix, Figure 14: a) TGA thermogram of **mPEG-Ia**. Degradation starts at 233 °C; a) TGA thermogram of **mPEG-Ib**. Degradation starts at 236 °C

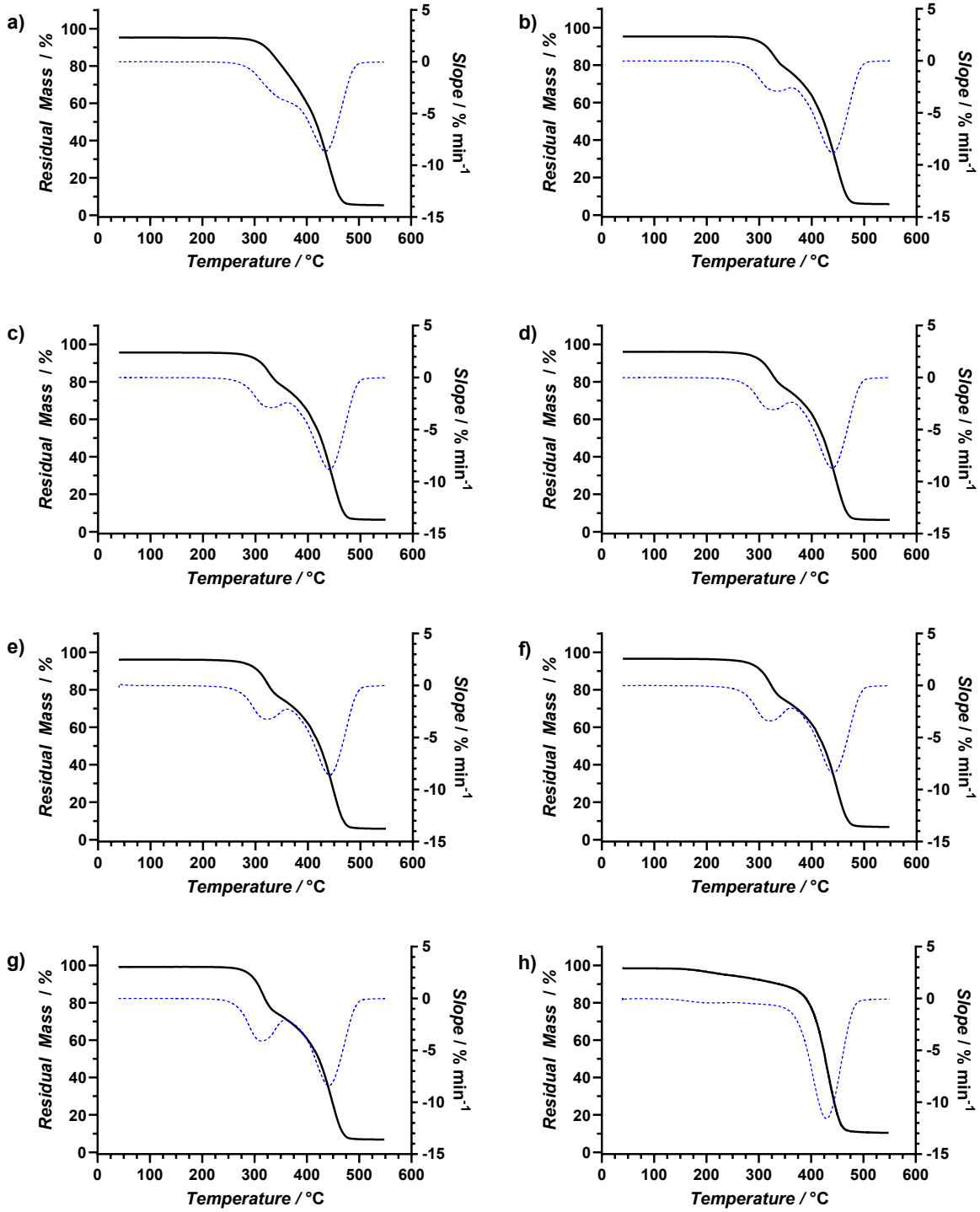

Appendix, Figure 15 TGA **mPEG-II a-h**. Degradation temperatures can be found at the end of the respective chapter.

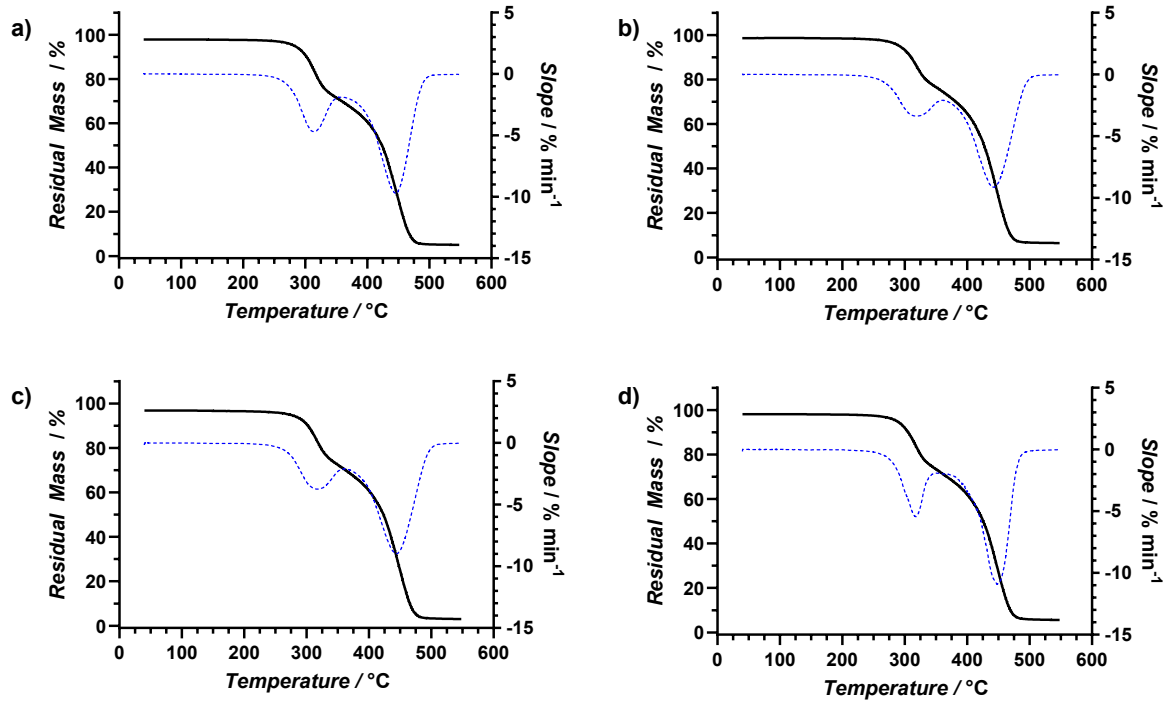

Appendix, Figure 16: TGA results of **mPEG-II** modified polymers at large scale. Degradation temperatures can be found at the end of the respective chapter.

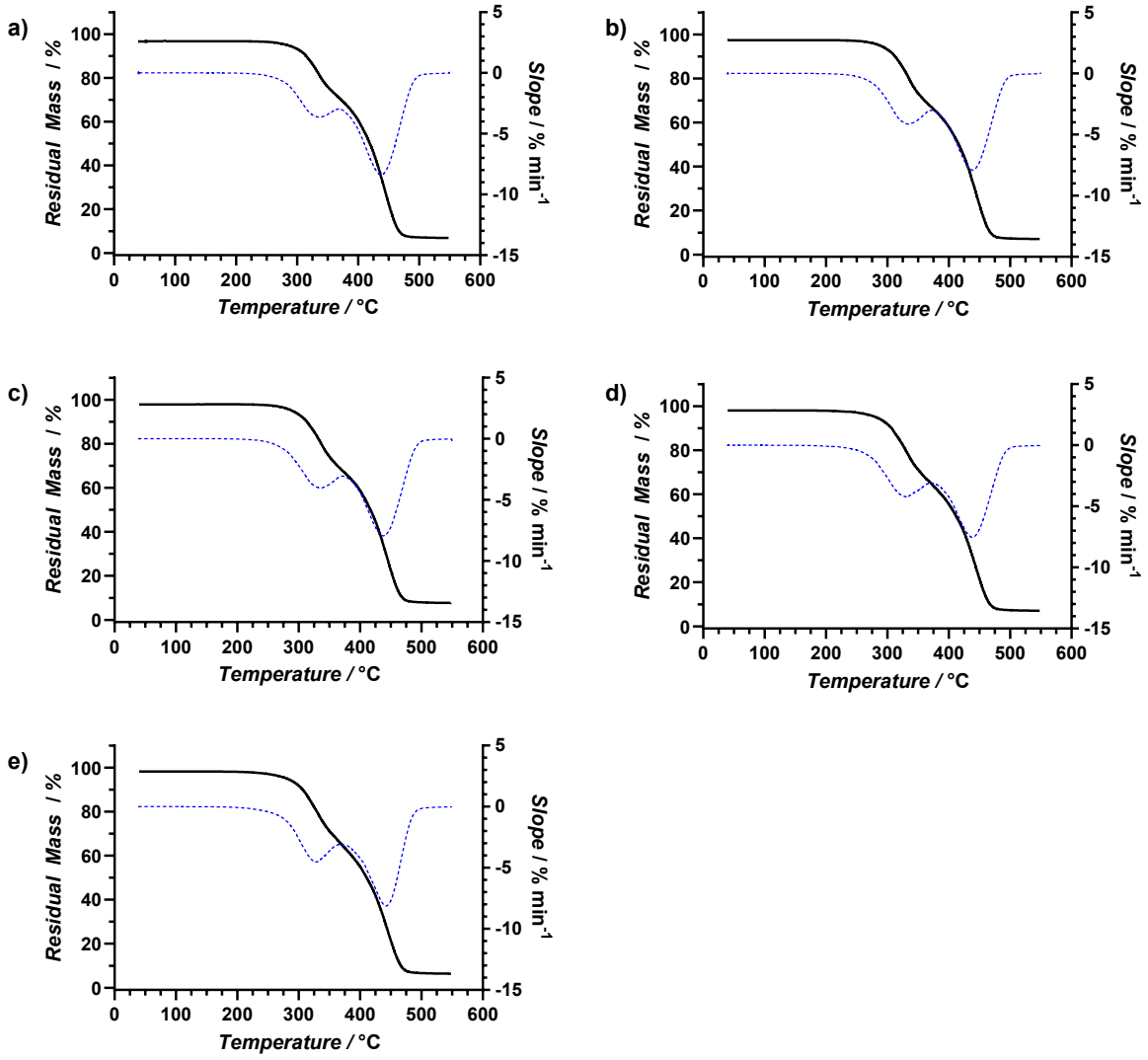

Appendix, Figure 17: TGA results of **mPEG-III** modified polymers at large scale. Degradation temperatures can be found at the end of the respective chapter.

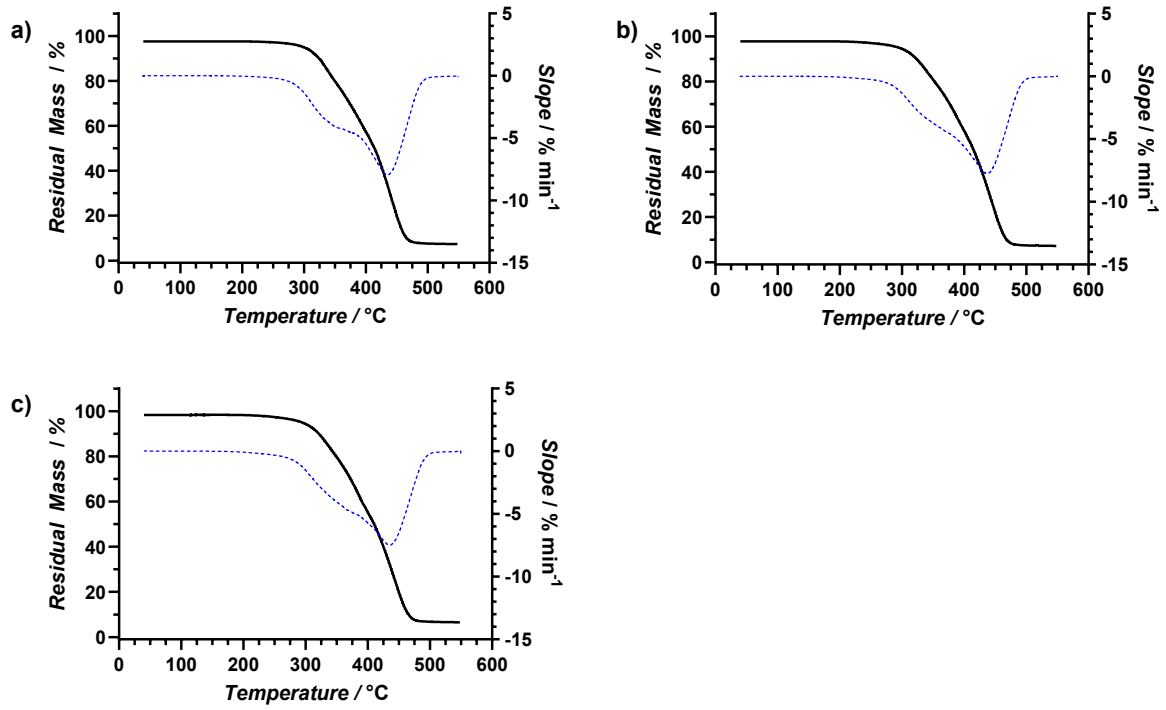

Appendix, Figure 18: TGA results of **mPEG-IV** modified polymers at large scale. Degradation temperatures can be found at the end of the respective chapter.

12.1.2.4 GPC

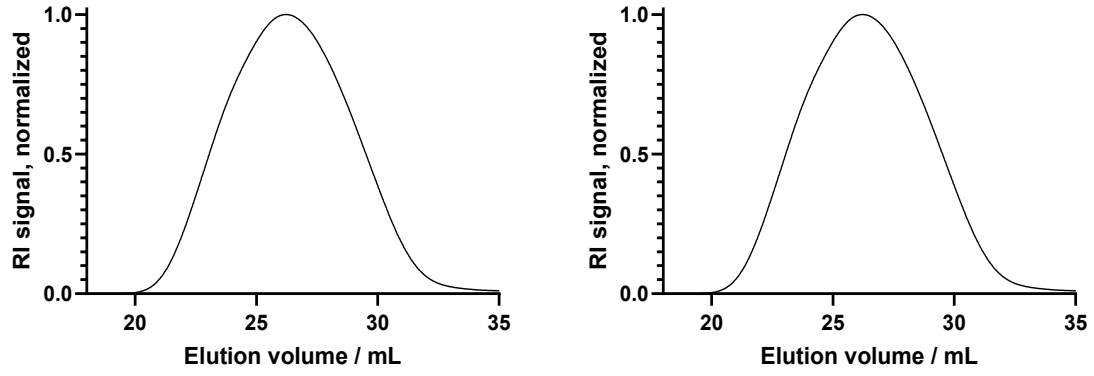

Appendix, Figure 19: GPC elugram of **mPEG-I** modified polymers with normalized RI signal. Measurement calibrated against PMMA standards in DMAc with 0.6 g L^{-1}LiBr; a) **mPEG-Ia**, M_w = 28000 g mol, Đ = 3.2; b) **mPEG-Ib**, M_w = 33000 g mol, Đ = 3.3.

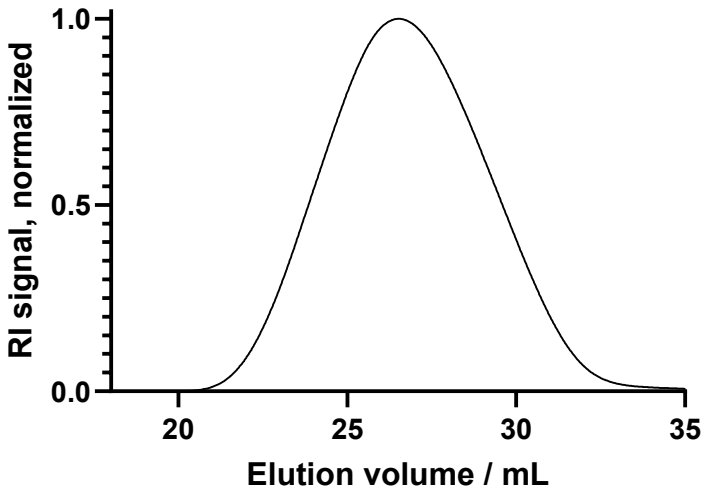

Appendix, Figure 20 GPC elugram of mPEG-IId modified polymers with normalized RI signal. Measurement calibrated against PMMA standards in DMAc with 0.6 g L^{-1}LiBr; **mPEG-IId**, M_w = 35000 g mol, Đ = 2.6.

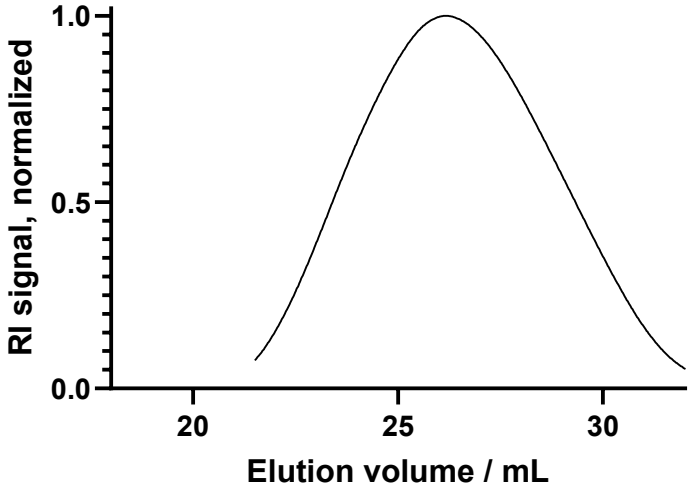

Appendix, Figure 21: GPC elugram of mPEG-III modified polymer with normalized RI signal. Measurement calibrated against PMMA standards in DMAc with 0.6 g L^{-1}LiBr; **mPEG-IIId**, M_w = 40000 g mol, Đ = 3.1.

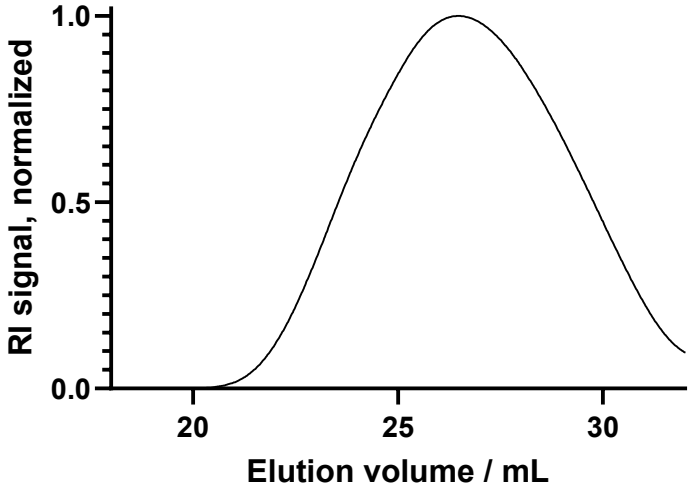

Appendix, Figure 22: GPC elugram of mPEG-IV modified polymers with normalized RI signal. Measurement calibrated against PMMA standards in DMAc with 0.6 g L^{-1}LiBr; a) **mPEG-IVc**, M_w = 34000 g mol, Đ = 5.8.

12.1.2.5 Melt Rheology

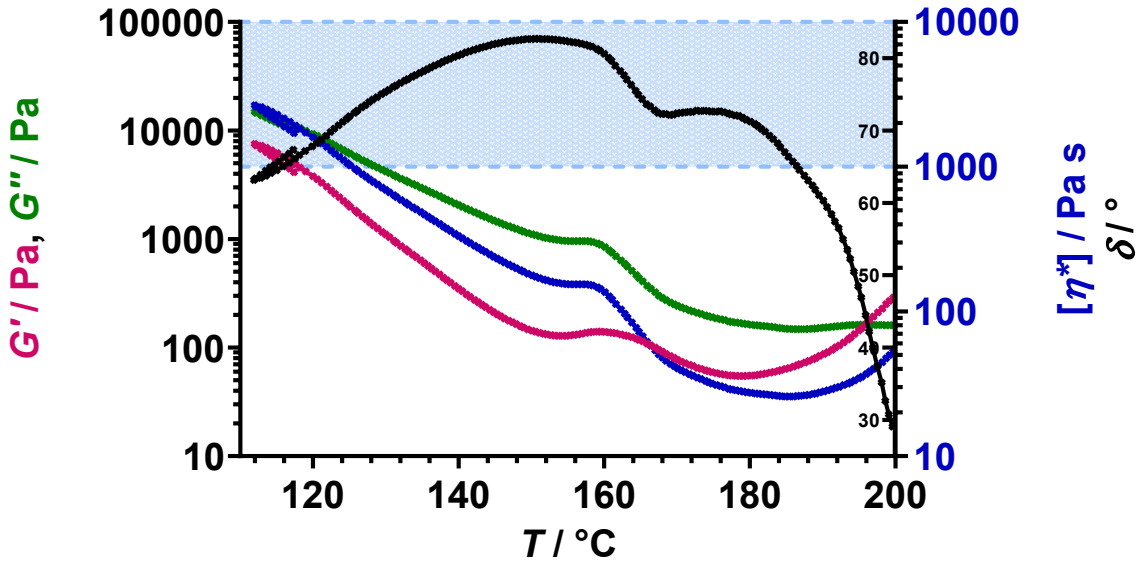

Figure 94: Melt rheological measurements **mPEG-IIId**.

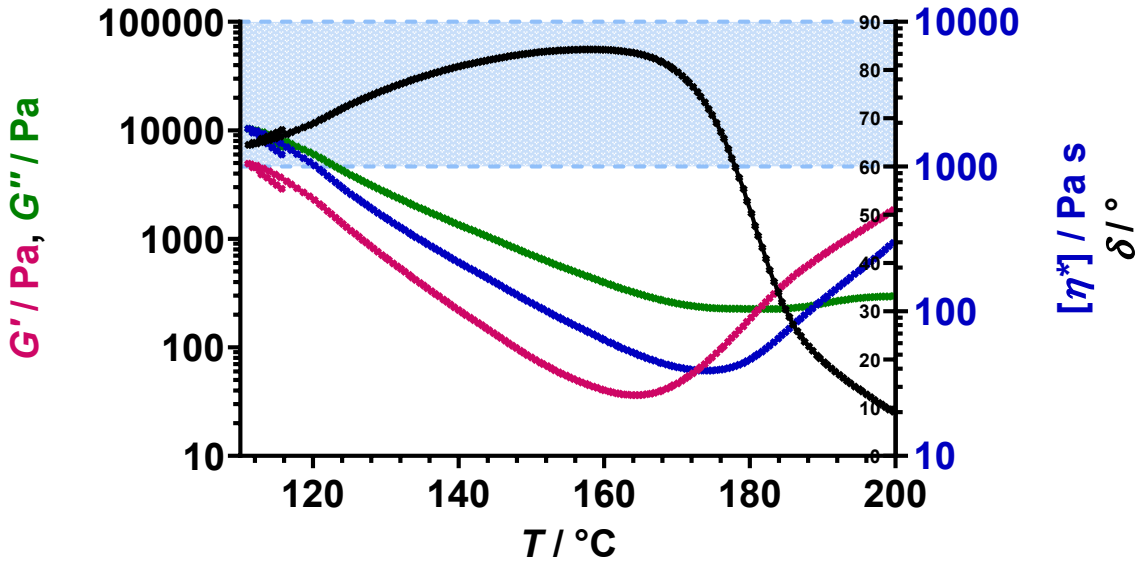

Figure 95: Melt rheological measurements **mPEG-IVc**.

12.1.3 Additional analytical data amine modifications

12.1.3.1 NMR

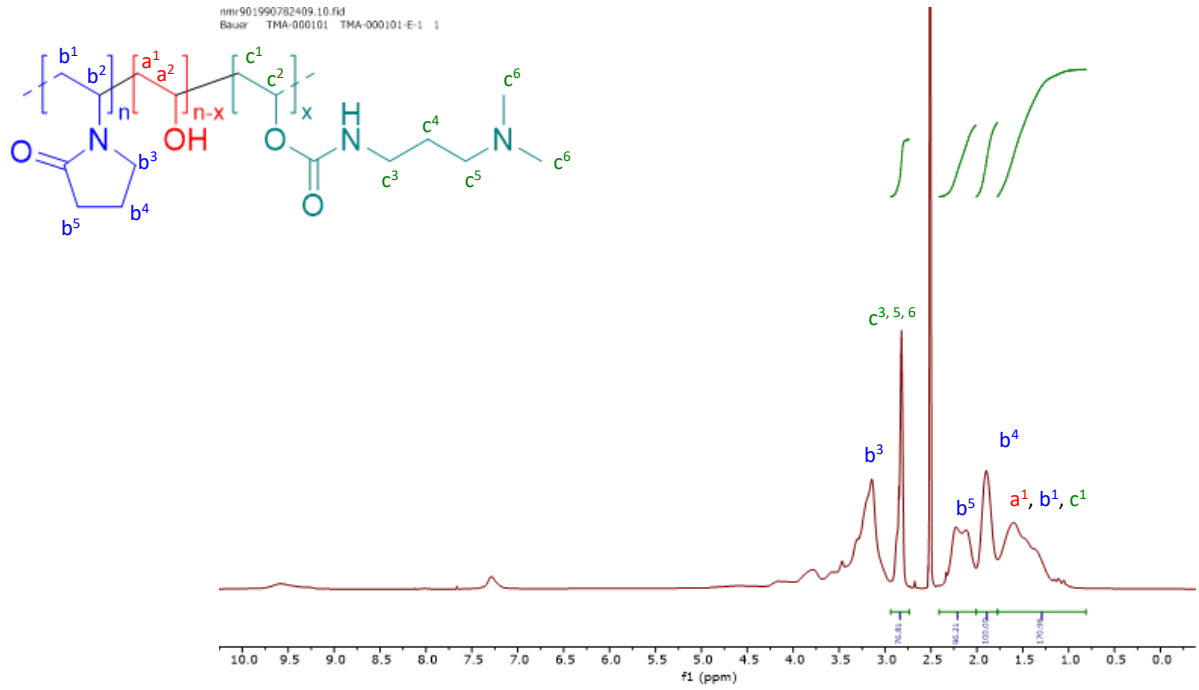

Appendix, Figure 23: Exemplary ^{1}H NMR spectrum of **amine-Ie.** Modification degree 9.4%.

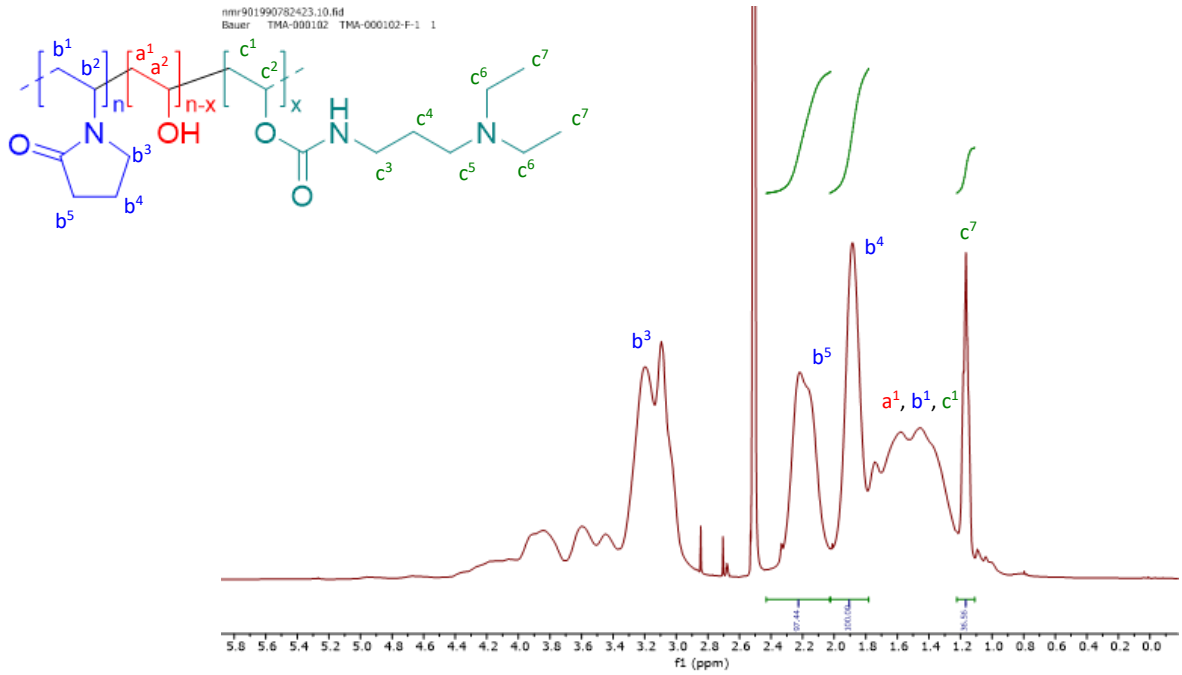

Appendix, Figure 24: Exemplary ^{1}H NMR of **amine-IIf.** Modification degree 7.4%

12.1.3.2 DSC

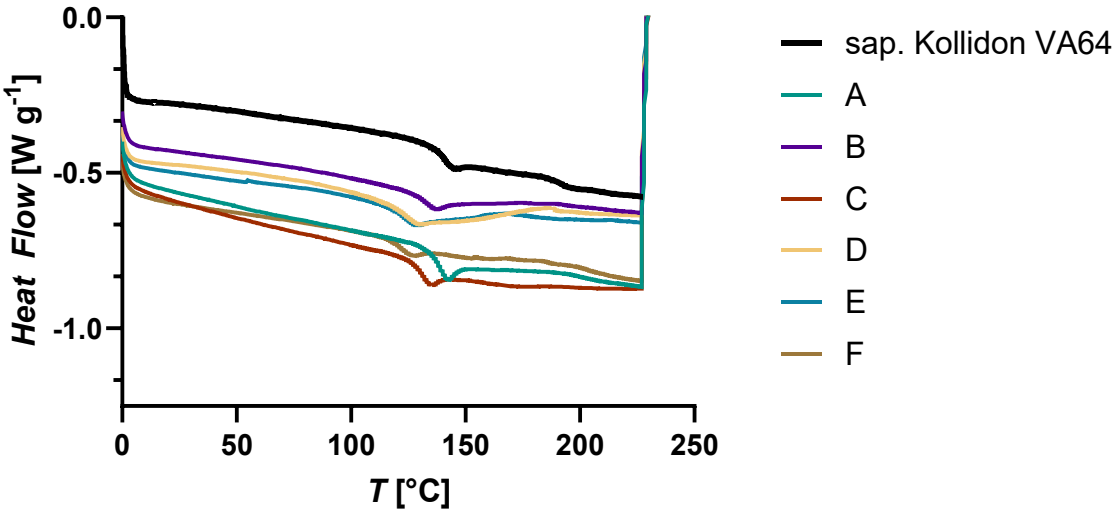

Appendix, Figure 25: DSC thermograms of all modifications using **amine-I**; T_g(a) = 137 °C; T_g (b) = 133 °C; T_g (c) = 130 °C; T_g (d) = 125 °C; T_g (e) = 123 °C; T_g (f) = 124 °C

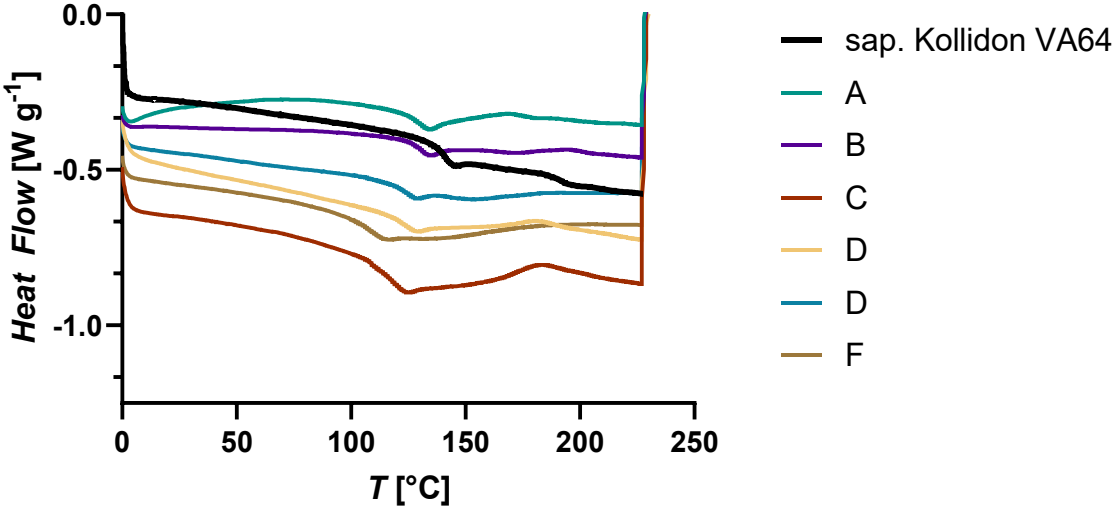

Appendix, Figure 26: DSC thermograms of all modifications using **amine-II**; T_g (a) = 129 °C; T_g (b) = 128 °C; T_g (c)= 118 °C; T_g (d)= 124 °C; T_g (e)= 122 °C; T_g (f)= 108 °C.

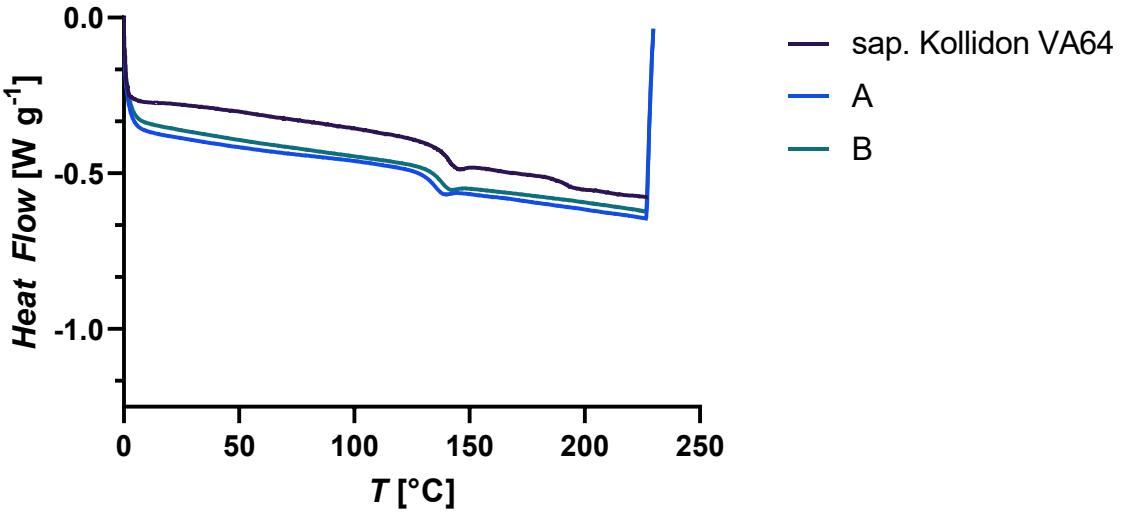

Appendix, Figure 27: DSC thermograms of all modifications using **amine-III** Acid; T_g (a) = 134 °C; T_g (b) = 132 °C.

12.1.3.3 TGA

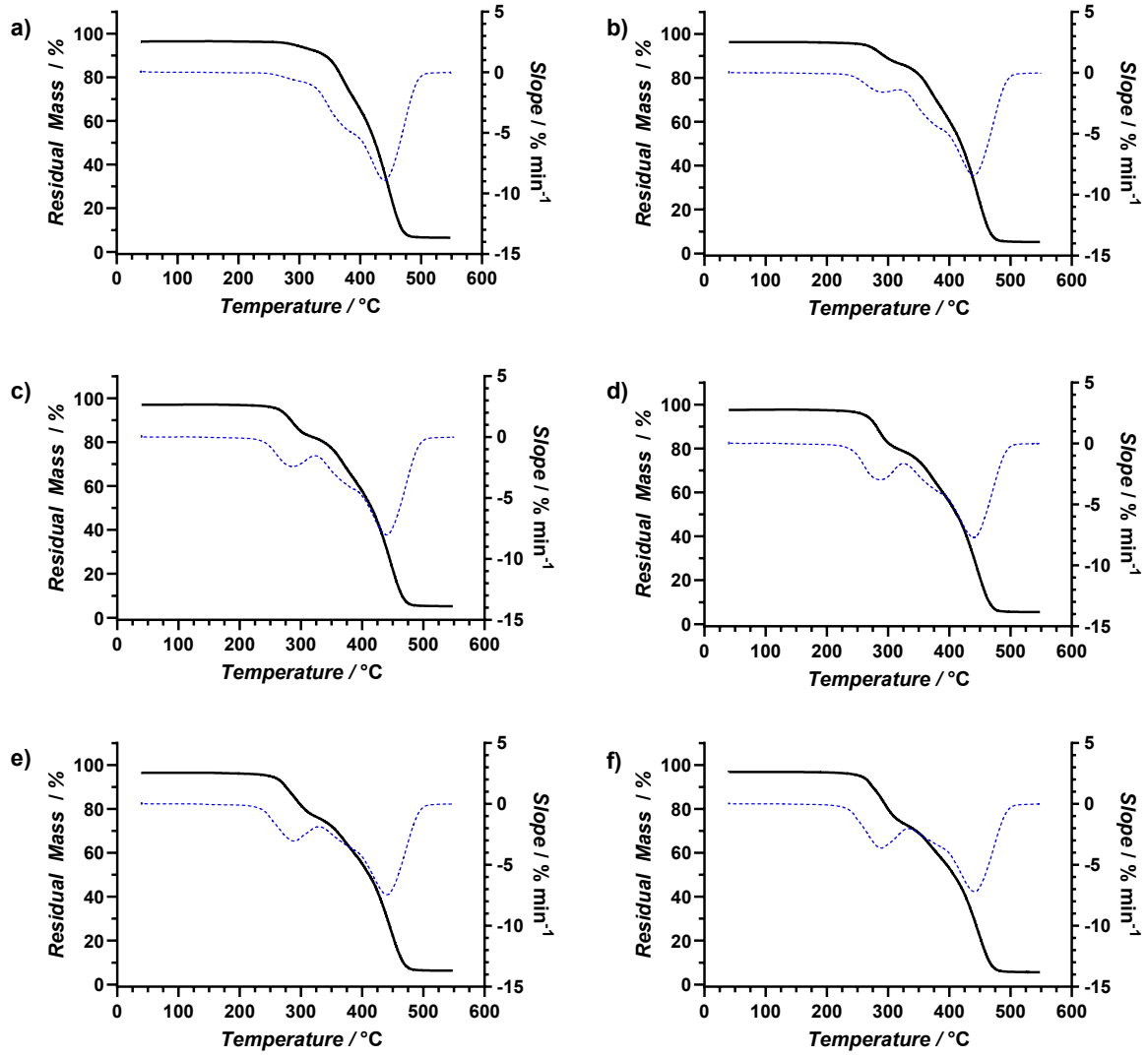

Appendix, Figure 28: TGA **amine-I a-f**. Degradation temperatures can be found at the end of the respective chapter.

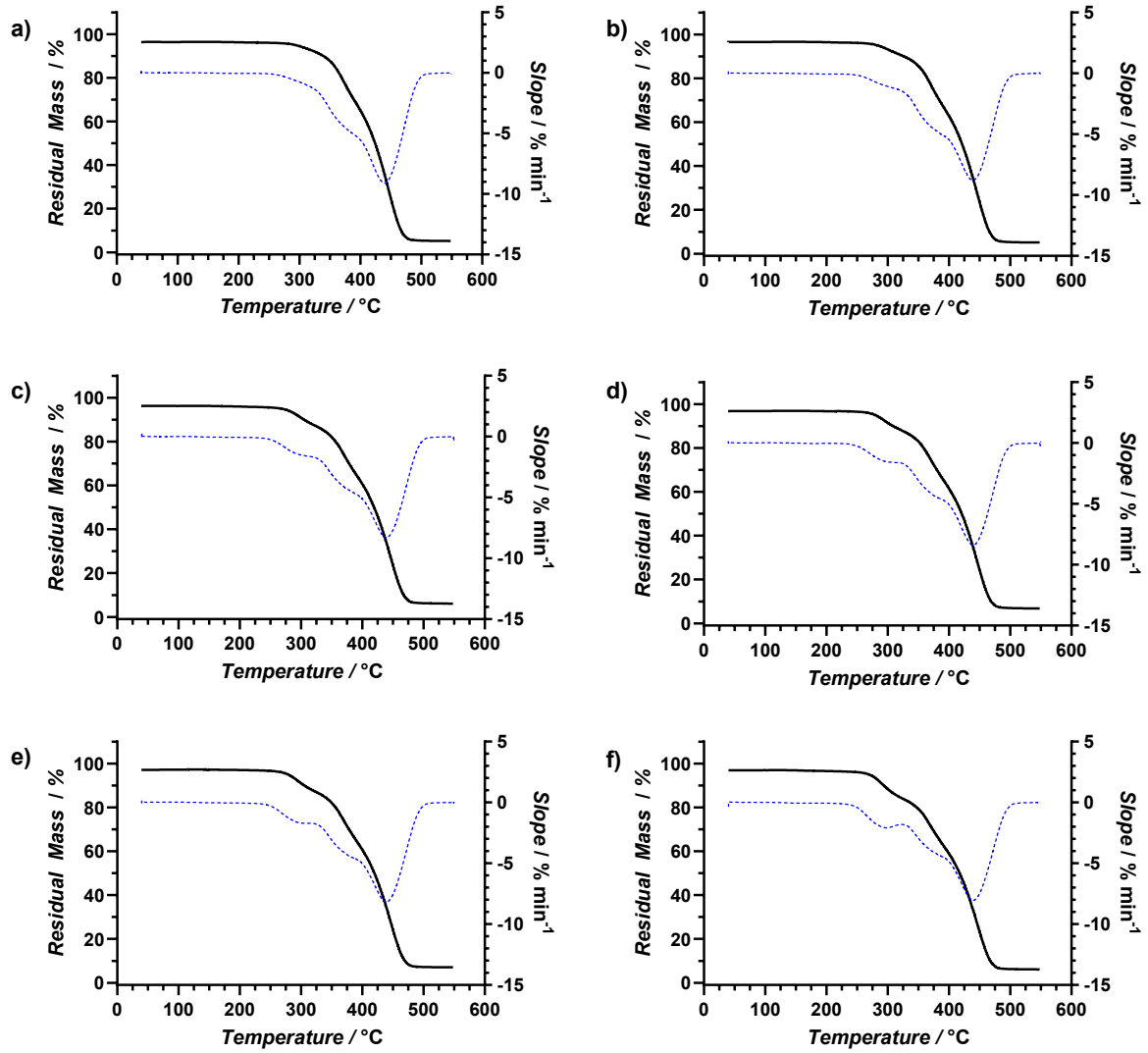

Appendix, Figure 29: TGA **amine-II a-f**. Degradation temperatures can be found at the end of the respective chapter.

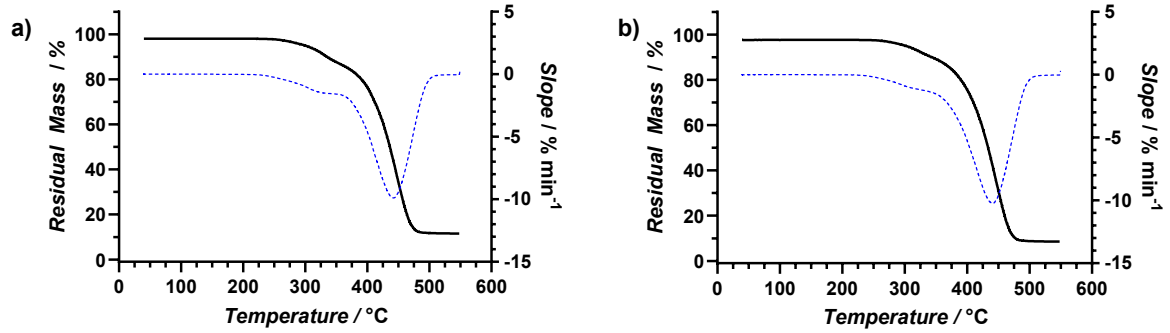

Appendix, Figure 30: TGA **amine-III a-b**. Degradation temperatures can be found at the end of the respective chapter.

12.1.3.4 GPC

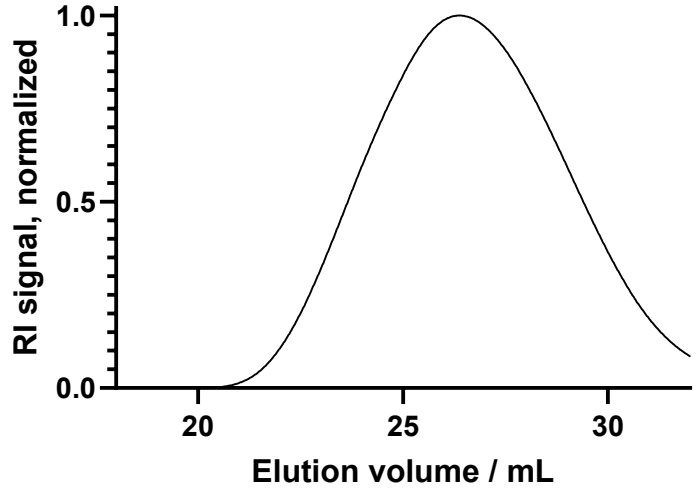

Appendix, Figure 31: GPC elugram of amine-I modified polymers with normalized RI signal. Measurement calibrated against PMMA standards in DMAc with 0.6 g L^{-1}LiBr; a) **amine-Ie**, M_w = 37000 g mol, Đ = 2.9.

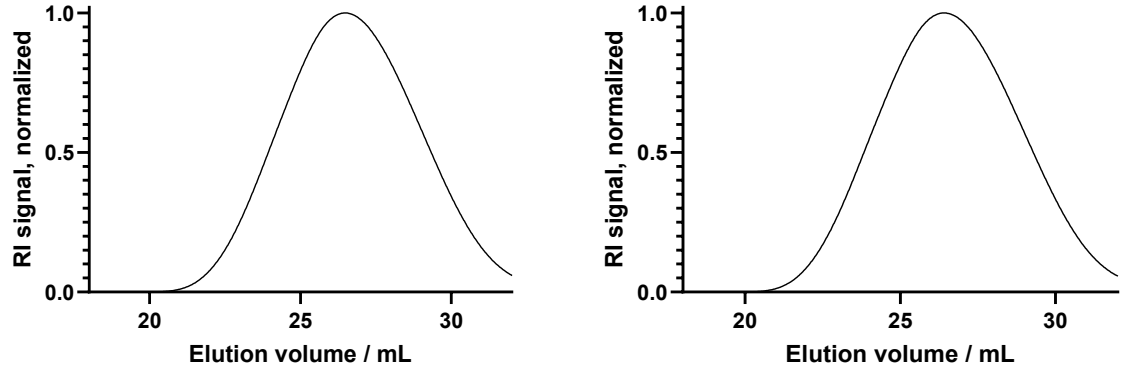

Appendix, Figure 32: GPC elugram of amine-II modified polymers with normalized RI signal. Measurement calibrated against PMMA standards in DMAc with 0.6 g L^{-1}LiBr; a) **amine-IIe**, M_w = 35000 g mol, Đ = 2.5; b) **amine-IIf** M_w = 36000 g mol, Đ = 2.5.

12.1.4 Additional analytical data hydrophobic modifications

12.1.4.1 NMR

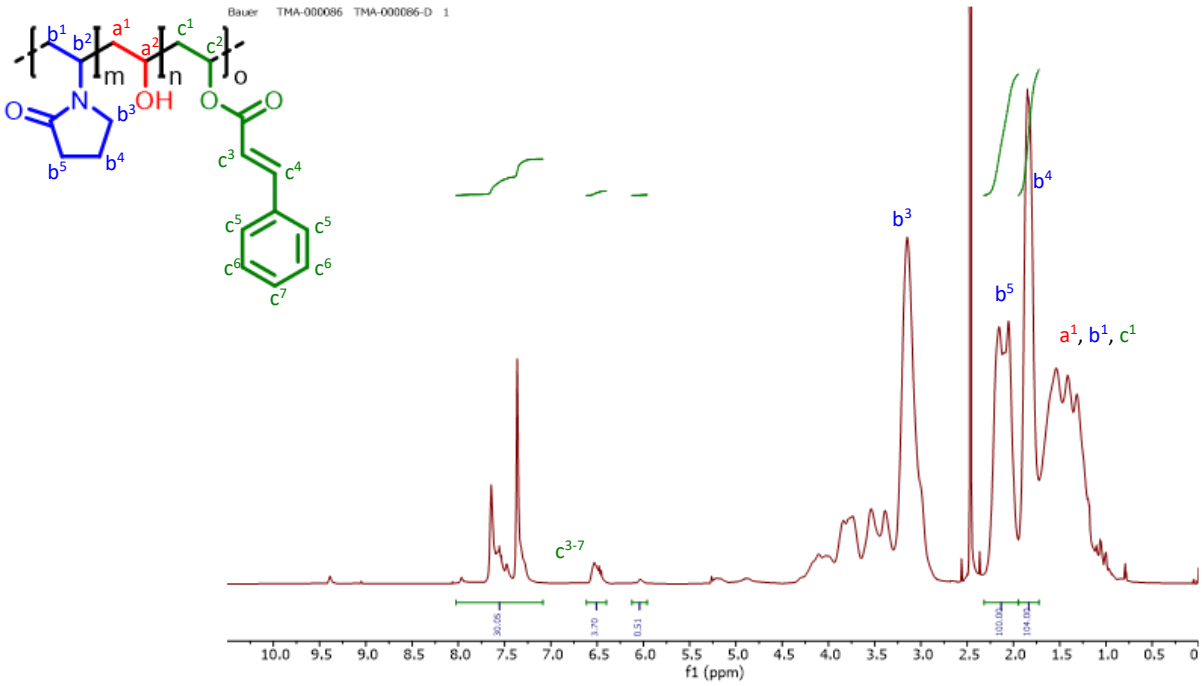

Appendix, Figure 33: ^{1}H NMR **apolar-Id**. Modification degree 6.0%

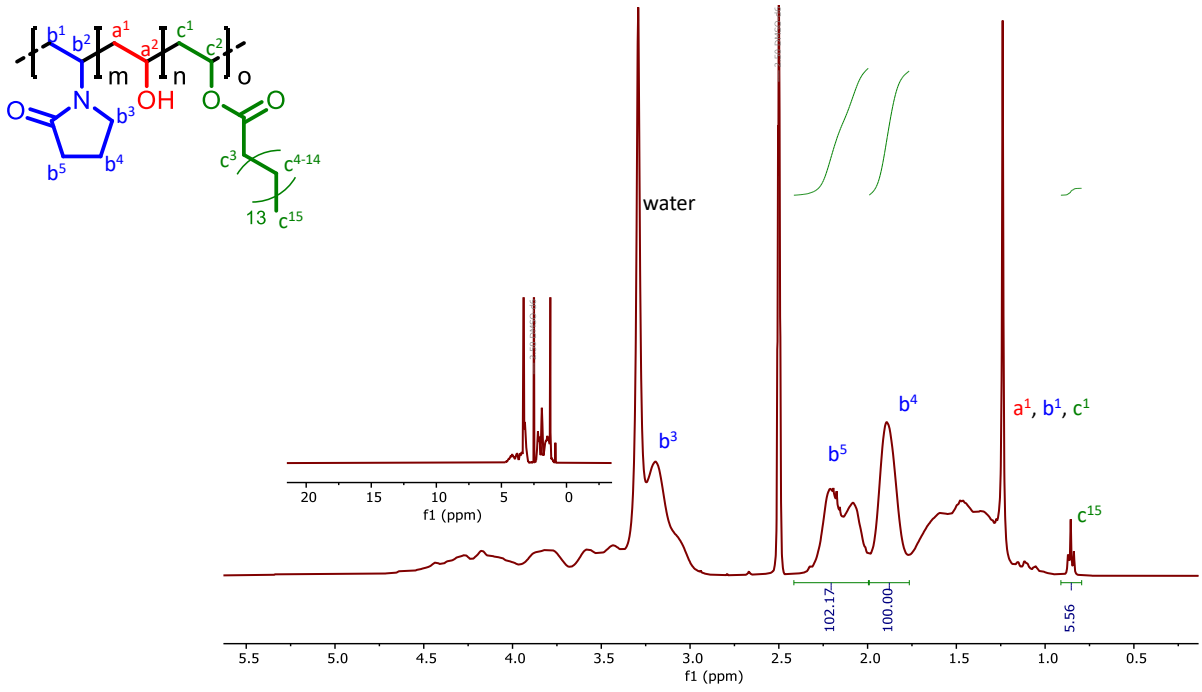

Appendix, Figure 34: ^{1}H NMR **apolar-IIIa**; Modification degree 4.2%

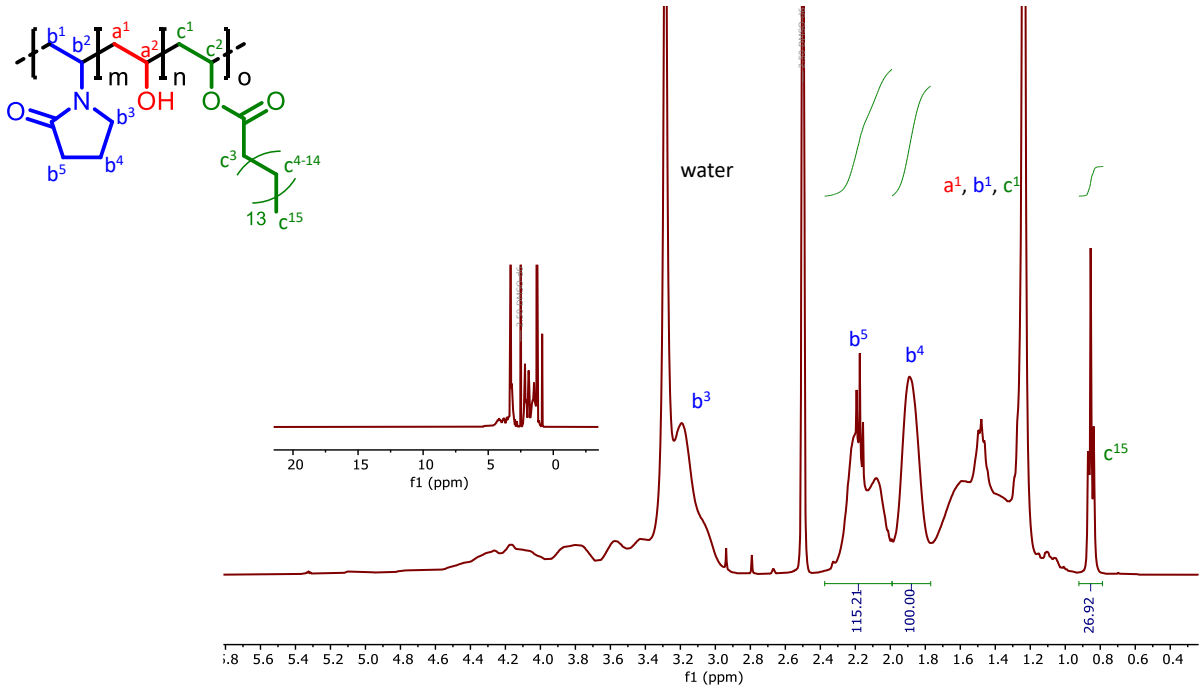

Appendix, Figure 35: ^{1}H NMR **apolar-IIIb**; Modification degree 18%

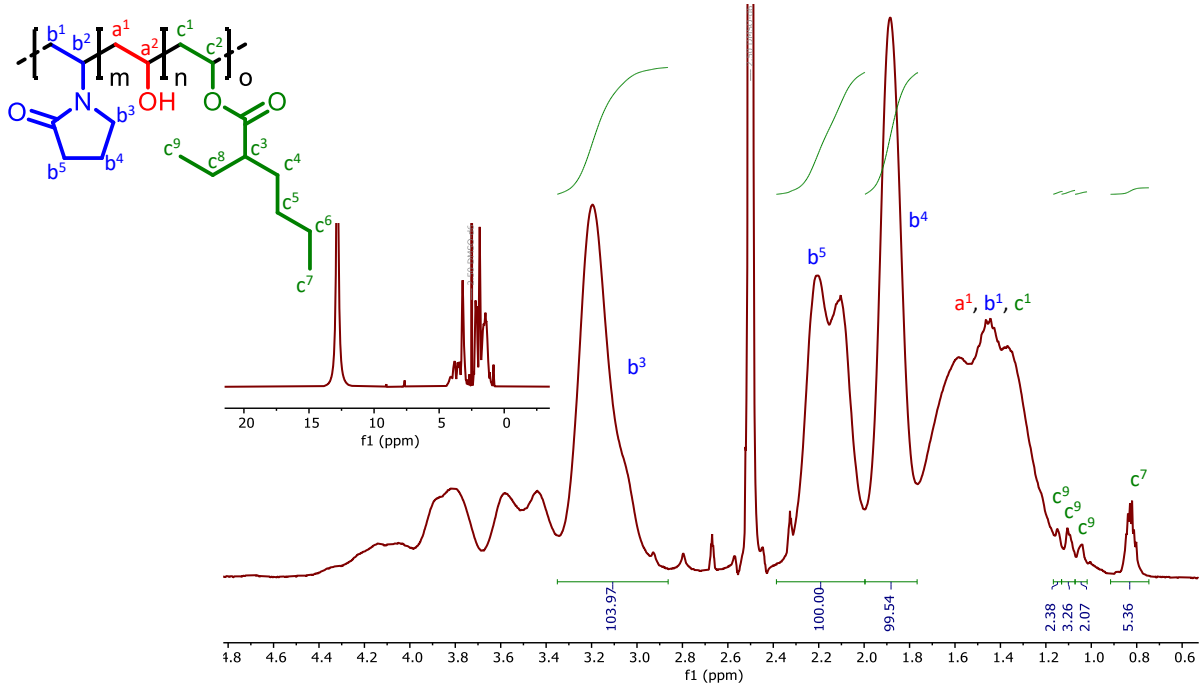

Appendix, Figure 36: ^{1}H NMR **apolar-IVa**. Modification degree 2%

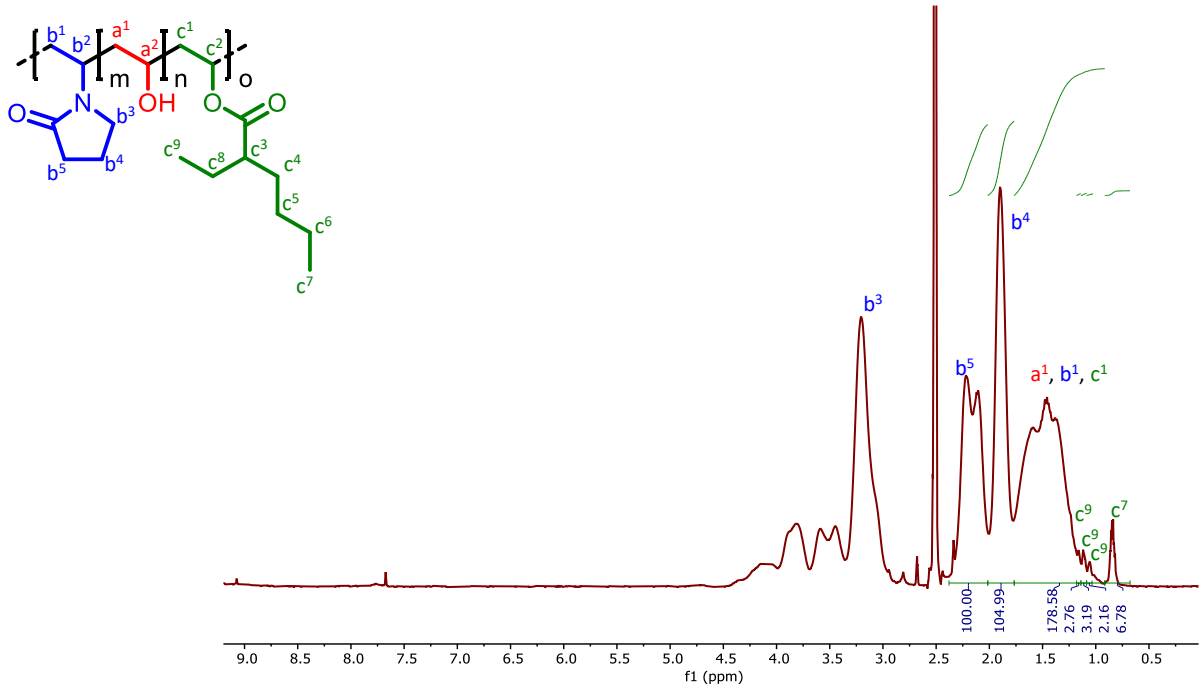

Appendix, Figure 37: [1]H NMR **apolar-IVb**. Modification degree 2%.

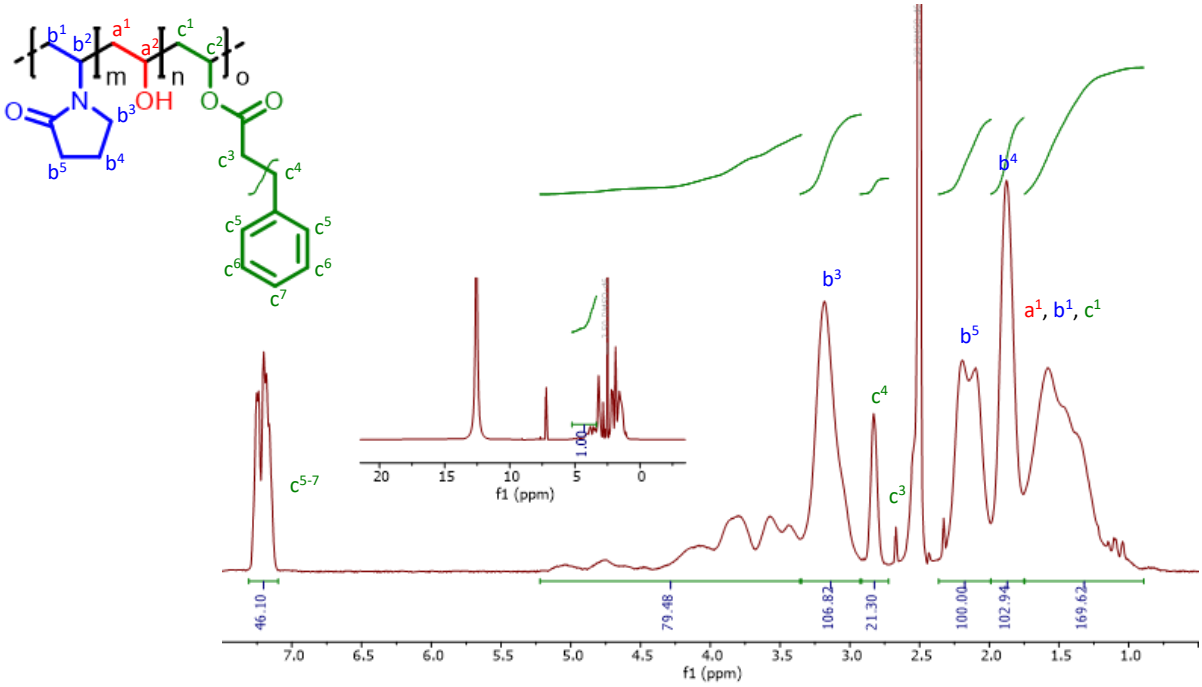

Appendix, Figure 38: [1]H NMR **apolar-IIa.** Modification degree 1.0%

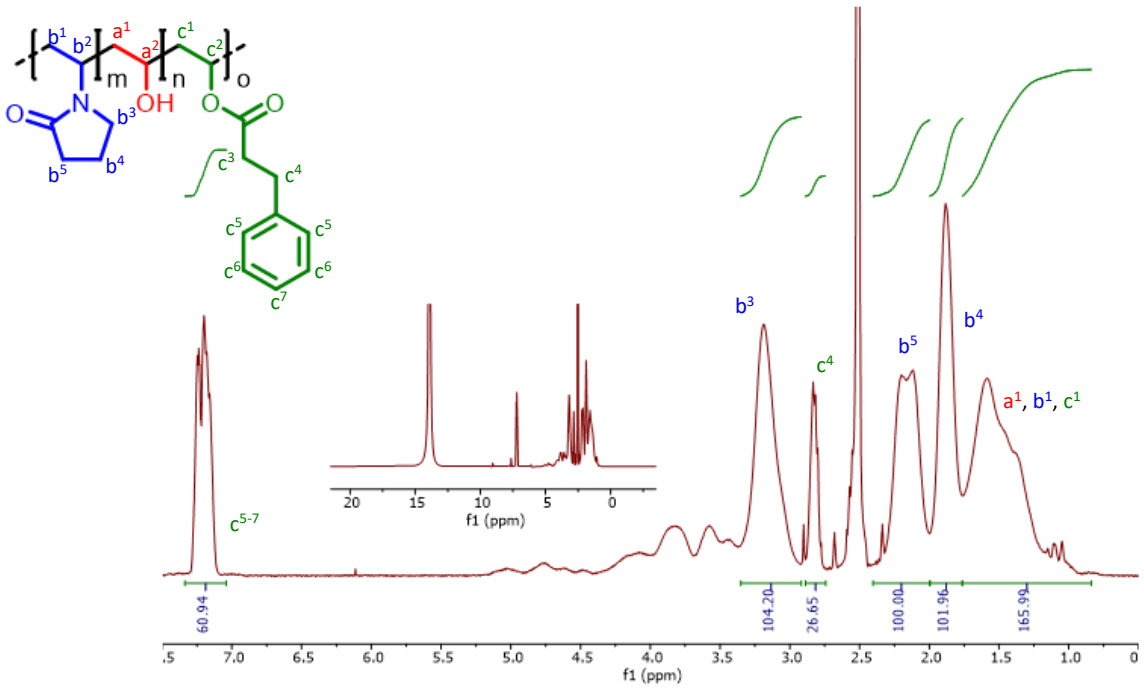

Appendix, Figure 39: ^{1}H NMR **apolar-IIa.** Modification degree 2.0%

12.1.4.2 DSC

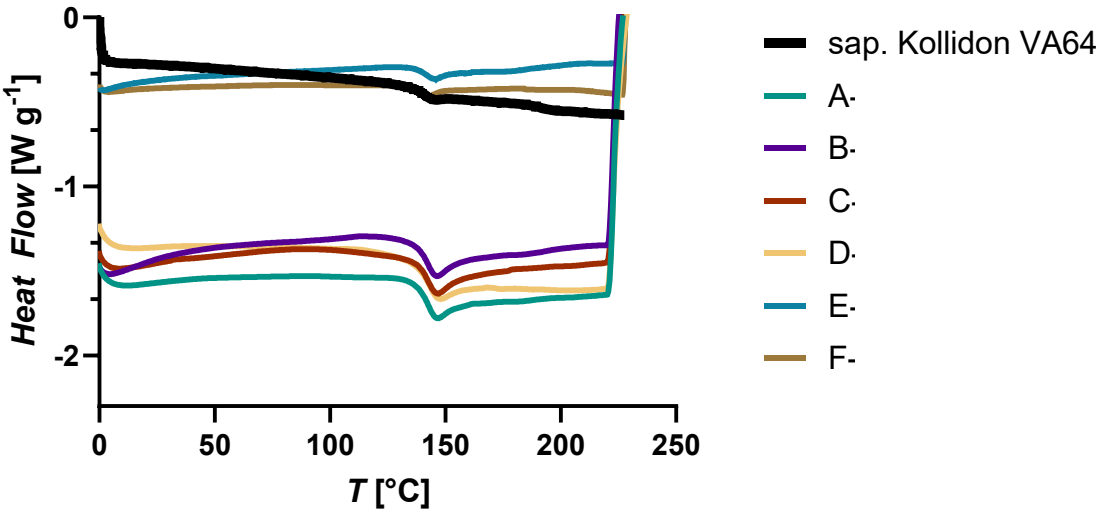

Appendix, Figure 40: DSC thermograms of all modifications using **apolar-I**; T_g(a) = 142 °C; T_g (b) = 141 °C; T_g (c) = 142 °C; T_g (d) = 142 °C; T_g (e) = 140 °C; T_g (f) = 137 °C.

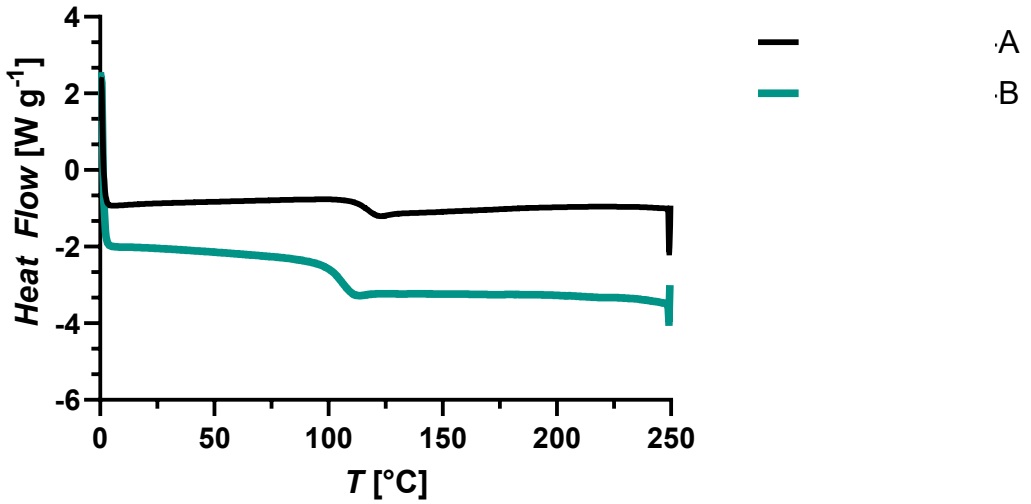

Appendix, Figure 41: DSC thermograms of all modifications using **apolar-II**; T_g(a) = 115 °C; T_g (b) = 106 °C.

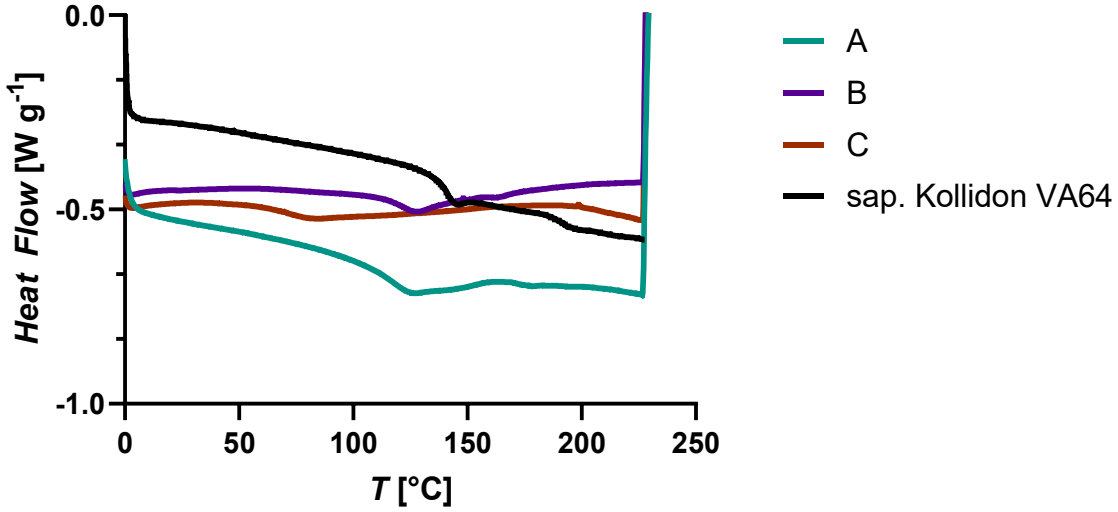

Appendix, Figure 42: DSC thermograms of all modifications using **apolar-III**; T_g(a) = 121 °C; T_g (b) = 123 °C; T_g (c) = 75 °C.

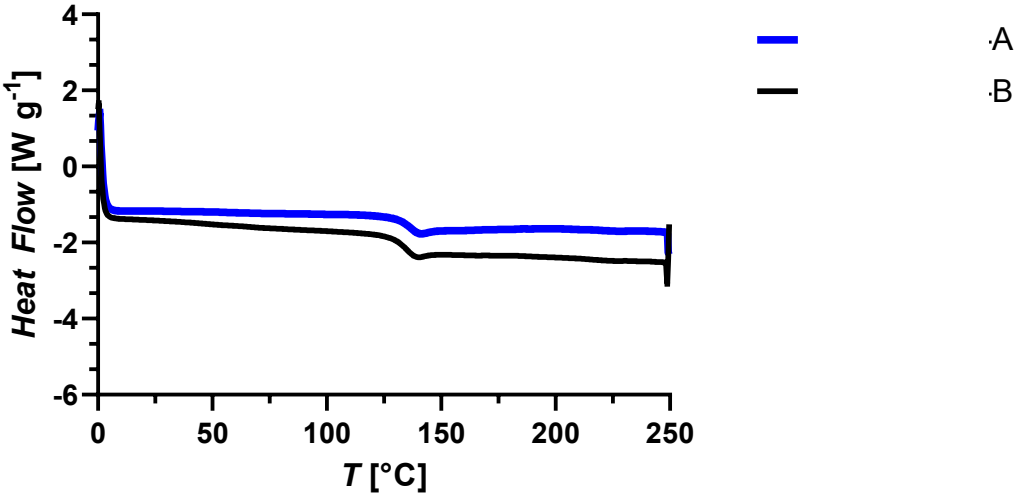

Appendix, Figure 43: DSC thermograms of all modifications using **apolar-IV**; T_g(a) = 210 °C; T_g (b) = 220 °C.

12.1.4.3 TGA

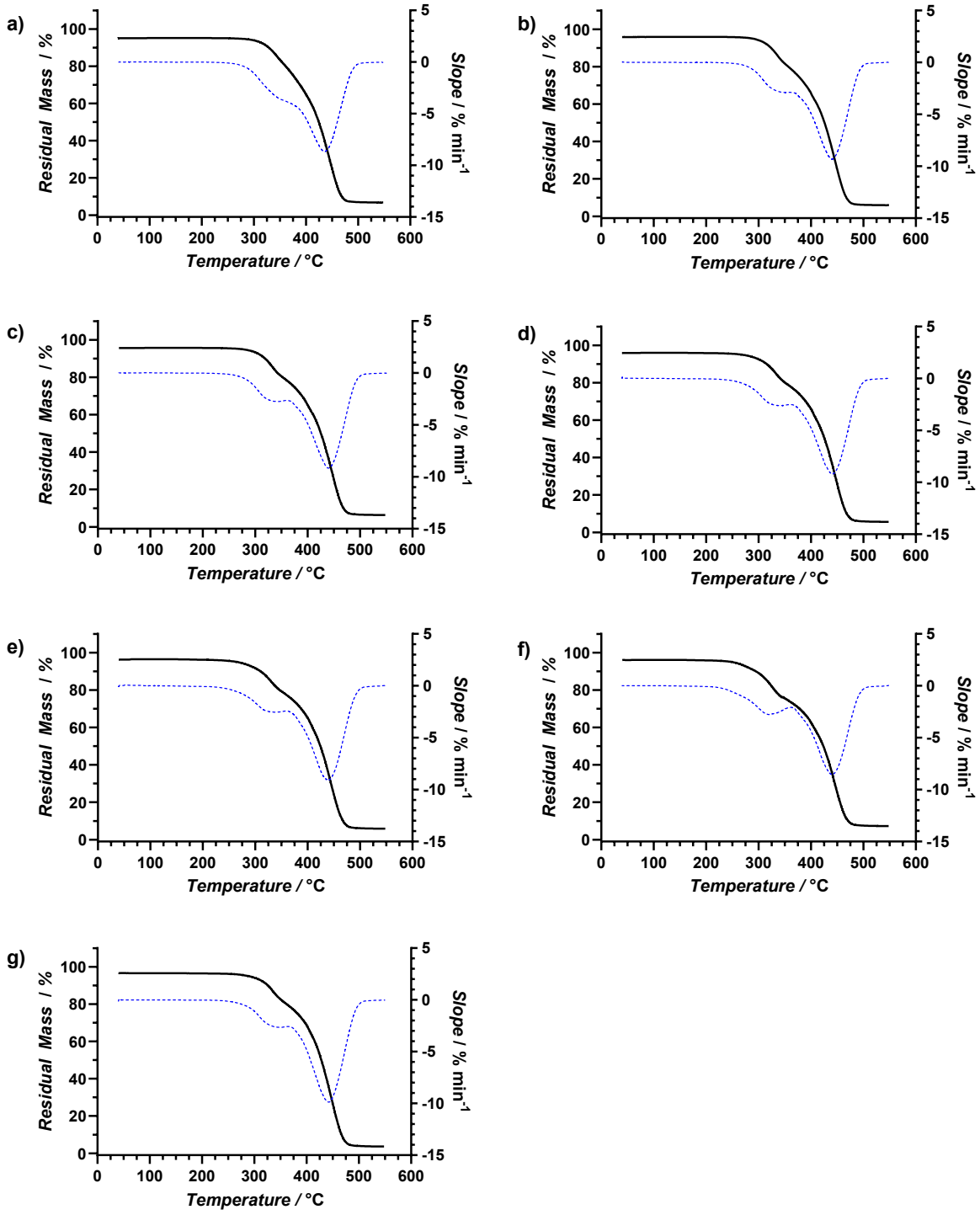

Appendix, Figure 44: TGA **apolar-I a-g**. Degradation temperatures can be found at the end of the respective chapter.

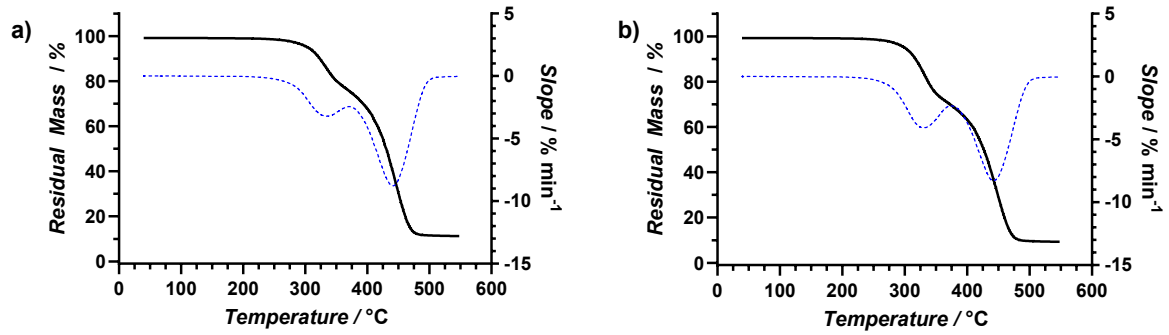

Appendix, Figure 45: TGA **apolar-II a-b**. Degradation temperatures can be found at the end of the respective chapter.

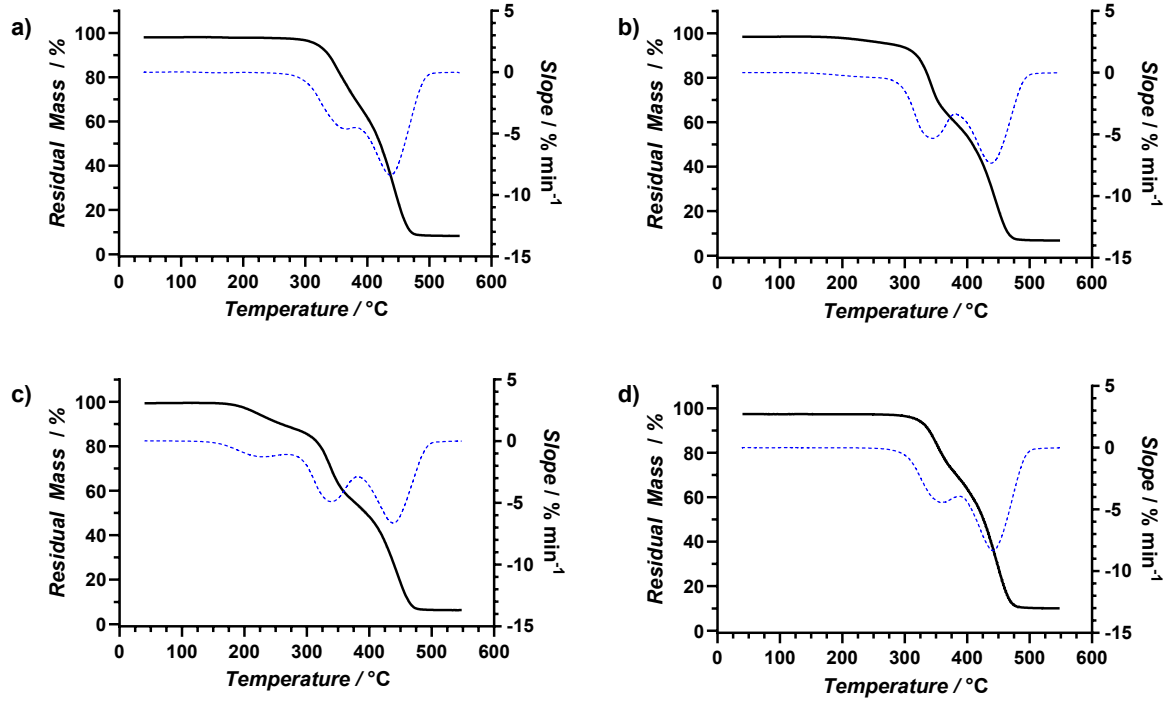

Appendix, Figure 46: TGA **apolar-III a-d**. Degradation temperatures can be found at the end of the respective chapter.

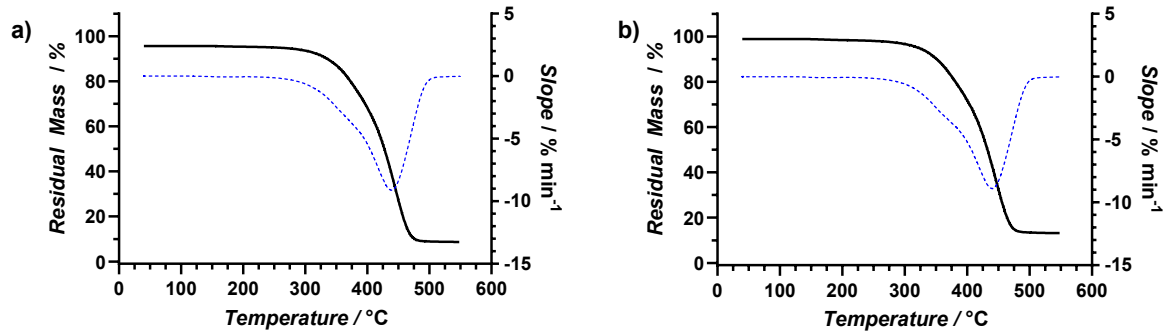

Appendix, Figure 47: TGA **apolar-IV a-b**. Degradation temperatures can be found at the end of the respective chapter.

12.1.4.4 GPC

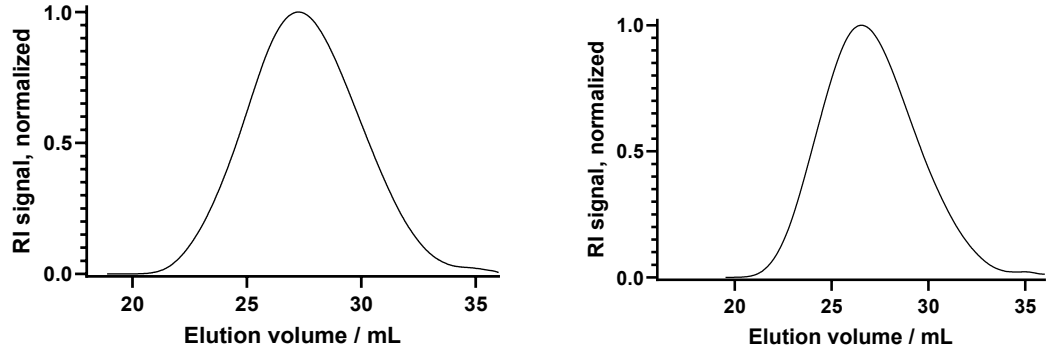

Appendix, Figure 48: GPC elugram of apolarII modified polymers with normalized RI signal. Measurement calibrated against PMMA standards in DMAc with 0.6 g L^{-1}LiBr; a) **apolar-IIa**, M_w = 28000 g mol, Đ = 3.2; b) **apolar-IIb**, M_w = 33000 g mol, Đ = 3.3.

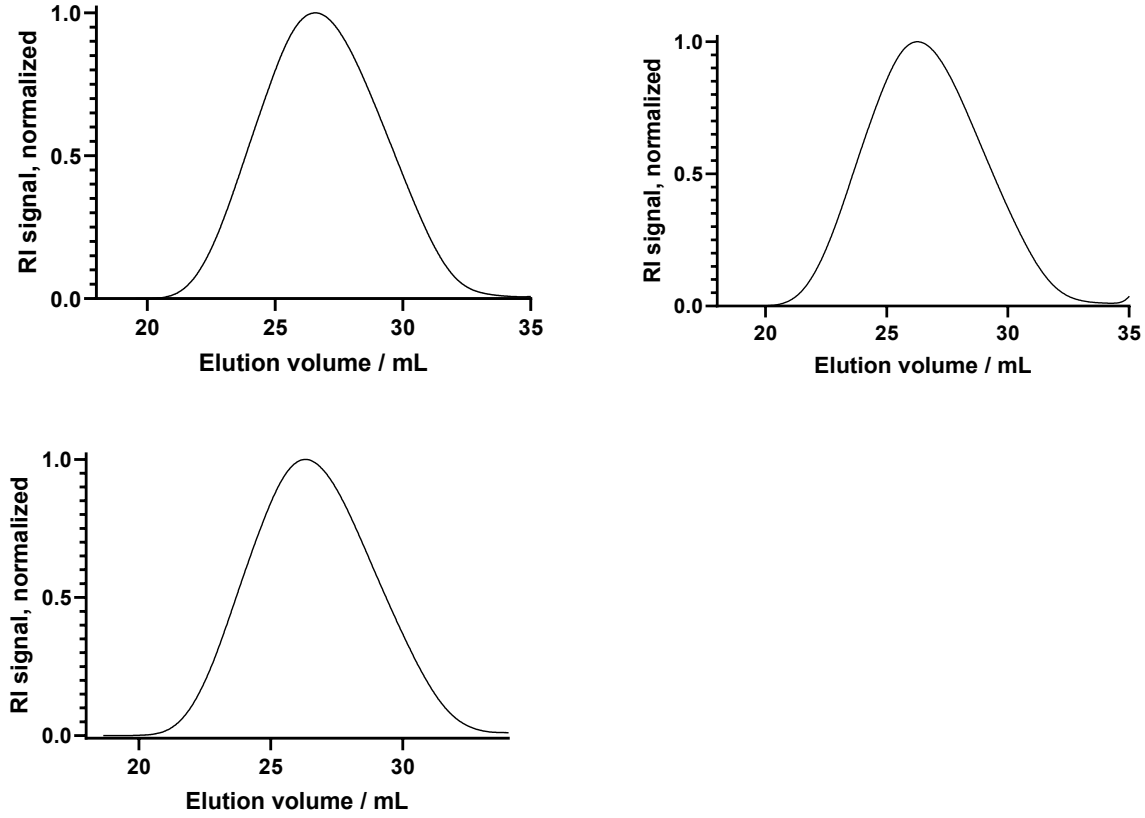

Appendix, Figure 49: GPC elugram of apolarIII modified polymers with normalized RI signal. Measurement calibrated against PMMA standards in DMAc with 0.6 g L^{-1}LiBr; a) **apolar-IIIa**, M_w = 35000 g mol, Đ = 2.5; b) **apolar-IIIb**, M_w = 38000 g mol, Đ = 2.5; c) **apolar-IIIc**, M_w = 37000 g mol, Đ = 2.4.

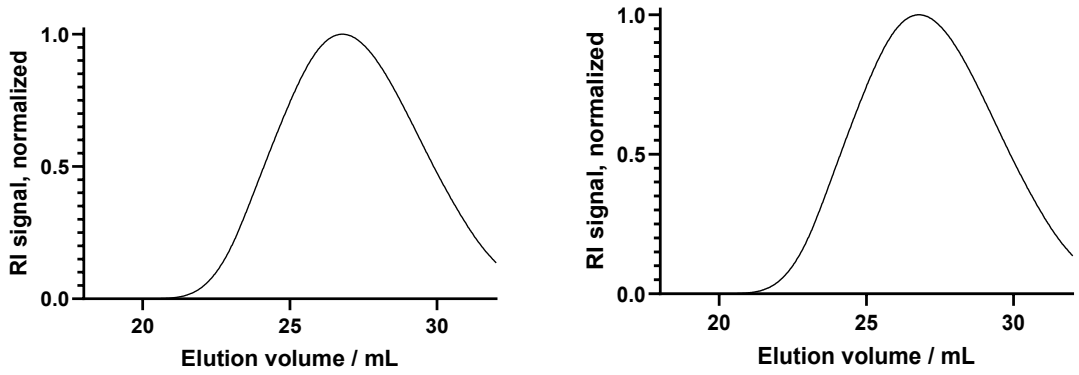

Appendix, Figure 50: GPC elugram of apolarIV modified polymers with normalized RI signal. Measurement calibrated against PMMA standards in DMAc with 0.6 g L^{-1}LiBr; a) **apolar-IVa**, M_w = 30000 g mol, Đ = 3.1; b) **apolar-IVb**, M_w = 31000 g mol, Đ = 3.1.

12.1.5 Additional analytical data other modifications

12.1.5.1 NMR

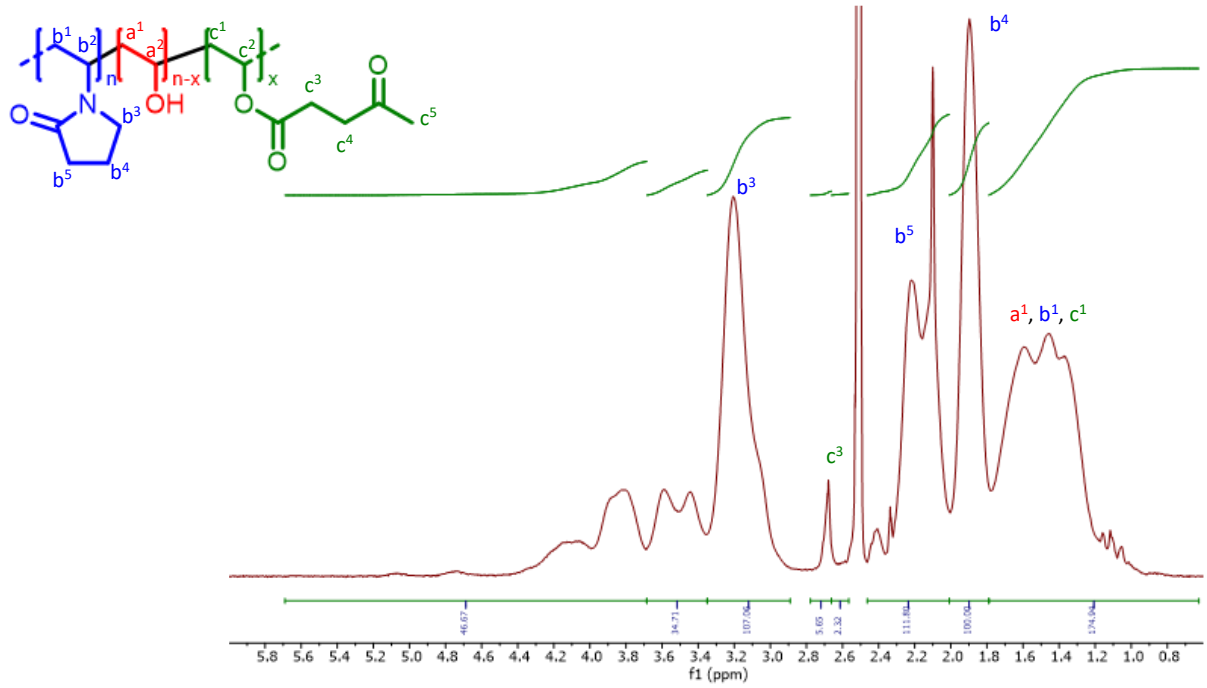

Appendix, Figure 51: ^{1}H NMR **misc-Ib**. Modification degree 2.0%

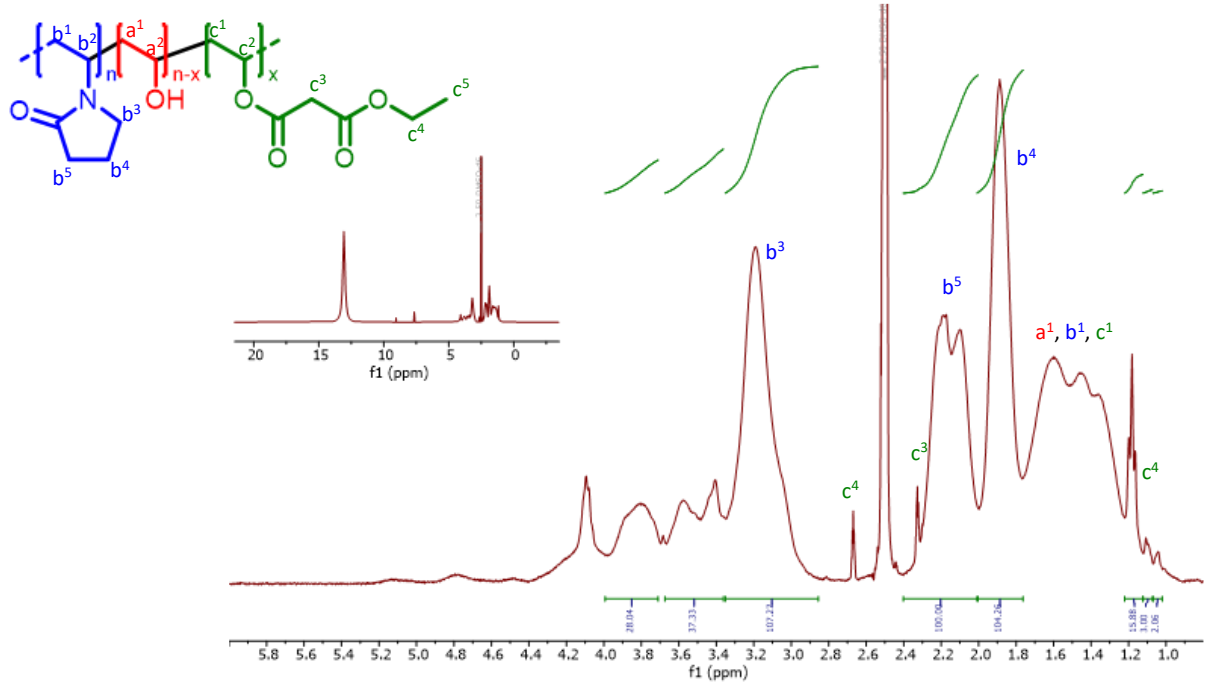

Appendix, Figure 52: ^{1}H NMR **misc-IIb**. Modification degree 7.0

12.1.5.2 TGA

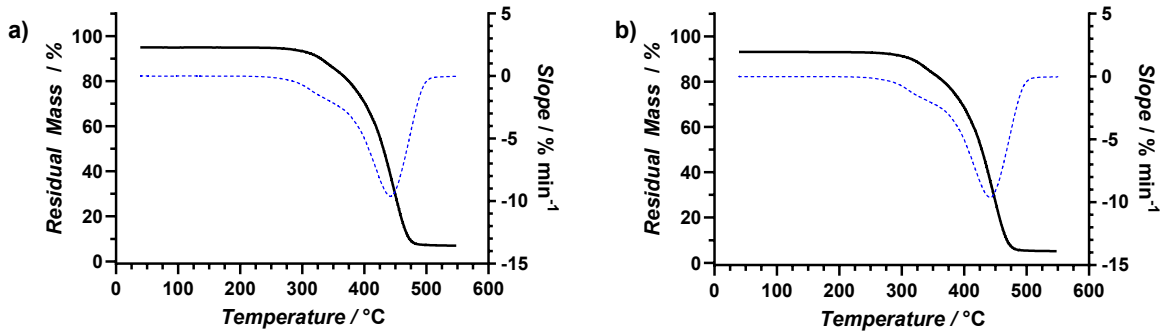

Appendix, Figure 53: TGA **misc-Ia-b**. Degradation temperatures can be found at the end of the respective chapter.

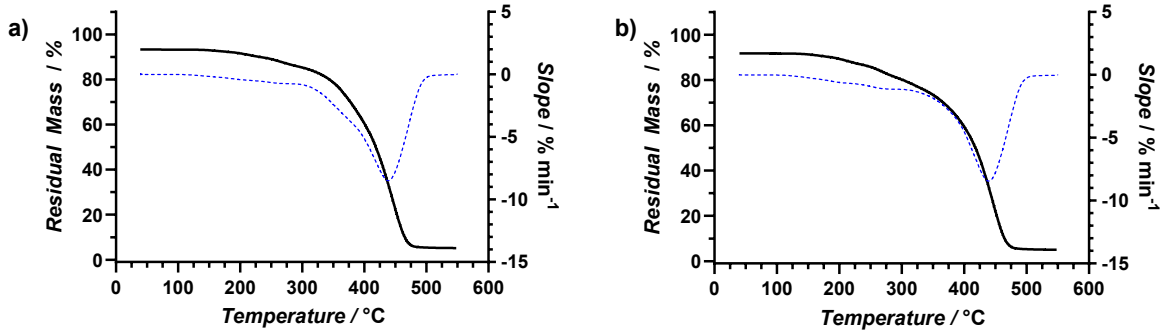

Appendix, Figure 54: TGA **misc-IIa-b**. Degradation temperatures can be found at the end of the respective chapter.

12.1.5.3 GPC

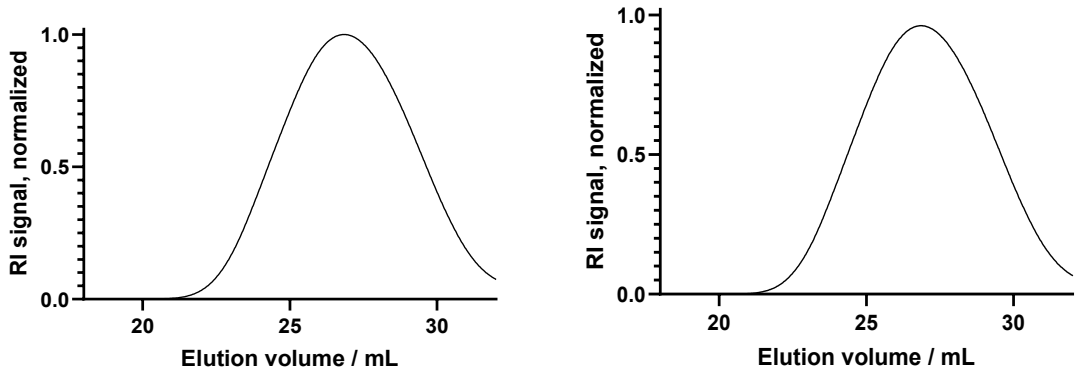

Appendix, Figure 55: GPC elugram of misc-I modified polymers with normalized RI signal. Measurement calibrated against PMMA standards in DMAc with 0.6 g L^{-1}LiBr; a) **misc-Ia**, M_w = 31000 g mol, Đ = 3.1; b) **misc-Ib**, M_w = 31000 g mol, Đ = 2.6.

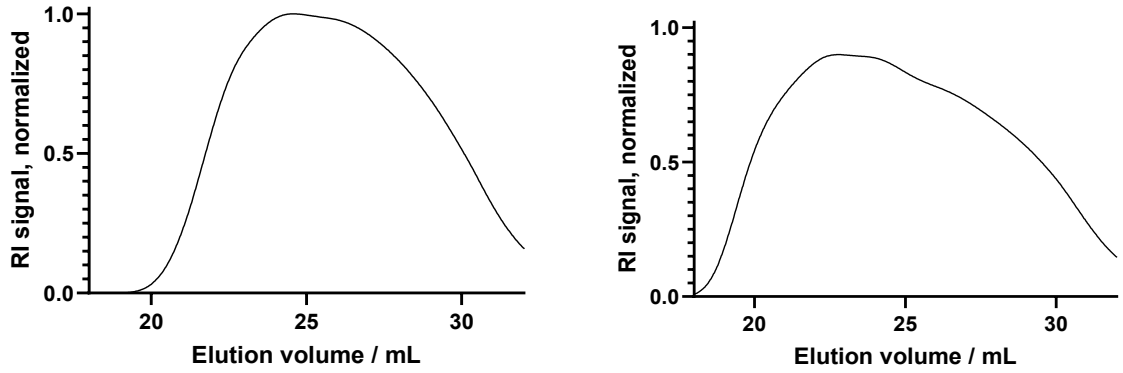

Appendix, Figure 56: GPC elugram of misc-II modified polymers with normalized RI signal. Measurement calibrated against PMMA standards in DMAc with 0.6 g L^{-1}LiBr; a) **misc-IIa**, M_w = 60000 g mol, Đ = 4.9; b) **misc-IIb**, M_w = 138000 g mol, Đ = 9.4.

12.1.6 Additional analytical data combined modifications

12.1.6.1 NMR

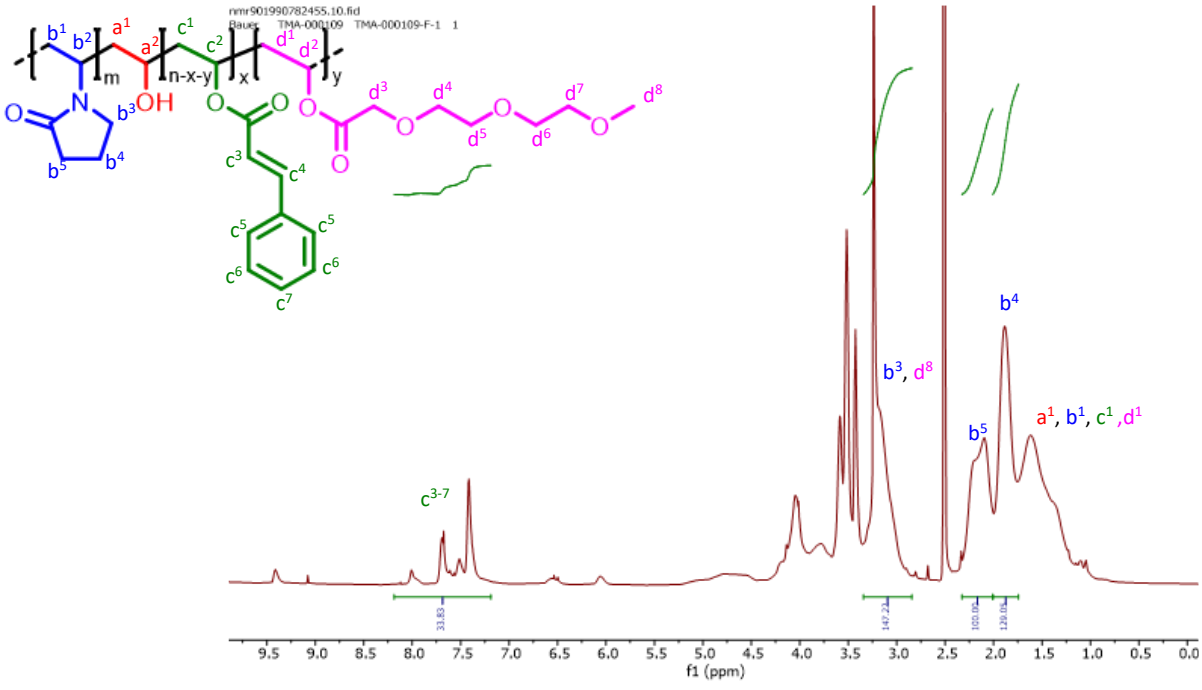

Appendix, Figure 57: ^{1}H NMR **mPEG-II/apolar-If**. Modification degree **mPEG-II** 8.5%; Modification degree **apolar-I** 4.9%

12.1.6.2 DSC

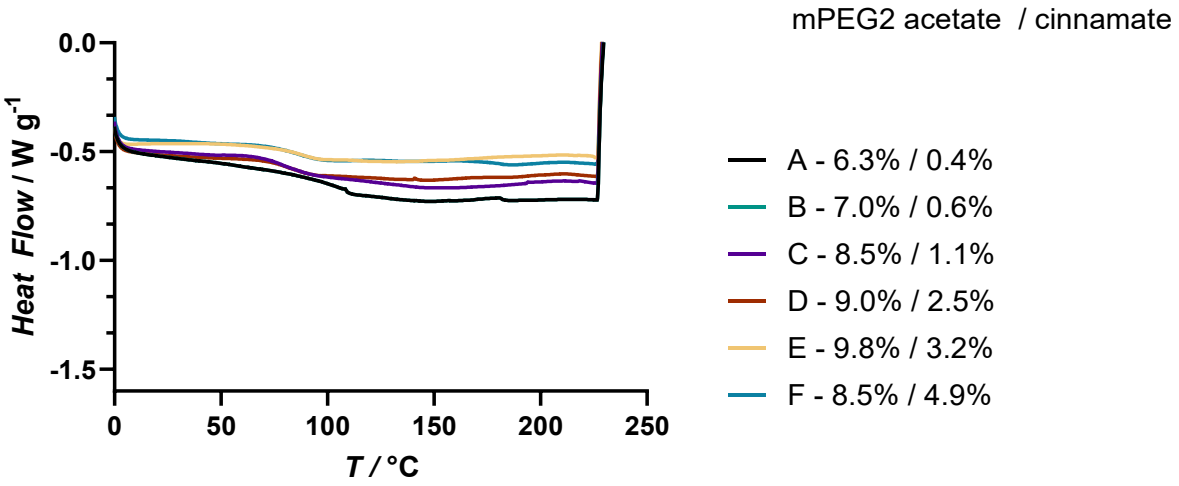

Appendix, Figure 58: DSC thermograms of all modifications using **mPEG-II/apolar-I**; T_g(a) = 109 °C; T_g (b) = 104 °C; T_g (c) = 87 °C; T_g (d) = 82 °C; T_g (e) = 89 °C; T_g (f) = 88 °C.

12.1.6.3 TGA

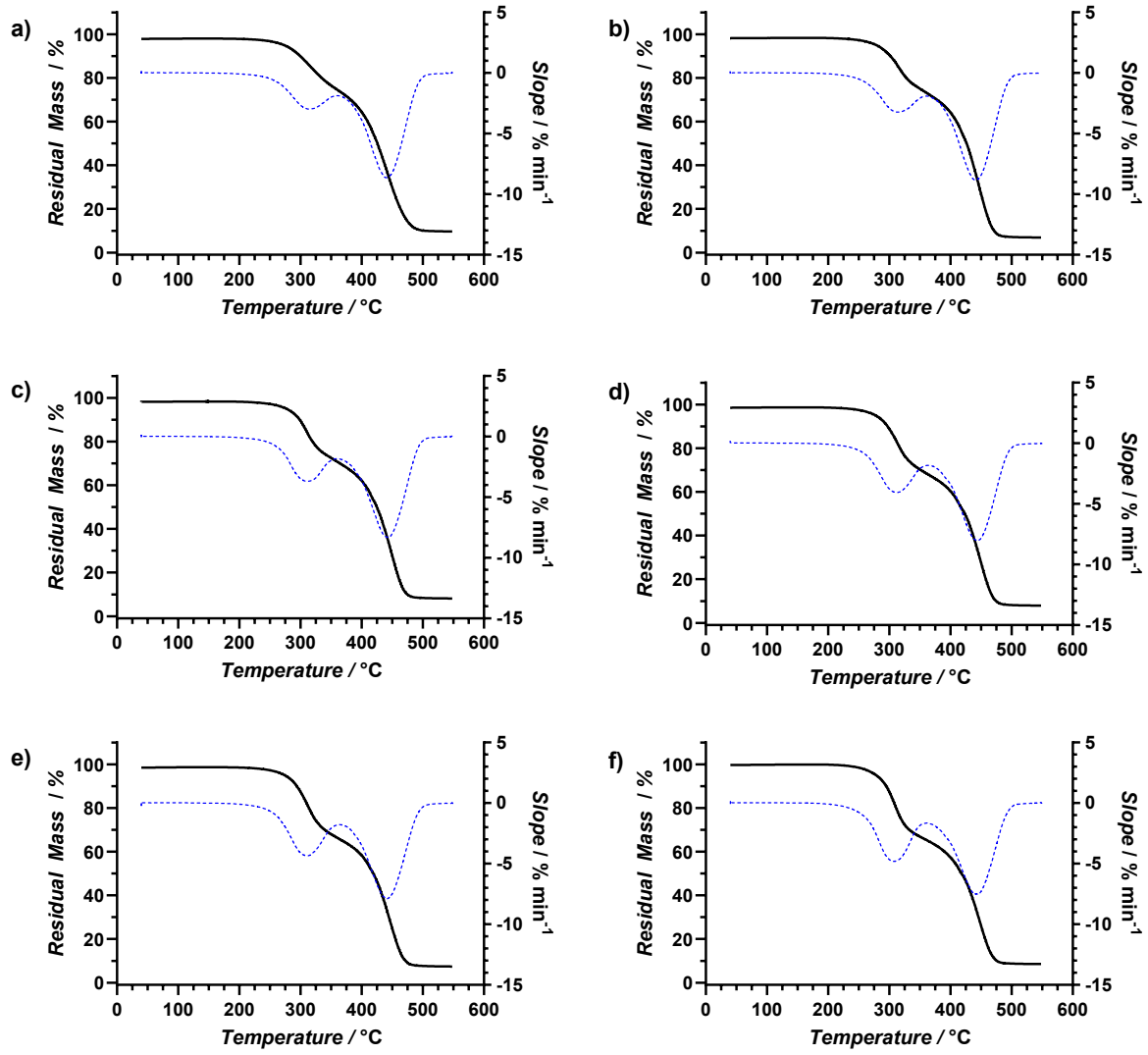

Appendix, Figure 59: TGA **mPEG-II/apolar-Ia-f**. Degradation temperatures can be found at the end of the respective chapter.

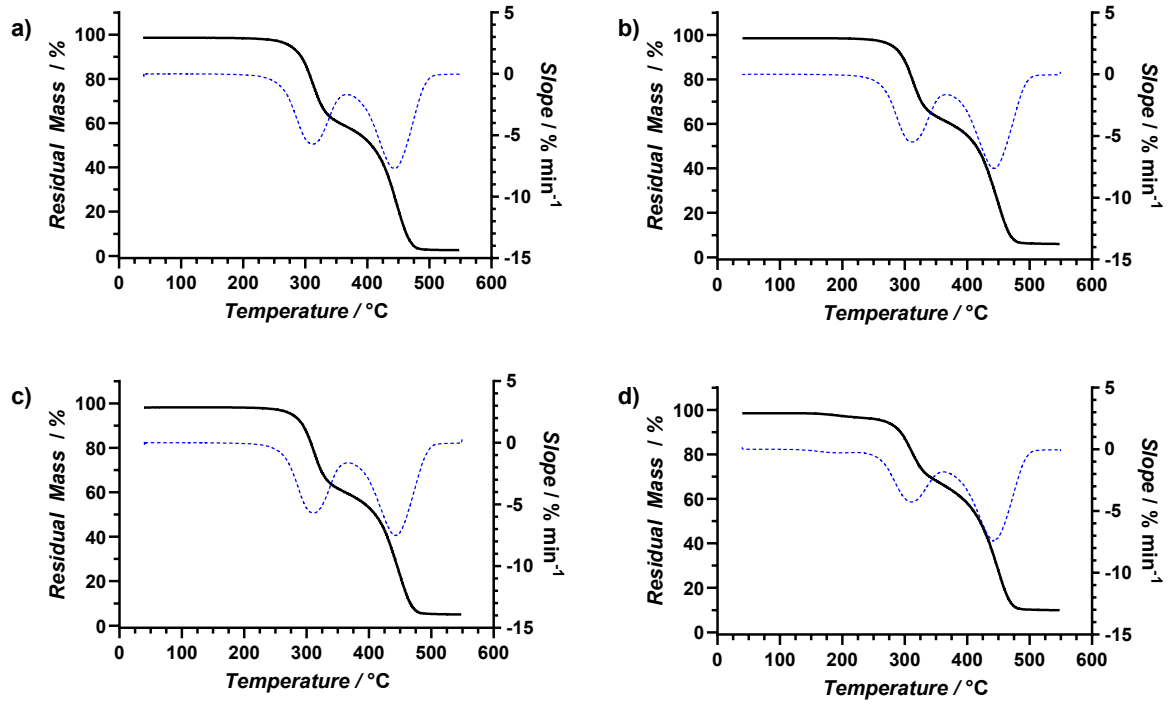

Appendix, Figure 60: TGA **mPEG-II/apolar-Ig-j**. Degradation temperatures can be found at the end of the respective chapter.

12.2 Section 6: Synthesis of optimized polymers

12.2.1 Radical Polymerization - Additional analytical data

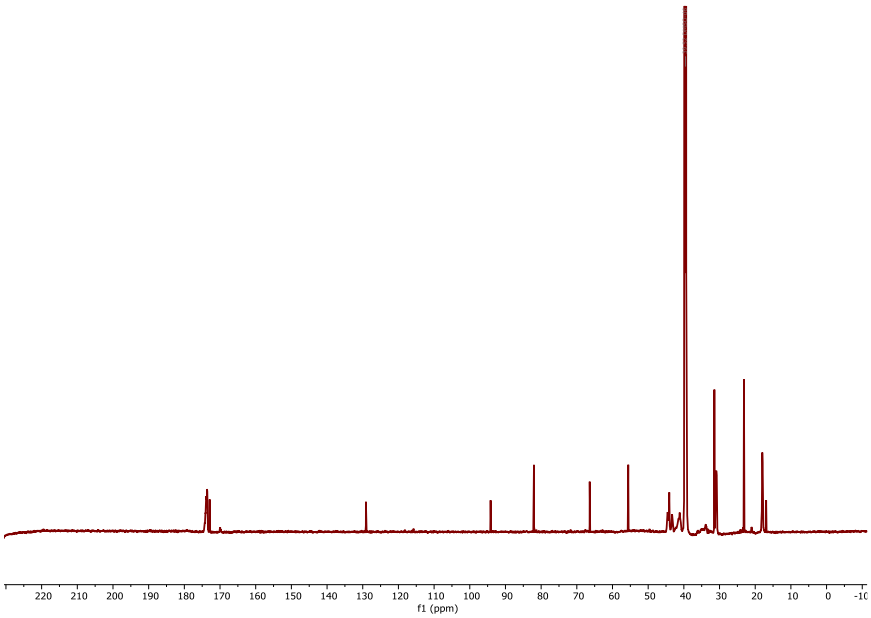

Appendix, Figure 61: Quantitative ^{13}C-NMR spectrum of commercially obtained batch of **RAD-I** at a concentration of 200 mg mL^{-1}. 512 scans with addition of Cr(acac)$_3$ as relaxation agent to reduce T_2 relaxation and increase resolution at a relaxation delay of 15 s.

12.2.1.1 Process Development

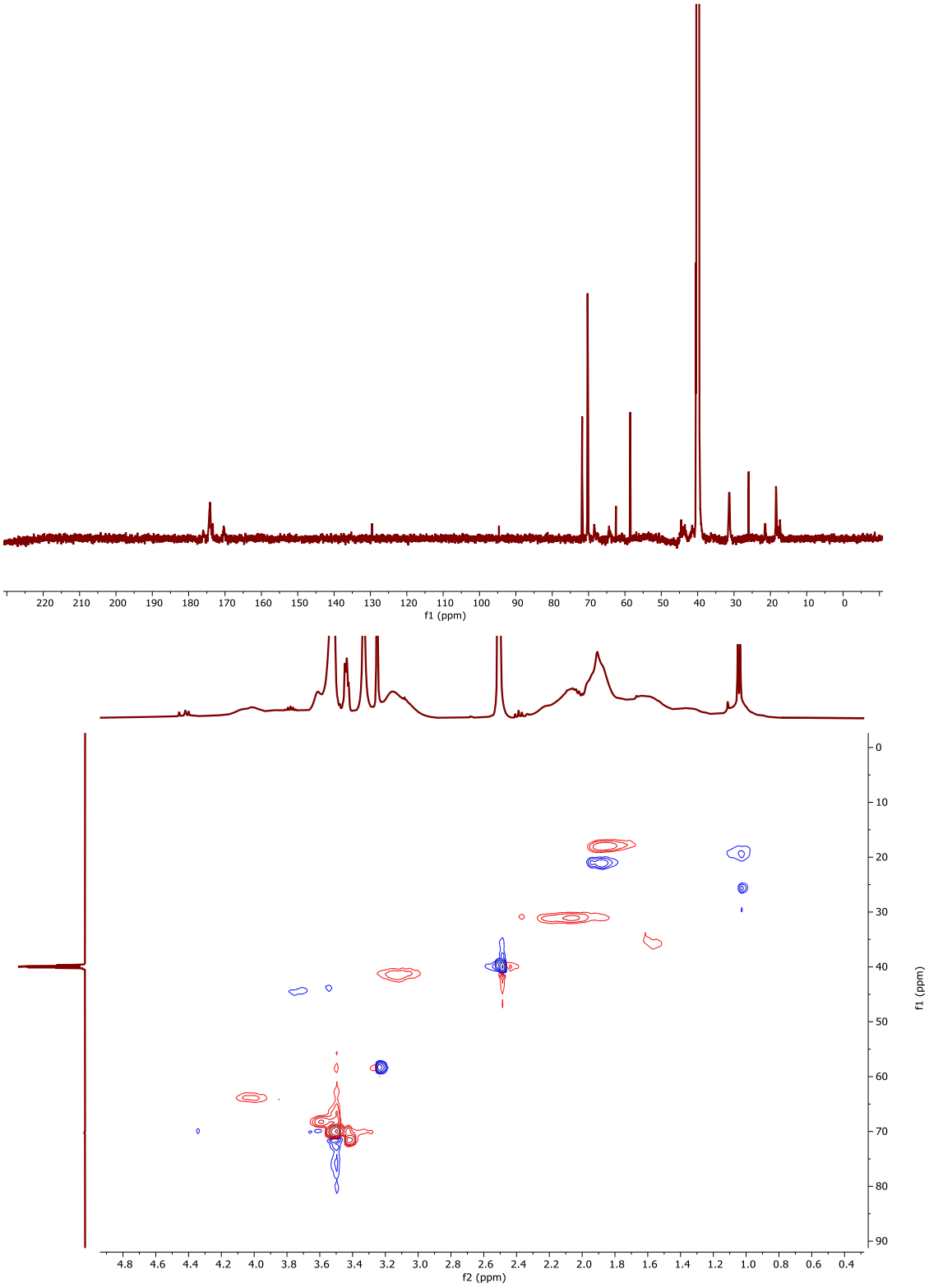

Appendix, Figure 62: RAD-III 13C NMR (top) and HSQC NMR (bottom).

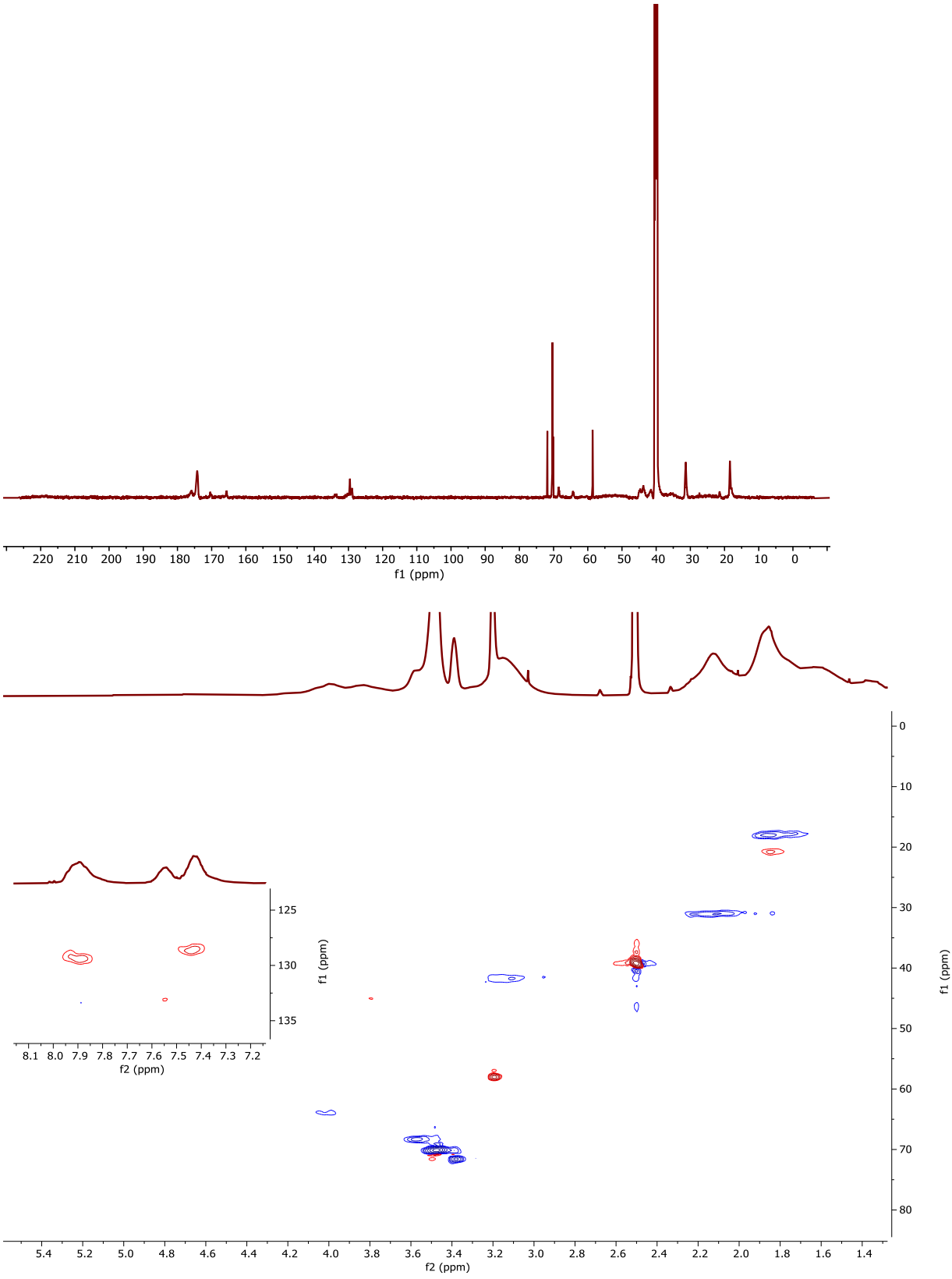

Appendix, Figure 63:RAD-IV 13C NMR in(top) and HSQC NMR (bottom).

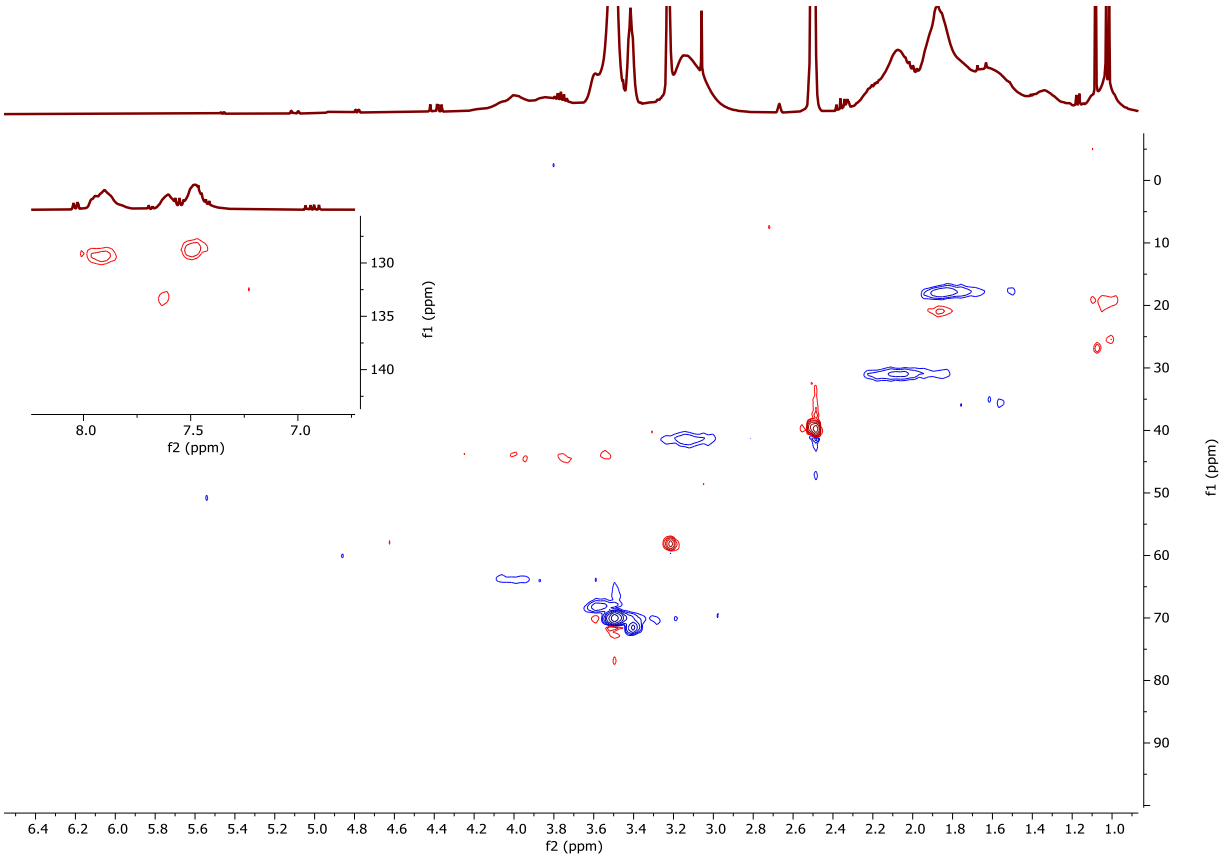

Appendix, Figure 64:RAD-V HSQC NMR.

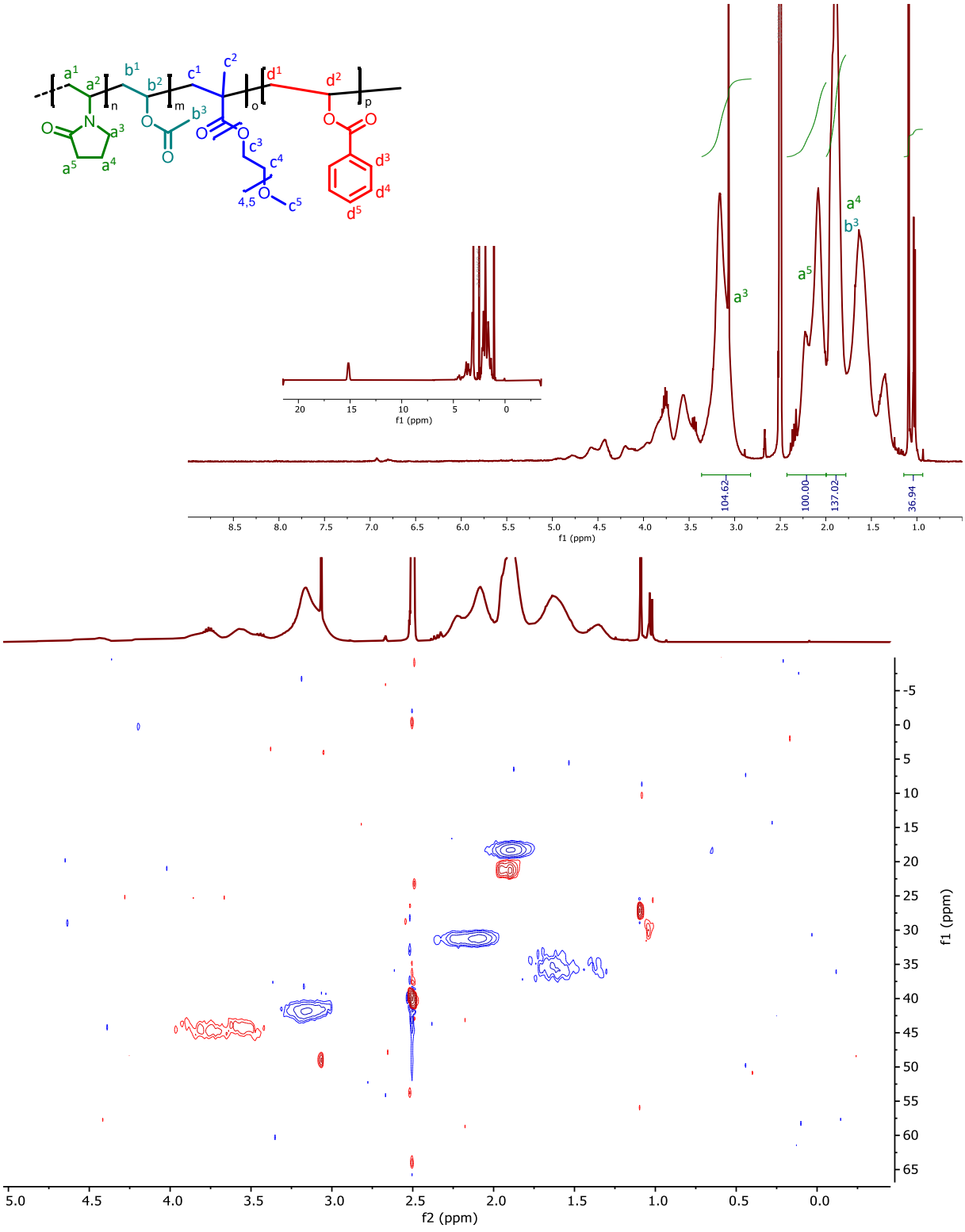

Appendix, Figure 65: ^{1}H-NMR spectrum of **RAD-VII**, monomer distribution **M-I/M-II/M-III/M-IV** 69%/27%/0%/4% (top). HSQC spectrum (bottom) with the addition of TFA. Referenced to the solvent d_6-DMSO.

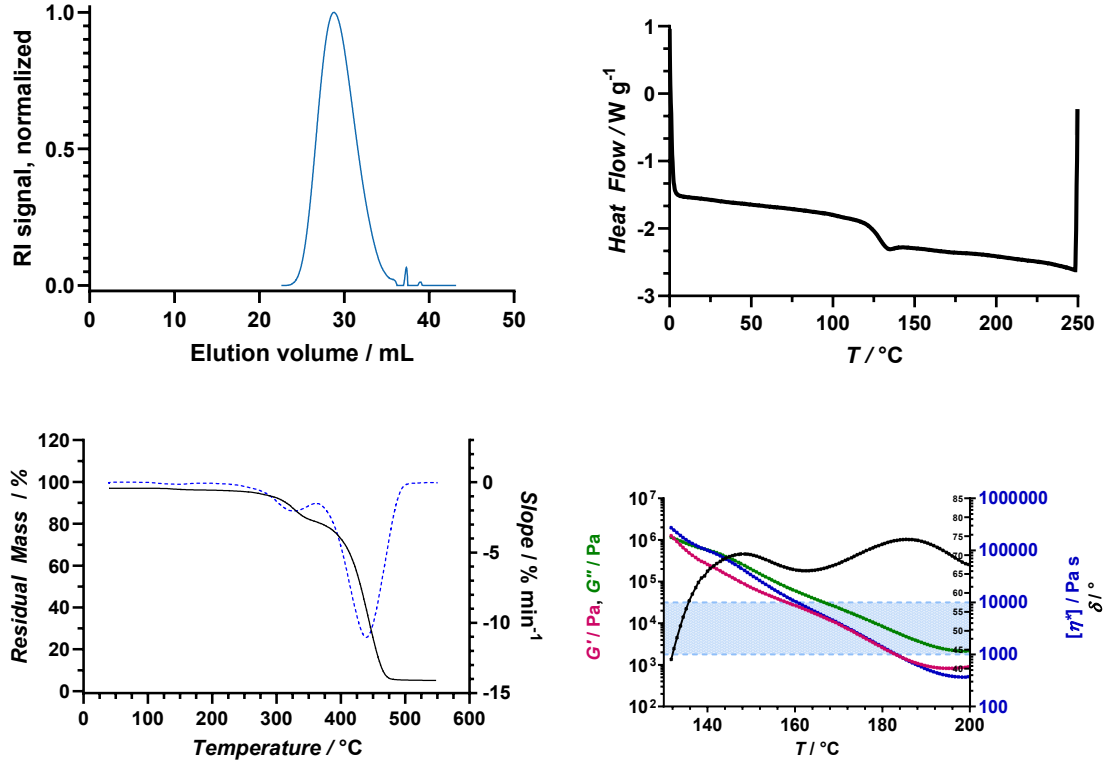

Appendix, Figure 66: Characterization of **RAD-VII**: a) GPC-Elugram of **RAD-VII** with normalized RI signal. Measurement calibrated against PMMA standards in DMAc with 0.6 g L^{-1}LiBr; M_w = 12000 g mol^{-1} b) DSC thermogram of **RAD-VII** with a T_g = 131 °C c) TGA thermogram of **RAD-VII** (black) and the respective 1st derivative (blue) with a T_{deg} = 226 °C. d) Melt rheogram of **RAD-VII**, $T_{1,10000\ Pa\ s}$ = 160 °C $T_{2,1000\ Pa\ s}$ = 183 °C blue area confined by dashed lines indicates melt viscosity between η_{melt} = 1000 Pa s and η_{melt} = 10000 Pa s, blue: melt viscosity η_{melt}, red: G', blue: G'', black: phase angle.

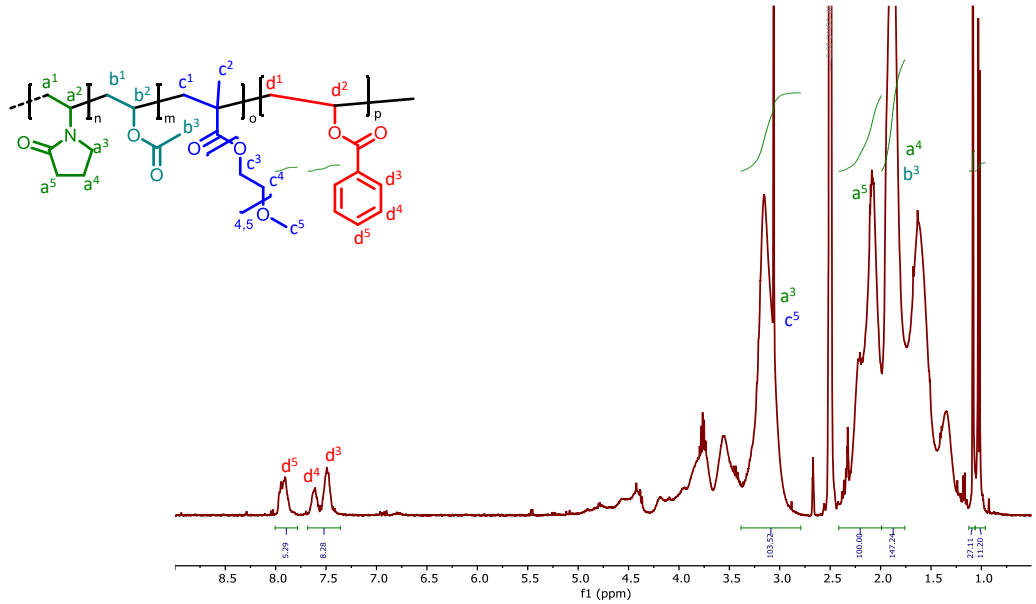

Appendix, Figure 67: ^{1}H-NMR spectrum of **RAD-VIII** (top) and HSQC spectrum (bottom) with the addition of TFA. Referenced to the solvent d_6-DMSO.

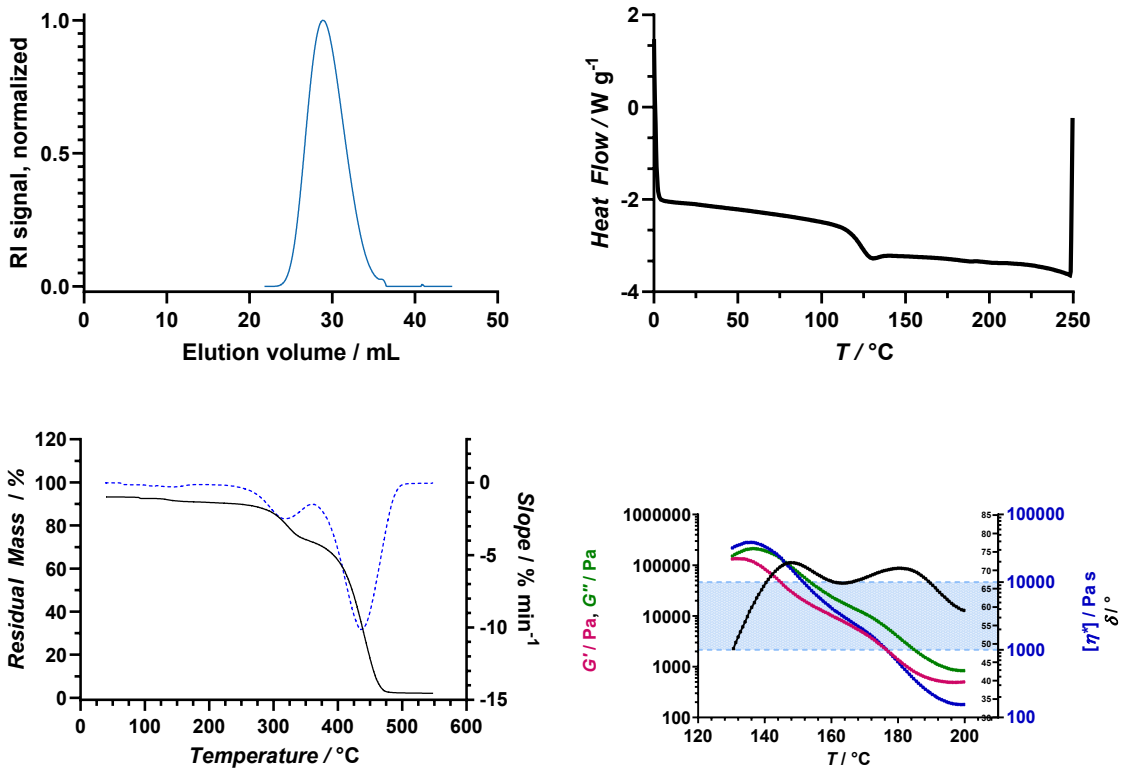

Appendix, Figure 68: Characterization of **RAD-VIII**: a) GPC-Elugram of **RAD-VIII** with normalized RI signal. Measurement calibrated against PMMA standards in DMAc with 0.6 g L^{-1}LiBr; M_w = 11000 g mol^{-1} b) DSC thermogram of **RAD-VIII** with a T_g = 121 °C c) TGA thermogram of **RAD-VIII** (black) and the respective 1st derivative (blue) with a T_{deg} = 212 °C. d) Melt rheogram of **RAD-VIII**, $T_{1,10000\ Pa\ s}$ = 152 °C $T_{2,1000\ Pa\ s}$ = 176 °C blue area confined by dashed lines indicates melt viscosity between η_{melt} = 1000 Pa s and η_{melt} = 10000 Pa s, blue: melt viscosity η_{melt}, red: G', blue: G'', black: phase angle.

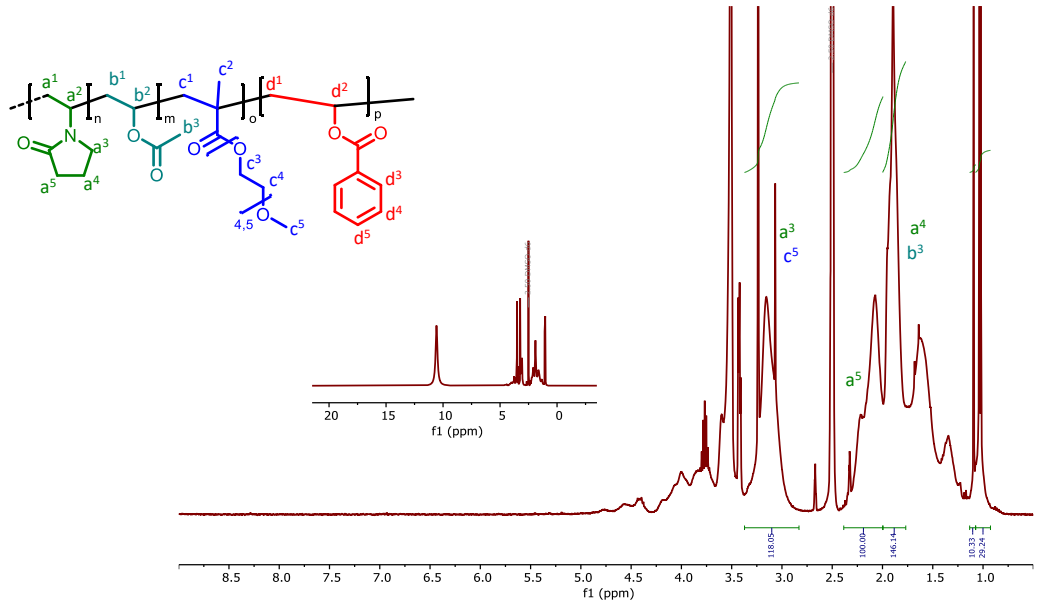

Appendix, Figure 69: ^{1}H-NMR spectrum of **RAD-IX** (top) and HSQC spectrum (bottom) with the addition of TFA. Referenced to the solvent d_6-DMSO.

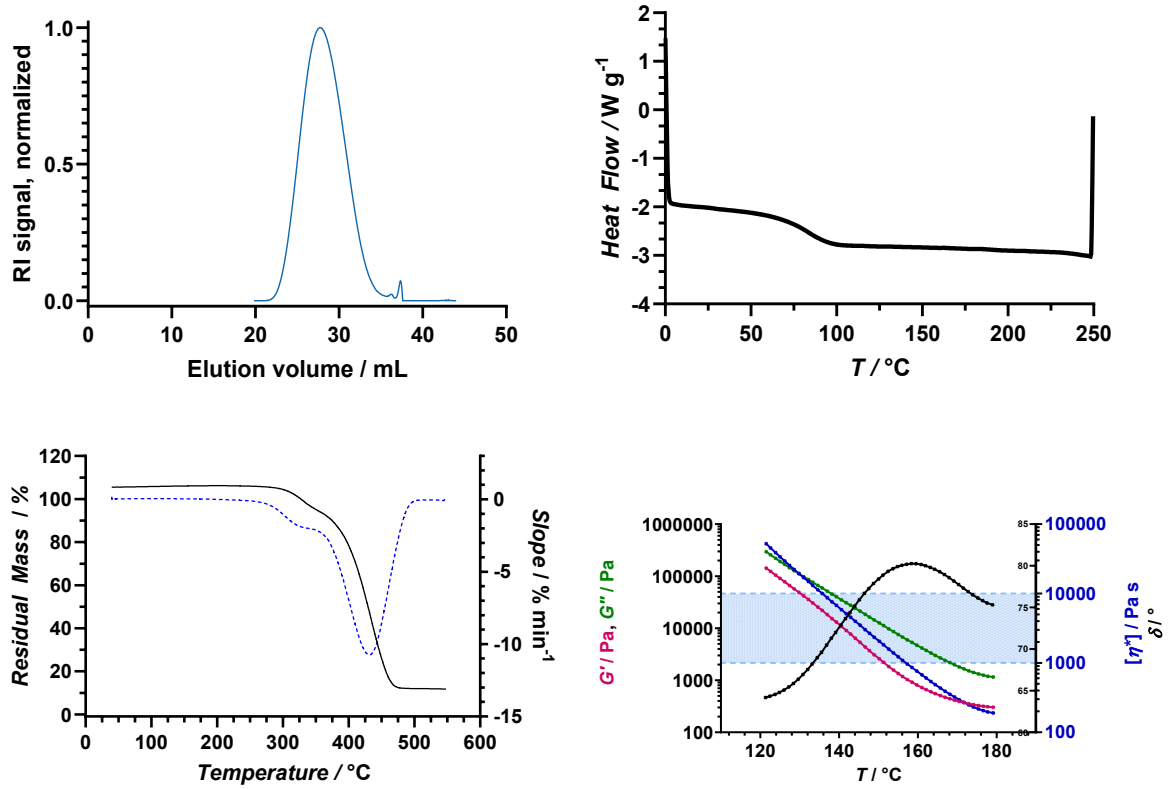

Appendix, Figure 70: Characterization of **RAD-IX**: a) GPC-Elugram of **RAD-IX** with normalized RI signal. Measurement calibrated against PMMA standards in DMAc with 0.6 g L^{-1}LiBr; M_w = 21000 g mol^{-1} b) DSC thermogram of **RAD-IX** with a T_g = 87 °C c) TGA thermogram of **RAD-IX** (black) and the respective 1st derivative (blue) with a T_{deg} = 223 °C. d) Melt rheogram of **RAD-IX**, $T_{1,10000\ Pa\ s}$ = 136 °C $T_{2,1000\ Pa\ s}$ = 157 °C blue area confined by dashed lines indicates melt viscosity between η_{melt} = 1000 Pa s and η_{melt} = 10000 Pa s, blue: melt viscosity η_{melt}, red: G', blue: G'', black: phase angle.

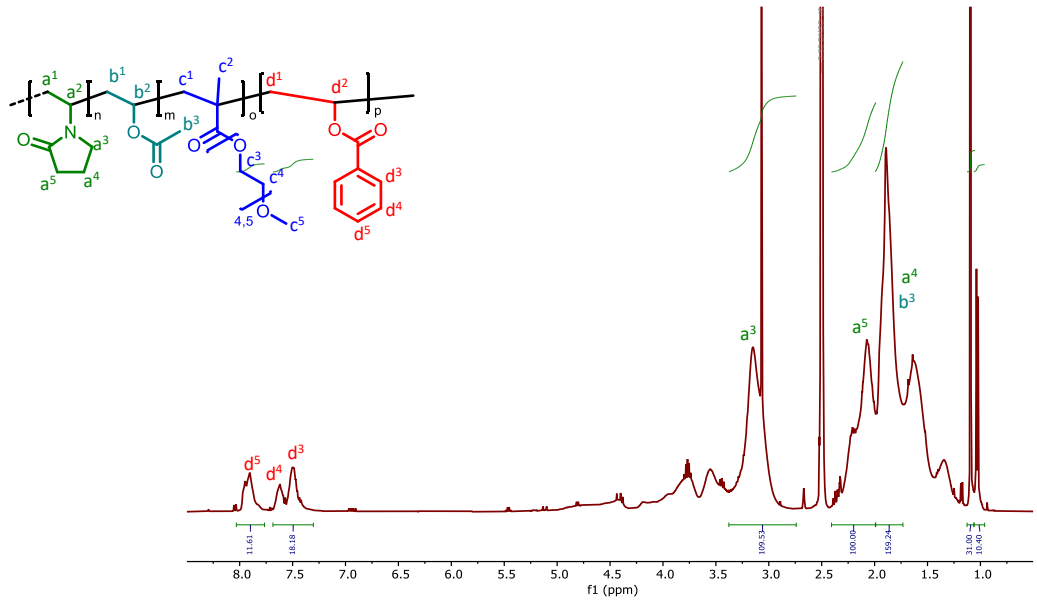

Appendix, Figure 71: 1H-NMR spectrum of **RAD-X**, monomer distribution M-I/M-II/M-III/M-IV 66%/26%/0%/8% measured in d6-DMSO with the addition of TFA.

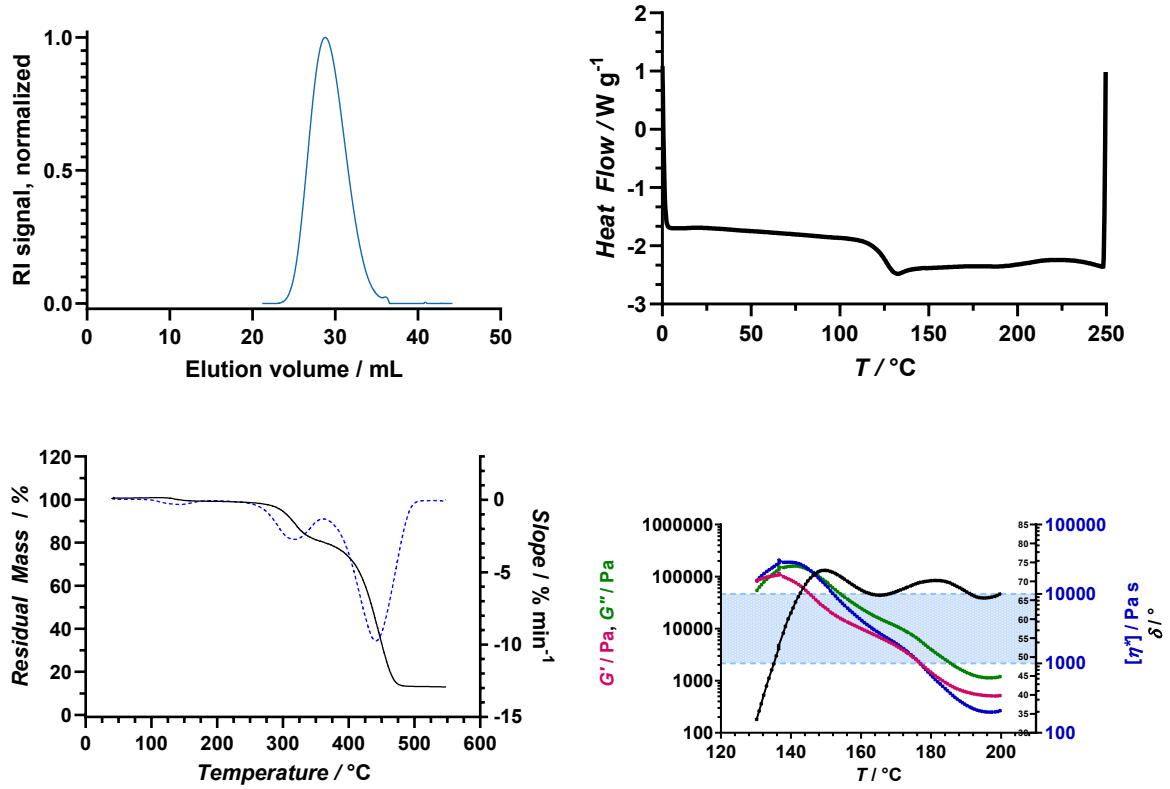

Appendix, Figure 72: Characterization of **RAD-X**: a) GPC-Elugram of **RAD-X** with normalized RI signal. Measurement calibrated against PMMA standards in DMAc with 0.6 g L^{-1}LiBr; M_w = 12000 g mol^{-1} b) DSC thermogram of **RAD-X** with a T_g = 126 °C c) TGA thermogram of **RAD-X** (black) and the respective 1st derivative (blue) with a T_{deg} = 226 °C. d) Melt rheogram of **RAD-X**, $T_{1,10000\ Pa\ s}$ = 152 °C $T_{2,1000\ Pa\ s}$ = 177 °C blue area confined by dashed lines indicates melt viscosity between η_{melt} = 1000 Pa s and η_{melt} = 10000 Pa s, blue: melt viscosity η_{melt}, red: G', blue: G'', black: phase angle.

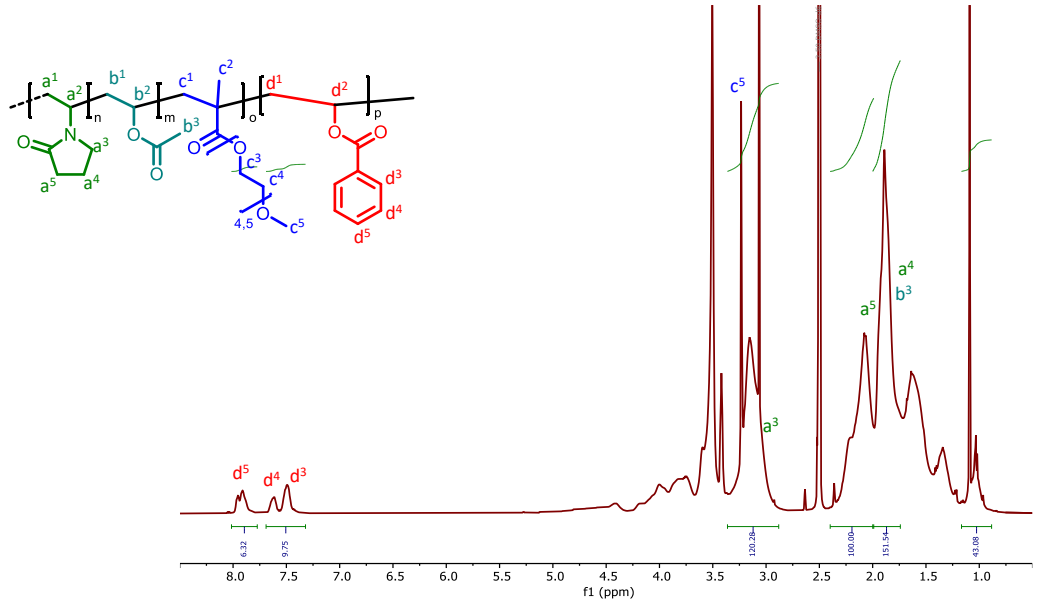

Appendix, Figure 73: 1H-NMR spectrum of **RAD-XI**, monomer distribution M-I/M-II/M-III/M-IV 66%/25%/5%/4% measured in d6-DMSO with the addition of TFA.

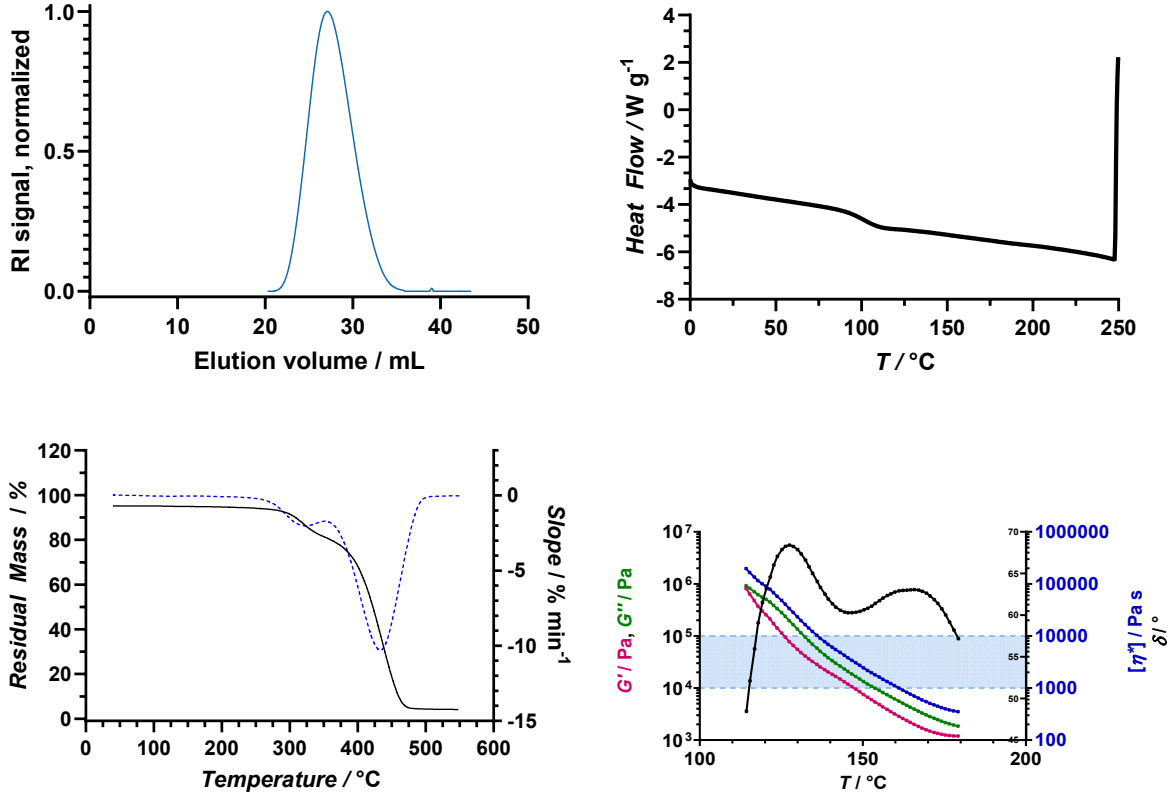

Appendix, Figure 74: Characterization of **RAD-XI**: a) GPC-Elugram of **RAD-XI** with normalized RI signal. Measurement calibrated against PMMA standards in DMAc with 0.6 g L^{-1}LiBr; M_w = 26000 g mol^{-1} b) DSC thermogram of **RAD-XI** with a T_g = 94 °C c) TGA thermogram of **RAD-XI** (black) and the respective 1st derivative (blue) with a T_{deg} = 225 °C. d) Melt rheogram of **RAD-XI**, $T_{1,10000\ Pa\ s}$ = 126 °C $T_{2,1000\ Pa\ s}$ = 146 °C blue area confined by dashed lines indicates melt viscosity between η_{melt} = 1000 Pa s and η_{melt} = 10000 Pa s, blue: melt viscosity η_{melt}, red: G', blue: G'', black: phase angle.

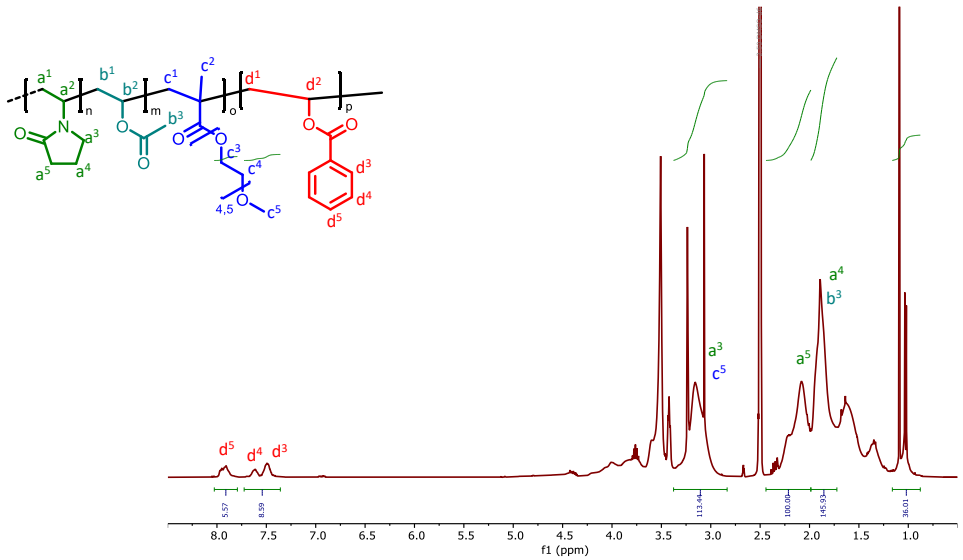

Appendix, Figure 75: 1H-NMR spectrum of **RAD-XII**, monomer distribution M-I/M-II/M-III/M-IV 65%/24%/7%/4% measured in d6-DMSO with the addition of TFA.

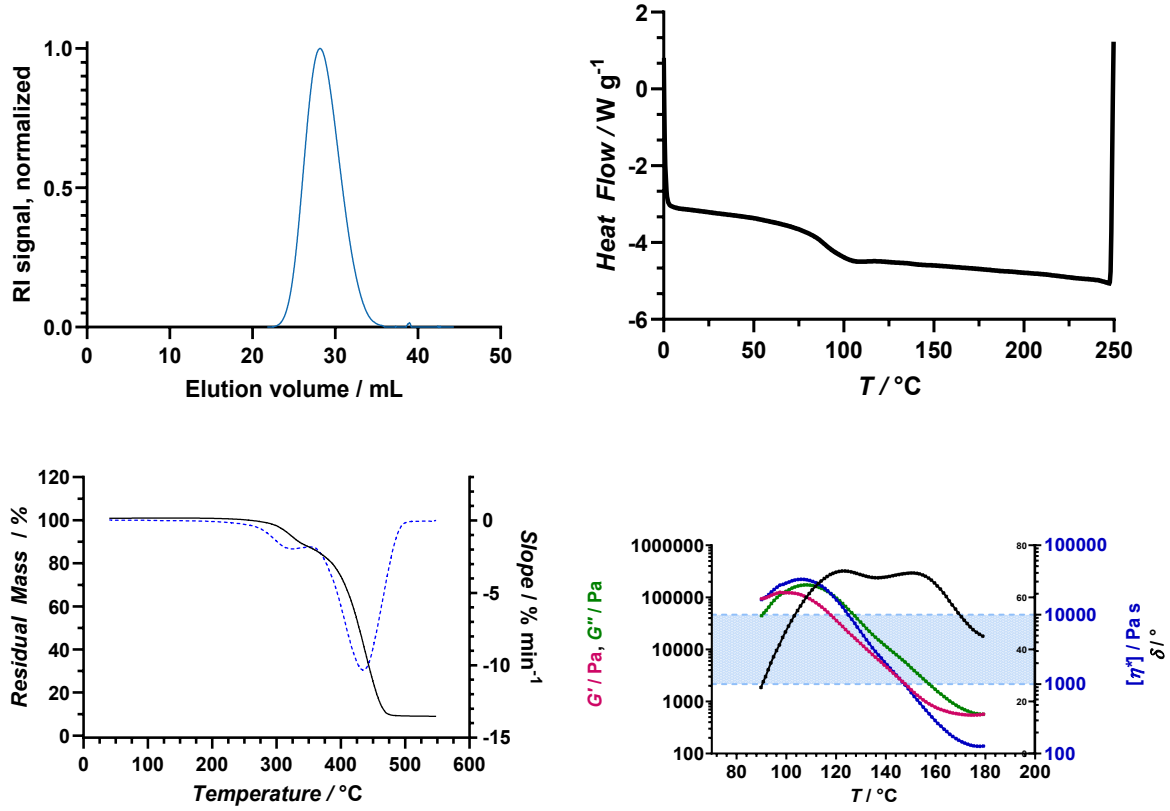

Appendix, Figure 76: Characterization of **RAD-XII**: a) GPC-Elugram of **RAD-XII** with normalized RI signal. Measurement calibrated against PMMA standards in DMAc with 0.6 g L^{-1}LiBr; M_w = 16000 g mol^{-1} b) DSC thermogram of **RAD-XII** with a T_g = 97 °C c) TGA thermogram of **RAD-XII** (black) and the respective 1st derivative (blue) with a T_{deg} = 200 °C. d) Melt rheogram of **RAD-XII**, $T_{1,10000\ Pa\ s}$ = 125 °C $T_{2,1000\ Pa\ s}$ = 148 °C blue area confined by dashed lines indicates melt viscosity between η_{melt} = 1000 Pa s and η_{melt} = 10000 Pa s, blue: melt viscosity η_{melt}, red: G', blue: G'', black: phase angle.

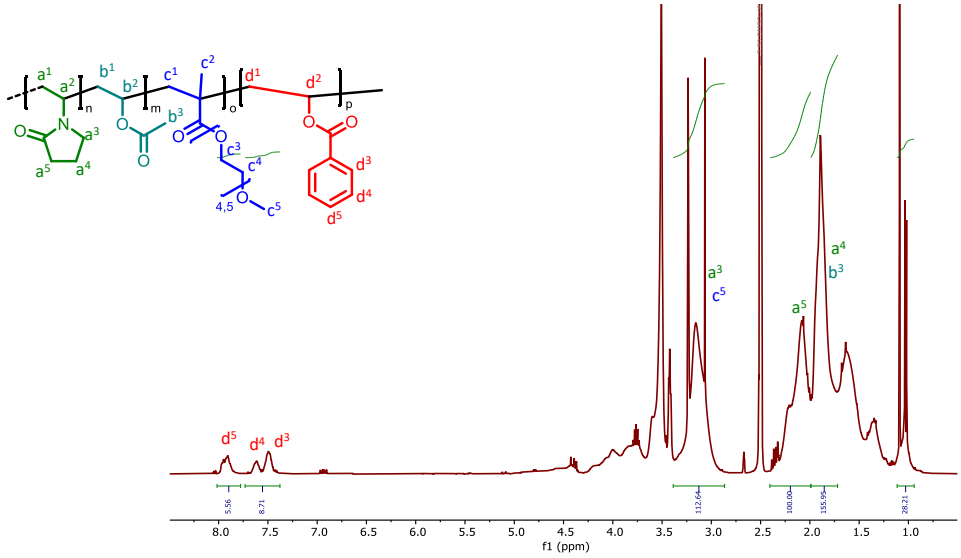

Appendix, Figure 77: 1H-NMR spectrum of RAD-XIII, monomer distribution M-I/M-II/M-III/M-IV 70%/21%/5%/4% measured in d6-DMSO with the addition of TFA.

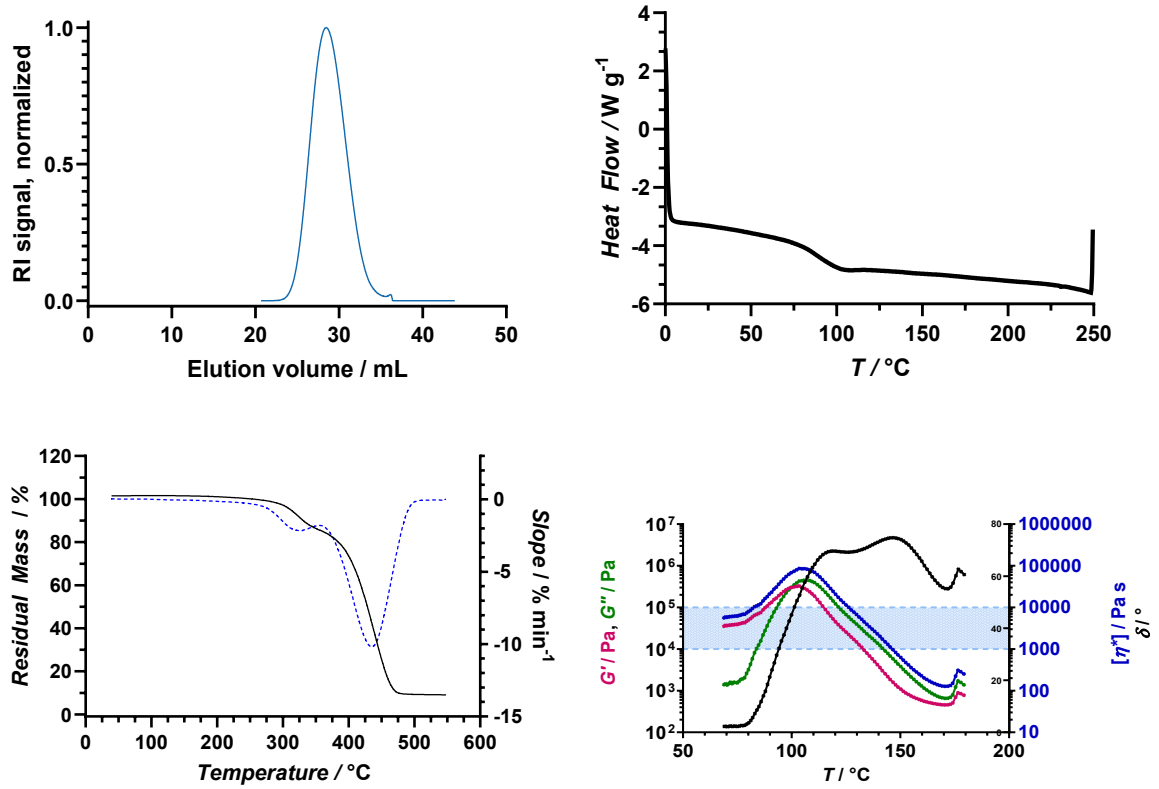

Appendix, Figure 78: Characterization of **RAD-XIII**: a) GPC-Elugram of **RAD-XIII** with normalized RI signal. Measurement calibrated against PMMA standards in DMAc with 0.6 g L^{-1}LiBr; M_w = 14000 g mol^{-1} b) DSC thermogram of **RAD-XIII** with a T_g = 103 °C c) TGA thermogram of **RAD-XIII** (black) and the respective 1st derivative (blue) with a T_{deg} = 192 °C. d) Melt rheogram of **RAD-XIII**, $T_{1,10000\ Pa\ s}$ = 136 °C $T_{2,1000\ Pa\ s}$ = 161 °C blue area confined by dashed lines indicates melt viscosity between η_{melt} = 1000 Pa s and η_{melt} = 10000 Pa s, blue: melt viscosity η_{melt}, red: G', blue: G'', black: phase angle.

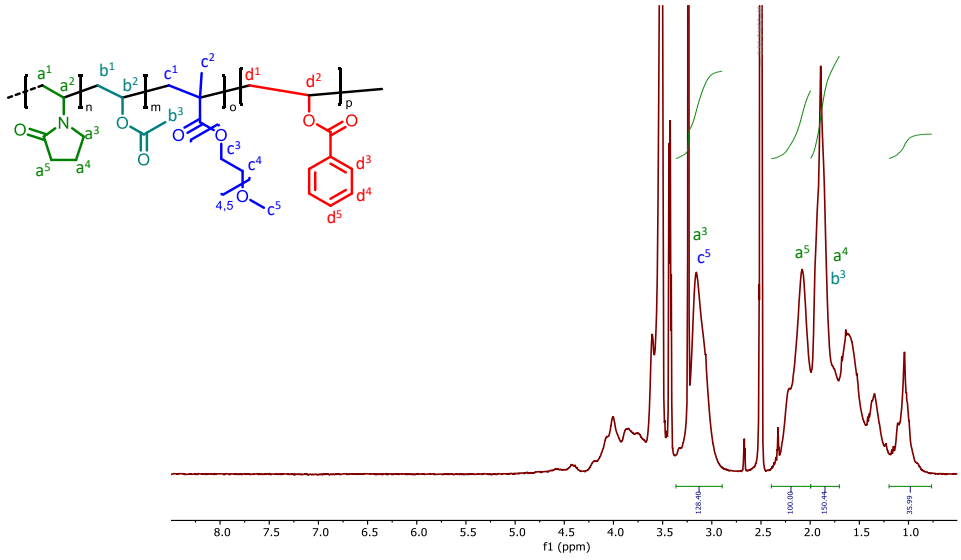

Appendix, Figure 79: 1H-NMR spectrum of RAD-XIV, monomer distribution M-I/M-II/M-III/M-IV 64%/23%/13%/0% measured in d6-DMSO with the addition of TFA.

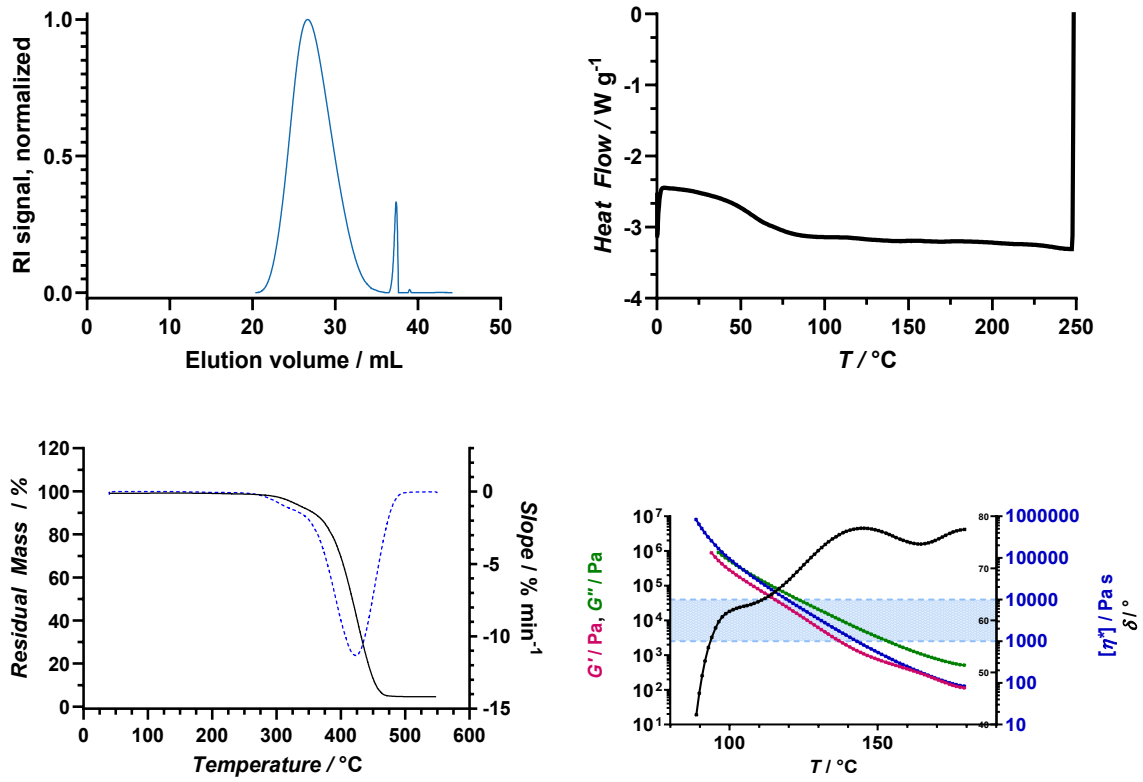

Appendix, Figure 80: Characterization of **RAD-XIV**: a) GPC-Elugram of **RAD-XIV** with normalized RI signal. Measurement calibrated against PMMA standards in DMAc with 0.6 g L^{-1}LiBr; M_w = 30000 g mol^{-1} b) DSC thermogram of **RAD-XIV** with a T_g = 66 °C c) TGA thermogram of **RAD-XIV** (black) and the respective 1st derivative (blue) with a T_{deg} = 214 °C. d) Melt rheogram of **RAD-XIV**, $T_{1,10000\ Pa\ s}$ = 119 °C $T_{2,1000\ Pa\ s}$ = 143 °C blue area confined by dashed lines indicates melt viscosity between η_{melt} = 1000 Pa s and η_{melt} = 10000 Pa s, blue: melt viscosity η_{melt}, red: G', blue: G'', black: phase angle.

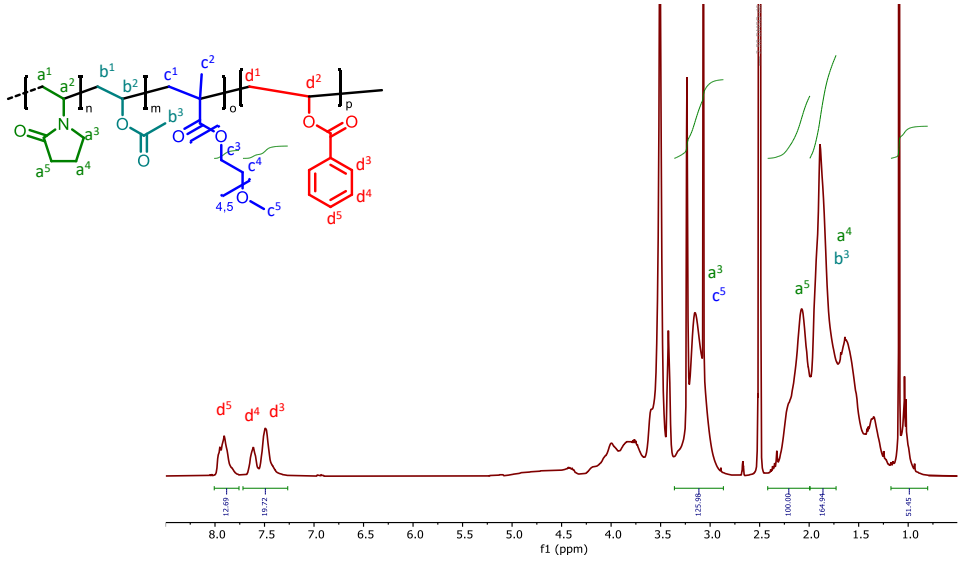

Appendix, Figure 81: 1H-NMR spectrum of RAD-XV, monomer distribution M-I/M-II/M-III/M-IV 60%/25%/7%/8% measured in d6-DMSO with the addition of TFA.

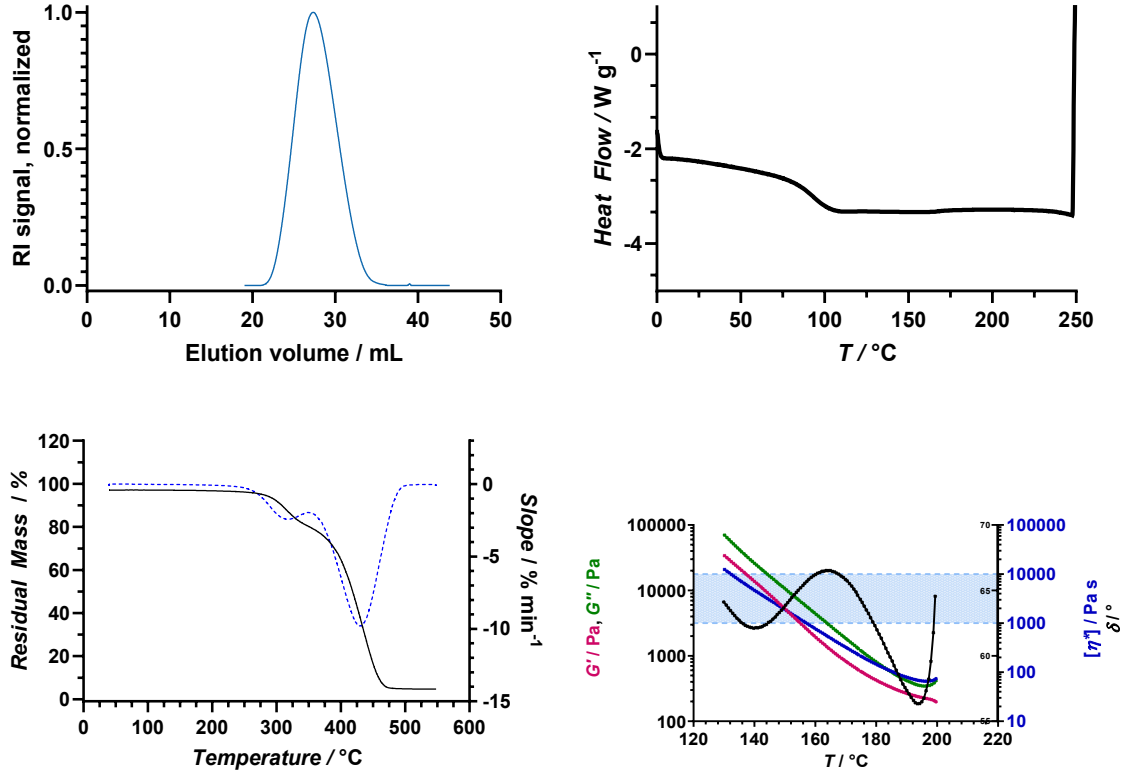

Appendix, Figure 82: Characterization of **RAD-XV**: a) GPC-Elugram of **RAD-XV** with normalized RI signal. Measurement calibrated against PMMA standards in DMAc with 0.6 g L^{-1}LiBr; M_w = 25000 g mol^{-1} b) DSC thermogram of **RAD-XV** with a T_g = 97 °C c) TGA thermogram of **RAD-XV** (black) and the respective 1st derivative (blue) with a T_{deg} = 221 °C. d) Melt rheogram of **RAD-XV**, $T_{1,10000\ Pa\ s}$ = 132 °C $T_{2,1000\ Pa\ s}$ = 157 °C blue area confined by dashed lines indicates melt viscosity between η_{melt} = 1000 Pa s and η_{melt} = 10000 Pa s, blue: melt viscosity η_{melt}, red: G', blue: G'', black: phase angle.

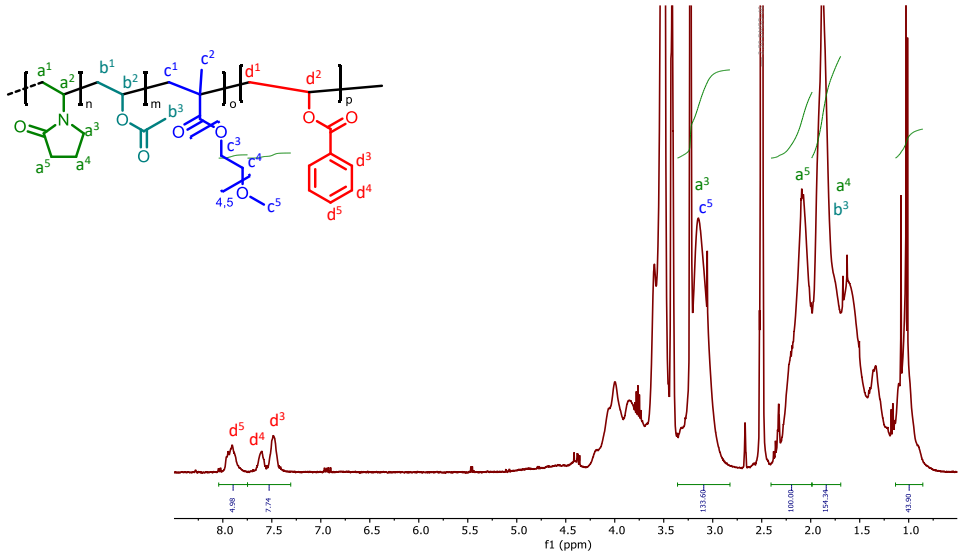

Appendix, Figure 83: 1H-NMR spectrum of RAD-XVI, monomer distribution M-I/M-II/M-III/M-IV 60%/23%/14%/3% measured in d6-DMSO with the addition of TFA.

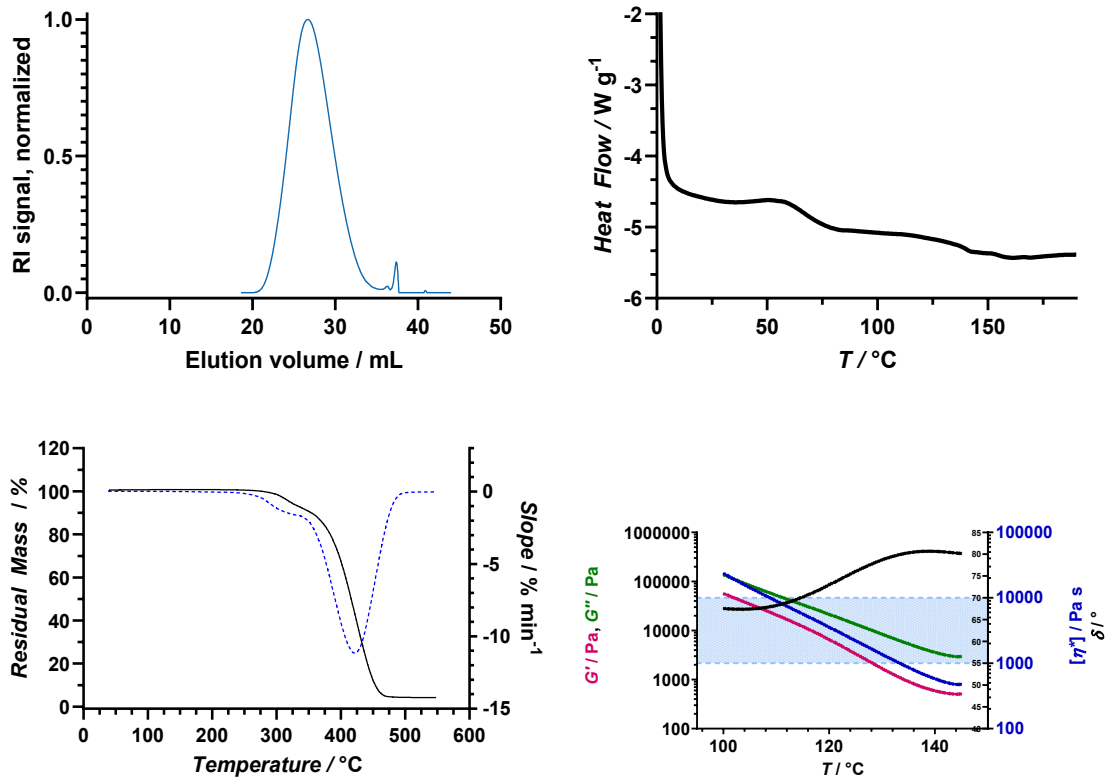

Appendix, Figure 84: Characterization of **RAD-XVI**: a) GPC-Elugram of **RAD-XVI** with normalized RI signal. Measurement calibrated against PMMA standards in DMAc with 0.6 g L^{-1}LiBr; M_w = 32000 g mol^{-1} b) DSC thermogram of **RAD-XVI** with a T_g = 68 °C c) TGA thermogram of **RAD-XVI** (black) and the respective 1st derivative (blue) with a T_{deg} = 224 °C. d) Melt rheogram of **RAD-XVI**, $T_{1,10000\ Pa\ s}$ = 109 °C $T_{2,1000\ Pa\ s}$ = 133 °C blue area confined by dashed lines indicates melt viscosity between η_{melt} = 1000 Pa s and η_{melt} = 10000 Pa s, blue: melt viscosity η_{melt}, red: G', blue: G'', black: phase angle.

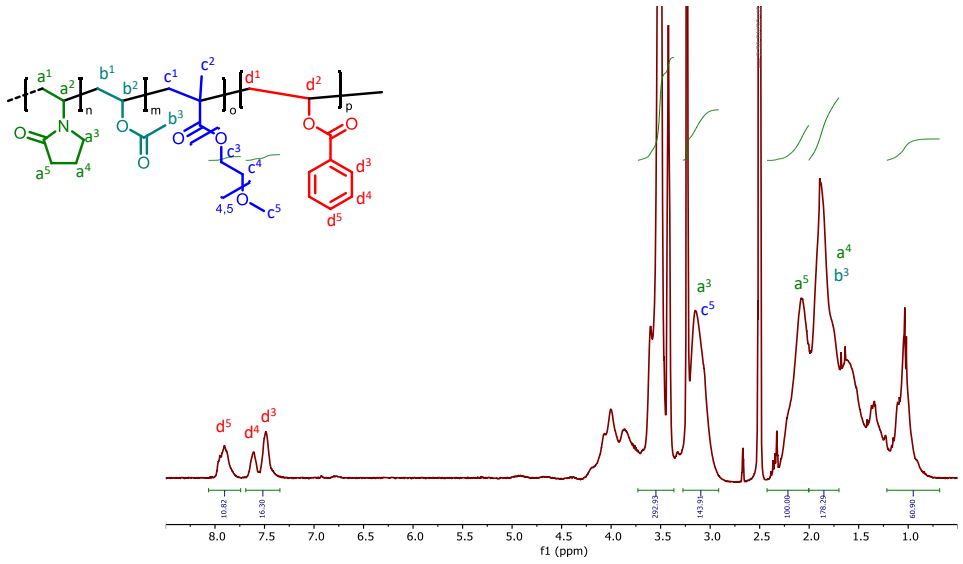

Appendix, Figure 85: 1H-NMR spectrum of RAD-XVI, monomer distribution M-I/M-II/M-III/M-IV 60%/23%/14%/3% measured in d6-DMSO with the addition of TFA.

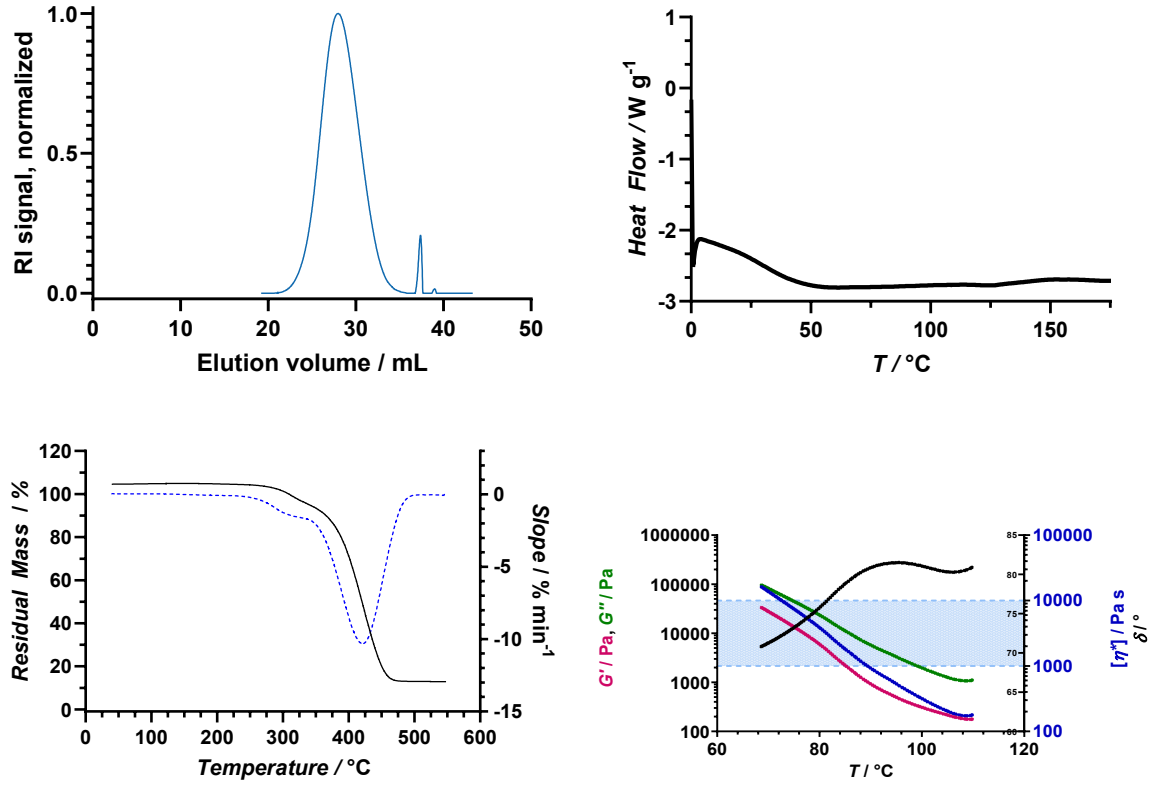

Appendix, Figure 86: Characterization of **RAD-XVII**: a) GPC-Elugram of **RAD-XVII** with normalized RI signal. Measurement calibrated against PMMA standards in DMAc with 0.6 g L^{-1}LiBr; M_w = 19000 g mol^{-1} b) DSC thermogram of **RAD-XVII** with a T_g = 38 °C c) TGA thermogram of **RAD-XVII** (black) and the respective 1st derivative (blue) with a T_{deg} = 220 °C. d) Melt rheogram of **RAD-XVII**, $T_{1,10000\ Pa\ s}$ = 73 °C $T_{2,1000\ Pa\ s}$ = 89 °C blue area confined by dashed lines indicates melt viscosity between η_{melt} = 1000 Pa s and η_{melt} = 10000 Pa s, blue: melt viscosity η_{melt}, red: G', blue: G'', black: phase angle.

12.2.2 Design of Experiments: Additional Figures

12.2.2.1 DoE Evaluation

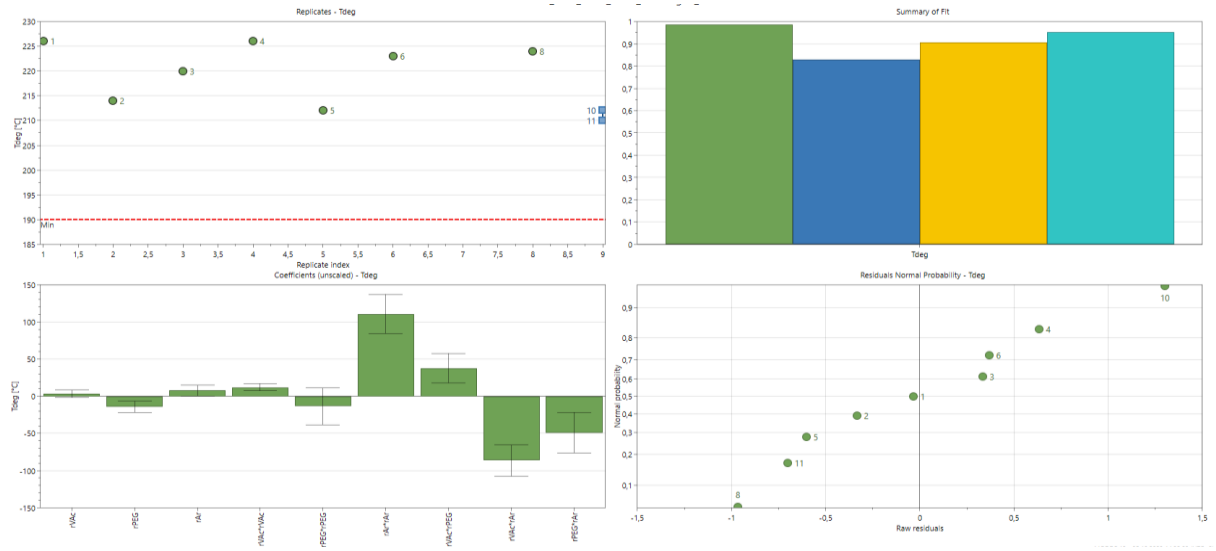

Appendix, Figure 87: Tdeg Replicates Residuals Summary. Experiment 9 excluded.

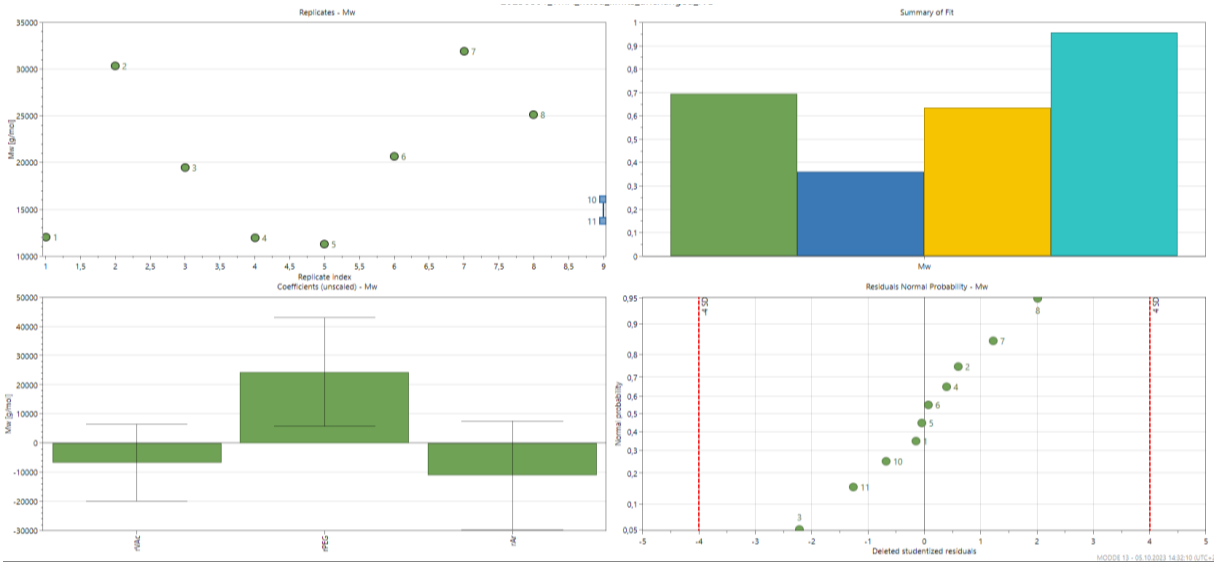

Appendix, Figure 88: Mw Replicates Residuals Summary

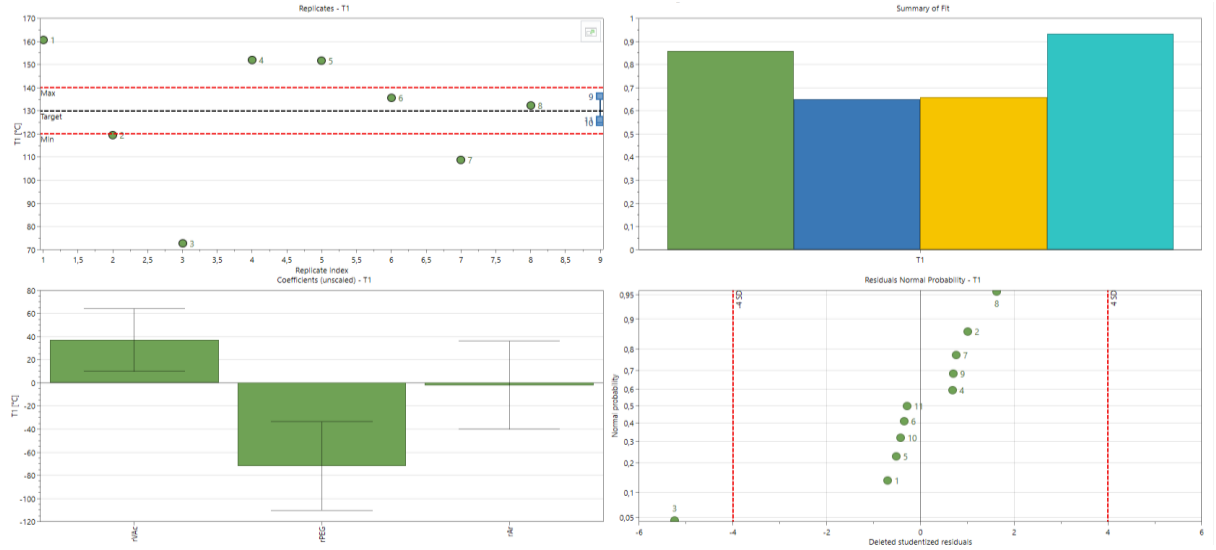

Appendix, Figure 89: T1 Replicates Residuals Summary

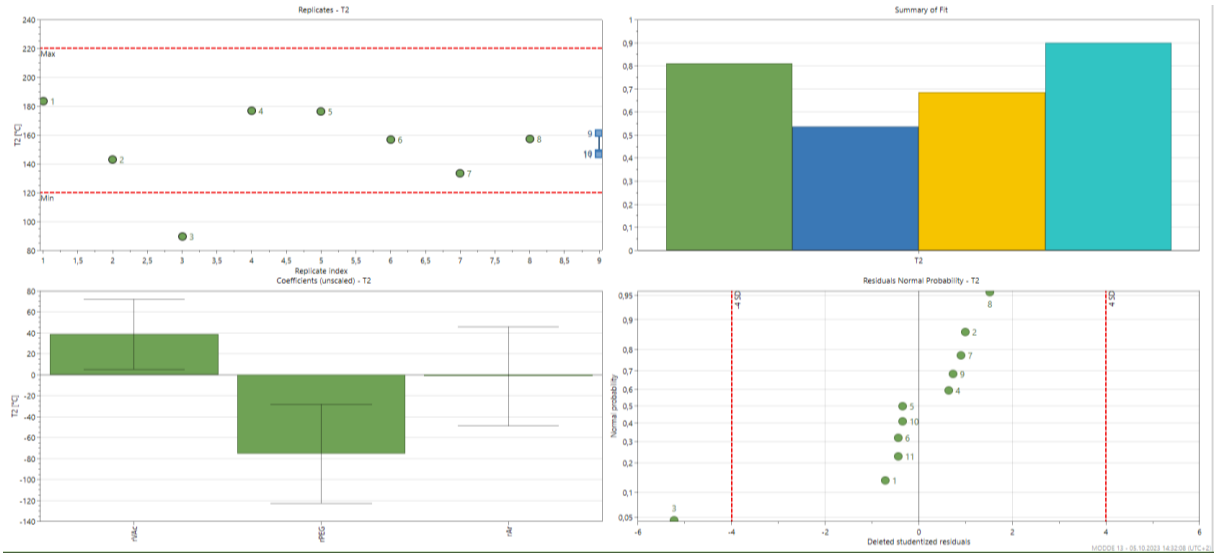

Appendix, Figure 90: T2 Replicates Residuals Summary

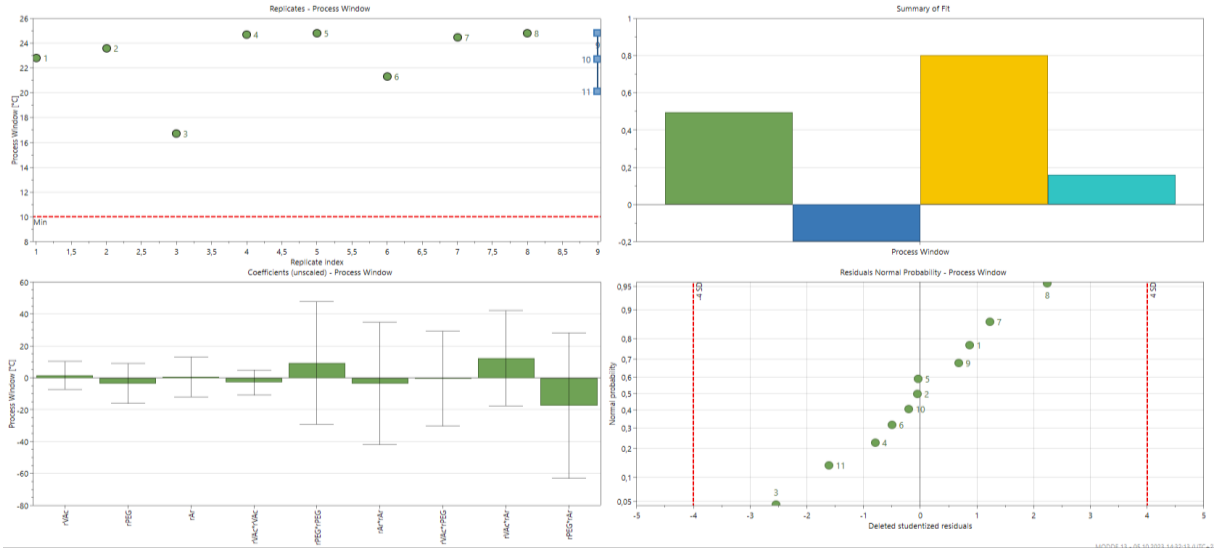

Appendix, Figure 91: Process Window Replicates Residuals Summary

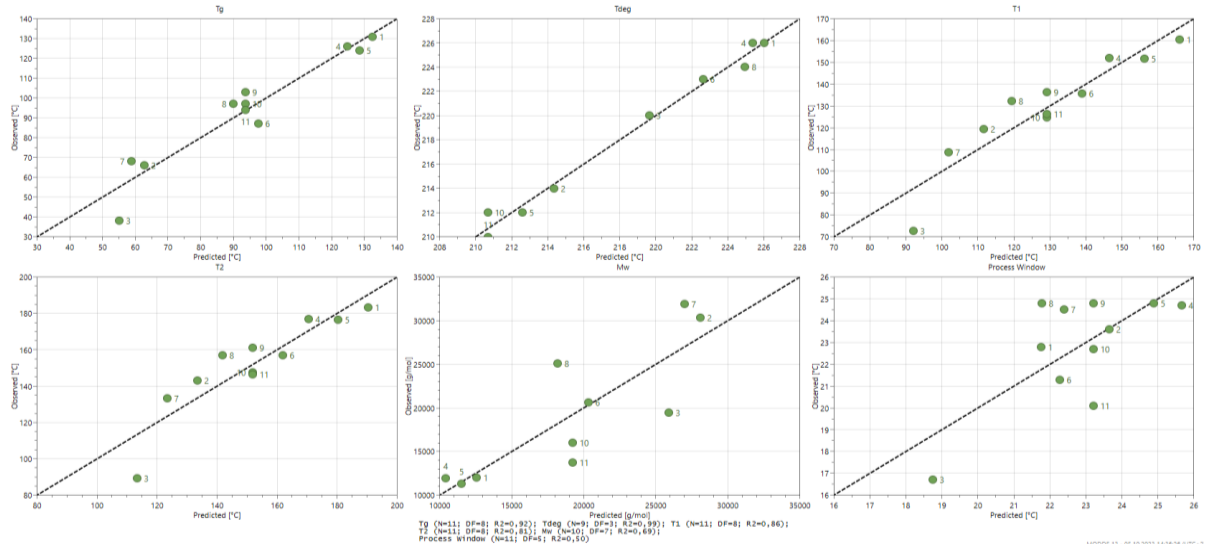

Appendix, Figure 92: Observed vs Predicted Summary Responses

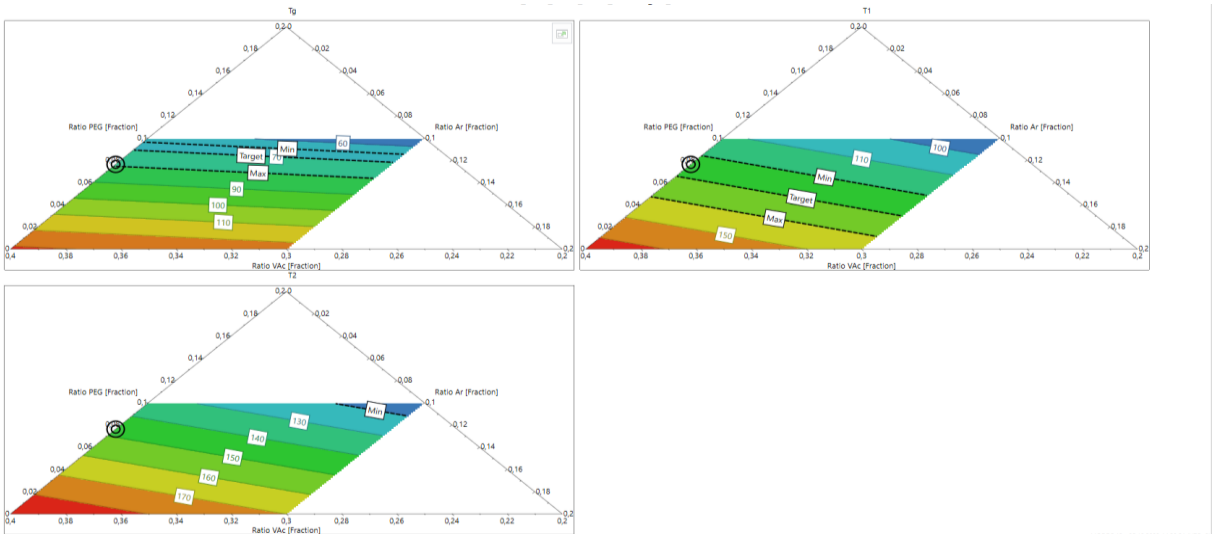

Appendix, Figure 93: Response Contour Plot

12.2.2.2 Sweet Spot analysis and Upscale

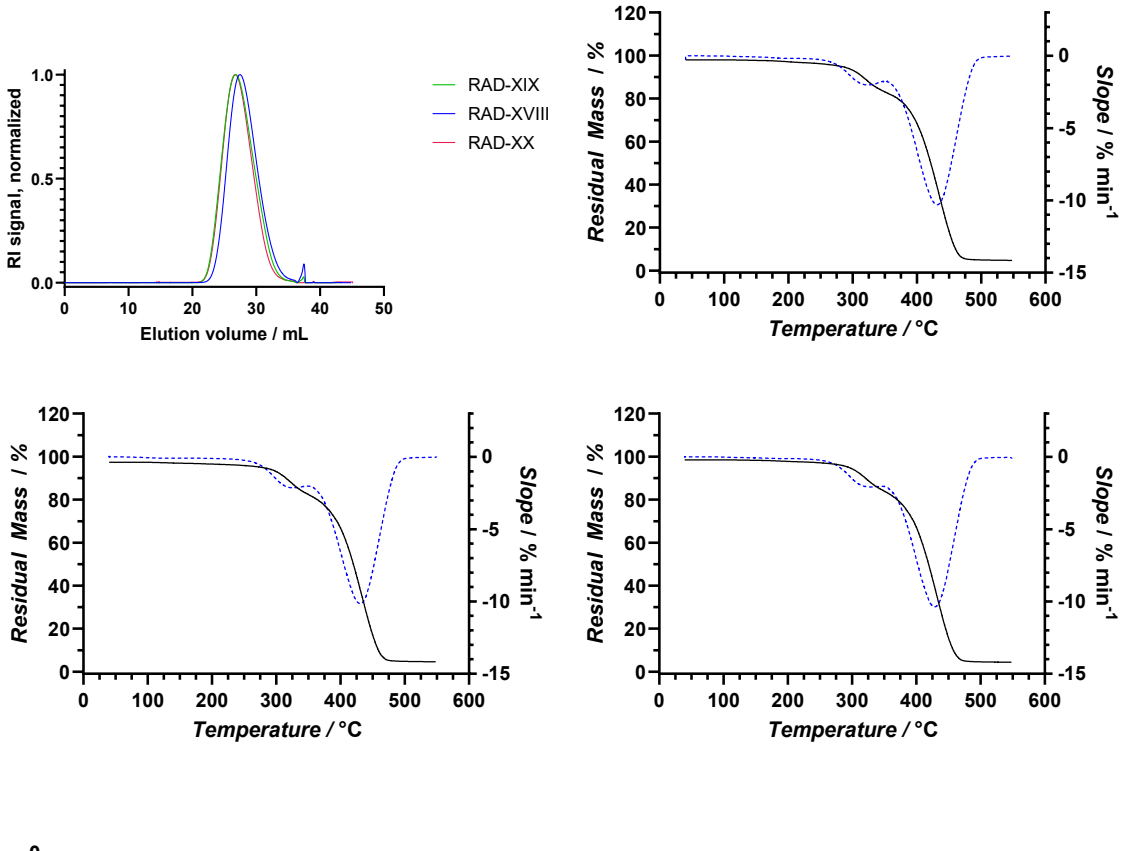

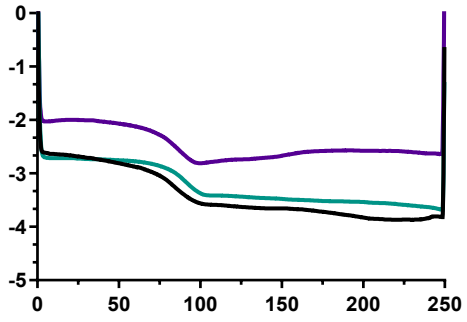

Parameter	Target	Achieved	
Ratio M-I	60 %	62%	± 2%
Ratio M-II	30%	24%	± 2%
Ratio M-III	5%	9%	± 1%
Ratio M-IV	5%	4%	± 0%
M_W / g mol^{-1}		28000	± 4000
$Đ$		3.0	± 0.3
T_g / °C	80-90	88	± 2
T_{deg} / °C	>200	225	± 5

Appendix, Figure 94: Characterization of **RAD-XVIII**, **RAD-XIX**, and **RAD-XX**: a) Overlay of GPC-Elugrams with normalized RI signal. Measurement calibrated against PMMA standards in DMAc with 0.6 g L^{-1}LiBr with M_w(**RAD-XVIII**) = 22000 g mol^{-1} M_w(**RAD-XIX**) = 30000 g mol^{-1} M_w(**RAD-XX**) = 31000 g mol^{-1} b) TGA thermogram of **RAD-XVIII** (black) and the respective 1st derivative (blue) with a T_{deg} = 233 °C. c) TGA thermogram of **RAD-XIX** (black) and the respective 1st derivative (blue) with a T_{deg} = 227 °C. d) TGA thermogram of **RAD-XX** (black) and the respective 1st derivative (blue) with a T_{deg} = 222 °C. e) Overlay of DSC thermograms with T_g(**RAD-XVIII**) = 89 °C, T_g(**RAD-XIX**) = 90 °C, T_g(**RAD-XX**) = 86 °C f) Summary of data with variation ranges.

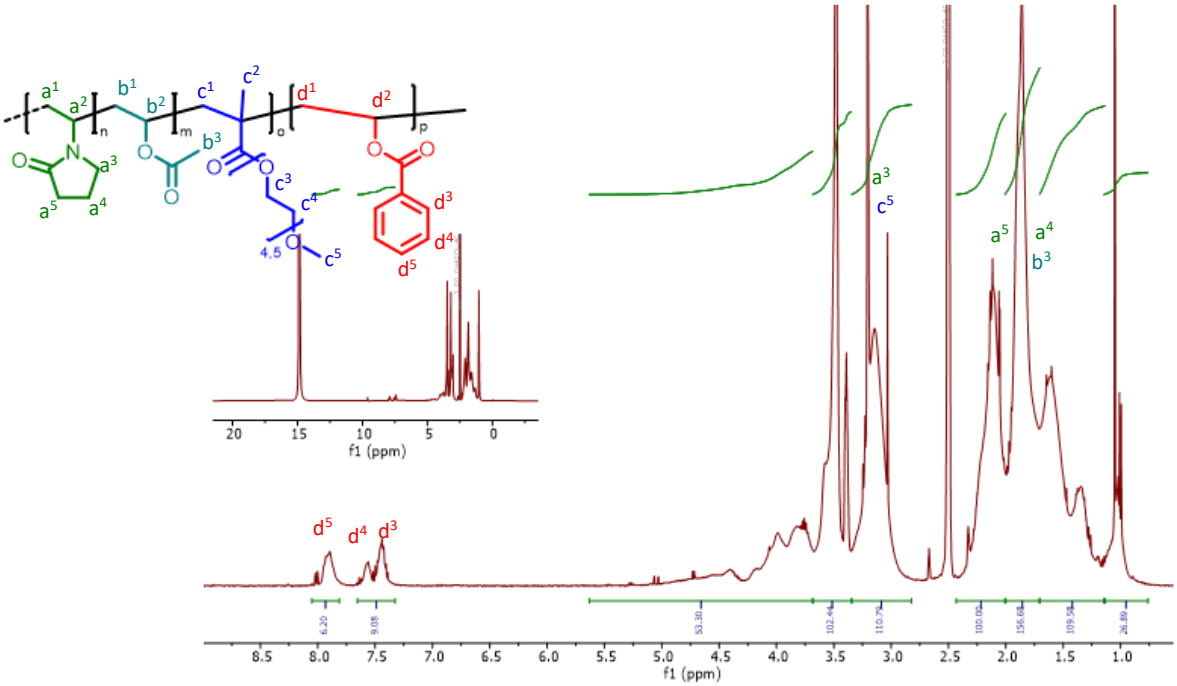

Appendix, Figure 95: ^{1}H-NMR spectrum of **RAD-XVII**, monomer distribution M-I/M-II/M-III/M-IV 64%/22%/9%/4% measured in d_6-DMSO with the addition of TFA.

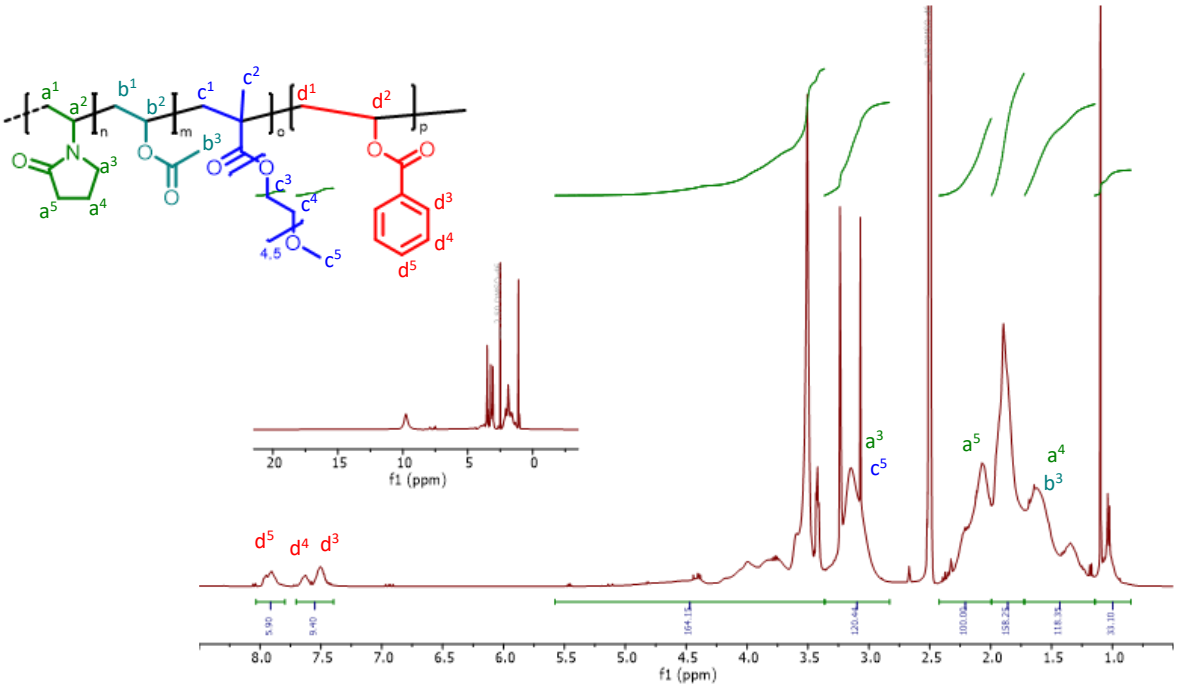

Appendix, Figure 96: ^{1}H-NMR spectrum of **RAD-XVIII**, monomer distribution M-I/M-II/M-III/M-IV 63%/24%/9%/4% measured in d_6-DMSO with the addition of TFA.

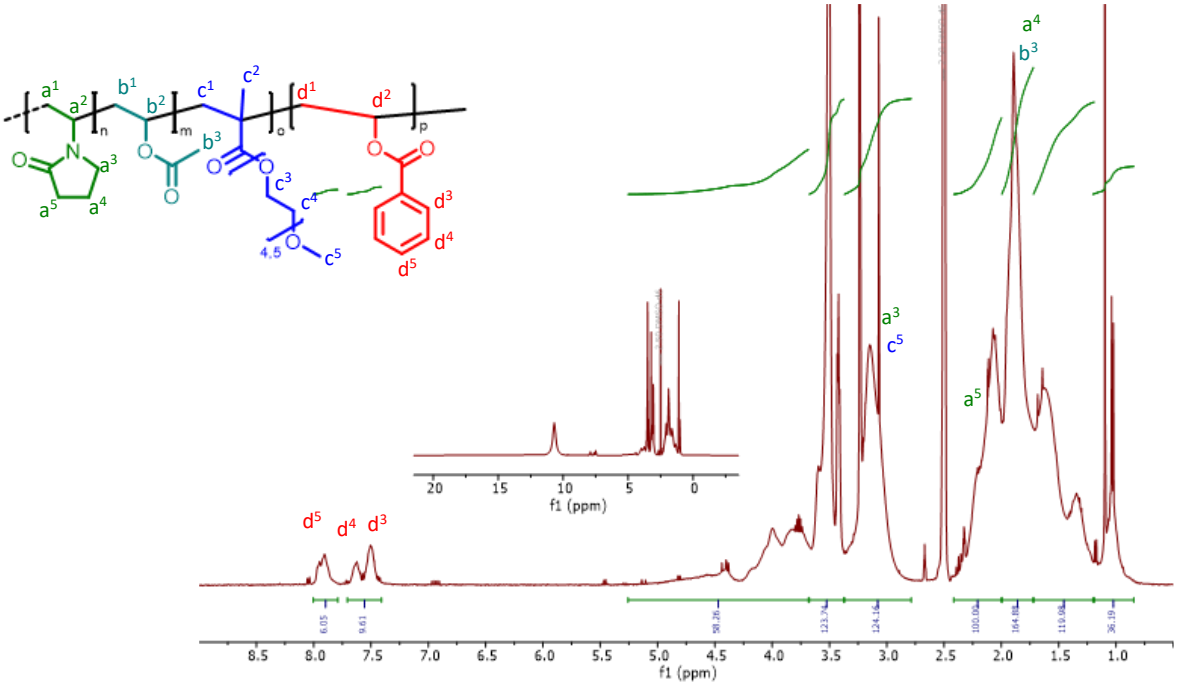

Appendix, Figure 97: ^{1}H-NMR spectrum of **RAD-XIX**, monomer distribution M-I/M-II/M-III/M-IV 60%/26%/10%/4% measured in d_6-DMSO with the addition of TFA.

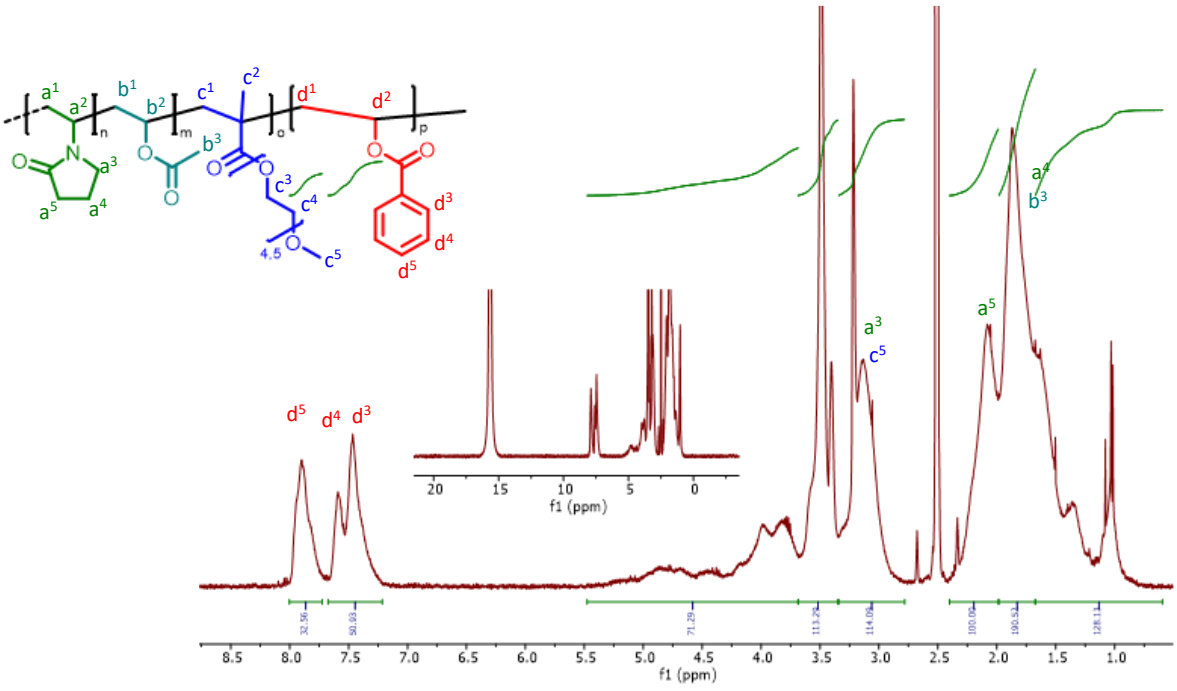

Appendix, Figure 98: ^{1}H-NMR spectrum of **RAD-XX**, monomer distribution M-I/M-II/M-III/M-IV 49%/30%/5%/16% measured in d_6-DMSO with the addition of TFA.

12.2.3 Extrusion Data

Table 72: Summary table for Extrusion Data for PVAc-co-PVP and RAD-VII.

Sample	**PVAc-co-PVP**	**PVAc-co-PVP**	**PVAc-co-PVP**	**RAD-VII**	**RAD-VII**	**RAD-VII**	**RAD-VII**
Temperature / °C	100/110/110	100/120/120	100/130/130	120/160/160	120/170/170	120/180/180	130/190/190
RPM	300	300	300	300	300	300	300
Average Torque / Nm	2.50	1.50	1.50	1.45	1.40	1.40	1.40
Nozzle	1.5	1.5	1.5	1.5	1.5	1.5	1.5
Appearance	yellow	yellow	yellow	colorless	colorless	colorless	colorless
Translucence	transparent	transparent	transparent	transparent	transparent	transparent	transparent
Flexibility	brittle	brittle	brittle	brittle	brittle	brittle	brittle
Extrusion possible	yes	yes	yes	yes	yes	yes	yes
Filament	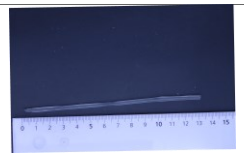	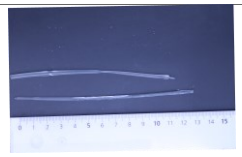	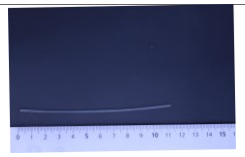	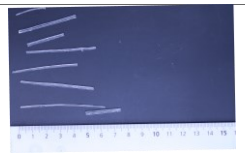	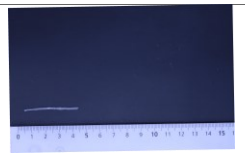	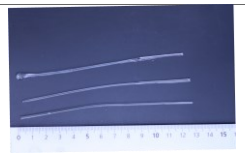	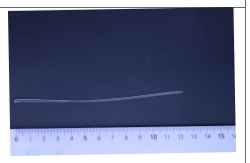

Table 73: Summary table for Extrusion Data for RAD-VIII and RAD-IX.

Sample	**RAD-VIII**	**RAD-VIII**	**RAD-VIII**	**RAD-IX**	**RAD-IX**	**RAD-IX**	**RAD-IX**
Temperature / °C	120/140/140	120/150/150	120/160/160	100/135/135	100/145/145	100/155/155	100/165/165
RPM	300	300	300	300	300	300	300
Average Torque / Nm	1.50	1.10	1.00	1.20	1.20	1.15	1.15
Nozzle	1.5	1.5	1.5	1.5	1.5	1.5	1.5
Appearance	colorless	colorless	colorless	yellowish/colorless	yellowish/colorless	yellowish/colorless	yellowish/colorless
Translucence	transparent	transparent	transparent	opaque	transparent	transparent	transparent
Flexibility	brittle	brittle	brittle	flexible	flexible	flexible	flexible
Extrusion possible	yes	yes	yes	yes	yes	yes	yes
Filament	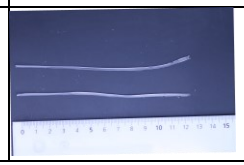	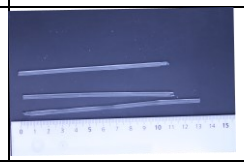	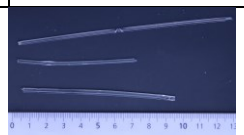	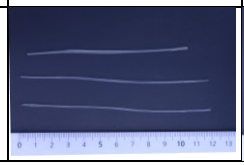	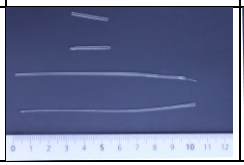	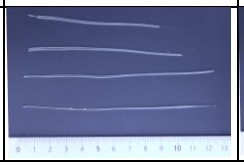	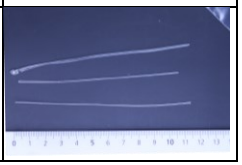

Table 74: Summary table for Extrusion Data for RAD-X and RAD-XI.

Sample	**RAD-X**	**RAD-X**	**RAD-X**	**RAD-XI**	**RAD-XI**	**RAD-XI**	**RAD-XI**
Temperature / °C	120/140/140	120/150/150	130/160/160	95/130/130	105/140/140	105/150/150	115/160/160
RPM	300	300	300	300	300	300	300
Average Torque / Nm	1.50	1.40	1.30	1.60	1.30	1.30	1.10
Nozzle	1.5	1.5	1.5	1.5	1.5	1.5	1.5
Appearance	colorless	colorless	colorless	yellowish/colorless	yellowish/colorless	yellowish/colorless	yellowish/colorless
Translucence	transparent	transparent	transparent	transparent	transparent	transparent	transparent
Flexibility	brittle	brittle	brittle	brittle	flexible	flexible	flexible
Extrusion possible	yes	yes	yes	yes	yes	yes	yes
	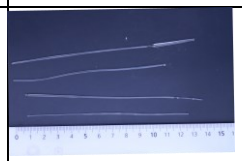	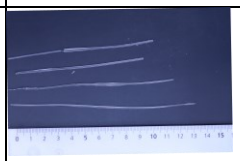		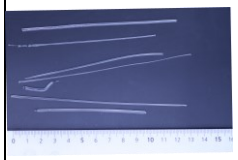	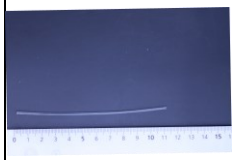	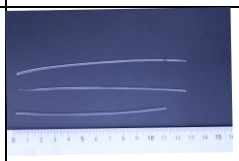	

Table 75: Summary table for Extrusion Data for RAD-XII and RAD-XIII.

Sample	**RAD-XII**	**RAD-XII**	**RAD-XII**	**RAD-XII**	**RAD-XIII**	**RAD-XIII**	**RAD-XIII**
Temperature / °C	100/150/150	90/120/120	90/130/130	95/140/140	90/120/120	90/130/130	95/140/140
RPM	300	300	300	300	300	300	300
Average Torque / Nm	1.10	1.50	1.30	1.20	1.30	1.20	1.10
Nozzle	1.5	1.5	1.5	1.5	1.5	1.5	1.5
Appearance	yellow	yellow	yellow	yellow	colorless	colorless	colorless
Translucence	transparent	transparent	transparent	transparent	transparent	transparent	transparent
Flexibility	brittle	brittle	brittle	brittle	flexible	flexible	flexible
Extrusion possible	yes	yes	yes	yes	yes	yes	yes
	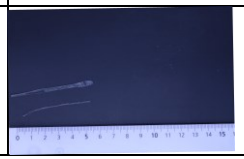	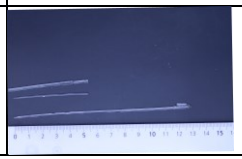	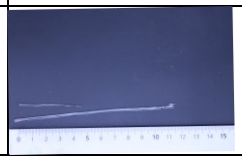	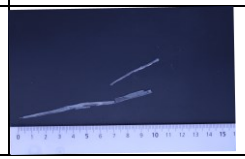	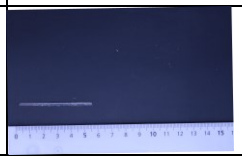	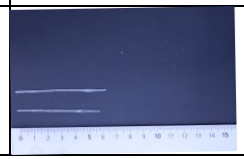	

Table 76: Summary table for Extrusion Data for RAD-XIV and RAD-XV.

Sample	**RAD-XIV**	**RAD-XIV**	**RAD-XIV**	**RAD-XV**	**RAD-XV**	**RAD-XV**	**RAD-XV**
Temperature / °C	85/130/130	85/140/140	95/150/150	90/125/125	90/135/135	90/145/145	90/155/155
RPM	300	300	300	300	300	300	300
Average Torque / Nm	1.20	1.20	1.10	1.40	1.30	1.40	1.20
Nozzle	1.5	1.5	1.5	1.5	1.5	1.5	1.5
Appearance	yellow	yellow	yellow	colorless	colorless	colorless	colorless
Translucence	transparent	transparent	transparent	transparent	transparent	transparent	transparent
Flexibility	brittle	flexible	flexible	flexible	flexible	flexible	flexible
Extrusion possible	yes	yes	yes	yes	yes	yes	yes
	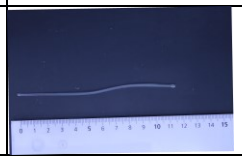	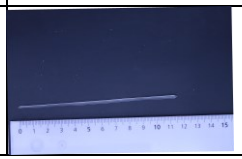	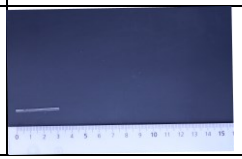	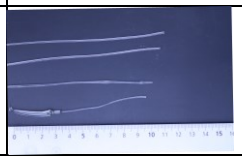	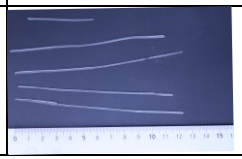	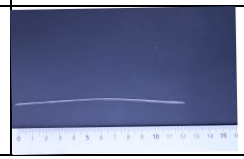	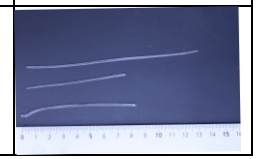

Table 77: Summary table for Extrusion Data for RAD-XVI and RAD-XVII.

Sample	**RAD-XVI**	**RAD-XVI**	**RAD-XVI**	**RAD-XVI**	**RAD-XVII**	**RAD-XVII**	**RAD-XVII**
Temperature / °C	90/100/100	90/110/110	90/120/120	100/140/140	35/45/45	45/60/60	50/70/70
RPM	300	300	300	300	300	300	300
Average Torque / Nm	1.20	1.10	1.10	1.00	1.90	1.65	1.60
Nozzle	1.5	1.5	1.5	1.5	1.5	1.5	1.5
Appearance	grey/yellowish	grey/yellowish	grey/yellowish	grey/yellowish	colorless	colorless	colorless
Translucence	opaque	transparent	transparent	transparent	transparent	transparent	transparent
Flexibility	flexible	flexible	flexible	flexible	flexible	flexible	flexible
Extrusion possible	yes	yes	yes	yes	yes	yes	yes